De Gruyter Studies in Mathematical Physics 14

Oleg N. Kirillov

Nonconservative Stability Problems of Modern Physics

De Gruyter

Physics and Astronomy Classification Scheme 2010: 02.30.Oz, 02.30.Tb, 02.40.Yy, 03.65.Vf, 05.45.-a, 45.20.-d, 45.30.+s, 46.40.-f, 47.20.-k, 47.65.-d.

Author
Dr. Oleg N. Kirillov
Helmholtz-Zentrum Dresden-Rossendorf
Institut für Fluiddynamik
Abteilung Magnetohydrodynamik
Postfach 510119
01314 Dresden
Germany
o.kirillov@hzdr.de

ISBN 978-3-11-027034-1
e-ISBN 978-3-11-027043-3
Set-ISBN 978-3-11-027044-0

Library of Congress Cataloging-in-Publication Data
A CIP catalog record for this book has been applied for at the Library of Congress.

Bibliographic information published by the Deutsche Nationalbibliothek
The Deutsche Nationalbibliothek lists this publication in the Deutsche Nationalbibliografie; detailed bibliographic data are available in the Internet at http://dnb.dnb.de.

Typesetting: PTP-Berlin Protago-TEX-Production GmbH, www.ptp-berlin.de
Printing and binding: Hubert & Co. GmbH & Co. KG, Göttingen
♾ Printed on acid-free paper

Printed in Germany

www.degruyter.com

To the memory of my parents Alevtina and Nikolai

Contents

Preface

Hubs are special. They dominate the structure of all networks in which they are present, making them look like small worlds. While two pages on the Web are 19 clicks away, Yahoo.com, a giant hub, is reachable from most Webpages in 2 to 3 clicks. From the perspective of the hubs the world is indeed very tiny.

A.-L. Barabási, *Linked*

Almost half a century ago, the seminal book by V.V. Bolotin, *Nonconservative problems of the theory of elastic stability*, came into print [75]. It summarized the experience of engineers in the analysis of nonconservative systems accumulated since the 1920s when the first attempts to take into account dissipative effects in rotor dynamics and to explain such dangerous instabilities as aerodynamic flutter and shimmy in aircraft landing gear were undertaken. Despite the many excellent books on stability theory that were published during the next fifty years [22, 60, 121, 127, 141, 150, 162, 168, 182, 213, 239, 346, 367, 369, 371, 394, 400, 412, 423, 437, 470, 503, 518, 528, 570, 590, 626], Bolotin's monograph still remains the only one devoted solely to the methods and challenges of nonconservative stability. Its only drawback is that this book cannot take into account the dramatic developments in mathematics, engineering and physics that have been made since 1963.

The book [75] was motivated mainly by the problems of stability of slender structures under follower forces and of rotating flexible shafts. Already these models deal with the two fundamental nonconservative perturbations – viscous dissipation and nonpotential positional forces [332, 333].

Last five decades extended considerably the range of applications in which such nonconservative forces play a crucial role. We mention friction-induced instabilities causing the flipping of the tippe top [84] and the problems of the acoustics of friction related to the excitation of audible vibrations in brakes and clutches [268], paper calenders [92, 537], prostheses of hip joints [255] and even in the singing glasses of Benjamin Franklin's glass harmonica [6, 293].

Nonconservative models appear in modern studies of landslides on gentle slopes when the constitutive relation of a nonassociated geomaterial, such as loose sand, is described by a nonsymmetric matrix [59, 60, 117].

In hydrodynamics and plasma physics, the counter-intuitive destabilizing influence of dissipation on negative energy waves [115, 168, 446, 552] is an important ingredient in the theories of boundary layer [349], flow control [111, 112, 171] and stability of wave propagation [90]. In rotating fluids, interplay of the nonconservative and gyroscopic forces may lead to the paradoxical discontinuous change in the stability boundary as happens in the case of the baroclinic instability when the Ekman layer dissipation is infinitesimally small [334, 501, 563].

In magnetohydrodynamics, the Velikhov–Chandrasekhar paradox [120,581] occurs in the theory of magnetorotational instability when for infinite electrical conductivity of the differentially rotating fluid the limit of the vanishing axial magnetic field does not trace back to the Rayleigh threshold of hydrodynamics [1, 28, 199]. Nonconservative forces play an increasing role in celestial mechanics, e.g., in the modeling of tethered satellite systems, satellite and planetary rings [43, 44, 87].

A rich source of nonconservative problems is modern robotics and automatic control [41] and biomechanics [216] – for example, the spine is frequently modeled as a column loaded by a distributed follower force [500]. Of course, traditional areas such as aerospace engineering and structural mechanics remain one of the biggest consumers of the nonconservative stability theory [224, 240].

Already in the 1960s Bolotin emphasized that progress in the nonconservative stability theory depends on developments in the theory of nonself-adjoint operators. Important contributions to the latter motivated mainly by mechanical applications were made, e.g., in the 1940s by S. L. Sobolev [536] and L. S. Pontryagin [483], in the 1950s by M. V. Keldysh [261] and M. G. Krein [336, 337] and since then by many other authors.

The needs of optimal design and rational experiment planning required consideration of multiparameter families of nonself-adjoint boundary eigenvalue problems. In the 1970s, the studies by V. I. Arnold and his co-workers established a sharp correspondence between the multiple eigenvalues of nonsymmetric matrices and geometric singularities on the boundary of the asymptotic stability domain of a matrix family [17, 18, 374, 375]. An immediate consequence of this result is the resolution of the famous Ziegler's paradox (1952) of destabilization of a reversible system by small dissipation [622] by means of the Whitney umbrella singularity, which was done independently by a number of authors starting with O. Bottema in 1955–56 [80, 81].

Since the 1950s, the concept of the symplectic or Krein signature of eigenvalues has been widely used in hydro- and magnetohydrodynamics to describe waves of positive and negative energy [264, 320, 390, 392, 606, 607]. In the 1990s, the influence of non-Hamiltonian perturbations on the stability of Hamiltonian systems became a topic for a systematic investigation [391, 395] that gave birth to the area of research known

as 'dissipation-induced instabilities' [74] – a concept that touches a broad variety of physical applications [333].

Though very excellent, a network of these results is chaotically scattered at present throughout the specialized journals. Many brilliant physical phenomena that could crown the nonconservative stability theory are almost unknown to the stability theorists with a classical mechanical background. On the other hand, achievements of the theory of nonself-adjoint operators [421, 611], the theory of operators in the spaces with indefinite metric (Krein and Pontryagin spaces) [202], Lidskii–Vishik–Lyusternik perturbation theory for multiple eigenvalues [428], theory of multiparameter eigenvalue problems [24, 585], modern results of applied linear algebra [576] as well as singularity theory appear to be still not familiar to many engineers, physicists and even stability theorists working with nonconservative stability problems.

However, the combination of these approaches of modern applied mathematics with the complex fundamental nonconservative phenomena of physics and mechanics seems to be the only way to understand the latter and to create a rather complete and unified constructive theory of stability of nonconservative systems and of dissipation-induced instabilities. That is why there is a strong need for a detailed exposition which would bring together the scattered results of the last fifty years and which would endeavor to unify and to systematize both the results and the methods of treatment of the nonconservative stability problems of modern physics. This book is an attempt to fill this need.

In it an effort is made to present the subject of nonconservative stability from the modern point of view as completely as possible within the allotted space. It presents relevant mathematical concepts, both already familiar and the new ones for this subject as well as rigorous stability results and numerous classical and contemporary examples from mechanics and physics. The book is substantially based on the results of the author; although by necessity it contains some results of other authors without which it is impossible to create a self-consistent exposition. It is hoped that this book will serve the present and prospective specialist in the field by acquainting him with the current state of knowledge in this actively developing field.

The book has 12 chapters. After a number of examples accompanied by a historical overview in the Introduction, the first six chapters deal with the finite dimensional nonconservative systems, while the rest of the book is dedicated to the infinite dimensional ones. Naturally, the first part of the book contains fundamentals of the theory and more general results because of the wide variety of mathematical tools available in finite dimensions. The center of gravity in the second part is shifted to studies of concrete physical problems. All chapters contain illustrative physical examples.

I would like to express my warmest gratitude to all the colleagues and collaborators whose support, friendly advice, encouraging discussions and fruitful joint research were among the main inspirational factors driving my work on this project: Abd Rahim Abu Bakar, Sergei Agafonov, Vadim Anischenko, Teodor Atanackovic, Vladimir Beletsky, Carl Bender, Michael Berry, Noël Challamel, Gengdong

Cheng, Richard Cushman, Felix Darve, Barbara Dietz, Mikhail Efroimsky, Yasuhide Fukumoto, Gunter Gerbeth, Valentin Glavardanov, Yuanxian Gu, Eva-Maria Graefe, Samvel Grigorian, Uwe Günther, Peter Hagedorn, Hanns-Ludwig Harney, Daniel Hochlenert, Norbert Hoffmann, Igor Hoveijn, Wolfhard Kliem, Anthony Kounadis, Yuri Leschinski, Alexei Mailybaev, Vadim Marchenko, Jerrold Marsden, Maxim Miski-Oglu, Oliver O'Reilly, Huajiang Ouyang, Pauli Pedersen, Dmitry Pelinovsky, Alexandra Perlova, Karl Popp, Achim Richter, Ingrid Rotter, Florian Schäfer, Guido Schneider, Alexander Seyranian, Sergei Sorokin, Gottfried Spelsberg-Korspeter, Frank Stefani, Ferdinand Verhulst, Alexander Zevin, and Miloslav Znojil.

I learned a lot from the lectures and seminars given during my studies at the Moscow Institute of Physics and Technology in 1989–1995 by Alexander Abramov, Oleg Besov, Boris Fedosov, Victor Galactionov, Victor Lidskii, Boris Rauschenbach, Victor Zhuravlev, and other brilliant professors and lecturers of my Alma Mater whose enthusiastic work in the 'stormy 1990s' in Russia was an impressive example of a noble dedication to students and the profession that deeply influenced my formation as a scientist.

I thank the Russian Foundation for Basic Research (RFBR, Russia), the National Natural Science Foundation of China (NSFC, China), INTAS (EU), the Civilian Research and Development Foundation (CRDF, USA), the Alexander von Humboldt Foundation (Germany), Deutsche Forschungsgemeinschaft (DFG, Germany), Saxon Ministry of Science (Germany) and the Japan Society for the Promotion of Science (JSPS, Japan) for their most valuable funding.

I am indebted to my wife Ksenia and to my daughter Marina and son Nikolai who generously gifted me time, support, and understanding.

Dresden, 12 April 2012

Chapter 1

Introduction

I never satisfy myself until I can make a mechanical model of a thing. If I can make a mechanical model, I understand it.

W. Thomson (Lord Kelvin) [436]

Recent years have seen tremendous activity related to non-Hermitian Hamiltonians in physics and, in particular, to the physics of non-Hermitian degeneracies – so called diabolical and exceptional points [50, 154, 166, 218, 426]. In mechanics, these spectral singularities correspond to semisimple and nonsemisimple $1:1$ resonances that in many cases determine peculiar stability properties of a mechanical system. Guided by the above motto of Lord Kelvin we would like to invite a reader into a labyrinth of modern concepts such as a non-Hermitian Hamiltonian, exceptional points, the geometric phase, and $\mathcal{PT}$-symmetry, looking at them through the prism of classical mechanics and stability theory. Mathematical and historical parallels discussed in this chapter should convince the reader that positions occupied by non-Hermitian physics and nonconservative mechanics are closer to each other than one might expect. A simple but paradigmatic model of Brouwer's rotating saddle trap will serve us as an Ariadne's thread in this adventure.

1.1 Gyroscopic stabilization on a rotating surface

In 1918 Luitzen Egbertus (Bertus) Jan Brouwer (1881–1966) – a founder of modern topology who established, for example, the topological invariance of dimension and the fixed point theorem – considered stability of equilibrium of a heavy particle in a rotating vessel [82, 93, 94, 304].[1]

[1] Curiously enough, in 1917 motivated by meteorological applications Francis John Welsh Whipple (1876–1943) studied a not unrelated problem on the motion of a particle on the surface of a rotating globe [594].

1.1.1 Brouwer's mechanical model

Let us imagine a particle of unit mass moving on a surface that has a horizontal tangent plane at some point O and rotates with a constant angular velocity Ω around a vertical axis through O in a counter-clockwise direction, Figure 1.1.

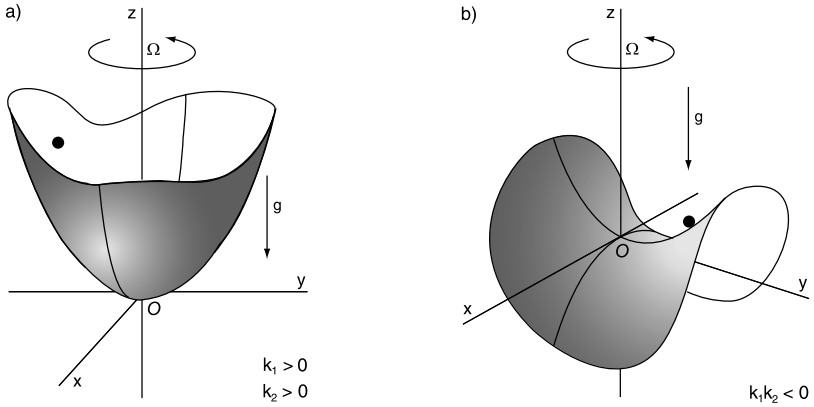

Figure 1.1. Brouwer's particle on a rotating (a) cavity and (b) saddle [299].

In the co-rotating frame (x, y, z), the (x, z)- and (y, z)-plane of which coincide with the principal normal sections of the surface at the origin O, a potential function of the particle is $V = gz$ and a kinetic energy is $T = \frac{1}{2}[(\dot{x} - y\Omega)^2 + (\dot{y} + x\Omega)^2 + \dot{z}^2]$, where g is the gravity acceleration. In the assumption that the particle moves without friction, the equations of motion linearized about the equilibrium position O, have the form [93]

$$\begin{aligned} \ddot{x} - 2\Omega\dot{y} + \left(k_1 - \Omega^2\right) x = 0, \\ \ddot{y} + 2\Omega\dot{x} + \left(k_2 - \Omega^2\right) y = 0, \end{aligned} \tag{1.1}$$

where dot indicates time differentiation, $k_{1,2} = g/r_{1,2}$, and r_1 and r_2 are the radii of curvature of the intersection of the surface with the (x, z)- and (y, z)-plane, respectively, $r_1 \neq r_2$.

Brouwer's innovation was that he not only allowed the radii of curvature to be nonequal, which was already the state of the art of his time, but he also did not impose restrictions on the sign of k_1 and k_2 and considered both concave (Figure 1.1 (a)) and saddle-like (Figure 1.1 (b)) surfaces, ahead of his contemporaries.

1.1.2 Eigenvalue problems and the characteristic equation

Assuming solution of the linear system of differential equations (1.1) in the form $x = X\exp(\lambda t)$ and $y = Y\exp(\lambda t)$, we arrive at the homogeneous system of algebraic

equations with respect to X and Y

$$\mathbf{L}\mathbf{u} = 0, \tag{1.2}$$

where the *matrix polynomial* [200] with respect to the *spectral parameter* λ is

$$\mathbf{L}(\lambda) = \mathbf{I}\lambda^2 + 2\Omega\mathbf{J}\lambda + \mathbf{K} + (\Omega\mathbf{J})^2 \tag{1.3}$$

and

$$\mathbf{u} = \begin{pmatrix} X \\ Y \end{pmatrix}, \quad \mathbf{I} = \begin{pmatrix} 1 & 0 \\ 0 & 1 \end{pmatrix}, \quad \mathbf{J} = \begin{pmatrix} 0 & -1 \\ 1 & 0 \end{pmatrix}, \quad \mathbf{K} = \begin{pmatrix} k_1 & 0 \\ 0 & k_2 \end{pmatrix}. \tag{1.4}$$

Equation (1.2) is one of the standard forms of eigenvalue problems associated with gyroscopic systems [234, 238]. It has a nontrivial solution if and only if

$$\det(\mathbf{L}(\lambda)) = 0, \tag{1.5}$$

which results in the *characteristic equation* for λ

$$a_0\lambda^4 + a_1\lambda^2 + a_2 = 0. \tag{1.6}$$

with

$$a_0 = 1, \quad a_1 = k_1 + k_2 + 2\Omega^2, \quad a_2 = (k_1 - \Omega^2)(k_2 - \Omega^2). \tag{1.7}$$

The roots of equation (1.6) are *eigenvalues* of the *eigenvalue problem* (1.2). Together with the *eigenvectors* $\mathbf{u}$ that are the corresponding solutions of equation (1.2) and the generalized eigenvectors that will be introduced in the following, they determine time evolution of the solutions of the linear system (1.1).

Biquadratic equation (1.6) can be solved exactly

$$\lambda^2 = -\frac{k_1 + k_2 + 2\Omega^2}{2} \pm \frac{1}{2}\sqrt{(k_1 - k_2)^2 + 8\Omega^2(k_1 + k_2)}. \tag{1.8}$$

A necessary and sufficient condition for all λ^2s to be real is that the discriminant of the polynomial (the radicand in (1.8)) is nonnegative [3, 187]

$$D := (k_1 - k_2)^2 + 8\Omega^2(k_1 + k_2) \geq 0. \tag{1.9}$$

Moreover, the real λ^2s are all nonpositive if and only if $a_1 \geq 0$ and $a_2 \geq 0$, which after taking into account expressions (1.7), yields

$$k_1 + k_2 + 2\Omega^2 \geq 0, \quad (k_1 - \Omega^2)(k_2 - \Omega^2) \geq 0. \tag{1.10}$$

Inequalities (1.9) and (1.10) form a criterion for the eigenvalues λ to be all pure imaginary, i.e. $\lambda = \pm i\omega$, where $\omega \geq 0$ is real (*spectral stability*). This is however only a necessary condition for all the solutions to the linear equation (1.1) to be bounded and thus to be *marginally (linearly) stable* [390].

1.1.3 Eigencurves and bifurcation of multiple eigenvalues

Among the pure imaginary or zero eigenvalues, repeated roots of the characteristic equation (1.6) may occur. Indeed, according to equation (1.8), the eigenvalues are double in the discriminant set $D = 0$, being pure imaginary when $a_1 \neq 0$ and zero when $a_1 = 0$. This set bounds the light gray domains in the (k_1, Ω)-plane in Figure 1.2 while the set $a_2 = 0$ corresponds to the double eigenvalues $\lambda = 0$ and bounds the dark gray domains. The eigenvalues that are repeated roots of the characteristic equation are said to have an *algebraic multiplicity* [258, 428].

Evolution of eigenvalues when the white and gray domains in Figure 1.2 are crossed with the variation of parameters, is presented as *eigencurves* [64] in the $(\mathrm{Re}\lambda, \mathrm{Im}\lambda, \Omega)$-space in Figure 1.3. When $k_1 = 0.25$ and $k_2 = -0.3$ the surface is a saddle and the equilibrium of the Brouwer particle is unstable without rotation. Indeed, when $\Omega = 0$, there exist a complex-conjugate pair of pure imaginary eigenvalues and two

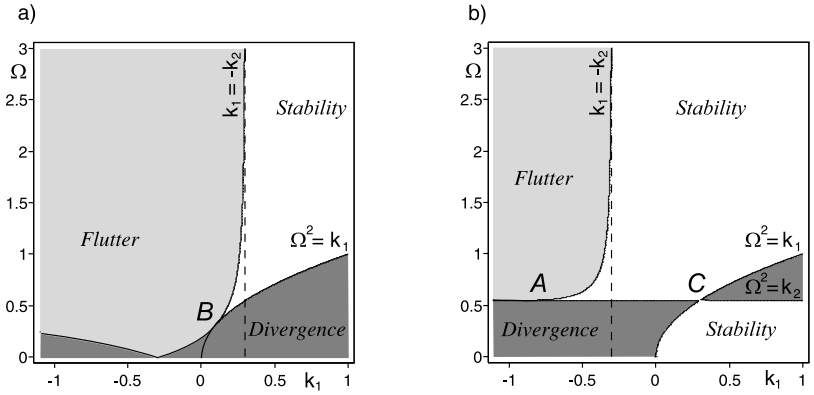

Figure 1.2. Stability diagram of Brouwer's problem in the (k_1, Ω)-plane for (a) $k_2 = -0.3$ and (b) $k_2 = 0.3$ [304].

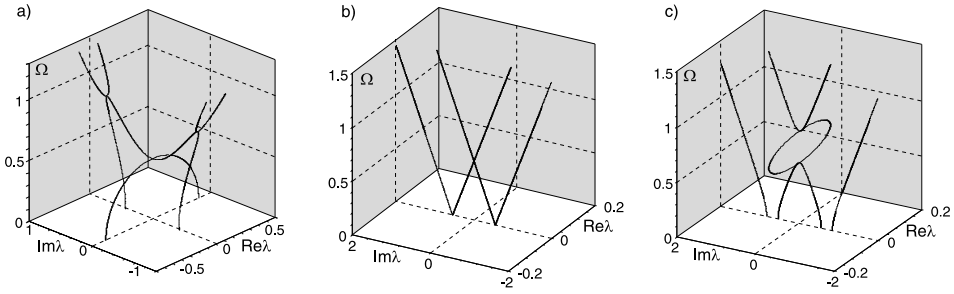

Figure 1.3. Evolution of eigenvalues with the variation of the rotation speed for (a) a saddle with $k_1 = 0.25$ and $k_2 = -0.3$ (gyroscopic stabilization), (b) symmetric concave surface with $k_1 = k_2 = 0.3$ (Campbell diagram), and (c) nonsymmetric concave surface with $k_1 = 0.7$ and $k_2 = 0.3$ (bubble of instability and avoided crossings) [304].

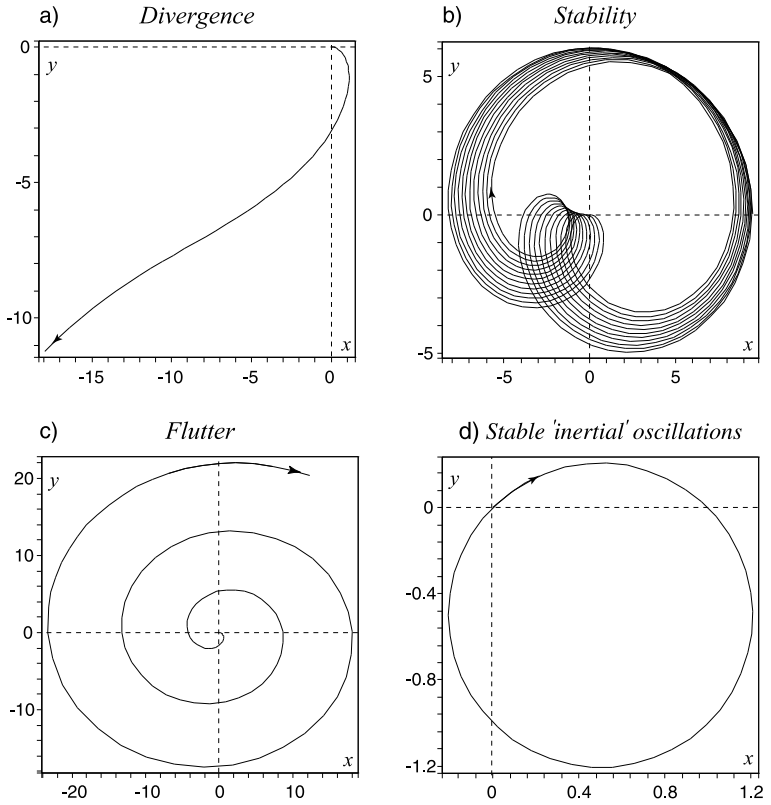

Figure 1.4. Tracks of the Brouwer particle in (x, y)-plane at $k_1 = 0.25$, $k_2 = -0.3$, $x(0) = 0$, $\dot{x} = 1$, $y(0) = 0$ and $\dot{y}(0) = 0$: (a) escaping by divergence at $\Omega = 0.4$ when $0 \le t \le 8$, (b) trapping at $\Omega = 0.6$ when $0 \le t \le 200$, (c) escaping by flutter at $\Omega = 0.9$ when $0 \le t \le 20$. (d) Stable inertial oscillations at the point C with $k_1 = k_2 = 1$ and $\Omega = 1$ when $x(0) = 0$, $\dot{x}(0) = 1$, $y(0) = 0$, $\dot{y}(0) = 1$ and $0 \le t \le \pi$ [304].

real ones of different signs, Figure 1.3 (a). A positive real eigenvalue corresponds to an exponentially growing nonoscillatory solution which is known as *divergence* or *static instability* [239], see Figure 1.4 (a).

With increasing angular velocity, the magnitude of the real eigenvalues becomes smaller until they collide at the origin and form a zero eigenvalue of algebraic multiplicity 2. If Ω grows further, the double eigenvalue splits into two pure imaginary eigenvalues, Figure 1.3 (a). Then, all the eigenvalues are pure imaginary of algebraic multiplicity 1 (i.e. *simple*) and the equilibrium is marginally stable.

Therefore, a sufficiently fast rotation of a saddle results in the *gyroscopic stabilization* [325] or *trapping* [571] of the particle, Figure 1.4 (b). The curve $a_2 = 0$, corresponding to double zero eigenvalues, forms a boundary between the domains of divergence (dark gray) and stability (white), Figure 1.2 (a).

What are the eigenvectors at the double zero eigenvalues? On the curve $k_1 = \Omega^2$ when $\Omega^2 \neq k_2$ every eigenvector is of the form $\mathbf{u}_0^T = C_1(1, 0)$, where C_1 is an arbitrary constant. Any two such vectors are linearly dependent. The number of linearly independent eigenvectors at the eigenvalue is its *geometric multiplicity*. Thus, at the points of the boundary $k_1 = \Omega^2$ when $\Omega^2 \neq k_2$, zero eigenvalues have algebraic multiplicity 2 and geometric multiplicity 1 and the *defect*, i.e. the difference between the multiplicities, is equal to one [258, 428].

Nevertheless, such a *defective eigenvalue* possesses another vector,

$$\mathbf{u}_1^T = (C_2, 2\Omega C_1/(\Omega^2 - k_2))$$

that satisfies the nonhomogeneous equation [200]

$$\mathbf{L}\mathbf{u}_1 + \frac{\partial \mathbf{L}}{\partial \lambda}\mathbf{u}_0\bigg|_{\lambda=0} = 0. \tag{1.11}$$

The eigenvector $\mathbf{u}_0$ and the *generalized eigenvector* $\mathbf{u}_1$ constitute what is known as the *Keldysh chain* in the theory of matrix polynomials [200, 261, 421] and the *Jordan chain* in the matrix theory [548]. The solution, corresponding to a double eigenvalue with the defect 1, involves both vectors of the chain

$$\mathbf{z}(t) = (\mathbf{u}_1 + \mathbf{u}_0 t)e^{\lambda t}, \tag{1.12}$$

where $\mathbf{z}^T = (x, y)$. The linear in t *secular term* makes the solution (1.12) grow even if λ is vanishing or pure imaginary, in contrast to the case of a simple eigenvalue when $\mathbf{z}(t) = \mathbf{u}_0 e^{\lambda t}$. Therefore, although at the line $a_2 = 0$ separating the stability and divergence domains, double eigenvalues are vanishing, the corresponding solutions are still statically unstable with the linear growth in time when a double eigenvalue has the Keldysh chain. The growth is exponential at the inner points of the dark gray divergence domain in Figure 1.2.

The gyroscopically trapped Brouwer's particle can escape the *rotating saddle trap* when $k_1 < -k_2$ and the speed Ω is high enough, Figure 1.2 (a). Approaching the upper bound for Ω, two pure imaginary eigenvalues merge into a double one with the defect 1 (a *nonsemisimple* $1:1$ *resonance* [231]). When Ω comes inside the light gray domain in Figure 1.2 (a), the double eigenvalue splits into two complex eigenvalues, one of them with $\mathrm{Re}\lambda > 0$, Figure 1.3 (a). This eigenvalue corresponds to an oscillatory solution with exponentially growing amplitude (*flutter*), see Figure 1.4 (c). At the flutter boundary the amplitude of the oscillatory solution is growing linearly in time owing to the secular term. This scenario of transition from stability to flutter is known as the *Krein collision* [337, 430] or the linear *Hamiltonian–Hopf bifurcation* [579].

The stability gap between the flutter and divergence domains decreases when the parameter $k_1 > 0$ approaches the point B in Figure 1.2 (a). At this point the boundaries of the two instability domains touch each other, forming a cuspidal singularity. At the *cuspidal point* there exists a defective zero eigenvalue of algebraic multiplicity 4 and

geometric multiplicity 1. The same singularity occurs for $k_1 < 0$ and $k_2 > 0$ at the point A in Figure 1.2 (b). At the singular points the equilibrium is unstable because of secular terms.

At the singular point C in Figure 1.2 (b) the divergence boundaries $k_1 = \Omega^2$ and $k_2 = \Omega^2$ intersect each other. The curvatures k_1 and k_2 are equal at this self-intersection. When they are nonvanishing, there exist a pair of pure imaginary eigenvalues and a double zero one at C. In this symmetric case the eigenvalues as functions of Ω remain pure imaginary in the vicinity of the zero double eigenvalue, see Figure 1.3 (b). For $k_1 = k_2 > 0$ the eigenvalues are *passing* [146] through each other at zero when Ω is varying without *splitting*, see Figure 1.3 (b). The latter however is typical at any other point of the divergence boundary, Figure 1.3 (a, c).

The rotating symmetric cavity does not have a preferable less steep direction that could provoke the Brouwer particle to escape. Indeed, the solution corresponding to the double zero eigenvalue is free from secular terms. This happens because there are two linearly independent eigenvectors at the double eigenvalue, which is a *semisimple eigenvalue* [428] with algebraic and geometric multiplicity 2. The point C in Figure 1.2 (b) thus belongs to the stability domain.

Since at C the gravitational and centrifugal forces are in balance, the sole Coriolis force causes the Brouwer particle to rotate along an eccentric circle with the frequency 2Ω, see Figure 1.4 (d). In geophysics such a motion is known as *inertial oscillations* or *inertial waves* that would occur in the atmosphere or in the ocean in the case when the Coriolis force would not have a dependence on the latitude (the β-effect), see e.g. [140, 464].

When $k_1 = k_2 = 0$, which happens when either gravity is absent or the surface is flat, the point C is at the origin in the (k_1, k_2, Ω)-space. However, the equilibrium of the particle on the flat nonrotating surface is unstable: any perturbation in its velocity yields a linear in time increase in the coordinate. These secular terms correspond to two double zero eigenvalues, each of geometric multiplicity 1, which was suggested by the physical reasoning quite in the spirit of the insightful book by Mark Levi [376].

Indeed, at $\Omega = 0$ and $k_1 = k_2 = 0$ Brouwer's equations (1.1) decouple. With the new variables $x_1 = x$, $x_2 = \dot{x}$ and $y_1 = y$, $y_2 = \dot{y}$, the equations $\ddot{x} = 0$ and $\ddot{y} = 0$ take the form $\dot{\mathbf{q}} = \mathbf{A}\mathbf{q}$, where $\mathbf{q}^T = (x_1, x_2, y_1, y_2)$, and

$$\mathbf{A} = \begin{pmatrix} 0 & 1 & 0 & 0 \\ 0 & 0 & 0 & 0 \\ 0 & 0 & 0 & 1 \\ 0 & 0 & 0 & 0 \end{pmatrix}.$$

The matrix $\mathbf{A}$ contains a pair of Jordan blocks with double zero eigenvalues ($0^2 0^2$ in notation proposed by Arnold [17]). Assuming $k_2 = \kappa k_1$ in equation (1.1) we find that the two double eigenvalues at $\Omega = 0$ split as $\lambda_{1,2} = \pm i\sqrt{k_1}$ and $\lambda_{3,4} = \pm i\sqrt{\kappa k_1}$, see Figure 1.5 (a). This type of splitting was observed in the spectrum of the Couette–Taylor flow and of the Bose–Hubbard model, see [308] and references therein. At $\Omega \neq$

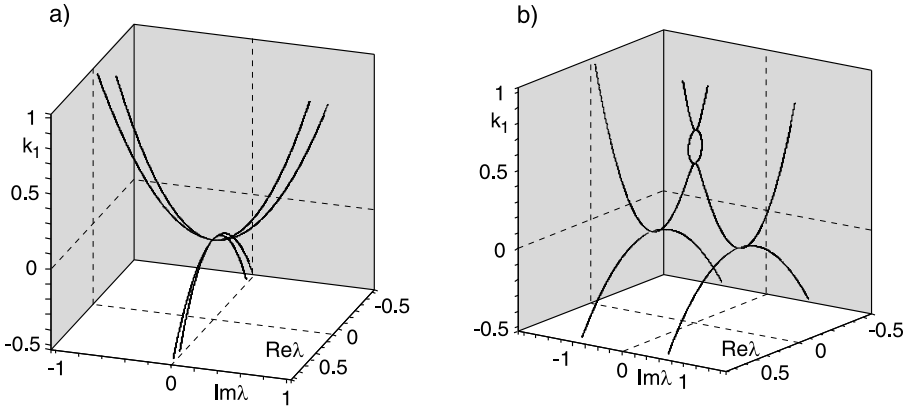

Figure 1.5. Evolution of eigenvalues with the variation of k_1 in the $(\mathrm{Re}\lambda, \mathrm{Im}\lambda, k_1)$-space when $k_2 = \kappa k_1$ and $\kappa = 0.7$ at (a) $\Omega = 0$ and (b) $\Omega = 0.7$ [304].

0, the degeneracy is removed and the eigencurves develop a bubble of (divergence) instability, Figure 1.5 (b).

1.1.4 Singular stability boundary of the rotating saddle trap

The analysis of eigenvalues and eigenvectors performed above suggests the necessary and sufficient conditions for marginal stability of the linear system (1.1)

$$D > 0, \quad a_2 > 0, \quad k_1 = k_2 = \Omega^2 \ \forall \ \Omega \neq 0. \tag{1.13}$$

In the (k_1, k_2, Ω)-space the parabolic cylinders $k_1 = \Omega^2$ and $k_2 = \Omega^2$ intersect along the parabola SC that lies in the plane $k_1 = k_2$, see Figure 1.6. This parabola smoothly touches the surface $D = 0$ at the origin (S). In its turn, the latter surface smoothly touches both of the parabolic cylinders $k_1 = \Omega^2$ and $k_2 = \Omega^2$ along spacial curves SA and SB that project into the lines $k_2 = -3k_1$ and $k_1 = -3k_2$ in the (k_1, k_2)-plane shown by dashed lines in Figure 1.6. The stability domain thus consists of the two compartments joined along the line SC. The boundary of the first part has the form of a trihedral spike with the cuspidal edges SA and SB and the transversal intersection SC. All three curves touch each other at the origin. The boundary of another part has only a dihedral angle singularity along SC. The system is stable at the inner points of the domains as well as on the edge SC when $\Omega \neq 0$.

The trihedral spike corresponds to the stability for large angular velocities according to Brouwer's classification. Indeed, both the stability region in Figure 1.2 (a) and the upper stability region in Figure 1.2 (b) are slices of it. In Brouwer's interpretation "as long as in O the principal curvature, concave in an upward direction, is less than three times the one concave in a downward direction, there are rotation velocities for which the motion of the particle on the rotating saddle yields formal stability" [93, 94].

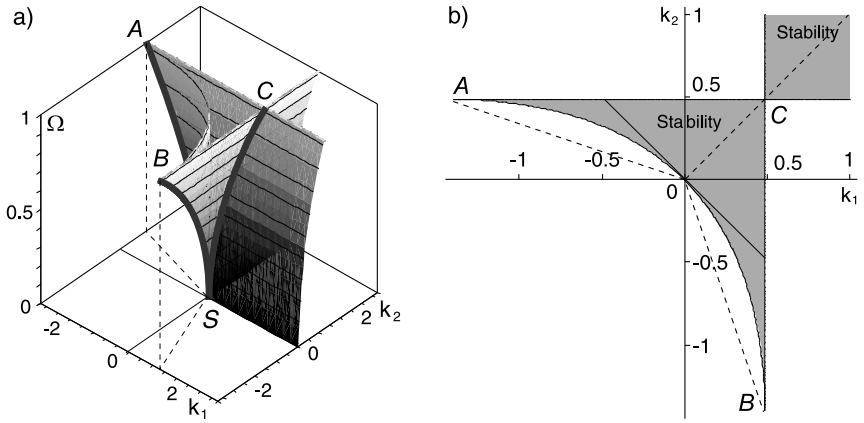

Figure 1.6. (a) Stability boundary of Brouwer's problem with the swallowtail-like singularity at the origin in the (k_1, k_2, Ω)-space and (b) the domain of marginal stability in the (k_1, k_2)-plane for $\Omega = 0.7$ with the dashed lines indicating projections of the two cuspidal edges SA and SB and the line of self-intersection SC [299, 304].

This challenging to common sense conclusion of Brouwer follows from the proportions of the cross-section of the spike by the $\Omega = const$ plane that has the form of a curvilinear triangle ABC, Figure 1.6 (b). Similar planar stability domains were observed in numerous problems of gyroscopic stabilization, e.g. for a mass mounted on a noncircular weightless rotating shaft subject to a constant axial compression force [238, 241, 518] or in a recent study of levitation of a rotating body carrying a point electrical charge in the field of a fixed point charge of the same sign [151].

A beautiful connection exists between the boundaries of the domain of the gyroscopic stabilization and the eigenvalues $\sigma_{1,2}(\mathbf{K})$ of the matrix $\mathbf{K}$ of potential forces and those of the rotationally symmetric matrix $\mathbf{K}_A$

$$\mathbf{K}_A = \frac{1}{2}(\mathbf{K} - \mathbf{JKJ}) = \frac{k_1 + k_2}{2}\mathbf{I}, \tag{1.14}$$

representing a sort of 'averaged' $\mathbf{K}$ around the rotation axis [582].

Already in Figure 1.2 (b) it is visible that the lower bound of the region of gyroscopic stabilization at large angular velocities is determined by $\sigma_{1,2}(\mathbf{K})$ as

$$\Omega_d^2 = \max(\sigma_1(\mathbf{K}), \sigma_2(\mathbf{K})). \tag{1.15}$$

According to Veselić [582], $\mathbf{K}_A > 0$ is a necessary and sufficient condition for the absence of the upper bound on the gyroscopic parameter Ω. Hence, the gyroscopically stabilized Brouwer particle will not escape the trap with the arbitrary increase of $|\Omega| > |\Omega_d|$ if and only if $k_1 + k_2 > 0$. This condition defines the vertical asymptotes to the flutter domain in Figure 1.2. Hence, at low rotation speeds of a saddle, it is negative eigenvalues of $\mathbf{K}_A$ that determine the existence of the upper bound for the gyroscopic

stabilization, which is necessary for the origination of the cuspidal singularities on the stability boundary [582].

The triangle ABC in Figure 1.6 (b) is connected at the corner C to the domain of stability for small angular velocities given by the inequalities $k_1 > \Omega^2$ and $k_2 > \Omega^2$ (cf. the lower stability region in Figure 1.2 (b)). This part of the stability diagram was found already in 1869 by Rankine[2] [491], whereas the triangle ABC was reconstructed by joint efforts of Föppl[3] (1895) [172], von Kármán[4] (1910) [586], Prandtl[5] (1918) [485], Brouwer (1918) [93], and Jeffcott[6] (1919) [244].

The *swallowtail*-like surface bounding the stability domain of the Brouwer heavy particle in a rotating vessel perfectly symbolizes the variety of applications to which this mechanical model is connected. Almost literally at every corner of the surface shown in Figure 1.6 (a) lives a physical phenomenon.

1.2 Manifestations of Brouwer's model in physics

1.2.1 Stability of deformable rotors

With the equal positive coefficients $k_1 = k_2 > 0$, the Brouwer equations (1.1) coincide with that of the idealized model of the classical rotor dynamics problem of shaft whirl by Föppl [172], von Kármán [586], and Jeffcott [244], written in the rotating (x, y)-frame.

Indeed, a deformable shaft carrying, e.g. a turbine wheel, and rotating with the angular speed Ω about its axis of symmetry can be modeled as a planar oscillator on a rotating plate [73], i.e. as a unit mass point that is suspended symmetrically by massless springs with the effective stiffness coefficients $k_1 = k_2 = k$ from the frame that rotates with the angular velocity Ω [137, 139], see Figure 1.7 (a). On the other hand, this model arises in the theory of modern micro-mechanical Coriolis vibratory gyroscopes (CVG) [16].

For the stationary ($\Omega = 0$) symmetrical Föppl–von Kármán–Jeffcott rotor the transverse bending modes occur in pairs with equal natural frequencies $\omega = \sqrt{k}$ for vibrations in orthogonal diametral planes. When the vibrations of such a pair are combined with equal amplitudes and a quarter period phase difference, the result is a *circularly polarized* vibration – a clockwise or counter-clockwise circular *whirling* motion with

[2] William John Macquorn Rankine (1820–1872) – a Scottish engineer and physicist, an author e.g. of the Rankine vortex model and Rankine–Hugoniot conditions in gas dynamics and at the same time of one of the first studies on stability of bicycles.

[3] August Otto Föppl (1854–1924) – a German civil engineer, a student of C. Mohr and an advisor of L. Prandtl; well known are e.g. the Föppl–von Kármán equations for large deflections of thin flat plates.

[4] Theodore von Kármán (1881–1963) – a Hungarian-German-American aerospace engineer and hydrodynamicist, one of the founders of the Jet Propulsion Laboratory.

[5] Ludwig Prandtl (1875–1953) – a German scientist, one of the creators of aerodynamics.

[6] Henry Homan Jeffcott (1877–1937) – an Irish engineer developed the *Jeffcott rotor* model.

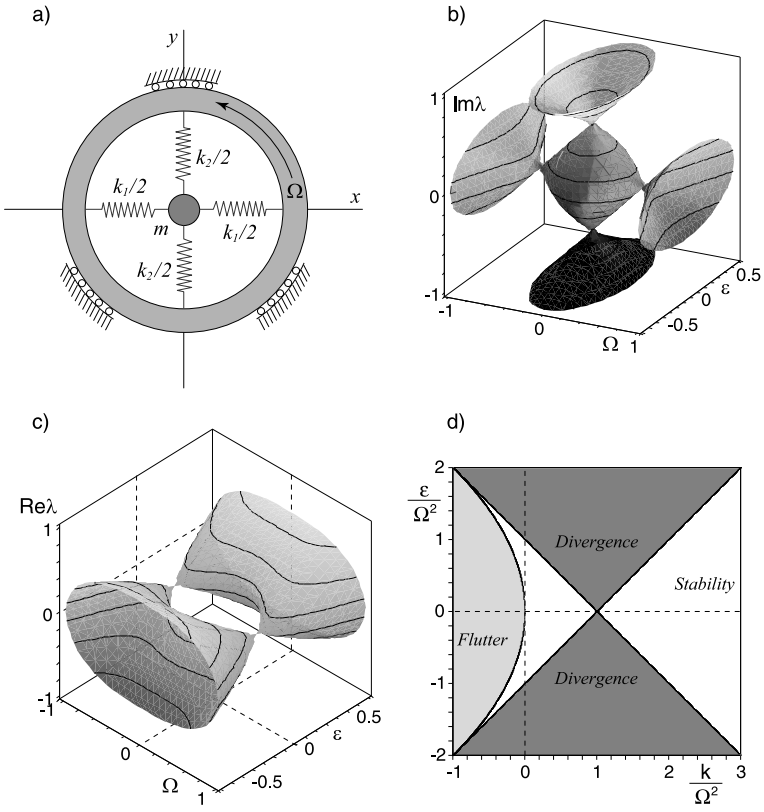

Figure 1.7. (a) A Prandtl–Smith model of whirling shaft [137, 139]: A point mass $m = 1$ suspended by the springs from the frame that rotates with the angular velocity Ω. (b) Whirling frequencies of the Prandtl–Smith rotor with $k_1 = k + \varepsilon$, $k_2 = k - \varepsilon$, and $k = 0.3$ as a function of Ω and ε form a singular surface with four conical points in the plane $\varepsilon = 0$. (c) Growth rates of the Prandtl–Smith rotor showing instability due to stiffness detuning near the critical speeds $\Omega = \pm\sqrt{k}$. (d) The corresponding stability diagram in the $(\varepsilon\Omega^{-2}, k\Omega^{-2})$-plane given by the conditions (1.19) and (1.20) [304]. The parameter $k\Omega^{-2}$ has the meaning of the squared *Rossby number* $\mathrm{Ro} = k^{1/2}\Omega^{-1}$. In geophysics it is a measure of the relative strength of the Coriolis force.

the whirl rate $\omega > 0$ [137, 139]. This phenomenon is related to the *Doppler splitting* of the repeated eigenvalues into the forward and backward traveling waves propagating along the circumferential direction of a rotating elastic solid of revolution, known already to Bryan[7] in 1890 [96, 248, 439].

According to Brouwer's stability conditions (1.13), the symmetrical Föppl–von Kármán–Jeffcott rotor is marginally stable at any speed Ω. Indeed, the part of the

[7] George Hartley Bryan (1864–1928) – a British physicist, discoverer of the *wave inertia effect* (Bryan's effect) in rotating shells and originator of the equations of airplane motion.

plane $k_1 = k_2$ corresponding to $k_{1,2} > 0$ belongs to the domain of marginal stability, as seen in the stability diagrams of Figure 1.6.

The symmetry of the Föppl–von Kármán–Jeffcott rotor is, however, a latent source of its instability. Destabilization can be caused already by constraining the mass point to vibrate along a rotating diameter. For example, if a guide rail is installed along the x-axis so that y is constrained to vanish identically, equation (1.1) reduces to the 1869 model by Rankine [491]

$$\ddot{x} + (k_1 - \Omega^2)x = 0, \tag{1.16}$$

which predicts unbounded growth for x as soon as $\Omega^2 > k_1$, i.e. as soon as the centrifugal field overpowers the elastic field [137, 139]. In the diagram comprising Figure 1.6 (b) Rankine's instability threshold (critical rotating speed) bounds the infinite stability domain with the corner at the point C showing that the constraint could also be achieved by tending one of the stiffness coefficients to infinity. Note that recently Baillieul and Levi, motivated by stabilization of satellites with flexible parts, studied the dynamical effects of imposing constraints on the relative motions of component parts in a rotating mechanical system or structure and in particular in the Brouwer equations [27].

After successful demonstration by De Laval[8] in 1889 of a well-balanced gas turbine running stably at supercritical, i.e. unstable by Rankine, speeds Ω, the model of Rankine [491] has been recognized as inadequate [137,139]. Nevertheless, its instability threshold is just a part of the singular stability boundary of the Brouwer equations shown in Figure 1.6.

Soon after the success of the symmetric Föppl–von Kármán–Jeffcott model of De Laval's rotor, in 1918 Prandtl [485] noted that if the elastic or inertia properties of a rotor are not symmetric about the axis of rotation there may be speed ranges where the rotor whirl is unstable. He pointed out the analogy between a rotor whose shaft had unequal principal stiffness coefficients ($k_1 \neq k_2$) and a pendulum mounted asymmetrically on a turntable.[9] The pendulum was unstable when the turntable rotation rate Ω was between the pendulum natural frequencies in the soft and stiff directions [137, 139]. Similar instability due to inertia asymmetry was discussed by Smith[10]

[8] Karl Gustaf Patrik de Laval (1845–1913) – a Swedish engineer and inventor, founder of the Alpha Laval Company. Rankine's pessimistic predictions of instabilities at high speeds were widely accepted among engineers and discouraged the development of high speed rotors until De Laval's invention of 1889. Being inspired by De Laval's success, Föppl proposed in 1895 a model that is now known as the Jeffcott rotor [172]. In 1916 further experimental evidence of a rotor operating stably above the Rankine threshold was published by Kerr [262]. This publication motivated the Royal Society of London to commission Jeffcott to resolve the conflict between Rankine's theory and the practice of Kerr and De Laval [444, 492]. Jeffcott's work came into print in 1919 [244].

[9] When $k_1 = k_2 > 0$ and the 'turntable' is the Earth, Brouwer's equations describe small oscillations of *Foucault's pendulum* [18].

[10] David MacLeish Smith (1900–1986) – a Scottish engineer participated in the development of the first British axial flow jet engine for aircraft.

in 1933 [534]. For positive coefficients $k_1 \neq k_2$, the Brouwer equations (1.1) constitute exactly the undamped model by Prandtl and Smith, Figure 1.7 (a).

Let us assume in the equation (1.1) that $k_1 = k + \varepsilon$ and $k_2 = k - \varepsilon$ [137, 139]. Calculating imaginary parts of the roots of the equation (1.6), we find the implicit equation for the whirling frequencies in the Prandtl–Smith model

$$((\mathrm{Im}\lambda)^2 - k - \Omega^2)^2 - 4\Omega^2 k = \varepsilon^2. \tag{1.17}$$

In the $(\Omega, \varepsilon, \mathrm{Im}\lambda)$-space the whirling frequencies form a singular surface with four conical points, Figure 1.7 (b). The slice of this surface by the plane $\varepsilon = 0$ shows four straight lines intersecting each other at the conical points at $\Omega = 0$ and at the critical speeds $\Omega = \pm\sqrt{k}$; see Figure 1.3 (b). These eigencurves constitute the *Campbell* [11] *diagram* [109] of the ideal Föppl–von Kármán–Jeffcott rotor.

Stiffness modification with the variation of ε corresponds to the eigencurves in a slice of the eigenvalue surface by the plane that departs from the conical singularities by a distance $\varepsilon \neq 0$. In the vicinity of $\Omega = 0$ the eigencurves demonstrate *avoided crossings* or *veering*, while near the critical speeds $\Omega = \pm\sqrt{k}$ the eigenvalues are real with zero frequency, Figure 1.3 (c). As Figure 1.7 (c) shows, the real eigenvalues (growth rates) lie on a singular eigenvalue surface with two conical points at the critical speeds

$$((\mathrm{Re}\lambda)^2 + k + \Omega^2)^2 - 4\Omega^2 k = \varepsilon^2. \tag{1.18}$$

The slices of the surface (1.18) by the planes $\varepsilon \neq 0$ in the vicinity of the apexes of the cones are closed loops named *bubbles of instability* by MacKay in 1986 [390], see Figure 1.3 (c). Hence, for $\varepsilon \neq 0$, the Prandtl–Smith rotor is unstable by divergence at the speeds in the interval

$$\sqrt{k - \varepsilon} < |\Omega| < \sqrt{k + \varepsilon}, \tag{1.19}$$

provided that

$$\varepsilon^2 + 4\Omega^2 k > 0. \tag{1.20}$$

The stability diagram in the $(\varepsilon\Omega^{-2}, k\Omega^{-2})$-plane corresponding to the inequalities (1.19) and (1.20) is actually a rotated by an angle $\frac{\pi}{4}$ diagram given by the conditions (1.13), cf. Figure 1.6 (b) and Figure 1.7 (d). In this orientation Brouwer's stability diagram also appears frequently in *accelerator physics*, see e.g. [498, 522].

The amount of kinetic energy available in the rotor is usually orders of magnitude greater than the deformational energy which any internal mode can absorb. Therefore, already small deviations from the ideal conditions yield coupling between modes that by transferring even a tiny fraction of the rotational energy can initiate failure in the vibratory mode [137, 139].

[11] Wilfred Campbell (1884–1924) – an engineer at the General Electric Company who first proposed the frequency-rotation speed diagram for predicting the critical speeds of rotors.

The conical singularities on the surfaces of frequencies and growth rates arise as a result of unfolding of double semisimple eigenvalues of the Föppl–von Kármán–Jeffcott rotor that exist at $\Omega = 0$ ($\lambda = \pm i\omega$) and at the critical speeds $\Omega = \pm\sqrt{k}$ ($\lambda = 0$), where $i = \sqrt{-1}$. The double eigenvalues originate at the crossings of the branches of the Campbell diagram corresponding to $\varepsilon = 0$, Figure 1.3 (b),

$$\lambda_p^+ = i\omega + i\Omega, \quad \lambda_n^+ = i\omega - i\Omega, \quad \lambda_p^- = -i\omega + i\Omega, \quad \lambda_n^- = -i\omega - i\Omega. \tag{1.21}$$

The eigenvectors at the eigenvalues (1.21) are

$$\mathbf{u}_p^+ = \begin{pmatrix} -i \\ 1 \end{pmatrix}, \quad \mathbf{u}_n^+ = \begin{pmatrix} i \\ 1 \end{pmatrix}, \quad \mathbf{u}_p^- = \begin{pmatrix} -i \\ 1 \end{pmatrix}, \quad \mathbf{u}_n^- = \begin{pmatrix} i \\ 1 \end{pmatrix}. \tag{1.22}$$

The eigenvalue problem (1.2) can be rewritten in the form $\mathbf{A}\mathbf{a} = \lambda\mathbf{a}$ with the Hamiltonian[12] matrix $\mathbf{A}$ and the vector $\mathbf{a}$ defined as [603]

$$\mathbf{A} = \begin{pmatrix} -\Omega\mathbf{J} & \mathbf{I} \\ -\mathbf{K} & -\Omega\mathbf{J} \end{pmatrix} = \mathbf{S}\mathbf{A}^T\mathbf{S}, \ \mathbf{S} = \begin{pmatrix} 0 & -\mathbf{I} \\ \mathbf{I} & 0 \end{pmatrix}, \ \mathbf{a} = \begin{pmatrix} \mathbf{u} \\ \lambda\mathbf{u} + \Omega\mathbf{J}\mathbf{u} \end{pmatrix}. \tag{1.23}$$

For every eigenvalue in (1.21), the sign of the quantity $i\overline{\mathbf{a}}^T\mathbf{S}\mathbf{a}$, where overbar denotes complex conjugate and $\mathbf{a}$ is constructed by means of the corresponding eigenvectors of (1.22), defines its *Krein signature* [431,603] known also as *symplectic signature* in the more narrow context of Hamiltonian systems [390, 393]. The eigenvalues λ_p^+ and λ_n^+ branching from the double eigenvalue $i\omega$ have the positive signature, while for λ_p^- and λ_n^- that branch from $-i\omega$, it is negative. Indeed,

$$i\overline{\mathbf{a}_p^+}^T\mathbf{S}\mathbf{a}_p^+ = 4\omega, \ i\overline{\mathbf{a}_n^+}^T\mathbf{S}\mathbf{a}_n^+ = 4\omega, \ i\overline{\mathbf{a}_p^-}^T\mathbf{S}\mathbf{a}_p^- = -4\omega, \ i\overline{\mathbf{a}_n^-}^T\mathbf{S}\mathbf{a}_n^- = -4\omega. \tag{1.24}$$

In 1986, MacKay [390] studied unfoldings of the semisimple double pure imaginary and zero eigenvalues in general Hamiltonian systems and demonstrated that the orientation of the cones depends on the Krein signature [430] of the double eigenvalues. At $\Omega = 0$ the double eigenvalues at the crossing of the branches λ_p^+ and λ_n^+ have definite [603] Krein signature. Then, according to MacKay, the frequency cones are oriented vertically in the $(\Omega, \varepsilon, \mathrm{Im}\lambda)$-space that yields avoided crossings in their slices and thus stability, see Figure 1.7 (b). If the double eigenvalue has a mixed [603] Krein signature, as happens at the crossing of the branches λ_n^+ and λ_p^-, there appears a differently oriented eigenvalue cone for the real parts of the perturbed eigenvalues that possesses bubbles of instability in its cross-sections, Figure 1.7 (c).

Therefore, definiteness of the Krein signature of the double eigenvalues at $\Omega = 0$ prohibits their unstable unfolding in the region of low angular velocities by the perturbations such as the stiffness modification that preserve the Hamiltonian structure of the equations of motion of the gyroscopic system (1.1).

[12] Also known as the *infinitesimally symplectic* matrix [394].

1.2.2 Foucault's pendulum, Bryan's effect, Coriolis vibratory gyroscopes, and the Hannay–Berry phase

A general solution corresponding to the symmetric Brouwer's cavity with the eigenvalues (1.21) and eigenvectors (1.22) is

$$\mathbf{z}(t) = C_1\mathbf{u}_p^+ e^{\lambda_p^+ t} + C_2\mathbf{u}_n^+ e^{\lambda_n^+ t} + C_3\mathbf{u}_p^- e^{\lambda_p^- t} + C_4\mathbf{u}_n^- e^{\lambda_n^- t}. \tag{1.25}$$

For example, initial conditions $x(0) = y(0) = 0$ and $\dot{x}(0) = \dot{y}(0) = 1$ yield

$$\begin{aligned} x(t) &= (\cos\Omega t + \sin\Omega t)\omega^{-1}\sin\omega t, \\ y(t) &= (\cos\Omega t - \sin\Omega t)\omega^{-1}\sin\omega t. \end{aligned} \tag{1.26}$$

In the low speed region when $\Omega \ll \omega$, equations (1.25) and (1.26) describe *modulated oscillations* with the modulation frequency Ω and the carrier frequency ω. In the (x, y)-plane of the rotating frame the particle traces narrow petals of a rose curve (1.26) drawing new petals in the clockwise direction; see Figure 1.8 (a). This means that the swing plane of the particle in the cavity slowly precesses with the angular velocity $\Omega_p = -\Omega$. This angular shift should not be surprising if we remember Prandtl's remark that Brouwer's equations (1.1) describe small oscillations of a pendulum on a turntable. The symmetric case when $k_1 = k_2$ corresponds to the well-known Foucault's[13] pendulum [18, 339].

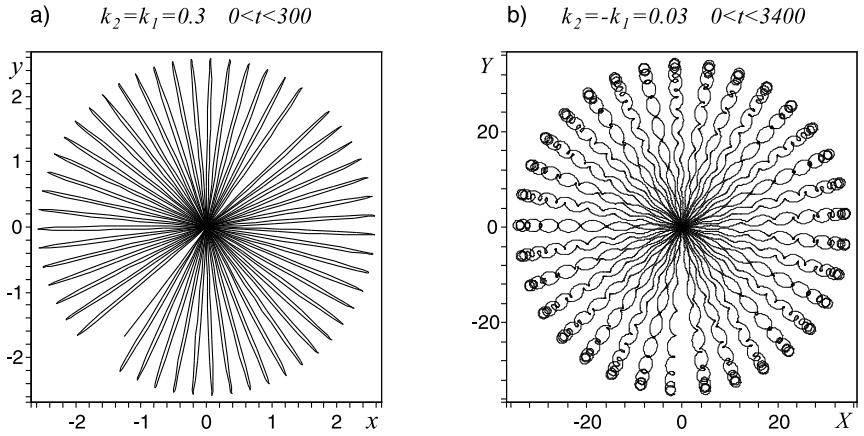

Figure 1.8. (a) A *rhodonea curve* represents a retrograde precession (*Bryan's effect*) with $\Omega_p = -\Omega$ in the rotating frame (x, y) of the plane of oscillations of the Brouwer particle in a cavity rotating counter-clockwise with $\Omega = 0.01$ when $x(0) = y(0) = 0$ and $\dot{x}(0) = \dot{y}(0) = 1$; (b) A prograde precession with $\Omega_p = 2k_1^2\Omega$ in the laboratory frame (X, Y) of the orbit of the Brouwer particle trapped in a saddle rotating with $\Omega = 0.5$ when $X(0) = Y(0) = 0$, $\dot{X}(0) = 0$ and $\dot{Y}(0) = 1$ [304, 571].

[13] Jean Bernard Léon Foucault (1819–1868) – a French physicist who in 1851 first observed the Bryan's effect caused by the rotation of the Earth and proposed the very term 'gyroscope'.

An effect analogous to the precession of the swing plane of Foucault's pendulum due to the Coriolis force exists in vibrating solids of revolution such as disks, rings, cylinders or shells subjected to a rotation with the speed Ω about the symmetry axis. In 1890 Bryan was the first to observe that the vibrating pattern of standing waves rotates with respect to such a structure at a rate proportional to Ω [96].

Bryan's effect of inertia of standing waves is a working principle of Coriolis vibratory gyroscopes (CVG) that sense the imposed rotation. A wide variety of designs including micro-electro-mechanical systems (MEMS) have been proposed and built since the 1960s [13, 16, 248, 523, 601]. Remarkably, most modern analyses of CVGs are *linear* in nature and view the Coriolis force as providing a coupling between two vibratory modes of the system [13]. For example, a single mass MEMS-based CVG without decoupling frame is described by the Brouwer model (1.1) and its perturbation [16].

In 2003–2004 Andersson and Krishnaprasad [12, 13] demonstrated that the Bryan's effect of imposed slow rotatory motion on a rapidly vibrating structure is geometrical in nature. The angle of the retrograde precession of the nodal points of vibration with respect to the structure itself, and hence the precession angle of the orbit of the Brouwer particle in Figure 1.8 (a), is exactly the *geometric phase* [410,411] in the sense of Berry and Hannay [49, 214].

A converse statement came recently from optics where the very *Berry phase* accumulated by a light wave as it propagates along a helical ray in a cylindrical medium was shown to represent the Coriolis effect in a noninertial coordinate frame accompanying the ray trajectory [69–72, 382]. According to Bliokh "the Berry phase describes a sort of inertia of the electric field which remains locally nonrotating about the ray" [69]. This observation gives a link to the effect of inertia of the standing wave pattern in vibrating mechanical structures subjected to slow rotation. It should not be surprising then that the Brouwer model (1.1) can be encountered in optics.

1.2.3 Polarized light within a cholesteric liquid crystal

Indeed, following Marathay [408] let us consider the state of polarization of a plane light wave as it propagates along the helical axis within a nonmagnetic cholesteric liquid crystal. Assume that the Z-axis of a right-handed laboratory frame is parallel to the helical axis. The molecular planes of the structure are parallel to the (X, Y)-plane of the laboratory frame. The principal axes of each molecular plane are gradually rotated as one proceeds along the Z-direction. Define the pitch p as the minimum distance between the two planes whose principal axes are parallel and introduce the parameter $\Omega = 2\pi/p$. Restricting ourselves by the plane waves that propagate normally to the crystal planes, i.e. along the helical axis, we find from the Maxwell equations that

$$\partial_Z^2 \mathbf{E} = \frac{\varepsilon(Z)}{c^2} \partial_t^2 \mathbf{E}, \quad \mathbf{E} = \begin{pmatrix} E_X \\ E_Y \end{pmatrix}, \tag{1.27}$$

where $\mathbf{E} = \mathbf{E}(Z,t)$ is the Jones[14] vector [408]. The 2×2 matrix $\varepsilon(Z)$ describes the dielectric properties of the layer at Z in the laboratory frame and for a right-handed structure in terms of the principal dielectric constants $\varepsilon_{11}^0 > 0$ and $\varepsilon_{22}^0 > 0$ it can be expressed as

$$\varepsilon(Z) = \mathbf{R}(\Omega Z)\mathbf{T}\mathbf{R}^{-1}(\Omega Z), \tag{1.28}$$

where $\mathbf{T} = \text{diag}\,(\varepsilon_{11}^0, \varepsilon_{22}^0)$ and $\mathbf{R}$ is the rotation matrix

$$\mathbf{R} = \begin{pmatrix} \cos(\Omega Z) & -\sin(\Omega Z) \\ \sin(\Omega Z) & \cos(\Omega Z) \end{pmatrix}. \tag{1.29}$$

Looking for a time-harmonic solution of equation (1.27) of the form $\mathbf{E}(Z,t) = \mathbf{F}(Z)exp(-i\omega t)$ and transforming to a space-rotating coordinate system by

$$\mathbf{f}(Z) = \mathbf{R}(-\Omega Z)\mathbf{F}(Z), \tag{1.30}$$

we find that in the space-rotating frame (x, y, z) the dynamics of the state of polarization $\mathbf{f}$ is governed by the autonomous equation

$$\ddot{\mathbf{f}} + 2\Omega\mathbf{J}\dot{\mathbf{f}} + (\mu^2\mathbf{T} + (\Omega\mathbf{J})^2)\mathbf{f} = 0, \tag{1.31}$$

where $\mu^2 = \omega^2/c^2$, the dot stands for the derivative d/dz, and $z = Z$. Equation (1.31) is the system (1.1) with $k_1 = \mu^2\varepsilon_{11}^0$ and $k_2 = \mu^2\varepsilon_{22}^0$ corresponding to the Brouwer particle in a cavity.

A medium with properties that are helically varying in space, or with *chirality*, can therefore introduce *gyroscopic* terms in the equations of motion where a spacial variable plays the role of time. In accelerator physics such a chiral environment can be created artificially with the use of the twisted electrostatic [131,605] or magnetic [15,522] quadrupole lenses as happens, e.g. in a betatron with stellarator fields [498]. In this case, as will be shown below, equations of the Brouwer particle on a rotating saddle naturally appear.

1.2.4 Helical magnetic quadrupole focussing systems

Already in 1914 Brouwer discussed a possibility of experimental verification of stabilization of a heavy ball on a rotating saddle [93, 94]. Nowadays such mechanical demonstrations are available as teaching laboratory experiments [571]. However, the prospects for the first nontrivial physical application of this effect had arisen as early as 1936 when Penning[15] proposed using the quadrupole electric field to confine the charged particles [475].

[14] Robert Clark Jones (1916–2004) – an American physicist who worked at the Bell Labs.
[15] Frans Michel Penning (1894–1953) – a Dutch physicist who worked at the Philips Laboratory.

In the RF-electric-quadrupole *Paul trap*[16] invented in 1953 [471], a saddle-shaped field created to trap a charged ion is not rotating about the ion in the center. The Paul-trap potential can only 'flap' the field up and down, which yields two decoupled Mathieu equations describing the motion of a single ion in the trap. Nevertheless, comparing the rotating saddle trap and the Paul trap, Shapiro [522] and Thompson et al. [571] demonstrated that the former mimics most of the characteristics of the Paul trap, such as regions of stability and instability, micromotion and secular oscillation frequency [571]. Although Brouwer's problem is not only a mechanical analogy to the Paul trap, the equations of the two models are substantially different. Brouwer's system is autonomous, which greatly simplifies its solution. It originates, however, in accelerator physics where it describes strong focussing of the charged particles by a helical magnetic quadrupole lens [472, 498].

Linearized equations of motion in the laboratory (X, Y, Z)-frame of a particle of momentum p and charge e in the helical quadrupole magnetic field rotating with distance along the Z-axis and completing one rotation in an axial distance Λ, in the assumption that $X, Y \ll \Lambda$, are [472]

$$\begin{aligned} \ddot{X} &= -\varepsilon(X\cos Z + Y\sin Z), \\ \ddot{Y} &= -\varepsilon(X\sin Z - Y\cos Z), \end{aligned} \tag{1.32}$$

where dot stands for the derivative d/dZ,

$$\varepsilon = \frac{\Lambda^2\nu^2}{16\pi^2}, \quad \nu^2 = \frac{eG}{pc}, \tag{1.33}$$

and c is the speed of light. The downstream distance Z is measured in units of $\Lambda/(4\pi)$. At $Z = 0$, the components of the magnetic field in the laboratory frame are $B_X = GY$, $B_Y = GX$, $B_Z = 0$ as for the conventional quadrupole.

Changing the basis similar to as in the *rotating wave approximation* [363, 571]

$$\begin{aligned} x &= \ X\cos\frac{Z}{2} + Y\sin\frac{Z}{2}, \\ y &= -X\sin\frac{Z}{2} + Y\cos\frac{Z}{2}, \end{aligned} \tag{1.34}$$

transforms periodic equations (1.32) into the system that is autonomous in the co-moving frame (x, y, z) rotating with the mechanical rotation of the helix

$$\ddot{\mathbf{v}} + \mathbf{J}\dot{\mathbf{v}} + (\mathbf{K} + (\mathbf{J}/2)^2)\mathbf{v} = 0, \tag{1.35}$$

where dot denotes d/dz, $z = Z$, and

$$\mathbf{v} = \begin{pmatrix} x \\ y \end{pmatrix}, \quad \mathbf{J} = \begin{pmatrix} 0 & -1 \\ 1 & 0 \end{pmatrix}, \quad \mathbf{K} = \begin{pmatrix} \varepsilon & 0 \\ 0 & -\varepsilon \end{pmatrix}. \tag{1.36}$$

[16] Named after Wolfgang Paul (1913–1993) – a German physicist who was awarded the Nobel Prize in Physics in 1989 for the development of the ion trap technique.

Equations (1.35), following from (1.1) when $\Omega = 1/2$ and $k_1 = -k_2 = \varepsilon$, correspond to a rotating saddle. On the stability diagram of the Prandtl–Smith rotor shown in Figure 1.7 (d) the rotating saddle trap corresponds to the vertical dashed line $k = 0$. The same diagram determines stability of a high current betatron with stellarator field [498]. Since in the laboratory frame the Brouwer equations (1.1) transform to those of the two coupled oscillators with periodically varying parameters, such as equations (1.32), the divergence and flutter domains in the diagram in Figure 1.7 (d) are often interpreted as the zones of *parametric resonance* [110, 118, 522].

Figure 1.7 (d) demonstrates that when $|\varepsilon| < \Omega^2$, the quadrupole lens is focussing or the rotating saddle is trapping. When $|\varepsilon| \ll \Omega^2$, the orbit of the particle in the laboratory frame is a fast oscillation of the frequency $2\varepsilon\Omega$ with the imposed micromotions. The average plane of the oscillations experiences a slow prograde precession with the angular velocity $\Omega_p = 2\varepsilon^2\Omega$ [571]. Figure 1.8 (b) illustrates this precession for $\Omega = 0.5$ and $\varepsilon = -0.03$.

Therefore, if rotational and vibrational time scales are widely separated, the orbit of the Brouwer particle exhibits similar precession patterns both in a cavity, Figure 1.8 (a), and on a saddle, Figure 1.8 (b). Adiabatically slow rotation or vibration yields accumulation of the geometric phase that manifests itself in the particle's orbit precession [13, 45, 54].

1.2.5 Modulational instability

A monochromatic plane wave with a finite amplitude propagating in a nonlinear and dispersive medium can be disrupted into a train of short pulses (called *solitons*) when the amplitude exceeds some threshold [313]. This process develops due to an unbounded increase in the percentage amplitude modulation of the wave, i.e. instability of the carrier wave with respect to the modulations. This is the fundamental for modern fluid dynamics, nonlinear optics and plasma physics *modulational instability*.[17]

Without dissipation, a slow varying in time envelope A of the rapidly oscillating carrier wave is described by the *nonlinear Schrödinger equation* (NLS)

$$iA_t + \alpha A_{xx} + \gamma|A|^2 A = 0 \tag{1.37}$$

that can be derived in the rotating wave approximation [313]. In the equation (1.37), α and γ are positive real numbers, $i = \sqrt{-1}$, and the modulations are restricted to one space dimension x. The equation (1.37) has a solution in the form of a *monochromatic wave*

$$A = A_0 e^{ikx - i\omega t}, \tag{1.38}$$

[17] Known as the *Benjamin–Feir instability* in hydrodynamics [48] and as the *Bespalov–Talanov instability* in nonlinear optics [57].

where the frequency of the modulation, ω, depends on the amplitude $A_0 = u_1^0 + iu_2^0$ and spacial wave number k as

$$\omega = \alpha k^2 - \gamma \|\mathbf{u}_0\|^2 \tag{1.39}$$

with $\mathbf{u}_0^T = (u_1^0, u_2^0)$ [90, 609].

Introducing into equation (1.37) dispersive and viscous losses with the coefficients a and b, respectively, we arrive at the *dissipatively-perturbed NLS*

$$iA_t + (\alpha - ia)A_{xx} + ibA + \gamma |A|^2 A = 0. \tag{1.40}$$

Separating the real and imaginary parts of the complex amplitude $A = u_1 + iu_2$, we rewrite equation (1.40) as [90]

$$\mathbf{J}\mathbf{u}_t + \alpha \mathbf{u}_{xx} + \gamma \|\mathbf{u}\|^2 \mathbf{u} - a\mathbf{J}\mathbf{u}_{xx} + b\mathbf{J}\mathbf{u} = 0, \tag{1.41}$$

where $\mathbf{u}^T = (u_1, u_2)$ and $\mathbf{J} = \left(\begin{smallmatrix} 0 & -1 \\ 1 & 0 \end{smallmatrix}\right)$. Assuming a solution to equation (1.41) in the form $\mathbf{u} = \mathbf{R}(\mathbf{u}_0 + \mathbf{z}(x,t))$, where [90]

$$\mathbf{R} = \begin{pmatrix} \cos(kx - \omega t) & -\sin(kx - \omega t) \\ \sin(kx - \omega t) & \cos(kx - \omega t) \end{pmatrix}, \tag{1.42}$$

and $\mathbf{z}$ is a perturbation to the traveling wave solution of the undamped NLS with the amplitude vector $\mathbf{u}_0$, we obtain a linearization of equation (1.41)

$$\mathbf{J}\mathbf{z}_t + 2\alpha k \mathbf{J}\mathbf{z}_x + \alpha \mathbf{z}_{xx} + 2\gamma \mathbf{u}_0 \mathbf{u}_0^T \mathbf{z} + ak^2 \mathbf{J}\mathbf{z} + 2ak\mathbf{z}_x - a\mathbf{J}\mathbf{z}_{xx} + b\mathbf{J}\mathbf{z} = 0, \tag{1.43}$$

where the dyad $\mathbf{u}_0\mathbf{u}_0^T$ is a 2×2 symmetric matrix. Note that we have taken into account the relation (1.39) and following [90] assumed that the dissipation is a second-order effect in a sense that the traveling wave exists for a sufficiently long time before the effects of dissipation become significant.

Looking for a solution to equation (1.43) that has a form $\mathbf{z}(x,t) \sim \mathbf{v}(t)\cos\sigma x + \mathbf{w}(t)\sin\sigma x$, we arrive at the two coupled equations

$$\begin{aligned} \mathbf{J}\dot{\mathbf{v}} + 2\alpha k\sigma \mathbf{J}\mathbf{w} - \alpha\sigma^2 \mathbf{v} + 2\gamma \mathbf{u}_0\mathbf{u}_0^T \mathbf{v} + 2ka\sigma \mathbf{w} + (a(\sigma^2 + k^2) + b)\mathbf{J}\mathbf{v} = 0, \\ \mathbf{J}\dot{\mathbf{w}} - 2\alpha k\sigma \mathbf{J}\mathbf{v} - \alpha\sigma^2 \mathbf{w} + 2\gamma \mathbf{u}_0\mathbf{u}_0^T \mathbf{w} - 2ka\sigma \mathbf{v} + (a(\sigma^2 + k^2) + b)\mathbf{J}\mathbf{w} = 0, \end{aligned} \tag{1.44}$$

Note that equations (1.43) and (1.44) contain terms proportional to ak^2 that are missing in the corresponding equations derived in [90].

Differentiating the first of equations (1.44) once and using the second one in order to extract $\mathbf{w}$ and its derivative, we decouple the equation for the vector $\mathbf{v}$

$$\begin{aligned} \ddot{\mathbf{v}} + 2((a(\sigma^2 + k^2) + b)\mathbf{I} + q\mathbf{J})\dot{\mathbf{v}} + \mathbf{P}\mathbf{v} + ((a(\sigma^2 + k^2) + b)\mathbf{I} + q\mathbf{J})^2 \mathbf{v} \\ - \frac{2\gamma(\alpha\mathbf{J} + a\mathbf{I})(\alpha\mathbf{J}\mathbf{D}(\dot{\mathbf{v}} + (b + ak^2)\mathbf{v}) + 2a\gamma \|\mathbf{u}_0\|^2 \mathbf{u}_0\mathbf{u}_0^T \mathbf{v})}{\alpha^2 + a^2} = 0, \end{aligned} \tag{1.45}$$

where $\mathbf{I}$ is a unit matrix, $q = \alpha\sigma^2 - \gamma\|\mathbf{u}_0\|^2$ and

$$\mathbf{P} = \gamma^2\|\mathbf{u}_0\|^4\mathbf{I} - 4k^2\sigma^2(\alpha\mathbf{J} + a\mathbf{I})^2, \quad \mathbf{D} = \mathbf{u}_0\mathbf{u}_0^T\mathbf{J} - \mathbf{J}\mathbf{u}_0\mathbf{u}_0^T. \tag{1.46}$$

In the absence of the dispersive and viscous losses, i.e. when $a = 0$ and $b = 0$, equation (1.45) reduces to a standard form for gyroscopic systems [238, 239, 299]

$$\ddot{\mathbf{v}} + 2q\mathbf{J}\dot{\mathbf{v}} + 2\gamma\mathbf{D}\dot{\mathbf{v}} + (\mathbf{P}_0 + (q\mathbf{J})^2)\mathbf{v} = 0, \tag{1.47}$$

where $\mathbf{P}_0 = (\gamma^2\|\mathbf{u}_0\|^4 + 4\alpha^2k^2\sigma^2)\mathbf{I}$, cf. also [10].

Equation (1.47) is the damped version of the Brouwer equation (1.1) with $\Omega = q$ and $k_1 = k_2 = 4\alpha^2k^2\sigma^2 + \gamma^2\|\mathbf{u}_0\|^4$. The 'damping' matrix $\mathbf{D}$ is symmetric and traceless, i.e. it is *indefinite* with the eigenvalues $\mu_{1,2} = \pm\|\mathbf{u}_0\|^2$. The characteristic equation of the system (1.47)

$$\lambda^4 + 2\alpha\sigma^2(4\alpha k^2 + \alpha\sigma^2 - 2\gamma\|\mathbf{u}_0\|^2)\lambda^2 + \alpha^2\sigma^4(4\alpha k^2 - \alpha\sigma^2 + 2\gamma\|\mathbf{u}_0\|^2)^2 = 0 \tag{1.48}$$

determines the frequency and the growth rate of the perturbed modulation [90]

$$\lambda = \pm i2\alpha k\sigma \pm i\sigma\sqrt{\alpha^2\sigma^2 - 2\alpha\gamma\|\mathbf{u}_0\|^2}. \tag{1.49}$$

When the amplitude of the unperturbed modulation is vanishing, $\|\mathbf{u}_0\| = 0$, the equation (1.47) formally coincides with that of the Jeffcott rotor and therefore its eigenvalues are pure imaginary: $\lambda = \pm i\alpha\sigma(\sigma \pm 2k)$. The eigencurves $\lambda(k)$ exhibit crossings at *diabolical points* [270] where double semisimple eigenvalues originate, cf. Figure 1.3 (b).

What looks a bit more surprising is that at $\|\mathbf{u}_0\| \neq 0$ the spectrum of the gyroscopic system with the traceless indefinite 'damping' matrix (1.46) remains Hamiltonian [174], i.e. symmetric with respect to both real and imaginary axis of the complex plane.[18] At small amplitudes of the modulation, the eigenvalues are pure imaginary. With an increase in the amplitude, the modes with the opposite Krein signature collide at the threshold $\|\mathbf{u}_0\| = \|\mathbf{u}_0\|_i$, where [90, 610]

$$\|\mathbf{u}_0\|_i^2 = \frac{\alpha\sigma^2}{2\gamma}. \tag{1.50}$$

At $\|\mathbf{u}_0\| > \|\mathbf{u}_0\|_i$ the double eigenvalue splits into complex-conjugate eigenvalues, one of which has a positive real part that corresponds to the modulational instability in the ideal (undamped) case Figure 1.9 (b, c).

The form of equation (1.47) allows us to treat the modulational instability as the destabilization of a gyroscopic system by indefinite damping [174, 314]. This destabilization mechanism is well known in rotor dynamics, where the indefinite damping matrix produced by the falling dependence of the friction coefficient on the sliding

[18] Note that the Hamiltonian form of the NLS equation is well known [90, 609, 610]. Equation (1.47) is also $\mathcal{PT}$-symmetric, i.e. invariant under transformations $t \leftrightarrow -t$ and $v_1 \leftrightarrow v_2$ [47].

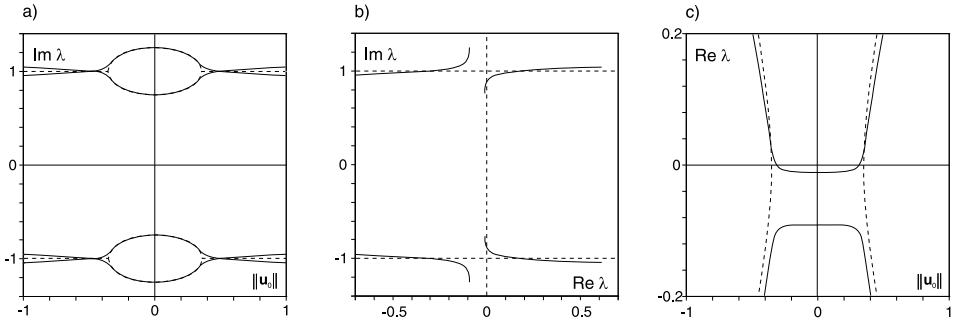

Figure 1.9. $\alpha = 1$, $k = 1$, $\sigma = 0.5$, $\gamma = 1$ and (dashed line) $a = 0$ and $b = 0$ or (solid line) $a = 0.04$ and $b = 0.0008$: (a) Frequency of the perturbation in dependence on $\|\mathbf{u}_0\|$; (b) Movement of eigenvalues in the complex plane; (c) Growth rates of the perturbation in the presence of dissipation (solid line) become positive at lower values of $\|\mathbf{u}_0\|$ than in the undamped case (dashed line) (*dissipation-enhanced modulational instability*) [304].

velocity provokes vibrations in rotating elastic continua in frictional contact, e.g. in the singing wine glass [293, 314, 541].

The dispersive and viscous losses change the mechanism of the onset of the modulational instability as the evolution of eigenvalues shown by solid lines in Figure 1.9 demonstrates. First, the eigenvalues do not merge into a double one anymore and simply pass in close proximity of each other, Figure 1.9 (a, b). Now, the modulational instability takes place when a pair of complex eigenvalues with the smaller absolute value of the imaginary part moves to the right in the complex plane. Second, the amplitude, $\|\mathbf{u}_0\|$, at the instability threshold can be lower than that in the undamped case, Figure 1.9 (c). This is the effect of enhancement of the modulational instability with dissipation described by Bridges and Dias [90].

Writing the Routh–Hurwitz conditions [470] for the characteristic polynomial of the system (1.44), which coincides with that of equation (1.45), to have all its roots with negative real parts (*asymptotic stability*), we find the threshold of the modulational instability in the presence of dissipation

$$4\sigma^2 a^2 k^2 \gamma^2 \|\mathbf{u}_0\|^4 + 2\sigma^2 \alpha\gamma r \|\mathbf{u}_0\|^2 - r((b + a(\sigma^2 + k^2))^2 + \alpha^2\sigma^4) = 0, \quad (1.51)$$

where $r = (b + a(\sigma^2 + k^2))^2 - 4a^2\sigma^2k^2$. The threshold (1.51) plotted in the $(a, b, \|\mathbf{u}_0\|)$-space is shown in Figure 1.10 (a). The surface has a self-intersection along an interval of the $\|\mathbf{u}_0\|$-axis. At the points of this interval the stability boundary is efficiently described by its linear approximation. Indeed, resolving the equation (1.51) with respect to b and expanding the solution in a, we find a linear approximation of the region of asymptotic stability in the (a, b)-plane

$$b = \left[-\sigma^2 - k^2 \pm \frac{k\sigma(2\|\mathbf{u}_0\|_i^2 - \|\mathbf{u}_0\|^2)}{\|\mathbf{u}_0\|_i \sqrt{\|\mathbf{u}_0\|_i^2 - \|\mathbf{u}_0\|^2}} \right] a + o(a). \quad (1.52)$$

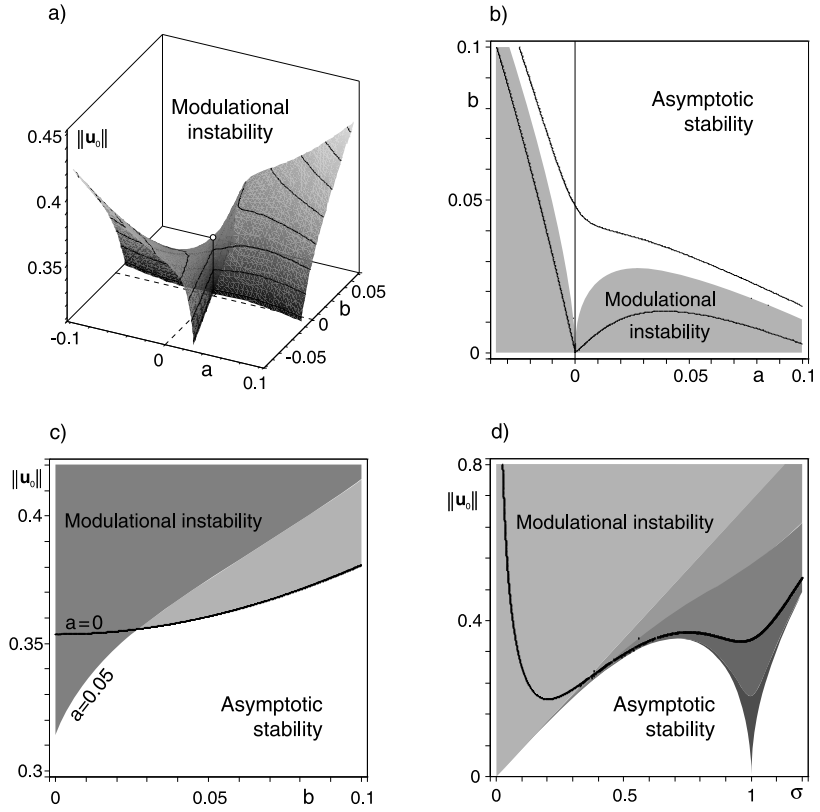

Figure 1.10. For $\alpha = 1$, $\gamma = 1$, and $k = 1$: (a) The threshold (1.51) at $\sigma = 0.5$; (b) its cross-sections in the (a, b)-plane at (lower black curve) $\|\mathbf{u}_0\| = 0.34$, (gray domain) $\|\mathbf{u}_0\| = \|\mathbf{u}_0\|_i$, and (upper black curve) $\|\mathbf{u}_0\| = 0.36$ and (c) in the $(b, \|\mathbf{u}_0\|)$-plane at (black curve) $a = 0$ and (dark gray domain) $a = 0.05$; (d) in the $(\sigma, \|\mathbf{u}_0\|)$-plane the threshold (1.51) in the limit $a \to 0$ for (the lightest gray domain) $\beta := a/b = 0$ and (subsequent darker gray areas) $\beta = 5, 50, 500, \infty$ given by equations (1.52) and (1.55); the black curve is the threshold (1.51) at $a = 0.04$ and $b = 0.0008$ [304].

The linear approximation (1.52) consists of two straight lines. The angle between them decreases when $\|\mathbf{u}_0\|$ approaches $\|\mathbf{u}_0\|_i$. At the exceptional point $\|\mathbf{u}_0\| = \|\mathbf{u}_0\|_i$ the linear approximation (1.52) degenerates into a single line $a = 0$.

For $a \ll b$, equation (1.52) yields a simple estimate of the threshold of the dissipative modulational instability in the vicinity of the exceptional point $(a, b, \|\mathbf{u}_0\|_i)$

$$\|\mathbf{u}_0\|_d \approx \|\mathbf{u}_0\|_i \left(1 - \frac{k^2\sigma^2}{2}\frac{a^2}{b^2}\right) \leq \|\mathbf{u}_0\|_i . \tag{1.53}$$

Equation (1.53) has the form $Y = X^2/Z^2$ that is canonical for the *Whitney umbrella* surface [312]. As is visible in Figure 1.10 (a), the instability threshold (1.51) indeed

possesses the Whitney umbrella singularity at $a = 0$, $b = 0$ and $\|\mathbf{u}_0\| = \|\mathbf{u}_0\|_i$ in the $(a, b, \|\mathbf{u}_0\|)$-space.

The presence of the singularity on the stability boundary explains why at every small $a \neq 0$ there exists a domain of modulational instability at smaller values of $\|\mathbf{u}_0\|$ with respect to that for $a = 0$, Figure 1.10 (c). This enhancement of the modulational instability with dissipation discussed in [90] is clearly seen in the approximation (1.53). On the other hand, some combinations of a and b yield positive increments to the stability domain shown in light gray in Figure 1.10 (c). For example, at $\|\mathbf{u}_0\| = \|\mathbf{u}_0\|_i$ there exists a stability domain in the (a, b)-plane that has a cuspidal point singularity at the origin, Figure 1.10 (b). Quadratic approximation to the cusp follows from the expression (1.51) as

$$b = \sigma\sqrt{\sigma}\sqrt{\alpha k|a|} - a(\sigma^2 + k^2) + o(a). \tag{1.54}$$

Figure 1.10 (d) demonstrates how the existence of the Whitney umbrella singularity at the exceptional point influences the instability threshold in the $(\sigma, \|\mathbf{u}_0\|)$-plane. The lightest gray area in Figure 1.10 (d) is the undamped domain of instability with the threshold (1.50) that yields $\|\mathbf{u}_0\| = \sigma\sqrt{\frac{\alpha}{2\gamma}}$; the black curve here shows the stability boundary (1.51) at $a = 0.04$ and $b = 0.0008$ so that $\beta := ab^{-1} = 50$. We see that the black line intersects the instability threshold in the undamped case, i.e. dissipation both increases and decreases the critical amplitude. However, when β is fixed and $a \to 0$, the stability boundary tends to a limiting curve that is below the undamped threshold for all $\sigma > 0$ and thus does not coincide with the line $\|\mathbf{u}_0\| = \sigma\sqrt{\frac{\alpha}{2\gamma}}$. This limiting curve is described by the equation (1.52). In Figure 1.10 (d) such limiting curves are plotted for $\beta = 5, 50, 500$ and for $\beta \to \infty$ and are visible as the boundaries between the gray areas of different darkness. In the case $\beta \to \infty$, the equation (1.52) yields [305]

$$\|\mathbf{u}_0\| = \pm\frac{\sigma}{k}\sqrt{\frac{\alpha}{2\gamma}(k^2 - \sigma^2)}, \quad \|\mathbf{u}_0\| = \pm\sqrt{\frac{\alpha}{2\gamma}(\sigma^2 - k^2)}. \tag{1.55}$$

The curves (1.55) form a cusp at $\|\mathbf{u}_0\| = 0$ when $\sigma = k$, indicating a kind of resonance between the wave numbers σ and k of the perturbation and modulation, Figure 1.10 (d). Note, however, that the modulational instability is characterized by $\sigma < k$ [90].

1.3 Brouwer's problem with damping and circulatory forces

Enhancement of the modulational instability with dissipation is a manifestation of one of the most fundamental phenomena that characterize nonconservative systems – the effect of *dissipation-induced instabilities* [74, 312, 333]. This connection becomes

more explicit if we look closer at the structure of equation (1.45), where dispersive and viscous losses contribute to the terms proportional both to $\dot{\mathbf{v}}$ and $\mathbf{v}$. Among the latter we focus our attention on the term $2q(a(\sigma^2+k^2)+b)\mathbf{J}\mathbf{v}$ with the skew-symmetric matrix $\mathbf{J}$, which can be formally interpreted as a nonpotential positional perturbation if $\mathbf{v}$ is treated as a position vector. In 1953, Ziegler, who studied stability of rods in solid mechanics, proposed the name *circulatory* for the nonpotential positional forces to which a skew-symmetric matrix corresponds in the linearized equations of motion [623]. Remarkably, Ziegler borrowed the notation, as he admitted, "from a similar case in hydrodynamics'. Velocity-dependent damping forces and positional circulatory forces are two fundamental *nonconservative forces* [55, 332]. Formally, equation (1.45) is a perturbation of the gyroscopic system of Brouwer's type (1.47) by velocity-dependent forces as well as by potential and circulatory forces.

1.3.1 Circulatory forces

Circulatory terms appear in the linearization (1.45) of the dissipatively-perturbed NLS about the periodic in time traveling wave solution quite similarly to how they historically originated in the equations of rotor dynamics when dissipation both in rotor and stator was taken into account. The two types of damping were introduced in 1923–25 by Kimball[19] [266] in order to explain a new type of supercritical instability in built-up rotors in the early 1920s.

In 1933 Smith [534] implemented this idea in a model of a rotor carried by a flexible shaft in flexible bearings with the linearization given by the equation

$$\ddot{\mathbf{z}} + \mathbf{D}\dot{\mathbf{z}} + 2\Omega\mathbf{G}\dot{\mathbf{z}} + (\mathbf{K} + (\Omega\mathbf{G})^2)\mathbf{z} + \nu\mathbf{N}\mathbf{z} = 0 \tag{1.56}$$

where $\mathbf{z}^T = (x, y)$ is the position vector in the frame rotating with the shaft's angular velocity Ω, $\mathbf{D} = \mathrm{diag}\,(\delta+\nu, \delta+\nu)$, $\mathbf{G} = \mathbf{J}$, $\mathbf{K} = \mathrm{diag}\,(k_1, k_2)$, and $\mathbf{N} = \Omega\mathbf{J}$. In Smith's model (1.56) the *stationary* (in the laboratory frame, and thus *external* with respect to the shaft) damping coefficient $\nu \geq 0$ represents the effect of viscous damping in bearing supports while the *rotating* damping coefficient $\delta \geq 0$ represents the effect of viscous damping in the shaft itself (*internal* damping) [137, 267]. The term $\nu\Omega\mathbf{J}\mathbf{z}$ in equation (1.56) corresponds to circulatory forces exactly as the term $2q(a(\sigma^2 + k^2) + b)\mathbf{J}\mathbf{v}$ formally does in equation (1.45). In 1976, equation (1.56) re-appeared in the work of Bottema [82] where it described the motion on a rotating surface of the Brouwer particle perturbed by internal and external damping.

1.3.2 Dissipation-induced instability of negative energy modes

Quite in agreement with Prandtl [485], Smith concluded that when $\delta = 0$ and $\nu = 0$, the asymmetry of the bearing stiffness ($k_1 \neq k_2$) extends the interval of divergence

[19] Arthur Livingstone Kimball (1886–1943) – an American engineer who worked at the General Electric Co. [329] and in fact also introduced the notion of the *follower force* in solid mechanics [267].

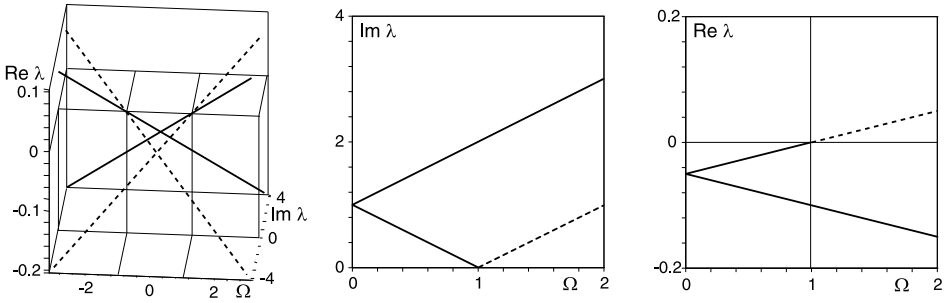

Figure 1.11. Imaginary and real parts of the eigenvalues of the Jeffcott rotor with internal and external damping according to Smith [534] in the case when $k_1 = k_2 = 1$, $\nu = 0$, and $\delta = 0.1$. (a) Evolution of eigenvalues in the $(\Omega, \mathrm{Im}\lambda, \mathrm{Re}\lambda)$-space. (b) Frequencies and (c) growth rates where dashed (solid) lines denote eigenvalues perturbed from the eigenvalues of the Jeffcott rotor with negative (positive) Krein signature. Internal damping, δ, destabilizes the eigenvalues with the negative Krein signature in the supercritical for the Jeffcott rotor speed range $|\Omega| > 1$.

instability (1.19) so that the second speed of transition from divergence to stability is higher (*supercritical*) than the critical speed $|\Omega| = \sqrt{k}$ of the perfectly symmetric (Jeffcott) rotor with $k_1 = k_2 = k > 0$. Another of Smith's conclusion sounded rather counter-intuitive: Internal damping in the shaft induces flutter instability of the Jeffcott rotor when (see Figure 1.11)

$$|\Omega| > \Omega_{cr} := \left(1 + \frac{\nu}{\delta}\right)\sqrt{k} \geq \sqrt{k}. \tag{1.57}$$

The critical speed, Ω_{cr}, at the onset of flutter, is always supercritical and increases with the increase of excess of the intensity of the external damping (ν) over the magnitude of the internal damping (δ) [534]. Since the minimum value of the critical speed is realized when there is no stationary damping, it was concluded that internal (rotating) damping indeed has a destabilizing effect while external (stationary) damping is a stabilizing factor [138].

At $|\Omega| > \Omega_{cr}$ the undamped Jeffcott rotor is a gyroscopically stabilized system (see Figure 1.6) and its destabilization by internal damping should not be surprising in view of the Kelvin–Tait–Chetaev theorem [127, 573, 608]. More interestingly, in the laboratory frame the motion of the shaft at any Ω consists of two spiral whirls, one with the direction of rotation (forward whirl) and the other against it (backward whirl). At $|\Omega| < \Omega_{cr}$ the amplitude of both spirals decreases, whereas at $|\Omega| > \Omega_{cr}$ it is the amplitude of the forward whirl that increases with time, as was established already in 1908 by H. Lamb[20] [343], see also [534]. This physical picture sharply corresponds to the behavior of eigencurves of the system (1.56) shown in Figure 1.11.

[20] Horace Lamb (1849–1934) – a British mathematician who studied, in particular, the dynamics of rotating shells containing fluid and wave motion in spinning flexible disks.

Recall that eigenvalues (1.21) of the system (1.56) without damping ($\delta = 0, \nu = 0$) have according to equations (1.24) an invariant (Krein signature) that does not change with the variation of Ω. Figure 1.11 demonstrates that the eigenvalues λ_p^+ and λ_n^+, both with positive Krein signature, existing at $|\Omega| < \Omega_{cr}$ acquire negative real parts (asymptotic stability) due to the action of pure internal damping. In the supercritical speed range $|\Omega| > \Omega_{cr}$, the pure internal damping stabilizes the eigenvalue λ_p^+ with positive Krein signature but destabilizes the eigenvalue λ_p^- with negative Krein signature. Therefore, destabilization of the forward whirl by internal damping corresponds to the movement of a pure imaginary eigenvalue with the negative Krein signature of the Hamiltonian system to the right in the complex plane due to non-Hamiltonian dissipative perturbation.

This particular observation turned out to be rather general, as was established in 1990s by MacKay [391], Bloch et al. [74] and Maddocks and Overton [395], who also explicitly expressed the perturbation of a simple eigenvalue by means of the energy and its rate of change of the corresponding mode. Their results clearly explain the effect of destabilization of negative energy modes well-known in rotor dynamics [139, 343, 574], fluid dynamics [90, 108, 168, 349, 462], plasma physics [446, 551, 552] and magnetohydrodynamics [264].

1.3.3 Circulatory systems and the destabilization paradox

In a more general model of the rotating shaft by Shieh and Masur [524], the damping matrix in equation (1.56) is allowed to be $\mathbf{D} = \operatorname{diag}(\delta_1, \delta_2)$ while the matrix of the nonconservative positional forces is simply $\mathbf{N} = \mathbf{J}$. Already this setting allows us to illustrate several nontrivial situations arising in stability analysis of nonconservative systems.

If we let $\Omega = 0$ in equation (1.56) within the Shieh and Masur model, the asymptotic stability domain given by the criterion of Routh and Hurwitz is

$$(\delta_1 + \delta_2)^2(\delta_1\delta_2 k_1 - \nu^2) + \delta_1\delta_2\kappa(\kappa + \delta_1(\delta_1 + \delta_2)) > 0, \quad \delta_1 + \delta_2 > 0, \qquad (1.58)$$

where $\kappa = k_2 - k_1$. The domain (1.58) in the $(\delta_1, \delta_2, \kappa)$-space at the given $\nu \neq 0$ is shown in Figure 1.12 (a). Its boundary has two self-intersections along the intervals $(0, 0, \pm 2\nu)$. These intervals are regions of marginal stability of the ideal system without dissipation ($\delta_{1,2} = 0$), which is under action of potential and circulatory forces only. Such nonconservative systems are called *circulatory* [239, 623]. Their equations of motion respect the *time-reversal* symmetry [459, 575]. As a consequence, the eigenvalues of circulatory systems are located symmetrically with respect to both axes in the complex plane, i.e. these systems can only be marginally stable when all eigenvalues are pure imaginary and semisimple [344, 514]. The transition from marginal stability to flutter instability in circulatory systems occurs when two pure imaginary eigenvalues experience the nonsemisimple $1:1$ resonance and then split into a complex-conjugate pair (*reversible Hopf bifurcation*). Exactly this process takes place when the parameter

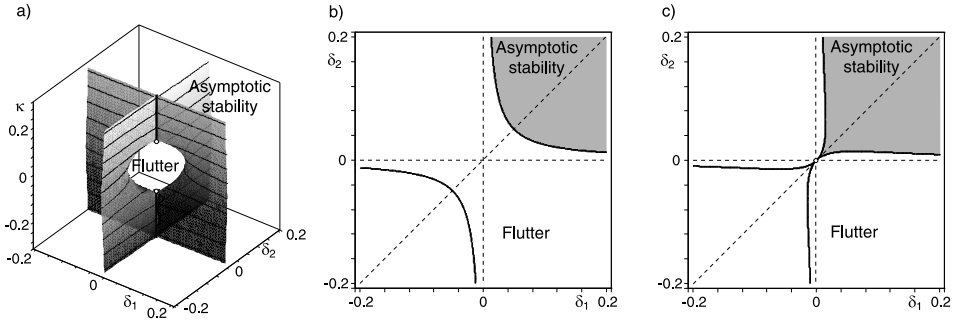

Figure 1.12. Stability domain of the rotating shaft by Shieh and Masur [524] for $k_1 = 1$, $\Omega = 0$, and $\nu = 0.05$ (a) in the $(\delta_1, \delta_2, \kappa)$-space. Its slices in the (δ_1, δ_2)-plane with (b) $\kappa = 0$ and (c) $\kappa = 2\nu = 0.1$. Open circles show locations of exceptional points where the eigenvalues of the ideal circulatory system experience the nonsemisimple 1 : 1 resonance [301].

κ varies along the intervals of self-intersection shown in black in Figure 1.12 (a). The end points of the intervals with the coordinates $(0, 0, \pm 2\nu)$, marked by open circles, correspond to the nonsemisimple 1 : 1 resonances. At the same time, these *exceptional points* are singular points of the boundary of the domain of asymptotic stability of the nonideal circulatory system with dissipation. In 1956, Bottema[21] [81] established that such points of the stability boundary correspond to the Whitney umbrella singularity.

In the $(\kappa = 2\nu)$-plane the cross-section of the domain of asymptotic stability has a cuspidal singularity at the exceptional point, Figure 1.12 (c). As a consequence, along the line $\delta_1 = \delta_2$ (dashed in Figure 1.12 (c)) we can trace the damping parameters until the origin staying all the time in the domain of asymptotic stability. However, moving towards the origin along any other line we unavoidably cross the stability boundary and come to the flutter domain before the origin is reached. This means that in the limit we end up at the origin generically with the higher value of $|\kappa|$ than $2|\nu|$. Such an enhancement of the flutter domain of a circulatory system in the limit of vanishing dissipation discovered by Ziegler in 1952 [622] and explained via the Whitney umbrella singularity by Bottema in 1955–56 [80,81], is well known as *Ziegler's paradox*, which is more correctly called the *Ziegler–Bottema destabilization paradox*.

1.3.4 Merkin's theorem, Nicolai's paradox, and subcritical flutter

The destabilization paradox reflects the existence of flutter at $|\kappa| > |2\nu|$ in the presence of weak dissipation ($\delta_1 > 0, \delta_2 > 0$). When $|\kappa| < |2\nu|$, the flutter domain of the ideal circulatory system situated between the exceptional points $(0, 0, -2\nu)$ and $(0, 0, 2\nu)$ continues to a neighborhood of the origin when the damping coefficients are sufficiently small. For example, in the $(\kappa = 0)$-plane the asymptotic stability is inside

[21] Oene Bottema (1901–1992) – a Dutch mathematician who was the Rector Magnificus of the Technical University of Delft in the 1950s.

a branch of a hyperbola selected by the condition $\delta_1 + \delta_2 > 0$:

$$\delta_1 \delta_2 > \frac{\nu^2}{k_1}, \tag{1.59}$$

see Figure 1.12 (b). At $\delta_1 = \delta_2 = \delta$ and $k_1 = k_2 = k$ the stabilization condition (1.59) reduces to $\delta > \nu/\sqrt{k}$ obtained by Kapitsa in 1939 [256].

The singular stability diagram in Figure 1.12 illustrates several remarkable facts observed already in the early studies of nonconservative stability problems.

First, there is the instability of the ideal circulatory system with symmetric potential ($k_1 = k_2$) when $\nu \neq 0$. On the one hand, this is a consequence of the general theorem by Merkin [333, 423] that states that a potential system with all its eigenvalues coinciding into a multiple semisimple one with algebraic multiplicity equal to the dimension of the system is destabilized by an arbitrary circulatory perturbation, see Theorem 5.16.

On the other hand, in 1928 Nicolai [75, 196, 448, 519] interpreted this instability as a paradox when he considered stability of a rod of a perfect circular cross-section compressed by a potential force and simultaneously twisted by a follower torque, i.e. a torque which is always directed along the neutral line of the rod. The rod is unstable no matter how small the torque is. The follower torque adds circulatory terms in the equations of motion of the rod. In two dimensions, the latter take the form of the Shieh and Masur model [524] with $\Omega = 0$, $k_1 = k_2$, and $\delta_{1,2} = 0$ [519]. As we have seen, this circulatory system is unstable by Merkin's theorem. Nevertheless, breaking the symmetry of the potential ($k_1 \neq k_2$) or adding large enough damping can stabilize it, as Figure 1.12 (a, b) demonstrates. Indeed, later on, Nicolai found that rods of noncircular cross-section can be stable at sufficiently small values of the follower torque[22] [75, 196, 449, 624].

Finally, we mention that Merkin's theorem and Nicolai's paradox are directly related to some models of friction-induced flutter in rotating disks of car brakes, where gyroscopic effects are neglected in the assumption that the speed of rotation is small [254]. The spectrum of perfectly symmetric solids of revolution contains double semisimple pure imaginary eigenvalues that under a circulatory perturbation can acquire from the frictional contact a positive real part causing flutter [293, 294]. In two dimensions, such models frequently yield linearized equations (1.56) in the form of Shieh

[22] We note that the settings considered by Nicolai go back to the work of Greenhill of 1883 [206] on the buckling of screw-shafts of steamers under a compressive load and a torque. On the other hand, Nicolai was aware of the works of Kimball, see e.g. [450]. Thus, such settings could be considered as simplified models serving for better understanding the stability of rotors with internal and external damping [75, 624]. They were found to be challenging from the mathematical point of view and were investigated quite extensively in their own right which in the 1950s resulted in the formulation of new problems on stability of slender structures under the action of not only follower torques but also follower forces [39, 75, 196, 623, 624]. Since then the nonconservative stability problems of structural mechanics became a separate branch of research to such an extent that in the 1990s Crandall had to recall their origin in rotor dynamics [138, 139].

and Masur [524] that in the absence of rotation $\Omega = 0$ have the singular stability diagram shown in Figure 1.12 (a) [299, 301].

1.3.5 Indefinite damping and parity-time ($\mathcal{PT}$) symmetry

Let in equation (1.56) with the damping matrix $\mathbf{D} = \operatorname{diag}(\delta_1, \delta_2)$ the effect of nonconservative positional forces be negligible ($\nu = 0$). Although the literal meaning of the word 'damping' prescribes the coefficients δ_1 and δ_2 to be nonnegative, it is instructive to act similarly to Brouwer did with respect to the stiffness coefficients k_1 and k_2 and relax this sign convention. Therefore, we consider a gyroscopic system

$$\begin{aligned} \ddot{x} + \delta_1 \dot{x} - 2\Omega \dot{y} + (k_1 - \Omega^2)x = 0, \\ \ddot{y} + \delta_2 \dot{y} + 2\Omega \dot{x} + (k_2 - \Omega^2)y = 0, \end{aligned} \tag{1.60}$$

where the negative sign of the damping coefficient corresponds to a gain and the positive one to a loss, see [177].

In mechanics, negative damping terms enter the equations of motion of moving continua in frictional contact when the dependence of the frictional coefficient on the relative velocity has a negative slope, which can be observed already in the tabletop experiments with the singing wine glass [340, 541]. In physics, a pair of coupled oscillators, one with gain and the other with loss, can naturally be implemented as an LRC-circuit [511] or as an optical system [507]. Since the gyroscopic effects can be introduced in LRC-circuits by means of commercially available Tellegen's *gyrators*[23] [170, 303, 567], it should be possible to realize the gyroscopic system (1.60) with gain and loss in an extended laboratory experiment of Schindler et al. [511].

When $\delta_1 = -\delta_2 = \delta > 0$ the gain and loss in equation (1.60) are in perfect balance. Let us further assume that $k_1 = k_2 = k$ and consider the dissipative Brouwer equations in this special case

$$\begin{aligned} \ddot{x} + \delta \dot{x} - 2\Omega \dot{y} + (k - \Omega^2)x = 0, \\ \ddot{y} - \delta \dot{y} + 2\Omega \dot{x} + (k - \Omega^2)y = 0. \end{aligned} \tag{1.61}$$

Let us look at what happens with these equations when we change the direction of time, assuming $t \leftrightarrow -t$. Then,

$$\begin{aligned} \ddot{x} - \delta \dot{x} + 2\Omega \dot{y} + (k - \Omega^2)x = 0, \\ \ddot{y} + \delta \dot{y} - 2\Omega \dot{x} + (k - \Omega^2)y = 0 \end{aligned} \tag{1.62}$$

and we see that equations (1.61) are not invariant to the time reversal transformation ($\mathcal{T}$). The interchange of the coordinates as $x \leftrightarrow y$ in equations (1.61) results again in equations (1.62), which do not coincide with the original. Hence, the equations (1.61) are not invariant with respect to the *parity* transformation ($\mathcal{P}$).

[23] The gyrator (a linear electrical network element) was invented in 1948 by Bernard Tellegen (1900–1990) – a Dutch electrical engineer who worked at Philips Research Laboratories.

Nevertheless, two negatives make an affirmative, and the combined $\mathcal{PT}$-transformation leaves the equations (1.61) invariant despite the $\mathcal{T}$-symmetry and $\mathcal{P}$-symmetry not being respected separately. The spectrum of the $\mathcal{PT}$*-symmetric* [47] system (1.61) with *indefinite damping* is symmetrical with respect to the imaginary axis on the complex plane as happens in Hamiltonian and reversible systems [174, 175].

To see this, let us consider the eigenvalues λ of the problem (1.60) introducing the new parameters $\Delta_1 = \delta_1 + \delta_2$, $\Delta_2 = \delta_1 - \delta_2$ and $\kappa = k_2 - k_1$. Then, at $\Delta_1 = 0$ and $\kappa = 0$ they represent the spectrum of the problem (1.61)

$$\lambda = \pm\frac{1}{4}\sqrt{2\Delta_2^2 - 16k_1 - 16\Omega^2 \pm 2\sqrt{(16\Omega^2 - \Delta_2^2)(16k_1 - \Delta_2^2)}}, \qquad (1.63)$$

where $k_1 = k$ and $\Delta_2 = 2\delta$. In Figure 1.13 the eigenvalues (1.63) are shown by dashed lines. They are pure imaginary when $|\Delta_2| < 4|\Omega|$. At the exceptional points (EPs), $\Delta_2 = \pm 4\Omega$, the pure imaginary eigenvalues collide into a double defective one which with the further increase in Δ_2 splits into a complex-conjugate pair (flutter instability). Qualitatively, the eigenvalues (1.63) evolve as in the case of the undamped modulational instability, Figure 1.9, which is not surprising in view of the fact that equation (1.47) and equation (1.61) have the same form and are $\mathcal{PT}$-symmetric.

$\mathcal{PT}$-symmetry can be violated by the asymmetry both in the stiffness distribution ($\kappa \neq 0$) and in the balance of gain and loss ($\Delta_1 \neq 0$). In such a situation, the merging of eigenvalues that was perfect for the $\mathcal{PT}$-symmetric system (1.61) is destroyed. The solid eigencurves in Figure 1.13 demonstrate the *imperfect merging of modes* [226] that causes a decrease of the stability interval with respect to that of the symmetric system (the effect similar to the Ziegler–Bottema destabilization paradox).

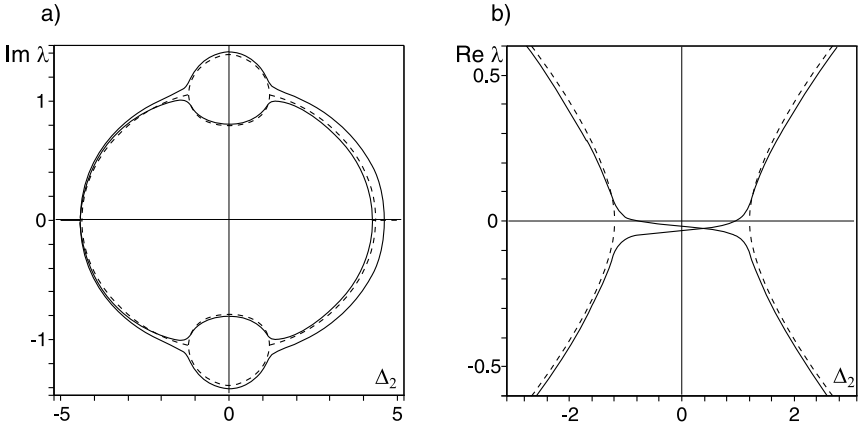

Figure 1.13. Given $\Omega = 0.3$, dashed lines depict (a) imaginary and (b) real parts of the eigenvalues of the $\mathcal{PT}$-symmetric Brouwer problem with indefinite damping (1.61) as functions of the parameter $\Delta_2 = \delta_1 - \delta_2 = 2\delta$ when $k = 1$. Solid lines correspond to the eigenvalues of the problem (1.60) with $k_1 = 1$, $\kappa = k_2 - k_1 = 0.1$ and $\Delta_1 = \delta_1 + \delta_2 = 0.1$.

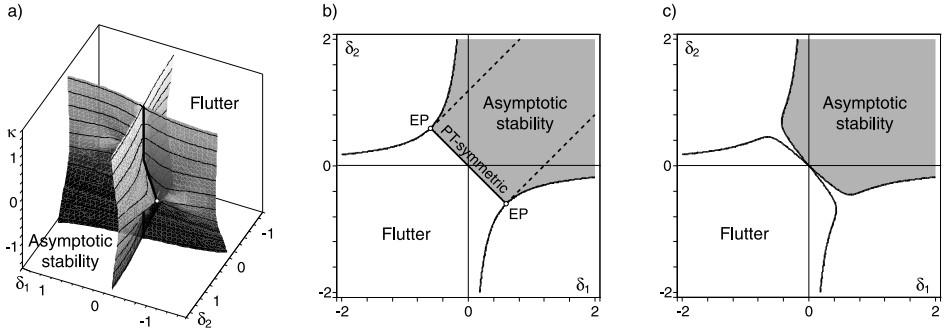

Figure 1.14. Stability domain of the rotating shaft by Shieh and Masur for $k_1 = 1$, $\Omega = 0.3$, and $\nu = 0$. (a) The Plücker conoid in the $(\delta_1, \delta_2, \kappa)$-space and its slices in the (δ_1, δ_2)-plane with (b) $\kappa = 0$ and (c) $\kappa = 0.1$. Open circles show locations of exceptional points (EPs) where pure imaginary eigenvalues of the ideal $\mathcal{PT}$-symmetric system (1.61) experience the nonsemisimple $1 : 1$ resonance; dashed lines are locations of the exceptional points where double nonsemisimple eigenvalues have negative real parts [301, 303].

The Routh–Hurwitz conditions applied to the characteristic polynomial of the system (1.60) yield the domain of the asymptotic stability

$$\delta_1\delta_2\kappa^2 + (\delta_1+\delta_2)(\delta_1\delta_2+4\Omega^2)(\delta_1\kappa + (\delta_1+\delta_2)(k_1-\Omega^2)) > 0, \;\; \delta_1+\delta_2 > 0, \;\; (1.64)$$

shown in Figure 1.14 (a) in the $(\delta_1, \delta_2, \kappa)$-space. The surface has a self-intersection along the κ-axis that corresponds to a marginally stable conservative gyroscopic (Hamiltonian) system. More intriguing is that in the $(\kappa = 0)$-plane there exists another self-intersection along the interval of the line $\delta_1 + \delta_2 = 0$ with the ends at the exceptional points $(\delta_1 = 2\Omega, \delta_2 = -2\Omega)$ and $(\delta_1 = -2\Omega, \delta_2 = 2\Omega)$, see Figure 1.14 (b). This is the interval of marginal stability of the oscillatory damped ($\mathcal{PT}$-symmetric) gyroscopic system (1.61) with the perfect gain/loss balance. At the exceptional points, the stability boundary has the Whitney umbrella singularities, as in the case of modulational instability with damping.

In the vicinity of the interval of marginal stability of the $\mathcal{PT}$-symmetric system, the linear approximation to the boundary of the domain of asymptotic stability, shown in Figure 1.14 (a), is given by a *ruled surface* known as the *Plücker conoid*[24] of degree $n = 1$ [231, 303].

In the $(\kappa = 0)$-plane the range of stability is growing with the increase of the distance from the line $\delta_1 + \delta_2 = 0$, which is accompanied by detuning of the gain/loss balance, Figure 1.14 (b). Indeed, in this slice the boundary of the domain of asymptotic stability is the hyperbola

$$(\delta_1 - \delta_2)^2 - (\delta_1 + \delta_2)^2 = 16\Omega^2. \qquad (1.65)$$

[24] Named after the German mathematician Julius Plücker (1801–1868), a doctoral advisor of Felix Klein, known also for his studies of Hamilton's conical refraction [189].

At $\delta_1 + \delta_2 = 0$ it touches the two straight lines $\delta_1 - \delta_2 = \pm 4\Omega$, every point of which corresponds to a pair of double defective complex-conjugate eigenvalues with real parts that are negative when $\delta_1 + \delta_2 > 0$, positive[25] when $\delta_1 + \delta_2 < 0$, and zero when $\delta_1 + \delta_2 = 0$:

$$\lambda = -\frac{\delta_1 + \delta_2}{4} \pm \frac{1}{4}\sqrt{(\delta_1 + \delta_2)^2 - 16(k_1 - \Omega^2)}. \tag{1.66}$$

The two lines of exceptional points stem from the end points of the interval of marginal stability of the $\mathcal{PT}$-symmetric system and continue inside the asymptotic stability domain of the near-$\mathcal{PT}$-symmetric one (dashed lines in Figure 1.14 (b)).

The proximity of a set of defective eigenvalues to the boundary of the asymptotic stability, that generically is characterized by simple pure imaginary eigenvalues, plays an important role in modern nonconservative physical and mechanical problems. Near this set the eigenvalues can dramatically change their trajectories in the complex plane. For this reason, encountering double eigenvalues with the Jordan block and negative real parts is considered as a precursor to instability in electrical networks [157], hydrodynamics [246], and rotor dynamics [530]. Such applications stimulated the development of numerical methods of finding degenerate eigenvalues that are naturally connected to pseudospectrum and eigenvalue optimization [7,243,576] and geometric phase [153].

1.4 Scope of the book

Completing this short excursion into nonconservative problems of mechanics (non-Hermitian problems of physics), we can summarize our first experience:

- In the presence of dissipative and nonconservative positional forces, linear stability analysis already becomes nontrivial.
- The difficulties arise first of all from the nonself-adjoint nature of operators governing linearized equations of the nonconservative systems.
- Non-conservative problems contain deliberately more physical parameters.
- In n-parameter families of nonself-adjoint eigenvalue problems complicated spectral degeneracies become generic even if n is not large.
- By affecting the eigenvalue movement in the complex plane, the degeneracies determine geometry of the stability diagrams in the parameter space.
- The boundary of the domain of asymptotic stability is neither smooth nor convex; its singularities can correspond to various ideal systems such as Hamiltonian, reversible, or $\mathcal{PT}$-symmetric.

[25] A similar situation may take place in optics where the exceptional points can exist above the lasing threshold [380].

"Singularity is almost invariably a clue," remarked Sherlock Holmes during his investigation of the Boscombe Valley mystery [95].

Our book is about the relationship between marginal stability of the ideal systems and asymptotic stability of the dissipative nonconservative systems situated 'nearby'. Although the former cannot always be realized in practice, they considerably determine or even dictate the stability properties of the latter that, in contrast, naturally occur in real life. Keeping in mind as a clue the idea that the intricate behavior of eigenvalues or paradoxical limiting properties of stability diagrams of nonconservative systems most likely implies the proximity to a spectral singularity related to an ideal system, one can observe that among the latter the Hamiltonian, reversible, or $\mathcal{PT}$-symmetric ones occur most frequently as limiting cases. By studying arbitrary perturbation of these ideal cases systematically, we will deduce stability properties of dissipative nonconservative systems explicitly and reduce them to a finite number of relatively simple and natural rules.

We start the book in Chapter 2 with an overview of the Lyapunov stability theory, discuss linearization of autonomous and nonautonomous systems and linear stability analysis, formulate classical stability criteria and inertia theorems and establish relationships between them and, finally, describe the role of multiple eigenvalues in the robust stability.

Hamiltonian and gyroscopic systems are considered in Chapter 3, including the elements of Pontryagin and Krein space theory, the notion of the Krein signature of eigenvalues and its relation with negative and positive energy of the oscillation modes, the graphical interpretation of the Krein signature via eigencurves, strong stability and some extensions to Hamiltonian partial differential equations with the application to absolute and convective instability.

Reversible and circulatory systems are described in Chapter 4 with the classification of typical singularities of stability diagrams and their sensitivity analysis by means of the perturbation theory of multiple eigenvalues that is finally applied to a number of mechanical problems.

What happens with stability when dissipative, circulatory, potential, and gyroscopic forces are acting all together or in different combinations with each other? The most important results on the influence of structure of forces on stability, from the Kelvin–Tait–Chetaev theorem to recent achievements, including the overdamped and indefinitely damped systems, are presented in Chapter 5.

Chapter 6 is a detailed study of dissipation-induced instabilities in Hamiltonian and reversible systems, including an analytical description of movement of eigenvalues under dissipative and circulatory perturbations in dependence on the Krein signature of eigenvalues of ideal systems and explicit expressions approximating the drop in the stability threshold.

Chapter 7 develops a convenient perturbation theory of nonself-adjoint boundary eigenvalue problems for differential operator matrices with boundary conditions depending on both the spectral and physical parameters, laying a foundation for the sta-

bility analysis of continuous nonconservative systems considered in the rest of the book.

In Chapter 8 we present a theory of the Ziegler–Bottema destabilization paradox in continuous circulatory systems and illustrate it with examples from solid mechanics.

Chapter 9 demonstrates how the Krein signature of eigenvalues and variation of the boundary conditions control excitation of the oscillatory magnetohydrodynamics (MHD) dynamo – a destabilization of a heavily damped system in the presence of gyroscopic forces – that is responsible for the generation of magnetic fields in stars and planets.

A similar controlling role of the Krein signature in the destabilization of bending waves propagating in gyroscopic continua in frictional contact is discussed in Chapter 10, which also establishes how MacKay's eigenvalue cones unfold into the eigensurfaces known as the double-coffee-filter and viaduct, and thereby explains why the wine glass sings.

Chapter 11 discusses Hamilton's conical refraction, explicitly describes energy and width surfaces of general non-Hermitian Hamiltonians, and demonstrates how to calculate perturbatively the Berry phase around diabolical and exceptional points of singular dispersion surfaces arising in optics of birefringent absorptive and chiral media.

In Chapter 12, the geometrical optics approximation is applied to the stability analysis of the MHD equations describing the paradoxical noncommuting limiting behavior of the threshold of the Velikhov–Chandrasekhar magnetorotational instability that is the most probable trigger of turbulence in the disks of matter orbiting around gravitating astrophysical objects.

Chapter 2

Lyapunov stability and linear stability analysis

1875 March 6, the following subject for the Adams Prize to be adjudged in 1877 was agreed upon: The criterion of dynamical stability. ... what is required is a corresponding condition enabling us to decide when a dynamically possible motion is such, that if slightly deranged, the motion shall continue to be only slightly departed from.

J. Challis [417]

The examiners for the 1877 Adams Prize essay[1] at Cambridge who formulated its theme as "The criterion of dynamical stability" were J. C. Maxwell and G. G. Stokes. Twenty years earlier Maxwell himself won the Adams Prize competition by giving a solution to the problem on the nature of the Saturn's rings proposed by J. Challis and W. Thomson (Lord Kelvin). Solid or liquid rings turned out to be unstable which allowed him to conclude that "the only system of rings which can exist is one composed of an indefinite number of unconnected particles, revolving around a planet with different velocities according to their respective distances" [455]. In order to establish the instability or stability, Maxwell had to analyze whether the complex roots of an algebraic dispersion relation have positive or negative real parts, respectively. He encountered the same mathematical problem in the subsequent study of centrifugal governors of steam engines [416]. Intrigued by nontriviality of stability conditions already in particular cases, at a meeting of the London Mathematical Society on 23 January 1868 Maxwell asked if anyone in the audience could formulate the necessary and sufficient condition that "all the possible [real] roots and all the possible parts of the impossible [complex] roots of a certain equation shall be negative" [416,417]. This challenge was faced by E. J. Routh who in his Adams Prize essay of 1877 found such an algorithm for real polynomials [504, 505].

[1] The annual Adams Prize is named after the English astronomer John Couch Adams (1819–1892) who predicted the existence of the planet Neptune independently of the French mathematician Urbain Jean Joseph Leverrier (1811–1877). Despite Adams presenting his results to the then director of the Cambridge Observatory, James Challis (1803–1882), Neptune was actually discovered in Berlin with the use of the Leverrier's computations [455].

In an equivalent form, the Routh criterion was re-discovered in 1895 independently by A. Hurwitz[2] [236]. Both scientists were unaware of the criterion of C. Hermite[3] found already in 1856 [221]. The three equivalent algebraic criteria for all the roots of a real polynomial to have negative real parts were derived for the systems governed by *linear* ordinary differential equations with constant coefficients. In 1892, A. M. Lyapunov[4] developed the foundations of a rigorous stability theory of the processes described by the *nonlinear* differential equations, including a formal definition of stability of motion and justification of a linearization, that had been "courageously used" [371,372] in the XIXth century, in a neighborhood of stationary and nonstationary motions [387].

2.1 Main facts and definitions

Consider a nonlinear dynamical system [150, 253, 423]

$$\frac{d\mathbf{z}}{dt} = \mathbf{g}(\mathbf{z}, t), \quad \mathbf{z}(t_0) = \mathbf{z}_0, \tag{2.1}$$

where $\mathbf{g} : U \subseteq \mathbb{R}^n \times \mathbb{R} \to \mathbb{R}^n$ is a function that is continuously differentiable with respect to $\mathbf{z}$ and continuous with respect to t in an open domain U. Then, the initial-value problem (2.1) has a unique solution (*motion*) $\mathbf{z}(t)$ starting at any initial state $\mathbf{z}_0$ at any time t_0 (selected within U) that is defined on an open time interval around t_0 [150, 253].

Let $\mathbf{z}'(t)$ be a fixed (*unperturbed* in terms of Lyapunov [387]) motion of the system (2.1). Then, introducing the *deviation* about the unperturbed motion as $\mathbf{x}(t) = \mathbf{z}(t) - \mathbf{z}'(t)$, we find that [253, 503]

$$\frac{d\mathbf{z}}{dt} = \frac{d\mathbf{x}}{dt} + \frac{d\mathbf{z}'(t)}{dt} = \mathbf{g}(\mathbf{x} + \mathbf{z}'(t), t) = \mathbf{f}(\mathbf{x}, t) + \mathbf{g}(\mathbf{z}'(t), t).$$

In view of equation (2.1), the system describing the development of the deviation is

$$\frac{d\mathbf{x}}{dt} = \mathbf{f}(\mathbf{x}, t), \tag{2.2}$$

where $\mathbf{f}$ is continuously differentiable in $\mathbf{x}$ in an open set $\Omega \subseteq \mathbb{R}^n$ containing the origin, continuous in t in an open interval (τ, ∞), and $\mathbf{f}(0, t) = 0$, $\forall t \in (\tau, \infty)$, i.e.

[2] Adolf Hurwitz (1859–1919) – a German mathematician. During his work at the ETH Zurich he met a Slovak turbine engineer, Aurel Boleslaw Stodola (1859–1942), who in 1893–94 motivated Hurwitz to derive the stability criterion [66].

[3] Charles Hermite (1822–1901) – a French algebraist. In contrast to Routh and Hurwitz, who were inspired by practical applications, Hermite's work on the isolation of the roots of a polynomial in a region of a complex plane was primarily driven by his interest in finding explicit solutions to algebraic equations, e.g. to the general quintic equation [335].

[4] Alexandr Mikhailovich Lyapunov (1857–1918) – a Russian mathematician, founder of the modern stability theory [469].

the origin $\mathbf{x} = 0$ is an *equilibrium state* of the system (2.2). Hence, we have reduced the study of stability of the motion $\mathbf{z}'(t)$ of the system (2.1) to the study of stability of the equilibrium of equation (2.2).

2.1.1 Stability, instability, and uniform stability

Let $[t_0, \omega) \subset [t_0, \infty)$ be the right maximal interval of existence [420] of the solution $\mathbf{x}(t)$ of equation (2.2) and $\| \, . \, \|$ the Euclidean norm of a vector.

Definition 2.1 (A. M. Lyapunov, 1892 [387, 503]). The equilibrium $\mathbf{x} = 0$ of equation (2.2) is called *Lyapunov stable* if for every $\varepsilon > 0$ and $t_0 \in (\tau, \infty)$ there is a $\delta(\varepsilon, t_0) > 0$ such that $\|\mathbf{x}(t_0)\| < \delta$ implies $\|\mathbf{x}(t)\| < \varepsilon$ for all $t \in [t_0, \omega)$.

In Definition 2.1, ω is not assumed to be infinite which may result in the motions escaping to infinity in finite time. However, if $\overline{B}_\varepsilon \subset \Omega$, where $\overline{B}_\varepsilon = \{\mathbf{x} \in \mathbb{R}^n, \|\mathbf{x}\| \leq \varepsilon\}$, then the motion $\mathbf{x}(t)$ in this definition can be extended through the semiaxis $[t_0, \infty)$ so that $\omega = \infty$ [420, 503].

Definition 2.2 (A. M. Lyapunov, 1892 [387, 503]). The equilibrium $\mathbf{x} = 0$ of equation (2.2) is called *unstable* if it is not Lyapunov stable, i.e. for some $\varepsilon > 0$ and $t_0 \in (\tau, \infty)$ and any $\delta > 0$ there exist $\mathbf{x}(t_0)$ with $\|\mathbf{x}(t_0)\| < \delta$ and $t \in [t_0, \omega)$ such that $\|\mathbf{x}(t)\| \geq \varepsilon$.

Note that stability and instability in the sense of Lyapunov do not depend on the specific choice of t_0 [2, 150]. However, Lyapunov's definition of stability contains a rather gentle assumption that the deviations should start in a neighborhood of the equilibrium, whose size depends on the initial time instant, t_0. Sometimes, however, it is necessary to prove stability in a stronger assumption, for example, that such a dependence on t_0 does not exist.

Definition 2.3 (K. P. Persidskii, 1933 [503]). The equilibrium $\mathbf{x} = 0$ of equation (2.2) is called *uniformly stable* if for each $\varepsilon > 0$ there exists a $\delta(\varepsilon) > 0$ such that $\|\mathbf{x}(t)\| < \varepsilon$ for all $t_0 \in (\tau, \infty)$, $\|\mathbf{x}(t_0)\| < \delta$, and $t \in [t_0, \omega)$.

2.1.2 Attractivity and asymptotic stability

The concepts of the Lyapunov stability and uniform stability formalize the intuitive idea of Maxwell and Stokes that small initial errors should lead to small variations in the motion. In many situations, however, it is desirable that the small errors vanish as time goes to infinity in order for the deviation to approach the equilibrium asymptotically.

Definition 2.4 (W. Hahn, 1967 [470, 503]). The equilibrium $\mathbf{x} = 0$ of equation (2.2) is said to be *attractive* if for any $t_0 \in (\tau, \infty)$ there is a $\eta = \eta(t_0)$ and for each $\varepsilon > 0$ and $\mathbf{x}(t_0)$ satisfying $\|\mathbf{x}(t_0)\| < \eta$ there exists $\sigma = \sigma(t_0, \varepsilon, \mathbf{x}(t_0)) > 0$ such that $t_0 + \sigma \in [t_0, \omega)$ and $\|\mathbf{x}(t)\| < \varepsilon$ for all $t \geq t_0 + \sigma$.

If η and σ in Definition 2.4 do not depend on the initial data t_0 and $\mathbf{x}(t_0)$, the equilibrium becomes *uniformly attractive*. Notice that if $\overline{B}_\varepsilon \subset \Omega$, then the solution $\mathbf{x}(t)$ in these definitions can be extended[5] through the semiaxis $[t_0, \infty)$. Then, all the motions satisfying $\|\mathbf{x}(t_0)\| < \eta$ converge (uniformly in $\mathbf{x}(t_0)$ and t_0) as $t \to \infty$ to the (uniformly) attractive equilibrium $\mathbf{x} = 0$ [503].

Definition 2.5 (A. M. Lyapunov, 1892 [387]). The equilibrium $\mathbf{x} = 0$ of equation (2.2) is said to be *asymptotically stable* at $t = t_0$ if it is Lyapunov stable and attractive.

Definition 2.6 (I. G. Malkin, 1954 [400, 503]). The equilibrium $\mathbf{x} = 0$ of equation (2.2) is said to be *uniformly asymptotically stable* if it is Lyapunov stable and uniformly attractive.

All the points $\mathbf{x}(t_0)$ from which motions starting at t_0 converge to the equilibrium as $t \to \infty$ form the *domain of attraction* of the equilibrium [2]. The domain of attraction is uniform if it does not depend on t_0 [470, 503].

2.1.3 Autonomous, nonautonomous, and periodic systems

The dynamical system (2.2) is a time-invariant or *autonomous* system, if its right-hand side does not depend explicitly on time. Otherwise, it is *nonautonomous*. The nonautonomous system (2.2) with $\mathbf{f}(\mathbf{x}, t)$ periodic in t is referred to as a *periodic* dynamical system [253, 423].

Theorem 2.7 (T. Ioshizawa, 1966 [253, 503]). *Let the function* $\mathbf{f}(\mathbf{x}, t)$ *in equation* (2.2) *not depend explicitly on* t *or is periodic in* t. *Then the Lyapunov stability of the equilibrium* $\mathbf{x} = 0$ *implies uniform stability and the asymptotic stability implies uniform asymptotic stability.*

Therefore, the concept of uniformity makes sense only in application to general (nonperiodic) time-varying systems.[6] On the other hand, it is the autonomous and periodic systems that most frequently arise in physical and engineering models.

[5] In the following, we will always assume that solutions have this property.

[6] An interested reader can find other stability notions and relationships between them, e.g. in the comprehensive surveys [253, 372, 384] and monographs [371, 503].

2.2 The direct (second) method of Lyapunov

After the formal definitions of stability are established, a question arises how to judge stability taking into account that explicit solutions to nonlinear differential equations are rare and numerical methods do not give a proof.

2.2.1 Lyapunov functions

Lyapunov's direct method provides an answer by utilizing the given form of equations of motion but without their explicit integration. Our physical intuition suggests that if the isolated system lost its energy at every possible state except a single equilibrium point, then the energy of the system would finally decrease to a minimum and this would happen exactly at the equilibrium. Since for an abstract dynamical system its energy cannot always naturally be defined [253], Lyapunov proposed an alternative, which we now know as the *Lyapunov functions* [387].

Definition 2.8. A continuously differentiable scalar real-valued function $V(\mathbf{x},t) \in C^1(\Omega\times(\tau,\infty))$ is (locally) *positive definite* if for some continuous, strictly increasing scalar function $\alpha : \mathbb{R}^+ \to \mathbb{R}^+$ such that $\alpha(0) = 0$ we have $V(0,t) = 0$ and $V(\mathbf{x},t) \geq \alpha(\|\mathbf{x}\|)$ for all $(\mathbf{x},t) \in (\Omega\times(\tau,\infty))$.

The function $V(\mathbf{x},t)$ is *negative definite* if $-V(\mathbf{x},t)$ is positive definite. If for all $(\mathbf{x},t) \in (\Omega\times(\tau,\infty))$ we have $V(\mathbf{x},t) \geq 0$ (≤ 0), the function $V(\mathbf{x},t)$ is called positive (negative) *semidefinite*.

Definition 2.9. A continuously differentiable scalar real-valued function $V(\mathbf{x},t) \in C^1(\Omega\times(\tau,\infty))$ is *decrescent* if there is a continuous, strictly increasing scalar function $\beta : \mathbb{R}^+ \to \mathbb{R}^+$ such that $\beta(0) = 0$ and $V(\mathbf{x},t) \leq \beta(\|\mathbf{x}\|)$ for all $(\mathbf{x},t) \in (\Omega\times(\tau,\infty))$.

In order to be a Lyapunov function for the system (2.2), the function $V(\mathbf{x},t)$ together with its derivative taken along the motion of the system (2.2)

$$\dot{V}(\mathbf{x},t) := \frac{dV}{dt} = \partial_t V(\mathbf{x},t) + \sum_{i=1}^{n} \partial_{x_i} V(\mathbf{x},t)\, f_i(\mathbf{x},t) \tag{2.3}$$

should satisfy some of the definiteness properties introduced above.

2.2.2 Lyapunov and Persidskii theorems on stability

A sufficient condition for the equilibrium $\mathbf{x} = 0$ of the system (2.2) to be Lyapunov stable can be formulated in terms of the positive definite functions.

Theorem 2.10 (A. M. Lyapunov, 1892 [253, 387, 503]). *Suppose for the system* (2.2) *there exists a positive definite function* $V(\mathbf{x}, t)$ *and its derivative along the trajectories of this system is negative semidefinite:* $\dot{V}(\mathbf{x}, t) \leq 0$*, then the equilibrium* $\mathbf{x} = 0$ *is Lyapunov stable.*

To detect uniformly stable equilibria we must further constrain the Lyapunov function $V(\mathbf{x}, t)$, by requiring it to be decrescent.

Theorem 2.11 (K. P. Persidskii, 1933 [503]). *Let, for the system* (2.2)*, there exist a positive definite and decrescent function* $V(\mathbf{x}, t)$ *and its derivative along the trajectories of this system is negative semidefinite:* $\dot{V}(\mathbf{x}, t) \leq 0$*, then the equilibrium* $\mathbf{x} = 0$ *is uniformly stable.*

If, additionally, the derivative of the Lyapunov function along the trajectories of the system (2.2) is negative definite, it can serve for proving the uniform asymptotic stability of the equilibrium.

Theorem 2.12 (A. M. Lyapunov, 1892 [253, 387, 503]). *Suppose there exists for the system* (2.2) *a positive definite and decrescent function* $V(\mathbf{x}, t)$ *such that* $-\dot{V}(\mathbf{x}, t)$ *is positive definite, then the equilibrium* $\mathbf{x} = 0$ *is uniformly asymptotically stable.*

Remember that for autonomous and periodic systems the notions of the uniform Lyapunov stability and uniform asymptotic stability are equivalent to that of the Lyapunov stability and asymptotic stability, respectively [253, 503].

2.2.3 Chetaev and Lyapunov theorems on instability

The method of Lyapunov functions is also efficient for establishing sufficient conditions for instability. One of the most well-known results in this direction is the *Chetaev instability theorem* [127].

Theorem 2.13 (N. G. Chetaev, 1934 [503]). *Suppose that for the system* (2.2) *there exist* $t_0 \in (\tau, \infty)$, $\varepsilon > 0$ *so that* $\overline{B}_\varepsilon \subset \Omega$, *an open set* $Z \in B_\varepsilon$, *and a scalar function* $V(\mathbf{x}, t) \in C^1(B_\varepsilon \times (t_0, \infty))$ *such that in* $Z \times (t_0, \infty)$:

(1) $0 < V(\mathbf{x}, t) \leq k < \infty$ *for some* k;

(2) $\dot{V}(\mathbf{x}, t) \geq \alpha(V(\mathbf{x}, t))$, *where* $\alpha : \mathbb{R}^+ \to \mathbb{R}^+$, $\alpha(0) = 0$, *is a continuous, strictly increasing scalar function;*

(3) *the equilibrium* $\mathbf{x} = 0 \in \partial Z$, *where* ∂Z *is the boundary of* Z;

(4) $V(\mathbf{x}, t) = 0$ *in* $(\partial Z \bigcap B_\varepsilon) \times (t_0, \infty)$;

then the equilibrium is Lyapunov unstable.

With $V(\mathbf{x}, t) > 0$ being decrescent, Theorem 2.13 is known as the *first Lyapunov instability theorem* in the case when $\dot{V}(\mathbf{x}, t)$ is positive definite and as the *second Lyapunov instability theorem* in the case when $\dot{V}(\mathbf{x}, t) = cV(\mathbf{x}, t) + W(\mathbf{x}, t)$, $c > 0$, and $W(\mathbf{x}, t) \geq 0$ is a continuous function [387, 503].

The direct method of Lyapunov is a very powerful tool for proving stability of time-dependent nonlinear systems not only in a local sense but also in the case when the deviations can start far from the equilibrium (global stability).

Although a universally applicable algorithm of construction of the Lyapunov functions is not yet known, for many important classes of systems, including linear ones, methods of finding the Lyapunov functions have been developed. They enable, in particular, to justify the investigation of stability by linearization and to establish stability criteria. In the special cases when the linear approximation is not enough to judge nonlinear stability, the second method of Lyapunov often provides the only alternative [253, 503].

2.3 The indirect (first) method of Lyapunov

Although physical and engineering systems are invariably nonlinear and their linear description is by necessity accurate only within a restricted region of operation (local), the relative simplicity of linear differential equations suggests using information on the stability of a linearization in order to judge the stability of the original nonlinear system. Stability analysis by linearization is the essence of the first method of Lyapunov.

2.3.1 Linearization

Since by our initial assumption the function $\mathbf{f}(\mathbf{x}, t)$ in the nonlinear system (2.2) is continuously differentiable in $\mathbf{x}$ and continuous in t, we can extract the linear in $\mathbf{x}$ terms and write equation (2.2) in the *quasilinear* form

$$\frac{d\mathbf{x}}{dt} = \mathbf{A}(t)\mathbf{x} + \mathbf{r}(\mathbf{x}, t), \tag{2.4}$$

where $\mathbf{A}(t) \in C(\tau, \infty)$ is the real *Jacobian matrix* of $\mathbf{f}$ evaluated at the equilibrium $\mathbf{x} = 0$: $a_{ij} = \partial_{x_j} f_i(0, t)$, $i, j = 1, \ldots, n$. We suppose that

$$\sup_{t \in [t_0, \infty)} \|\mathbf{A}(t)\| \leq M < \infty. \tag{2.5}$$

The remainder $\mathbf{r}(\mathbf{x}, t) = \mathbf{f}(\mathbf{x}, t) - \mathbf{A}(t)\mathbf{x}$ is a C^1-function in $\mathbf{x}$ and continuous in t that is assumed to approach zero uniformly in t, i.e. [141, 150]:

$$\lim_{\|\mathbf{x}\| \to 0} \sup_{t \in [t_0, \infty)} \frac{\|\mathbf{r}(\mathbf{x}, t)\|}{\|\mathbf{x}\|} = 0. \tag{2.6}$$

With the use of the direct Lyapunov method the following result can be established.

Theorem 2.14 (W. Hahn, 1967 [213, 437]). *If* (2.6) *is fulfilled and* $\mathbf{x} = 0$ *is a uniformly asymptotically stable equilibrium of the* linearization

$$\frac{d\mathbf{x}}{dt} = \mathbf{A}(t)\mathbf{x} \tag{2.7}$$

of the nonlinear system (2.2)*, then the latter has at* $\mathbf{x} = 0$ *a (locally) uniformly asymptotically stable equilibrium.*

It is known that uniform asymptotic stability implies asymptotic stability [253]. In order to prove asymptotic stability by linearization directly, a careful examination of the linear system (2.7) with the matrix $\mathbf{A}(t)$ is required.

2.3.2 The characteristic exponent of a solution

Let $\mathbf{X}(t) = (\mathbf{x}_1(t), \ldots, \mathbf{x}_n(t))$ be a *fundamental matrix* of the linear system (2.7), i.e. a solution to the matrix differential equation

$$\frac{d\mathbf{X}(t)}{dt} = \mathbf{A}(t)\mathbf{X}(t). \tag{2.8}$$

The columns of the matrix $\mathbf{X}(t)$ are n linearly independent solutions of the system (2.7). Hence, $\det \mathbf{X}(t) \neq 0$. According to the Ostrogradsky–Liouville formula [150]

$$\det \mathbf{X}(t) = \det \mathbf{X}(t_0) \exp\left(\int_{t_0}^{t} \mathrm{tr}\mathbf{A}(s) ds \right), \tag{2.9}$$

where tr$\mathbf{A}$ stands for the trace of the matrix $\mathbf{A}$. Hence, $\mathbf{X}(t)$ is nonsingular if $\det \mathbf{X}(t_0) \neq 0$, i.e. when the initial vectors at the time instant t_0 are linearly independent. In the case when $\mathbf{X}(t_0) = \mathbf{I}$, where $\mathbf{I}$ is a unit $n \times n$ matrix, the fundamental matrix is called normalized at a point t_0 and is denoted as $\mathbf{X}(t) = \mathbf{\Phi}(t, t_0)$ [2]. In our subsequent considerations the fundamental matrix is assumed to be normalized.

Any solution $\mathbf{x}(t)$ of equation (2.7) can be represented in the form [2]

$$\mathbf{x}(t) = \mathbf{X}(t)\mathbf{X}^{-1}(t_0)\mathbf{x}(t_0) = \mathbf{\Phi}(t, t_0)\mathbf{x}(t_0). \tag{2.10}$$

By this reasoning the normalized fundamental matrix is frequently called the *state transition matrix* in the engineering literature [144, 427, 540].

Under the condition (2.5), any nontrivial solution $\mathbf{x}(t)$ of the linear system (2.7) has a finite *characteristic exponent* that is defined as [2, 150]

$$\chi[\mathbf{x}] := \lim_{t \to +\infty} \sup \frac{1}{t} \ln \|\mathbf{x}(t)\|. \tag{2.11}$$

A set of all different characteristic exponents of solutions of the system (2.7) is called its spectrum. The number N of elements of the spectrum does not exceed n. If a fundamental matrix $\mathbf{X}(t)$ contains $r_k \geq 0$ columns with the identical characteristic exponents equal to α_k, $k = 1, \ldots, N$, then the sum of the characteristic exponents of its columns is

$$\sigma_X = \sum_{j=1}^{n} \chi[\mathbf{x}_j] = \sum_{k=1}^{N} r_k \alpha_k. \tag{2.12}$$

A fundamental matrix is said to be *normal*, if σ_X is minimal in comparison with other fundamental matrices [150, 371]. For any fundamental matrix (including the normal ones) the *Lyapunov inequality* is valid:

$$\sigma_X \geq \lim_{t \to +\infty} \sup \frac{1}{t} \int_{t_0}^{t} \mathrm{tr}\mathbf{A}(s) ds. \tag{2.13}$$

Equality in (2.13) implies that $\mathbf{X}(t)$ is normal, the converse is not true [2, 150].

2.3.3 Lyapunov regularity of linearization

It is known [2, 150] that in all normal fundamental matrices the number $n_{k'}$ of columns with the characteristic exponent $\alpha_{k'}$, $k' = 1, \ldots, N'$, is the same, $\sum_{k'=1}^{N'} n_{k'} = n$, and each normal fundamental matrix realizes a spectrum of the linear system (2.7). The number $n_{k'}$ is the *multiplicity* of $\alpha_{k'}$ [2].

Definition 2.15 (B. P. Demidovich, 1967 [150]). A set of characteristic exponents $\chi[\mathbf{x}_1], \ldots, \chi[\mathbf{x}_n]$ of columns of a certain normal fundamental matrix of the linear system (2.7) is called a *complete spectrum* of the linear system and the number

$$\sigma = \sum_{j=1}^{n} \chi[\mathbf{x}_j] = \sum_{k'=1}^{N'} n_{k'} \alpha_{k'} \tag{2.14}$$

is a sum of characteristic exponents of the linear system (2.7).

Note that any fundamental matrix can be reduced to a normal one by a linear transformation with a constant nonsingular triangular matrix [387].

Definition 2.16 (B. P. Demidovich, 1967 [150]). Linear system (2.7) is said to be *regular* in the sense of Lyapunov, if

$$\sigma = \lim_{t \to +\infty} \inf \frac{1}{t} \int_{t_0}^{t} \mathrm{tr}\mathbf{A}(s) ds. \tag{2.15}$$

The linear system

$$\frac{d\mathbf{y}}{dt} = -\mathbf{A}^T(t)\mathbf{y}, \tag{2.16}$$

is adjoint to the system (2.7). Let

$$+\infty > \eta_1 \geq \eta_2 \geq \cdots \geq \eta_n > -\infty$$

be a complete spectrum of the system (2.16) and that of the system (2.7) be

$$-\infty < \chi_1 \leq \chi_2 \leq \cdots \leq \chi_n < +\infty.$$

Theorem 2.17 (O. Perron, 1930 [2, 150]). *The linear system* (2.7) *is regular if and only if*

$$\chi_s + \eta_s = 0, \quad s = 1, \ldots, n.$$

A linear system is irregular if it is not regular.

Definition 2.18 (B. P. Demidovich, 1967 [150]). The number

$$\gamma = \sigma - \lim_{t \to +\infty} \inf \frac{1}{t} \int_{t_0}^{t} \mathrm{tr}\mathbf{A}(s) ds \tag{2.17}$$

is called the *coefficient of irregularity* of the linear system (2.7).

The coefficient of irregularity vanishes ($\gamma = 0$) if and only if the system is regular in the sense of Lyapunov [2].

2.3.4 Stability and instability in the first approximation

Let the remainder of the quasilinear system (2.4) be such that

$$\|\mathbf{r}(\mathbf{x}, t)\| \leq c\|\mathbf{x}\|^{\nu}, \quad \nu > 1, \quad c > 0. \tag{2.18}$$

With the use of the properties of the characteristic exponents and the second method of Lyapunov a sufficient condition for asymptotic stability in the first approximation can be obtained.

Theorem 2.19 (A. M. Lyapunov, 1892 [150, 213]). *If the linearization* (2.7) *is regular in the sense of Lyapunov, all its characteristic exponents are negative, and the condition* (2.18) *is fulfilled, then the equilibrium* $\mathbf{x} = 0$ *of the nonlinear system* (2.2) *is asymptotically stable.*

The Lyapunov sufficient condition of asymptotic stability given by Theorem 2.19 was extended to the irregular case by a number of authors including Malkin (1938), Chetaev (1948), and Massera (1956), see e.g. [150, 372]. A variant of their result can be formulated as follows.

Theorem 2.20 (B. P. Demidovich, 1967 [150, 213]). *Let, for the nonlinear system* (2.4)*, the condition* (2.18) *be fulfilled and the characteristic exponents* χ_1, $\chi_2, \ldots, \chi_n$ *of its linearization* (2.7) *satisfy the inequality*

$$\max_k \chi_k < -\frac{\gamma}{\nu - 1} \leq 0, \tag{2.19}$$

where γ *is the coefficient of irregularity of the linear system* (2.7)*, then the equilibrium* $\mathbf{x} = 0$ *of the nonlinear system* (2.2) *is asymptotically stable.*

Sufficient conditions for instability in the sense of Lyapunov of the nonlinear system (2.2) via the characteristic exponents of its linearization is a delicate question in the case of general nonautonomous systems. Recent results in this direction as well as a discussion of the state of the art in this field can be found by an interested reader in the works of Leonov and Kuznetsov [371, 372].

Recall that asymptotic stability implies uniform asymptotic stability for periodic and autonomous systems [253, 503]. Below we will see that these systems are also Lyapunov regular.

2.4 Linear stability analysis

Regular linear systems have nice properties reducing the question of asymptotic stability of the original nonlinear system to the placement of the characteristic exponents in the open left half-plane of the complex plane. What do regular systems, in the sense of Lyapunov, look like?

2.4.1 Autonomous systems

It is straightforward to show that a linear system with constant coefficients is regular. Indeed, if in equation (2.7) the real matrix $\mathbf{A}$ is constant, then the state transition matrix is

$$\mathbf{\Phi}(t,t_0) = \mathbf{I} + \mathbf{A}(t-t_0) + \mathbf{A}^2(t-t_0)^2/2! + \ldots =: e^{\mathbf{A}(t-t_0)}. \tag{2.20}$$

Hence, $\mathbf{x}(t) = e^{\mathbf{A}(t-t_0)}\mathbf{x}(t_0)$.

It is known that there exists a real nondegenerate matrix $\mathbf{S}$, transforming $\mathbf{A}$ to the *Jordan canonical form* that yields $e^{\mathbf{A}t} = \mathbf{S}e^{\mathbf{J}t}\mathbf{S}^{-1}$ with

$$e^{\mathbf{J}t} = \operatorname{diag}\left(e^{\mathbf{J}_{k_1}(\lambda_1)t}, \ldots, e^{\mathbf{J}_{k_m}(\lambda_m)t}, e^{\mathbf{B}_{2\nu_{m+1}}(\lambda_{m+1})t}, \ldots, e^{\mathbf{B}_{2\nu_{N-1}}(\lambda_{N-1})t}\right). \tag{2.21}$$

Matrix exponentials associated with the $k_s \times k_s$ *Jordan blocks* $\mathbf{J}_{k_s}(\lambda_s)$

$$e^{\mathbf{J}_{k_s}(\lambda_s)t} = e^{\lambda_s t}\begin{pmatrix} 1 & 0 & \cdots & 0 \\ t & 1 & \ddots & \vdots \\ \vdots & \ddots & \ddots & 0 \\ \frac{t^{k_s-1}}{(k_s-1)!} & \cdots & t & 1 \end{pmatrix}, \quad s = 1, 2, \ldots, m,$$

correspond to the real eigenvalues $\lambda_s(\mathbf{A})$ of the matrix $\mathbf{A}$. The remaining $(N-m)/2$ products of $2\nu_s \times 2\nu_s$ block matrices [2]

$$e^{\mathbf{B}_{2\nu_s}(\lambda_s)t} = \begin{pmatrix} e^{\mathbf{J}_{\nu_s}(\alpha_s)t} & 0 \\ 0 & e^{\mathbf{J}_{\nu_s}(\alpha_s)t} \end{pmatrix}\begin{pmatrix} \mathbf{I}_{\nu_s}\cos(\beta_s t) & -\mathbf{I}_{\nu_s}\sin(\beta_s t) \\ \mathbf{I}_{\nu_s}\sin(\beta_s t) & \mathbf{I}_{\nu_s}\cos(\beta_s t) \end{pmatrix}$$

represent the contribution of $(N-m)/2$ pairs of complex-conjugate eigenvalues $\lambda_s = \alpha_s + i\beta_s$ and $\lambda_{s+1} = \alpha_s - i\beta_s$, where $s = m+1, m+3, \ldots, N-1$. Note that the number of the Jordan blocks $N \le n$ and $\sum_{s=1}^{m} k_s + 2\sum_{j=0}^{(N-m)/2-1} \nu_{m+2j+1} = n$. Real eigenvalues or complex-conjugate pairs corresponding to different blocks in equation (2.21) may coincide [2]. Then, the sum of the sizes of the respective Jordan blocks is an algebraic multiplicity of the eigenvalue and the number of the Jordan blocks is its geometric multiplicity.

Writing $\mathbf{S}^{-1}\mathbf{x}(t) = e^{\mathbf{J}(t-t_0)}\mathbf{S}^{-1}\mathbf{x}(t_0)$, we see that the characteristic exponents of nontrivial solutions of the system (2.7) with time-independent matrix $\mathbf{A}$ are $\chi_j =$

$\mathrm{Re}\lambda_j(\mathbf{A})$, where the eigenvalues $\lambda_j = \lambda_j(\mathbf{A})$ (some of them may be equal to each other) are solutions to the characteristic equation $\det(\mathbf{A} - \lambda\mathbf{I}) = 0$ [150]. Therefore,

$$\lim_{t\to+\infty} \inf \frac{1}{t}\int_{t_0}^{t} \mathrm{tr}\mathbf{A}(s)ds = \mathrm{tr}\mathbf{A} = \sum_{j=1}^{n} \mathrm{Re}\lambda_j = \sigma, \tag{2.22}$$

which according to Definitions 2.15 and 2.16 implies regularity [2].

Theorem 2.21 (A. M. Lyapunov, 1892 [150]). *The linear system* (2.7) *with time-independent matrix* $\mathbf{A}$ *is Lyapunov stable if and only if all its eigenvalues* $\lambda_j = \lambda_j(\mathbf{A})$ *have nonpositive real parts*

$$\mathrm{Re}\lambda_j(\mathbf{A}) \le 0$$

and the algebraic and geometric multiplicity of the eigenvalues with the vanishing real part coincide. The system (2.7) *with time-independent matrix* $\mathbf{A}$ *is asymptotically stable if and only if for all* $\lambda_j = \lambda_j(\mathbf{A})$

$$\mathrm{Re}\lambda_j(\mathbf{A}) < 0.$$

As a consequence of the regularity of autonomous systems, Theorem 2.21, and Theorem 2.19, the equilibrium $\mathbf{x} = 0$ of a nonlinear autonomous system is locally asymptotically stable, if all eigenvalues of the matrix of its linearization are in the open left half-plane of the complex plane [2, 150].

The case when all the eigenvalues of the linearization do not have positive real part and some of them are pure imaginary is *critical* in the sense of Lyapunov, because stability (instability) of the linear system does not generally imply stability (instability) of the original nonlinear one. The critical cases require taking into account either higher order terms in the Taylor expansion of the right-hand side of the nonlinear equation, if it is smooth enough, or application of the direct method of Lyapunov [127, 387, 400, 423].

2.4.2 Lyapunov transformation and reducibility

Consider the linear system (2.7) with the matrix $\mathbf{A}(t)$ satisfying the condition (2.5). Let

$$\mathbf{x} = \mathbf{L}(t)\mathbf{q} \tag{2.23}$$

be a transformation with the nonsingular matrix $\mathbf{L}(t)$ that is continuously differentiable for $t \in [t_0, \infty)$. The transformation (2.23) reduces the system (2.7) to another linear system

$$\frac{d\mathbf{q}}{dt} = \mathbf{B}(t)\mathbf{q}, \tag{2.24}$$

where

$$\mathbf{B}(t) = \mathbf{L}^{-1}(t)\mathbf{A}(t)\mathbf{L}(t) - \mathbf{L}^{-1}(t)\frac{d\mathbf{L}(t)}{dt}. \tag{2.25}$$

Definition 2.22 (N. P. Erugin, 1946 [2, 91]). The transformation (2.23) is the *Lyapunov transformation* if $\mathbf{L} \in C^1([t_0, \infty))$ and $\mathbf{L}(t)$, $\mathbf{L}^{-1}(t)$, and $\dot{\mathbf{L}}(t)$ are bounded for $t \in [t_0, \infty)$. The matrix $\mathbf{L}(t)$ is called the *Lyapunov matrix*.

The Lyapunov transformation is symmetrical in a sense that if the system (2.7) is reducible to (2.24), then the system (2.24) is reducible to (2.7). Moreover, Lyapunov transformations do not change characteristic exponents of a linear system and preserve its regularity [2].

If there exists a Lyapunov transformation (2.23) such that the matrix $\mathbf{B}(t)$ can be expressed as in equation (2.25), then the system (2.7) is said to be *reducible* to the system (2.24). If, additionally, the matrix $\mathbf{B}$ in equation (2.25) does not depend on t, the system (2.7) is called reducible to an autonomous system [2, 91]. A criterion of reducibility to a time-independent system involves a possibility of a certain factorization of the fundamental matrix.

Theorem 2.23 (N. P. Erugin, 1946 [2, 150]). *A linear system* (2.7) *is reducible to a system with constant coefficients if and only if it has a fundamental matrix* $\mathbf{X}(t)$ *of the form*

$$\mathbf{X}(t) = \mathbf{L}(t)e^{\mathbf{B}t} \tag{2.26}$$

where $\mathbf{L}(t)$ *is a Lyapunov matrix and* $\mathbf{B}$ *is a constant matrix.*

From the regularity of linear autonomous systems, symmetry of the Lyapunov transformation, and invariance of the regularity under the Lyapunov transformation it follows that any linear nonautonomous system reducible to a system with constant coefficients is regular [2].

A system reducible to an autonomous system is Lyapunov stable if and only if all its characteristic exponents, understood as the real parts of the eigenvalues of the constant matrix $\mathbf{B}$, are nonpositive, and zero characteristic exponents correspond to the eigenvalues of $\mathbf{B}$ with coinciding algebraic and geometric multiplicities (semisimple eigenvalues [428]). Such a reducible system is asymptotically stable if and only if all its characteristic exponents are negative [150].

2.4.3 Periodic systems

Let in the equation (2.7) the matrix $\mathbf{A}(t)$ be a T-periodic function of time, i.e. $\mathbf{A}(t + T) = \mathbf{A}(t)$, $T > 0$, for all t. According to the following *Floquet representation theo-*

rem, the state transition matrix of the periodic system can be factorized into periodic and exponential parts.

Theorem 2.24 (G. Floquet, 1883 [2,150]). *The normalized at $t_0 = 0$ fundamental matrix of the linear system* (2.7) *with periodic coefficients can be represented in the form*

$$\mathbf{\Phi}(t,0) = \mathbf{L}(t)e^{\mathbf{F}t} \tag{2.27}$$

where $\mathbf{F} = \frac{1}{T}\mathrm{Ln}\mathbf{\Phi}(T,0)$ *and* $\mathbf{L}(t) = \mathbf{L}(t+T)$ *with* $\mathbf{L}(0) = \mathbf{I}$.

The value $\mathbf{\Phi}(T,0)$ of the state transition matrix after one period is called the *monodromy matrix*. The eigenvalues of the monodromy matrix, i.e. the roots, ρ, of the characteristic equation $\det(\mathbf{\Phi}(T,0) - \rho\mathbf{I}) = 0$, are known as the *Floquet multipliers* of the periodic system whereas the eigenvalues, λ, of the *Floquet factor* $\mathbf{F}$ are its *Floquet exponents*. The Floquet exponents are related to the Floquet multipliers via the formula

$$\lambda_k = \frac{1}{T}\mathrm{Ln}\rho_k = \frac{1}{T}\left(\ln|\rho_k| + i\left(\arg\rho_k + 2\pi m\right)\right), \tag{2.28}$$

where $m = 0, \pm 1, \ldots$ and $k = 1, \ldots, n$. The real parts of the Floquet exponents are characteristic exponents of nontrivial solutions of the periodic system (2.7).

It can be shown that Theorem 2.24 is valid for any T-periodic fundamental matrix $\mathbf{X}(t)$ and that $\mathbf{L}(t)$ is a Lyapunov matrix [2,603]. Hence, by Theorem 2.23 we obtain the *Lyapunov reducibility theorem* which implies regularity of the linear systems with periodic coefficients.

Theorem 2.25 (A. M. Lyapunov, 1892 [2,150]). *Linear system* (2.7) *with periodic C^1-matrix $\mathbf{A}(t)$ is reducible to a system with constant coefficients.*

In general, the constant Floquet factor $\mathbf{F}$ and the periodic Lyapunov matrix $\mathbf{L}(t)$ of the real periodic system (2.7) are complex-valued. However, it is always possible to obtain the real factorizations by considering the matrix $\mathbf{\Phi}(t,0)$ over a doubled period [2,540]:

$$\mathbf{F}_{2T} = \frac{1}{2T}\mathrm{Ln}\mathbf{\Phi}(2T,0), \quad \mathbf{L}_{2T}(t) = \mathbf{L}_{2T}(t+2T), \quad \mathbf{L}(0) = \mathbf{I}. \tag{2.29}$$

Existence and construction of real factorizations with T-periodic real Lyapunov matrices were discussed in [603] and recently in [427,540,616].

Theorem 2.26 (G. Floquet, 1883 [2, 150]). *Linear system* (2.7) *with periodic coefficients is Lyapunov stable if and only if all its multipliers* $\rho_j = \rho_j(\mathbf{\Phi}(T,0))$ *belong to the closed unit disk* $|\rho| \le 1$ *in the complex plane, and the multipliers lying on the unit circle* $|\rho| = 1$ *are semisimple. For asymptotic stability it is necessary and sufficient that all the multipliers be located in the interior of the unit disk* $|\rho| < 1$.

Indeed, according to the formula (2.28) the condition $|\rho_j| \le 1$ is equivalent to $\mathrm{Re}\lambda_j \le 0$. The necessary and sufficient conditions for all the roots of a polynomial with real (complex) coefficients to be inside the unit circle are given by the Schur–Cohn (Bilharz) criterion [62, 409].

2.4.4 Example. Coupled parametric oscillators

Equations of two coupled parametric oscillators arise in problems of particle transport and wave propagation in structures rotating in time or space [522]

$$\begin{aligned} \ddot{\xi}_1 + 2h\dot{\xi}_1 + (a - 2\kappa\cos(2\Omega t))\xi_1 &= 2\kappa\xi_2\sin(2\Omega t), \\ \ddot{\xi}_2 + 2h\dot{\xi}_2 + (a + 2\kappa\cos(2\Omega t))\xi_2 &= 2\kappa\xi_1\sin(2\Omega t), \end{aligned} \tag{2.30}$$

where $\Omega > 0$ and the dot stands for time differentiation. The equations (2.30) can be written in the form $\dot{\mathbf{x}} = \mathbf{A}(t)\mathbf{x}$ with $\mathbf{x}^T = (\xi_1, \xi_2, \dot{\xi}_1, \dot{\xi}_2)$ and

$$\mathbf{A}(t) = \begin{pmatrix} 0 & 0 & 1 & 0 \\ 0 & 0 & 0 & 1 \\ -a + 2\kappa\cos(2\Omega t) & 2\kappa\sin(2\Omega t) & -2h & 0 \\ 2\kappa\sin(2\Omega t) & -a - 2\kappa\cos(2\Omega t) & 0 & -2h \end{pmatrix}. \tag{2.31}$$

The real matrix $\mathbf{A}(t)$ is periodic with the period $T = \pi/\Omega$. The Lyapunov transformation (2.23) with the $2T$-periodic matrix [325, 522, 529]

$$\mathbf{L}_{2T}(t) = \begin{pmatrix} \cos(\Omega t) & -\sin(\Omega t) & 0 & 0 \\ \sin(\Omega t) & \cos(\Omega t) & 0 & 0 \\ 0 & 0 & \cos(\Omega t) & -\sin(\Omega t) \\ 0 & 0 & \sin(\Omega t) & \cos(\Omega t) \end{pmatrix} \tag{2.32}$$

reduces the original periodic system to (2.24) with the constant matrix $\mathbf{B}$ (2.25)

$$\mathbf{B} = \begin{pmatrix} 0 & \Omega & 1 & 0 \\ -\Omega & 0 & 0 & 1 \\ -a + 2\kappa & 0 & -2h & \Omega \\ 0 & -a - 2\kappa & -\Omega & -2h \end{pmatrix}. \tag{2.33}$$

This implies that the evolution of the first two components of the vector $\mathbf{q}$ is governed by the following system of second-order linear differential equations

$$\begin{aligned} \ddot{q}_1 + 2h\dot{q}_1 - 2\Omega\dot{q}_2 + (a - 2\kappa - \Omega^2)q_1 - 2h\Omega q_2 = 0, \\ \ddot{q}_2 + 2h\dot{q}_2 + 2\Omega\dot{q}_1 + (a + 2\kappa - \Omega^2)q_2 + 2h\Omega q_1 = 0, \end{aligned} \tag{2.34}$$

which is nothing else but the gyroscopic system with damping and circulatory forces[7] (1.56) corresponding to Smith's model of a rotating shaft with the external and internal damping, where the stiffness coefficients are $k_1 = a - 2\kappa$ and $k_2 = a + 2\kappa$, the coefficient of internal damping is $\delta = 0$, and the coefficient of external damping is $\nu = 2h$. When $h = 0$, equation (2.34) describes the already familiar to us from Chapter 1, Brouwer's particle in a rotating vessel [93, 94, 304], cf. equation (1.1).

When $h = 0$, $\kappa = 0$, and $a > 0$, Brouwer's particle moves in the cavity rotating with the angular velocity Ω. Then, the monodromy matrix of the $(T = \pi/\Omega)$-periodic system with the matrix (2.31), is

$$\mathbf{\Phi}(T, 0) = \mathbf{L}_{2T}(T)e^{\mathbf{B}T} = \mathbf{S}\,\mathrm{diag}\,(\rho_+, \rho_-, \rho_+, \rho_-)\,\mathbf{S}^{-1}, \tag{2.35}$$

where $\mathbf{L}_{2T}(t)$ and $\mathbf{B}$ are given by equations (2.32) and (2.33) and the matrix $\mathbf{S}$ is

$$\mathbf{S} = \frac{1}{2}\begin{pmatrix} 1 & 1 & 0 & 0 \\ 1 & 1 & 1 & 1 \\ i\sqrt{a} & -i\sqrt{a} & 0 & 0 \\ i\sqrt{a} & -i\sqrt{a} & i\sqrt{a} & -i\sqrt{a} \end{pmatrix}. \tag{2.36}$$

By means of equation (2.28), the Floquet multipliers

$$\rho_\pm = e^{\pm i\frac{\pi\sqrt{a}}{\Omega}} = e^{\pm iT\sqrt{a}} \tag{2.37}$$

living on the unit circle, yield the Floquet exponents $\lambda_\pm$

$$\lambda_\pm = \frac{i}{T}(\pm T\sqrt{a} + 2\pi m) = \pm i\sqrt{a} + 2i\Omega m, \quad m = \pm 1, \tag{2.38}$$

that are the eigenvalues of the complex Floquet factor

$$\mathbf{F} = \begin{pmatrix} -2i\Omega & 0 & 1 & 0 \\ 0 & 2i\Omega & 0 & 1 \\ -a^2 & 0 & -2i\Omega & 0 \\ 0 & -a^2 & 0 & 2i\Omega \end{pmatrix}. \tag{2.39}$$

The monodromy matrix decomposition is thus $\mathbf{\Phi}(T, 0) = \mathbf{L}_T(T)e^{\mathbf{F}T}$, where $\mathbf{L}_T(t) = e^{i2\Omega t\,\mathrm{diag}\,(1,-1,1,-1)}$ is the complex T-periodic Lyapunov matrix. The Floquet exponents (2.38) differ by $\pm i\Omega$ from the eigenvalues of the matrix (2.33), evaluated at

[7] Conversely, in some cases a suitable Lyapunov transformation can be found that eliminates gyroscopic or circulatory terms from the linear equations of motion of an autonomous mechanical system, see e.g. [322, 325, 437, 529].

$\kappa = 0$ and $h = 0$, because the Lyapunov matrix $\mathbf{L}_T(t)$ has the same period as the parametric excitation ($T = \pi/\Omega$), whereas $\mathbf{L}_{2T}(t)$ is of the double period, $2\pi/\Omega$ [522].

Notice that at $\Omega = \sqrt{a}$ the Floquet multipliers $\rho_\pm = -1$, implying existence of the $2T$-periodic solution to equation (2.30) with $\kappa = 0$ and $h = 0$ [2, 603]. For the Brouwer particle in a rotating cavity this means oscillations with the frequency Ω in the nonrotating frame, corresponding to the motion along an *inertial circle* with the frequency 2Ω in the rotating frame, see Figure 1.4 (d).

A number of interesting finite-dimensional time-periodic systems originate in the field of hydrodynamic stability, in particular, in vortex dynamics, as a result of consideration of linear partial differential equations in the short-wavelength approximation that represents solutions in the form of a rapid oscillation with slowly varying amplitude of its envelope [38, 45, 179, 215].

On the other hand, the Floquet representation theorem can be applied to solutions of the equations describing the wave propagation in spatially-periodic media. Such solutions, known as the *Bloch waves*, represent the plane waves modulated in space coordinates by a function that has the periodicity of the spatial pattern (*Bloch function*). Then, the characteristic equation for the Floquet factor determines the Floquet exponents that in the spatially-periodic case are components of the wave vector multiplied by the imaginary unit [338]. In accordance with equation (2.28), the branches of the complex logarithm determine what is known as the *Brillouin zones* for the components of the wave vector (spatial exponents) that in general depend on the time frequency (temporal exponent) of the plane wave (*dispersion*), see e.g. [165, 315]. For this reason the characteristic equation for the Floquet exponents in the spatially-periodic case is known as the dispersion relation while the dependencies of the time frequencies on the wave vector are referred to as the *dispersion curves*[8] (also known as the *energy bands* [315]).

Note that considering the dispersion relation in the limit when the wavelength of the Bloch waves is large in comparison with the spatial period of the pattern is a standard way of determination of the macroscopic properties of a periodic on small scales material. In this limit, the Bloch wave behaves almost as a plane wave that perceives the periodic medium as a homogeneous substance with its own material properties which are referred to as effective material parameters [143, 386, 484]. For example, dielectric tensors of both natural and artificial chiral (optically active) [52] crystals[9] can be obtained by this *homogenization* scheme that is based in fact on the Floquet representation theorem [482, 533].

[8] With the spatial and temporal exponents considered as spectral parameters, the corresponding eigenvalue problem becomes a *multiparameter* one [89] (see also [24, 63, 585]) where the dispersion curves are treated as the *eigencurves* [64, 319]. Extension of the Floquet approach to partial differential equations can be found by an interested reader, e.g. in [141, 341].

[9] The optics of such homogeneous media will be discussed in Chapter 11 of this book.

2.5 Algebraic criteria for asymptotic stability

As we have just seen, both real and complex linear autonomous systems naturally originate in physical and engineering applications, in particular, in the wave propagation problems, frequently after (sometimes implicit) use of the Lyapunov transformations. The practical efficacy of the linear stability analysis critically depends on the ability to judge the location of eigenvalues of real and complex matrices in the given region of the complex plane directly in terms of the entries of a matrix. Two useful tools – algebraic criteria and sensitivity analysis – will be discussed briefly in the sequel to this chapter.

2.5.1 Lyapunov's matrix equation and stability criterion

Assume that the matrix $\mathbf{A}$ of the linear system (2.7) does not depend on time. Consider a function

$$V(\mathbf{x}) = \mathbf{x}^T \mathbf{P} \mathbf{x}, \tag{2.40}$$

where $\mathbf{P} = \mathbf{P}^T > 0$ is a real symmetric positive-definite matrix. Then $V(\mathbf{x})$ is a positive-definite and decrescent function in the sense of Definitions 2.8 and 2.9, because $\lambda(\mathbf{P})\|\mathbf{x}\|^2 \leq V(\mathbf{x}) \leq \Lambda(\mathbf{P})\|\mathbf{x}\|^2$, where $\lambda(\mathbf{P}) > 0$ and $\Lambda(\mathbf{P}) > 0$ are, respectively, the minimal and the maximal eigenvalues of $\mathbf{P}$.

According to equation (2.3), the derivative of $V(\mathbf{x})$ taken along the motion of the linear system (2.7) is

$$\dot{V}(\mathbf{x}) = \dot{\mathbf{x}}^T \mathbf{P} \mathbf{x} + \mathbf{x}^T \mathbf{P} \dot{\mathbf{x}} = \mathbf{x}^T (\mathbf{A}^T \mathbf{P} + \mathbf{P}\mathbf{A}) \mathbf{x}.$$

If $\mathbf{P}$ satisfies the *matrix Lyapunov equation*

$$\mathbf{A}^T \mathbf{P} + \mathbf{P}\mathbf{A} = -\mathbf{Q}, \tag{2.41}$$

where $\mathbf{Q} = \mathbf{Q}^T > 0$ is a symmetric positive-definite matrix, then $\dot{V}(\mathbf{x})$ is negative definite. Consequently, $V(\mathbf{x})$ is a Lyapunov function for the linear autonomous system (2.7) and according to Theorem 2.12, its equilibrium $\mathbf{x} = 0$ is asymptotically stable [437, 470].

Theorem 2.27 (A. M. Lyapunov, 1892 [253, 387]). *The equilibrium state* $\mathbf{x} = 0$ *of the linear system* (2.7) *with the constant matrix* $\mathbf{A}$ *is asymptotically stable if and only if given any symmetric, positive-definite matrix* $\mathbf{Q}$ *there exists a symmetric, positive definite matrix* $\mathbf{P}$ *which is the unique solution of the set of* $n(n+1)/2$ *linear equations* (2.41) *and* $V(\mathbf{x}) = \mathbf{x}^T \mathbf{P} \mathbf{x}$ *is a Lyapunov function for equation* (2.7).

Indeed, if the eigenvalues of $\mathbf{A}$ have negative real parts, then the equation (2.41) has a unique solution given by the integral [91, 141, 345]

$$\mathbf{P} = \int_0^\infty e^{\mathbf{A}^T t}\mathbf{Q}e^{\mathbf{A}t}dt = \mathbf{P}^T > 0 \tag{2.42}$$

that is convergent in view of the representation (2.21). By equations (2.20) and (2.7)

$$\dot{\mathbf{x}} = \mathbf{A}\mathbf{x} = \mathbf{A}e^{\mathbf{A}(t-t_0)}\mathbf{x}(t_0) = \frac{d}{dt}e^{\mathbf{A}(t-t_0)}\mathbf{x}(t_0)$$

and thus

$$\mathbf{A}^T\int_0^\infty e^{\mathbf{A}^T t}\mathbf{Q}e^{\mathbf{A}t}dt + \int_0^\infty e^{\mathbf{A}^T t}\mathbf{Q}e^{\mathbf{A}t}dt\,\mathbf{A} = \int_0^\infty \frac{d}{dt}\left(e^{\mathbf{A}^T t}\mathbf{Q}e^{\mathbf{A}t}\right) = -\mathbf{Q}.$$

Consequently, $\mathbf{P}$ given by the formula (2.42) is a solution to the matrix Lyapunov equation. If $\mathbf{P}_1$ and $\mathbf{P}_2$ are two solutions of equation (2.41), then

$$\mathbf{A}^T(\mathbf{P}_1 - \mathbf{P}_2) + (\mathbf{P}_1 - \mathbf{P}_2)\mathbf{A} = 0$$

and

$$\frac{d}{dt}\left(e^{\mathbf{A}^T t}(\mathbf{P}_1 - \mathbf{P}_2)e^{\mathbf{A}t}\right) = 0,$$

implying that $e^{\mathbf{A}^T t}(\mathbf{P}_1 - \mathbf{P}_2)e^{\mathbf{A}t} = const$ at all t. Since at $t = 0$ the constant is equal to $\mathbf{P}_1 - \mathbf{P}_2$ whereas at $t = +\infty$ it vanishes, we conclude that $\mathbf{P}_1 = \mathbf{P}_2$ and that the solution (2.42) is unique [142, 253].

2.5.2 The Leverrier–Faddeev algorithm and Lewin's formula

Consider a characteristic polynomial $p(\lambda) = \det(\mathbf{A} - \lambda\mathbf{I})$ of the matrix $\mathbf{A}$

$$p(\lambda) = \lambda^n + a_1\lambda^{n-1} + \ldots + a_{n-1}\lambda + a_n. \tag{2.43}$$

and let

$$(\mathbf{A} - \lambda\mathbf{I})^{-1} = \frac{\lambda^{n-1}\mathbf{I} + \lambda^{n-2}\mathbf{A}_1 + \ldots\lambda\mathbf{A}_{n-2} + \mathbf{A}_{n-1}}{p(\lambda)}. \tag{2.44}$$

The coefficients a_k as well as the matrices $\mathbf{A}_k$ are simultaneously determined via the recurrent formulas of the *Leverrier–Faddeev algorithm* [36, 437]

$$\begin{aligned} a_k &= -\frac{1}{k}\mathrm{tr}(\mathbf{A}\mathbf{A}_{k-1}), \quad a_0 = 1, \quad \mathbf{A}_0 = \mathbf{I}, \\ \mathbf{A}_k &= \mathbf{A}\mathbf{A}_{k-1} + a_k\mathbf{I}, \quad k = 1, \ldots, n. \end{aligned} \tag{2.45}$$

Define a partition of a positive integer k as

$$k = r_1 + r_1 + \cdots + r_1 + r_2 + \cdots + r_2 + \cdots + r_j + \cdots + r_j = \sum_{i=1}^{j} r_i s_i \quad (2.46)$$

with $r_1 > r_2 > \ldots > r_j > 0$. Then, with use of the Leverrier–Faddeev algorithm all the coefficients of the characteristic polynomial can be expressed explicitly by *Lewin's formula* [377].

Theorem 2.28 (M. Lewin, 1994 [377]). *Let* $\mathbf{A}$ *be an* n*-square (real or complex) matrix, and let its characteristic polynomial be given by* (2.43)*. Then*

$$a_k = \sum \prod_{i=1}^{j} \frac{(-\mathrm{tr}\mathbf{A}^{r_i})^{s_i}}{r_i^{s_i} s_i!}, \quad (2.47)$$

the summation being taken over all the partitions of k*.*

Particularly, $a_1 = -\mathrm{tr}\mathbf{A}$, $a_2 = \left[(\mathrm{tr}\mathbf{A})^2 - \mathrm{tr}\mathbf{A}^2\right]/2$, and $a_n = (-1)^n \det \mathbf{A}$. For example, in the case of $n = 2$

$$p(\lambda) = \lambda^2 - \lambda \mathrm{tr}\mathbf{A} + \left[(\mathrm{tr}\mathbf{A})^2 - \mathrm{tr}\mathbf{A}^2\right]/2 = \lambda^2 - \lambda \mathrm{tr}\mathbf{A} + \det \mathbf{A}.$$

2.5.3 Müller's solution to the matrix Lyapunov equation

In general, a solution to the matrix Lyapunov equation (2.41) exists uniquely if and only if the matrices $\mathbf{A}^T$ and $-\mathbf{A}$ have no common eigenvalues, i.e. [253, 437]

$$\lambda_i(\mathbf{A}) + \lambda_j(\mathbf{A}) \neq 0 \quad \forall \quad i, j. \quad (2.48)$$

In particular, the condition (2.48) is fulfilled when all eigenvalues of $\mathbf{A}$ have negative real parts. Assuming (2.48), with use of the Leverrier–Faddeev algorithm it is possible to express the solution to the matrix Lyapunov equation more explicitly in terms of the elements of the matrices $\mathbf{A}$ and $\mathbf{Q}$ [437]:

$$\mathbf{P} = \sum_{k=0}^{n-1} c_{k+1} \sum_{l=0}^{2k} (-1)^l \mathbf{A}_l^T \mathbf{Q} \mathbf{A}_{2k-l}. \quad (2.49)$$

The vector $\mathbf{c} = (c_1, c_2, \ldots, c_n)^T$ composed of the coefficients c_i of equation (2.49), is found from the equation

$$2\mathbf{H}^T\mathbf{c} = \mathbf{e}, \quad \mathbf{e}^T = (1, 0, \ldots, 0), \tag{2.50}$$

where $\mathbf{H}$ is an $n \times n$ *Hurwitz matrix* [236, 409] of the polynomial (2.43)

$$\mathbf{H} = \begin{pmatrix} a_1 & 1 & 0 & 0 & 0 & 0 & \cdots & 0 \\ a_3 & a_2 & a_1 & 1 & 0 & 0 & \cdots & 0 \\ a_5 & a_4 & a_3 & a_2 & a_1 & 1 & \cdots & 0 \\ \vdots & \vdots & \vdots & \vdots & \vdots & \vdots & \cdots & \vdots \\ a_{2n-1} & a_{2n-2} & a_{2n-3} & a_{2n-4} & a_{2n-5} & a_{2n-6} & \cdots & a_n \end{pmatrix} \tag{2.51}$$

with $a_s = 0$ for $s > n$. Introducing the *Hurwitz determinants*

$$h_1 = a_1, \quad h_2 = \det \begin{pmatrix} a_1 & 1 \\ a_3 & a_2 \end{pmatrix}, \quad \ldots, \quad h_n = \det \mathbf{H}, \tag{2.52}$$

we find by Cramer's rule that in equation (2.49)

$$c_{k+1} = \frac{(-1)^k M_{k+1,1}(\mathbf{H})}{2h_n}, \tag{2.53}$$

where $M_{k+1,1}(\mathbf{H})$ is the $(k+1, 1)$-minor of the Hurwitz matrix, i.e. the determinant of a $(n-1) \times (n-1)$ matrix obtained by striking out the row $k+1$ and the column 1 of $\mathbf{H}$.

Note that the unique solvability condition (2.48) implies $h_n \neq 0$ [437]. Below we will see that in the case when the system (2.7) with the constant matrix $\mathbf{A}$ is asymptotically stable, the determinant of the Hurwitz matrix does not vanish.

2.5.4 Inertia theorems and observability index

Inertia theorems generalize the Lyapunov stability criterion given by Theorem 2.27 and provide information on eigenvalue distribution of a nonsymmetric matrix $\mathbf{A}$ in the complex plane from the knowledge of the eigenvalue distribution of a symmetric matrix $\mathbf{P}$ related to $\mathbf{A}$ via the matrix Lyapunov equation.

Definition 2.29 (A. Ostrowski and H. Schneider, 1962 [142, 437]). The *inertia of a matrix* $\mathbf{A}$ of order n, denoted by $\mathrm{In}\mathbf{A}$ is the triplet $(\pi(\mathbf{A}), \nu(\mathbf{A}), \delta(\mathbf{A}))$ where $\pi(\mathbf{A})$, $\nu(\mathbf{A})$, and $\delta(\mathbf{A})$ are, respectively, the number of eigenvalues of $\mathbf{A}$ with positive, negative, and zero real parts, counting multiplicities.

Naturally, $\pi(\mathbf{A}) + \nu(\mathbf{A}) + \delta(\mathbf{A}) = n$.

Theorem 2.30 (A. Ostrowski and H. Schneider, 1962 [142]). *A necessary and sufficient condition that there exists a real matrix* $\mathbf{R} = \mathbf{R}^T$ *such that*

$$\mathbf{A}^T\mathbf{R} + \mathbf{R}\mathbf{A} = \mathbf{Q}, \quad \mathbf{Q} > 0 \tag{2.54}$$

is that $\delta(\mathbf{A}) = 0$. *For a real symmetric solution to equation* (2.54), $\mathrm{In}\mathbf{A} = \mathrm{In}\mathbf{R}$.

Hence, $\nu(\mathbf{A}) = n$ if and only if there exists a real symmetric matrix $\mathbf{R} = -\mathbf{P} < 0$ satisfying equation (2.54). The matrix $\mathbf{A}$ is then referred to as the *strictly* $\mathbf{P}$*-dissipative* [141, 202]. Remembering that the matrix Lyapunov equation has a unique solution when $\nu(\mathbf{A}) = n$, we recover Theorem (2.27).

For a pair of $n \times n$ matrices $(\mathbf{A}, \mathbf{Q})$ we consider the $n \times n^2$ block matrix

$$\mathbf{T}_O = \left(\mathbf{Q}, \mathbf{A}^T\mathbf{Q}, \ldots, (\mathbf{A}^T)^{n-1}\mathbf{Q}\right), \tag{2.55}$$

which is known as the *observability matrix* [142, 600]. The number $l = \mathrm{rank}\mathbf{T}_O$ is referred to as the *observability index* ($l \leq n$). *Full observability* means $l = n$.

Theorem 2.31 (H. K. Wimmer, 1974 [142, 600]). *If a real matrix* $\mathbf{R} = \mathbf{R}^T > 0$ *is such that*

$$\mathbf{A}^T\mathbf{R} + \mathbf{R}\mathbf{A} = \mathbf{Q} \geq 0,$$

then $\nu(\mathbf{A}) = 0$, $\delta(\mathbf{A}) = n - l$, *and* $\pi(\mathbf{A}) = l$. *If, additionally,* $(\mathbf{A}, \mathbf{Q})$ *is fully observable, then* $\delta(\mathbf{A}) = 0$ *and* $\mathrm{In}(\mathbf{A}) = \mathrm{In}(\mathbf{R})$.

Consequently, if $\mathbf{A}^T\mathbf{P} + \mathbf{P}\mathbf{A} = -\mathbf{Q}$, $\mathbf{Q} \geq 0$, and $\mathbf{P} > 0$, then all eigenvalues of $\mathbf{A}$ have a negative real part, if and only if $(\mathbf{A}, \mathbf{Q})$ is fully observable [596, 600].

2.5.5 Hermite's criterion via the matrix Lyapunov equation

Consider a *companion matrix* for the characteristic polynomial (2.43) of the matrix $\mathbf{A}$, which is given by the *Frobenius matrix*

$$\mathbf{A}_F = \begin{pmatrix} 0 & 1 & 0 & \cdots & 0 \\ 0 & 0 & 1 & \cdots & 0 \\ \vdots & \vdots & \vdots & \ddots & \vdots \\ 0 & 0 & 0 & \cdots & 1 \\ -a_n & -a_{n-1} & -a_{n-2} & \cdots & -a_1 \end{pmatrix}. \tag{2.56}$$

One can check, for example, by the Leverrier–Faddeev algorithm (2.45), that

$$\det(\mathbf{A} - \lambda\mathbf{I}) = \det(\mathbf{A}_F - \lambda\mathbf{I}) = p(\lambda),$$

As was noted already by Kalman and Bertram [253], the matrix Lyapunov criterion written for the matrix (2.56) should recover the criteria for the roots of the characteristic polynomial to have negative real parts in terms of the coefficients of the polynomial.

Following Parks [468, 469], let us choose the matrix $\mathbf{Q}$ in the Lyapunov equation (2.41) as a dyad: $\mathbf{Q} = \mathbf{q}\mathbf{q}^T$, where

$$\begin{aligned} \mathbf{q}^T &= (0, a_{n-1}, 0, \ldots, a_3, 0, a_1), \quad n \text{ even} \\ \mathbf{q}^T &= (a_n, 0, a_{n-2}, \ldots, a_3, 0, a_1), \quad n \text{ odd}. \end{aligned} \tag{2.57}$$

Then, according to *Müller's formula* (2.49) the solution to the Lyapunov equation is $\mathbf{P} = \frac{1}{2}\mathbf{P}_H$, where $\mathbf{P}_H$ is *Hermite's matrix* [221, 437, 468]

$$\mathbf{P}_H = \begin{pmatrix} a_n a_{n-1} & 0 & a_n a_{n-3} & \vdots & \vdots & \vdots & \vdots \\ 0 & -a_n a_{n-3} + a_{n-1} a_{n-2} & 0 & \vdots & \vdots & \vdots & \vdots \\ a_n a_{n-3} & 0 & \vdots & \vdots & \vdots & \vdots & \vdots \\ \vdots & \vdots & \vdots & \vdots & \vdots & \vdots & \vdots \\ \vdots & \vdots & \vdots & \vdots & \vdots & 0 & a_3 \\ \vdots & \vdots & \vdots & \vdots & 0 & -a_3 + a_2 a_1 & 0 \\ \vdots & \vdots & \vdots & \vdots & a_3 & 0 & a_1 \end{pmatrix}. \tag{2.58}$$

Let us demonstrate this for $n = 2$. According to the Leverrier–Faddeev algorithm (2.45), for the matrix $\mathbf{A}_F$, we obtain

$$\mathbf{A}_0 = \begin{pmatrix} 1 & 0 \\ 0 & 1 \end{pmatrix}, \quad \mathbf{A}_1 = \begin{pmatrix} a_1 & 1 \\ -a_2 & 0 \end{pmatrix}, \quad \mathbf{A}_2 = \begin{pmatrix} 0 & 0 \\ 0 & 0 \end{pmatrix}.$$

Using equation (2.53), we find

$$c_1 = \frac{1}{2a_1}, \quad c_2 = \frac{-1}{2a_1 a_2}.$$

Taking into account that Müller's formula (2.49) for $n = 2$ is

$$\mathbf{P} = c_1 \mathbf{A}_0^T \mathbf{Q} \mathbf{A}_0 + c_2 \big(\mathbf{A}_0^T \mathbf{Q} \mathbf{A}_2 - \mathbf{A}_1^T \mathbf{Q} \mathbf{A}_1 + \mathbf{A}_2^T \mathbf{Q} \mathbf{A}_0 \big),$$

finally, we arrive at the solution

$$\mathbf{P} = \frac{1}{2} \begin{pmatrix} a_2 a_1 & 0 \\ 0 & a_1 \end{pmatrix}$$

that also follows from equation (2.58) with $n = 2$.

Theorem 2.32 (Ch. Hermite, 1856 [221, 437, 468]). *A necessary and sufficient condition for the real polynomial* (2.43) *to have all its roots with negative real parts is that the Hermite matrix* (2.58) *is positive definite:*

$$\mathbf{P}_H > 0.$$

Indeed, the derivative of the function $V(\mathbf{x}) = \mathbf{x}^T \mathbf{P}_H \mathbf{x}$ along the motion of the system $\dot{\mathbf{x}} = \mathbf{A}_F \mathbf{x}$ is negative semidefinite

$$\dot{V} = -\mathbf{x}^T \mathbf{q}\mathbf{q}^T \mathbf{x} = -2(a_1 x_n + a_3 x_{n-2} + \ldots)^2 \leq 0.$$

By Theorem (2.31) we have to check the full observability of the pair consisting of the matrices $\mathbf{A}_F$ and $\mathbf{q}\mathbf{q}^T \geq 0$. For example, when $n = 2$ we can explicitly find that the observability matrix

$$(\mathbf{q}\mathbf{q}^T, \mathbf{A}_F^T \mathbf{q}\mathbf{q}^T) = \begin{pmatrix} 0 & 0 & 0 & -a_2 a_1^2 \\ 0 & a_1^2 & 0 & -a_1^3 \end{pmatrix}$$

has the rank equal to 2. In general, the pair $(\mathbf{A}_F, \mathbf{q}\mathbf{q}^T)$ is fully observable [437]. Hence, $\mathbf{P}_H > 0$ is equivalent to the localization of all the roots of the real polynomial (2.43) in the open left half-plane of the complex plane [437, 468].

2.5.6 Routh–Hurwitz, Liénard–Chipart, and Bilharz criteria

It was observed in the 1960s that the principal minors of the Hermite matrix $\mathbf{P}_H$ (given by equation (2.58)) starting from the bottom right-hand corner are

$$h_1, \quad h_1 h_2, \quad h_2 h_3, \quad \ldots, \quad h_{n-1} h_n,$$

where h_i, $i = 1, \ldots, n$, are the Hurwitz determinants (2.52) [490]. Combining this fact with the *Sylvester criterion* for $\mathbf{P}_H$ to be positive definite that requires positivity of all principal minors of a symmetric matrix, we recover the *Routh–Hurwitz criterion* [437, 468, 469].

Theorem 2.33 (A. Hurwitz, 1895 [236, 470]). *A necessary and sufficient condition for the real polynomial* (2.43) *to have all its roots with negative real parts is that the principal minors of the Hurwitz matrix* (2.51)*, i.e. the Hurwitz determinants* h_1*,* h_2*, …,* h_n *defined by equation* (2.52)*, are all positive.*

A polynomial satisfying the Hurwitz criterion is the *Hurwitz polynomial* [11]. The following *Liénard–Chipart criterion* simplifies the Routh–Hurwitz stability test by reducing the number of Hurwitz determinants in the sequence.

Theorem 2.34 (A. Liénard and M. H. Chipart, 1914 [11, 409, 437]). *The real polynomial* (2.43) *is Hurwitz if and only if one of the four following sets of inequalities holds:*

$$\begin{array}{lllllll}
(1) & a_n > 0, & a_{n-2} > 0, & a_{n-4} > 0, & \dots, & h_1 > 0, & h_3 > 0, \quad \dots \\
(2) & a_n > 0, & a_{n-2} > 0, & a_{n-4} > 0, & \dots, & h_2 > 0, & h_4 > 0, \quad \dots \\
(3) & a_n > 0, & a_{n-1} > 0, & a_{n-3} > 0, & \dots, & h_1 > 0, & h_3 > 0, \quad \dots \\
(4) & a_n > 0, & a_{n-1} > 0, & a_{n-3} > 0, & \dots, & h_2 > 0, & h_4 > 0, \quad \dots
\end{array}$$

Analogous criteria for the polynomials with complex coefficients were established independently by the efforts of Bilharz [62] (1944), Frank [173] (1946), Neimark [443] (1947), and Cotton and Yuan [134] (1948). Below we present the most popular *Bilharz criterion*. Other criteria of eigenvalue localization in a given domain of a complex plane as well as the discussion of the relationships between them and some unified formulations can be found by an interested reader, e.g. in the books by Marden [409] and Parks and Hahn [470] as well as in the articles by Barnett [35], Datta [142], and Henrion et al. [220].

Theorem 2.35 (H. Bilharz, 1944 [62]). *Let* $p(\lambda) = a_0 + a_1\lambda + \cdots + a_n\lambda^n$ *be a polynomial of degree n with complex coefficients* $a_k = a'_k + i\,a''_k$. *Let* $D_1, D_2, \cdots$ *be the even-ordered determinants*

$$D_1 = \begin{vmatrix} a'_0 & -a''_0 \\ a''_1 & a'_1 \end{vmatrix}, \quad D_2 = \begin{vmatrix} a'_0 & -a''_0 & 0 & 0 \\ a''_1 & a'_1 & a'_0 & -a''_0 \\ -a'_2 & a''_2 & a''_1 & a'_1 \\ -a''_3 & -a'_3 & -a'_2 & a''_2 \end{vmatrix}, \quad \dots, \qquad (2.59)$$

Then all the zeros of $p(\lambda)$ *have negative real parts if and only if all the determinants* D_k *are positive:* $D_k > 0$, $k = 1, \dots, n$.

2.6 Robust Hurwitz stability vs. structural instability

Even if a polynomial is Hurwitz, its roots can become positive if its coefficients deviate from the nominal values. Consider a real polynomial $p(\lambda) = \sum_{k=0}^{n} a_k\lambda^k$, with an uncertainty in its coefficients: $\underline{a}_k \le a_k \le \bar{a}_k$, for every k. If all the polynomials with the coefficients from the box $B := \{\mathbf{a} : \quad \mathbf{a} \in \mathbb{R}^{n+1}, \quad \underline{a}_k \le a_k \le \bar{a}_k, \quad k = 0, \dots, n\}$ are Hurwitz, the polynomial $p(\lambda)$ has the property of *robust Hurwitz stability* [58]. The following *Kharitonov theorem* that can be proved with the use of the matrix Lyapunov

equation [406, 407], reduces checking stability of an infinite number of polynomials from B to the stability test of just four extreme polynomials.

Theorem 2.36 (V. L. Kharitonov, 1978 [265, 407]). *The polynomials* $p(\lambda) = \sum_{k=0}^{n} a_k \lambda^k$ *(a_k real), in which a_k belongs to the interval $[\underline{a}_k, \bar{a}_k]$, are Hurwitz if and only if the following four extreme polynomials are Hurwitz:*

$$
\begin{aligned}
p_1(\lambda) &= \bar{a}_n\lambda^n + \underline{a}_{n-1}\lambda^{n-1} + \underline{a}_{n-2}\lambda^{n-2} + \bar{a}_{n-3}\lambda^{n-4} + \bar{a}_{n-4}\lambda^{n-4} + \dots,\\
p_2(\lambda) &= \bar{a}_n\lambda^n + \bar{a}_{n-1}\lambda^{n-1} + \underline{a}_{n-2}\lambda^{n-2} + \underline{a}_{n-3}\lambda^{n-4} + \bar{a}_{n-4}\lambda^{n-4} + \dots,\\
p_3(\lambda) &= \underline{a}_n\lambda^n + \underline{a}_{n-1}\lambda^{n-1} + \bar{a}_{n-2}\lambda^{n-2} + \bar{a}_{n-3}\lambda^{n-4} + \underline{a}_{n-4}\lambda^{n-4} + \dots,\\
p_4(\lambda) &= \underline{a}_n\lambda^n + \bar{a}_{n-1}\lambda^{n-1} + \bar{a}_{n-2}\lambda^{n-2} + \underline{a}_{n-3}\lambda^{n-4} + \underline{a}_{n-4}\lambda^{n-4} + \dots.
\end{aligned}
$$

Note that in Kharitonov's theorem it is assumed that the coefficients of the polynomial are independent parameters. How could the domain, where a real polynomial is Hurwitz, look like in the space of its coefficients? Apparently, the first nontrivial result was obtained in 1956 by O. Bottema [81].

2.6.1 Multiple eigenvalues: singularities and structural instabilities

Bottema observed that the necessary and sufficient conditions

$$
b_1 > 0, \quad b_2 > 0, \quad b_3 > 0, \quad b_4 > 0, \quad b_2 > \frac{b_1^2 b_4 + b_3^2}{b_1 b_3} \tag{2.60}
$$

for the polynomial $p(\mu) = \mu^4 + b_1\mu^3 + b_2\mu^2 + b_3\mu + b_4$ to be Hurwitz do not change after transformation of the spectral parameter $\mu = c\lambda$, where $c = \sqrt[4]{b_4}$, $b_4 > 0$. Indeed, denoting

$$
a_i = b_i c^{-i}, \quad i = 1, 2, 3, 4, \tag{2.61}
$$

we find that the inequalities (2.60) are equivalent to the conditions

$$
a_1 > 0, \quad a_3 > 0, \quad a_2 > \frac{a_1^2 + a_3^2}{a_1 a_3} > 0 \tag{2.62}
$$

that are necessary and sufficient for the polynomial

$$
\lambda^4 + a_1\lambda^3 + a_2\lambda^2 + a_3\lambda + 1 \tag{2.63}
$$

to be Hurwitz. The domain given by the conditions (2.62) was plotted by Bottema in the (a_1, a_3, a_2)-space, see Figure 2.1 (a).

Bottema, who studied general linear systems with the 4×4 constant real matrix $\mathbf{A}$ [80], realized that the boundary Γ of the asymptotic stability domain (2.62) is a *ruled surface* generated by straight lines $a_3 = ra_1$, $a_2 = r + 1/r$, where the parameter $r \in (0, \infty)$. The boundary Γ has a self-intersection along the ray $a_2 \geq 0$ of the a_2-axis.

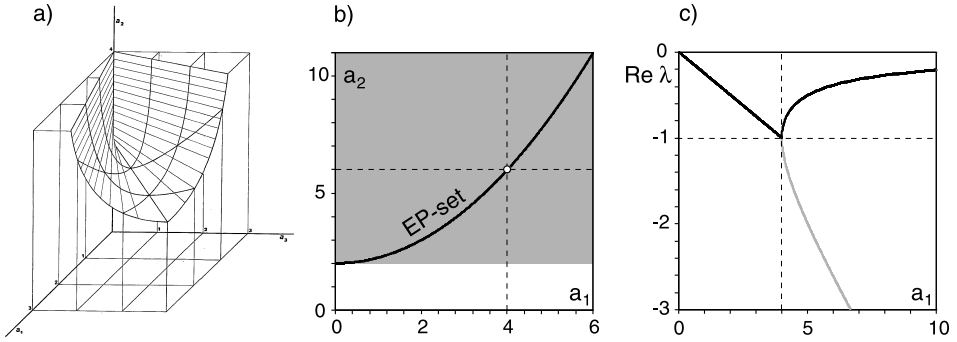

Figure 2.1. (a) A singular boundary Γ of the domain of asymptotic stability (2.62) of a real polynomial of fourth order as it appeared in the original work of Bottema [81], see also [312]. (b) Shown in gray is a tangent cone (2.68) to the domain of asymptotic stability that contains (black line) the EP-set (2.67). (c) The spectral abscissa (black line) attains its minimal value of -1 at $a_1 = a_3 = 4$ and $a_2 = 6$ (white dot in panel (b)) when parameters vary along the EP-set.

Two *generators* pass through each point of the ray; they coincide at $a_2 = 2$ ($r = 1$), and for $a_2 \to \infty$ their directions tend to those of the a_1- and a_3-axis ($r = 0, r = \infty$). Remarkably, the point $(0, 0, 2)$ is on Γ, but if one tends to the a_2-axis along the line $a_3 = ra_1$ the coordinate a_2 has the limit $r + 1/r > 2$ but for $r = 1$, when $a_2 = 2$ [81]. The point $(0, 0, 2)$ is the Whitney umbrella singularity [17, 312] already familiar to us from the Chapter 1.

In 1971, V. I. Arnold considered parametric families of real matrices and studied which singularities on the boundary of the asymptotic stability domain in the space of parameters are not destroyed by a small perturbation of the family, i.e. are *generic* singularities. He composed a list of generic singularities in parameter spaces of low dimension which revealed, in particular, that the Whitney umbrella persists on the stability boundary of a real matrix of arbitrary dimension if the number of parameters is not less than three, i.e. the singularity is of a *codimension* 3 [17]. As we see, in the case of 4×4 real matrices the latter result was in fact explicitly obtained by Bottema as early as 1956 [80, 81].

The singular point $(0, 0, 2)$ corresponds to a pair of double roots $\lambda = \pm i$ of the polynomial (2.63) that are double eigenvalues of the corresponding companion matrix (2.56) with the Jordan block of order 2 [17]. At the 'handle' of the Whitney umbrella formed by the ray $a_2 > 0$ of the a_2-axis there are two distinct complex-conjugate pairs of pure imaginary eigenvalues [81] indicating the Lyapunov stability. However, the threshold of the Lyapunov (or marginal) stability $a_2 = 2$ is extremely sensitive to the coefficients a_1 and a_3 as is seen from equation (2.62). Indeed, the stability threshold acquires an increment of order $O(1)$ even if the perturbation of these coefficients is of order ε (where $0 < \varepsilon \ll 1$) for almost all combinations of a_1 and a_3 but $a_1 = a_3$. The

minimal threshold of marginal stability $a_2 = 2$ at $a_1 = 0$ and $a_3 = 0$ corresponding to the double pure imaginary eigenvalue with the Jordan block is thus *structurally unstable*: it does not vary continuously under a small perturbation [81, 622].

Therefore, looking for extremal values of a parameter at the threshold of asymptotic stability (or, rather, instability, which is of interest first of all in *physical* applications, e.g. in hydrodynamics) may lead to structurally unstable configurations of parameters at the singular points of the stability boundary corresponding to multiple eigenvalues with zero real part. At first glance, nothing is father from the robust Hurwitz stability than this situation. For this reason, in *engineering* and control-theoretical applications a natural desire is to 'cut the singularities off' by constructing convex inner approximations to the domain of asymptotic stability [219, 220]. Nevertheless, there is a connection between the multiple eigenvalues on the stability boundary and those from the deep of the domain of asymptotic stability which is visible in the process of minimization of the so-called spectral abscissa that is intended to make asymptotic stability of a linear system more robust.

2.6.2 Multiple eigenvalues: spectral abscissa minimization and robust stability

The *spectral abscissa* of a matrix $\mathbf{A}$ is the maximal real part of its eigenvalues [580]:

$$\alpha(\mathbf{A}) = \max_k \mathrm{Re}\lambda_k(\mathbf{A}). \tag{2.64}$$

For a polynomial it is defined via the companion matrix (2.56). Generally, the spectral abscissa is a continuous nonsmooth and nonconvex function [103, 364]. For the polynomial (2.62) with $a_1 = a_3$ and $a_2 = 2 + \frac{a_1^2}{4}$ the spectral abscissa is shown as a function of a_1 in Figure 2.1 (c). The eigenvalues are then

$$\lambda_1 = \lambda_2 = -\frac{a_1}{4} - \frac{1}{4}\sqrt{a_1^2 - 16}, \quad \lambda_3 = \lambda_4 = -\frac{a_1}{4} + \frac{1}{4}\sqrt{a_1^2 - 16}. \tag{2.65}$$

When $0 \le a_1 < 4$ ($a_1 > 4$), the eigenvalues $\lambda_{1,2}$ and $\lambda_{3,4}$ are complex (real) and double with the Jordan block of order 2. At $a_1 = 4$ there is a quadruple real eigenvalue -1 with the Jordan block of order 4. Indeed, the companion matrix $\mathbf{A}_F$ with $a_1 = 4$, $a_2 = 6$, and $a_3 = 4$ has the Jordan form $\mathbf{J}_4(-1)$, where [176]

$$\mathbf{A}_F = \begin{pmatrix} 0 & 1 & 0 & 0 \\ 0 & 0 & 1 & 0 \\ 0 & 0 & 0 & 1 \\ -1 & -4 & -6 & -4 \end{pmatrix}, \quad \mathbf{J}_4(-1) = \begin{pmatrix} -1 & 1 & 0 & 0 \\ 0 & -1 & 1 & 0 \\ 0 & 0 & -1 & 1 \\ 0 & 0 & 0 & -1 \end{pmatrix}. \tag{2.66}$$

The set of exceptional points (or *EP-set*) where all the roots of the polynomial (2.62) are multiple, is therefore

$$\left\{(a_1, a_3, a_2): \quad a_1 = a_3, \quad a_2 = 2 + \frac{a_1^2}{4}\right\}. \tag{2.67}$$

As Figure 2.1 (b) demonstrates, when $a_1 > 0$, the set (2.67) lies within the *tangent cone* [374, 375] to the domain of asymptotic stability at the Whitney umbrella singularity $(0, 0, 2)$, which is a set of all directions leading from the singular point to the domain of asymptotic stability:

$$\{(a_1, a_3, a_2) : \quad a_1 = a_3, \quad a_1 > 0, \quad a_2 > 0\}. \tag{2.68}$$

Most of the points at the EP-set correspond to double eigenvalues (EP_2) but $(4, 4, 6)$, at which the eigenvalue is quadruple (EP_4), see Figure 2.1 (b).

The global minimum of the spectral abscissa of the polynomial (2.62) over all triplets (a_1, a_3, a_2), is attained at the EP-set inside the domain of asymptotic stability. Indeed, let us look at the movement of eigenvalues in the complex plane at the given a_1 and a_3 when a_2 increases from zero, Figure 2.2 (a). When $a_1 = a_3 < 4$, the unstable eigenvalues move along the unit circle to the left, cross the imaginary axis at $a_2 = 2$ and merge with another pair of complex eigenvalues at $a_2 = 2 + a_1^2/4$, i.e. at the EP-set. A further increase in a_2 leads to the splitting of the double eigenvalues. As a result there originates a pair of eigenvalues moving back to the imaginary axis. Thus, the spectral abscissa is minimal at the exceptional points (EP_2). When $a_1 \neq a_3$, i.e. when the variation of a_2 happens at a distance from the tangent cone, the $1:1$ resonance is destroyed and the eigenvalues turn back before they reach the location of the EP_2, see Figure 2.2 (a). Therefore, to further minimize the spectral abscissa we have to move the exceptional points EP_2 to the left along the unit circle, Figure 2.2 (b). This can be done by varying parameters along the EP-set (2.67) towards the point $(4, 4, 6)$

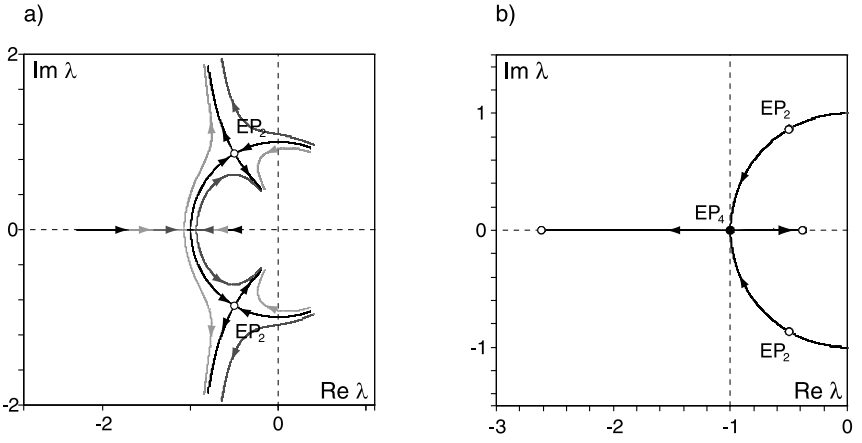

Figure 2.2. (a) Movement of eigenvalues of the Frobenius matrix of the polynomial (2.62) when a_2 increases from 0 to 6 and (black) $a_1 = a_3 = 2$, (dark gray) $a_1 = 1.7$, $a_3 = 2$, and (light gray) $a_1 = 2$, $a_3 = 1.7$. (b) Movement of double eigenvalues when parameters vary along the EP-set (2.67) and a_1 increases from 0 to 6, showing that the global minimum of the spectral abscissa corresponds to the coalescence of the two double eigenvalues (EP_2) into a quadruple one $\lambda = -1$ with the Jordan block of order 4 (EP_4).

shown as a white dot in Figure 2.1 (b). At this point the Frobenius matrix has the Jordan normal form $\mathbf{J}_4(-1)$, which corresponds to the real eigenvalue $\lambda = -1$ of the algebraic multiplicity 4 and geometric multiplicity 1. Thus,

$$\min_{a_1,a_2,a_3} \alpha(\mathbf{A}_F) = -1. \tag{2.69}$$

This value is a global minimum of the spectral abscissa because with the further increase of a_2 the EP_4 splits into two exceptional points EP_2, one of them inside the unit circle, Figure 2.2 (c).

Minimization of the spectral abscissa of an $n \times n$ matrix frequently ends up at such *nonderogatory matrices*, i.e. the matrices, all of whose eigenvalues have geometric multiplicity one (*nonderogatory eigenvalues* [17]). In particular, a minimizer could be a single Jordan block of order n, as in the above example [101, 102, 378]. We see that both the parametric optimization aiming to find extreme values of a parameter at the threshold of asymptotic stability and the minimization of the spectral abscissa directed inside the domain of asymptotic stability can lead to the matrices with multiple and defective eigenvalues (pure imaginary in the former case and complex in the latter). The EP-set (connecting such optima in our example) also plays a role in itself both in modern engineering and in non-Hermitian physics owing to the complicated transient behavior of associated dynamical systems with the parameters in the vicinity of exceptional points, see for instance [50, 157, 166, 246, 380, 426]. How to find this set in general?

Interestingly, some modern efficient algorithms of finding the set of defective matrices can be traced back to the question of what is the distance from a Kharitonov box to a nearest unstable polynomial. In general, the distance to instability for a given matrix $\mathbf{A}$ is $d = \inf\{\|\mathbf{A} - \mathbf{A}'\| : \det(\mathbf{A}' - \lambda\mathbf{I}) \; is \; Hurwitz\}$. Introducing the ε-pseudospectrum of $\mathbf{A}$, denoted $\Lambda_\varepsilon(\mathbf{A})$, as the set of numbers that are eigenvalues of some perturbed matrix $\mathbf{A} + \mathbf{E}$ with $\|\mathbf{E}\| < \varepsilon$ [7, 576]

$$\Lambda_\varepsilon(\mathbf{A}) = \{\lambda \in \mathbb{C} : \det(\mathbf{A} + \mathbf{E} - \lambda\mathbf{I}) = 0 \;\; for \; some \; \|\mathbf{E}\| < \varepsilon\},$$

we find that $d > \varepsilon$ if and only if $\Lambda_\varepsilon(\mathbf{A})$ lies within the open left half-plane of the complex plane. To maximize the distance to instability, the methods of minimizing the pseudospectral abscissa $\alpha_\varepsilon(\mathbf{A}) = \sup\{\mathrm{Re}\lambda : \lambda \in \Lambda_\varepsilon(\mathbf{A})\}$ were developed [103]. Further studies in this direction have led to the development of numerical and analytical methods of finding the distance to the set of defective matrices [7] and computation of multiple eigenvalues [243]. Curiously enough, the pseudospectral approach was recently applied to Ziegler's paradox [622] – a problem that motivated Bottema to initiate his studies on the geometry of the boundary of asymptotic stability [263].

Chapter 3

Hamiltonian and gyroscopic systems

> *... for a uniformly travelling periodic water wave to lose spectral stability, it is necessary that there be for the linearized problem about it a collision of eigenvalues of opposite signature or at zero ... the signature of an eigenvalue ... is negative if ... the corresponding disturbance moves in the same direction as the wave but slower, and positive if it moves faster or in the opposite direction. If the signatures are the same we predict an avoided crossing; if they are opposite we predict a bubble of instability.*
>
> R. S. MacKay and P. G. Saffman [392]

An attempt to spin a hard-boiled egg always ends up successfully: when spun sufficiently rapidly, its symmetry axis can even rise to the vertical position demonstrating a gyroscopic stabilization. The mathematical model of this effect is the rotating solid prolate spheroid known as *Jellett's egg* [83, 290, 425]. In contrast, trying to spin a raw egg containing a yolk inside, surrounded by a liquid, will generally lead to its slow wobbling motion. Remarkably, already in 1877 Kelvin experimentally demonstrated that a thin-walled and slightly oblate spheroid completely filled with liquid remains stable if rotated fast enough about a fixed point, which does not happen if the spheroid is slightly prolate [572]. In 1880 this observation was confirmed theoretically by Greenhill [205], who found that rotation around the center of gravity of the top in the form of a weightless ellipsoidal shell completely filled with an ideal and incompressible fluid, is unstable when $a < c < 3a$, where c is the length of the semiaxis of the ellipsoid along the axis of rotation and the lengths of the two other semiaxes are equal to a [549].

Quite similarly, bullets and projectiles fired from barreled weapons can relatively easily be stabilized by rotation, if they are solid inside. In 1942 when the Second World War in Russia was in full swing and thus using even chemical weapons did not seem impossible, researchers at the Steklov Mathematical Institute (then evacuated to the city of Kazan, far to the east of Moscow) had to resolve a problem of instability of chemical artillery shells.[1] These shells, containing a liquid substance inside, had a

[1] According to Boris Isaakovich Rabinovich (1924–2010) – a Russian aerospace engineer who worked on dynamics and stability of liquid-fuel rockets and spacecrafts [488], see also [451].

tendency to turn over despite seeming to revolve fast enough to be gyroscopically stabilized [512].

In the 1940s, the investigation of the stability of a rotating container filled with a viscous fluid was considered extremely complicated. In order to save time, M. A. Lavrent'ev[2] proposed a simplified model in the form of a solid with a spherical cavity in which another solid, spherical in shape, is enclosed. The inner sphere was assumed to be separated from the cavity walls by a lubricating film. It turned out that this model of a rotating solid containing a spherical damper inside possessed certain mechanical properties of a solid with a cavity containing a viscous fluid and thus enabled to quickly obtain useful practical recommendations for mass distribution inside the shell: stable steady rotation of a free solid with a damper is possible only about the axis of the maximal principal moment of inertia of the system[3] [126, 488].

3.1 Sobolev's top and an indefinite metric

Motivated by the same artillery application, in 1942 S. L. Sobolev, then director of the Steklov Institute, considered stability of a rotating heavy top with a cavity entirely filled with an ideal incompressible fluid [21,536] – a problem that is directly connected to the classical XIXth century models of astronomical bodies with a crust surrounding a molten core[4] [388].

For simplicity, the solid shell of the top and the domain V occupied by the cavity inside it can be assumed to have a shape of a solid of revolution. They have a common symmetry axis where the fixed point of the top is located. The velocity profile of the stationary unperturbed motion of the fluid is that of a solid body rotating with the same angular velocity Ω as the shell around the symmetry axis [536, 606].

Following Sobolev [536], we denote by M_1 the mass of the shell, M_2 the mass of the fluid, ρ and p the density and the pressure of the fluid, g the gravity acceleration, and l_1 and l_2 the distances from the fixed point to the centers of mass of the shell and the fluid, respectively. The moments of inertia of the shell and the 'frozen' fluid with respect to the symmetry axis are C_1 and C_2, respectively; A_1 (A_2) stands for the moment of inertia of the shell (fluid) with respect to any axis that is orthogonal to the symmetry axis and passes through the fixed point. Let, additionally,

$$L = C_1 + C_2 - A_1 - A_2 - \frac{K}{\Omega^2}, \quad K = g(l_1 M_1 + l_2 M_2). \tag{3.1}$$

[2] Mikhail Alekseevich Lavrent'ev (1900–1980) – a Soviet mathematician and hydrodynamicist, one of the founders of the Moscow Institute of Physics and Technology.

[3] It is instructive that the same conclusion applies to the stabilization of spinning satellites that cannot rotate stably along the axis of the minimum moment of inertia because of the energy dissipation via small deformations of the satellite [86, 139, 333].

[4] Precession of a rotating planet can stimulate the magnetohydrodynamics dynamo action via the whirling motions of an electrically conducting and viscous melt and thus be a cause of planetary magnetism [401] – a hypothesis that is going to be tested in the laboratory DRESDYN experiment [544].

The solenoidal ($\operatorname{div}\mathbf{v} = 0$) velocity field $\mathbf{v}$ of the fluid is assumed to satisfy the no-flow condition on the boundary of the cavity: $\mathbf{v}_n|_{\partial V} = 0$.

Stability of the stationary rotation of the top around its vertically oriented symmetry axis is determined by the system of linear equations derived by Sobolev in the frame (x, y, z) that has its origin at the fixed point of the top and rotates with respect to an inertial frame around the vertical z-axis with the angular velocity of the unperturbed top, Ω. If the real and imaginary part of the complex number Z describe the deviation of the unit vector of the symmetry axis of the top in the coordinates x, y, and z, then these equations are [536, 606]:

$$\begin{aligned}
\frac{dZ}{dt} &= i\,\Omega W,\\
(A_1+\rho\kappa^2)\frac{dW}{dt} &= i\,\Omega L Z + i\,\Omega(C_1-2A_1+\rho E)W + i\rho\int_V\left(v_x\frac{\partial\chi}{\partial y} - v_y\frac{\partial\chi}{\partial x}\right)dV,\\
\partial_t v_x &= 2\Omega v_y - \rho^{-1}\partial_x p + 2i\,\Omega^2 W\partial_y\overline{\chi},\\
\partial_t v_y &= -2\Omega v_x - \rho^{-1}\partial_y p - 2i\,\Omega^2 W\partial_x\overline{\chi},\\
\partial_t v_z &= -\rho^{-1}\partial_z p,
\end{aligned} \tag{3.2}$$

where $2\kappa^2 = \int_V |\nabla\chi|^2 dV$, $E = i\int_V \left(\partial_x\overline{\chi}\partial_y\chi - \partial_y\overline{\chi}\partial_x\chi\right)dV$, and the function χ is determined by the conditions

$$\nabla^2\chi = 0, \quad \partial_n\chi|_{\partial V} = z(\cos nx + i\cos ny) - (x+iy)\cos nz, \tag{3.3}$$

with n the absolute value of a vector $\mathbf{n}$, normal to the boundary of the cavity.

Sobolev realized that some qualitative conclusions on the stability of the top can be drawn with the use of the bilinear form

$$Q(R_1, R_2) = L\Omega Z_1\overline{Z}_2 + (A_1+\rho\kappa^2)W_1\overline{W}_2 + \frac{\rho}{2\Omega^2}\int_V \overline{\mathbf{v}}_2^T\mathbf{v}_1 dV \tag{3.4}$$

on the elements R_1 and R_2 of the space $\{R\} = \{Z, W, \mathbf{v}\}$. The linear operator B defined by equations (3.2) that can be written as $\frac{dR}{dt} = iBR$ has all its eigenvalues real when $L > 0$, which yields Lyapunov stability of the top [320, 536]. The number of pairs of complex-conjugate eigenvalues of B (counting multiplicities) does not exceed the number of negative squares of the quadratic form $Q(R, R)$, which can be equal only to one when $L < 0$. Hence, for $L < 0$ an unstable solution $R = e^{i\lambda_0 t}R_0$ can exist with $\operatorname{Im}\lambda_0 < 0$; all real eigenvalues are simple except for maybe one [320, 536].

In the particular case when the cavity is an ellipsoid of rotation with the semiaxes a, a, and c, the space of the velocity fields of the fluid can be decomposed into a direct sum of subspaces, one of which is finite-dimensional. Only the movements from this subspace interact with the movements of the rigid shell, which yields a finite-dimensional system of ordinary differential equations that describes coupling between the shell and the fluid [320, 536].

Calculating the moments of inertia of the fluid in the ellipsoidal container

$$C_2 = \frac{8\pi\rho}{15}a^4c, \quad A_2 = l_2^2 M_2 + \frac{4\pi\rho}{15}a^2c(a^2+c^2),$$

denoting $m = \frac{c^2-a^2}{c^2+a^2}$, and assuming the field $\mathbf{v} = (v_x, v_y, v_z)^T$ in the form

$$v_x = (z-l_2)a^2m\xi, \quad v_y = -i(z-l_2)a^2m\xi, \quad v_z = -(x-iy)c^2m\xi,$$

one can eliminate the pressure in equations (3.2) and obtain the reduced model

$$\frac{d\mathbf{x}}{dt} = i\,\Omega\mathbf{A}^{-1}\mathbf{C}\mathbf{x} = i\,\Omega\mathbf{B}\mathbf{x}, \tag{3.5}$$

where $\mathbf{x} = (Z, W, \xi)^T \in \mathbb{C}^3$ and [536]

$$\mathbf{A} = \begin{pmatrix} 1 & 0 & 0 \\ 0 & A_1 + l_2^2 M_2 + \dfrac{4\pi\rho}{15}a^2c\dfrac{(c^2-a^2)^2}{c^2+a^2} & 0 \\ 0 & 0 & c^2+a^2 \end{pmatrix},$$

$$\mathbf{C} = \begin{pmatrix} 0 & 1 & 0 \\ L & C_1 - 2A_1 - 2l_2^2M_2 - \dfrac{8\pi\rho}{15}a^2c^3m^2 & -\dfrac{8\pi\rho}{15}a^4c^3m^2 \\ 0 & -2 & -2a^2 \end{pmatrix}. \tag{3.6}$$

The matrix $\mathbf{B} \neq \mathbf{B}^T$ in equation (3.5) after multiplication by a symmetric matrix

$$\mathbf{G} = \begin{pmatrix} L & 0 & 0 \\ 0 & A_1 + l_2^2 M_2 + \dfrac{4\pi\rho}{15}a^2c\dfrac{(c^2-a^2)^2}{c^2+a^2} & 0 \\ 0 & 0 & \dfrac{4\pi\rho}{15}a^4c^3\dfrac{(c^2-a^2)^2}{c^2+a^2} \end{pmatrix} \tag{3.7}$$

yields a Hermitian matrix $\mathbf{GB} = \overline{(\mathbf{GB})}^T$, i.e. $\mathbf{B}$ is a self-adjoint operator in the space $\mathbb{C}^3$ endowed with the metric

$$[\mathbf{u}, \mathbf{u}] := (\mathbf{G}\mathbf{u}, \mathbf{u}) = \overline{\mathbf{u}}^T\mathbf{G}\mathbf{u}, \quad \mathbf{u} \in \mathbb{C}^3, \tag{3.8}$$

which is *definite* when $L > 0$ and *indefinite* with one negative square when $L < 0$. If λ is an eigenvalue of the matrix $\mathbf{B}$, i.e. $\mathbf{B}\mathbf{u} = \lambda\mathbf{u}$, then $\overline{\mathbf{u}}^T\mathbf{G}\mathbf{B}\mathbf{u} = \lambda\overline{\mathbf{u}}^T\mathbf{G}\mathbf{u}$. On the other hand, $\overline{\mathbf{u}}^T(\overline{\mathbf{G}\mathbf{B}})^T\mathbf{u} = \overline{\lambda}\,\overline{\mathbf{u}}^T\mathbf{G}\mathbf{u} = \overline{\lambda}\,\overline{\mathbf{u}}^T\mathbf{G}\mathbf{u}$. Hence,

$$(\lambda - \overline{\lambda})\overline{\mathbf{u}}^T\mathbf{G}\mathbf{u} = 0,$$

implying $\overline{\mathbf{u}}^T \mathbf{G}\mathbf{u} = 0$ on the eigenvector $\mathbf{u}$ of the complex $\lambda \neq \overline{\lambda}$. For real eigenvalues $\lambda = \overline{\lambda}$ and $\overline{\mathbf{u}}^T \mathbf{G}\mathbf{u} \neq 0$. The sign of the quantity $\overline{\mathbf{u}}^T \mathbf{G}\mathbf{u}$ can be different for different real eigenvalues.

For example, when the ellipsoidal shell is massless and the supporting point is at the center of mass of the system, then $A_1 = 0, C_1 = 0, M_1 = 0, l_2 = 0$. The matrix $\mathbf{B}$ thus has one real eigenvalue ($\lambda_1^+ = -1$, $\overline{\mathbf{u}_1^+}^T \mathbf{G}\mathbf{u}_1^+ > 0$) and the pair of eigenvalues

$$\lambda_2^{\pm} = -\frac{1}{2} \pm \frac{1}{2}\sqrt{1 + \frac{32\pi\rho}{15}\frac{ca^4}{L}}, \quad L = \frac{4\pi\rho}{15}a^2c(a^2 - c^2), \tag{3.9}$$

which are real if $L > 0$ and can be complex if $L < 0$. The latter condition together with the requirement that the radicand in equation (3.9) is negative, reproduces Greenhill's instability zone: $a < c < 3a$ [205, 388, 536]. With the change of c, the real eigenvalue λ_2^+ with $\overline{\mathbf{u}_2^+}^T \mathbf{G}\mathbf{u}_2^+ > 0$ collides at $c = 3a$ with the real eigenvalue λ_2^- with $\overline{\mathbf{u}_2^-}^T \mathbf{G}\mathbf{u}_2^- < 0$ into a real double defective eigenvalue λ_d with the algebraic multiplicity two and geometric multiplicity one, see Figure 3.1. Note that $\overline{\mathbf{u}_d}^T \mathbf{G}\mathbf{u}_d = 0$, where $\mathbf{u}_d$ is the eigenvector at λ_d.

Therefore, in the case of the ellipsoidal shapes of the shell and the cavity, the Hilbert space $\{R\} = \{Z, W, \mathbf{v}\}$ of the Sobolev problem endowed with the indefinite metric ($L < 0$) decomposes into the three-dimensional space of the reduced model (3.5), where the self-adjoint operator B can have complex eigenvalues and real defective eigenvalues, and a complementary infinite-dimensional space, which is free of these complications. The very idea that the signature of the indefinite metric can serve for counting unstable eigenvalues of an operator that is self-adjoint in a functional space

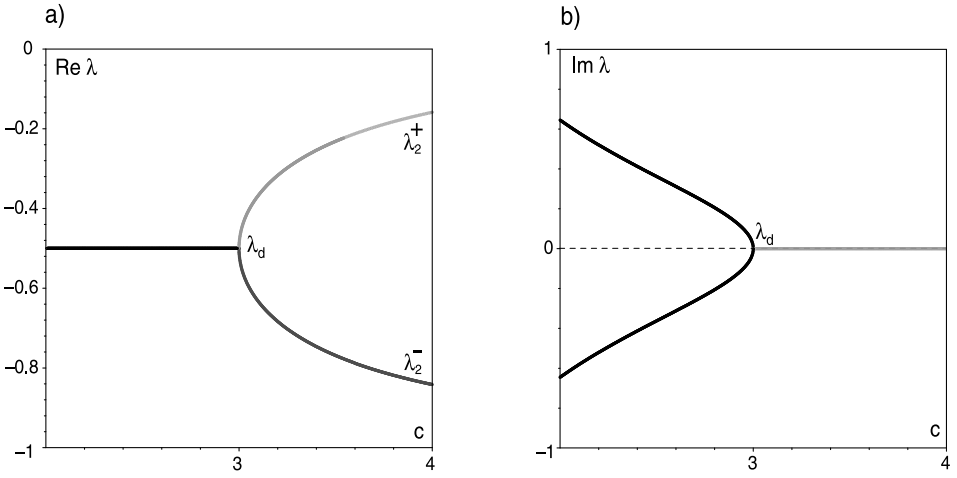

Figure 3.1. (a) Simple real eigenvalues (3.9) of Sobolev's top in the Greenhill case for $a = 1$ with (light gray) $\overline{\mathbf{u}}^T \mathbf{G}\mathbf{u} > 0$ and (dark gray) $\overline{\mathbf{u}}^T \mathbf{G}\mathbf{u} < 0$. (b) At simple complex-conjugate eigenvalues (black) and at the double real eigenvalue λ_d we have $\overline{\mathbf{u}}^T \mathbf{G}\mathbf{u} = 0$.

equipped with such a metric, see e.g. [129], turned out to be a concept of rather universal character possessing powerful generalizations that were initiated by Pontryagin in 1944 [483].

3.2 Elements of Pontryagin and Krein space theory

Let $\mathcal{H}$ be a Hilbert space, i.e. an infinite-dimensional linear space (or *lineal*) over $\mathbb{C}$, which is complete with respect to a *norm* $\|\cdot\| = \sqrt{(\cdot,\cdot)}$, where $(\cdot,\cdot)$ is an inner product. Two elements x and y of $\mathcal{H}$ are orthogonal if $(x, y) = 0$. Recall that two subspaces $\mathcal{H}_1$ and $\mathcal{H}_2$ of $\mathcal{H}$ are orthogonal if each element of $\mathcal{H}_1$ is orthogonal to every element of $\mathcal{H}_2$. If $\mathcal{H}_2$ is a collection of all elements of $\mathcal{H}$ that are orthogonal to $\mathcal{H}_1$, then $\mathcal{H} = \mathcal{H}_1 \oplus \mathcal{H}_2$, i.e. the whole Hilbert space is split into a subspace $\mathcal{H}_1$ and its *orthogonal complement* $\mathcal{H}_2$. If $\mathcal{H}_2$ is of finite dimension $k \geq 1$, then $\mathcal{H}_1$ is said to be of *codimension* k, see e.g. [320].

A linear mapping $A : \mathcal{H} \mapsto \mathcal{H}$ is called a *linear operator*. The linear operator A is *bounded* if there exists a constant c such that $\|Ax\| \leq c\|x\|$ for all $x \in \mathcal{H}$. An operator $A^\dagger$ that is *adjoint* to A is defined by the equality

$$(Ax, y) = (x, A^\dagger y), \quad x, y \in \mathcal{H}, \tag{3.10}$$

where (Ax, y) is the *bilinear form* of A ((Ax, x) is then a *quadratic form* of A).

If the bounded operator A coincides with its adjoint, i.e. $A = A^\dagger$, implying

$$(Ax, y) = (x, Ay), \quad x, y \in \mathcal{H},$$

then A is called *self-adjoint* in the Hilbert space $\mathcal{H}$. An *orthogonal projector* P_s from $\mathcal{H} = \mathcal{H}_1 \oplus \mathcal{H}_2$ onto $\mathcal{H}_s$, $s = 1, 2$, is a self-adjoint operator with $\|P_s\| = 1$ that transforms every element $x \in \mathcal{H}$ to $y = P_s x \in \mathcal{H}_s$ and has the property $(P_s)^2 = P_s$. A quadratic form of a self-adjoint operator A is a real-valued functional. Hence, if $(Ax, x) \geq 0$ for every $x \in \mathcal{H}$, then A is called nonnegative ($A \geq 0$); it is positive ($A > 0$) if $(Ax, x) > 0$ for any $x \neq 0$ from $\mathcal{H}$ [320, 442].

Definition 3.1 (A. A. Shkalikov, 2004 [526]). The Hilbert space $\mathcal{H}$ is said to be endowed with a *fundamental symmetry* (*indefinite metric*) if a quadratic form $[x, x] = (Gx, x)$ is introduced in $\mathcal{H}$, where G is a bounded and invertible self-adjoint operator in $\mathcal{H}$ with the bounded inverse.

Without loss of generality one can consider that the metric is generated by the operator $J = P_+ - P_-$, where $P_\pm$ are orthogonal projectors in $\mathcal{H}$ such that $P_+ + P_- = I$, where I is the identity. $J = J^\dagger = J^{-1}$ with $J^2 = I$. There is a decomposition of $\mathcal{H}$ into an orthogonal sum $\mathcal{H} = \mathcal{H}_+ \oplus \mathcal{H}_-$, such that

$$[x, y] = (P_+ x, P_+ y) - (P_- x, P_- y).$$

Suppose that $\dim\mathcal{H}_- = k < \infty$. Hence, P_- is a k-dimensional orthogonal projection and $\dim \mathcal{H}_+ = \infty$ [526]. In the Sobolev problem (3.2), $k = 1$.

Definition 3.2 (L. S. Pontryagin, 1944 [129, 483]). The Hilbert space $\mathcal{H}$ endowed with the indefinite inner product $[\cdot,\cdot] = (J\cdot,\cdot)$ is called a *Pontryagin space* with the rank of negativity $k < \infty$ and is denoted by $\Pi_k = \{\mathcal{H}, J\}$.

If both the operators P_+ and P_- are infinite dimensional, then the space $\mathcal{H}$ equipped with the indefinite inner product is referred to as the *Krein space* and is denoted as $\mathcal{K} = \{\mathcal{H}, J\}$ [526].

The elements x and y of $\mathcal{H}$ are called J-orthogonal, if $[x, y] = 0$. Every element x from $\mathcal{H}$ is either positive ($[x, x] > 0$), or negative ($[x, x] < 0$), or neutral ($[x, x] = 0$). If for all elements $x \neq 0$ of a linear subset (subspace) $L \subseteq \mathcal{H}$ we have $[x, x] > 0$, then it is called a positive lineal (subspace) [2, 320]. The lineal (subspace) is nonnegative if $[x, x] \geq 0$, and neutral if $[x, x] = 0$. A nonnegative (nonpositive) subspace is called maximal if it does not lie within a larger nonnegative (nonpositive) subspace. Every nonnegative (nonpositive) subspace can be extended to a maximal subspace [320].

The operator A^+ is J-adjoint to the linear operator A if

$$[Ax, y] = [x, A^+ y].$$

The operator A^+ and the operator $A^\dagger$ defined in (3.10) are related as $A^+ = JA^\dagger J$. An operator A is called *J-self-adjoint* or a self-adjoint operator in a space with the indefinite metric if [320]

$$(JA)^\dagger = JA. \tag{3.11}$$

A set $\rho(A)$ of all points λ of the complex plane at which there exists a bounded inverse operator $(A - \lambda I)^{-1}$ is referred to as the *resolvent set* of A [320, 442]. The *spectrum* $\sigma(A) = \mathbb{C} \setminus \rho(A)$ of a J-self-adjoint operator A is symmetric with respect to the real axis in the complex plane. If A is a J-self-adjoint nonnegative operator ($JA \geq 0$), i.e. an operator with the property $[Ax, x] = (JAx, x) \geq 0$, then $\sigma(A) \subset \mathbb{R}$ and, moreover, there exist two maximal J-orthogonal subspaces L_+ and L_-, which are invariant relatively to the operator A, such that [320]

$$\sigma(A|L_+) \subset [0, \infty), \quad \sigma(A|L_-) \subset (-\infty, 0]. \tag{3.12}$$

A nonzero element $x \in \mathcal{H}$ is called a *root element* corresponding to an *eigenvalue* $\lambda_0 \in \mathbb{C}$ of an operator A acting on $x \in \mathcal{H}$, if $(A - \lambda_0 I)^n x = 0$ for some $n \in \mathbb{N}$. If $x = x_0$ and $n = 1$, then x_0 is an *eigenelement* of the operator A at the eigenvalue λ_0. If $x = x_m$ is such that $(A - \lambda_0 I)^n x \neq 0$ for $n \leq m$ and $(A - \lambda_0 I)^n x = 0$ for $n > m$, then x_m is an m-th *associated element* to the eigenelement x_0. The (finite or infinite) sequence $x_0, x_1, \ldots, x_m, \ldots$ is a *Jordan chain* at the eigenelement x_0. The linear hull of all eigen- and associated elements of A corresponding to the same eigenvalue λ_0 forms the *root lineal* $L_{\lambda_0}(A)$. Its dimension is called the *algebraic multiplicity* of the

eigenvalue λ_0. If the algebraic multiplicity is finite, the root lineal $L_{\lambda_0}(A)$ is a *root subspace* corresponding to λ_0 [320].

The set of all eigenvalues of the operator A forms its *point spectrum*, $\sigma_p(A) \subset \sigma(A)$. If a pair $\{\lambda, \mu\}$ belongs to a point spectrum of A and $\lambda \neq \overline{\mu}$ then the root lineals $L_\lambda(A)$ and $L_\mu(A)$ are J-orthogonal. In particular, if $\lambda \neq \overline{\lambda}$, then L_λ is a neutral lineal, i.e. $[x, x] = 0$ for all $x \in L_\lambda$ $(x \neq 0)$ [320].

In the Pontryagin space Π_k all nonpositive lineals L_- have $\dim L_- \leq k$ and thus are subspaces. All k-dimensional nonpositive subspaces are maximal nonpositive and vice versa. A J-self-adjoint operator A acting on Π_k has at least one eigenvalue, and the entire spectrum of the operator $A = A^+$ lies on the real axis, except for no more than k pairs of nonreal eigenvalues (counting multiplicities) which are located symmetrically relatively to the real axis [320]. Let the nonreal spectrum of A be a union of two disjoint parts Λ and $\overline{\Lambda}$, which are symmetric with respect to the real axis: $\sigma_{non}(A) = \Lambda \cup \overline{\Lambda}$.

Theorem 3.3 (L. S. Pontryagin, 1944 [129, 320, 483, 526]). *For every J-self-adjoint operator A on Π_k there exist the maximal nonnegative and nonpositive subspaces L_+ and L_-, which are invariant for A and, in addition, satisfy the spectral conditions*

$$\sigma_{non}(A|L_+) = \Lambda, \quad \sigma_{non}(A|L_-) = \overline{\Lambda}. \tag{3.13}$$

The subspace L_+ can be chosen in such a way that the linear hull $L_\Lambda(A) \subset L_+$ of all the root lineals corresponding to eigenvalues with $\mathrm{Im}\lambda > 0$ has the dimension $\dim L_\Lambda(A) \leq k$. A similar assertion is true for the root lineal $L_{\overline{\Lambda}}(A)$, corresponding to eigenvalues λ with $\mathrm{Im}\lambda < 0$.

Thus, complex eigenvalues (e.g. destabilizing Sobolev's top) of a J-self-adjoint operator are concentrated in a finite-dimensional part of Π_k. As we will see in the following, an important role in stability questions is played by self-adjoint operators acting even in finite-dimensional spaces with indefinite metric.

3.3 Canonical and Hamiltonian equations

Following [603], we consider a complex vector space $\mathbb{C}^n$ with the inner product $(\mathbf{x}, \mathbf{y}) = \overline{\mathbf{y}}^T \mathbf{x}$. Define an indefinite inner product in $\mathbb{C}^n$ as

$$[\mathbf{x}, \mathbf{y}] = (\mathbf{G}\mathbf{x}, \mathbf{y}) = \overline{\mathbf{y}}^T \mathbf{G}\mathbf{x}, \tag{3.14}$$

where $\mathbf{G} = \overline{\mathbf{G}}^T$ ($\det \mathbf{G} \neq 0$) is an arbitrary (neither positive nor negative definite) Hermitian $n \times n$ matrix. Hence, $[\mathbf{x}, \mathbf{x}]$ is real but in contrast to $(\mathbf{x}, \mathbf{x})$ it can be positive, negative, or zero for $\mathbf{x} \neq 0$ [603].

The matrix $\mathbf{A}^+$ with the property

$$[\mathbf{A}\mathbf{x}, \mathbf{y}] = [\mathbf{x}, \mathbf{A}^+\mathbf{y}] \tag{3.15}$$

is said to be $\mathbf{G}$-adjoint to $\mathbf{A}$. From equation (3.15) it follows that

$$\mathbf{A}^+ = \mathbf{G}^{-1}\overline{\mathbf{A}}^T\mathbf{G}. \tag{3.16}$$

A differential equation

$$i^{-1}\mathbf{G}\frac{d\mathbf{z}}{dt} = \mathbf{H}\mathbf{z}, \tag{3.17}$$

where $\mathbf{H}$ is Hermitian, is called a *Hamiltonian equation*. The matrix $\mathbf{A} = i\mathbf{G}^{-1}\mathbf{H}$ yields

$$[\mathbf{A}\mathbf{x}, \mathbf{y}] = -[\mathbf{x}, \mathbf{A}\mathbf{y}], \tag{3.18}$$

i.e. $\mathbf{A}^+ = -\mathbf{A}$, and is called the $\mathbf{G}$-Hamiltonian matrix [603]. In terms of the $\mathbf{G}$-Hamiltonian matrix $\mathbf{A}$, the Hamiltonian system (3.17) takes the form

$$\frac{d\mathbf{z}}{dt} = \mathbf{A}\mathbf{z}. \tag{3.19}$$

Since $\mathbf{A} = -\mathbf{G}^{-1}\overline{\mathbf{A}}^T\mathbf{G}$, the matrices $-\overline{\mathbf{A}}^T$ and $\mathbf{A}$ have the same spectrum. Consequently, if λ is an eigenvalue of $\mathbf{A}$, then so is $-\overline{\lambda}$. Hence, the spectrum of a $\mathbf{G}$-Hamiltonian matrix is symmetric about the imaginary axis. The eigenvalue λ lies on the imaginary axis if and only if $\lambda = -\overline{\lambda}$ [603].

Let $\mathbf{I}$ be the unit $k \times k$-matrix and

$$\mathbf{J} = \begin{pmatrix} 0 & -\mathbf{I} \\ \mathbf{I} & 0 \end{pmatrix} = -\mathbf{J}^{-1}, \tag{3.20}$$

the canonical *symplectic matrix* [89]. The $n \times n$ matrix $\mathbf{G} = i\mathbf{J}$, where $n = 2k$, is Hermitian: $\overline{\mathbf{G}}^T = \overline{i\mathbf{J}^T} = -i(-\mathbf{J}) = i\mathbf{J} = \mathbf{G}$. With $\mathbf{G} = i\mathbf{J}$ and $\mathbf{H} = \mathbf{H}^T$ real, the Hamiltonian equation (3.17) reduces to

$$\mathbf{J}\frac{d\mathbf{x}}{dt} = \mathbf{H}\mathbf{x} \tag{3.21}$$

that is referred to as the *canonical equation*, whereas the indefinite inner product takes the form [431, 603].

$$[\mathbf{x}, \mathbf{y}] = \overline{\mathbf{y}}^T(i\mathbf{J})\mathbf{x} = i\overline{\mathbf{y}}^T\mathbf{J}\mathbf{x}. \tag{3.22}$$

The canonical Hamiltonian linear equations (3.21) describe motion of a system with k degrees of freedom

$$\frac{dx_s}{dt} = \frac{\partial H}{\partial x_{k+s}}, \quad \frac{dx_{k+s}}{dt} = -\frac{\partial H}{\partial x_s}, \quad s = 1, \ldots, k, \tag{3.23}$$

where x_s are *generalized coordinates* and x_{k+s} are *generalized momenta*. The quadratic form $H = \frac{1}{2}(\mathbf{Hx}, \mathbf{x})$, where $\mathbf{x}^T = (x_1, \ldots, x_{2k})$, is referred to as a *Hamiltonian function*. The real symmetric $2k \times 2k$-matrix $\mathbf{H}$ of the quadratic form H is called the *Hamiltonian* [394, 603].

Seeking for the solution to equation (3.21) in the form $\mathbf{x} = \mathbf{u}\exp(\lambda t)$, we find

$$\mathbf{Hu} = \lambda \mathbf{Ju}. \tag{3.24}$$

From equation (3.22) and equation (3.24) it follows that if λ is a pure imaginary eigenvalue with the eigenvector $\mathbf{u}$ of the $(i\mathbf{J})$-Hamiltonian matrix $\mathbf{J}^{-1}\mathbf{H}$, then

$$(\mathbf{Hu}, \mathbf{u}) = \mathrm{Im}\lambda\, [\mathbf{u}, \mathbf{u}]. \tag{3.25}$$

Since $\mathbf{J}$ and $\mathbf{H}$ are real matrices and the eigenvalues of a $(i\mathbf{J})$-Hamiltonian matrix are symmetric with respect to the imaginary axis, the spectrum of the matrix $\mathbf{J}^{-1}\mathbf{H}$ is symmetric with respect to both real and imaginary axes of the complex plane.

Theorem 3.4 (J. H. Maddocks, 1998 [394]). *Let λ be an eigenvalue of the eigenvalue problem* (3.24). *Then so is its complex conjugate, $\overline{\lambda}$, and $-\lambda$. Hence, for a canonical Hamiltonian linear equation* (3.21) *the eigenvalues come in singlets* $\{0\}$, *doublets* $\{\lambda, -\lambda\}$ *with* $\lambda \in \mathbb{R}$ *or* $\lambda \in i\,\mathbb{R}$, *or quadruplets* $\{\lambda, -\lambda, \overline{\lambda}, -\overline{\lambda}\}$. *The algebraic multiplicity of the eigenvalue* $\lambda = 0$ *is even.*

Consequently, the equilibrium $\mathbf{x} = 0$ of the system (3.21) is Lyapunov stable, if and only if the eigenvalues λ of the eigenvalue problem (3.24) are pure imaginary and semisimple [603].

3.3.1 Krein signature of eigenvalues

Let λ ($\mathrm{Re}\lambda = 0$) be a simple pure imaginary eigenvalue of a $\mathbf{G}$-Hamiltonian matrix $\mathbf{A}$ and $\mathbf{u}$ be a corresponding eigenvector:

$$\mathbf{Au} = \lambda \mathbf{u}. \tag{3.26}$$

Definition 3.5 (V. A. Yakubovich and V. M. Starzhinskii, 1975 [89, 603]). A simple pure imaginary eigenvalue $\lambda = i\omega$ with the eigenvector $\mathbf{u}$ is said to have *positive Krein signature* if $[\mathbf{u}, \mathbf{u}] > 0$ and *negative Krein signature* if $[\mathbf{u}, \mathbf{u}] < 0$.

Let, further, λ ($\mathrm{Re}\lambda = 0$) be a multiple pure imaginary eigenvalue of a $\mathbf{G}$-Hamiltonian matrix $\mathbf{A}$, and let $\mathbf{L}_\lambda$ be the eigensubspace of $\mathbf{A}$ belonging to the eigenvalue λ, i.e. the set of all $\mathbf{u} \in \mathbb{C}^n$ satisfying equation (3.26). If $[\mathbf{u}, \mathbf{u}] > 0$ for any $\mathbf{u} \in \mathbf{L}_\lambda$ ($\mathbf{u} \neq 0$), then λ is a multiple eigenvalue with positive Krein signature and the

eigensubspace $\mathbf{L}_\lambda$ is positive definite; if $[\mathbf{u},\mathbf{u}] < 0$, λ is a multiple eigenvalue with negative Krein signature and the eigensubspace $\mathbf{L}_\lambda$ is negative definite. In such cases the multiple eigenvalue is said to have *definite Krein signature*. If there exists a vector $\mathbf{u} \in \mathbf{L}_\lambda$ ($\mathbf{u} \neq 0$) such that $[\mathbf{u},\mathbf{u}] = 0$, the multiple pure imaginary eigenvalue λ is said to have *mixed Krein signature* [390, 603].

Note that in the case when a multiple pure imaginary eigenvalue λ_0 of $\mathbf{A}$ has geometric multiplicity that is less than its algebraic multiplicity, then there is an eigenvector $\mathbf{u}_0$ at λ_0 such that $[\mathbf{u}_0,\mathbf{u}_0] = 0$, i.e. λ_0 has mixed Krein signature. Indeed, there exists at least one *associated vector* $\mathbf{u}_1$: $\mathbf{A}\mathbf{u}_1 = \lambda_0\mathbf{u}_1 + \mathbf{u}_0$, where $\mathbf{A}\mathbf{u}_0 = \lambda_0\mathbf{u}_0$. Taking into account the property (3.18), we obtain

$$\begin{aligned}[\mathbf{A}\mathbf{u}_0, \mathbf{A}\mathbf{u}_1] &= -\left[\mathbf{u}_0, \mathbf{A}^2\mathbf{u}_1\right] = -\overline{\lambda}_0^2[\mathbf{u}_0,\mathbf{u}_1] - 2\overline{\lambda}_0[\mathbf{u}_0,\mathbf{u}_0] \\ &= \lambda_0\overline{\lambda}_0\,[\mathbf{u}_0,\mathbf{u}_1] + \lambda_0\,[\mathbf{u}_0,\mathbf{u}_0]\,, \end{aligned} \tag{3.27}$$

which yields

$$[\mathbf{u}_0,\mathbf{u}_0] = 0 \tag{3.28}$$

since $\lambda_0 = -\overline{\lambda}_0$ [603]. On the other hand, if $\lambda_0 \neq -\overline{\lambda}_0$ then $[\mathbf{u}_0,\mathbf{u}_0] = 0$ for any eigenvector $\mathbf{u}_0$ at λ_0, which follows from the identity

$$[\mathbf{A}\mathbf{u}_0, \mathbf{A}\mathbf{u}_0] = \lambda_0\overline{\lambda}_0\,[\mathbf{u}_0,\mathbf{u}_0] = -\left[\mathbf{u}_0, \mathbf{A}^2\mathbf{u}_0\right] = \overline{\lambda}_0^2\,[\mathbf{u}_0,\mathbf{u}_0]\,.$$

Therefore, a multiple pure imaginary eigenvalue can have definite Krein signature only if it is semisimple [525].

3.3.2 Krein collision or linear Hamiltonian–Hopf bifurcation

Let in the eigenvalue problem (3.24) the matrix $\mathbf{H}$ smoothly depend on a vector of real parameters $\mathbf{p} \in \mathbb{R}^m$: $\mathbf{H} = \mathbf{H}(\mathbf{p})$. Let at $\mathbf{p} = \mathbf{p}_0$ the matrix $\mathbf{H}_0 = \mathbf{H}(\mathbf{p}_0)$ have a double pure imaginary eigenvalue $\lambda = i\omega_0$ ($\omega_0 \geq 0$) with the Jordan chain consisting of the eigenvector $\mathbf{u}_0$ and the associated vector $\mathbf{u}_1$. Hence,

$$\mathbf{H}_0\mathbf{u}_0 = i\omega_0\mathbf{J}\mathbf{u}_0, \quad \mathbf{H}_0\mathbf{u}_1 = i\omega_0\mathbf{J}\mathbf{u}_1 + \mathbf{J}\mathbf{u}_0. \tag{3.29}$$

Transposing equations (3.29) and applying the complex conjugation yields

$$\overline{\mathbf{u}}_0^T\mathbf{H}_0 = i\omega_0\overline{\mathbf{u}}_0^T\mathbf{J}, \quad \overline{\mathbf{u}}_1^T\mathbf{H}_0 = i\omega_0\overline{\mathbf{u}}_1^T\mathbf{J} - \overline{\mathbf{u}}_0^T\mathbf{J}. \tag{3.30}$$

As a consequence, $\overline{\mathbf{u}}_1^T\mathbf{J}\mathbf{u}_0 + \overline{\mathbf{u}}_0^T\mathbf{J}\mathbf{u}_1 = 0$, i.e.

$$[\mathbf{u}_0,\mathbf{u}_1] = -[\mathbf{u}_1,\mathbf{u}_0]. \tag{3.31}$$

Varying the vector of parameters along the curve $\mathbf{p} = \mathbf{p}(\varepsilon)$ ($\mathbf{p}(0) = \mathbf{p}_0$) and applying the perturbation formulas for double eigenvalues that can be found e.g. in [288, 395], we obtain

$$\lambda_\pm = i\omega_0 \pm i\omega_1\sqrt{\varepsilon} + o(\varepsilon^{1/2}), \quad \mathbf{u}_\pm = \mathbf{u}_0 \pm i\omega_1\mathbf{u}_1\sqrt{\varepsilon} + o(\varepsilon^{1/2}) \tag{3.32}$$

under the assumption

$$\omega_1 = \sqrt{\frac{\overline{\mathbf{u}}_0^T \mathbf{H}_1 \mathbf{u}_0}{\overline{\mathbf{u}}_1^T \mathbf{J} \mathbf{u}_0}} > 0, \tag{3.33}$$

where

$$\mathbf{H}_1 = \sum_{s=1}^{m} \frac{\partial \mathbf{H}}{\partial p_s} \frac{dp_s}{d\varepsilon}\bigg|_{\varepsilon=0}. \tag{3.34}$$

When $\varepsilon > 0$, the double eigenvalue $i\omega_0$ splits into two pure imaginary ones according to the formulas (3.32). Calculating the indefinite inner product for the perturbed eigenvectors $\mathbf{u}_\pm$ by equation (3.22) and taking into account the conditions (3.28) and (3.31), we find

$$[\mathbf{u}_\pm, \mathbf{u}_\pm] = \pm 2\omega_1 \overline{\mathbf{u}}_1^T \mathbf{J} \mathbf{u}_0 \sqrt{\varepsilon} + o(\varepsilon^{1/2}), \tag{3.35}$$

i.e. the simple pure imaginary eigenvalues λ_+ and λ_- have opposite Krein signatures. When ε decreases from positive values to negative ones, the pure imaginary eigenvalues of opposite Krein signatures merge at $\varepsilon = 0$ to the double pure imaginary eigenvalue $i\omega_0$ with the Jordan chain of length 2 that further splits[5] into two complex eigenvalues, one of them with the positive real part. When $\omega_0 \neq 0$, this process is known as the linear Hamiltonian–Hopf bifurcation [354, 579], the onset of flutter [239], nonsemisimple $1:1$ resonance [146] or the Krein collision [133, 430], see e.g. Figure 3.1 for an illustration. When $\omega_0 = 0$, a pair of pure imaginary eigenvalues of opposite Krein signatures colliding at zero and splitting then into a pair of real eigenvalues of different sign means the onset of the nonoscillatory instability or divergence [239] known also as the linear *steady-state bifurcation* [146].

3.3.3 MacKay's cones, veering, and instability bubbles

The eigensubspace $\mathbf{L}_\lambda$ of a semisimple r-fold eigenvalue λ ($\mathrm{Re}\lambda = 0$) is positive (negative) definite if and only if its *Gram matrix*, $\mathbf{\Gamma}$, relative to a basis of eigenvectors $\mathbf{u}_1, \ldots, \mathbf{u}_r$ is positive (negative) definite [603], where

$$\mathbf{\Gamma} = \begin{pmatrix} [\mathbf{u}_1, \mathbf{u}_1] & \cdots & [\mathbf{u}_1, \mathbf{u}_r] \\ \vdots & \ddots & \vdots \\ [\mathbf{u}_r, \mathbf{u}_1] & \cdots & [\mathbf{u}_r, \mathbf{u}_r] \end{pmatrix} = \overline{\mathbf{\Gamma}}^T. \tag{3.36}$$

Hence, the eigenvalues of the matrix $\mathbf{\Gamma}$ are real. If all of them are positive (negative), the semisimple eigenvalue λ of the eigenvalue problem (3.24) has definite Krein signature. If $\mathbf{\Gamma}$ has eigenvalues of different sign, λ has mixed Krein signature [390, 603].

Let $r = 2$, and the matrix $\mathbf{H} = \mathbf{H}(\mathbf{p}(\varepsilon))$ be such that at $\varepsilon = 0$ the matrix $\mathbf{H}_0 = \mathbf{H}(\mathbf{p}_0) = \mathbf{H}(\mathbf{p}(0))$ has a double pure imaginary semisimple eigenvalue $\lambda_0 = i\omega_0$ with

[5] Generically. In the presence of additional symmetries the splitting may not happen and the eigenvalues can pass through each other remaining on the imaginary axis, see [146] for the general results on eigenvalue movement in equivariant Hamiltonian systems.

the two linearly independent eigenvectors $\mathbf{u}_1$ and $\mathbf{u}_2$. Then, eigenvalues and eigenvectors of the matrix $\mathbf{H} = \mathbf{H}(\mathbf{p}(\varepsilon))$ at small ε are [155]

$$\lambda = i\omega_0 + i\omega_1\varepsilon + o(\varepsilon), \quad \mathbf{u} = a_1\mathbf{u}_1 + a_2\mathbf{u}_2 + o(1).$$

The coefficients a_1 and a_2 are determined from the eigenvalue problem $\mathbf{F}^T\mathbf{a} = \omega_1\mathbf{\Gamma}^T\mathbf{a}$, where $\mathbf{a} = (a_1, a_2)^T$. The coefficient ω_1 is a root of the equation [592]

$$\det(\mathbf{F} - \omega_1\mathbf{\Gamma}) = \omega_1^2 \det\mathbf{\Gamma} - \omega_1(\mathrm{tr}\mathbf{\Gamma}\,\mathrm{tr}\mathbf{F} - \mathrm{tr}\mathbf{\Gamma}\,\mathbf{F}) + \det\mathbf{F} = 0, \tag{3.37}$$

with the Hermitian matrices

$$\mathbf{\Gamma} = \begin{pmatrix} [\mathbf{u}_1, \mathbf{u}_1] & [\mathbf{u}_1, \mathbf{u}_2] \\ [\mathbf{u}_2, \mathbf{u}_1] & [\mathbf{u}_2, \mathbf{u}_2] \end{pmatrix}, \quad \mathbf{F} = (F_{ij})_1^2 = \begin{pmatrix} \overline{\mathbf{u}}_1^T\mathbf{H}_1\mathbf{u}_1 & \overline{\mathbf{u}}_2^T\mathbf{H}_1\mathbf{u}_1 \\ \overline{\mathbf{u}}_1^T\mathbf{H}_1\mathbf{u}_2 & \overline{\mathbf{u}}_2^T\mathbf{H}_1\mathbf{u}_2 \end{pmatrix} \tag{3.38}$$

and the real symmetric matrix $\mathbf{H}_1$ defined in equation (3.34):

$$\omega_1 = \frac{\mathrm{tr}\mathbf{\Gamma}\,\mathrm{tr}\mathbf{F} - \mathrm{tr}\mathbf{\Gamma}\,\mathbf{F} \pm \sqrt{(\mathrm{tr}\mathbf{\Gamma}\,\mathrm{tr}\mathbf{F} - \mathrm{tr}\mathbf{\Gamma}\,\mathbf{F})^2 - 4\det\mathbf{\Gamma}\det\mathbf{F}}}{2\det\mathbf{\Gamma}}.$$

The eigenvectors $\mathbf{u}_1$ and $\mathbf{u}_2$ can be orthonormalized such that $[\mathbf{u}_1, \mathbf{u}_1] = \alpha$, $[\mathbf{u}_2, \mathbf{u}_2] = \beta$, $[\mathbf{u}_1, \mathbf{u}_2] = 0$, $[\mathbf{u}_2, \mathbf{u}_1] = 0$, where $\alpha, \beta = \pm 1$ [603]. Then,

$$\omega_1 = \frac{\alpha F_{22} + \beta F_{11} \pm \sqrt{(\alpha F_{22} - \beta F_{11})^2 + 4\alpha\beta|F_{12}|^2}}{2\alpha\beta} \tag{3.39}$$

and ω_1 is real when $\alpha\beta > 0$ (definite Krein signature) and complex when $\alpha\beta < 0$ (mixed Krein signature). Introducing the real m-vectors $\mathbf{f}_{11}$ and $\mathbf{f}_{22}$ and the complex m-vector $\mathbf{f}_{12}$ with the components

$$f_{11}^s = \overline{\mathbf{u}}_1^T\frac{\partial\mathbf{H}}{\partial p_s}\mathbf{u}_1, \quad f_{22}^s = \overline{\mathbf{u}}_2^T\frac{\partial\mathbf{H}}{\partial p_s}\mathbf{u}_2, \quad f_{12}^s = \overline{\mathbf{u}}_2^T\frac{\partial\mathbf{H}}{\partial p_s}\mathbf{u}_1,$$

where the derivatives are evaluated at $\mathbf{p} = \mathbf{p}_0$, and denoting $\Delta\mathbf{p} = \mathbf{p}(\varepsilon) - \mathbf{p}_0$ we rewrite the expression (3.39) as

$$\lambda = i\omega_0 + \frac{i}{2}(\alpha\langle\mathbf{f}_{11}, \Delta\mathbf{p}\rangle + \beta\langle\mathbf{f}_{22}, \Delta\mathbf{p}\rangle) \tag{3.40}$$
$$\pm \frac{i}{2}\sqrt{(\alpha\langle\mathbf{f}_{11}, \Delta\mathbf{p}\rangle - \beta\langle\mathbf{f}_{22}, \Delta\mathbf{p}\rangle)^2 + 4\alpha\beta(\langle\mathrm{Re}\mathbf{f}_{12}, \Delta\mathbf{p}\rangle^2 + \langle\mathrm{Im}\mathbf{f}_{12}, \Delta\mathbf{p}\rangle^2)} + o(\|\Delta\mathbf{p}\|)$$

with $\langle\mathbf{f}, \mathbf{p}\rangle = \mathbf{f}^T\mathbf{p}$. We see that when the double semisimple eigenvalue $i\omega_0$ of the canonical Hamiltonian linear system (3.21) has definite Krein signature ($\alpha\beta > 0$), it splits into two pure imaginary eigenvalues (3.40) under a generic variation of parameters. Moreover, the vanishing radicand in equation (3.40) yields three nonsplitting conditions for $i\omega_0$. Hence, this spectral degeneracy is a codimension 3 phenomenon

[97,146,186] in a family of canonical Hamiltonian linear systems (3.21) and its unfolding is described by the three-dimensional hypercone in the $(\xi, \eta, \zeta, \mathrm{Im}\lambda)$-space [390]:

$$\left(\mathrm{Im}\lambda - \omega_0 - \frac{\kappa}{2}\right)^2 = \frac{\xi^2}{4} + \eta^2 + \zeta^2. \tag{3.41}$$

The meaning of the parameters κ, ξ, η, and ζ easily follows from equation (3.40). Almost every slice of *MacKay's eigenvalue cone* (3.41) by a two-dimensional plane parallel to the $\mathrm{Im}\lambda$-axis yields a pair of hyperbolic eigencurves that do not intersect, demonstrating veering or avoided crossing [370, 389, 476, 583]. Therefore, perturbation of a double semisimple pure imaginary eigenvalue with the definite Krein signature under a real symmetric variation of the Hamiltonian $\mathbf{H}$ keeps the eigenvalues on the imaginary axis of the complex plane and cannot be a reason for instability [603]. This is not the case when the Krein signature is mixed ($\alpha\beta < 0$).

If the semisimple eigenvalue $i\omega_0$ has mixed Krein signature ($\alpha\beta < 0$), then its unfolding can be accompanied by the origination of complex eigenvalues (oscillatory instability or flutter) provided that $\xi^2 < 4(\eta^2 + \zeta^2)$, i.e. when the parameters are inside the conical *flutter domain* in the (ξ, η, ζ)-space [186]. The complex eigenvalues have $\mathrm{Im}\lambda = \omega_0 + \frac{\kappa}{2}$. Their real parts belong to the hypersurface in the $(\xi, \eta, \zeta, \mathrm{Re}\lambda)$-space [390]:

$$(\mathrm{Re}\lambda)^2 = -\frac{\xi^2}{4} + \eta^2 + \zeta^2. \tag{3.42}$$

Many cross-sections of the eigenvalue hypersurface (3.42) by the two-dimensional planes that are parallel to the $\mathrm{Re}\lambda$-axis are eigencurves of elliptical shape well known as instability bubbles [390, 392]. The reader has already seen two-dimensional[6] versions of MacKay's eigenvalue surfaces (3.41) and (3.42) in Figure 1.7 (b) and Figure 1.7 (c), respectively.

3.3.4 Instability degree and count of eigenvalues

Let λ, $\mathrm{Re}\lambda = 0$, be an r-fold eigenvalue of a $\mathbf{G}$-Hamiltonian matrix $\mathbf{A}$ and the Gram matrix $\mathbf{\Gamma}$ of the corresponding root subspace have r_1 positive and r_2 negative eigenvalues $r_1 + r_2 = r$. When $r_1 = 0$ and $r_2 = r$ or when $r_1 = r$ and $r_2 = 0$, the r-fold eigenvalue λ has definite Krein signature. When $r_1 \neq 0$ and $r_2 \neq 0$, the r-fold eigenvalue λ has mixed Krein signature. One can interpret this as a collision at λ of r_1 eigenvalues with positive Krein signature and r_2 eigenvalues with negative Krein signature. Then [603], the number of pure imaginary eigenvalues with such understood positive (negative) Krein signature plus the number of eigenvalues in the open left (right) half-plane of the complex plane of any $\mathbf{G}$-Hamiltonian matrix $\mathbf{A} = i\mathbf{G}^{-1}\mathbf{H}$ is equal to the number p (q) of positive (negative) eigenvalues, respectively, of the nonsingular Hermitian $n \times n$ matrix $\mathbf{G}$ in the indefinite inner product (3.14), provided that $p + q = n$.

[6] Because of the additional rotational symmetry of the corresponding problem [146, 147].

In particular, if $\mathbf{G} = i\mathbf{J}$, where $\mathbf{J}$ is the $2k \times 2k$ matrix (3.20), then the number of eigenvalues (counting multiplicities) of the matrix $\mathbf{J}^{-1}\mathbf{H}$ in the open left (right) half-plane of the complex plane plus the number of pure imaginary eigenvalues with positive (negative) Krein signature, is k [603].

Theorem 3.6 (V. A. Yakubovich and V. M. Starzhinskii, 1975 [603]). *The canonical equation* (3.21) *with a positive definite real Hamiltonian* $\mathbf{H} = \mathbf{H}^T > 0$ *is Lyapunov stable and the* $(i\mathbf{J})$*-Hamiltonian matrix* $\mathbf{A} = \mathbf{J}^{-1}\mathbf{H}$ *has only semisimple pure imaginary nonzero eigenvalues. Let* $\pm i\omega_1, \ldots, \pm i\omega_k$ *be the eigenvalues of the matrix* $\mathbf{J}^{-1}\mathbf{H}$*, with the sign so chosen that* $\omega_j > 0$*. Then,* $i\omega_1$*,* $\ldots$*,* $i\omega_k$ *are the eigenvalues with positive Krein signature and* $-i\omega_1, \ldots, -i\omega_k$ *are those with negative one.*

Indeed, from the stability of the trivial solution of the system (3.21) it follows that all the eigenvalues of the matrix $\mathbf{J}^{-1}\mathbf{H}$ are pure imaginary and semisimple. If $\mathbf{u}_j$ is an eigenvector of a simple eigenvalue $\lambda_j = i\omega_j$ $(\omega_j > 0)$ such that $\mathbf{J}^{-1}\mathbf{H}\mathbf{u}_j = i\omega_j\mathbf{u}_j$, then, according to equation (3.25) we have $[\mathbf{u}_j, \mathbf{u}_j] = \omega_j^{-1}(\mathbf{H}\mathbf{u}_j, \mathbf{u}_j) > 0$, i.e. $\lambda_j = i\omega_j$ is an eigenvalue with positive Krein signature.

If $i\omega_1 = \ldots = i\omega_r = i\omega$ $(\omega > 0)$ is a semisimple eigenvalue of multiplicity $r \le n$, then the Gram matrix of the corresponding eigensubspace

$$\mathbf{\Gamma} = \begin{pmatrix} [\mathbf{u}_1, \mathbf{u}_1] & \cdots & [\mathbf{u}_1, \mathbf{u}_r] \\ \vdots & \ddots & \vdots \\ [\mathbf{u}_r, \mathbf{u}_1] & \cdots & [\mathbf{u}_r, \mathbf{u}_r] \end{pmatrix} = \frac{1}{\omega}\begin{pmatrix} (\mathbf{H}\mathbf{u}_1, \mathbf{u}_1) & \cdots & (\mathbf{H}\mathbf{u}_1, \mathbf{u}_r) \\ \vdots & \ddots & \vdots \\ (\mathbf{H}\mathbf{u}_r, \mathbf{u}_1) & \cdots & (\mathbf{H}\mathbf{u}_r, \mathbf{u}_r) \end{pmatrix}$$

is positive definite since $\mathbf{H} > 0$ and $\omega > 0$. Therefore the r-fold semisimple eigenvalue $\lambda = i\omega$ has positive Krein signature [603].

Note that Theorem 3.6 exactly describes the distribution of the eigenvalues with positive and negative Krein signature of the Jeffcott rotor when its angular velocity is in the subcritical speed range, see Section 1.2.1 and in particular equation (1.24).

Note that when the Hamiltonian $\mathbf{H} = \mathbf{H}^T > 0$ is perturbed as $\mathbf{H} + \Delta\mathbf{H}$ with $(\Delta\mathbf{H}) = (\Delta\mathbf{H})^T > 0$, then a simple eigenvalue $i\omega$ gets an increment $i\omega + i\Delta\omega$, where according to equations (3.37) and (3.38)

$$\Delta\omega = \frac{(\Delta\mathbf{H}\mathbf{u}, \mathbf{u})}{[\mathbf{u}, \mathbf{u}]} = \omega\frac{(\Delta\mathbf{H}\mathbf{u}, \mathbf{u})}{(\mathbf{H}\mathbf{u}, \mathbf{u})}. \tag{3.43}$$

Therefore, with the increase of the Hamiltonian the positive pure imaginary eigenvalues $i\omega$ increase while their complex conjugates $-i\omega$ decrease or, equivalently, according to Theorem 3.6 the eigenvalues with the positive Krein signature increase while those with the negative Krein signature decrease. This statement goes back to the result of Rayleigh from 1894 [613].

Definition 3.7 (V. V. Kozlov and A. A. Karapetyan, 2005 [330]). The *instability degree* u of the canonical system (3.21) is the number of roots (counting multiplicities) of the characteristic equation of $\mathbf{A} = \mathbf{J}^{-1}\mathbf{H}$ in the open right half-plane of the complex plane; the number of positive pure imaginary roots (counting multiplicities) is the *stability degree* s.

The following theorem, going back to the works of Kelvin and Tait [573] and Chetaev [127], establishes a relation of the instability degree with the number of negative eigenvalues of the Hamiltonian $\mathbf{H}$.

Theorem 3.8 (V. V. Kozlov and A. A. Karapetyan, 2005 [330, 525, 613]). *Let in equation* (3.21) *the matrix* $\mathbf{H}$ *be nondegenerate and* $\pi(\mathbf{H})$ *and* $\nu(\mathbf{H})$ *denote the number of positive and negative eigenvalues of* $\mathbf{H}$*, respectively. Then,*

$$(a) \quad u \equiv \nu(\mathbf{H}) \mod 2;$$
$$(b) \quad |\pi(\mathbf{H}) - \nu(\mathbf{H})| \leq 2s.$$

According to Theorems 3.6 and 3.8, for a nondegenerate equilibrium $\mathbf{x} = 0$ of the Hamiltonian system (3.21) with $\mathbf{H} > 0$, the instability degree is $u = 0$, the eigenvalues are pure imaginary and semisimple, and the equilibrium is linearly (Lyapunov) stable. When the instability degree is odd, there exists a positive real eigenvalue (instability). A nondegenerate equilibrium with even and nonzero degree u can be either stable or unstable [573, 613].

Theorem 3.9 (A. A. Zevin, 1996 [613]). *The quantity* $s - |k - \pi(\mathbf{H})|$ *is even:* $(s + \pi(\mathbf{H}) - k)/2$ *positive pure imaginary eigenvalues (as well as their complex conjugates) have positive Krein signature and* $(s - \pi(\mathbf{H}) + k)/2$ *positive pure imaginary eigenvalues (and their complex conjugates) have negative Krein signature.*

3.3.5 Graphical interpretation of the Krein signature

With the Hermitian matrix $\mathbf{G} = i\mathbf{J} = \overline{\mathbf{G}}^T$ and new eigenvalue parameter $\nu = i\lambda$, the eigenvalue problem (3.24) is reduced to the eigenvalue problem for a self-adjoint (Hermitian) matrix pencil [202, 319]

$$\mathbf{L}(\nu)\mathbf{u} := (\mathbf{H} + \nu\mathbf{G})\mathbf{u} = 0. \tag{3.44}$$

Notice that a pure imaginary eigenvalue $\lambda = i\omega$ of the generalized eigenvalue problem (3.24) is the real eigenvalue $\nu = -\omega$ of the eigenvalue problem (3.44).

Interpreting the pencil $\mathbf{L}(\nu)$ as a matrix family parameterized by the distinguished parameter ν, we consider an auxiliary eigenvalue problem

$$\mathbf{L}(\nu)\mathbf{u} = \mu\mathbf{u} \tag{3.45}$$

where the eigenvalue parameter is μ. In the theory of *multiparameter eigenvalue problems* [24, 63, 585] one has the freedom to consider any distinguished parameter as an eigenvalue parameter and to study it as a function of other distinguished parameters. In the two-parameter eigenvalue problems such a function defines an eigencurve [64].

It turns out that the pure imaginary eigenvalues $\lambda = i\omega$ of the Hamiltonian matrix $\mathbf{J}^{-1}\mathbf{H}$ and their Krein signatures as well as the real eigenvalues ν of the generalized eigenvalue problem (3.44) can be found by means of the real-valued eigencurves $\mu(\nu)$ of the matrix family $\mathbf{L}(\nu)$ [64, 202, 319].

First, there exists a one-to-one correspondence between the pure imaginary eigenvalues of the matrix $\mathbf{J}^{-1}\mathbf{H}$ and the values of the parameter ν at which $\mu(\nu) = 0$ [64, 202, 319]. The eigenvalues $\lambda = i\omega$ with $\omega > 0$ correspond to $\nu < 0$, their complex conjugates to $\nu > 0$, and $\lambda = 0$ to $\nu = 0$.

On the other hand, the characteristic polynomial of the eigenvalue problem (3.45) is the *Evans–Krein function* for the self-adjoint matrix pencil $\mathbf{L}(\nu)$ [319]

$$E(\nu;\mu) = \det\left(\mathbf{L}(\nu) - \mu\mathbf{I}\right), \tag{3.46}$$

where $\mathbf{I}$ is the $2k \times 2k$ identity matrix. An isolated simple root $\nu = \nu_0$ of the function $\det(\mathbf{L}(\nu))$, corresponding to a simple eigenvalue $\lambda_0 = i\omega_0$ of $\mathbf{J}^{-1}\mathbf{H}$, is a point of a transversal intersection of the ν-axis in the (ν, μ)-plane by a single eigencurve $\mu(\nu)$. The slope of the eigencurve at the point ν_0 is

$$\mu'(\nu_0) = -\frac{\partial_\nu E(\nu_0; 0)}{\partial_\mu E(\nu_0; 0)}, \tag{3.47}$$

where prime denotes differentiation with respect to ν.

Theorem 3.10 (R. Kollár and P. D. Miller, 2012 [319]). *The Krein signature of a simple eigenvalue $\lambda_0 = i\omega_0$ of the Hamiltonian matrix $\mathbf{J}^{-1}\mathbf{H}$ coincides with the sign of the slope of the eigencurve $\mu(\nu)$ at the point $\nu_0 = -\omega_0$, where $\mu(\nu_0) = 0$:*

$$\operatorname{sign}\left(i\overline{\mathbf{u}}^T\mathbf{J}\mathbf{u}\right) = \kappa(\nu_0) := \operatorname{sign}\left(\mu'(\nu_0)\right). \tag{3.48}$$

Moreover, if $\lambda_0 = i\omega_0$ is a multiple semisimple eigenvalue of $\mathbf{J}^{-1}\mathbf{H}$, then its multiplicity, r, is equal to the number of eigencurves simultaneously intersecting the ν-axis

at $\nu = \nu_0$. If all the r eigencurves have at ν_0 slopes of the same sign, the eigenvalue λ_0 has definite Krein signature. If r_1 eigencurves have positive slopes and r_2 negative ones ($r_1 + r_2 = r$), then at the r-fold semisimple eigenvalue λ_0 with mixed Krein signature, r_1 simple eigenvalues with positive Krein signature and r_2 with negative one collide [319].

If a single eigencurve $\mu(\nu)$ touches the ν-axis at $\nu = \nu_0$ and $\mu^{(s)} = 0$ for $s = 0, 1, 2, \ldots, r-1$ whereas $\mu^{(r)} \neq 0$, then $\nu_0 = -\omega_0$ corresponds to the eigenvalue $\lambda = i\omega_0$ of the Hamiltonian system (3.21) with the geometric multiplicity 1 and algebraic multiplicity r. This graphical interpretation is naturally extendable to the eigenvalues with arbitrary algebraic and geometric multiplicities [319]. Elegant proofs of the results on the instability degree, such as Theorem 3.8 and its refinements, based on the representation of the multiplicities and Krein signature of eigenvalues via the analytical properties of the corresponding eigencurves can be found by an interested reader in the surveys by Kollár and Miller [319] and Binding and Volkmer [64].

Let us illustrate the graphical approach to the Krein signature on the example of the already familiar Brouwer particle in a rotating vessel. In the absence of nonconservative dissipative and positional forces, its equations (1.1) with $k_1 = k + \varepsilon$ and $k_2 = k - \varepsilon$ can be presented in the Hamiltonian form (3.21) with the matrices

$$\mathbf{H} = \begin{pmatrix} k+\varepsilon & 0 & 0 & -\Omega \\ 0 & k-\varepsilon & \Omega & 0 \\ 0 & \Omega & 1 & 0 \\ -\Omega & 0 & 0 & 1 \end{pmatrix}, \quad \mathbf{J} = \begin{pmatrix} 0 & 0 & -1 & 0 \\ 0 & 0 & 0 & -1 \\ 1 & 0 & 0 & 0 \\ 0 & 1 & 0 & 0 \end{pmatrix}. \tag{3.49}$$

Numerical computation of the roots of the Evans–Krein function (3.46) for different values of the parameters k, ε, and Ω yields the real eigencurves $\mu(\nu)$ that are presented in Figure 3.2.

In the case of an axially symmetric Brouwer's cavity with $k = 1$ and $\varepsilon = 0$, the eigencurves $\mu(\nu)$ in the (ν, μ)-plane are straight lines, see Figure 3.2 (a–c). According to the *Motzkin–Taussky theorem*, this implies commutativity of the Hermitian matrices $\mathbf{H}$ and $\mathbf{G} = i\mathbf{J}$ [434, 435]; when $k \neq 1$ this property is lost even if $\varepsilon = 0$. The eigencurves for $k \neq 1$ are shown in Figure 3.2 (d, e).

At $k = 1$ and $\varepsilon = 0$, the Evans–Krein function (3.46) factors out as

$$E(\nu; \mu) = ((\mu + \Omega - 1)^2 - \nu^2)((\mu - \Omega - 1)^2 - \nu^2). \tag{3.50}$$

The linear eigencurves $\mu = \pm\nu + 1 - \Omega$ and $\mu = \pm\nu + 1 + \Omega$ vanish at the points

$$\nu_1^{\pm} = \pm(\Omega - 1), \quad \nu_2^{\pm} = \pm(\Omega + 1). \tag{3.51}$$

The slopes of the linear eigencurves

$$\mu'(\nu) = \nu \frac{\Omega^2 + 1 - \nu^2}{\Omega^2 - 1 + \nu^2}$$

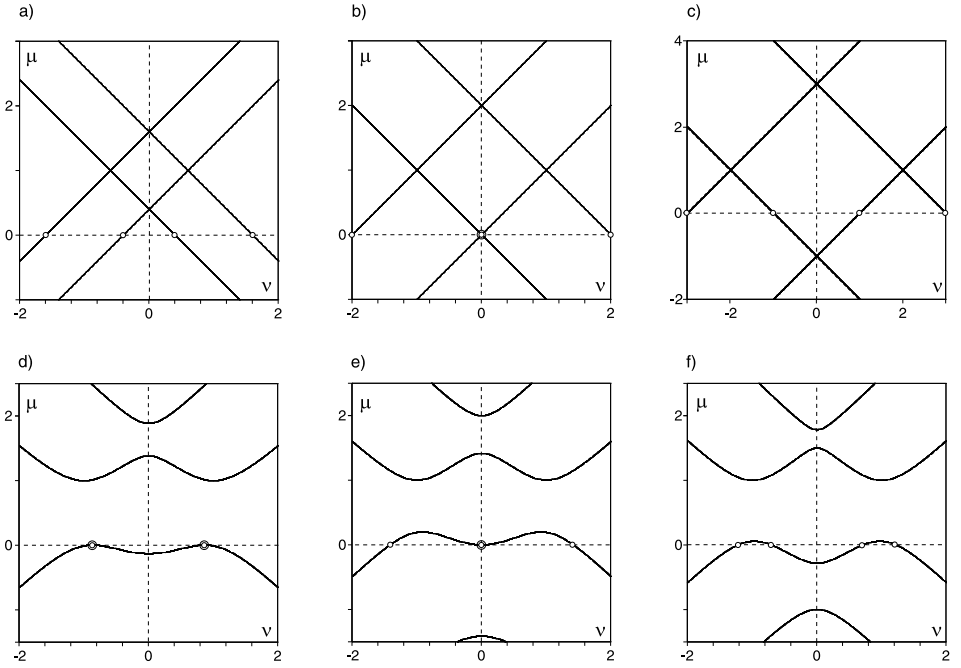

Figure 3.2. Eigencurves $\mu(\nu)$ of the Hamiltonian system (3.22) with the matrices (3.49) corresponding to the Brouwer cavity with $k = 1$, $\varepsilon = 0$ rotating at the angular velocities (a) $\Omega = 0.6$, (b) $\Omega = 1$, (c) $\Omega = 2$. The eigencurves of Brouwer's saddle rotating with the velocity $\Omega = 1$ with the parameters (d) $k = -0.25$, $\varepsilon = 1$, (e) $k = 0$, $\varepsilon = 1$, and (f) $k = 0$, $\varepsilon = 0.5$. Open circles mark simple eigenvalues of the Hamiltonian system (3.22), double circles correspond to the eigenvalues with the algebraic multiplicity 2 and geometric multiplicity (b) 2 or (d, e) 1.

at the points (3.51) are

$$\mu'(\nu_1^{\pm}) = \pm 1, \quad \mu'(\nu_2^{\pm}) = \mp 1. \tag{3.52}$$

The eigencurves of Figure 3.2 (a) correspond to the case of small angular velocities of the Brouwer system situated in the right (subcritical, because $\Omega = 0.6 < 1$) compartment of the stability domain shown in Figure 1.7 (d). The matrix $\mathbf{H}$ in equation (3.49) is then positive definite and according to Theorem 3.6 two pure imaginary eigenvalues with positive imaginary parts have positive Krein signature while their complex conjugates have the negative one.

Indeed, according to equation (3.52) at $\nu = \nu_1^+ < 0$ and $\nu = \nu_2^- < 0$ the slopes of the eigencurves are positive whereas at $\nu = \nu_1^- > 0$ and $\nu = \nu_2^+ > 0$ they are negative, Figure 3.2 (a).

With the increase in the angular velocity to $\Omega = 1$ two characteristic values $\nu_1^{\pm}$ of different signs collide at zero. This corresponds to a double zero semisimple eigen-

value of the matrix $\mathbf{J}^{-1}\mathbf{H}$ of the mixed type because two eigencurves with the opposite slopes intersect each other at $\nu = 0$, see Figure 3.2 (b). The system is stable because the other two eigenvalues are simple and pure imaginary at the conical intersection of Figure 1.7 (d).

In the supercritical speed range ($\Omega = 2 > 1$), the eigencurves with the opposite slopes (3.52) intersect the ν-axis at the values $\nu_1^- = -1$, $\nu_2^- = -3$ and $\nu_1^+ = 1$, $\nu_2^+ = 3$ of the same sign, Figure 3.2 (c). Here the matrix $\mathbf{H}$ is indefinite with the number of negative eigenvalues $\nu(\mathbf{H}) = 2$. According to Theorem 3.8, the instability degree should be either $u = 2$ or $u = 0$. In our case, all eigenvalues are on the imaginary axis ($u = 0$). However, potentially two eigenvalues of opposite Krein signature can collide under additional perturbation of $\mathbf{H}$ that, e.g., breaks the rotational symmetry of the system.

The panels (d–f) of Figure 3.2 correspond to a rotating saddle. The matrix $\mathbf{H}$ is indefinite in all three cases. In the case (e) we have $\nu(\mathbf{H}) = 1$ but Theorem 3.8 is not applicable because $\det \mathbf{H} = 0$. In Figure 3.2 (e) a single eigencurve touches the ν-axis at $\nu = 0$, which corresponds to a double zero eigenvalue of the matrix $\mathbf{J}^{-1}\mathbf{H}$ with the algebraic multiplicity 2 and geometric multiplicity 1 (divergence instability due to secular terms linearly dependent on time). Note that the eigencurve has opposite slopes in the vicinity of $\nu = 0$, which means that the double eigenvalue $\lambda = 0$ with the mixed Krein signature is formed due to collision of two simple pure imaginary eigenvalues $\pm i\,\omega$ that have opposite Krein signatures.

In the cases (d) and (f), the number of negative eigenvalues of the Hamiltonian $\nu(\mathbf{H}) = 2$ and $\det \mathbf{H} \neq 0$ and according to Theorem 3.8 the equilibrium can be either unstable (d) or stable (f). The latter corresponds to the gyroscopic stabilization in the supercritical speed range of the stability diagram of Figure 1.7 (d). Indeed, in Figure 3.2 (d) a single eigencurve touches the ν-axis at the two points $\pm\nu_0$, yielding two pure imaginary eigenvalues $\mp i\,\omega_0$ with algebraic multiplicity 2 and geometric multiplicity 1 (flutter instability due to secular terms linearly dependent on time). In Figure 3.2 (f) the eigencurve has four transversal intersections corresponding to four simple pure imaginary eigenvalues (stability). When ε tends to 1, two eigenvalues of different Krein signature collide at zero (divergence); when ε vanishes, two pairs of pure imaginary eigenvalues, each pair containing eigenvalues with opposite Krein signature, merge into double ones with the mixed Krein signature (flutter), in accordance with the stability diagram of Figure 1.7 (d).

3.3.6 Strong stability: robustness to Hamiltonian's variation

Lyapunov stability of the equilibrium $\mathbf{x} = 0$ of the canonical system (3.21) is equivalent to the requirement that all the eigenvalues λ of the eigenvalue problem (3.24) are pure imaginary and semisimple [603]. Nevertheless, as we have seen in Section 3.3.3, perturbation of the Hamiltonian $\mathbf{H} = \mathbf{H}_0 + \mathbf{H}_1$, where $\mathbf{H}_0$ and $\mathbf{H}_1$ are real symmetric matrices, may lead to the destabilizing splitting of double semisimple pure imaginary

eigenvalues of the matrix $\mathbf{J}^{-1}\mathbf{H}_0$ with mixed Krein signature, see e.g. equation (3.39). If the equilibrium of the perturbed canonical system is Lyapunov stable for a sufficiently small $\|\mathbf{H}_1\|$, then the equilibrium of the nonperturbed canonical system (3.21) with the Hamiltonian $\mathbf{H}_0$ is called *strongly stable* [193, 394, 603].

According to the classical *Krein–Gelfand–Lidskii theorem*, the canonical Hamiltonian linear system (3.21) is strongly stable if and only if it is Lyapunov stable and, additionally, all its eigenvalues have definite Krein signature [193, 337].

Theorem 3.11 (V. A. Yakubovich and V. M. Starzhinskii, 1975 [603]). *Canonical equation* (3.21) *is strongly stable if and only if there is a real nonsingular matrix* $\mathbf{S}$ *such that*

$$\mathbf{S}^{-1}\mathbf{J}\mathbf{H}\mathbf{S} = \operatorname{diag}(\omega_1\mathbf{J}_2, \ldots, \omega_k\mathbf{J}_2), \quad \mathbf{S}^T\mathbf{J}\mathbf{S} = \operatorname{diag}(\mathbf{J}_2, \ldots, \mathbf{J}_2),$$

where $\mathbf{J}_2 = \begin{pmatrix} 0 & -1 \\ 1 & 0 \end{pmatrix}$, $\omega_1, \ldots, \omega_k$ *are any numbers such that* $(\omega_j + \omega_h)T \neq 2\pi$ *for all* j, h. *The numbers* $i\omega_1, \ldots, i\omega_k$ *are then the eigenvalues with positive Krein signature of the matrix* $\mathbf{J}^{-1}\mathbf{H}$ *and their complex conjugates* $-i\omega_1, \ldots, -i\omega_k$ *have negative Krein signature.*

For example, the equilibrium of the Brouwer particle in the rotating symmetric cavity is strongly stable if and only if $\Omega \neq \sqrt{k}$. Indeed, at $\Omega = \sqrt{k}$ the matrix $\mathbf{J}^{-1}\mathbf{H}$ with $\mathbf{H}$ and $\mathbf{J}$ given by equation (3.49) where $\varepsilon = 0$ has a double zero eigenvalue with mixed Krein signature, see Figure 3.2 (b). On the other hand, there exists a matrix

$$\mathbf{S} = \frac{1}{\sqrt[4]{4k}} \begin{pmatrix} 0 & 1 & 0 & -1 \\ 1 & 0 & 1 & 0 \\ -\sqrt{k} & 0 & \sqrt{k} & 0 \\ 0 & \sqrt{k} & 0 & \sqrt{k} \end{pmatrix} \tag{3.53}$$

satisfying Theorem 3.11 with $\omega_1 = \sqrt{k} - \Omega$, $\omega_2 = \sqrt{k} + \Omega$, and $T = \pi/\Omega$, which yields $\omega_1 + \omega_2 = 2\sqrt{k} \neq 2\pi/T = 2\Omega$, i.e. strong stability at $\Omega \neq \sqrt{k}$.

3.3.7 Inertia theorems and stability of gyroscopic systems

Consider equations of motion of a k-degrees-of-freedom mechanical system under the action of potential and *gyroscopic forces*

$$\ddot{\mathbf{z}} + \mathbf{G}\dot{\mathbf{z}} + \mathbf{K}\mathbf{z} = 0, \tag{3.54}$$

where dot stands for time differentiation, the real $k \times k$ matrix $\mathbf{G} = -\mathbf{G}^T$ is associated with the gyroscopic forces and $\mathbf{K} = \mathbf{K}^T$ ($\det \mathbf{K} \neq 0$) is the real $k \times k$ matrix of

potential forces [328,330]. The *kinetic* (T) and *potential* (U) energy of the *gyroscopic system* (3.54)

$$T = \frac{1}{2}\dot{\mathbf{z}}^T\dot{\mathbf{z}}, \quad U = \frac{1}{2}\mathbf{z}^T\mathbf{K}\mathbf{z}, \tag{3.55}$$

yield its first integral of motion: $H = T + U$. Introducing the vector of generalized momenta as [326]

$$\mathbf{y} = \dot{\mathbf{z}} + \frac{1}{2}\mathbf{G}\mathbf{z}$$

and denoting $\mathbf{x} = (z_1, z_2, \ldots, z_k, y_1, y_2, \ldots, y_k)^T$, we arrive at the equations (3.23) with the Hamiltonian function $H = T + U$, i.e. to the canonical Hamiltonian system (3.21) with the Hamiltonian [290]

$$\mathbf{H} = \begin{pmatrix} \mathbf{K} - \frac{1}{4}\mathbf{G}^2 & \frac{1}{2}\mathbf{G} \\ -\frac{1}{2}\mathbf{G} & \mathbf{I} \end{pmatrix}. \tag{3.56}$$

Since we have

$$H = \frac{1}{2}\mathbf{x}^T\mathbf{H}\mathbf{x} = \frac{1}{2}\dot{\mathbf{z}}^T\dot{\mathbf{z}} + \frac{1}{2}\mathbf{z}^T\mathbf{K}\mathbf{z},$$

the kinetic energy is given by a positive definite quadratic form, and $\mathbf{K}$ is not degenerate, then the Hamiltonian $\mathbf{H}$ has $\pi(\mathbf{H}) = k + k - \nu(\mathbf{K})$ positive eigenvalues and $\nu(\mathbf{H}) = \nu(\mathbf{K})$ negative eigenvalues. The number of negative eigenvalues of the matrix of potential forces, $\nu(\mathbf{K})$, is known as the *Poincaré instability degree* whereas the number $\pi(\mathbf{K}) = k - \nu(\mathbf{K})$ is the stability degree of the potential system in the absence of gyroscopic forces [330].

Let s and u be stability and instability degrees, respectively, of the gyroscopic system (3.54) in the sense of Definition 3.7. According to Theorem 3.8

$$|\pi(\mathbf{H}) - \nu(\mathbf{H})| = |k + k - \nu(\mathbf{K}) - \nu(\mathbf{K})| = 2|\pi(\mathbf{K})| \le 2s,$$

implying that $\pi(\mathbf{K}) \le s$. Moreover, $u \le \nu(\mathbf{K})$ [330,525].

Theorem 3.12 (V. V. Kozlov and A. A. Karapetyan, 2005 [330]). *The addition of gyroscopic forces does not diminish the stability degree $\pi(\mathbf{K})$ of a potential system: $s \ge \pi(\mathbf{K})$.*

3.3.8 Positive and negative energy modes and Krein signature

The Krein signature $\kappa(\lambda) := \text{sign}\,([\mathbf{u}, \mathbf{u}])$ of a simple pure imaginary eigenvalue $\lambda = i\omega$ with the eigenvector $\mathbf{u}$ of the canonical Hamiltonian system (3.21) is related via equation (3.25) to the sign of the energy $\mathcal{E} := (\mathbf{H}\mathbf{u}, \mathbf{u})$ of the corresponding vibration mode as [319,338,564]:

$$\text{sign}\,(\mathcal{E}) = \kappa(\lambda)\text{sign}\,(\text{Im}\lambda). \tag{3.57}$$

Therefore, the sign of the energy of a mode depends both on the Krein signature of the mode and on the sign of its frequency $\omega = \mathrm{Im}\lambda$. For the *positive energy modes (PEMs)*, $\mathcal{E} > 0$ and $\mathcal{E} < 0$ for the *negative energy modes (NEMs)* [564].

If all eigenvalues of the canonical system (3.21) are simple and pure imaginary, there exists a canonical transformation $\mathbf{X} = \mathbf{T}^{-1}\mathbf{x}$ such that $\mathbf{T}^T\mathbf{J}\mathbf{T} = \mathbf{J}$ and $\mathbf{T}^T\mathbf{H}\mathbf{T} = \mathrm{diag}\,(\omega_1, \ldots, \omega_k, \omega_1, \ldots, \omega_k)$ that reduces the Hamiltonian function of the system (3.21) to the following *Williamson's normal form* [597, 598]

$$H := \frac{1}{2}\mathbf{x}^T\mathbf{H}\mathbf{x} = \frac{1}{2}\mathbf{X}^T\mathbf{T}^T\mathbf{H}\mathbf{T}\mathbf{X} = \frac{1}{2}\sum_{s=1}^{k}\kappa(\lambda_s)\omega_s(X_s^2 + X_{k+s}^2) \tag{3.58}$$

where $\kappa(\lambda_s) \in \{-1, 1\}$ is the Krein signature of the mode [89, 324, 390, 564]. The Hamiltonian function (3.58) represents a system of k harmonic oscillators with different frequencies. The modes for which $\kappa(\lambda_s)\omega_s < 0$ give a negative contribution to the total energy and thus correspond to NEMs, while those corresponding to $\kappa(\lambda_s)\omega_s > 0$ are PEMs [564].

For the canonical system with the Hamiltonian (3.49) describing the Brouwer particle in a rotating nonsymmetric cavity, the matrix $\mathbf{T}$ at $\varepsilon = 0$ is

$$\mathbf{T} = \frac{1}{\sqrt[4]{4k}}\begin{pmatrix} 0 & 0 & 1 & -1 \\ 1 & 1 & 0 & 0 \\ -\sqrt{k} & \sqrt{k} & 0 & 0 \\ 0 & 0 & \sqrt{k} & \sqrt{k} \end{pmatrix}.$$

It reduces the Hamiltonian (3.49) to the above described diagonal form with $\omega_1 = \sqrt{k} - \Omega$ and $\omega_2 = \sqrt{k} + \Omega$. According to equation (1.24) we have $\kappa(i\omega_1) = 1$, $\kappa(i\omega_2) = 1$ and $\kappa(i\omega_1) = -1$, $\kappa(i\omega_2) = -1$. These eigencurves are shown in Figure 3.3 (a) where the light (dark) gray color marks the eigenvalues with the positive (negative) Krein signature. In the subcritical range ($\Omega < \sqrt{k}$) we have $\omega_1 > 0$ and $\omega_2 > 0$ and all the eigencurves correspond to PEMs. In the supercritical speed range ($\Omega > \sqrt{k}$) the frequency $\omega_1 < 0$ while $\kappa(i\omega_1) = 1$ (similarly, $-\omega_1 > 0$ but $\kappa(-i\omega_1) = -1$), hence these modes are NEMs. The higher modes in the supercritical range are PEMs.

Note that it is the negative energy modes in the supercritical region that are destabilized by infinitesimally small internal damping whereas PEMs become asymptotically stable both in the sub- and supercritical speed ranges, see Figure 1.11. However, it is the two modes with opposite Krein signatures (both corresponding to PEMs in the subcritical speed range or NEMs in the supercritical speed range) that collide into a double zero eigenvalue with the Jordan block at small variation of the symmetry of the cavity ($\varepsilon \neq 0$), see Figure 3.3 (b).

Recall that the oscillation of the Brouwer particle in a symmetric cavity in the absence of rotation is a superposition of two circular whirling motions, one with the angular frequency $\sqrt{k}$ (forward whirl) and another one with the angular frequency $-\sqrt{k}$

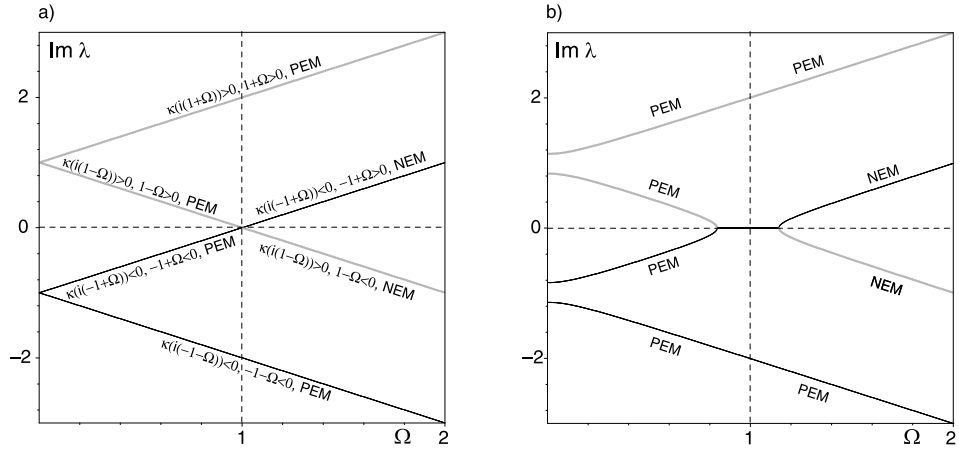

Figure 3.3. Eigencurves $\mathrm{Im}\lambda(\Omega)$ of the Brouwer problem on a particle in a rotating cavity (3.49) with $k = 1$ and (a) $\varepsilon = 0$ and (b) $\varepsilon = 0.3$. The light (dark) gray curves correspond to the modes with positive (negative) Krein signature. In the subcritical speed range ($\Omega < 1$) all the modes are PEMs; in the supercritical range ($\Omega > 1$) the lower modes are NEMs and the higher are PEMs.

(backward whirl) [137,138]. If the cavity rotates in the sense of the forward whirl, then when Ω is in the supercritical speed range ($\Omega > \sqrt{k}$), the particle in the stationary frame appears to move in the same direction as the cavity, having, however, lower angular velocity. It is this slow prograde motion that corresponds to the negative energy modes shown in Figure 3.3 (a). If, for example, a drag force existed between the cavity and the particle, the forward whirl in the supercritical speed range would be accelerated (dissipation just further decreases the negative value of energy thus causing the mode to grow), see Figure 1.11. This early (1908) observation of Lamb [343] turned out to be valid also for wave propagation in dispersive media.

3.3.9 Dispersive wave propagation in conservative systems

In 1960 Sturrock [552] found that waves of arbitrary physical nature can carry negative energy if they propagate in the media moving at velocities that exceed the characteristic velocity of small disturbances. Indeed, let for simplicity the medium be one-dimensional and its velocity with respect to the stationary frame be v. Consider two waves with the same wave number k and frequency ω that propagate in opposite directions with respect to the moving frame: the *forward wave* with the phase velocity $u = \omega/k > 0$ and the *backward wave* with the phase velocity $-u < 0$.

In the stationary frame both waves appear to be propagating forward, i.e. in the same direction that the medium is moving, if $v > u$. The wave with the phase velocity $v + u$

in the stationary frame propagates faster than the medium (the fast wave) whereas that with $v - u$ follows the medium (the slow wave). Assuming that the energy carried by each wave in the nonmoving medium is E, we conclude that with respect to the stationary frame the energy of the fast wave $E_f = E(v + u)/u$ and that of the slow wave $E_s = -E(v-u)/u$, are of opposite signs. When $E > 0$, the energy of the slow wave in the stationary frame is negative, provided that v is great enough to convert the backward wave of the moving frame to the forward wave of the stationary frame [552]. Such a wave is also known as a *reflected wave*, e.g. in rotor dynamics [109, 433, 604].

A negative energy wave is a potential source of instability because the energy needs to be withdrawn from the wave in order to enhance it. For example, instability of the wave can be induced by dissipation, which in the finite-dimensional case is established by the Kelvin–Tait–Chetaev theorem [127, 573, 608]. In a conservative system, coupling between waves of positive and negative energy leads to the power flow from the negative to the positive energy waves, allowing them to grow, which means instability [108, 264, 358, 386, 564].

In the 1990s, Bridges demonstrated that dispersive wave propagation in conservative systems is naturally described when the governing partial differential equations are reformulated as Hamiltonian systems on a so-called *multisymplectic structure* [89]. To illustrate this method, we consider the equation

$$\xi_{tt} + 2m\xi_{xt} + \delta\xi_{xx} - 2\alpha\xi = 0, \tag{3.59}$$

where the subscripts denote partial derivatives with respect to time (t) and the spacial coordinate (x), the parameters $\alpha, m, \delta \in \mathbb{R}$, $m^2 > \delta$, and $\delta = \pm 1$. Introducing the vector $\mathbf{z} = (\xi, \eta, \zeta)^T$ where $\eta = \xi_t$ and $\zeta = \xi_x$, we write [89]

$$\mathbf{M}\mathbf{z}_t + \mathbf{K}\mathbf{z}_x = \mathbf{H}\mathbf{z} \tag{3.60}$$

where $\mathbf{M}$ and $\mathbf{K}$ are real skew-symmetric matrices

$$\mathbf{M} = \begin{pmatrix} 0 & -1 & -m \\ 1 & 0 & 0 \\ m & 0 & 0 \end{pmatrix}, \quad \mathbf{K} = \begin{pmatrix} 0 & -m & -\delta \\ m & 0 & 0 \\ \delta & 0 & 0 \end{pmatrix} \tag{3.61}$$

and $\mathbf{H}$ is a real symmetric matrix

$$\mathbf{H} = \begin{pmatrix} -2\alpha & 0 & 0 \\ 0 & 1 & m \\ 0 & m & \delta \end{pmatrix}. \tag{3.62}$$

Looking for a solution in the form $\mathbf{z}(x, t) = \mathbf{u}e^{\lambda t + \mu x}$, where $\lambda, \mu \in \mathbb{C}$ and $\mathbf{u} \in \mathbb{C}^3$, we arrive at the two-parameter eigenvalue problem [63]

$$(\mathbf{H} - \lambda\mathbf{M} - \mu\mathbf{K})\mathbf{u} = 0. \tag{3.63}$$

Following Bridges [89], for the system (3.60) we define the temporal and spatial Krein signatures

$$\kappa_1 = \text{sign}\,(i\overline{\mathbf{u}}^T\mathbf{M}\mathbf{u}), \quad \kappa_2 = \text{sign}\,(i\overline{\mathbf{u}}^T\mathbf{K}\mathbf{u}), \tag{3.64}$$

as well as the *energy density* $\mathcal{E}$ and the *energy flux* $\mathcal{F}$

$$\mathcal{E} = \frac{1}{2}\mathbf{z}^T\mathbf{H}\mathbf{z} - \frac{1}{2}\mathbf{z}^T\mathbf{K}\mathbf{z}_x, \quad \mathcal{F} = \frac{1}{2}\mathbf{z}^T\mathbf{K}\mathbf{z}_t. \tag{3.65}$$

The system (3.60) has thus the energy *conservation law* [89]:

$$\frac{\partial\mathcal{E}}{\partial t} + \frac{\partial\mathcal{F}}{\partial x} = 0. \tag{3.66}$$

Evaluating $\mathcal{E}$ and $\mathcal{F}$ at the solution $\mathbf{z} = \mathbf{u}e^{i\omega t+ikx} + \overline{\mathbf{u}}e^{-i\omega t-ikx}$, we find that

$$\mathcal{E} = \omega i\overline{\mathbf{u}}^T\mathbf{M}\mathbf{u}, \quad \mathcal{F} = \omega i\overline{\mathbf{u}}^T\mathbf{K}\mathbf{u}. \tag{3.67}$$

Assuming $\lambda = i\omega$ and $\mu = ik$ and taking the derivative of equation (3.63) with respect to k, we obtain the equation

$$(\mathbf{H} - i\omega\mathbf{M} - ik\mathbf{K})\partial_k\mathbf{u} = i\,\partial_k\omega\mathbf{M}\mathbf{u} + i\mathbf{K}\mathbf{u},$$

that has a nontrivial solution if and only if [89]

$$c_g := \frac{\partial\omega}{\partial k} = -\frac{i\overline{\mathbf{u}}^T\mathbf{K}\mathbf{u}}{i\overline{\mathbf{u}}^T\mathbf{M}\mathbf{u}} = -\frac{\mathcal{F}}{\mathcal{E}}. \tag{3.68}$$

Therefore, the group velocity, c_g, of the wave is proportional to the energy flux $\mathcal{F}$, and via equations (3.64) and (3.67) to the spatial signature κ_2 – the result going back to the 1961 work by Krein and Liubarskii [338], see also [603].

3.3.10 Absolute and convective instability

A solvability condition written for equation (3.63) yields the *dispersion relation*

$$D(\omega, k) := \det(\mathbf{H} - i\omega\mathbf{M} - ik\mathbf{K}) = 0. \tag{3.69}$$

With the matrices given by equations (3.61) and (3.62), the function $D(\omega, k)$ is

$$D(\omega, k) = (m^2 - \delta)(\omega^2 + 2m\omega k + \delta k^2 + 2\alpha), \tag{3.70}$$

and its roots yield the *dispersion curves* [389]

$$\omega(k) = -km \pm \sqrt{k^2(m^2 - \delta) - 2\alpha} \tag{3.71}$$

that are shown in Figure 3.4 (a). When $\alpha < 0$, the temporal eigenvalue $i\omega$ is simple and pure imaginary with the eigenvector $\mathbf{u} = (1, i\omega, ik)^T$ at all k. Hence,

$$i\overline{\mathbf{u}}^T\mathbf{M}\mathbf{u} = 2(\omega + km), \quad i\overline{\mathbf{u}}^T\mathbf{K}\mathbf{u} = 2(\omega m + k\delta) \tag{3.72}$$

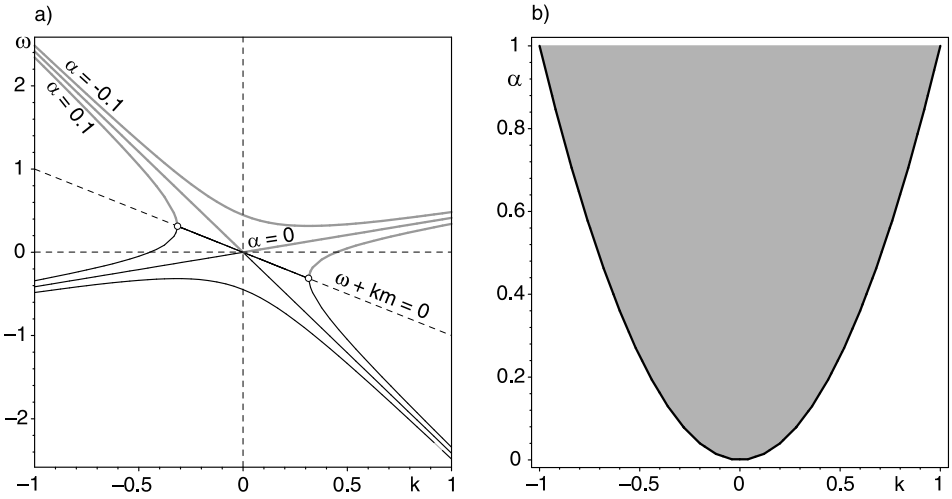

Figure 3.4. (a) Dispersion curves $\omega(k)$ according to equation (3.71) and (b) shown in gray the instability domain $\alpha > k^2(m^2 - \delta)/2$ corresponding to $\omega \in \mathbb{C}$ for $m = 1$, $\delta = -1$.

and according to the defining equations (3.64) the dispersion curve lying above the line $\omega + km = 0$ in the (k, ω)-plane corresponds to the eigenvalues $i\omega$ with positive temporal Krein signature $\kappa_1 > 0$ while that below this line corresponds to the eigenvalues $i\omega$ with $\kappa_1 < 0$. These two dispersion curves marked by light and dark gray colors, respectively, demonstrate an avoided crossing in Figure 3.4 (a). At $\alpha = 0$ they cross and at $\alpha > 0$ overlap with the origination of the bubble of instability consisting of complex ω when $k^2 < 2\alpha/(m^2 - \delta)$, see the black line in Figure 3.4 (a). Therefore, at the given $\alpha > 0$, two existing at $k^2 > 2\alpha/(m^2 - \delta)$ simple pure imaginary eigenvalues with the opposite signs of energy density $\mathcal{E}$ move toward each other when $k > 0$ is decreasing until they collide into the double pure imaginary eigenvalue $-ikm$, which further splits into a couple of complex eigenvalues (instability) in accordance with the usual scenario of the Krein collision, see Figure 3.4 (a).

The spatial Krein signature κ_2 can provide additional information about the temporal instability for the waves in one space dimension. Since the energies, i.e. the temporal Krein signatures κ_1, of the two waves in the Krein collision are of opposite sign, then if the signs of the energy flux, i.e. the spatial Krein signatures κ_2, are the same, the energy spreads in opposite spatial directions and the instability is *absolute* [88, 235, 506, 551]. If the signs of the energy flux, i.e. κ_2, are opposite, then the energy spreads in the same direction and the instability is convected away (*convective instability*) [88, 235, 506, 551].

By equation (3.68) the sign of the group velocity of the wave is determined by both signatures: $\operatorname{sign}(c_g) = -\kappa_1\kappa_2$. Hence, interaction of the two waves with the opposite temporal Krein signatures κ_1 can lead to the absolute instability if their spatial

Krein signatures κ_2 are the same, which yields opposite group velocities of the waves [577]. The group velocity is the slope of the dispersion curve $\omega(k)$. For example, in Figure 3.4 (a) the interacting light gray (positive energy) and dark gray (negative energy) waves also have opposite slopes so that their Krein collision results in the absolute instability [89].

Chapter 4

Reversible and circulatory systems

In the case of complicated structures there may appear different shapes of characteristic curves, and only an analysis in the [load-frequency] plane may assure the correct results for the design of structures subjected to nonconservative loads.

O. Mahrenholtz, R. Bogacz [396]

4.1 Reversible systems

Equations of *reversible* dynamical systems are invariant under a particular type of coordinate transformation which is accompanied, e.g, by *time reversal* [344,459]. We define the dynamical system

$$\frac{d\mathbf{x}}{dt} = \mathbf{f}(\mathbf{x}), \tag{4.1}$$

where $\mathbf{x}, \mathbf{f} \in \mathbb{R}^q$, to be reversible if there exists an involution of the state variables $\mathbf{R} = \mathbf{R}^{-1}$ such that [460,575]

$$\frac{d\mathbf{x}}{dt} = -\mathbf{R}\mathbf{f}(\mathbf{R}\mathbf{x}) = \mathbf{f}(\mathbf{x}), \tag{4.2}$$

leaving equation (4.1) invariant under the transformation[1] $\mathbf{x} \to \mathbf{R}\mathbf{x}$ and $t \to -t$.

In particular, all oscillation equations of the following form are reversible

$$\frac{d^2\mathbf{z}}{dt^2} = \mathbf{g}(\mathbf{z}), \tag{4.3}$$

where $\mathbf{z}, \mathbf{g} \in \mathbb{R}^m$. When (4.3) is rewritten as a first order system in the variables z_s and dz_s/dt in $\mathbb{R}^q$, $q = 2m$, the involution changes the signs of dz_s/dt [344].

From reversibility, at an equilibrium $\mathbf{x}_0$ of equation (4.1) the Jacobian

$$\mathbf{A} := D\mathbf{f}(\mathbf{x}_0) = -\mathbf{R}\mathbf{A}\mathbf{R}, \tag{4.4}$$

[1] In quantum mechanics, Wigner's time reversal operation [158,595] leaves the 'Schrödinger equation' $\frac{d\mathbf{x}}{dt} = i\,\mathbf{A}\mathbf{x}$ invariant under the transformation $\mathbf{x} \to \mathbf{U}\overline{\mathbf{x}}$ and $t \to -t$, where $i = \sqrt{-1}$, the overbar denotes complex conjugation, and $\mathbf{U}$ is a unitary matrix, $\mathbf{U}\overline{\mathbf{U}}^T = \overline{\mathbf{U}}^T\mathbf{U} = \mathbf{I}$. Indeed, the *anti-unitary symmetry*, $\mathbf{A} = \mathbf{U}\,\overline{\mathbf{A}}\,\overline{\mathbf{U}}^T$, transforms the equation $\frac{d\mathbf{U}\overline{\mathbf{x}}}{dt} = -i\,\mathbf{A}\mathbf{U}\overline{\mathbf{x}}$, into $\frac{d\mathbf{x}}{dt} = i\,\mathbf{U}^T\,\overline{\mathbf{A}}\,\overline{\mathbf{U}}\mathbf{x} = i\,\mathbf{A}\mathbf{x}$. The operator, $\mathbf{A}$, of the time reversible 'quantum' system $\frac{d\mathbf{x}}{dt} = i\,\mathbf{A}\mathbf{x}$, can be a real or complex symmetric matrix $\mathbf{A} = \mathbf{A}^T$ [212,595].

implying similarity of the eigenvalue structure of linear reversible systems to those of Hamiltonian systems:

Theorem 4.1 (J. S. W. Lamb and J. A. G. Roberts, 1998 [344]). *Let λ be an eigenvalue of a linear reversible vector field. Then so is its complex conjugate, $\overline{\lambda}$, and $-\lambda$. Hence, for linear flows the eigenvalues come in singlets $\{0\}$, doublets $\{\lambda, -\lambda\}$ with $\lambda \in \mathbb{R}$ or $\lambda \in i\mathbb{R}$, or quadruplets $\{\lambda, -\lambda, \overline{\lambda}, -\overline{\lambda}\}$.*

Consequently, an equilibrium of an autonomous reversible dynamical system is either unstable or all its eigenvalues λ lie on the imaginary axis of the complex plane, i.e., it can never be asymptotically stable. For equilibria of nonlinear systems whose eigenspectrum is of the latter type, a nonlinear analysis is necessary to determine stability [344, 459, 460].

In the absence of equivariance, the pure imaginary eigenvalues λ of the linearized vector field at an equilibrium point of a reversible autonomous flow are typically simple (no two eigenvalues are the same). Also, typically, they are nonresonant (no eigenvalues are positive integer multiples of others). However, such situations may arise in generic one-parameter families for suitable values of the parameter [344].

The collision at zero of pure imaginary eigenvalues of the linearized vector field at an equilibrium point of a flow corresponds to a *steady-state bifurcation*. In another bifurcation of codimension one, two pairs of pure imaginary (nonzero) eigenvalues $\lambda = \pm i\omega_1$, $\lambda = \pm i\omega_2$ collide when a parameter is varied. Then, typically, after such a collision they originate a quadruplet in the complex plane. In Hamiltonian systems, such a bifurcation is known as a linear Hamiltonian–Hopf bifurcation. In reversible systems, by analogy, it is called a linear *reversible Hopf bifurcation* or *reversible (non-semisimple) 1 : 1 resonance* [344].

4.2 Nonconservative positional forces

Consider a finite dimensional *Langrangian mechanical system*

$$\frac{d}{dt}\frac{\partial L}{\partial \dot{q}_k} - \frac{\partial L}{\partial q_k} + Q_k'' = 0, \quad k = 1, \ldots, m, \tag{4.5}$$

where dot stands for time differentiation, $L = T(\mathbf{q}, \dot{\mathbf{q}}) - U(\mathbf{q})$ is the *Lagrangian*, T and U the kinetic and potential energy, respectively, and $Q_k'' = Q_k''(\mathbf{q}, \dot{\mathbf{q}}, t)$ the nonpotential generalized forces [459, 575]. Assuming T is a quadratic function of the generalized velocities, the system (4.5) is reversible under the involution $t \to -t$, $\mathbf{q} \to \mathbf{q}$, and $\dot{\mathbf{q}} \to -\dot{\mathbf{q}}$, if Q_k'' is also invariant

$$Q_k'' = Q_k''(\mathbf{q}, \dot{\mathbf{q}}, t) = Q_k''(\mathbf{q}, -\dot{\mathbf{q}}, -t). \tag{4.6}$$

A generalized force having this invariance is, e.g., a *follower force* [61, 356] that became popular in the engineering community after the works of Ziegler[2] on elastic stability [622, 626].

The follower force has positional character, i.e. depends only on time and the generalized coordinates. In the linear case such forces can be written as follows

$$\mathbf{Q} = \mathbf{P}\mathbf{q} = \mathbf{K}\mathbf{q} + \mathbf{N}\mathbf{q}, \tag{4.7}$$

where $\mathbf{K}^T = \mathbf{K}$ and $\mathbf{N}^T = -\mathbf{N}$. The forces $\mathbf{Q}' = \mathbf{K}\mathbf{q}$ are said to be potential, or conservative. For these forces, there exists a potential function $U = \frac{1}{2}\mathbf{q}^T\mathbf{K}\mathbf{q}$ such that $Q'_k = \partial U/\partial q_k$. Usually, the existence of a potential for these forces is taken as their definition [618, 619].

The forces $\mathbf{Q}'' = \mathbf{N}\mathbf{q}$ are known in the literature as *nonconservative positional*, or *pseudo-gyroscopic*, or *circulatory* forces [239, 423, 623]. They are orthogonal to the vector $\mathbf{q}$ of generalized coordinates, $\mathbf{Q}''\mathbf{q} = 0$, because $\mathbf{q}^T\mathbf{N}\mathbf{q} = -\mathbf{q}^T\mathbf{N}\mathbf{q}$ for a skew-symmetric matrix $\mathbf{N}$, which explains the origin of the word 'circulatory' in the terminology [18, 623], see also [55].

In control problems for mechanical systems, a more detailed classification of linear generalized forces is used as well. The symmetric matrix $\mathbf{K}$ of arbitrary potential forces can be uniquely decomposed into a scalar matrix and a *deviator* matrix with zero trace, $\mathbf{K} = \mathbf{C} + \mathbf{H}$, where $\mathbf{C} = c\mathbf{I}$, $c = \mathrm{tr}\mathbf{K}/m$, and $\mathbf{H} = \mathbf{K} - c\mathbf{I}$, where $\mathbf{I}$ is the identity matrix. Accordingly, the forces $\mathbf{C}\mathbf{q}$ are called *potential forces of spherical type*, and the forces $\mathbf{H}\mathbf{q}$ are called *potential forces of hyperbolic type* [618, 619].

The nonlinear generalized forces are said to be potential if they have a potential, and circulatory if they are orthogonal to the vector of generalized coordinates, see [618, 619], where decomposition of arbitrary nonlinear positional forces into potential and circulatory parts is discussed in detail. Circulatory forces are fundamental nonconservative forces [332, 423].

4.3 Circulatory systems

A *circulatory system* [4, 75, 239, 423, 626] is a reversible linear autonomous mechanical system under the action of nonconservative positional forces

$$\mathbf{M}\ddot{\mathbf{q}} + \mathbf{P}\mathbf{q} = 0, \tag{4.8}$$

[2] Hans Ziegler (1910–1985) – a Swiss scientist who worked in the field of continuum and structural mechanics. Well-known is the *Ziegler's paradox* of destabilization by small dissipation of a two-link pendulum loaded by a follower force (*Ziegler's pendulum*) – an important early example of *dissipation-induced instabilities* [312, 622]. *Ziegler's principle* of maximum entropy production [625], which he established first as a means to derive nonlinear constitutive relations for solids and fluids, is being discussed nowadays [413, 414] as a fundamental variational principle for all *nonequilibrium thermodynamics* generalizing the results of Onsager [114, 457] on the irreversibility of the collective dynamics of a macroscopic number of classical particles despite the time-reversal symmetry of the equations of motion of an individual particle (microscopic reversibility [229]).

where $\mathbf{M} = \mathbf{M}^T \in \mathbb{R}^{m^2}$ and $\mathbf{P} \neq \mathbf{P}^T \in \mathbb{R}^{m^2}$ are matrices of mass and stiffness, and $\mathbf{q}$ is a real vector of generalized coordinates.

A variety of physical and technical processes, the modeling of which results in circulatory systems, extends from the phenomenon of intense angular self-oscillations of a carriage wheel (*shimmy*) [499, 620], controlled motion of a two-legged walking robot [41], and the destabilizing effect of viscous damping in bearing supports of turbine rotors [256, 266, 534] to squealing brakes [226, 254, 268, 531], self-excited vibrations in paper calenders that cause a specific wear phenomenon of the expensive rollers known as the *calender barring* [92, 537], flutter of flexible structures (such as wings, airfoils, flags, paper, solar sails) interacting with inviscid flows [75, 161, 366, 405, 499], physiology of blood and air flow [216, 614], magnetohydrodynamics [565] and dynamics of nonholonomic systems [79, 324].

4.3.1 Divergence and flutter instabilities

Assuming for the solutions of the system (4.8) the form $\mathbf{q} = \mathbf{u} \exp\left(i\sqrt{\sigma}t\right)$ and denoting $\mathbf{A} = \mathbf{M}^{-1}\mathbf{P}$, we arrive at the eigenvalue problem

$$\mathbf{A}\mathbf{u} = \sigma\mathbf{u}, \tag{4.9}$$

where σ is an eigenvalue and $\mathbf{u}$ is the corresponding eigenvector. The matrix $\mathbf{A}$ is real and nonsymmetric. In accordance with Theorem 4.1 (with $\sigma = -\lambda^2$), the circulatory system (4.8) is stable if and only if all the eigenvalues σ of the matrix $\mathbf{A}$ are positive and semisimple (algebraic and geometric multiplicities of σ coincide), because the origination of the Jordan block leads to instability owing to the polynomial in time secular terms. If all the eigenvalues σ are real and some of them negative, then the system (4.8) loses stability because of the existence of the solutions $\mathbf{q} = \mathbf{u}\exp(\sqrt{|\sigma|}t)$ (static instability or divergence). If at least one of the eigenvalues σ of the matrix $\mathbf{A}$ is complex, then the system (4.8) is unstable owing to the solutions $\mathbf{q} = \mathbf{u}\exp(\mathrm{Im}\sqrt{\sigma}\,t \pm i\,\mathrm{Re}\sqrt{\sigma}\,t)$ (oscillatory instability or flutter) [75, 239, 626].

4.3.2 Multiple parameter families of circulatory systems

Assume now that the matrices $\mathbf{M}$ and $\mathbf{P}$ of the circulatory system (4.8), and hence the matrix $\mathbf{A}$ in the eigenvalue problem (4.9), smoothly depend on the vector of real parameters $\mathbf{p}^T = (p_1, p_2, \ldots p_n)$. As a consequence of Theorem 4.1, the space of parameters is subdivided into the regions of stability, flutter and divergence. A point $\mathbf{p} = \mathbf{p}_0$ in the parameter space, where all the eigenvalues σ of the matrix $\mathbf{A}(\mathbf{p}_0)$ are simple and nonzero, is located inside one of these domains because simple eigenvalues of $\mathbf{A}$ smoothly depend on $\mathbf{p}$ [548]. The points of the boundaries between these domains may correspond to the matrices with zero simple or multiple eigenvalues σ as well as to the matrices that contain real nonzero multiple eigenvalues [516, 521].

In one-parameter circulatory systems ($n = 1$), the value of the parameter p, corresponding to the matrix $\mathbf{A}(p)$ with a simple zero eigenvalue and other eigenvalues positive and simple, separates the regions of stability and divergence. A point $p = p_0$, at which the matrix $\mathbf{A}(p_0)$ has a Jordan block of order 2 with the double real eigenvalue σ_0, is a boundary between the domains of stability and flutter when $\sigma_0 > 0$ and between the domains of divergence and flutter when $\sigma_0 < 0$. At $p = p_0$, an eigenvalue σ leaves the real axis after its collision with another real one, which in case of $\sigma_0 > 0$ corresponds to the reversible Hopf bifurcation in terms of λ, where $\lambda^2 = -\sigma$; transition of the real σ through zero from positive to negative values corresponds to the steady-state bifurcation. The two spectral singularities are *structurally stable* in one-parameter circulatory systems, i.e. they do not disappear under small deformations of the matrix family [17]. Matrices with the more complicated Jordan structure are not generic in a one-parameter family of circulatory systems [516].

When $n > 1$, the points of the above described two types are smooth hypersurfaces of codimension 1 in the parameter space. The points of the boundary corresponding to the matrices with more complicated Jordan form constitute *singularities* of higher codimension on these hypersurfaces [17]. How many different kinds of generic singularities are inherent to n-parameter circulatory systems? The answer follows, e.g., from the works on versal deformations of general reversible systems by Sevryuk and Hoveijn [230, 515]. We will deduce it studying Galin's bifurcation diagrams of real matrix families [185].

4.3.3 Generic singularities on the stability boundary

The matrix $\mathbf{A}(\mathbf{p})$ in the problem (4.9) maps the parameter space $\mathbb{R}^n$ into the space $\mathbb{R}^{m^2}$ of all real square matrices of order m. Let us divide the space $\mathbb{R}^{m^2}$ to the parts (*bundles*) in accordance with the *type* of eigenvalue and the dimension of the Jordan block corresponding to each eigenvalue σ [515]. The type of the eigenvalue determines whether σ is real nonzero, complex, or zero [515]. Therefore, a bundle consists of the matrices with the same types of eigenvalues and the same Jordan structure. Preimages of the bundles subdivide the parameter space $\mathbb{R}^n$ into the regions where the matrices have the same Jordan structure and the same types of eigenvalues. This partition is a *bifurcation diagram* of the family $\mathbf{A}(\mathbf{p})$ [17,185]. Generic n-parameter families do not contain matrices from the bundles of codimension higher than n [17].

The bundles consist of *orbits* containing the matrices with the same eigenvalues and the same Jordan blocks. The codimension d of an orbit of $\mathbf{A}$ is

$$d = \sum_{\sigma} [n_1(\sigma) + 3n_2(\sigma) + 5n_3(\sigma) + \cdots], \tag{4.10}$$

where $n_1(\sigma) \geq n_2(\sigma) \geq \cdots$ are the dimensions of the Jordan blocks of $\mathbf{A}$ corresponding to the eigenvalue σ [17, 185]. Thus the codimension c of the bundle is not higher than the codimension d of its orbits. If all eigenvalues of the matrix $\mathbf{A}$ were zero,

then the bundle would consist of one orbit and $c = d$. Let μ be a number of nonzero eigenvalues. Then the codimension of the bundle is smaller than the codimension of the orbit by $\mu = \sum_{\sigma \neq 0} 1$ [284]

$$c = [n_1(0) + 3n_2(0) + 5n_3(0) + \cdots] + \sum_{\sigma \neq 0} [-1 + n_1(\sigma) + 3n_2(\sigma) + 5n_3(\sigma) + \cdots]. \tag{4.11}$$

It is convenient to denote a bundle by the product of determinants of its Jordan blocks [17]. Different real nonzero eigenvalues are denoted by $\alpha, \beta, \gamma, \ldots$; the product of the complex eigenvalues $x \pm iy$ is written in the form $(x^2 + y^2)^2$, which reflects the fact of simultaneous origination of two Jordan blocks, one for a complex eigenvalue and another for its complex conjugate. We distinguish zero eigenvalues separately. The matrices with simple nonzero eigenvalues constitute generically a set of codimension zero in the space $\mathbb{R}^{m^2}$. Using the formula (4.11) we list all the bundles of codimension $c \leq 3$ [284]

$$\begin{aligned} c = 1: &\quad 0, \alpha^2 \\ c = 2: &\quad 0^2, 0\alpha^2, \alpha^3, \alpha^2\beta^2, \left(x^2 + y^2\right)^2 \\ c = 3: &\quad 0^3, 0^2\alpha^2, 0\alpha^3, 0\alpha^2\beta^2, 0\left(x^2 + y^2\right)^2, \\ &\quad \alpha\alpha, \alpha^4, \alpha^3\beta^2, \alpha^2\beta^2\gamma^2, \alpha^2\left(x^2 + y^2\right)^2. \end{aligned} \tag{4.12}$$

The bifurcation diagrams of the families of real matrices become *stability diagrams*, i.e. partitions of the parameter space of the families of circulatory systems into the domains of stability, flutter and divergence, by excluding points corresponding to the matrices with multiple complex eigenvalues that belong to the flutter domain. The boundaries of the domains of stability, flutter and divergence consist of the points where the matrices have simple or multiple zero eigenvalues or multiple real eigenvalues [284, 521].

Theorem 4.2 (O. N. Kirillov, 2000 [284]). *Stability diagrams of circulatory systems with $n \leq 3$ parameters possess the following generic singularities*

$$\begin{aligned} n = 1: &\quad 0, \alpha^2 \\ n = 2: &\quad 0^2, 0\alpha^2, \alpha^3, \alpha^2\beta^2 \\ n = 3: &\quad 0^3, 0^2\alpha^2, 0\alpha^3, 0\alpha^2\beta^2, \alpha\alpha, \alpha^4, \alpha^3\beta^2, \alpha^2\beta^2\gamma^2. \end{aligned} \tag{4.13}$$

The number N of types of singular points on the boundaries of the domains of stability, flutter and divergence rapidly increases with the increase in the number of

parameters n [284]:

n	1	2	3	4	5	6	7	8	9
N	2	4	8	16	28	49	83	142	228

The list (4.13) gives a qualitative understanding of what the boundaries of the domains of stability, flutter and divergence of generic circulatory systems look like if the number of parameters $n \leq 3$. Sensitivity analysis of multiple eigenvalues [548] is one of the means to provide quantitative information on the geometry of the boundaries near the singularities [459, 460, 518].

4.4 Perturbation of eigenvalues

Suppose that at a point $\mathbf{p}_0 \in \mathbb{R}^n$ the spectrum of the matrix $\mathbf{A}(\mathbf{p}_0)$ contains an eigenvalue σ_0. Considering a smooth one-parameter curve issuing from the point $\mathbf{p}_0$, say $\mathbf{p}(\varepsilon)$, $\varepsilon \geq 0$, let us expand the function $\mathbf{p}(\varepsilon)$ in Taylor series in the neighborhood of $\varepsilon = 0$

$$\mathbf{p}(\varepsilon) = \mathbf{p}_0 + \varepsilon \frac{d\mathbf{p}}{d\varepsilon} + \frac{\varepsilon^2}{2}\frac{d^2\mathbf{p}}{d\varepsilon^2} + o(\varepsilon^2), \tag{4.14}$$

where the derivatives are evaluated at $\varepsilon = 0$. Then,

$$\mathbf{A}=\mathbf{A}(\mathbf{p}_0)+\varepsilon\sum_{s=1}^{n}\frac{dp_s}{d\varepsilon}\partial_{p_s}\mathbf{A}+\frac{1}{2}\varepsilon^2\left(\sum_{s=1}^{n}\frac{d^2p_s}{d\varepsilon^2}\partial_{p_s}\mathbf{A}+\sum_{s,t=1}^{n}\frac{dp_s}{d\varepsilon}\frac{dp_t}{d\varepsilon}\partial_{p_s}\partial_{p_t}\mathbf{A}\right)+o(\varepsilon^2). \tag{4.15}$$

The derivatives of $\mathbf{A}$ with respect to the parameters are evaluated at the point $\mathbf{p}_0$ and may be expressed via $\mathbf{M}$ and $\mathbf{C}$ as [274]

$$\partial_{p_s}\mathbf{A} = \mathbf{M}_0\partial_{p_s}\mathbf{C} - \mathbf{M}_0^{-1}\partial_{p_s}\mathbf{M}\mathbf{M}_0^{-1}\mathbf{C}_0, \quad \mathbf{M}_0 = \mathbf{M}(\mathbf{p}_0), \quad \mathbf{C}_0 = \mathbf{C}(\mathbf{p}_0). \tag{4.16}$$

Let $\mathbf{A}_k$ denote the coefficient of ε^k in expansion (4.15), and let

$$\mathbf{e} = \left.\frac{d\mathbf{p}}{d\varepsilon}\right|_{\varepsilon=0}, \quad \mathbf{d} = \left.\frac{1}{2}\frac{d^2\mathbf{p}}{d\varepsilon^2}\right|_{\varepsilon=0}, \tag{4.17}$$

where $\mathbf{e},\ \mathbf{d} \in \mathbb{R}^n$. Then,

$$\mathbf{A}_0 = \mathbf{A}(\mathbf{p}_0), \quad \mathbf{A}_1 = \sum_{s=1}^{n}\partial_{p_s}\mathbf{A}e_s, \quad \mathbf{A}_2 = \sum_{s=1}^{n}\partial_{p_s}\mathbf{A}d_s + \frac{1}{2}\sum_{s,t=1}^{n}\partial^2_{p_s,p_t}\mathbf{A}e_se_t. \tag{4.18}$$

When the vector $\mathbf{p}_0$ is varied as in (4.14), the eigenvalue σ_0 and the eigenvector $\mathbf{u}_0$ get increments that may be expressed as series in integer or fractional powers of ε, depending on the Jordan structure corresponding to σ_0 [258, 379, 548, 584].

4.4.1 Simple eigenvalue

If σ_0 is a simple real eigenvalue of $\mathbf{A}_0$ with the eigenvector $\mathbf{u}_0$, the perturbed eigenvalue $\sigma(\varepsilon)$ and eigenvector $\mathbf{u}(\varepsilon)$ expand into Taylor series [548, 584]

$$\sigma = \sigma_0 + \varepsilon\sigma_1 + \varepsilon^2\sigma_2 + \cdots, \quad \mathbf{u} = \mathbf{u}_0 + \varepsilon\mathbf{w}_1 + \varepsilon^2\mathbf{w}_2 + \cdots. \tag{4.19}$$

Substituting expansions (4.15) and (4.19) into equation (4.9) and equating terms with the same powers of ε, we obtain an eigenvalue problem

$$(\mathbf{A}_0 - \sigma_0\mathbf{I})\mathbf{u}_0 = 0 \tag{4.20}$$

and equations determining corrections to σ_0 and $\mathbf{u}_0$ [274]

$$\begin{aligned}(\mathbf{A}_0 - \sigma_0\mathbf{I})\mathbf{w}_1 &= \sigma_1\mathbf{u}_0 - \mathbf{A}_1\mathbf{u}_0,\\ (\mathbf{A}_0 - \sigma_0\mathbf{I})\mathbf{w}_2 &= \sigma_1\mathbf{w}_1 - \mathbf{A}_1\mathbf{w}_1 + \sigma_2\mathbf{u}_0 - \mathbf{A}_2\mathbf{u}_0.\end{aligned} \tag{4.21}$$

Let $(\mathbf{a}, \mathbf{b}) = \overline{\mathbf{b}}^T\mathbf{a}$ denote the scalar product of vectors $\mathbf{a}, \mathbf{b} \in \mathbb{C}^m$. Together with the problem (4.20), we consider the adjoint eigenvalue problem

$$(\mathbf{A}_0^T - \overline{\sigma}_0\mathbf{I})\mathbf{v}_0 = 0. \tag{4.22}$$

We require the vector $\mathbf{v}_0$ to satisfy the following normalization condition

$$(\mathbf{u}_0, \mathbf{v}_0) = 1. \tag{4.23}$$

Given the vector $\mathbf{u}_0$, condition (4.23) enables us to determine the vector $\mathbf{v}_0$ uniquely. For the perturbed vector $\mathbf{u}$ we use the normalization condition

$$(\mathbf{u}, \mathbf{v}_0) = 1, \tag{4.24}$$

which uniquely determines all the terms σ_i and $\mathbf{w}_i$ in expansions (4.19).

Equations (4.21) are solvable if and only if their right-hand sides are orthogonal to the solution of the homogeneous adjoint eigenvalue problem (4.22). Hence, also using the normalization conditions (4.23) and (4.24), we obtain expressions for the coefficients σ_1 and σ_2 [274, 518]

$$\sigma_1 = (\mathbf{A}_1\mathbf{u}_0, \mathbf{v}_0), \quad \sigma_2 = (\mathbf{A}_2\mathbf{u}_0, \mathbf{v}_0) + (\mathbf{A}_1\mathbf{w}_1, \mathbf{v}_0). \tag{4.25}$$

The vector $\mathbf{w}_1$ is found from the first of equations (4.21) as

$$\mathbf{w}_1 = \mathbf{G}_0(\sigma_1\mathbf{I} - \mathbf{A}_1), \tag{4.26}$$

The first equality of (4.25) is a necessary and sufficient condition for the existence of the inverse operator $\mathbf{G}_0$, which is expressed via a nonsingular matrix

$$\mathbf{G}_0 = [\mathbf{A}_0 - \sigma_0\mathbf{I} - \overline{\mathbf{v}}_0\mathbf{v}_0^T]^{-1}. \tag{4.27}$$

Let $\langle \mathbf{a}, \mathbf{b} \rangle = \mathbf{b}^T \mathbf{a}$ be a scalar product of the vectors $\mathbf{a}$,$\mathbf{b} \in \mathbb{R}^n$. Introducing the real vector $\mathbf{g}$ with the components

$$g_s = \left(\partial_{p_s} \mathbf{A} \mathbf{u}_0, \mathbf{v}_0 \right), \tag{4.28}$$

we find

$$\sigma_1 = \langle \mathbf{g}, \mathbf{e} \rangle . \tag{4.29}$$

When $\mathbf{e} = \mathbf{e}_*$ is determined by the constraint $\langle \mathbf{g}, \mathbf{e}_* \rangle = 0$, then

$$\sigma_2 = - \langle \mathbf{E} \mathbf{e}_*, \mathbf{e}_* \rangle + \langle \mathbf{g}, \mathbf{d} \rangle , \tag{4.30}$$

where the real symmetric $n \times n$ matrix $\mathbf{E}$ has the entries E_{jk}, $j, k = 1, \ldots, n$,

$$\begin{aligned} 2E_{jk} = &-(\partial^2_{p_k, p_j} \mathbf{A} \mathbf{u}_0, \mathbf{v}_0) \\ &+ (\mathbf{G}_0(\partial_{p_k} \mathbf{A}, \mathbf{u}_0), \partial_{p_j} \mathbf{A}^T \mathbf{v}_0) + (\mathbf{G}_0(\partial_{p_j} \mathbf{A}, \mathbf{u}_0), \partial_{p_k} \mathbf{A}^T \mathbf{v}_0). \end{aligned} \tag{4.31}$$

4.4.2 Double eigenvalue of geometric multiplicity 1

If σ_0 is a two-fold real eigenvalue with the Jordan chain of length 2, an eigenvector $\mathbf{u}_0$ and an associated vector $\mathbf{u}_1$ exist satisfying the equations

$$(\mathbf{A}_0 - \sigma_0 \mathbf{I}) \mathbf{u}_0 = 0, \quad (\mathbf{A}_0 - \sigma_0 \mathbf{I}) \mathbf{u}_1 = \mathbf{u}_0, \tag{4.32}$$

as well as an eigenvector and an associated vector of the adjoint system

$$(\mathbf{A}_0^T - \overline{\sigma}_0 \mathbf{I}) \mathbf{v}_0 = 0, \quad (\mathbf{A}_0^T - \overline{\sigma}_0 \mathbf{I}) \mathbf{v}_1 = \mathbf{v}_0. \tag{4.33}$$

The vectors $\mathbf{u}_0$, $\mathbf{u}_1$, $\mathbf{v}_0$ and $\mathbf{v}_1$ are orthonormalized as

$$(\mathbf{u}_0, \mathbf{v}_0) = 0, \quad (\mathbf{u}_1, \mathbf{v}_0) = (\mathbf{u}_0, \mathbf{v}_1) = 1. \tag{4.34}$$

Generic case

With the variation of parameters (4.14), the perturbed double eigenvalue and its eigenvector are represented by the Newton–Puiseux series [258, 584]

$$\begin{aligned} \sigma &= \sigma_0 + \varepsilon^{1/2} \sigma_1 + \varepsilon \sigma_2 + \varepsilon^{3/2} \sigma_3 + \cdots , \\ \mathbf{u} &= \mathbf{u}_0 + \varepsilon^{1/2} \mathbf{w}_1 + \varepsilon \mathbf{w}_2 + \varepsilon^{3/2} \mathbf{w}_3 + \cdots , \end{aligned} \tag{4.35}$$

where $\mathbf{u}$ is assumed to satisfy the normalization condition

$$(\mathbf{u}, \mathbf{v}_1) = 1. \tag{4.36}$$

Substituting expressions (4.15) and (4.35) into eigenvalue problem (4.9), we obtain equations determining the corrections to σ_0 and $\mathbf{u}_0$

$$\begin{aligned}
&(\mathbf{A}_0 - \sigma_0\mathbf{I})\mathbf{w}_1 = \sigma_1\mathbf{u}_0, \\
&(\mathbf{A}_0 - \sigma_0\mathbf{I})\mathbf{w}_2 = -\mathbf{A}_1\mathbf{u}_0 + \sigma_1\mathbf{w}_1 + \sigma_2\mathbf{u}_0, \\
&(\mathbf{A}_0 - \sigma_0\mathbf{I})\mathbf{w}_4 = -\mathbf{A}_1\mathbf{w}_2 - \mathbf{A}_2\mathbf{u}_0 + \sigma_1\mathbf{w}_3 + \sigma_2\mathbf{w}_2 + \sigma_3\mathbf{w}_1 + \sigma_4\mathbf{u}_0.
\end{aligned} \tag{4.37}$$

An expression for the vector $\mathbf{w}_1$ follows from the first of equations (4.37)

$$\mathbf{w}_1 = \sigma_1(\mathbf{u}_1 - \mathbf{u}_0(\mathbf{u}_1, \mathbf{v}_1)). \tag{4.38}$$

The second of equations (4.37) is solvable if and only if its right-hand side is orthogonal to the vector $\mathbf{v}_0$. By (4.34) and (4.38), this condition takes the form

$$\sigma_1^2 = (\mathbf{A}_1\mathbf{u}_0, \mathbf{v}_0). \tag{4.39}$$

By means of equation (4.27), the third of equations (4.37) yields the vector $\mathbf{w}_2$

$$\mathbf{w}_2 = \mathbf{G}_0(\sigma_1\mathbf{w}_1 + \sigma_2\mathbf{u}_0 - \mathbf{A}_1\mathbf{u}_0). \tag{4.40}$$

Introducing the real vector $\mathbf{f} \in \mathbb{R}^n$ with the coefficients

$$f_s = \left(\partial_{p_s}\mathbf{A}\mathbf{u}_0, \mathbf{v}_0\right) \tag{4.41}$$

we write equation (4.39) in the form

$$\sigma_1^2 = \langle \mathbf{f}, \mathbf{e} \rangle . \tag{4.42}$$

equations (4.42) and (4.35) describe splitting of the double eigenvalue σ_0 with the Jordan chain of second order in the generic case when $(\mathbf{A}_1\mathbf{u}_0, \mathbf{v}_0) \neq 0$.

Degenerate case

In the degenerate case, when

$$(\mathbf{A}_1\mathbf{u}_0, \mathbf{v}_0) = 0, \tag{4.43}$$

the perturbed eigenvector $\mathbf{u}$ and eigenvalue σ are determined by terms of order ε [32, 33, 584], i.e. by the coefficients $\mathbf{w}_2$ and σ_2, since now in (4.35) we have

$$\sigma_1 = 0, \quad \mathbf{w}_1 = 0. \tag{4.44}$$

In order to find the coefficient σ_2, we write down the condition for the third of equations (4.37) to be solvable. Taking the normalization condition (4.34) and degeneracy condition (4.43) into consideration, we obtain

$$\sigma_2(\mathbf{w}_2, \mathbf{v}_0) - (\mathbf{A}_1\mathbf{w}_2, \mathbf{v}_0) - (\mathbf{A}_2\mathbf{u}_0, \mathbf{v}_0) = 0. \tag{4.45}$$

Multiplying both sides of the second of equations (4.37) by $\mathbf{v}_1$, we get

$$(\mathbf{w}_2, \mathbf{v}_0) = \sigma_2 - (\mathbf{A}_1\mathbf{u}_0, \mathbf{v}_1). \tag{4.46}$$

Substituting expressions (4.40) and (4.46) into equation (4.45), we find that in the degenerate case the coefficient σ_2 is determined by the equation [32, 33, 284, 521]

$$\sigma_2^2 - \sigma_2[(\mathbf{A}_1\mathbf{u}_0, \mathbf{v}_1) + (\mathbf{A}_1\mathbf{u}_1, \mathbf{v}_0)] - (\mathbf{A}_2\mathbf{u}_0, \mathbf{v}_0) + (\mathbf{G}_0(\mathbf{A}_1\mathbf{u}_0), \mathbf{A}_1^T\mathbf{v}_0) = 0. \tag{4.47}$$

If the discriminant of equation (4.46) does not vanish, i.e.

$$2\sigma_2 \neq (\mathbf{A}_1\mathbf{u}_0, \mathbf{v}_1) + (\mathbf{A}_1\mathbf{u}_1, \mathbf{v}_0), \tag{4.48}$$

the two-fold eigenvalue σ_0 splits in the degenerate case (4.43). When conditions (4.43) and (4.48) hold simultaneously, all the odd coefficients σ_{2i-1}, $\mathbf{w}_{2i-1}$ in expansions (4.35) vanish. The proof is by induction, see [274].

Introducing a real vector $\mathbf{h}$ with the components

$$2h_s = (\partial_{p_s}\mathbf{A}\mathbf{u}_0, \mathbf{v}_1) + (\partial_{p_s}\mathbf{A}\mathbf{u}_1, \mathbf{v}_0), \tag{4.49}$$

where $s = 1, \ldots, n$, and a real symmetric $n \times n$ matrix $\mathbf{H}$ with the elements

$$\begin{aligned} 2H_{jk} = &-(\partial^2_{p_k,p_j}\mathbf{A}\mathbf{u}_0, \mathbf{v}_0) \\ &+(\mathbf{G}_0(\partial_{p_k}\mathbf{A}, \mathbf{u}_0), \partial_{p_j}\mathbf{A}^T\mathbf{v}_0) + (\mathbf{G}_0(\partial_{p_j}\mathbf{A}, \mathbf{u}_0), \partial_{p_k}\mathbf{A}^T\mathbf{v}_0), \end{aligned} \tag{4.50}$$

we find

$$\begin{aligned} (\mathbf{A}\mathbf{u}_1, \mathbf{v}_0) + (\mathbf{A}_1\mathbf{u}_0, \mathbf{v}_1) &= 2\langle \mathbf{h}, \mathbf{e}_* \rangle, \\ -(\mathbf{A}_2\mathbf{u}_0, \mathbf{v}_0) + (\mathbf{G}_0(\mathbf{A}_1\mathbf{u}_0), \mathbf{A}_1^T\mathbf{v}_0) &= \langle \mathbf{H}\mathbf{e}_*, \mathbf{e}_* \rangle - \langle \mathbf{f}, \mathbf{d} \rangle, \end{aligned} \tag{4.51}$$

where the vector $\mathbf{e}_*$ is determined by the condition $\langle \mathbf{f}, \mathbf{e}_* \rangle = 0$.

4.4.3 Double eigenvalue of geometric multiplicity 2

Let at $\mathbf{p}_0$ the double real eigenvalue σ_0 have two linearly independent eigenvectors $\mathbf{u}_1$ and $\mathbf{u}_2$, which corresponds to the reversible semisimple $1:1$ resonance. Let $\mathbf{v}_1$ and $\mathbf{v}_2$ be linearly independent eigenvectors of the adjoint problem. Any linear combination of the vectors $\mathbf{u}_1, \mathbf{u}_2$ or $\mathbf{v}_1, \mathbf{v}_2$ is an eigenvector of the corresponding eigenvalue problem. In the assumption $(\mathbf{u}_i, \mathbf{v}_j) = \delta_{ij}$, where δ_{ij} is the Kronecker symbol and $i, j = 1, 2$, the perturbation theory yields $\sigma = \sigma_0 + \varepsilon\sigma_1 + o(\varepsilon)$ with σ_1 determined by the quadratic equation [155, 284]

$$[\sigma_1 - (\mathbf{A}_1\mathbf{u}_1, \mathbf{v}_1)]\,[\sigma_1 - (\mathbf{A}_1\mathbf{u}_2, \mathbf{v}_2)] - (\mathbf{A}_1\mathbf{u}_1, \mathbf{v}_2)\,(\mathbf{A}_1\mathbf{u}_2, \mathbf{v}_1) = 0. \tag{4.52}$$

Therefore,

$$\sigma = \sigma_0 + \varepsilon\frac{(\mathbf{A}_1\mathbf{u}_1, \mathbf{v}_1) + (\mathbf{A}_1\mathbf{u}_2, \mathbf{v}_2)}{2} \pm \frac{\varepsilon}{2}\sqrt{D} + o(\varepsilon), \tag{4.53}$$

where $D = \langle \mathbf{f}_*, \mathbf{e}\rangle^2 + \langle \mathbf{f}_+, \mathbf{e}\rangle^2 - \langle \mathbf{f}_-, \mathbf{e}\rangle^2$, the matrix $\mathbf{A}_1$ is determined in (4.18), and the s-th components of the real vectors $\mathbf{f}_*$, $\mathbf{f}_+$, and $\mathbf{f}_-$ are

$$f_{*,s} = \left(\partial_{p_s}\mathbf{A}\mathbf{u}_1, \mathbf{v}_1\right) - \left(\partial_{p_s}\mathbf{A}\mathbf{u}_2, \mathbf{v}_2\right), \quad f_{\pm,s} = \left(\partial_{p_s}\mathbf{A}\mathbf{u}_1, \mathbf{v}_2\right) \pm \left(\partial_{p_s}\mathbf{A}\mathbf{u}_2, \mathbf{v}_1\right). \tag{4.54}$$

4.4.4 Triple eigenvalue of geometric multiplicity 1

Let a triple real eigenvalue σ_0 have the Jordan chains consisting of the right and left eigenvectors $\mathbf{u}_0$ and $\mathbf{v}_0$, and associated vectors $\mathbf{u}_1$, $\mathbf{u}_2$ and $\mathbf{v}_1$, $\mathbf{v}_2$

$$\begin{aligned} &(\mathbf{A}_0 - \sigma_0\mathbf{I})\,\mathbf{u}_0 = 0, \quad &&\left(\mathbf{A}_0^T - \overline{\sigma}_0\mathbf{I}\right)\mathbf{v}_0 = 0,\\ &(\mathbf{A}_0 - \sigma_0\mathbf{I})\,\mathbf{u}_1 = \mathbf{u}_0, \quad &&\left(\mathbf{A}_0^T - \overline{\sigma}_0\mathbf{I}\right)\mathbf{v}_1 = \mathbf{v}_0,\\ &(\mathbf{A}_0 - \sigma_0\mathbf{I})\,\mathbf{u}_2 = \mathbf{u}_1, \quad &&\left(\mathbf{A}_0^T - \overline{\sigma}_0\mathbf{I}\right)\mathbf{v}_2 = \mathbf{v}_1, \end{aligned} \tag{4.55}$$

where

$$\begin{aligned} &(\mathbf{u}_0, \mathbf{v}_0) = 0, \quad (\mathbf{u}_1, \mathbf{v}_0) = 0, \quad (\mathbf{u}_0, \mathbf{v}_1) = 0,\\ &(\mathbf{u}_2, \mathbf{v}_1) = (\mathbf{u}_1, \mathbf{v}_2), \quad (\mathbf{u}_2, \mathbf{v}_0) = (\mathbf{u}_1, \mathbf{v}_1) = (\mathbf{u}_0, \mathbf{v}_2). \end{aligned} \tag{4.56}$$

Additionally, we assume that

$$(\mathbf{u}_0, \mathbf{v}_2) = 1, \quad (\mathbf{u}, \mathbf{v}_2) = 1. \tag{4.57}$$

Generic case

Generically, perturbation $\mathbf{p} = \mathbf{p}_0 + \varepsilon\mathbf{e} + \varepsilon^2\mathbf{d}$ yields splitting of the triple eigenvalue σ_0 into three simple eigenvalues [584]

$$\begin{aligned} &\sigma = \sigma_0 + \varepsilon^{1/3}\sigma_1 + \varepsilon^{2/3}\sigma_2 + \varepsilon\sigma_3 + \ldots,\\ &\mathbf{u} = \mathbf{u}_0 + \varepsilon^{1/3}\mathbf{w}_1 + \varepsilon^{2/3}\mathbf{w}_2 + \varepsilon\mathbf{w}_3 + \ldots. \end{aligned} \tag{4.58}$$

Proceeding similarly to the case of a double eigenvalue we find σ_1

$$\sigma_1^3 = (\mathbf{A}_1\mathbf{u}_0, \mathbf{v}_0) \equiv \langle \mathbf{q}, \mathbf{e}\rangle, \tag{4.59}$$

where the s-th component of the real vector $\mathbf{q}$ is

$$q_s = \left(\partial_{p_s}\mathbf{A}\mathbf{u}_0, \mathbf{v}_0\right). \tag{4.60}$$

Primary degeneracy

When the right-hand side of equation (4.59) vanishes, the triple eigenvalue splits into three simple ones in other ways. Two of the three perturbed eigenvalues and the corresponding eigenvectors expand as

$$\begin{aligned} &\sigma = \sigma_0 + \varepsilon^{1/2}\sigma_1 + \varepsilon\sigma_2 + \varepsilon^{3/2}\sigma_3 + \cdots,\\ &\mathbf{u} = \mathbf{u}_0 + \varepsilon^{1/2}\mathbf{w}_1 + \varepsilon\mathbf{w}_2 + \varepsilon^{3/2}\mathbf{w}_3 + \cdots, \end{aligned} \tag{4.61}$$

while for the third perturbed eigenvalue and its eigenvector we have

$$\sigma = \sigma_0 + \varepsilon\mu_1 + \varepsilon^2\mu_2 + \cdots, \quad \mathbf{u} = \mathbf{u}_0 + \varepsilon\mathbf{z}_1 + \varepsilon^2\mathbf{z}_2 + \cdots. \tag{4.62}$$

Substituting (4.61) and (4.15) into (4.9) yields

$$\begin{aligned}
&(\mathbf{A}_0 - \sigma_0\mathbf{I})\,\mathbf{w}_1 = \sigma_1\mathbf{u}_0,\\
&(\mathbf{A}_0 - \sigma_0\mathbf{I})\,\mathbf{w}_2 = \sigma_1\mathbf{w}_1 - \mathbf{A}_1\mathbf{u}_0 + \sigma_2\mathbf{u}_0,\\
&(\mathbf{A}_0 - \sigma_0\mathbf{I})\,\mathbf{w}_3 = \sigma_1\mathbf{w}_2 - \mathbf{A}_1\mathbf{w}_1 + \sigma_2\mathbf{w}_1 + \sigma_3\mathbf{u}_0.
\end{aligned} \tag{4.63}$$

The vector $\mathbf{w}_1 = \mathbf{G}_0(\sigma_1\mathbf{u}_0) = \sigma_1\mathbf{u}_1 + c\mathbf{u}_0$ is found with the use of the first of the equations (4.63). The coefficient $c = -\sigma_1(\mathbf{u}_1, \mathbf{v}_2)$ is determined from the normalization conditions (4.57). The solvability condition written for the third of the equations (4.63), with the use of (4.56) yields

$$(\mathbf{w}_2, \mathbf{v}_0) = (\mathbf{A}_1\mathbf{u}_1, \mathbf{v}_0). \tag{4.64}$$

Multiplying the second of the equations (4.63) by $\mathbf{v}_1$ and using equations (4.56) and (4.57) and the expression for the vector $\mathbf{w}_1$, we get

$$\sigma_1^2 = (\mathbf{w}_2, \mathbf{v}_0) + (\mathbf{A}_1\mathbf{u}_0, \mathbf{v}_1). \tag{4.65}$$

Expressions (4.64) and (4.65) yield the coefficient σ_1 in equation (4.61)

$$\sigma_1^2 = (\mathbf{A}_1\mathbf{u}_1, \mathbf{v}_0) + (\mathbf{A}_1\mathbf{u}_0, \mathbf{v}_1). \tag{4.66}$$

Introducing the real vector $\mathbf{r}$ with the components

$$r_s = \left(\partial_{p_s}\mathbf{A}\mathbf{u}_1, \mathbf{v}_0\right) + \left(\partial_{p_s}\mathbf{A}\mathbf{u}_0, \mathbf{v}_1\right), \tag{4.67}$$

we rewrite the equation (4.66) in the form [284]

$$\sigma_1 = \pm\sqrt{\langle\mathbf{r}, \mathbf{e}_*\rangle}, \tag{4.68}$$

where the vector $\mathbf{e}_*$ is determined by the condition $\langle\mathbf{q}, \mathbf{e}_*\rangle = 0$. Similarly, we obtain the coefficient μ_1 in the expansions (4.62) [284]

$$\mu_1 = \frac{\left(\mathbf{G}_0(\mathbf{A}_1\mathbf{u}_0), \mathbf{A}_1^T\mathbf{v}_0\right) - (\mathbf{A}_2\mathbf{u}_0, \mathbf{v}_0)}{(\mathbf{A}_1\mathbf{u}_1, \mathbf{v}_0) + (\mathbf{A}_1\mathbf{u}_0, \mathbf{v}_1)}. \tag{4.69}$$

This formula can be expressed by means of a real matrix $\mathbf{R}$ as

$$\mu_1 = \frac{\langle\mathbf{R}\mathbf{e}_*, \mathbf{e}_*\rangle - \langle\mathbf{q}, \mathbf{d}\rangle}{\langle\mathbf{r}, \mathbf{e}_*\rangle}. \tag{4.70}$$

Equations (4.61) and (4.62) with the coefficients (4.68) and (4.70) describe the splitting of the triple real eigenvalue σ_0 in the degenerate case $(\mathbf{A}_1\mathbf{u}_0, \mathbf{v}_0) \equiv \langle\mathbf{q}, \mathbf{e}_*\rangle = 0$ where $\langle\mathbf{r}, \mathbf{e}_*\rangle \neq 0$.

Secondary degeneracy

In case of the double degeneracy when simultaneously the right-hand sides in both equation (4.59) and equation (4.66) vanish, the triple eigenvalue expands as $\sigma = \sigma_0 + \varepsilon\sigma_1 + o(\varepsilon)$, where σ_1 is one of the roots of the equation

$$\sigma_1^3 + a_1\sigma_1^2 + a_2\sigma_1 + a_3 = 0, \tag{4.71}$$

with the coefficients [284]

$$\begin{aligned}
a_1 &= -(\mathbf{A}_1\mathbf{u}_0, \mathbf{v}_2) - (\mathbf{A}_1\mathbf{u}_1, \mathbf{v}_1) - (\mathbf{A}_1\mathbf{u}_2, \mathbf{v}_0),\\
a_2 &= -(\mathbf{A}_2\mathbf{u}_0, \mathbf{v}_1) - (\mathbf{A}_2\mathbf{u}_1, \mathbf{v}_0) + \left(\mathbf{G}_0(\mathbf{A}_1\mathbf{u}_0), \mathbf{A}_1^T\mathbf{v}_1\right)\\
&\quad + \left(\mathbf{G}_0(\mathbf{A}_1\mathbf{u}_1), \mathbf{A}_1^T\mathbf{v}_0\right) + \left(\mathbf{G}_0\mathbf{G}_0(\mathbf{A}_1\mathbf{u}_0), \mathbf{A}_1^T\mathbf{v}_0\right),\\
a_3 &= -(\mathbf{A}_3\mathbf{u}_0, \mathbf{v}_0) + \left(\mathbf{G}_0(\mathbf{A}_2\mathbf{u}_0), \mathbf{A}_1^T\mathbf{v}_0\right) + \left(\mathbf{G}_0(\mathbf{A}_1\mathbf{u}_0), \mathbf{A}_2^T\mathbf{v}_0\right)\\
&\quad - \left(\mathbf{G}_0\mathbf{A}_1\mathbf{G}_0(\mathbf{A}_1\mathbf{u}_0), \mathbf{A}_1^T\mathbf{v}_0\right).
\end{aligned} \tag{4.72}$$

We can write $a_1 = -\langle \mathbf{k}, \mathbf{e}_* \rangle$, where the real vector $\mathbf{k}$ has the components

$$k_s = \left(\partial_{p_s}\mathbf{A}\mathbf{u}_0, \mathbf{v}_2\right) + \left(\partial_{p_s}\mathbf{A}\mathbf{u}_1, \mathbf{v}_1\right) + \left(\partial_{p_s}\mathbf{A}\mathbf{u}_2, \mathbf{v}_0\right). \tag{4.73}$$

4.5 Geometry of the stability boundary

Now we are prepared for probing the parameter space in the vicinity of the points with multiple eigenvalues in order to find directions of parameters variation leading either to the domain of stability or to that of flutter/divergence.

4.5.1 Linear and quadratic approximations at smooth points

Consider a point $\mathbf{p}_0$ on the hypersurfaces of the type α^2 and 0 in the space of parameters, where there exists either a double real eigenvalue $\sigma_0 > 0$ with the Jordan chain of length 2 or a simple zero eigenvalue while all the remaining eigenvalues are simple and positive. Then, the vectors $\mathbf{g} \neq 0$ and $\mathbf{f} \neq 0$ are normals at $\mathbf{p}_0$ to the stability boundary in its smooth parts [274].

Indeed, according to equations (4.19), (4.29) and equations (4.35), (4.42)

$$\sigma(\varepsilon) = \langle \mathbf{g}, \mathbf{e} \rangle \varepsilon + o(\varepsilon), \quad \sigma(\varepsilon) = \sigma_0 \pm \sqrt{\langle \mathbf{f}, \mathbf{e} \rangle \varepsilon} + o(\varepsilon^{1/2}). \tag{4.74}$$

When $\langle \mathbf{g}, \mathbf{e} \rangle > 0$, a slight variation of the parameters along the curve (4.14), which generically is transversal to the stability boundary, turns zero eigenvalue into $\sigma(\varepsilon) > 0$, implying stability. Similarly, when $\langle \mathbf{f}, \mathbf{e} \rangle > 0$, the two-fold eigenvalue σ_0 bifurcates into two simple positive ones (stability). However, if $\langle \mathbf{g}, \mathbf{e} \rangle < 0$, we have $\sigma(\varepsilon) < 0$

(divergence) and if $\langle \mathbf{f}, \mathbf{e} \rangle < 0$, the double eigenvalue splits into a complex-conjugate pair (flutter). Thus, evaluated at a nonsingular point $\mathbf{p}_0$ of the stability boundary, the vectors $\mathbf{g}$ and $\mathbf{f}$ point into the stability domain along the normal to the boundary. A linear approximation to the stability boundary at $\mathbf{p}_0$ is given by the tangent planes

$$\langle \mathbf{g}, \Delta\mathbf{p} \rangle = 0 \ \text{ or } \ \langle \mathbf{f}, \Delta\mathbf{p} \rangle = 0, \tag{4.75}$$

where $\Delta\mathbf{p} = \mathbf{p} - \mathbf{p}_0$, provided that $\langle \mathbf{g}, \mathbf{e} \rangle \neq 0$ and $\langle \mathbf{f}, \mathbf{e} \rangle \neq 0$.

The geometrical meaning of the vector $\mathbf{h}$ and the matrices $\mathbf{E}$ and $\mathbf{H}$ defined by equations (4.49), (4.31) and (4.50) is related to the quadratic approximation of the stability domain. In order to establish it, consider the curves

$$\mathbf{p}(\varepsilon) = \mathbf{p}_0 + \varepsilon \mathbf{e}_* + \varepsilon^2 \mathbf{d} + o(\varepsilon^2), \tag{4.76}$$

which are tangent to the stability boundary at $\varepsilon = 0$, i.e. either

$$\langle \mathbf{g}, \mathbf{e}_* \rangle = 0, \quad or \quad \langle \mathbf{f}, \mathbf{e}_* \rangle = 0. \tag{4.77}$$

Let $\mathbf{p}_0$ be a point on the boundary between the stability and divergence domains. By condition (4.77), the coefficient σ_1 in series (4.19) vanishes, and

$$\sigma = \frac{1}{2} \left\langle \mathbf{g}, \frac{d^2\mathbf{p}}{d\varepsilon^2} \right\rangle \varepsilon^2 - \left\langle \mathbf{E} \frac{d\mathbf{p}}{d\varepsilon}, \frac{d\mathbf{p}}{d\varepsilon} \right\rangle \varepsilon^2 + o(\varepsilon^2) \tag{4.78}$$

Similarly, assuming $\mathbf{p}_0$ belongs to the boundary between stability and flutter domains, we find that the bifurcation of the two-fold eigenvalue σ_0 along the curves (4.76) tangent to the stability boundary is defined by the equation

$$\left(\sigma - \sigma_0 - \left\langle \mathbf{h}, \frac{d\mathbf{p}}{d\varepsilon} \right\rangle \varepsilon \right)^2 = \frac{1}{2} \left\langle \mathbf{f}, \frac{d^2\mathbf{p}}{d\varepsilon^2} \right\rangle \varepsilon^2 - \left\langle \mathbf{H} \frac{d\mathbf{p}}{d\varepsilon}, \frac{d\mathbf{p}}{d\varepsilon} \right\rangle \varepsilon^2 + \left\langle \mathbf{h}, \frac{d\mathbf{p}}{d\varepsilon} \right\rangle^2 \varepsilon^2 + o(\varepsilon^2). \tag{4.79}$$

Along the curves (4.76) lying on the stability boundary a simple zero eigenvalue remains equal to zero and a two-fold eigenvalue does not bifurcate. A necessary condition for this to occur is that the right-hand sides in equations (4.78) and (4.79) vanish. Taking into consideration that on these curves

$$\langle \mathbf{g}, \Delta\mathbf{p} \rangle = \frac{1}{2} \left\langle \mathbf{g}, \frac{d^2\mathbf{p}}{d\varepsilon^2} \right\rangle \varepsilon^2 + o(\varepsilon^2), \quad \langle \mathbf{f}, \Delta\mathbf{p} \rangle = \frac{1}{2} \left\langle \mathbf{f}, \frac{d^2\mathbf{p}}{d\varepsilon^2} \right\rangle \varepsilon^2 + o(\varepsilon^2), \tag{4.80}$$

we find that the stability boundary of the circulatory system (4.8) in the neighborhood of a nonsingular point is described up to $o(\|\Delta\mathbf{p}\|^2)$ by the equations

$$F_1(\Delta\mathbf{p}) := \langle \mathbf{g}, \Delta\mathbf{p} \rangle - G_1(\Delta\mathbf{p}) = 0, \quad F_2(\Delta\mathbf{p}) := \langle \mathbf{f}, \Delta\mathbf{p} \rangle - G_2(\Delta\mathbf{p}) = 0, \tag{4.81}$$

where

$$G_1(\Delta\mathbf{p}) = \langle \mathbf{E}\Delta\mathbf{p}, \Delta\mathbf{p} \rangle, \quad G_2(\Delta\mathbf{p}) = \langle (\mathbf{H} - \mathbf{h}\mathbf{h}^T)\Delta\mathbf{p}, \Delta\mathbf{p} \rangle. \tag{4.82}$$

when the stability domain borders on the divergence domain or when it has a common boundary with the flutter domain, respectively. It follows from equation (4.79) that the flutter domain is defined by the inequality $F_2 < 0$, and the stability domain, accordingly, is defined by the inequality $F_2 > 0$.

Considering vectors $\Delta\mathbf{p}$ belonging to the tangent plane (4.75), we deduce from the condition $F_2 > 0$ that if the quadratic form $G_2(\Delta\mathbf{p})$ is negative- (positive-) definite in the set (4.75), then the stability domain is concave (convex) and the flutter domain is convex (concave), since the tangent plane is contained in the stability (flutter) domain. Using equation (4.78) and reasoning in a similar way, we conclude that if the quadratic form $G_1(\Delta\mathbf{p})$ is negative (positive) definite in the set (4.75), the divergence domain $F_1 < 0$ is convex (concave) and the stability domain $F_1 > 0$ is concave (convex) [274].

4.5.2 Singularities in two-parameter circulatory systems

Theorem 4.3 (A. P. Seyranian and O. N. Kirillov, 2001 [284, 521]). *Let the circulatory system* (4.8) *depend on two parameters p_1 and p_2. Then, the boundary between the domain of stability and the domains of flutter and divergence in the (p_1, p_2)-plane is piecewise smooth. It consists of smooth curves of the types α^2 and 0 that generically are connected to each other at the singular points of the four types:*

$$0^2, \alpha^3 \quad (\textit{cuspidal points}) \quad \textit{and} \quad 0\alpha^2, \alpha^2\beta^2 \quad (\textit{transversal intersections}).$$

The singularities listed in Theorem 4.3 are generic in two-parameter circulatory systems and cannot be removed by small variations of the family $\mathbf{A}(p_1, p_2)$.

Definition 4.4 (L. V. Levantovskii, 1980 [374, 375]). A *tangent cone* to a set Z at the points of its boundary is a set of directions in which from the given point one can send a curve that lies in the set Z. The tangent cone is generic if it cuts a set of nonzero measure on a sphere. Otherwise, it is degenerate.

A smooth curve α^2, $\alpha > 0$

Consider a point $\mathbf{p}_0$ on the curve α^2 in the (p_1, p_2)-plane, corresponding to the double real eigenvalue $\sigma_0 = \alpha > 0$ with the Jordan chain of length 2, while other eigenvalues σ are simple and positive, Figure 4.1 (a). Then, from equation (4.74) it follows that if $\langle \mathbf{f}, \mathbf{e} \rangle > 0$, then at sufficiently small ε the vectors $\varepsilon\mathbf{e}$ are in the stability domain and if $\langle \mathbf{f}, \mathbf{e} \rangle < 0$, then the vectors $\varepsilon\mathbf{e}$ belong to the flutter domain. The tangent cone to the stability domain is a half-plane

$$K_S = \{\mathbf{e} : \ \langle \mathbf{f}, \mathbf{e} \rangle > 0\}.$$

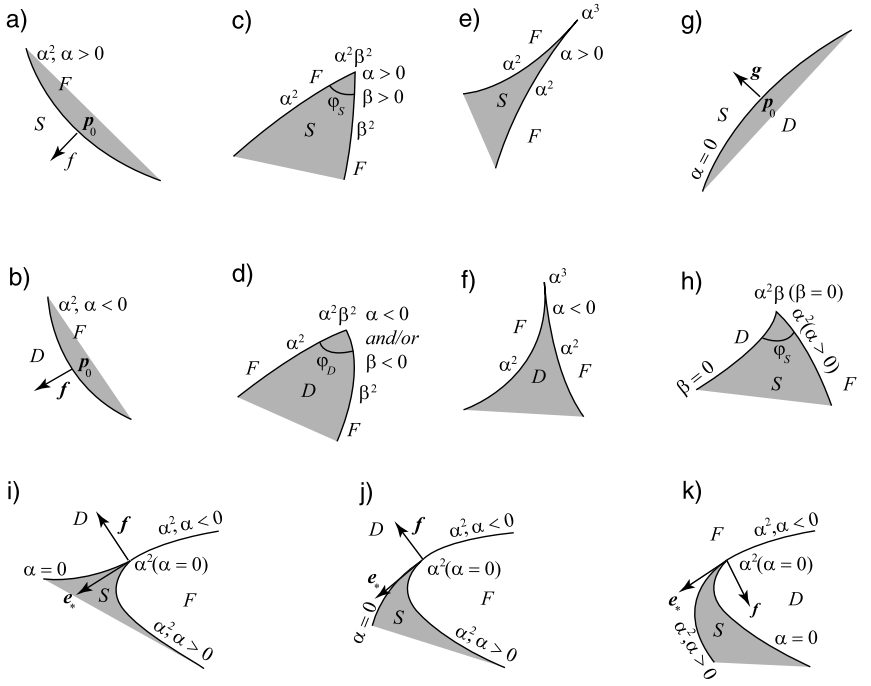

Figure 4.1. Boundaries between domains of stability (S), divergence (D), and flutter (F) and their generic singularities in two-parameter circulatory systems [284, 521].

Therefore, the curve α^2 ($\alpha > 0$) is a boundary between the domains of stability and flutter and the normal $\mathbf{f}$ points to the stability domain, Figure 4.1 (a).

If $G_2(\mathbf{e}_*) < 0$ for the vector of variation $\mathbf{e}_*$ tangent to the boundary ($\langle \mathbf{f}, \mathbf{e}_* \rangle = 0$), then the double eigenvalue α splits into two real ones; hence $\mathbf{e}_*$ points to the stability domain, which is thus concave. If $G_2(\mathbf{e}_*) > 0$, then $\mathbf{e}_*$ points to the flutter domain because α splits into a complex-conjugate pair. The stability domain at $\mathbf{p} = \mathbf{p}_0$ is then convex.

A smooth curve α^2, $\alpha < 0$

Let $\alpha < 0$ at the points of the curve α^2 while other eigenvalues σ are simple and positive, Figure 4.1 (b). Then, the set $K_D = \{\mathbf{e} : \langle \mathbf{f}, \mathbf{e} \rangle < 0\}$ is a tangent cone to the divergence domain and the inequality $\langle \mathbf{f}, \mathbf{e} \rangle < 0$ defines the tangent cone to the flutter domain at the point $\mathbf{p} = \mathbf{p}_0$. Therefore, the curve α^2 ($\alpha < 0$) is the boundary between the domains of flutter and divergence. The vector $\mathbf{f}$ is orthogonal to the boundary and points to the domain of divergence, Figure 4.1 (b). The flutter domain is convex at $\mathbf{p}_0$, if $G_2(\mathbf{e}_*) < 0$ and concave otherwise.

Transversal intersection $\alpha^2\beta^2$

At the singularity $\alpha^2\beta^2$ two smooth curves of the types α^2 and β^2 intersect each other under a nonzero angle, i.e. *transversally* [17], so that the boundary between stability (or divergence) and flutter is broken, Figure 4.1(c, d). The matrix $\mathbf{A}$ then contains two Jordan blocks of second order with the different real eigenvalues α and β.

Let us denote by $\mathbf{f}^\alpha$ ($\mathbf{f}^\beta$) the vector $\mathbf{f}$ corresponding to the eigenvalue α (β). In accordance with (4.74) the variation of parameters along the vectors $\mathbf{e}$, satisfying the inequalities $\langle \mathbf{f}^\alpha, \mathbf{e}\rangle < 0$ or $\langle \mathbf{f}^\beta, \mathbf{e}\rangle < 0$, yields splitting of α (or β) into pairs of complex-conjugate eigenvalues (flutter) and into two positive real ones otherwise (stability) when $\alpha > 0$ and $\beta > 0$. Therefore, at the point $\alpha^2\beta^2$ ($\alpha > 0, \beta > 0$) with other eigenvalues being simple and positive, the stability domain intrudes into the flutter domain in such a manner that the angle of the wedge $\varphi_S < \pi$, Figure 4.1 (c). The tangent cone to the stability domain is then

$$K_S = \left\{\mathbf{e} :\ \langle \mathbf{f}^\alpha, \mathbf{e}\rangle > 0,\ \langle \mathbf{f}^\beta, \mathbf{e}\rangle > 0\right\}. \tag{4.83}$$

When at least one of the eigenvalues α or β is negative and the remaining eigenvalues σ are simple and positive, the singularity $\alpha^2\beta^2$ is on the boundary between the domains of flutter and divergence, Figure 4.1 (d). The divergence domain at this point intrudes into the flutter domain with the angle $\varphi_D < \pi$. The $\langle \mathbf{f}^\alpha, \mathbf{e}\rangle > 0$ and $\langle \mathbf{f}^\beta, \mathbf{e}\rangle > 0$ is a tangent cone to the divergence domain.

The cuspidal point α^3

At this point $\mathbf{A}$ has a Jordan block of order 3 with the real eigenvalue α. Equations (4.58) and (4.59) show that the variation of parameters along a direction $\mathbf{e}$, such that $\langle \mathbf{q}, \mathbf{e}\rangle \neq 0$, is accompanied by the splitting of the triple eigenvalue α into one real and two complex ones (flutter) according to the formula

$$\sigma = \alpha + \sqrt[3]{\langle \mathbf{q}, \mathbf{e}\rangle\, \varepsilon} + o(\varepsilon^{1/3}). \tag{4.84}$$

The primary degeneracy condition $\langle \mathbf{q}, \mathbf{e}_*\rangle = 0$ selects a line in the (p_1, p_2)-plane. When the parameters vary along this line, the triple eigenvalue α splits in accordance with equations (4.61) and (4.68) into a couple of real or complex ones

$$\sigma_\pm = \alpha \pm \sqrt{\langle \mathbf{r}, \mathbf{e}_*\rangle\, \varepsilon} + O\left(\varepsilon\right), \tag{4.85}$$

and a simple real eigenvalue, which according to equations (4.62) and (4.70) is

$$\widetilde{\sigma} = \alpha + \varepsilon \frac{\langle \mathbf{R}\mathbf{e}_*, \mathbf{e}_*\rangle}{\langle \mathbf{r}, \mathbf{e}_*\rangle} + o\left(\varepsilon\right). \tag{4.86}$$

The eigenvalue $\widetilde{\sigma}$ remains real irrespectively of $\mathbf{e}_*$. The direction that stabilizes or destabilizes the system is determined by equation (4.85). If for instance $\langle \mathbf{r}, \mathbf{e}_*\rangle > 0$,

then from (4.85) it follows that the vector $\mathbf{e}_*$ is in the stability domain when $\alpha > 0$ and in the divergence domain when $\alpha < 0$. The vector $-\mathbf{e}_*$ is then in the flutter domain for any sign of α, since the variations in this direction yield a pair of complex-conjugate eigenvalues $\sigma_\pm$. Therefore, at the point α^3 the tangent cone to the domain of stability ($\alpha > 0$) or divergence ($\alpha < 0$) is a ray and is therefore degenerate

$$K_{S,D} = \left\{\mathbf{e} : \ \langle \mathbf{q}, \mathbf{e}\rangle = 0, \ \langle \mathbf{r}, \mathbf{e}\rangle > 0\right\}. \tag{4.87}$$

The domain of stability ($\alpha > 0$) or divergence ($\alpha < 0$) at the singularity α^3 intrudes by a narrow tongue into the flutter domain forming a cusp, Figure 4.1 (e, f).

A smooth curve $\alpha = 0$

At the points of a curve of the type 0, the matrix $\mathbf{A}$ contains a simple zero eigenvalue that changes under variation of parameters in accordance with equation (4.74). The set of directions $\mathbf{e}$ in the parameter space such that $\langle \mathbf{g}, \mathbf{e}\rangle > 0$ corresponds to transition to a positive eigenvalue; when $\langle \mathbf{g}, \mathbf{e}\rangle < 0$ the zero eigenvalue becomes a real negative one. If all other eigenvalues are simple and positive, the vector $\mathbf{g}$ is orthogonal to the boundary between the domains of divergence and stability and points to the stability domain, Figure 4.1 (g). The stability domain is concave when $G_1(\mathbf{e}_*) < 0$ and convex otherwise, where $\mathbf{e}_*$ is a tangent vector determined by the condition $\langle \mathbf{g}, \mathbf{e}_*\rangle = 0$ and G_1 is defined by equation (4.82).

Transversal intersection $0\alpha^2$

At the singularity $0\alpha^2$ the matrix $\mathbf{A}$ has the Jordan block of order 2 with the real eigenvalue α and a simple zero eigenvalue. When other eigenvalues are simple and positive and $\alpha > 0$, then from equations (4.74) the tangent cone to the stability domain follows in the form

$$K_S = \{\mathbf{e} : \ \langle \mathbf{f}, \mathbf{e}\rangle > 0, \ \langle \mathbf{g}, \mathbf{e}\rangle > 0\}. \tag{4.88}$$

The opening angle of the tangent cone $\varphi_S < \pi$, Figure 4.1 (h). In the case when $\alpha < 0$, a point of the type $0\alpha^2$ is on the boundary α^2 between the domains of flutter and divergence and does not originate a singularity.

The cuspidal point 0^2

The singular point 0^2 corresponds to the matrix $\mathbf{A}$ with the Jordan block of order 2 with zero eigenvalue. According to equation (4.74) determining splitting of the double eigenvalue $\sigma_0 = 0$, the vectors $\mathbf{e}$ satisfying the inequality $\langle \mathbf{f}, \mathbf{e}\rangle > 0$ are in the divergence domain. The inequality $\langle \mathbf{f}, \mathbf{e}\rangle < 0$ determines the tangent cone to the flutter domain, Figure 4.1 (i–k).

Let the vector $\mathbf{e}_*$ satisfy the condition $\langle \mathbf{f}, \mathbf{e}_* \rangle = 0$, i.e. it is a tangent vector to the boundary. Then from equation (4.79) it follows that for a given vector $\mathbf{e}_*$ it is possible to choose vectors $\mathbf{d}$ such that along the curves (4.76) the double zero eigenvalue will split into two simple positive ones (stability). This happens in the following three different cases.

In the case when $G_2(\mathbf{e}_*) < 0$ and $\langle \mathbf{H}\mathbf{e}_*, \mathbf{e}_* \rangle > 0$, the curves satisfying the inequalities $\langle \mathbf{h}, \mathbf{e}_* \rangle < 0$ and $2G_2(\mathbf{e}_*) < \langle \mathbf{f}, \mathbf{d} \rangle < 2\langle \mathbf{H}\mathbf{e}_*, \mathbf{e}_* \rangle$ lead to the stability domain. The stability domain is on both sides of the tangent vector $\mathbf{e}_*$, the flutter domain being convex, Figure 4.1 (i).

When $G_2(\mathbf{e}_*) < 0$ and $\langle \mathbf{H}\mathbf{e}_*, \mathbf{e}_* \rangle \leq 0$, the curves leading to the stability domain satisfy the inequalities $\langle \mathbf{h}, \mathbf{e}_* \rangle < 0$ and $2G_2(\mathbf{e}_*) < \langle \mathbf{f}, \mathbf{d} \rangle < 2\langle \mathbf{H}\mathbf{e}_*, \mathbf{e}_* \rangle \leq 0$. The stability domain is within the half-plane $\langle \mathbf{f}, \mathbf{d} \rangle < 0$ with respect to the tangent vector $\mathbf{e}_*$, and the flutter domain is convex, Figure 4.1 (j).

Finally, in the case when $G_2(\mathbf{e}_*) > 0$, in the stability domain are the curves that satisfy the conditions $\langle \mathbf{h}, \mathbf{e}_* \rangle < 0$ and $0 < 2G_2(\mathbf{e}_*) < \langle \mathbf{f}, \mathbf{d} \rangle < 2\langle \mathbf{H}\mathbf{e}_*, \mathbf{e}_* \rangle$. The stability domain is within the half-plane $\langle \mathbf{f}, \mathbf{d} \rangle > 0$ with respect to the tangent vector $\mathbf{e}_*$, and the flutter domain is concave, Figure 4.1 (k).

In all the three cases the stability domain touches the domains of flutter and divergence at the point 0^2 by a narrow tongue, Figure 4.1 (i–k). The tangent cone to the stability domain is degenerate

$$K_S = \{\mathbf{e} : \ \langle \mathbf{f}, \mathbf{e} \rangle = 0, \ \langle \mathbf{h}, \mathbf{e} \rangle < 0\}, \tag{4.89}$$

where generically the vectors $\mathbf{h}$ and $\mathbf{f}$ are linearly independent.

4.5.3 Example. Stabilization of comfortable walking

In [41] Beletsky considered a two-legged walking robot consisting of the massive body and a pair of weightless legs that are connected to the body by the joints at the point O, Figure 4.2 (a). During walking one leg of the robot is in a pointwise contact with the ground, Figure 4.2 (a). Let ρ be the distance between the mass center C to the point O that is elevated to the height h above the ground, M the mass of the body, I the moment of inertia of the body relative to the mass center, T the duration of one step, θ the angle of inclination of the body with respect to the vertical, u and q the momenta acting in the knee and the hip joints, respectively. Oscillations of the body with respect to the point O are described by the dimensionless nonlinear equation [41]

$$\begin{aligned}(1 + \mu_2 (\cos\theta - 1) + \mu_1 (\lambda\varphi(\tau) + \kappa) \sin\theta)\, \ddot{\theta} - \sin\theta - (\lambda\varphi(\tau) + \kappa) \\ + (\mu_1 (\lambda\varphi(\tau) + \kappa) \cos\theta - \mu_2 \sin\theta)\, \dot{\theta}^2 + (\mu_1 \cos\theta + \mu_2)\, \ddot{\kappa} = 0,\end{aligned} \tag{4.90}$$

where dot denotes differentiation with respect to time τ and

$$\kappa = ((x - x_\nu) - L\varphi(\tau))\, \rho^{-1}, \quad \varphi(\tau) = \tau/\tau_0 - [\tau/\tau_0] - S/L, \tag{4.91}$$

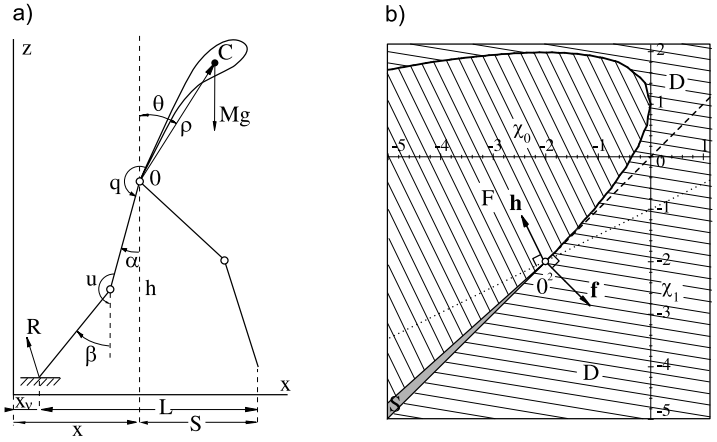

Figure 4.2. (a) A two-legged walking robot [41] and (b) its stability diagram when $\mu = \mu_1 + \mu_2 = 0.5$ [284].

with $\tau_0 = \omega T$ a nondimensional step duration and $[n]$ the integer part of n,

$$d\tau = \omega dt, \quad \omega = \sqrt{\frac{\mu_1 g}{\rho}}, \quad \mu_1 = \frac{M\rho^2}{I + M\rho\,(\rho + h)}, \quad \mu_2 = \frac{\mu_1 h}{\rho}. \quad (4.92)$$

The equation (4.90) describes oscillations of the body of the robot, given the motion of the hip joint $x = x\,(\tau)$, $z = h = const$, and the process of contact (α, β, x_v) of a leg with the ground, Figure 4.2 (a).

The coordinate $\kappa\,(\tau)$ is a deviation of the coordinate of the hip joint $x\,(\tau)$. If the horizontal motion of the joint is regular ($\kappa \equiv 0$), then the walking is called *comfortable* [41]. In this case the body oscillates with the period τ_0, equal to the duration of the step: $\theta = \hat{\theta}\,(\tau)$, $\hat{\theta}\,(\tau + \tau_0) = \hat{\theta}\,(\tau)$. The hip joint then moves with the constant speed at the constant height h above the ground, whereas the legs take steps of equal length and duration. This motion, generally, is unstable.

As it was shown in [41], stabilization of the motion and of the oscillations of the body is possible by a linear feedback with respect to the deviations $\vartheta = \theta - \hat{\theta}\,(\tau)$ and κ from the periodic motion $\hat{\theta}\,(\tau)$ and from the regular motion of the joint. The equations of motion of the system (4.90) linearized with respect to the variables ϑ and κ with the linear feedback taken into account are [41]

$$\begin{pmatrix} \ddot{\vartheta} \\ \ddot{\kappa} \end{pmatrix} + \mathbf{A} \begin{pmatrix} \vartheta \\ \kappa \end{pmatrix} = 0, \quad \mathbf{A} = \begin{pmatrix} \mu\chi_0 - 1 & \mu\chi_1 - 1 \\ -\chi_0 & -\chi_1 \end{pmatrix}, \quad (4.93)$$

where $\mu = \mu_1 + \mu_2 < 1$, and χ_0 and χ_1 are the feedback coefficients corresponding to the controlling moments at the joints.

Given μ, the circulatory system (4.93) depends on the two parameters χ_0 and χ_1. If these parameters (drive moments at the hip and knee joints) are in the stability do-

main, the feedback stabilizes the comfortable walking. Assuming solutions to equation (4.93) in the form $\vartheta, \kappa \sim \exp(\sqrt{\sigma}\, t)$, we find the eigenvalues

$$\sigma_{\pm} = \frac{\mu\chi_0 - \chi_1 - 1}{2} \pm \frac{1}{2}\sqrt{(1 - \mu\chi_0 + \chi_1)^2 - 4\,(\chi_1 - \chi_0)}. \qquad (4.94)$$

Along the straight line $\chi_1 = \chi_0$ one of the eigenvalues, $\sigma_+ = 0$, whereas σ_- remains positive when $\chi_1 = \chi_0 < 1/(\mu - 1)$, vanishes at the point $\mathbf{p}_0 = (1/(\mu - 1), 1/(\mu - 1))$ and is negative at the rest of the line. Hence, for $\chi_1 = \chi_0 < 1/(\mu - 1)$ this line divides the domains of stability and divergence. At $\mathbf{p}_0$ there is a double zero eigenvalue with the Jordan block, 0^2, and the remaining part of the line belongs to the divergence domain, Figure 4.2 (b).

The vanishing radicand in equation (4.94) means that the eigenvalues are double and real along the parabola $(1 + \chi_1 - \mu\chi_0)^2 = 4\,(\chi_1 - \chi_0)$. At the point $\mathbf{p}_0$, where the parabola touches the line $\chi_1 = \chi_0$, the double eigenvalue is zero, Figure 4.2 (b). A part of the parabola below the line $\chi_1 = \mu\chi_0 - 1$, is the boundary between the domains of stability and flutter, because here the double eigenvalues are positive. The remaining part of the parabola separates the domains of flutter and divergence, Figure 4.2 (b), because above the line $\chi_1 = \mu\chi_0 - 1$ the double eigenvalues $\sigma_{1,2} < 0$. Therefore, the stability domain is

$$\mu\chi_0 - \chi_1 - 1 > 0, \quad \chi_1 > \chi_0, \quad (1 + \chi_1 - \mu\chi_0)^2 - 4\,(\chi_1 - \chi_0) > 0. \qquad (4.95)$$

The eigenvectors and associated vectors of the double zero eigenvalue of the matrix $\mathbf{A}$ determined by equation (4.93) are

$$\mathbf{u}_0 = \frac{2}{1-\mu}\begin{pmatrix} 1 \\ -1 \end{pmatrix}, \quad \mathbf{v}_0 = -\frac{1}{2}\begin{pmatrix} 1 \\ 1 \end{pmatrix},$$
$$\mathbf{u}_1 = \begin{pmatrix} 0 \\ -2 \end{pmatrix}, \qquad \mathbf{v}_1 = \frac{1-\mu}{2}\begin{pmatrix} 1 \\ 0 \end{pmatrix}. \qquad (4.96)$$

In the (χ_0, χ_1)-plane the point 0^2 belongs to the boundary between the domains of stability (gray) and instability, originating a singularity. At this point three domains contact with each other: stability, flutter and divergence, Figure 4.2 (b). The singularities α^3, $\alpha^2\beta^2$, $0\alpha^2$, and $\alpha^2\beta^2$ cannot take place in this system because their origination requires more than two degrees of freedom.

Substituting the eigenvectors (4.96) into equation (4.41), we get the normal vector to the flutter boundary at the point 0^2: $\mathbf{f}^T = (1, -1)$. The vector $\mathbf{f}$ points to the divergence domain that in the vicinity of the point 0^2 is defined by the inequality $\langle \mathbf{f}, \mathbf{e} \rangle > 0$, i.e. $e_1 > e_2$, where $\mathbf{e}^T = (e_1, e_2)$. The vectors $\mathbf{e}$ that satisfy the condition $e_1 < e_2$ are directed to the flutter domain. The equality $e_1 = e_2$ selects the line $\chi_1 = \chi_0$, along which the splitting of the double zero eigenvalue is described by the quadratic equation (4.47).

In the degenerate case $e_1 = e_2 = e_*$, we find that $2\langle \mathbf{h}, \mathbf{e}_* \rangle = (\mu - 1)e_*$, where the vector $2\mathbf{h}^T = (\mu, -1)$, whereas $\langle \mathbf{H}\mathbf{e}_*, \mathbf{e}_* \rangle = 0$. Then, in the degenerate direction the

double zero eigenvalue splits as $\sigma_-(\varepsilon) = 0 + o(\varepsilon)$ and $\sigma_+(\varepsilon) = (\mu - 1)e_*\varepsilon + o(\varepsilon)$, in accordance with equation (4.94). Since $G_2(\mathbf{e}_*) = -\langle \mathbf{h}\mathbf{h}^T\mathbf{e}_*, \mathbf{e}_*\rangle < 0$, the flutter domain is convex at the point $(1/(\mu-1), 1/(\mu-1))$ and the stability domain is above the line $\chi_1 = \chi_0$, cf. Figure 4.2 (b) and Figure 4.1 (j). The quadratic approximation to the stability domain is $F_2 = \langle \mathbf{f}, \Delta\mathbf{p}\rangle + \langle \mathbf{h}\mathbf{h}^T\Delta\mathbf{p}, \Delta\mathbf{p}\rangle > 0$, i.e. $4(\chi_0 - \chi_1) + (\mu\chi_0 - \chi_1 - 1)^2 > 0$, coinciding with the third of the conditions (4.95). The tangent cone (4.89) to the stability domain is thus degenerate

$$K_S = \{\mathbf{e} : \ e_1 = e_2, \ e_2 < \mu e_1\}, \ \mu < 1.$$

In Figure 4.2 (b) the line $\chi_1 = \mu\chi_0 - 1$ is shown dotted whereas the dashed line denotes the part of the line $\chi_1 = \chi_0$ that lies in the divergence domain. The vector $\mathbf{f}$ is orthogonal to the line $\chi_1 = \chi_0$ and is directed to the divergence domain, while the vector $\mathbf{h}$ is orthogonal to the line $\chi_1 = \mu\chi_0 - 1$ at the point 0^2. Therefore, all the three stability conditions (4.95) are exactly reproduced by the sensitivity analysis of the double zero eigenvalue. We see in Figure 4.2 (b) that the stability tongue is very narrow. In the absence of control ($\chi_0 = \chi_1 = 0$), comfortable walking is unstable. Moreover, the control with respect to any single channel (when either $\chi_0 = 0$ or $\chi_1 = 0$) does not guarantee stability either. Stabilization of comfortable walking is only possible by simultaneously controlling both channels under very restrictive choice of the feedback coefficients [41].

4.5.4 Singularities in three-parameter circulatory systems

Theorem 4.5 (O. N. Kirillov, 2000 [284]). *The boundary between the domain of stability and the domains of flutter and divergence in the (p_1, p_2, p_3)-plane of a three-parameter circulatory system* (4.8) *is piecewise smooth. It consists of smooth surfaces of the types* 0 *and* α^2 *that generically are connected to each other along the curves of the four types*

$$0^2, \ \alpha^3 \ (\textit{cuspidal edges}) \ \textit{and} \ 0\alpha^2\,(\alpha > 0), \ \alpha^2\beta^2 \ (\textit{dihedral edges})$$

and at points of eight types

$$0^2\alpha^2\,(\alpha > 0), \ 0\alpha^3\,(\alpha > 0), \ \alpha^3\beta^2$$
$$(\textit{transversal intersections of cuspidal edges})$$
$$0\alpha^2\beta^2\,(\alpha > 0, \beta > 0), \ \alpha^2\beta^2\gamma^2 \ (\textit{trihedral angles})$$
$$\alpha\alpha \ (\textit{cone}), \ \alpha^4 \ (\textit{swallowtail}), \ \textit{and} \ 0^3 \ (\textit{trihedral spike}).$$

Smooth surfaces α^2 and 0

The surface α^2 is a smooth part of the boundary between the domains of stability and flutter when $\alpha > 0$ and between the domains of flutter and divergence when $\alpha < 0$, Figure 4.3 (a). The vector $\mathbf{f}$, defined in (4.41), is normal to the surface that separates the domains of flutter and stability (flutter and divergence) and lies in the domain of stability (divergence).

On the surface of the type 0, the matrix $\mathbf{A}$ contains a simple zero eigenvalue. If all other eigenvalues are positive and simple, the surface separates the domains of stability and divergence in the (p_1, p_2, p_3)-space. The normal vector $\mathbf{g}$, defined by equation (4.28), points to the domain of stability, Figure 4.3 (b).

Singular lines 0^2, $0\alpha^2$, α^3, and $\alpha^2\beta^2$

The points in the (p_1, p_2, p_3)-space corresponding to the matrices with eigenvalues of types 0^2, $0\alpha^2$, α^3, and $\alpha^2\beta^2$, other eigenvalues being positive and simple, constitute singular curves on the stability boundary. The curves $0\alpha^2(\alpha > 0)$ and $\alpha^2\beta^2$ exist at transversal intersections of two smooth surfaces forming edges of dihedral angles, Figure 4.3 (c, d). The tangent cones to the domains of stability and divergence at the points of these curves are (4.88) and (4.83), respectively. When $\alpha < 0$, the curve $0\alpha^2$ belongs to the boundary between the domains of flutter and divergence and does not create a singularity. When $\alpha > 0$ the edge $0\alpha^2$ is the summit of the domains of stability, flutter and divergence, Figure 4.3 (c). The singularity $\alpha^2\beta^2$ occurs on the boundary between the domains of stability and flutter for $\alpha > 0$, $\beta > 0$ and on the boundary between the domains of divergence and flutter when at least one of the eigenvalues α, β, is negative, Figure 4.3 (d).

A triple real eigenvalue α with the Jordan chain of length 3 existing at a point of the curve α^3 splits according to equation (4.84) for almost all directions of variation of parameters. Therefore, the condition $\langle \mathbf{q}, \mathbf{e} \rangle \neq 0$ determines the linear approximation to the flutter domain. Under variation of parameters in the particular direction specified by the condition $\langle \mathbf{q}, \mathbf{e} \rangle = 0$, one of the three eigenvalues remains real and close to α, while the other two split according to equation (4.85). The condition $\langle \mathbf{r}, \mathbf{e} \rangle > 0$ together with the degeneration condition select stabilizing variations for $\alpha > 0$ (destabilizing for $\alpha < 0$) and define degenerate tangent cones to the domains of stability (divergence) that are given by equation (4.87). Therefore, α^3 is a *cuspidal edge* in the (p_1, p_2, p_3)-space, Figure 4.3 (e).

The singularity 0^2 is a curve where the domains of stability, flutter and divergence meet, Figure 4.3 (f). Equation (4.89) defines a degenerate tangent cone to the stability domain at the points of this cuspidal edge.

Intersection points $0^2\alpha^2$, $0\alpha^3$, $0\alpha^2\beta^2$, $\alpha^3\beta^2$, $\alpha^2\beta^2\gamma^2$

Intersection of the edges shown in Figure 4.3 (c–f) by the surfaces of the types 0 and α^2, Figure 4.3 (a, b), creates the singularities $0^2\alpha^2$, $0\alpha^3$, $0\alpha^2\beta^2$, $\alpha^3\beta^2$, $\alpha^2\beta^2\gamma^2$ that have codimension 3, see Figure 4.4. For example, the singularity $\alpha^3\beta^2$ occurs when the cuspidal edge α^3 is transversally intersected by the surface β^2. The tangent cone to the domain of stability for $\alpha > 0, \beta > 0$, or divergence if at least one of the eigenvalues α, β is negative, follows from equation (4.87) by adding a condition $\langle \mathbf{f}, \mathbf{e} \rangle \geq 0$, where the vector $\mathbf{f}$ is related to the eigenvalue β

$$\alpha^3\beta^2: \quad K_{S,D} = \{\mathbf{e} : \langle \mathbf{q}, \mathbf{e} \rangle = 0, \langle \mathbf{r}, \mathbf{e} \rangle > 0, \langle \mathbf{f}, \mathbf{e} \rangle > 0\}. \tag{4.97}$$

Similarly, we derive the tangent cones at other singular points

$$\begin{aligned}
0^2\alpha^2\ (\alpha > 0): &\qquad K_S = \{\mathbf{e} : \langle \mathbf{f}^0, \mathbf{e} \rangle = 0, \langle \mathbf{h}^0, \mathbf{e} \rangle < 0, \langle \mathbf{f}^\alpha, \mathbf{e} \rangle > 0\};\\
\alpha^2\beta^2\gamma^2: &\qquad K_{S,D} = \{\mathbf{e} : \langle \mathbf{f}^\alpha, \mathbf{e} \rangle > 0, \langle \mathbf{f}^\beta, \mathbf{e} \rangle > 0, \langle \mathbf{f}^\gamma, \mathbf{e} \rangle > 0\};\\
0\alpha^2\beta^2\ (\alpha > 0, \beta > 0): &\qquad K_S = \{\mathbf{e} : \langle \mathbf{f}^\alpha, \mathbf{e} \rangle > 0, \langle \mathbf{g}, \mathbf{e} \rangle > 0, \langle \mathbf{f}^\beta, \mathbf{e} \rangle > 0\},\\
&\qquad K_D = \{\mathbf{e} : \langle \mathbf{f}^\alpha, \mathbf{e} \rangle > 0, \langle \mathbf{g}, \mathbf{e} \rangle < 0, \langle \mathbf{f}^\beta, \mathbf{e} \rangle > 0\};\\
0\alpha^3\ (\alpha > 0): &\qquad K_S = \{\mathbf{e} : \langle \mathbf{q}, \mathbf{e} \rangle = 0, \langle \mathbf{r}, \mathbf{e} \rangle > 0, \langle \mathbf{g}, \mathbf{e} \rangle > 0\},\\
&\qquad K_D = \{\mathbf{e} : \langle \mathbf{q}, \mathbf{e} \rangle = 0, \langle \mathbf{r}, \mathbf{e} \rangle > 0, \langle \mathbf{g}, \mathbf{e} \rangle < 0\},
\end{aligned} \tag{4.98}$$

where real vectors $\mathbf{g}, \mathbf{f}, \mathbf{h}, \mathbf{q}$, and $\mathbf{r}$ are defined in equations (4.28), (4.41), (4.49), (4.60), and (4.67), respectively. Hence, the tangent cones (4.97), (4.98) to the domains of stability or divergence at the points $\alpha^3\beta^2, 0^2\alpha^2\ (\alpha > 0), 0\alpha^3\ (\alpha > 0)$ are plane angles and

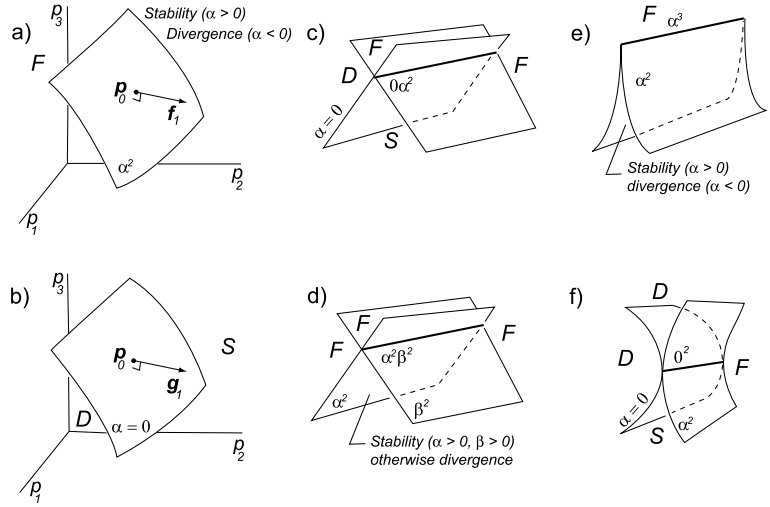

Figure 4.3. Smooth surfaces of types (a) α^2 and (b) 0; the dihedral angles (c) $0\alpha^2\ (\alpha > 0)$ and (d) $\alpha^2\beta^2$; the cuspidal edges (e) α^3 and (f) 0^2 [284].

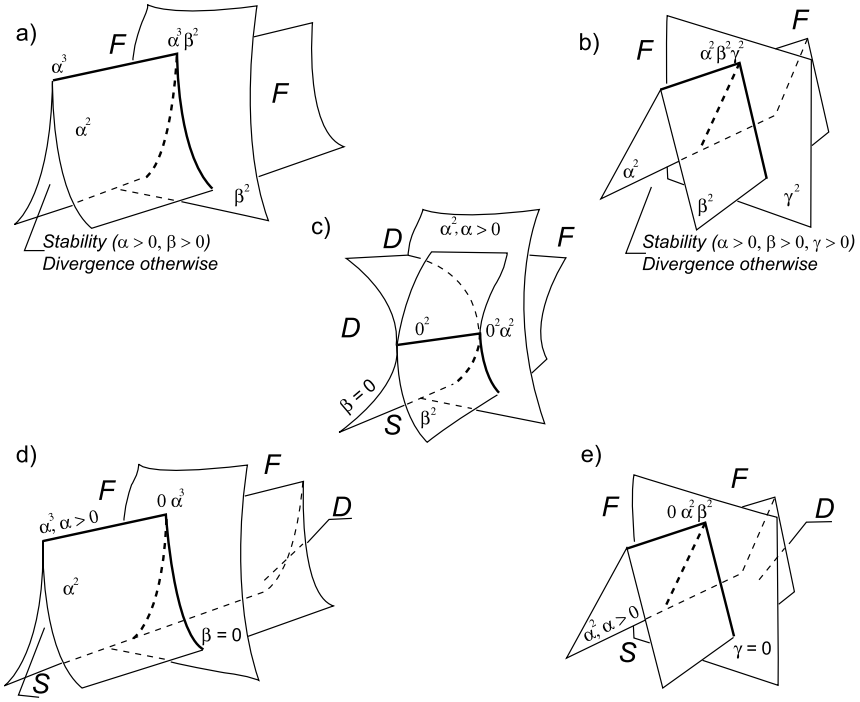

Figure 4.4. The singularities $\alpha^3\beta^2$, $0^2\alpha^2$ ($\alpha > 0$), $0\alpha^3$ ($\alpha > 0$). Trihedral angles $\alpha^2\beta^2\gamma^2$ and $0\alpha^2\beta^2$ ($\alpha > 0, \beta > 0$) [284].

are thus degenerate. The tangent cones at the points $\alpha^2\beta^2\gamma^2$ and $0\alpha^2\beta^2$ ($\alpha > 0, \beta > 0$) are trihedral angles. Note that the codimension 3 singularities do not occur at the points $0^2\alpha^2$ ($\alpha < 0$), $0\alpha^3$ ($\alpha < 0$), and at the point $0\alpha^2\beta^2$, when one of the eigenvalues α, β is negative.

Conical singularity $\alpha\alpha$

The points of the type $\alpha\alpha$ in the (p_1, p_2, p_3)-space correspond to the matrices with the double semisimple real eigenvalue $\sigma_0 = \alpha$. As follows from equation (4.53), the condition $D < 0$ selects the flutter domain while the condition $D > 0$ corresponds to the stability domain for $\alpha > 0$ and to the divergence domain for $\alpha < 0$. Equation $D := x^2 + y^2 - z^2 = 0$ determines the conical surface in the space of the parameters

$$x = \langle \mathbf{f}_*, \mathbf{e} \rangle\,, \quad y = \langle \mathbf{f}_+, \mathbf{e} \rangle\,, \quad z = \langle \mathbf{f}_-, \mathbf{e} \rangle\,, \tag{4.99}$$

see Figure 4.5 (b). Hence, independently of the sign of α flutter is inside the cone while the domains of stability or divergence are adjacent to the cone.

In order to describe the tangent cone to the stability or divergence domains at $\alpha\alpha$ in the (p_1, p_2, p_3)-space, we introduce the polar angle φ, Figure 4.5 (a). Then, taking

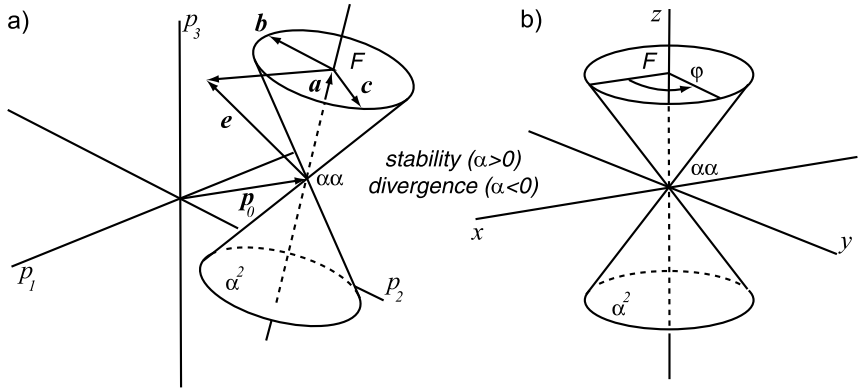

Figure 4.5. The singularity $\alpha\alpha$ [277, 284] on the boundary between the domain of flutter (F, inside the cone) and (outside the cone) stability (when $\alpha > 0$) or divergence (when $\alpha < 0$). The skirts of the cone correspond to the surfaces of type α^2.

into account that $x = z\cos\varphi$ and $y = z\sin\varphi$, we find

$$\langle \mathbf{f}_* - \mathbf{f}_- \cos\varphi, \mathbf{e}_* \rangle = 0, \quad \langle \mathbf{f}_+ - \mathbf{f}_- \sin\varphi, \mathbf{e}_* \rangle = 0. \tag{4.100}$$

Hence, a tangent vector to the conical surface at the apex of the cone is

$$\mathbf{e}_* = t\,(\mathbf{f}_* - \mathbf{f}_- \cos\varphi) \times (\mathbf{f}_+ - \mathbf{f}_- \sin\varphi)\,, \tag{4.101}$$

where $t \in \mathbb{R}$ is a real parameter. Expanding the inner product in (4.101) and introducing the new vectors $\mathbf{a} = \mathbf{f}_* \times \mathbf{f}_+$, $\mathbf{b} = \mathbf{f}_* \times \mathbf{f}_-$, $\mathbf{c} = \mathbf{f}_- \times \mathbf{f}_+$, yields

$$\mathbf{e}_* = t\,(\mathbf{a} + \mathbf{b}\sin\varphi + \mathbf{c}\cos\varphi)\,. \tag{4.102}$$

Therefore, at the point $\alpha\alpha$ in the (p_1, p_2, p_3)-space the tangent cone to the domain of stability ($\alpha > 0$) or divergence ($\alpha < 0$) is

$$K_{S,D} = \{\mathbf{e} : \mathbf{e} = t\,(\mathbf{a} + d\,(\mathbf{b}\sin\varphi + \mathbf{c}\cos\varphi))\,, t \in \mathbb{R}, \varphi \in [0, 2\pi]\,, d \in [1, \infty)\}\,. \tag{4.103}$$

Singular points α^4 and 0^3

Sensitivity analysis of eigenvalues becomes less efficient in cases that correspond to eigenvalues of higher multiplicity. By this reason, for the investigation of singularities $0^3, \alpha^4$ we will use a method proposed in [399] based on the investigation of a bifurcation diagram of the *versal deformation* [17] of a matrix.

A versal deformation of a matrix $\mathbf{A}_0$ is a matrix family $\tilde{\mathbf{A}}\,(\tilde{\mathbf{p}})$, that smoothly depends on the vector of parameters $\tilde{\mathbf{p}} \in \mathbb{R}^d$, such that any smooth family $\mathbf{A}\,(\mathbf{p})$, $(\mathbf{A}\,(\mathbf{p}_0) = \mathbf{A}_0)$ in the vicinity of the point $\mathbf{p} = \mathbf{p}_0$ has the form

$$\mathbf{A}\,(\mathbf{p}) = \mathbf{C}\,(\mathbf{p})\,\tilde{\mathbf{A}}\,(\varphi\,(\mathbf{p}))\,\mathbf{C}^{-1}\,(\mathbf{p})\,, \tag{4.104}$$

where $\mathbf{C}(\mathbf{p})$, $\mathbf{C}(\mathbf{p}_0) = \mathbf{C}_0$ is the family of nondegenerate matrices smoothly dependent on $\mathbf{p}$, $\mathbf{C}_0$ is the nondegenerate matrix that transforms the matrix $\mathbf{A}_0$ to the upper triangular Jordan form, i.e. $\mathbf{A}_0 = \mathbf{C}_0\mathbf{J}\mathbf{C}_0^{-1}$, and $\tilde{\mathbf{p}} = \varphi(\mathbf{p})$ is a smooth map of the neighborhood of the point $\mathbf{p}_0$ in the space $\mathbb{R}^3$ to the vicinity of the origin in the space $\mathbb{R}^d$. Versal deformation with the minimal possible number of parameters is called *miniversal* [17].

Let at $\mathbf{p} = \mathbf{p}_0$ the real matrix $\mathbf{A}$ of the eigenvalue problem (4.9) have the Jordan block of third order with the zero eigenvalue, 0^3. Let all other eigenvalues be positive and simple. The miniversal deformation of $\mathbf{A}_0 = \mathbf{A}(\mathbf{p}_0)$ can be chosen in the form [17, 185]

$$\tilde{\mathbf{A}}(\tilde{\mathbf{p}}) = \mathbf{J} + \mathbf{B}(\tilde{\mathbf{p}}), \tag{4.105}$$

where $\mathbf{J}$ is the Jordan upper triangular form of $\mathbf{A}_0$, and $\mathbf{B}(\tilde{\mathbf{p}})$ is the block diagonal matrix with the blocks corresponding to the eigenvalues of the matrix $\mathbf{A}_0$. The first block of the matrix $\tilde{\mathbf{A}}(\tilde{\mathbf{p}})$, that corresponds to the triple zero eigenvalue, is [17, 185]

$$\begin{pmatrix} 0 & 1 & 0 \\ 0 & 0 & 1 \\ \tilde{p}_1 & \tilde{p}_2 & \tilde{p}_3 \end{pmatrix}. \tag{4.106}$$

Since in view of (4.104) the characteristic equations for the matrices $\mathbf{A}(\mathbf{p})$ and $\tilde{\mathbf{A}}(\tilde{\mathbf{p}})$ coincide, one can investigate the stability of a circulatory system using the miniversal deformation. Stability of the matrix $\tilde{\mathbf{A}}(\tilde{\mathbf{p}})$ in view of its block-diagonal structure is determined by its first block (4.106) that has the following characteristic equation

$$-\sigma^3 + \sigma^2\tilde{p}_3 + \sigma\tilde{p}_2 + \tilde{p}_1 = 0. \tag{4.107}$$

In the $(\tilde{p}_1, \tilde{p}_2, \tilde{p}_3)$-space of the miniversal deformation the matrix $\tilde{\mathbf{A}}$ has a triple zero eigenvalue at the origin. From (4.107) it follows that the $(\tilde{p}_2, \tilde{p}_3)$-plane corresponds to the matrices with the simple zero eigenvalues and the axis $\tilde{p}_3$ corresponds to that with the double zero eigenvalue. Other multiple eigenvalues live on the discriminant surface [23]

$$27\tilde{p}_1^2 + 18\tilde{p}_1\tilde{p}_2\tilde{p}_3 - \tilde{p}_2^2\tilde{p}_3^2 + 4\tilde{p}_3^3\tilde{p}_1 - 4\tilde{p}_2^3 = 0, \tag{4.108}$$

shown in Figure 4.6 (a). The cuspidal edge, α^3 ($\alpha > 0$), of the surface lies above the plane of simple zero eigenvalues, intersecting it at the origin. After that, α changes the sign and the edge α^3 ($\alpha < 0$) goes below the $(\tilde{p}_2, \tilde{p}_3)$-plane. One of the surfaces α^2, $\alpha > 0$, which is adjacent to the cuspidal edge α^3, intersects the plane of zero eigenvalues and forms the dihedral angle $0\alpha^2$ ($\alpha > 0$). The second surface α^2 ($\alpha > 0$) touches this plane along the axis $\tilde{p}_3$ and forms the cuspidal edge 0^2. Therefore, the stability domain is inside the *trihedral spike* that is bounded by the surfaces (4.108) and the $(\tilde{p}_2, \tilde{p}_3)$-plane. The curves α^3 ($\alpha < 0$), $0\alpha^2$ ($\alpha > 0$) and 0^2 are the edges of the trihedral spike.

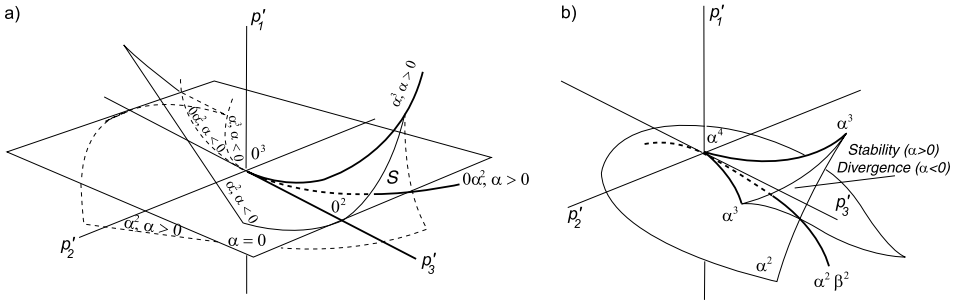

Figure 4.6. Singularities (a) 0^3 and (b) α^4 on the boundary of the stability (S) or divergence domains that are inside the trihedral spikes [284].

The vectors $\tilde{\mathbf{e}}$, that satisfy the conditions

$$\tilde{e}_1 = 0, \quad \tilde{e}_2 = 0, \quad \tilde{e}_3 > 0. \tag{4.109}$$

lead to the stability domain from the origin in the $(\tilde{p}_1, \tilde{p}_2, \tilde{p}_3)$-space, thus forming a degenerate tangent cone to the stability domain at the point 0^3.

Taking into account that

$$\tilde{e}_i = \frac{d\,\tilde{p}_i}{d\,\varepsilon} = \sum_{j=1}^{3} \frac{\partial \varphi_i}{\partial p_j} \frac{dp_j}{d\,\varepsilon} = \sum_{j=1}^{3} \frac{\partial \varphi_i}{\partial p_j} e_j, \tag{4.110}$$

we conclude that the vectors $\tilde{\mathbf{e}}$ and $\mathbf{e}$ determining the tangent cones in the spaces of parameters of the miniversal deformation and that of the original matrix family are related via the Jacobi matrix of the map $\tilde{\mathbf{p}} = \varphi(\mathbf{p})$. The derivatives $\frac{\partial \tilde{p}_i}{\partial p_j}$ can be found as linear combinations of the elements of the matrix $\mathbf{F}^j = \mathbf{C}_0^{-1} \frac{\partial \mathbf{A}}{\partial p_j} \mathbf{C}_0$, see [399]. The matrices $\mathbf{F}^j$, are subdivided into blocks in accordance with the Jordan form of the matrix $\mathbf{A}_0$

$$\mathbf{F}^j = \left(\begin{array}{ccc|c} \left(\frac{\partial \mathbf{A}}{\partial p_j}\mathbf{u}_0, \mathbf{v}_2\right) & \left(\frac{\partial \mathbf{A}}{\partial p_j}\mathbf{u}_1, \mathbf{v}_2\right) & \left(\frac{\partial \mathbf{A}}{\partial p_j}\mathbf{u}_2, \mathbf{v}_2\right) & \\ \left(\frac{\partial \mathbf{A}}{\partial p_j}\mathbf{u}_0, \mathbf{v}_1\right) & \left(\frac{\partial \mathbf{A}}{\partial p_j}\mathbf{u}_1, \mathbf{v}_1\right) & \left(\frac{\partial \mathbf{A}}{\partial p_j}\mathbf{u}_2, \mathbf{v}_1\right) & \vdots \\ \left(\frac{\partial \mathbf{A}}{\partial p_j}\mathbf{u}_0, \mathbf{v}_0\right) & \left(\frac{\partial \mathbf{A}}{\partial p_j}\mathbf{u}_1, \mathbf{v}_0\right) & \left(\frac{\partial \mathbf{A}}{\partial p_j}\mathbf{u}_2, \mathbf{v}_0\right) & \\ \hline \multicolumn{3}{c|}{\cdots} & \ddots \end{array}\right). \tag{4.111}$$

Here $\mathbf{u}_0, \mathbf{u}_1, \mathbf{u}_2, \mathbf{v}_0, \mathbf{v}_1, \mathbf{v}_2$ are eigenvectors and associated vectors of the triple eigenvalue that satisfy the equations (4.55) and conditions (4.56) and (4.57). The derivatives $\frac{\partial \tilde{p}_i}{\partial p_j}$ are expressed through the components f_{pq}^j of the matrices $\mathbf{F}^j$

$$\frac{\partial \tilde{p}_1}{\partial p_j} = f_{31}^j, \quad \frac{\partial \tilde{p}_2}{\partial p_j} = f_{21}^j + f_{32}^j, \quad \frac{\partial \tilde{p}_3}{\partial p_j} = f_{11}^j + f_{22}^j + f_{33}^j, \tag{4.112}$$

Substituting (4.112) into (4.110), we obtain

$$\tilde{e}_1 = f_{31}^1 e_1 + f_{31}^2 e_2 + f_{31}^3 e_3. \tag{4.113}$$

The vector with the components f_{31}^j is the vector $\mathbf{q}$ defined in (4.60). Therefore, equation (4.113) yields $\tilde{e}_1 = \langle \mathbf{q}, \mathbf{e} \rangle$. Similarly, $\tilde{e}_2 = \langle \mathbf{r}, \mathbf{e} \rangle$ and $\tilde{e}_3 = \langle \mathbf{k}, \mathbf{e} \rangle$, because the components of the vectors $\mathbf{r}$ and $\mathbf{k}$, defined in (4.67) and (4.73), respectively, are related to the elements of matrices $\mathbf{F}^j$ as $r^j = f_{21}^j + f_{32}^j$ and $k^j = f_{11}^j + f_{22}^j + f_{33}^j$. Then, the relations (4.109) yield the degenerate tangent cone to the stability domain at the point 0^3 in the (p_1, p_2, p_3)-space

$$K_S = \{\mathbf{e} : \ \langle \mathbf{q}, \mathbf{e} \rangle = 0, \ \langle \mathbf{r}, \mathbf{e} \rangle = 0, \ \langle \mathbf{k}, \mathbf{e} \rangle > 0\}. \tag{4.114}$$

Similarly we study the singularity α^4, meaning that the matrix $\mathbf{A}$ contains a Jordan block of order 4 with the real eigenvalue α. Let $\mathbf{u}_k$,$\mathbf{v}_k$, $k = 0...3$ be eigenvectors and associated vectors that satisfy the natural normality conditions. The first block of the miniversal deformation has the form [185]

$$\begin{pmatrix} \alpha & 1 & 0 & 0 \\ 0 & \alpha & 1 & 0 \\ 0 & 0 & \alpha & 1 \\ \tilde{p}_1 & \tilde{p}_2 & \tilde{p}_3 & \alpha \end{pmatrix}. \tag{4.115}$$

Stability of the circulatory system in the vicinity of α^4 is determined by the characteristic equation

$$(\alpha - \sigma)^4 - \tilde{p}_3 (\alpha - \sigma)^2 + \tilde{p}_2 (\alpha - \sigma) - \tilde{p}_1 = 0 \tag{4.116}$$

and its discriminant set. The singularity of the stability boundary at the point α^4 is known as the *swallowtail* [23], Figure 4.6 (b). Stability domains for $\alpha > 0$ (or divergence for $\alpha < 0$) are inside the trihedral spike, formed by the surfaces α^2 and the cuspidal edges α^3 and $\alpha^2\beta^2$. The tangent cone at the point α^4 to the domain of stability or divergence is degenerate [284]

$$K_{S,D} = \{\mathbf{e} : \ \langle \mathbf{l}, \mathbf{e} \rangle = 0, \ \langle \mathbf{m}, \mathbf{e} \rangle = 0, \ \langle \mathbf{n}, \mathbf{e} \rangle > 0\}. \tag{4.117}$$

The components of the real vectors $\mathbf{l}$, $\mathbf{m}$, and $\mathbf{n}$ in (4.117) are expressed through the elements $f_{pq}^j = \left(\frac{\partial \mathbf{A}}{\partial p_j} \mathbf{u}_{q-1}, \mathbf{v}_{4-p} \right)$, of the matrices $\mathbf{F}^j$ as [284]

$$l_1^j = f_{41}^j, \quad m_1^j = f_{31}^j + f_{42}^j, \quad n_1^j = f_{21}^j + f_{32}^j + f_{43}^j. \tag{4.118}$$

This completes our study of singularities on the stability boundaries in generic three-parameter families of circulatory systems.

4.5.5 The cone $\alpha\alpha$ and Merkin's instability theorem

Let in equation (4.8) the matrix $\mathbf{M} = \mathbf{I}$, where $\mathbf{I}$ is a unit matrix. Then, the matrix $\mathbf{A}$ in the eigenvalue problem (4.9) is $\mathbf{A} = \mathbf{K} + \mathbf{N}$, where $\mathbf{K} = \mathbf{K}^T$ and $\mathbf{N} = -\mathbf{N}^T$.

When $m = 2$, we can represent the matrix $\mathbf{A}$ in the eigenvalue problem (4.9) as a sum of the matrices corresponding to the potential forces of spherical and hyperbolical types and that of nonconservative positional forces [618, 619]

$$\mathbf{A} = \frac{1}{2}\begin{pmatrix} k_{11}+k_{22} & 0 \\ 0 & k_{11}+k_{22} \end{pmatrix} + \frac{1}{2}\begin{pmatrix} k_{11}-k_{22} & 2k_{12} \\ 2k_{12} & k_{22}-k_{11} \end{pmatrix} + \nu\begin{pmatrix} 0 & -1 \\ 1 & 0 \end{pmatrix}. \tag{4.119}$$

Consider the matrix (4.119) as a three-parameter matrix family $\mathbf{A}(k_{22}, k_{12}, \nu)$ that at $k_{22} = k_{11}$, $k_{12} = 0$, and $\nu = 0$ reduces to $\mathbf{A}_0 = k_{11}\mathbf{I}$ with the double semisimple eigenvalue $\sigma_0 = k_{11}$ that has two linearly independent eigenvectors

$$\mathbf{u}_1 = \begin{pmatrix} 0 \\ 1 \end{pmatrix}, \quad \mathbf{u}_2 = \begin{pmatrix} 1 \\ 0 \end{pmatrix}. \tag{4.120}$$

Therefore, the point $(k_{11}, 0, 0)$ in the (k_{22}, k_{12}, ν)-space is a conical singular point of type $\alpha\alpha$ on the boundary between the domains of flutter and stability when $k_{11} > 0$.

The vectors in the equations (4.101) and (4.103) that determine the tangent cone to the stability domain at the singular point in the (k_{22}, k_{12}, ν)-space, follow from equations (4.54) where the eigenvectors (4.120) are taken into account

$$\mathbf{f}_*^T = (1, 0, 0), \quad \mathbf{f}_+^T = (0, 2, 0), \quad \mathbf{f}_-^T = (0, 0, -2). \tag{4.121}$$

The linear dependence of the matrix (4.119) on parameters allows us to choose $\mathbf{e} = (k_{22} - k_{11}, k_{12}, \nu)$ and, in combination with the vectors (4.121), to calculate the coefficients in the expression $D := \langle \mathbf{f}_*, \mathbf{e}\rangle^2 + \langle \mathbf{f}_+, \mathbf{e}\rangle^2 - \langle \mathbf{f}_-, \mathbf{e}\rangle^2$. The stability domain in the (k_{22}, k_{12}, ν)-space is thus approximated by the cone

$$D = (k_{22} - k_{11})^2 + 4k_{12}^2 - 4\nu^2 > 0, \tag{4.122}$$

which coincides with the exact solution following from the explicit expressions for the eigenvalues of the matrix (4.119). Note that by inverting the inequality in equation (4.122) we get a sufficient condition for the dynamical instability that, if represented in the equivalent invariant form [100, 290]

$$\|\mathbf{N}\|^2 > \|\mathbf{K}\|^2 - \frac{1}{m}(\mathrm{tr}\mathbf{K})^2, \tag{4.123}$$

where $\|\mathbf{N}^2\| := \mathrm{tr}(\mathbf{N}^T\mathbf{N})$ and $\|\mathbf{K}^2\| := \mathrm{tr}(\mathbf{K}^T\mathbf{K})$, is valid for any number of degrees of freedom $m \geq 2$ (*Bulatovic's flutter condition* [100], see Theorem 5.17).

In the (k_{22}, k_{12}, ν)-space, the apex of the cone at the point $(k_{11}, 0, 0)$ corresponds to a stable system under the action of potential forces of spherical type only. When $\nu = 0$, any sufficiently small deviation expressed by the potential forces of hyperbolic type does not change the marginal stability.

The cone $D = 0$ has a vertical axis given by the equations $k_{22} = k_{11}$ and $k_{12} = 0$ and has elliptical cross-sections in the planes perpendicular to this line, cf.

Figure 4.5 (b). Inside the cone, i.e. when $D < 0$, the circulatory system with the matrix $\mathbf{A}(k_{22}, k_{12}, \nu)$ is unstable by flutter. Outside, it is marginally stable, cf. Figure 4.5. Thus, for any perturbation of the system with potential forces of spherical type by the potential forces of hyperbolic type, there exists a nontrivial critical value of the parameter ν, above which the potential system is destabilized by circulatory forces. This threshold vanishes only when the potential forces of hyperbolic type are absent, i.e. when $k_{22} = k_{11}$ and $k_{12} = 0$.

Therefore, the nonconservative positional forces destroy the marginal stability of the system with potential forces of spherical type. Such a statement is valid also in case of $m > 2$ degrees of freedom and is known as *Merkin's theorem*, see Theorem 5.16 [332, 333, 423]. In the case of $m = 2$ degrees of freedom,[3] this theorem is an obvious consequence of the conical geometry of the flutter domain in the vicinity of the singular point of the $\alpha\alpha$ type on the stability boundary, Figure 4.5.

4.5.6 Example: a brake disk in distributed frictional contact

A natural source of circulatory systems, where the conical singularity $\alpha\alpha$ as well as Merkin's theorem play a part, is rotor dynamics. In this section we consider a model that describes onset of flutter in an automotive disk brake.

Recently, Kang, Krousgrill, and Sadeghi investigated the dynamic instability due to circumferential friction between a stationary thin annular plate and two fixed annular sector contact interfaces under steady-sliding conditions, see [254, 301]. The effects of rotation and damping were neglected in their model.

After linearization of the governing PDEs and truncation of the modal expansions, the governing equations were obtained in [254] in the form of the linear circulatory system (4.8) with $\mathbf{M} = \mathbf{I}$ and $\mathbf{P} = \mathbf{C} + \mathbf{H} + \mathbf{N}$, where

$$\mathbf{C} = \frac{\omega_{2n}^2 + \omega_{2n-1}^2 + k_c \tilde{R}_n^z \theta_c}{2}\mathbf{I}, \quad \mathbf{N} = \nu \begin{pmatrix} 0 & -1 \\ 1 & 0 \end{pmatrix}, \quad \nu = \frac{\mu k_c n \tilde{R}_n^\theta \theta_c}{2},$$
$$\mathbf{H} = \frac{k_c \sin(n\theta_c)}{2n} \begin{pmatrix} \tilde{R}_n^z & \mu n \tilde{R}_n^\theta \\ \mu n \tilde{R}_n^\theta & -\tilde{R}_n^z \end{pmatrix} + \frac{\omega_{2n-1}^2 - \omega_{2n}^2}{2} \begin{pmatrix} 1 & 0 \\ 0 & -1 \end{pmatrix}. \tag{4.124}$$

In equation (4.124), n is the number of nodal diameters on a vibrating annular plate and is referred to as the mode number. The two neighboring circular natural frequencies of the stationary disk are denoted as ω_{2n} and ω_{2n-1}. The friction coefficient μ is assumed to be uniformly constant over the contact area of the disk with the contact span angle $0 \le \theta_c \le 2\pi$, Figure 4.7 (a). The stiffness of the contact is also uniformly constant and equal to k_c, Figure 4.7 (a). The coefficients $\tilde{R}_n^\theta$ and $\tilde{R}_n^z$ are integrals involving the

[3] In 1939 Pyotr Leonidovich Kapitsa (1894–1984) – a Russian physicist, who was awarded the Nobel Prize in Physics in 1978 for his experiments with liquid helium – derived Merkin's theorem in the case $m = 2$ in his study of transition to supercritical speeds in a special high-efficiency expansion turbine that he developed for liquefaction of air [256].

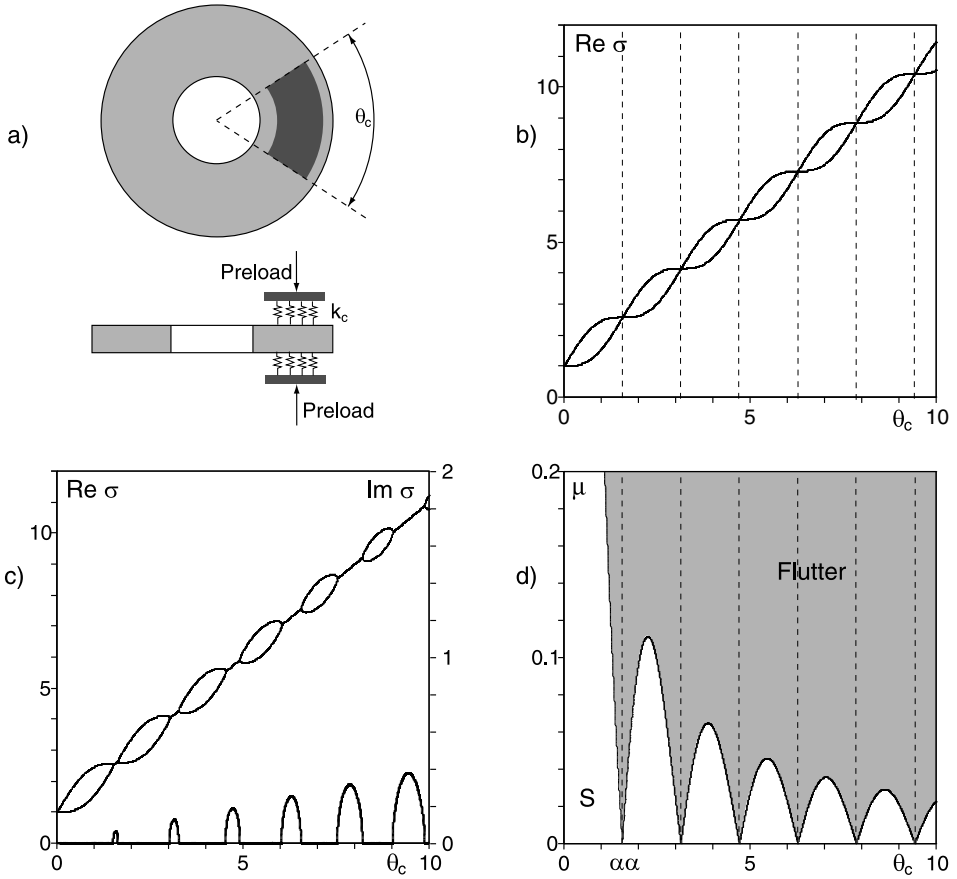

Figure 4.7. (a) A stationary thin annular plate with an annular sector friction interface under steady-sliding conditions; the preload acting on the top pad and the bottom pad, symmetrically, creates the vertical contact and horizontal friction forces on the top and bottom contact areas [254]. For $n = 2$, $k_c = 1$, $\omega_{2n} = \omega_{2n-1} = 1$, $\tilde{R}_n^\theta = \tilde{R}_n^z = 2$ (b) shows the real parts of the eigenvalues σ of the two modes of the plate as functions of the contact span angle, θ_c, when friction is absent (the friction coefficient $\mu = 0$); at the intersections the real eigenvalues σ are in the semisimple $1 : 1$ resonance. (c) The real (thin lines) and imaginary (bold lines) parts of the eigenvalues σ of the plate in frictional contact when $\mu = 0.02$. (d) Domains of marginal stability and flutter for the disk in the (θ_c, μ)-plane with the conical singularities $\alpha\alpha$ at $\theta_c = \pi s/n$, $s = 1, 2, \ldots$.

squared radial functions of order n in the modal expansions of the transverse displacement of the disk [254].

Since the matrix of positional forces, $\mathbf{P}$, is a sum of potential forces of spherical and hyperbolic type and circulatory forces as in equation (4.119), we can directly apply the formula (4.122) to find the stability domain. Equation (4.122) for the matrices given

by equation (4.124) takes the form [254, 301]

$$\mu^2 < \mu_{cr}^2 := \frac{\left(\omega_{2n}^2 - \omega_{2n-1}^2 - k_c \tilde{R}_n^z \frac{\sin(n\theta_c)}{n}\right)^2}{(k_c \tilde{R}_n^\theta)^2 (n^2\theta_c^2 - \sin^2(n\theta_c))}. \tag{4.125}$$

The domains of flutter and stability separated by the curve $\mu = \mu_{cr}(\theta_c)$ are shown in Figure 4.7 (d) in the (θ_c, μ)-plane in gray and white colors, respectively. When the friction coefficient vanishes, $\mu = 0$, the flutter boundary has conical singularities. The flutter domain is inside the instability tongues, Figure 4.7 (d).

The apexes of the cones correspond to the intersections shown in Figure 4.7 (b) of the real eigenvalues

$$\sigma = \omega_{2n}^2 + \frac{k_c \tilde{R}_n^z}{2}\left(\theta_c - \frac{\sin(n\theta_c)}{n}\right), \quad \sigma = \omega_{2n-1}^2 + \frac{k_c \tilde{R}_n^z}{2}\left(\theta_c + \frac{\sin(n\theta_c)}{n}\right). \tag{4.126}$$

The intersections of the eigencurves happen when

$$k_c \tilde{R}_n^z \sin(n\theta_c) = n(\omega_{2n}^2 - \omega_{2n-1}^2) \tag{4.127}$$

and are associated with the double real semisimple eigenvalues of the type $\alpha\alpha$.

An initially rotationally symmetrical disk is characterized by the coinciding frequencies $\omega_{2n} = \omega_{2n-1}$ [254, 293, 294]. Then, the condition (4.127) reduces to $\sin(n\theta_c) = 0$ which yields $\alpha\alpha$ singularities at every

$$\theta_c = \pi s/n, \quad s = 1, 2, \ldots . \tag{4.128}$$

At the resonances (4.128), the contact span angle is such that even when the preload is turned on ($k_c \neq 0$) the matrix of potential forces of hyperbolic type vanishes, $\mathbf{H} = 0$. Therefore, according to Merkin's theorem, the friction induces vibrations in the disk at any $\mu > 0$. Indeed, the dashed vertical lines that start at the $\alpha\alpha$ points in Figure 4.7 (d) lie in the flutter domain.[4]

[4] In early studies of nonconservative stability problems of structural mechanics, such an absence of the upper bound for the magnitude of the circulatory forces was regarded as paradoxical [75]. For example, in 1928 a Russian engineer, Evgenii Nicolai (1880–1950), motivated by rotor dynamics applications [196, 450], considered stability of a compressed flexible rod of a perfect circular cross-section loaded by a *follower torque* that corresponded to circulatory forces [448]. Surprisingly, he found that the rod lost stability however small the magnitude of the torque was (*Nicolai's paradox*) [75]. However, the rods of noncircular cross-sections were found to be stable if the follower torque did not exceed some threshold [449]. A natural but for a long time missing link of Nicolai's paradox to the $\alpha\alpha$ conical singularity on the stability boundary of circulatory systems (described in [284]) was given recently in [519]. Stability problems of this type motivated Hans Ziegler to take the next step and to introduce the notion of the *follower force* into structural mechanics and to single out the very nonconservative positional (circulatory) forces [622, 623]. We notice that some nonconservative problems were studied even in the XIXth century and early in the XXth century, for example a problem of Greenhill of 1883 on a buckling of a flexible rod under a conservative compressing force and a torque with a constant direction of its vector [206] or a problem considered by Nicolai in 1918 on the stability of a circular arch under a hydrostatic load [447]. Nevertheless, neither author realized at that time that they encountered nonconservative positional forces [116, 196, 368, 621, 626].

As soon as the size of the brake pads deviates from the resonant one, the matrix of potential forces of hyperbolic type ($\mathbf{H} \neq 0$) destroys the symmetry of the potential. Then, Bulatovic's flutter condition (4.123) and the conical geometry of the flutter domain near the $\alpha\alpha$ singularity allow the friction-induced destabilization only after μ exceeds the threshold $\mu_{cr}(\theta_c) > 0$, Figure 4.7 (d).

Smooth parts of the stability boundary in Figure 4.7 (d) are constituted by the α^2 points. Consequently, the eigencurves $\sigma(\theta_c)$ at $\mu \neq 0$ show numerous interactions at the nonsemisimple $1:1$ resonances, Figure 4.7 (c). The bubbles of pure imaginary eigenvalues shown in bold black lines in Figure 4.7 (c) correspond to the gray flutter tongues of Figure 4.7 (d). Thus, perturbation by circulatory forces transforms the crossed eigencurves of the conservative system of Figure 4.7 (b) into the overlapped ones of Figure 4.7 (c). The next example will demonstrate similar metamorphoses of eigencurves even in the absence of the $\alpha\alpha$ points on the stability boundary.

4.5.7 Example: stability of an airfoil in an inviscid flow

Consider stability of a rigid plate of infinite span in air flow using a simplified model by Panovko and Gubanova [465]. The plate rests on two elastic supports with stiffness coefficients c_1 and c_2 per unit span and has two degrees of freedom: a vertical displacement y and an angle of deviation φ, Figure 4.8 (a). A lifting force, Y, acting on the plate, is proportional to φ, velocity of the flow, v, and the width, b, of the plate: $Y = c_y^{\alpha} \frac{\rho v^2}{2} b\varphi$, where c_y^{α} is the derivative of the lifting force with respect to the angle of attack and ρ is the density of the flow. Small oscillations of the plate are governed by the equations

$$\begin{gathered} \ddot{y} + \frac{c_1 + c_2}{mb} y + \left(\frac{c_1 - c_2}{2m} - c_y^{\alpha} \frac{\rho v^2}{2m} \right) \varphi = 0, \\ \ddot{\varphi} + 6\frac{c_1 - c_2}{mb^2} y + 3 \left(\frac{c_1 + c_2}{mb} + c_y^{\alpha} \rho v^2 \frac{b - 2a}{mb^2} \right) \varphi = 0, \end{gathered} \tag{4.129}$$

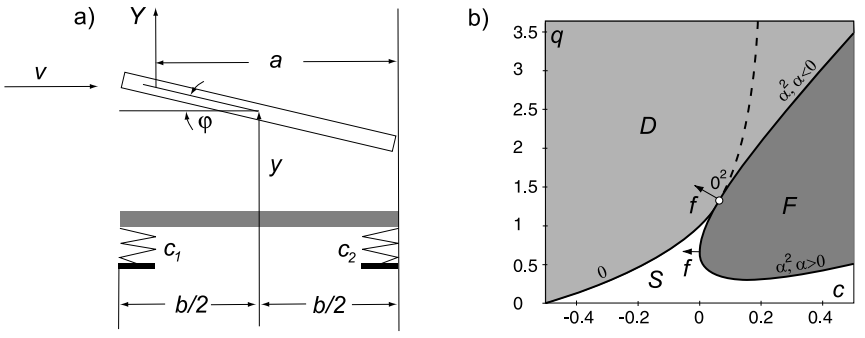

Figure 4.8. (a) An airfoil in a flow [465] and (b) its stability diagram [284, 521].

where mb is a mass of the plate per unit span and a is the distance between the trailing edge and the point of application of the lifting force. Taking b as a length scale, we put $z = y/b$ and define

$$c = \frac{c_1 - c_2}{2(c_1 + c_2)}, \quad \gamma = 6\left(\frac{2a}{b} - 1\right), \quad q = \frac{c_y^a \rho v^2}{2(c_1 + c_2)}, \quad \tau = t\sqrt{\frac{c_1 + c_2}{mb}}. \quad (4.130)$$

Assuming that $(z, \varphi)^T = \mathbf{u}^T e^{i\sqrt{\sigma}\tau}$, we get the eigenvalue problem (4.9) with

$$\mathbf{A} = \begin{pmatrix} 1 & c - q \\ 12c & 3 - \gamma q \end{pmatrix}. \quad (4.131)$$

Setting $c_y^\alpha > 0$, we obtain $q \geq 0$. It follows from physical considerations that $|c| \leq 1/2$. For thin profiles in the incompressible flow one can put $\gamma = 3$, and $a/b = 0.75$ [465]. Then, the characteristic equation for the matrix $\mathbf{A}$ is

$$\sigma^2 + (3q - 4)\sigma + 12cq - 3q - 12c^2 + 3 = 0. \quad (4.132)$$

Equating the free term in equation (4.132) to zero, we find the curve $q_d(c)$, that corresponds to $\sigma = 0$, i.e. defines the divergence boundary [284, 521]

$$q_d(c) = \frac{1 - 4c^2}{1 - 4c}. \quad (4.133)$$

Since $|c| \leq \frac{1}{2}$, $q \geq 0$, the curve $q_d(c)$ is in the stripe $c < \frac{1}{4}$. At its points

$$\sigma_1(c) \equiv 0, \quad \sigma_2(c) = \frac{1 - 16c + 12c^2}{1 - 4c}. \quad (4.134)$$

When $c < \frac{4-\sqrt{13}}{6}$, the eigenvalue $\sigma_2 > 0$ and the curve $q_d(c)$ separate the domains of stability and divergence, Figure 4.8 (b). When $\frac{4-\sqrt{13}}{6} < c < \frac{1}{4}$, the curve $q_d(c)$ belongs to the domain of divergence because $\sigma_2 < 0$. This part of the curve $q_d(c)$ is shown in Figure 4.8 (b) as the dashed line. At the 0^2 singular point ($c = \frac{4-\sqrt{13}}{6}, q = \frac{4}{3}$) both eigenvalues coalesce at zero, $\sigma_1 = \sigma_2 = 0$, and the stability domain by a narrow tongue touches the domains of flutter and divergence, Figure 4.8 (b).

When the discriminant of the polynomial (4.132) is negative, the eigenvalues are complex (flutter). The vanishing discriminant yields the flutter boundaries

$$q_f(c) = \frac{2}{3}\left(1 + 4c \pm 2\sqrt{c(c + 2)}\right). \quad (4.135)$$

The flutter domain is within the stripe $c \geq 0$, Figure 4.8 (b). The plus and minus signs correspond to the upper and lower boundaries of the flutter domain. The flutter boundary is a curve of double real eigenvalues with the Jordan chain of length 2: $\sigma_{1,2} = \frac{4-3q}{2}$. Therefore, for $q > \frac{4}{3}$ the curve $q_f(c)$ is a boundary between the flutter and divergence domains. In the case $q < \frac{4}{3}$, the curve $q_f(c)$ separates the domains of

stability and flutter. Partition of the plane of parameters into stability (S), flutter (F) and divergence (D) domains is shown in Figure 4.8 (b).

If the stiffness of the support of the leading edge, c_1, is lower than that of the trailing edge, c_2, i.e. when $c < 0$, then the plate loses stability statically by divergence. When $c > 0$, i.e. when the spring at the trailing edge is weaker, the stability is lost by flutter, which qualitatively correctly describes the instability of an airfoil in a flow, see also [405, 499].

Let us consider the point $(c = 0, q = 2/3)$ on the boundary between the stability and flutter domains that corresponds to the double eigenvalue $\sigma = 1$, Figure 4.8 (b). Note that equation (4.132) can be transformed into[5]

$$\left(\sigma - 1 + \frac{3}{2}q - 1\right)^2 - \left(-4c + \frac{3}{2}q - 1\right)^2 = -8c - 4c^2. \tag{4.139}$$

When $c \neq 0$, equation (4.139) describes a hyperbola with two asymptotes

$$\mathrm{Re}\sigma = 1 - 4c, \quad \mathrm{Re}\sigma = 3 - 3q + 4c, \tag{4.140}$$

that intersect at the point $(2(1 + 4c)/3, 1 - 4c)$ in the $(q, \mathrm{Re}\sigma)$-plane, Figure 4.9 (a). For $-1/2 < c < 0$, the solutions $\sigma(q)$ of equation (4.140) are real. One branch of the hyperbola remains positive when $q > 0$, while the second intersects the line $\mathrm{Re}\sigma = 0$ at some $q_d < 1$, as show the dark gray lines in Figure 4.9 (a). Hence, for $c < 0$ and $q > q_d, q_d < 1$, the airfoil is statically unstable (divergence).

When $c = 0$, the hyperbolas degenerate into two straight lines intersecting at the point $(2/3, 1)$ in the $(q, \mathrm{Re}\sigma)$-plane that are shown in black in Figure 4.9 (a). Therefore, the crossing of the eigencurves happens at the regular point of type α^2 of the flutter boundary, see Figure 4.8 (b). The double eigenvalue splits linearly with respect to q (which is nongeneric!) because at the point $(c = 0, q = 2/3)$ the flutter boundary has a vertical tangent which makes the splitting of the double nonsemisimple eigenvalue $\sigma = 1$ degenerate in the q direction.

---

[5] The eigencurves (4.139) are well approximated by equation (4.161) via the eigenvectors and associated vectors of the double eigenvalue $\sigma_0 = 1$ at the point $\mathbf{p}_0 = (0, 2/3)$

$$\mathbf{u}_0 = \begin{pmatrix} 1 \\ 0 \end{pmatrix}, \quad \mathbf{v}_0 = \begin{pmatrix} 0 \\ -2/3 \end{pmatrix}, \quad \mathbf{u}_1 = \begin{pmatrix} 0 \\ -3/2 \end{pmatrix}, \quad \mathbf{v}_1 = \begin{pmatrix} 1 \\ 0 \end{pmatrix}. \tag{4.136}$$

Indeed, at the point $\mathbf{p}_0$ in the (c, q)-plane the condition (4.159) is fulfilled, because $\mathbf{v}_0^T \partial_q \mathbf{A}\mathbf{u}_0 = 0$. Taking into account that $\Delta p_1 = c$, $\Delta p_2 = q - 2/3$ and

$$\begin{aligned} &\mathbf{v}_0^T \partial_c \mathbf{A}\mathbf{u}_0 = -8, \quad \mathbf{v}_0^T \partial_q \mathbf{A}\mathbf{G}_0 \partial_q \mathbf{A}\mathbf{u}_0 = 0, \\ &\mathbf{v}_1^T \partial_q \mathbf{A}\mathbf{u}_0 = 0, \quad \mathbf{v}_0^T \partial_q \mathbf{A}\mathbf{u}_1 = -3, \quad \mathbf{v}_0^T \partial_q^2 \mathbf{A}\mathbf{u}_0 = 0, \end{aligned} \tag{4.137}$$

equation (4.161) yields the approximation corresponding to a convex flutter domain, Figure 4.8 (b)

$$\left(\lambda - 1 + \frac{3}{2}q - 1\right)^2 - \left(\frac{3}{2}q - 1\right)^2 = -8c. \tag{4.138}$$

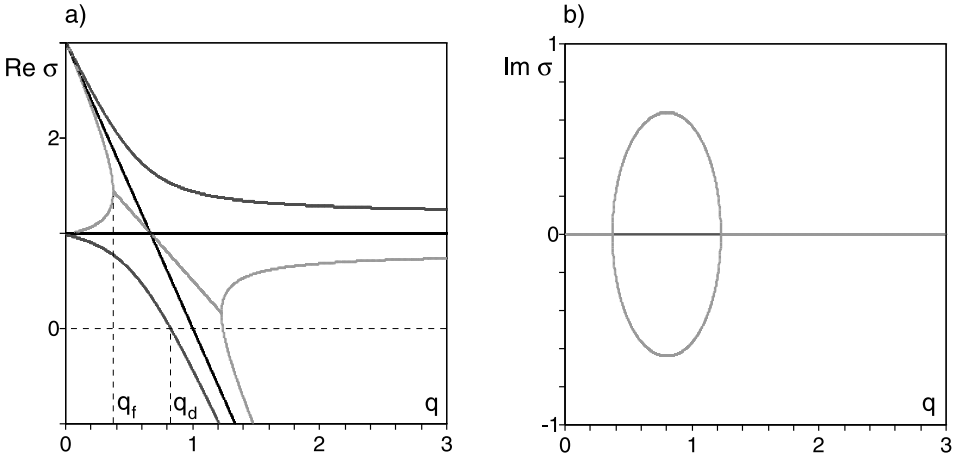

Figure 4.9. (a) Real parts of the eigenvalues σ demonstrating (dark gray lines) *veering* with $c = -0.05$, (black) *crossing* with $c = 0$, and (light gray lines) *overlapping* with $c = 0.05$; (b) the corresponding imaginary parts [284, 521].

Indeed, calculating the eigenvectors and associated vectors corresponding to the double eigenvalue $\sigma = \frac{4-3q}{2}$ at a point (c, q) on the curve $q_f\ (c)$

$$\mathbf{u}_0 = \begin{pmatrix} \frac{2(q-c)}{3q-2} \\ 1 \end{pmatrix}, \quad \mathbf{v}_0 = \begin{pmatrix} 12c \\ \frac{2-3q}{2} \end{pmatrix}, \quad \mathbf{u}_1 = \begin{pmatrix} 0 \\ \frac{2}{2-3q} \end{pmatrix}, \quad \mathbf{v}_1 = \begin{pmatrix} 0 \\ 1 \end{pmatrix} \tag{4.141}$$

we find the normal vector to the boundary

$$\mathbf{f} = \begin{pmatrix} 12\,(2c-q) \\ -12c + \frac{3}{2}\,(3q-2) \end{pmatrix}. \tag{4.142}$$

In particular, at the point $\left(c = 0, q = \frac{2}{3}\right)$ the vector $\mathbf{f}^T = (-8, 0)$ is directed to the stability domain orthogonal to the q-axis, Figure 4.8 (b).

The change of sign in the parameter c entails passage to hyperbolas laying in the adjacent angles formed by asymptotes (4.140), as demonstrated by the light gray curves in Figure 4.9 (a). The modification of the eigencurves originates a zone of complex eigenvalues (flutter), Figure 4.9 (b). This causes a sudden fall in the critical load ($q_f < q_d$), which is accompanied by a change of the nonoscillatory character of instability to an oscillatory one.

Comparing Figure 4.7 (b) and Figure 4.9 (a) we see that the similar crossing of eigencurves may happen both in the vicinity of the singularity $\alpha\alpha$ and in the vicinity of the regular point, α^2, on the flutter boundary. In the latter case parameters should vary along the tangent direction to the boundary. In the next section we describe the unfolding of the eigencurves in these two typical situations in the general setting.

4.6 Eigencurves, their crossing and veering

An eigencurve [64] is a one-parameter family of eigenvalues. When in the eigenvalue problem (4.9) corresponding to the circulatory system (4.8) the matrix $\mathbf{A}$ is real symmetric, the eigencurves of the potential system are real and generically avoid crossing (the *veering* phenomenon [370, 583]). In the presence of symmetries, the eigencurves can cross each other forming multiple semisimple eigenvalues at distinct values of the parameter [147, 587]. Perturbation of the potential system by, e.g., gyroscopic forces, can force the eigencurves to overlap [146, 392] and form *bubbles of instability* [390] consisting of complex eigenvalues (flutter). The same overlapping happens in circulatory systems near a conical $\alpha\alpha$ point [254], because here the flutter domain is convex, see Figure 4.7 (c).

4.6.1 Convex flutter domain: conical point $\alpha\alpha$.

The eigenvalues in the vicinity of the double semisimple eigenvalue $\sigma_0 > 0$ are determined by the quadratic equation (4.52). Denoting $\Delta\sigma = \varepsilon\sigma_1$ and

$$\tilde{\sigma} = \varepsilon\frac{(\mathbf{A}_1\mathbf{u}_1, \mathbf{v}_1) + (\mathbf{A}_1\mathbf{u}_2, \mathbf{v}_2)}{2}, \tag{4.143}$$

then separating real and imaginary parts in equation (4.52), we find

$$(\mathrm{Im}\Delta\sigma)^2 + x^2 = -(y^2 - z^2), \tag{4.144}$$

when $\mathrm{Re}\Delta\sigma = \tilde{\sigma}$, and

$$(\mathrm{Re}\Delta\sigma - \tilde{\sigma})^2 - x^2 = y^2 - z^2, \tag{4.145}$$

when $\mathrm{Im}\Delta\sigma = 0$, where x, y, and z are determined by equation (4.99).

Taking into account the conical geometry of the flutter domain in the (x, y, z)-space of Figure 4.5 (b), we see that at the fixed y and z such that $y^2 - z^2 > 0$, the equation (4.145) describes two hyperbolic eigencurves $\mathrm{Re}\Delta\sigma(x)$ in the avoided crossing. Since $y^2 - z^2 > 0$ implies $D = x^2 + y^2 - z^2 > 0$, the chosen path, parameterized by x, in the (x, y, z)-space lies in the stability domain being close both to the apex and to the skirt of the cone, Figure 4.5 (b).

When $y^2 - z^2 < 0$, the one-parameter path intersects the conical stability boundary and partly belongs to the flutter domain. Then, in the interval $x^2 < -(y^2 - z^2)$ equation (4.144) defines an ellipse of imaginary parts $\mathrm{Im}\Delta\sigma(x)$ with the real parts $\mathrm{Re}\Delta\sigma = \tilde{\sigma}$, cf. bubbles of instability in Figure 4.7 (c). In the interval $x^2 > -(y^2 - z^2)$, the eigenvalues are real and are described by the adjacent hyperbola (4.145), cf. overlapping of the real eigencurves in Figure 4.7 (c).

When $y = z = 0$, the eigencurves $\mathrm{Re}\Delta\sigma(x)$ are two crossed lines (4.145) that pass through a modified semisimple eigenvalue $\sigma_0 + \tilde{\sigma}$. Moreover, the similarly looking

crossing happens also when the x-parameterized path touches the skirt of the cone,[6] so that $y^2 = z^2 \neq 0$, cf. the crossing in Figure 4.9 (a).

Therefore, using the eigenvalues and eigenvectors of the double semisimple real eigenvalue at the $\alpha\alpha$ point, we can describe the crossing, veering and overlapping of the eigencurves via the approximations (4.144) and (4.145). Nevertheless, in comparison with the α^2 points which generically require only one parameter to occur in a family of circulatory systems, the $\alpha\alpha$ singularity needs at least three, being a much rarer phenomenon. A practical need for parametric and structural optimization of nonconservative systems requires description of the metamorphoses of eigencurves near smooth points of the flutter and divergence boundaries by using spectral information at the very points of the α^2 type, see e.g. [182, 259, 323, 356, 357, 396, 497].

4.6.2 Convex/concave flutter domain: smooth points α^2

Formulas (4.74) describe the movement of eigenvalues of the n-parameter circulatory system (4.8) in transverse crossing of the stability boundary. How do the eigenvalues behave along a straight line tangent to the stability boundary at a nonsingular point $\mathbf{p}_0$ as well as along the lines parallel to the tangent at a short distance from the boundary? The answer is given by the following lemma.

Lemma 4.6 (O. N. Kirillov, A. P. Seyranian, 2002 [274]). *Let $\mathbf{p}_0$ be a nonsingular point on the boundary between the stability and flutter domains, $\mathbf{f}$ the normal vector* (4.41) *evaluated at $\mathbf{p}_0$, $\mathbf{n} = \mathbf{f}/\|\mathbf{f}\|$ the corresponding unit vector, and $\mathbf{t} = \mathbf{e}_*/\|\mathbf{e}_*\|$ the unit vector of an arbitrary tangent at the point $\mathbf{p}_0$. Then, the section of the stability domain by the plane Oxy spanned by the vectors $\mathbf{n}$ and $\mathbf{t}$, with origin at the point $\mathbf{p}_0$, is described by the inequality*

$$y > Qx^2/\|\mathbf{f}\|, \quad \text{where} \quad P = \langle \mathbf{H}\mathbf{t}, \mathbf{t}\rangle, \quad Q = P - R^2, \quad R = \langle \mathbf{h}, \mathbf{t}\rangle. \tag{4.146}$$

Under these conditions, the formula

$$(\sigma - \sigma_0 - Rx)^2 + Qx^2 = y\|\mathbf{f}\| + o(x^2) \tag{4.147}$$

describes bifurcation of the double real eigenvalue $\sigma_0 > 0$ with the Jordan chain of length 2 that exists at $\mathbf{p}_0$.

---

[6] In the example of Section 4.5.5 we have $x = k_{22} - k_{11}$, $y = 2k_{12}$, $z = 2\nu$, and $\tilde{\sigma} = (k_{22} - k_{11})/2$. Then, equations (4.144) and (4.145) take, respectively, the form:

$$(\mathrm{Im}\sigma)^2 + (k_{22} - k_{11})^2 = -4k_{12}^2 + 4\nu^2, \quad (\mathrm{Re}\sigma - (k_{11} + k_{22})/2)^2 - (k_{22} - k_{11})^2 = 4k_{12}^2 - 4\nu^2.$$

When $k_{12} = \nu$, the matrix (4.119) is $\mathbf{A} = \begin{pmatrix} k_{11} & 0 \\ 2\nu & k_{22} \end{pmatrix}$, which reduces to the Jordan block (α^2) when $k_{11} = k_{22}$. The latter becomes a matrix proportional to the unity $(\alpha\alpha)$ if $\nu = 0$.

Proof. The behavior of the double eigenvalue along the curves (4.76) is described by the formula (4.79). The curve (4.76) in the plane of the normal and tangent vectors may be expressed as

$$\mathbf{p}(\varepsilon) = \mathbf{p}_0 + x(\varepsilon)\mathbf{t} + y(\varepsilon)\mathbf{n} \tag{4.148}$$

where $x(\varepsilon)$ and $y(\varepsilon)$ are smooth functions of ε. By definition (4.17)

$$\mathbf{e}_* = \frac{d\mathbf{p}}{d\varepsilon} = \frac{dx}{d\varepsilon}\mathbf{t} + \frac{dy}{d\varepsilon}\mathbf{n}, \quad 2\mathbf{d} \equiv \frac{d^2\mathbf{p}}{d\varepsilon^2} = \frac{d^2x}{d\varepsilon^2}\mathbf{t} + \frac{d^2y}{d\varepsilon^2}\mathbf{n}, \tag{4.149}$$

where all the derivatives are evaluated at $\varepsilon = 0$. Hence,

$$\frac{dx}{d\varepsilon}(\varepsilon = 0) = \|\mathbf{e}_*\|, \quad \frac{dy}{d\varepsilon}(\varepsilon = 0) = 0, \quad \frac{d^2y}{d\varepsilon^2}(\varepsilon = 0) = 2\langle \mathbf{n}, \mathbf{d}\rangle. \tag{4.150}$$

With equations (4.149) and (4.150) the formula (4.79) takes the form

$$\left(\sigma - \sigma_0 - R\frac{dx}{d\varepsilon}\varepsilon\right)^2 + Q\left(\frac{dx}{d\varepsilon}\varepsilon\right)^2 = \frac{1}{2}\frac{d^2y}{d\varepsilon^2}\|\mathbf{f}\|\varepsilon^2 + o(\varepsilon^2). \tag{4.151}$$

Since the first differential of the function $y(\varepsilon)$ vanishes at $\varepsilon = 0$, its increment is determined by the term of order ε^2. Consequently, equation (4.147) holds in the neighborhood of the point $\mathbf{p}_0$ in the plane of the vectors $\mathbf{n}$ and $\mathbf{t}$, Figure 4.10 (a). The nonbifurcation condition, applied to equation (4.147), yields the second-order approximation (4.146) to the section of the stability domain by the plane Oxy. □

Given a tangent vector $\mathbf{t}$, equation (4.147) describes the eigenvalue $\sigma(x, y)$ that originates after splitting of the double eigenvalue $\sigma_0 > 0$ existing on the boundary between the stability and flutter domains. The function $\sigma(x, y)$ can be considered as a one-parameter family of eigencurves $\sigma(x)$ parameterized by y.

The shape of the eigencurves $\sigma(x)$ near the point $\mathbf{p}_0$ depends on whether the section of the stability domain by the plane through the normal and tangent vectors to its boundary at $\mathbf{p}_0$ is convex or concave. According to the inequality (4.146) for $Q < 0$, the section of the stability domain is concave and the flutter domain is convex, Figure 4.10 (b). Then, at $y > 0$, the eigencurves $\sigma(x)$ are given by the two branches of a hyperbola in the $(x, \mathrm{Re}\sigma)$-plane

$$(\mathrm{Re}\sigma - \sigma_0 - Rx)^2 + Qx^2 = y\|\mathbf{f}\|, \quad \mathrm{Im}\sigma = 0. \tag{4.152}$$

As the parameter y decreases, the curves $\sigma(x)$ approach one another until they cross at the point $(0, \mathrm{Re}\sigma)$ when $y = 0$, Figure 4.10 (b). In the neighborhood of this point, the eigencurves are

$$\mathrm{Re}\sigma = \sigma_0 + x(R \pm \sqrt{-Q}), \quad \mathrm{Im}\sigma = 0. \tag{4.153}$$

With the further reduction of y, an ellipse of complex eigenvalues originates (a bubble of instability [390])

$$\mathrm{Re}\sigma = \sigma_0 + xR, \quad (\mathrm{Im}\sigma)^2 - x^2Q = -y\|\mathbf{f}\|, \tag{4.154}$$

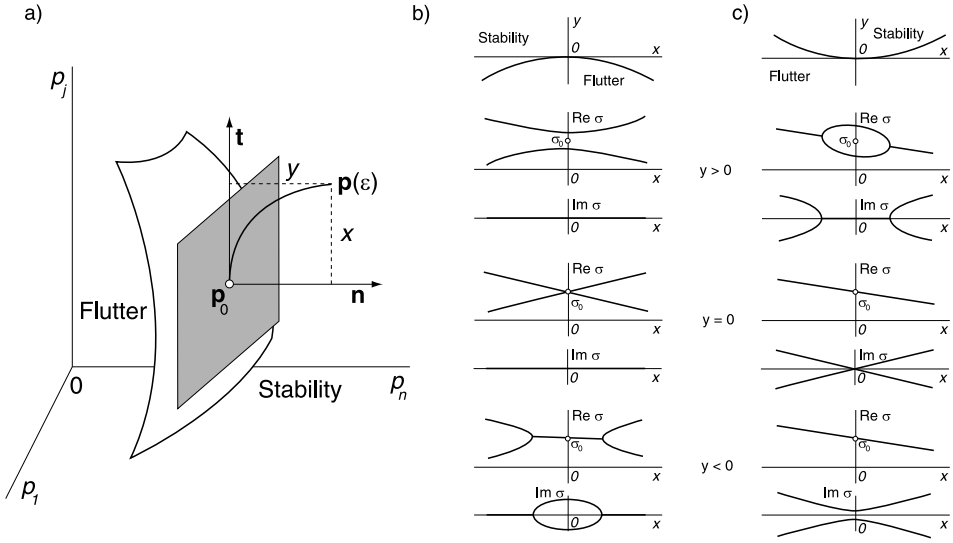

Figure 4.10. (a) A smooth part of the boundary between the stability and flutter domain with the local coordinate system Oxy in the normal plane spanned by the normal $\mathbf{n}$ and tangent $\mathbf{t}$ vector. (b) In the case of a convex cross-section of the flutter domain, the scenario of transformation of the eigencurves $\sigma(x)$ when y varies from positive values to negative ones. (c) Transformation of the eigencurves when the cross-section of the flutter domain is concave [274].

when x is inside the interval

$$x^2 < -\frac{y\|\mathbf{f}\|}{|Q|}. \tag{4.155}$$

Outside the interval (4.155), the eigencurves correspond to real eigenvalues that belong to the two branches of the adjacent hyperbola (4.152). In the $(\mathrm{Re}\sigma, \mathrm{Im}\sigma, x)$-space the ellipse and the hyperbola lie in the orthogonal planes. They touch one another at the exceptional points with $x = x_\pm := \pm\sqrt{\frac{y\|\mathbf{f}\|}{Q}}$, where the double real eigenvalues are formed

$$\sigma_\pm = \sigma_0 \pm R\sqrt{\frac{y\|\mathbf{f}\|}{Q}}. \tag{4.156}$$

Thus, as the parameter x varies, the eigenvalue bifurcates at the points x_- and x_+: two eigenvalues, being in one plane in the $(\mathrm{Re}\sigma, \mathrm{Im}\sigma, x)$-space, collide and take off in directions orthogonal to that plane. This is the reversible Hopf bifurcation that happens in transverse crossing of the boundary of the flutter domain. Note that inequality (4.155), which defines the boundaries of the instability bubble, is identical to the quadratic approximation to the section of the flutter domain (4.146). Thus, the overlapping of the eigencurves is closely related to the convexity of the flutter domain, Figure 4.10 (b).

When $Q > 0$, the section of the stability domain is convex and the flutter domain is concave. The corresponding unfolding of eigencurves is shown in Figure 4.10 (c). When $y > 0$, the real eigenvalues form an ellipse (4.152) in the interval

$$x^2 < \frac{y\|\mathbf{f}\|}{Q}. \tag{4.157}$$

The ellipse is connected to a hyperbola (4.154) of complex eigenvalues lying in the $(\mathrm{Re}\sigma, \mathrm{Im}\sigma, x)$-space. As the parameter y is reduced, the branches of the hyperbola approach one another and the stability bubble shrinks to a point $(0, \sigma_0)$ at $y = 0$. Then, the eigencurves are linear functions of x

$$\mathrm{Re}\sigma = \sigma_0 + Rx, \quad \mathrm{Im}\sigma = \pm x\sqrt{Q}. \tag{4.158}$$

Hyperbolas (4.154) consisting of complex-conjugate eigenvalues correspond to negative values of y, Figure 4.10 (c).

Let $\sigma_1(p_j)$ and $\sigma_2(p_j)$ be eigencurves of the n-parameter circulatory system (4.8). Assume that $\sigma_1(p_{0,j}) = \sigma_2(p_{0,j}) = \sigma_0$, where $\sigma_0 > 0$ is a double real eigenvalue with the right and left Jordan chains of vectors, $\mathbf{u}_0$, $\mathbf{u}_1$ and $\mathbf{v}_0$, $\mathbf{v}_1$, respectively, at a nonsingular point $\mathbf{p}_0^T = (p_{0,1}, \ldots, p_{0,n})$ of the boundary between the stability and flutter domains. Let, additionally,

$$\mathbf{v}_0^T \partial_{p_j} \mathbf{A}\mathbf{u}_0\Big|_{\mathbf{p}=\mathbf{p}_0} = 0. \tag{4.159}$$

Condition (4.159) implies that the j-th component of the normal vector $\mathbf{f}$ vanishes at the point $\mathbf{p}_0$. Since we are interested in the functions $\sigma(p_j)$, we have to take the unit tangent vector $\mathbf{t}$ parallel to the p_j axis, Figure 4.10 (a). All the components of this vector vanish, except for $t_j = 1$. Under these conditions

$$x = \Delta p_j, \quad y\|\mathbf{f}\| = \sum_{s=1, s\neq j}^{n} f_s \Delta p_s. \tag{4.160}$$

In addition, because of the special form of the unit tangent vector $\mathbf{t}$, the scalar products in formulae (4.146)–(4.147) degenerate and contain only the components H_{jj} and h_j of the matrix $\mathbf{H}$ and vector $\mathbf{h}$. Taking all this into consideration in (4.147) and expressing H_{jj}, h_j and f_s in terms of the derivatives of the matrix $\mathbf{A}$ with respect to the parameters and the vectors of the Jordan chain, we finally arrive at the following theorem:

Theorem 4.7 (O. N. Kirillov, A. P. Seyranian, 2002 [274]). *If in the eigenvalue problem* (4.9)*, the matrix* $\mathbf{A}(\mathbf{p})$ *satisfies equation* (4.159)*, then the eigencurves* $\sigma_1(p_j)$ *and* $\sigma_2(p_j)$ *are approximated by a hyperbola*

$$\left(\Delta\sigma - \frac{\mathbf{v}_1^T \partial_{p_j}\mathbf{A}\mathbf{u}_0 - \mathbf{v}_0^T \partial_{p_j}\mathbf{A}\mathbf{u}_1}{2}\Delta p_j\right)^2 - \sum_{s=1, s\neq j}^{n} \mathbf{v}_0^T \partial_{p_s}\mathbf{A}\mathbf{u}_0 \Delta p_s \quad (4.161)$$
$$= \left(\frac{\left(\mathbf{v}_1^T \partial_{p_j}\mathbf{A}\mathbf{u}_0 - \mathbf{v}_0^T \partial_{p_j}\mathbf{A}\mathbf{u}_1\right)^2}{4} - \mathbf{v}_0^T \left(\partial_{p_j}\mathbf{A}\mathbf{G}_0\partial_{p_j}\mathbf{A} - \frac{\partial^2_{p_j}\mathbf{A}}{2}\right)\mathbf{u}_0\right)(\Delta p_j)^2,$$

where $\Delta\sigma = \sigma - \sigma_0$, $\Delta p_k = p_k - p_{0,k}$, $\mathbf{G}_0 = [\mathbf{A}(\mathbf{p}_0) - \sigma_0\mathbf{I} - \mathbf{v}_0\mathbf{v}_0^T]^{-1}$, *and* $\mathbf{I}$ *is the identity matrix.*

A similar result on the eigencurves near a smooth point of the boundary between stability and divergence domains is established in [274]. Note that when $\sigma_0 < 0$, Theorem 4.7 describes the behavior of eigencurves near the divergence/flutter boundary. Such boundaries indicating transition from oscillatory to nonoscillatory instability are important, e.g. in the theory of MHD dynamos [307].

4.7 Parametric optimization of circulatory systems

Optimization of stability of conservative elastic systems [182], e.g. finding a shape of a column that would withstand the highest possible buckling load under a fixed volume constraint, is already nontrivial because some optimal solutions could be multi-modal and thus correspond to a multiple semisimple eigenvalue which creates a conical singularity of the merit functional [518]. Nevertheless, an increase in the critical divergence load attained at the optimal design is usually not very large in comparison with the initial design [182, 518].

In contrast to the potential systems, the circulatory ones can lose stability both by divergence and by flutter. It is known that mass and stiffness modification can increase the critical flutter load by hundreds percent, which is an order of magnitude higher than typical gains achieved in optimization of conservative systems [182,259,323,357,396, 497]. For example, Ringertz [497] reported an 838% increase of the critical flutter load for a Beck's column loaded by a follower force [113], from 20.05 for a uniform design to 188.1 for an optimized shape.

In both conservative and nonconservative problems of structural optimization of slender structures, their optimal or optimized shapes often possess places with small or even vanishing cross-sections [182, 259, 271, 284, 357, 497]. Another intriguing aspect of optimization of nonconservative systems is the 'wandering' critical frequency at

the optimal critical load. During the optimization the eigenvalue branches experience numerous mutual overlappings and veerings [259, 271, 284, 323, 357, 396, 497]. This puzzling behavior of the critical frequency is still awaiting its explanation.

In some problems, such as the optimal placement of a point mass along a uniform free-free rod moving under the follower thrust [467, 562], the local maximum was found at the α^3 singularity on the flutter boundary where a triple eigenvalue with the Jordan block exists [283, 284]. In order for the last phenomenon to happen, one needs at least three modes [283, 284] meaning that two-mode approximations [467, 562] are unable to detect such optima. This reflects a general question on model reduction and validity of low-dimensional approximations in nonconservative stability problems discussed already by Bolotin [75] and Gasparini et al. [191] and recently raised again in the context of friction-induced vibrations by Butlin and Woodhouse [107].

The above mentioned phenomena make rigorous proofs of the optimality in the nonconservative optimization problems substantially more difficult than in conservative ones. To the best of our knowledge, the rigorously proven optimal solutions in optimization problems for distributed circulatory systems have not been found. Although in the finite-dimensional case the situation is not much better, it looks reasonable to try to understand the nature of the observed difficulties of optimization on the final dimensional nonconservative systems that depend on a finite number of control parameters [272, 275, 300, 302].

4.7.1 Example: optimization of Ziegler's pendulum

Let us consider the classical Ziegler's pendulum consisting of two light and rigid links of equal length l. The pendulum is attached to a firm basement by an elastic revolute joint with the stiffness coefficient c_1. Another joint with the stiffness coefficient c_2 connects the two links, see Figure 4.11 (a). At the second revolute joint and at, respectively, the free end of the second link, the point masses m_1 and m_2 are located. The pendulum is subjected to a force P that is always directed along the second link (the follower force) [312, 622].

Small angular deviations θ_1 and θ_2 from the vertical equilibrium of Ziegler's pendulum are described by equation (4.8) with the matrices [312, 622]

$$\mathbf{M} = l^2 \begin{pmatrix} m_1 + m_2 & m_2 \\ m_2 & m_2 \end{pmatrix}, \quad \mathbf{P} = \begin{pmatrix} c_1 + c_2 - Pl & Pl - c_2 \\ -c_2 & c_2 \end{pmatrix}. \tag{4.162}$$

Calculating $\det(\mathbf{P} - \sigma\mathbf{M})$ we obtain the characteristic equation [302]

$$m_1 m_2 l^4 \sigma^2 - (m_1 c_2 + 4m_2 c_2 + c_1 m_2 - 2Plm_2) l^2 \sigma + c_1 c_2 = 0. \tag{4.163}$$

Using the Gallina criterion [187], we find that given positive m_1, m_2, and l, the pendulum is marginally stable when $c_1 \geq 0$, $c_2 \geq 0$, and $P < P_f^-(c_1, c_2)$, where

$$P_f^{\pm} := \frac{4m_2 c_2 + \left(\sqrt{m_1 c_2} \pm \sqrt{m_2 c_1}\right)^2}{2lm_2}. \tag{4.164}$$

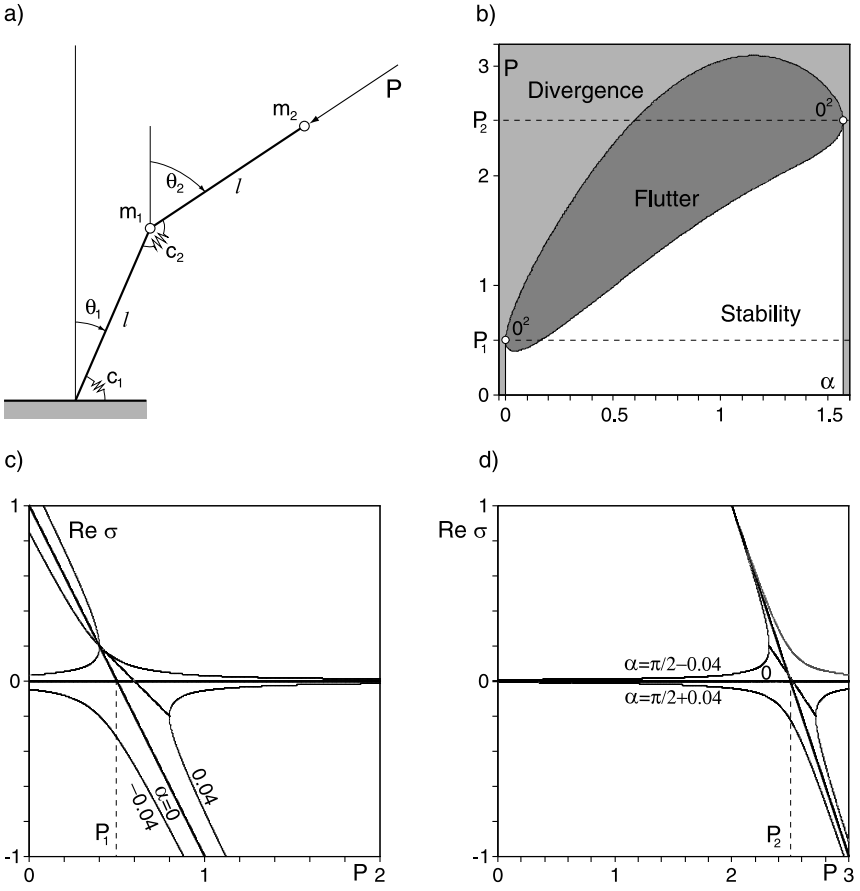

Figure 4.11. (a) Ziegler's pendulum. For $m_1 = m_2 = 1$ and $l = 1$: (b) the critical load $P(\alpha)$, where $c_1 = c\cos(\alpha)$, $c_2 = c\sin(\alpha)$, and $c = 1$; (c) the eigencurves near the point ($\alpha = 0, P = P_1 = 1/2$) of the local maximum and (d) near the point ($\alpha = \pi/2, P = P_2 = 5/2$) of the global maximum of P.

Note that

$$P_f^-(c_2 = 0) := P_1 = \frac{c_1}{2l}, \quad P_f^-(c_1 = 0) = P_2 := \frac{c_2}{2l}\left(4 + \frac{m_1}{m_2}\right). \tag{4.165}$$

Applying the *isoperimetric constraint* $c_1^2 + c_2^2 = c^2$, we can write $c_1 = c\cos(\alpha)$ and $c_2 = c\sin(\alpha)$. Then, for $m_1 = m_2 = 1$, $l = 1$, and $c = 1$, we get

$$P_f^{\pm}(\alpha) = \frac{5\sin(\alpha) + \cos(\alpha)}{2} \pm \sqrt{\sin(\alpha)\cos(\alpha)}. \tag{4.166}$$

In Figure 4.11 (b) the stability diagram of the pendulum is plotted in the (α, P)-plane. When $\alpha < 0$ or $\alpha > \pi/2$, the system is unstable by divergence. The flutter

domain is contained between the curves $P_f^-(\alpha)$ and $P_f^+(\alpha)$. Above the curve $P_f^+(\alpha)$, the pendulum is unstable by divergence. The divergence, stability and flutter domains meet at the two singular points (0^2) when $\alpha = 0$ ($c_2 = 0$) and $\alpha = \pi/2$ ($c_1 = 0$). At these points the critical flutter load, P_f^-, attains its maximal values given by equation (4.165), see Figure 4.11 (b). The global maximum is thus $P_f^- = 5/2$ at $\alpha = \pi/2$.

Note that at the both extremal points the flutter boundary has a vertical tangent. As a consequence, the eigencurves $\sigma(P)$, parameterized by α, bifurcate demonstrating subsequently the avoided crossing, crossing and overlapping, Figure 4.11 (c, d). The critical flutter load is maximal at the crossing of the eigencurves, corresponding to the double zero eigenvalue with the Jordan block. Another peculiarity is that at the optimal solutions found, either the first (c_1) or the second (c_2) stiffness becomes zero, reminding us of the vanishing cross-sections of the optimized solutions of continuous nonconservative elastic systems [182, 259, 271, 284, 357, 497].

Therefore, already the parametric optimization of the two degrees of freedom Ziegler's pendulum evidences that in circulatory systems the merit functional is nonsmooth and nonconvex. It may attain its maxima at the singular points of the stability boundary that correspond to the bimodal solutions. At these points the stability boundary has a vertical tangent and the eigencurves have a crossing. In the last sections of this chapter we will develop a method to judge whether the crossing of eigencurves is associated with a local extremum or an improving variation of the merit functional can be constructed.

4.7.2 A nonsmooth and nonconvex optimization problem

Let the circulatory system (4.8) depend on the vector of parameters $\mathbf{p}$ that is decomposed as $\mathbf{p}^T = (q, \mathbf{z}^T)$, where $q = p_1$ is the nonconservative load parameter and $\mathbf{z}^T = (p_2, \ldots, p_n)$ the vector of design parameters [275]. Assume that at $q = 0$ and for any $\mathbf{z}$ from an open domain $U \subset \mathbb{R}^{n-1}$ all eigenvalues of the matrix $\mathbf{A}(0, \mathbf{z})$ in the eigenvalue problem (4.9) are positive and simple (i.e. $(0, \mathbf{z})$ is an interior point of the stability domain).

The one-parameter family $\mathbf{A}(q)$ generically contains matrices with simple spectra (only at some isolated values of q may the matrix $\mathbf{A}$ have either a Jordan block of order 2 with a double real eigenvalue or a simple zero eigenvalue). If the vector $\mathbf{z}$ is varied, then we may expect that matrices of a more complicated Jordan structure can appear in the family $\mathbf{A}(q)$ (among them, only matrices whose spectra contain multiple positive and zero eigenvalues correspond to the boundary of the stability domain).

Definition 4.8 (O. N. Kirillov, A. P. Seyranian, 2002 [275]). Given the vector of design parameters $\mathbf{z} \subset U$. The parameter q takes its critical value q_j^* if the spectrum of $\mathbf{A}(q_j^*, \mathbf{z})$ with a Jordan structure J consists of real eigenvalues $\lambda \geq 0$ among which there exists at least one zero eigenvalue of algebraic multiplicity $k \geq 1$ or at least

one positive eigenvalue of algebraic multiplicity $k \geq 2$. The minimal element of the set $\Omega_{\mathbf{z}} = \{q^*_{J_1}, q^*_{J_2}, \ldots\}$ formed by all critical values of q is called the *critical load functional* and is denoted by $q^*(\mathbf{z})$.

Optimization of the circulatory system (4.8) with respect to stability criterion means to widen the interval of safe (in the sense of stability loss) values of q via the proper choice of $\mathbf{z}$

$$q^*(\mathbf{z}) \to \sup, \quad \mathbf{z} \in U \subset \mathbb{R}^{n-1}. \tag{4.167}$$

In the problems of optimum design [182, 259, 323, 356, 357, 396, 497], the vector $\mathbf{z}$ usually corresponds to the mass- or stiffness distribution of a structure. Additional restrictions may be imposed on $\mathbf{z}$ (e.g. an isoperimetric constraint). As is shown below, in our problem the main difficulty is that the merit functional is nonsmooth (therefore, we do not take into account such restrictions).

4.7.3 The gradient of the critical load

As a rule, the problem (4.167) is solved numerically; traditionally, the gradient method is used [182, 357, 396, 497]. Let us consider a point $\mathbf{p}_0 = (q^*_{\alpha^2}, \mathbf{z})$ belonging to the smooth part (a hypersurface) of the boundary between the stability and flutter domains, see e.g. Figure 4.10 (a). At this point of the boundary there exists a tangent plane such that an expression for the gradient of the critical load $q^*_{\alpha^2}$ follows from the equation (4.75) of this plane. With the decomposition $(\Delta\mathbf{p})^T = (\Delta q, (\Delta\mathbf{z})^T)$, the equation (4.75) takes the form $\Delta q = \langle \mathbf{g}_{\alpha^2}, \Delta\mathbf{z} \rangle$, where

$$\mathbf{g}_{\alpha^2} = -\frac{\mathbf{r}_{\alpha^2}}{f^1_{\alpha^2}}, \tag{4.168}$$

when $f^1_{\alpha^2} \neq 0$, is the gradient of the critical load $q^*_{\alpha^2}$ with respect to the design parameters $\mathbf{z}$. The normal vector to the boundary is $\mathbf{f}^T_{\alpha^2} = (f^1_{\alpha^2}, \mathbf{r}^T_{\alpha^2})$. The vector $\mathbf{r}^T_{\alpha^2} = (f^2_{\alpha^2}, \ldots, f^n_{\alpha^2})$ and the quantity $f^1_{\alpha^2}$ are determined as [275]

$$f^1_{\alpha^2} = \mathbf{v}_0^T \frac{\partial \mathbf{A}}{\partial q}\mathbf{u}_0, \quad f^s_{\alpha^2} = \mathbf{v}_0^T \frac{\partial \mathbf{A}}{\partial z_{s-1}}\mathbf{u}_0, \quad s = 2 \ldots n. \tag{4.169}$$

Let us assume that $q^*(\mathbf{z}) = q^*_{\alpha^2}$ with $\mathbf{z}$ given. If $\mathbf{g}_{\alpha^2} \neq 0$, then the variation $\Delta\mathbf{z} = \gamma \mathbf{g}_{\alpha^2}$ is an improving one, since the increment $\Delta q^* = \gamma |\mathbf{g}_{\alpha^2}|^2 > 0$ for a sufficiently small $\gamma > 0$. The condition $\mathbf{g}_{\alpha^2} = 0$ is necessary for the vector $\mathbf{z}$ to be a solution to problem (4.167) in those domains of its variation where the objective functional smoothly depends on the design parameters. In another frequently occurring situation, the gradient significantly grows in such a way that for some $\mathbf{z}$ the functional is discontinuous and $\mathbf{g}_{\alpha^2} \to \infty$ [323, 396].

4.7.4 An infinite gradient at the crossing of the eigencurves

Let $q^*(\mathbf{z}) = q^*_{\alpha^2}$ at some $\mathbf{z}$ and the gradient $\mathbf{g}_{\alpha^2}$ does not exist. According to equation (4.168), this is possible when $f^1_{\alpha^2} = 0$, i.e. when the normal vector to the stability boundary is orthogonal to the q-axis in the parameter space: $\mathbf{f}^T_{\alpha^2} = (0, \mathbf{r}^T_{\alpha^2})$. With the unit tangent vector $\mathbf{t}^T = (1, 0, \ldots, 0)$ at the point $\mathbf{p}_0 = (q^*_{\alpha^2}, \mathbf{z})$ we rewrite equation (4.147) as

$$(\Delta\sigma - h^1_{\alpha^2}\Delta q)^2 + Q(\Delta q)^2 = \langle \mathbf{r}_{\alpha^2}, \Delta\mathbf{z}\rangle + o((\Delta q)^2), \tag{4.170}$$

where $\Delta\sigma = \sigma - \alpha$, $\Delta q = q - q^*_{\alpha^2}$, $Q = H^{11}_{\alpha^2} - (h^1_{\alpha^2})^2$, and the coefficients $h^1_{\alpha^2}$ and $H^{11}_{\alpha^2}$ are specified in terms of the eigenvectors and associated vectors of the double eigenvalue α by the equations

$$2h^1_{\alpha^2} = \mathbf{v}_1^T \frac{\partial \mathbf{A}}{\partial q}\mathbf{u}_0 + \mathbf{v}_0^T \frac{\partial \mathbf{A}}{\partial q}\mathbf{u}_1, \quad H^{11}_{\alpha^2} = -\frac{1}{2}\mathbf{v}_0^T \frac{\partial^2 \mathbf{A}}{\partial q^2}\mathbf{u}_0 + \mathbf{v}_0^T \frac{\partial \mathbf{A}}{\partial q}\mathbf{G}_0 \frac{\partial \mathbf{A}}{\partial q}\mathbf{u}_0. \tag{4.171}$$

We restrict our further consideration to the case $Q < 0$, implying that the section of the flutter domain in the plane of the vectors $\mathbf{f}_{\alpha^2}$ and $\mathbf{t}$ is convex, Figure 4.10 (b). Then, at $\Delta\mathbf{z} = 0$ the eigencurves $\sigma(q)$ cross. At

$$\langle \mathbf{r}_{\alpha^2}, \Delta\mathbf{z}\rangle > 0, \tag{4.172}$$

they veer away and at $\langle \mathbf{r}_{\alpha^2}, \Delta\mathbf{z}\rangle < 0$ they overlap and form a ring of complex eigenvalues in the interval of variation of q that belongs to the flutter domain, Figure 4.10 (b). Note that the crossing of the eigencurves $\sigma(q)$ takes place at the point $(q^*_{\alpha^2}, \mathbf{z})$ where the gradient equation (4.168) tends to infinity because $f^1_{\alpha^2} = 0$.

4.7.5 Improving variations and necessary conditions for optimality in the case where the eigencurves cross

Suppose we are given a vector $\mathbf{z}$ and the first two minimal values $q^*_{\alpha^2}$ and $q^*_{\beta^2}$ corresponding to double eigenvalues α and β, respectively ($q^*_{\alpha^2} < q^*_{\beta^2}$). It is assumed that $\mathbf{g}_{\alpha^2} \to \infty$, i.e. ($f^1_{\alpha^2} = 0$) and $\mathbf{g}_{\beta^2} \neq 0$ ($f^1_{\beta^2} \neq 0$). Then, $q^*(\mathbf{z}) = q^*_{\alpha^2}$, Figure 4.12 (b). This value is not maximal, because according to equation (4.170) any small variation $\Delta\mathbf{z}$ satisfying equation (4.172) causes a stepwise increase in the functional by shifting the characteristic curves $\sigma(q)$ apart at the point $q = q^*_{\alpha^2}$ so that the critical value $q^*_{\alpha^2}$ disappears, Figure 4.12 (c). In contrast, generically, the critical value $q^*_{\beta^2}$ and its gradient $\mathbf{g}_{\beta^2}$ only slightly change.

The value of the functional at the point $\mathbf{z} + \Delta\mathbf{z}$ exceeds its value at the point $\mathbf{z}$ by a quantity of order $q^*_{\beta^2} - q^*_{\alpha^2}$. At the same time, the former may be less than the critical value $q^*_{\beta^2}$ computed at the point $\mathbf{z}$ if $q^*_{\beta^2}$ is the supremum of the functional q^* in a neighborhood of the point $\mathbf{z}$. Let us find the necessary conditions which are to be valid if it is known that at the point $\mathbf{z}$ we have

$$q^*(\mathbf{z}) = q^*_{\alpha^2}, \quad f^1_{\alpha^2} = 0, \quad q^*_{\alpha^2} < q^*_{\beta^2}, \quad f^1_{\beta^2} \neq 0, \quad \mathbf{g}_{\beta^2} \neq 0. \tag{4.173}$$

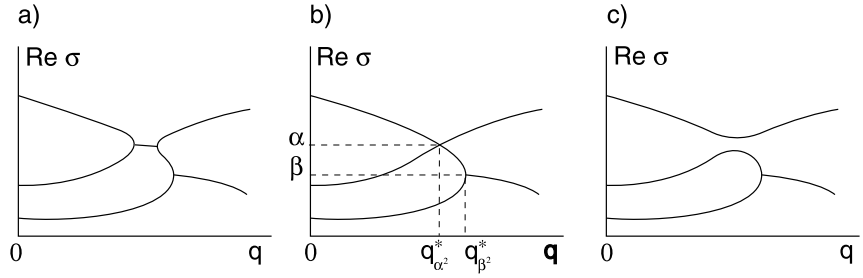

Figure 4.12. A discontinuity of $q^*(\mathbf{z})$ when the eigencurves (a) overlap ($\langle \mathbf{r}_{\alpha^2}, \Delta\mathbf{z}\rangle<0$) after (b) crossing ($\Delta\mathbf{z} = 0$) that is preceded by (c) their veering ($\langle \mathbf{r}_{\alpha^2}, \Delta\mathbf{z}\rangle>0$).

If $q^*_{\beta^2}$ is not a supremum, then it can be increased by moving along the gradient $\mathbf{g}_{\beta^2}$ and simultaneously preventing the eigencurves from converging. Hence, the improving variation $\Delta\mathbf{z}$ must satisfy the condition (4.172) and the inequality

$$\Delta q^*_{\beta^2} = \langle \mathbf{g}_{\beta^2}, \Delta\mathbf{z}\rangle > 0. \tag{4.174}$$

We shall look for this variation in the form of the linear combination

$$\Delta\mathbf{z} = c_1\mathbf{r}_{\alpha^2} + c_2\mathbf{g}_{\beta^2}. \tag{4.175}$$

Let the distance between the eigenvalues $\sigma_\pm = \alpha \pm \sqrt{\langle \mathbf{r}_{\alpha^2}, \Delta\mathbf{z}\rangle}$ at the point $(q^*_{\alpha^2}, \mathbf{z}+\Delta\mathbf{z})$ be equal to $2\sqrt{\varepsilon_1}$ ($\varepsilon_1 > 0$) and the increment $\Delta q^*_{\beta^2}$ be equal to $\varepsilon_2 > 0$. Substituting the variation (4.175) into equations (4.172) and (4.174), yields the equations determining c_1 and c_2

$$c_1\langle \mathbf{r}_{\alpha^2}, \mathbf{r}_{\alpha^2}\rangle + c_2\langle \mathbf{r}_{\alpha^2}, \mathbf{g}_{\beta^2}\rangle = \varepsilon_1, \quad c_1\langle \mathbf{g}_{\beta^2}, \mathbf{r}_{\alpha^2}\rangle + c_2\langle \mathbf{g}_{\beta^2}, \mathbf{g}_{\beta^2}\rangle = \varepsilon_2. \tag{4.176}$$

Since the matrix of the system (4.176) is the Gramian matrix of the vectors $\mathbf{r}_{\alpha^2}$ and $\mathbf{g}_{\beta^2}$, its determinant is not equal to zero (i.e. a nontrivial solution exists) if the vectors are linearly independent. Thus, the following lemma is valid [275]:

Lemma 4.9. *If the above vectors* $\mathbf{r}_{\alpha^2}$ *and* $\mathbf{g}_{\beta^2}$ *are linearly independent, then for any small* $\varepsilon_1 > 0$ *and* $\varepsilon_2 > 0$ *there exists an improving variation* (4.175) *preventing the characteristic curves from overlapping when* $q < q^*_{\beta^2}$ *whose coefficients* c_1 *and* c_2 *are solutions to the system* (4.176).

The vanishing determinant of the Gramian matrix means linear dependence of $\mathbf{r}_{\alpha^2}$ and $\mathbf{g}_{\beta^2}$. Then, equations (4.176) may have a solution only when the right-hand side of (4.176) is orthogonal to the solution of the homogeneous system obtained from (4.176). This condition of solvability is

$$\varepsilon_2 = \varepsilon_1 \frac{\langle \mathbf{r}_{\alpha^2}, \mathbf{g}_{\beta^2}\rangle}{\langle \mathbf{r}_{\alpha^2}, \mathbf{r}_{\alpha^2}\rangle}. \tag{4.177}$$

When the numerator in (4.177) is positive, a solution to system (4.176) exists with $\varepsilon_1 > 0$ and $\varepsilon_2 > 0$. Hence, an improving variation also exists. If

$$\langle \mathbf{r}_{\alpha^2}, \mathbf{g}_{\beta^2} \rangle < 0, \tag{4.178}$$

then ε_1 and ε_2 are opposite in sign and variation (4.175) is not improving. In this case an increase of $q^*_{\beta^2}$ ($\varepsilon_2 > 0$) causes an overlapping of the eigencurves ($\varepsilon_1 < 0$) and a stepwise decrease of the functional, Figure 4.12 (a). An attempt to move the eigencurves apart ($\varepsilon_1 > 0$) at the point $q^*_{\alpha^2}$ causes a decrease of the critical load $q^*_{\beta^2}$ ($\varepsilon_2 < 0$). Thus, from Lemma 4.9 and inequality (4.178) the necessary condition follows for a local extremum in the problem (4.167):

Theorem 4.10 (O. N. Kirillov, A. P. Seyranian, 2002 [275]). *Let conditions* (4.173) *be valid for a vector* $\mathbf{z}$. *In order for* $q^*_{\beta^2}$ *to be the supremum of the functional* $q^*(\mathbf{z})$ *in a small neighborhood of* $\mathbf{z}$, *it is necessary that the vectors* $\mathbf{r}_{\alpha^2}$ *and* $\mathbf{g}_{\beta^2}$ *be linearly dependent:* $\mathbf{r}_{\alpha^2} = \gamma \mathbf{g}_{\beta^2}$ *with* $\gamma < 0$.

Note that conditions (4.173) are generic for a circulatory system with two or more parameters. Therefore, a discontinuity of the critical load functional can often be observed in the problems of optimization of circulatory systems, see e.g. [323, 357, 396, 497] where all attempts to find an improving variation leading away from a point of discontinuity, or to prove the extremality of q^* at this point were unsuccessful. Theorem 4.10 allows one to detect an extremum or to move away from the point of discontinuity of the functional q^*.

Chapter 5

Influence of structure of forces on stability

Now conservative, circulatory, and gyroscopic forces are present. The pairwise interaction of arbitrary two of these results in the existence of stable domains in the parameter space. However, the simultaneous action of all three effects always results in instability!

V. V. Beletsky [41]

In this chapter we consider stability of equilibria of mechanical systems under the action of *positional* potential and circulatory forces and *velocity-dependent* damping and gyroscopic forces. Equations describing the linearized dynamics of such a system with m degrees of freedom have the form

$$\mathbf{M}\ddot{\mathbf{x}} + (\mathbf{G} + \mathbf{D})\dot{\mathbf{x}} + (\mathbf{K} + \mathbf{N})\mathbf{x} = 0, \quad \mathbf{x} \in \mathbb{R}^m, \tag{5.1}$$

where dot stands for time differentiation and the real $m \times m$ matrices $\mathbf{M} = \mathbf{M}^T$, $\mathbf{G} = -\mathbf{G}^T$, $\mathbf{D} = \mathbf{D}^T$, $\mathbf{K} = \mathbf{K}^T$, and $\mathbf{N} = -\mathbf{N}^T$ correspond to inertia, gyroscopic, damping, potential, and circulatory forces, respectively [239, 423, 460, 623]. Potential and gyroscopic forces are conservative forces while damping and circulatory forces are nonconservative ones [332, 333]. The matrices $\mathbf{M}$, $\mathbf{D}$, and $\mathbf{K}$ can be both definite and indefinite, and we will specify their properties in every particular case.

Frequently, the *general nonconservative system* (5.1) can be seen as a result of a small perturbation of an 'ideal' system. The latter could be:
the *undamped potential system* [423]

$$\mathbf{M}\ddot{\mathbf{x}} + \mathbf{K}\mathbf{x} = 0, \tag{5.2}$$

the *undamped gyroscopic system* [423]

$$\mathbf{M}\ddot{\mathbf{x}} + \mathbf{G}\dot{\mathbf{x}} + \mathbf{K}\mathbf{x} = 0, \tag{5.3}$$

the *circulatory system* [623]

$$\mathbf{M}\ddot{\mathbf{x}} + (\mathbf{K} + \mathbf{N})\mathbf{x} = 0, \tag{5.4}$$

and the *oscillatory damped system* [174]

$$\mathbf{M}\ddot{\mathbf{x}} + \mathbf{D}\dot{\mathbf{x}} + \mathbf{K}\mathbf{x} = 0, \tag{5.5}$$

where $\mathbf{D}$ is an indefinite matrix with properties that will be specified later.

Looking for a solution to equation (5.1) in the form $\mathbf{x} = \mathbf{u}e^{\lambda t}$, we obtain the eigenvalue problem

$$(\mathbf{M}\lambda^2 + (\mathbf{G} + \mathbf{D})\lambda + \mathbf{K} + \mathbf{N})\mathbf{u} = 0, \tag{5.6}$$

which has a nontrivial solution $\mathbf{u}$ if and only if

$$p(\lambda) := \det(\mathbf{M}\lambda^2 + (\mathbf{G} + \mathbf{D})\lambda + \mathbf{K} + \mathbf{N}) = 0. \tag{5.7}$$

The roots of the characteristic equation (5.7) are eigenvalues of the eigenvalue problem (5.6) corresponding to the eigenvectors $\mathbf{u}$.

Theorem 5.1 (S. Barnett, 1989 [36, 592]). *Let*

$$(s^2\mathbf{I} - s\mathbf{A}_1 - \mathbf{A}_2)^{-1} = \frac{s^{2m-2}\mathbf{I} + s^{2m-2}\mathbf{B}_1 + \cdots + \mathbf{B}_{2m-2}}{d(s)}$$

where $d(s) = s^{2m} + d_1 s^{2m-1} + \cdots + d_{2m-1}s + d_{2m}$. *Then,*

$$\begin{aligned} d_1 &= -\mathrm{tr}\mathbf{A}_1, \quad \mathbf{B}_1 = \mathbf{A}_1 + d_1\mathbf{I}, \\ d_i &= -\frac{\mathrm{tr}(\mathbf{A}_1\mathbf{B}_{i-1} + 2\mathbf{A}_2\mathbf{B}_{i-2})}{i}, \quad i = 2, 3, \ldots, 2m-2, \\ \mathbf{B}_i &= \mathbf{A}_1\mathbf{B}_{i-1} + \mathbf{A}_2\mathbf{B}_{i-2} + d_i\mathbf{I}, \quad i = 2, 3, \ldots, 2m-2, \end{aligned}$$

where $\mathbf{B}_0 = \mathbf{I}$, $d_{2m-1} = \mathrm{tr}(\mathbf{A}_1\mathbf{B}_{2m-2})$ *and* $d_{2m} = -\frac{\mathrm{tr}(\mathbf{A}_2\mathbf{B}_{2m-2})}{m}$.

The *Leverrier–Barnett algorithm* given by Theorem 5.1 allows us to find sequentially the coefficients of the characteristic polynomial $p(\lambda)$ in equation (5.7) if $\mathbf{M} = \mathbf{I}$, where $\mathbf{I}$ is the $m \times m$ unit matrix. For $m = 2$, we find [290, 459]

$$\begin{aligned} p(\lambda) = {} & \lambda^4 + \mathrm{tr}\mathbf{D}\lambda^3 + (\mathrm{tr}\mathbf{K} + \det\mathbf{D} + \det\mathbf{G})\lambda^2 \\ & + (\mathrm{tr}\mathbf{K}\mathrm{tr}\mathbf{D} - \mathrm{tr}\mathbf{K}\mathbf{D} - \mathrm{tr}\mathbf{N}\mathbf{G})\lambda + \det\mathbf{K} + \det\mathbf{N}. \end{aligned} \tag{5.8}$$

For arbitrary (including degenerate) matrix $\mathbf{M}$, the coefficients of the characteristic polynomial can be expressed by means of the extended version of the Leverrier–Barnett algorithm that can be found, e.g. in [592].

5.1 Undamped potential systems

Let in equation (5.2) the matrix of inertia forces $\mathbf{M}$ and the matrix of potential forces $\mathbf{K}$ be nondegenerate. Then, $\mathbf{x} = 0$ is an isolated equilibrium of the potential system. The total energy $H = T + U$ of the potential system is conserved ($\dot{H} = 0$), where

the kinetic and potential energy are, respectively

$$T = \frac{1}{2}\dot{\mathbf{x}}^T \mathbf{M}\dot{\mathbf{x}}, \quad U = \frac{1}{2}\mathbf{x}^T \mathbf{K}\mathbf{x}.$$

5.1.1 Lagrange's theorem and Poincaré instability degree

Assume that $\mathbf{M} > 0$, then the Poincaré instability degree is the negative inertia index of the potential energy $U(\mathbf{x})$ at the nondegenerate stationary point, i.e. the number $\nu(\mathbf{K})$ of negative eigenvalues of the matrix $\mathbf{K}$. If potential energy has a minimum at $\mathbf{x} = 0$, then $\nu(\mathbf{K}) = 0$ and the system (5.2) is Lyapunov stable – the result known as *Lagrange's stability theorem* [127]. If $\nu(\mathbf{K}) = 1$, then the characteristic polynomial $\det(\mathbf{M}\lambda^2 + \mathbf{K})$ of the system (5.2) has a unique real root in the open right half-plane of the complex plane (divergence instability) [327, 328]. For example, the cavity in Brouwer's problem (1.1) has $\nu(\mathbf{K}) = 0$ and the saddle has $\nu(\mathbf{K}) = 1$.

5.1.2 Rayleigh's theorem on movement of eigenvalues

Let two potential systems (5.2) have the same matrices of inertia forces ($\mathbf{M}_1 = \mathbf{M}_2$) and different matrices of potential forces: $\mathbf{K}_1 \neq \mathbf{K}_2$. If $\overline{\mathbf{u}}^T \mathbf{K}_2 \mathbf{u} > \overline{\mathbf{u}}^T \mathbf{K}_1 \mathbf{u}$ for all nonzero $\mathbf{u} \in \mathbb{C}^m$, then we say that the system with the matrix $\mathbf{K}_2$ has greater *rigidity* than that with the matrix $\mathbf{K}_1$ [613, 617].

Theorem 5.2 (J. W. S. Rayleigh, 1894 [613,617]). *All natural frequencies of the potential system* (5.2) *with* $\mathbf{M} > 0$ *and* $\mathbf{K} > 0$ *can only increase when there is an increase in its potential energy (rigidity) or a decrease in its kinetic energy.*

In other words, by Theorems 3.6 and 5.2, when the rigidity increases, all pure imaginary eigenvalues with the positive Krein signature move up whereas all those with the negative one move down along the imaginary axis, which prevents eigenvalues of the opposite signatures from colliding at zero [603].

5.1.3 Steady-state bifurcation

The steady-state bifurcation or divergence is characterized generically by a collision at zero of two simple eigenvalues with opposite Krein signatures [146]. This is the only mechanism for the potential system (5.2) to lose stability when $\mathbf{M} > 0$ [239,328]. After transition from one equilibrium to another, the Poincaré instability degree is changed by an odd number [127].

Let, for example, the matrix $\mathbf{K}$ of the system (5.2) continuously depend on a parameter ε and $U(\mathbf{x})$ has its minimum at $\mathbf{x} = 0$ if $\varepsilon < 0$, is degenerate ($\det \mathbf{K} = 0$)

when $\varepsilon = 0$, and loses the property of minimum if $\varepsilon > 0$, so that $\mathbf{K}(\varepsilon)$ acquires one negative eigenvalue at $\varepsilon > 0$. Then, after passing through the bifurcation point $\varepsilon = 0$, there appears exactly one positive real eigenvalue as a result of collision at zero of a pair of pure imaginary eigenvalues. The latter move toward the origin in the complex plane according to Rayleigh's theorem because the rigidity of the system decreases with the increase of ε [327, 328]. We note that in general, the number of eigenvalues of the potential system (5.2) with positive real parts depends both on the negative eigenvalues of the matrix $\mathbf{K}$ and the negative eigenvalues of the matrix $\mathbf{M}$ [142, 525, 600]. Hence, stability of equilibrium x=0 of the potential system can be lost not only when $\det \mathbf{K} = 0$, which is the standard divergence instability threshold, but also when $\det \mathbf{M} = 0$ [302, 445].

5.2 Damped potential systems

With $\mathbf{G} = 0$ and $\mathbf{N} = 0$ equation (5.1) describes a potential system with damping

$$\mathbf{M}\ddot{\mathbf{x}} + \mathbf{D}\dot{\mathbf{x}} + \mathbf{K}\mathbf{x} = 0. \tag{5.9}$$

Let us introduce the block matrices

$$\mathbf{A} = \begin{pmatrix} 0 & \mathbf{I} \\ -\mathbf{M}^{-1}\mathbf{K} & -\mathbf{M}^{-1}\mathbf{D} \end{pmatrix}, \quad \mathbf{P} = \frac{1}{2}\begin{pmatrix} \mathbf{K} & 0 \\ 0 & \mathbf{M} \end{pmatrix}, \quad \mathbf{Q} = \begin{pmatrix} 0 & 0 \\ 0 & \mathbf{D} \end{pmatrix} \tag{5.10}$$

and recall that $\pi(\mathbf{X})$ and $\nu(\mathbf{X})$ denote the number of eigenvalues (counting multiplicities) of a matrix $\mathbf{X}$ with positive and negative real part, respectively.

Theorem 5.3 (H. K. Wimmer, 1974 [142, 348, 437, 600]). *Let* $\mathbf{M}$ *and* $\mathbf{K}$ *be nonsingular,* $\mathbf{D} \geq 0$*, and* $\mathbf{A}$ *and* $\mathbf{Q}$ *be defined by equation* (5.10)*. Then*

$$\nu(\mathbf{L}(\lambda)) \leq \pi(\mathbf{M}) + \pi(\mathbf{K}), \quad \pi(\mathbf{L}(\lambda)) \leq \nu(\mathbf{M}) + \nu(\mathbf{K}), \tag{5.11}$$

where $\mathbf{L}(\lambda) = \mathbf{M}\lambda^2 + \mathbf{D}\lambda + \mathbf{K}$*. If, additionally, the pair* $(\mathbf{A}, \mathbf{Q})$ *is fully observable, then* $\mathbf{L}(\lambda)$ *has no pure imaginary eigenvalues and*

$$\nu(\mathbf{L}(\lambda)) = \pi(\mathbf{M}) + \pi(\mathbf{K}), \quad \pi(\mathbf{L}(\lambda)) = \nu(\mathbf{M}) + \nu(\mathbf{K}). \tag{5.12}$$

In particular, the equalities (5.12) take place also when $\mathbf{D} > 0$, see e.g. [342, 525, 608]. Therefore, if the damping matrix is positive definite and among the eigenvalues of matrices $\mathbf{M}$ and $\mathbf{K}$ there is at least one negative, then the system (5.9) is unstable. Theorem 5.3 follows from the inertia theorems of Ostrowski and Schneider (Theorem 2.30) and Wimmer (Theorem 2.31).

5.2.1 Overdamped and heavily damped systems

Assume that in equation (5.9) $\mathbf{M} > 0$, $\mathbf{D} > 0$, and $\mathbf{K} > 0$. If the magnitude of damping forces with $\mathbf{D} > 0$ is large enough, one can expect that all the eigenvalues of the matrix polynomial $\mathbf{M}\lambda^2 + \mathbf{D}\lambda + \mathbf{K}$ will not only be situated in the open left half-plane of the complex plane but, moreover, be real and negative. What additional conditions should the matrices of the system satisfy in order for this to happen?

If all eigenvalues of the system (5.9) are real, negative, and semisimple, and hence all its decaying solutions do not oscillate, then it is called a *heavily damped system* [99].

Theorem 5.4 (R. Bulatovic, 2004 [99]). *Let* $\mathbf{M} > 0$, $\mathbf{D} > 0$, *and* $\mathbf{K} > 0$ *in the damped potential system* (5.9). *Then it is heavily damped if*

$$\mathbf{D}\mathbf{M}^{-1}\mathbf{D} - 2(\mathbf{K} + \omega_{max}^2\mathbf{M}) > 0, \tag{5.13}$$

where $\lambda = i\omega_{max}$ *is the largest eigenvalue of the operator* $\mathbf{M}\lambda^2 + \mathbf{K}$.

In particular, if

$$\mathbf{D}\mathbf{M}^{-1}\mathbf{K} = \mathbf{K}\mathbf{M}^{-1}\mathbf{D}, \tag{5.14}$$

then the system (5.9) is heavily damped if and only if

$$\mathbf{D}\mathbf{M}^{-1}\mathbf{D} - 4\mathbf{K} > 0. \tag{5.15}$$

If the system (5.9) is heavily damped, then

$$\mathrm{tr}\left((\mathbf{M}^{-1}\mathbf{D})^2\right) > 2\mathrm{tr}(\mathbf{M}^{-1}\mathbf{K}). \tag{5.16}$$

A well-known sufficient [99] condition for the system (5.9) to be heavily damped is that for all nonzero $\mathbf{u} \in \mathbb{C}^m$

$$(\overline{\mathbf{u}}^T\mathbf{D}\mathbf{u})^2 > 4(\overline{\mathbf{u}}^T\mathbf{M}\mathbf{u})(\overline{\mathbf{u}}^T\mathbf{K}\mathbf{u}). \tag{5.17}$$

The inequality (5.17) serves as a definition of an *overdamped system* [34].

Theorem 5.5 (L. Barkwell and P. Lancaster, 1992 [34]). *System* (5.9) *with* $\mathbf{M}>0$, $\mathbf{D}>0$, *and* $\mathbf{K}>0$ *is overdamped, if and only if for some* $\varepsilon_0 > 0$

$$\mathbf{D} > \varepsilon_0\mathbf{M} + \varepsilon_0^{-1}\mathbf{K}. \tag{5.18}$$

It is instructive to understand how the domains of asymptotic stability and heavy damping are related to each other at least in the case when the number of degrees of freedom in (5.9) is $m = 2$.

Assuming $\mathbf{M} = \mathbf{I}$, where $\mathbf{I}$ is the $m \times m$ unit matrix, and introducing the quantities

$$a_1 = \frac{\mathrm{tr}\mathbf{D}}{\sqrt[4]{\det \mathbf{K}}}, \quad a_2 = \frac{\mathrm{tr}\mathbf{K} + \det \mathbf{D}}{\sqrt{\det \mathbf{K}}}, \quad a_3 = \frac{\mathrm{tr}\mathbf{K}\mathrm{tr}\mathbf{D} - \mathrm{tr}\mathbf{K}\mathbf{D}}{\sqrt[4]{(\det \mathbf{K})^3}}. \tag{5.19}$$

we reduce the characteristic polynomial (5.8) with $\mathbf{G} = 0$ and $\mathbf{N} = 0$ to the form (2.63). Conditions for asymptotic stability written for the polynomial (2.63) are given by equation (2.62). As was established by Bottema [81], in the (a_1, a_3, a_2)-space the domain of asymptotic stability lies inside a surface with the Whitney umbrella singularity at the point $(0, 0, 2)$, see Figure 2.1 (a).

Consider the *discriminant* Δ of the polynomial (2.63) and equate it to zero:

$$\begin{aligned}\Delta := {} & 16a_2^4 - 4(a_1^2 + a_3^2)a_2^3 + (a_1^2a_3^2 - 80a_1a_3 - 128)a_2^2 \\ & + 18(a_1a_3 + 8)(a_1^2 + a_3^2)a_2 \\ & + 256 - 27a_3^4 - 27a_1^4 - 6a_1^2a_3^2 - 192a_1a_3 - 4a_1^3a_3^3 = 0.\end{aligned} \tag{5.20}$$

In the (a_1, a_3, a_2)-space, the polynomial (2.63) has at least one multiple root at the points of the set given by equation (5.20). For example, in the plane $a_1 = a_3$

$$\Delta = (a_2 + 2 + 2a_3)(a_2 + 2 - 2a_3)(4a_2 - 8 - a_3^2)^2,$$

and equation $\Delta = 0$ yields the straight line $a_2 = 2(a_3 - 1)$ and parabola $a_2 = 2 + a_3^2/4$ that touch each other at $a_3 = 4$ and $a_2 = 6$, which corresponds to the EP_4 point in Figure 5.1 (a). According to equations (2.65), (2.66), and (2.69) the point EP_4 corresponds to the negative 4-fold real root -1 of the polynomial (2.63), which is a global minimum of its spectral abscissa.

Solving the system of equations $a_1 = 4$, $a_2 = 6$, $a_3 = 4$, where the coefficients a_1, a_2, and a_3 are defined by equation (5.19), yields an explicit expression for the damping matrix $\mathbf{D}$ that minimizes the spectral abscissa of the system (5.9) with $m = 2$ degrees of freedom in terms of the coefficients k_{11}, k_{22}, k_{12} and the eigenvalues ω_1^2 and ω_2^2 ($\omega_{1,2} > 0$) of the given matrix $\mathbf{K}$ when $\mathbf{M} = \mathbf{I}$ [176].

Theorem 5.6. *Given* $\mathbf{K} > 0$ *and* $\mathbf{M} = \mathbf{I}$*, the spectral abscissa of the system* (5.9) *with* $m = 2$ *degrees of freedom attains its global minimum at the real eigenvalue* $\lambda = -\sqrt[4]{\det \mathbf{K}} = -\sqrt{\omega_1\omega_2}$ *with the algebraic multiplicity* 4 *and geometric multiplicity* 1*, if* $\mathbf{D} = \mathbf{D}_+$ *or* $\mathbf{D} = \mathbf{D}_-$*, where*

$$\begin{aligned}\mathbf{D}_\pm = {} & \frac{4k_{12}\sqrt{\omega_1\omega_2} \pm (k_{11} - k_{22})(\omega_1 - \omega_2)}{(\omega_1 + \omega_2)^2} \begin{pmatrix} -\frac{2k_{12}}{k_{11}-k_{22}} & 1 \\ 1 & \frac{2k_{12}}{k_{11}-k_{22}} \end{pmatrix} \\ & + \begin{pmatrix} -\frac{4\sqrt{\omega_1\omega_2}(\omega_1\omega_2 - k_{11})}{k_{11}-k_{22}} & 0 \\ 0 & \frac{4\sqrt{\omega_1\omega_2}(\omega_1\omega_2 - k_{22})}{k_{11}-k_{22}} \end{pmatrix}.\end{aligned} \tag{5.21}$$

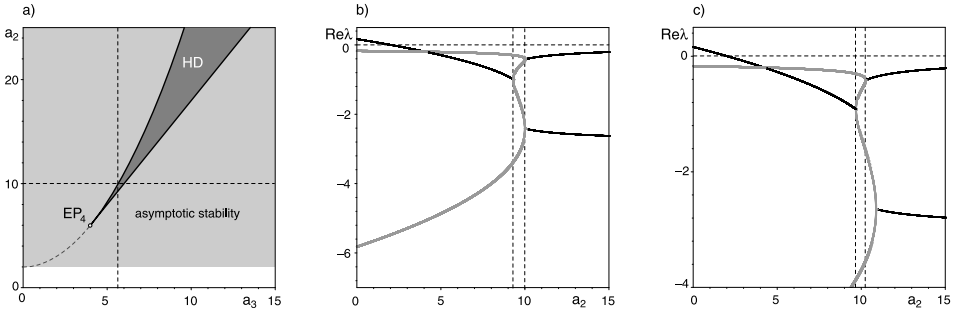

Figure 5.1. (a) Cross-section of the domains of asymptotic stability and heavy damping by the $(a_1 = a_3)$-plane; the dashed line shows a part of the EP-set (2.67), cf. Figure 2.1 (b). (b) Real parts of the eigenvalues of the polynomial (2.63) as functions of a_2 when $a_1 = 4\sqrt{2}$ and $a_3 = 4\sqrt{2}$ and (c) when $a_1 = 6$ and $a_3 = 5.7$. Light gray color marks real eigenvalues with $\mathrm{Im}\lambda = 0$ and black color denotes eigenvalues with $\mathrm{Im}\lambda \neq 0$.

Notice that $\mathbf{D}_\pm$ can be both positive definite and indefinite; $\mathbf{D}_+ = \mathbf{D}_-$ if and only if $\mathbf{K} = \kappa\mathbf{I}$, where κ is a scalar [176].

Taking into account that a single Jordan block of order $2m$ could be a minimizer of the spectral abscissa of a real $2m \times 2m$ matrix [101] and in view of Lemma 5.6, it is natural to expect that the eigenvalues of the potential system (5.2) with m degrees of freedom and $\mathbf{M} = \mathbf{I}$ cannot all be shifted by the dissipative perturbation with the matrix $\mathbf{D} = \mathbf{D}^T$ to the left with respect to the imaginary axis in the complex plane farther than $-\sqrt[2m]{\det \mathbf{K}}$.

Indeed, denote the spectral abscissa of the system (5.9) with $\mathbf{M} = \mathbf{I}$ as $\alpha(\mathbf{D}) = \max_k \mathrm{Re}\lambda_k(\mathbf{L})$, where $\mathbf{L}(\lambda) = \mathbf{I}\lambda^2 + \mathbf{D}\lambda + \mathbf{K}$.

Theorem 5.7 (P. Freitas and P. Lancaster, 1999 [176]). *The function $\alpha(\mathbf{D})$ is bounded from below and the optimal spectral abscissa satisfies*

$$\inf_{\mathbf{D}}(\alpha(\mathbf{D})) \geq -\sqrt[2m]{\det \mathbf{K}}.$$

Equality holds if and only if $\mathbf{L}(\lambda)$ has one single (real) eigenvalue with algebraic multiplicity $2m$ and, in this case, $\mathbf{L}(\lambda) \geq 0$ for all $\lambda \in \mathbb{R}$.

Returning to the stability diagram of Figure 5.1 (a), we see that the point EP_4 is a singular cuspidal point of the narrow domain (dark gray) situated inside the domain of asymptotic stability (light gray). At the points of the upper (parabolic) boundary of the dark gray domain there are two double real negative eigenvalues of geometric multiplicity 1, see Figure 5.1 (b). For example, at $a_1 = a_3 = 4\sqrt{2}$, and $a_2 = 10$ the

eigenvalues (2.65) of the polynomial (2.63) are

$$\lambda_{1,2} = 1 - \sqrt{2}, \quad \lambda_{3,4} = -1 - \sqrt{2}.$$

This is not surprising because the upper boundary is a part of the EP-set (2.67); at another part shown by the dashed line in Figure 5.1 (a) there are two double complex eigenvalues with the Jordan block, cf. Figure 2.2. At the lower boundary given by a part of the line $a_2 = 2(a_3 - 1)$, one negative real eigenvalue is double with the Jordan block and two are simple, Figure 5.1 (b). At the inner points of the dark gray domain in Figure 5.1 (a) all four eigenvalues are simple, real, and negative. Hence, this is the domain of heavy damping.

If we assume $a_1 \neq a_3$ and vary a_2, then the interval where all the eigenvalues are real and negative exists in the vicinity of the plane $a_1 = a_3$, see Figure 5.1 (c). Hence, the domain of heavy damping is three dimensional. Its boundary is a part of the surface defined by equation (5.20). It has a self-intersection along the parabolic curve

$$a_2 = 2 + \frac{a_3^2}{4}, \quad a_1 = a_3 \geq 4$$

and two semicubic cuspidal edges defined in the parametric form as

$$a_1 = \frac{a_2^2 \pm a_2\sqrt{a_2^2 - 36} - 12}{(a_2 \pm \sqrt{a_2^2 - 36})^{3/2}}\sqrt{6}, \quad a_3 = \frac{a_2^2 \pm a_2\sqrt{a_2^2 - 36} + 36}{3\sqrt{6a_2 \pm 6\sqrt{a_2^2 - 36}}}, \quad a_2 \geq 6.$$

At the cuspidal edges one root of the polynomial (2.63) is triple real and negative and the other one is simple and negative. For example, at the points $\left(\frac{28}{9}\sqrt{3}, 4\sqrt{3}, 10\right)$ and $\left(4\sqrt{3}, \frac{28}{9}\sqrt{3}, 10\right)$ we have, respectively,

$$\lambda_1 = -\frac{\sqrt{3}}{9}, \quad \lambda_{2,3,4} = -\sqrt{3}, \quad \text{and} \quad \lambda_1 = -3\sqrt{3}, \quad \lambda_{2,3,4} = -\frac{\sqrt{3}}{3}.$$

At the point EP_4 with the coordinates $(4, 4, 6)$ in the (a_1, a_3, a_2)-space the boundary of the domain of heavy damping has the swallowtail singularity described, e.g. in Section 4.5.4, see Figure 5.2 (a) and compare it with Figure 4.6 (b).

The domain of heavy damping is confined between three hypersurfaces and has the form of a trihedral spike with the swallowtail singularity at its tip that is situated inside the domain of asymptotic stability that has the Whitney umbrella singular point at $a_1 = 0$, $a_3 = 0$, and $a_2 = 2$, Figure 5.2 (a). The domain of heavy damping is relatively small and has a nonsmooth and nonconvex boundary, Figure 5.2 (a, b). The Whitney umbrella and the swallowtail singular points are connected by the EP-set given by equation (2.67). According to Lemma 5.6, at the swallowtail singularity, the spectral abscissa of the characteristic polynomial of the damped potential system attains its global minimum.

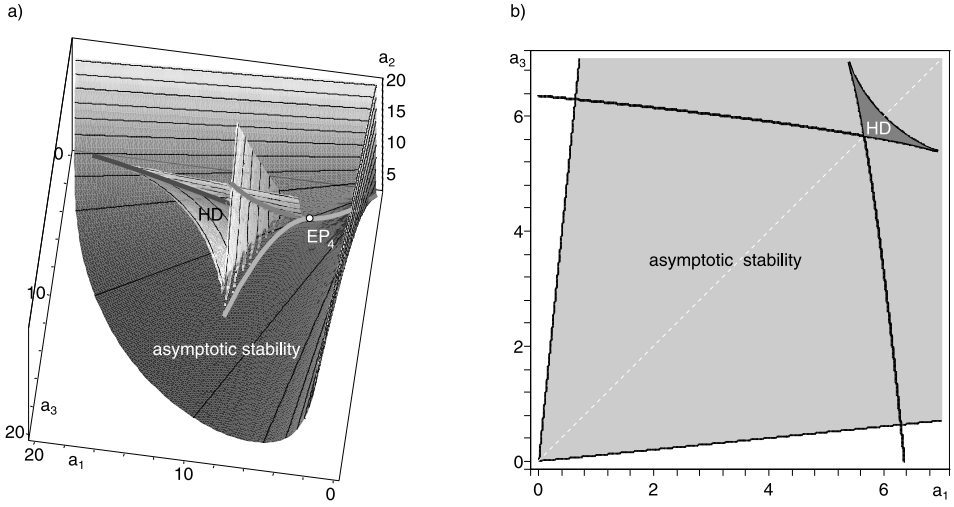

Figure 5.2. (a) The domain of asymptotic stability given by equation (2.62) with the Whitney umbrella singularity at the point $(0, 0, 2)$ and inside it the domain of heavy damping (HD) given by equation (5.20) with the swallowtail singularity (white dot) at the point $(4, 4, 6)$ for the polynomial (2.63) in the (a_1, a_3, a_2)-space. (b) The cross-section of these domains by the $(a_2 = 10)$-plane.

5.2.2 Indefinitely damped systems

The notion of indefinite damping originated in the problems of stability of solutions to the wave equation, e.g. [177]

$$u_{tt} + \varepsilon d(z) u_t = u_{zz}, \tag{5.22}$$

where the damping coefficient $d(z)$ is assumed to be a function changing its sign in the interval $z \in (0, 1)$. Such problems arise, e.g., in structural dynamics where the viscous damping material distributed over part of the vibrating structure can be used to control the vibration [122]. It turned out that for any sign-changing damping distribution $d(z)$, there exists $\varepsilon_0 > 0$, such that for all $0 < \varepsilon < \varepsilon_0$ the trivial solution of (5.22) is asymptotically stable, i.e. it is decaying with time [177]. The dependence of ε_0 on d is however very nontrivial. In order to understand it better, Freitas et al. [175] formulated a finite-dimensional version of the problem (5.22)

$$\ddot{\mathbf{x}} + \varepsilon \mathbf{D}\dot{\mathbf{x}} + \mathbf{K}\mathbf{x} = 0, \tag{5.23}$$

where dot is time differentiation, $\mathbf{x} \in \mathbb{R}^m$, $\mathbf{K}$ is a real diagonal matrix, and $\mathbf{D} = \mathbf{D}^T$ is a real indefinite matrix.

Theorem 5.8 (P. Freitas, M. Grinfeld and P. Knight, 1997 [175]). *Let* $\mathbf{K} > 0$ *and let* $\pi(\mathbf{D})$, $\nu(\mathbf{D})$, *and* $\delta(\mathbf{D})$ *be the numbers of positive, negative, and zero eigenvalues of the real symmetric matrix* $\mathbf{D}$. *Then there exist real numbers* $\varepsilon^{-}_{\pi(\mathbf{D})}$ *and* $\varepsilon^{+}_{\nu(\mathbf{D})}$ *such that for* $\varepsilon > \varepsilon^{-}_{\pi(\mathbf{D})}$ *there are at least* $2\pi(\mathbf{D})$ *real negative eigenvalues* λ *of the matrix polynomial* $\mathbf{I}\lambda^2 + \varepsilon\mathbf{D}\lambda + \mathbf{K}$ *while for* $\varepsilon > \varepsilon^{+}_{\nu(\mathbf{D})}$ *there are at least* $2\nu(\mathbf{D})$ *real positive eigenvalues* λ. *If* $\delta(\mathbf{D}) = 0$, *then for* $\varepsilon > \max\{\varepsilon^{-}_{\pi(\mathbf{D})}, \varepsilon^{+}_{\nu(\mathbf{D})}\}$ *there are* $2m$ *real eigenvalues, i.e. all eigenvalues* λ *are real.*

As an illustration of the sensitivity of ε_0 to the entries of the matrices, Freitas et al. [175] considered the following two-dimensional example: $d_{11} = 1$, $d_{12} = 1$, $d_{22} = 1/2$ and $k_{11} = 1$, $k_{22} = 4$, $k_{12} = 0$. Then $\varepsilon_0 \approx 1.15$. However, already an interchange of the diagonal entries of the matrix $\mathbf{K}$ leads to an increase in the interval of the asymptotic stability: $\varepsilon_0 \approx 1.41$. Nevertheless, even the instability threshold found in [175] for a two-degrees-of-freedom system (5.23) did not lead to a clear interpretation that would explain its "wild" dependence on the matrices $\mathbf{D}$ and $\mathbf{K}$.

A subsequent investigation made in [174] revealed an intriguing fact that with specifically chosen matrices $\mathbf{D}$ and $\mathbf{K}$, the eigenvalues of the system (5.23) behave like those of a Hamiltonian system, being located symmetrically to both the real and imaginary axis of the complex plane, see Theorem 3.4. Such a system can be marginally stable when $0 < \varepsilon < \varepsilon_0$ with all its eigenvalues pure imaginary and simple, which corresponds to the bounded oscillations. Then, the potential system with the indefinite damping is referred to as the oscillatory damped system [174]. The oscillations become unstable (flutter) when $\varepsilon \geq \varepsilon_0$.

Theorem 5.9 (P. Freitas, 1999 [174]). *For all real* $\mathbf{D} = \mathbf{D}^T$ *and diagonal* $\mathbf{K}$ *with real entries* k_{ii} ($k_{ii} \neq k_{jj}, i \neq j$), *the spectrum of* $\mathbf{L}(\lambda) = \mathbf{I}\lambda^2 + \mathbf{D}\lambda + \mathbf{K}$ *is symmetric with respect to both the real and imaginary axis of the complex plane if and only if there exists a matrix* $\mathbf{T} = \operatorname{diag}(t_{11}, \ldots, t_{mm})$ *with* $t_{ii} \in \{-1, +1\}$ *such that* $\mathbf{TDT} = -\mathbf{D}$. *The eigenvector* $\mathbf{u} = (u_1, \ldots, u_m)$ *at* $\lambda = i\omega$ *can be chosen to have* $\operatorname{Im} u_j = 0$ *if* $t_{jj} = +1$ *and* $\operatorname{Re} u_j = 0$ *if* $t_{jj} = -1$.

If, additionally, the diagonal matrix $\mathbf{K} > 0$, the solutions of equation (5.23) are bounded for ε in a neighborhood of the origin that depends on $\mathbf{D}$ and $\mathbf{K}$, i.e. equation (5.23) describes the oscillatory damped system [174].

Consider, for example, the equation $\ddot{\mathbf{q}} + \varepsilon\widetilde{\mathbf{D}}\dot{\mathbf{q}} + \widetilde{\mathbf{K}}\mathbf{q} = 0$ with the matrices

$$\widetilde{\mathbf{D}} = \begin{pmatrix} -1 & 0 \\ 0 & 1 \end{pmatrix}, \quad \widetilde{\mathbf{K}} = \frac{-1}{1-\mu^2}\begin{pmatrix} -1 & \mu \\ \mu & -1 \end{pmatrix} \tag{5.24}$$

that describe two coupled ideal LRC circuits, one with gain (realized by means of the voltage amplifier) and another with loss (resistance), where $0 < \mu < 1$ is the mutual inductance and $\varepsilon > 0$ is loss which perfectly matches the gain $(-\varepsilon)$. The components of the vector $\mathbf{q}$ have the meaning of electrical charge, see [511]. A coordinate transformation by means of the matrix $\mathbf{C}$ reduces this equation to the form (5.23) with $\mathbf{K} = \mathbf{C}\widetilde{\mathbf{K}}\mathbf{C}^{-1}$ and $\mathbf{D} = \mathbf{C}\widetilde{\mathbf{D}}\mathbf{C}^{-1}$, where

$$\mathbf{D} = \begin{pmatrix} 0 & -1 \\ -1 & 0 \end{pmatrix}, \quad \mathbf{K} = \begin{pmatrix} \frac{-1}{\mu-1} & 0 \\ 0 & \frac{1}{\mu+1} \end{pmatrix}, \quad \mathbf{C} = \begin{pmatrix} 1 & -1 \\ 1 & 1 \end{pmatrix}. \tag{5.25}$$

Since $\mathbf{TDT} = -\mathbf{D}$ with $\mathbf{T} = \operatorname{diag}(1, -1)$, the spectrum of the two coupled LRC circuits with perfectly matched gain and loss considered in [511] is Hamiltonian. When $0 < \varepsilon < \varepsilon_0 = 1/\sqrt{1-\mu} - 1/\sqrt{1+\mu}$ the system is marginally stable, i.e. it is an oscillatory damped system.

On the other hand, Schindler et al. [511] pointed out that their equations with the matrices (5.24) are invariant under a combined *parity* ($q_1 \leftrightarrow q_2$) and *time-reversal* ($t \leftrightarrow -t$) transformation. This immediately connects the "oscillatory damped systems" in the sense of [174] with the fundamental $\mathcal{PT}$*-symmetry*.

The notion of $\mathcal{PT}$-symmetry entered modern physics mainly from the side of quantum mechanics. Parametric families of non-Hermitian Hamiltonians having both parity ($\mathcal{P}$) and time-reversal ($\mathcal{T}$) symmetry possess pure real spectrum in some regions of the parameter space, which questions the need for the Hermiticity axiom in quantum theory [46, 47, 353]. First experimental evidence of $\mathcal{PT}$-symmetry came, however, from classical optics [507], where the properly designed imaginary part of the linear refractive index yields a gain and loss inhomogeneous in space.[1] The recently designed experiment with $\mathcal{PT}$-symmetric LRC circuits can be regarded as an analogue modeling of the optical systems [511]. Additional losses naturally arising in real electric circuits could be used to investigate the departure from the ideal $\mathcal{PT}$-symmetric system considered in [511] and thus experimentally observe the paradoxical behavior of the instability threshold of a potential system with the general indefinite damping matrix pointed out in [175].

In the case when $m = 2$, however, the connection between the domain of marginal stability of the oscillatory damped system and the domain of asymptotic stability of a general indefinitely damped system can be seen explicitly [303,305]. Indeed, assuming $\mathbf{M} = \mathbf{I}$ in equation (5.9) and denoting by $Y = \delta_2 - \delta_1$ the difference between the eigenvalues δ_1 and δ_2 of $\mathbf{D}$, we find

$$\det \mathbf{D} = \frac{1}{4}\left((\mathrm{tr}\mathbf{D})^2 - Y^2\right). \tag{5.26}$$

Given $\mathbf{K} > 0$, let $\mathbf{D}_{\mathcal{PT}}$ be a matrix satisfying the equalities

$$\mathrm{tr}\mathbf{D}_{\mathcal{PT}} = 0, \quad \mathrm{tr}\mathbf{K}\mathbf{D}_{\mathcal{PT}} = 0. \tag{5.27}$$

[1] Cf. the placement of dampers/actuators in engineering problems of vibration control [122].

Then, according to equation (5.8) the coefficients of the characteristic polynomial at λ and λ^3 vanish, $\det \mathbf{D}_{\mathcal{PT}} = -\frac{Y_{\mathcal{PT}}^2}{4} < 0$, and the eigenvalues of the operator $\mathbf{I}\lambda^2 + \mathbf{D}_{\mathcal{PT}}\lambda + \mathbf{K}$ can be found explicitly as

$$\lambda_{\mathcal{PT}}^2 = -\frac{\mathrm{tr}\mathbf{K}}{2} + \frac{Y_{\mathcal{PT}}^2}{8} \pm \frac{1}{8}\sqrt{\left((Y_{\mathcal{PT}})^2 - (Y_{\mathcal{PT}}^-)^2\right)\left((Y_{\mathcal{PT}})^2 - (Y_{\mathcal{PT}}^+)^2\right)}, \quad (5.28)$$

where

$$Y_{\mathcal{PT}}^{\pm} = 2\left(\sqrt{\kappa_2} \pm \sqrt{\kappa_1}\right) \quad (5.29)$$

and κ_1 and κ_2 are the eigenvalues of the matrix $\mathbf{K}$.

At $Y^2 = (Y_{\mathcal{PT}}^-)^2$ the eigenvalues $\lambda_{\mathcal{PT}}$ experience the nonsemisimple 1 : 1 resonance and originate a double pure imaginary eigenvalue with the Jordan block. Thus, the values $\pm Y_{\mathcal{PT}}^-$ are exceptional points (EPs) of the parameter Y. When Y^2 exceeds $(Y_{\mathcal{PT}}^-)^2$, the eigenvalues become complex with positive and negative real parts, which means oscillatory instability or flutter. A further increase in Y^2 results in the merging of complex-conjugate eigenvalues into the double real ones at $\pm Y_{\mathcal{PT}}^+$ that then split into simple real eigenvalues (divergence or static instability).

Therefore, the spectrum of the system (5.9) with the indefinite damping matrix $\mathbf{D} = \mathbf{D}_{\mathcal{PT}}$ is Hamiltonian, i.e. the eigenvalues are symmetric with respect to both real and imaginary axis of the complex plane [174]. The Hamiltonian symmetry of the spectrum is lost when the matrices $\mathbf{D}$ and $\mathbf{K}$ do not satisfy the conditions (5.27). In this case the system (5.9) can be asymptotically stable if and only if $\mathrm{tr}\mathbf{D} > 0$ and [175, 290, 305]

$$Y^2 > (\mathrm{tr}\mathbf{D})^2 + 4\frac{(\mathrm{tr}\mathbf{K}\mathbf{D} - \kappa_1\mathrm{tr}\mathbf{D})(\mathrm{tr}\mathbf{K}\mathbf{D} - \kappa_2\mathrm{tr}\mathbf{D})}{\mathrm{tr}\mathbf{D}(\mathrm{tr}\mathbf{K}\mathbf{D} - \mathrm{tr}\mathbf{K}\mathrm{tr}\mathbf{D})}. \quad (5.30)$$

Assuming equality in equation (5.30), we resolve it with respect to $\mathrm{tr}\mathbf{K}\mathbf{D}$ and write the threshold of asymptotic stability in the form

$$\mathrm{tr}\mathbf{K}\mathbf{D} = \frac{\left(Y_{\mathcal{PT}}^-\right)^2 + \left(Y_{\mathcal{PT}}^+\right)^2}{16}\mathrm{tr}\mathbf{D} \quad (5.31)$$
$$+ \frac{\mathrm{tr}\mathbf{D}}{8}\left[Y^2 - (\mathrm{tr}\mathbf{D})^2 \pm \sqrt{\left(Y^2 - (\mathrm{tr}\mathbf{D})^2 - \left(Y_{\mathcal{PT}}^-\right)^2\right)\left(Y^2 - (\mathrm{tr}\mathbf{D})^2 - \left(Y_{\mathcal{PT}}^+\right)^2\right)}\right].$$

In the $(\mathrm{tr}\mathbf{D}, \mathrm{tr}\mathbf{K}\mathbf{D}, Y)$-space, two sheets of the surface (5.31), corresponding to different signs before the square root, intersect each other along an interval of the Y axis, Figure 5.3 (a). When

$$Y^2 = \left(Y_{\mathcal{PT}}^-\right)^2 + (\mathrm{tr}\mathbf{D})^2, \quad (5.32)$$

the two sheets are connected along a space curve that projects into a line

$$\mathrm{tr}\mathbf{K}\mathbf{D} = \frac{\mathrm{tr}\mathbf{D}}{16}\left(3\left(Y_{\mathcal{PT}}^-\right)^2 + \left(Y_{\mathcal{PT}}^+\right)^2\right), \quad (5.33)$$

lying in the $(\mathrm{tr}\mathbf{D}, \mathrm{tr}\mathbf{K}\mathbf{D})$-plane. According to equation (5.32) the space curve lying on the surface (5.31) passes through the point $Y = Y_{\mathcal{PT}}^-$ when $\mathrm{tr}\mathbf{D} = 0$. Therefore,

the interval of self-intersection is determined by the inequality $Y^2 \le (Y^-_{\mathcal{PT}})^2$, which contains the interval of marginal stability $Y^2 < (Y^-_{\mathcal{PT}})^2$ of the oscillatory damped system, Figure 5.3 (a). Retaining only the terms of order $O(\mathrm{tr}\mathbf{D})$ in equation (5.31), we obtain a linear approximation to the intersecting sheets at the points of the interval $Y^2 \le (Y^-_{\mathcal{PT}})^2$ of the Y-axis

$$\mathrm{tr}\mathbf{KD} = \frac{\mathrm{tr}\mathbf{D}}{16}\left[\left(Y^-_{\mathcal{PT}}\right)^2 + \left(Y^+_{\mathcal{PT}}\right)^2 + 2Y^2 \pm 2\sqrt{\left(Y^2 - \left(Y^-_{\mathcal{PT}}\right)^2\right)\left(Y^2 - \left(Y^+_{\mathcal{PT}}\right)^2\right)}\right]. \tag{5.34}$$

Near the line (5.33) in the neighborhood of the exceptional point ($\mathrm{tr}\mathbf{D} = 0, \mathrm{tr}\mathbf{KD} = 0, Y = Y^-_{\mathcal{PT}}$) the linear approximation (5.34) yields a simple estimate of the instability threshold

$$Y \approx Y^-_{\mathcal{PT}} - \frac{\left(32\mathrm{tr}\mathbf{KD} - 2\left(3(Y^-_{\mathcal{PT}})^2 + (Y^+_{\mathcal{PT}})^2\right)\mathrm{tr}\mathbf{D}\right)^2}{Y^-_{\mathcal{PT}}\left|(Y^-_{\mathcal{PT}})^2 - (Y^+_{\mathcal{PT}})^2\right|(\mathrm{tr}\mathbf{D})^2}. \tag{5.35}$$

Note that the equation (5.35) is in the form $Y = X^2/Z^2$, which is canonical for the Whitney umbrella surface [17]. Therefore, the surface (5.31) contains the Whitney umbrella singularity at the exceptional point $(0, 0, Y^-_{\mathcal{PT}})$ of the $(\mathrm{tr}\mathbf{D}, \mathrm{tr}\mathbf{KD}, Y)$-space, which is a generic singularity of codimension 3 on the boundary of asymptotic stability of a general family of real matrices [17] that is associated with the double pure imaginary eigenvalue with the Jordan block [81, 232, 354].

A pocket of the singular surface (5.31) selected by the condition $\mathrm{tr}\mathbf{D} > 0$ bounds the domain of asymptotic stability of the indefinitely damped system with $m = 2$ degrees of freedom. The part of the plane (5.33) in the $(\mathrm{tr}\mathbf{D}, \mathrm{tr}\mathbf{KD}, Y)$-space under the constraints $\mathrm{tr}\mathbf{D} > 0$ and $Y < Y^-_{\mathcal{PT}}$ constitutes the tangent cone to the stability domain at the EP [375]. This tangent cone touching the stability boundary at the EP is shown in black in Figure 5.3 (a). It separates the stability pocket into the compartments marked by the letters 'g' and 'r' in Figure 5.3 (a). This subdivision controls the eigenvalue movement in the complex plane [288].

We first observe that the upper bound to the tangent cone, i.e. the ray specified by the expressions (5.33), $Y = Y^-_{\mathcal{PT}}$, and $\mathrm{tr}\mathbf{D} > 0$, consists of the exceptional points. Indeed, the spectrum of the indefinitely damped system with $m = 2$ degrees of freedom at the points of the ray shown as a white dashed line in Figure 5.3 (a) consists of a pair of double complex-conjugate eigenvalues

$$\lambda = -\frac{1}{4}\mathrm{tr}\mathbf{D} \pm \frac{i}{4}\sqrt{\left(Y^+_{\mathcal{PT}}\right)^2 - \left(Y^-_{\mathcal{PT}}\right)^2 - (\mathrm{tr}\mathbf{D})^2}. \tag{5.36}$$

The pair (5.36) lives in the complex plane on the circle

$$(\mathrm{Re}\lambda)^2 + (\mathrm{Im}\lambda)^2 = \frac{\left(Y^+_{\mathcal{PT}}\right)^2 - \left(Y^-_{\mathcal{PT}}\right)^2}{16}. \tag{5.37}$$

When Y increases within the black tangent cone in Figure 5.3 (a), $\mathrm{tr}\mathbf{D}$ and $\mathrm{tr}\mathbf{KD}$ fixed, two simple complex eigenvalues $\lambda(Y)$ are attracted to an exceptional point on the

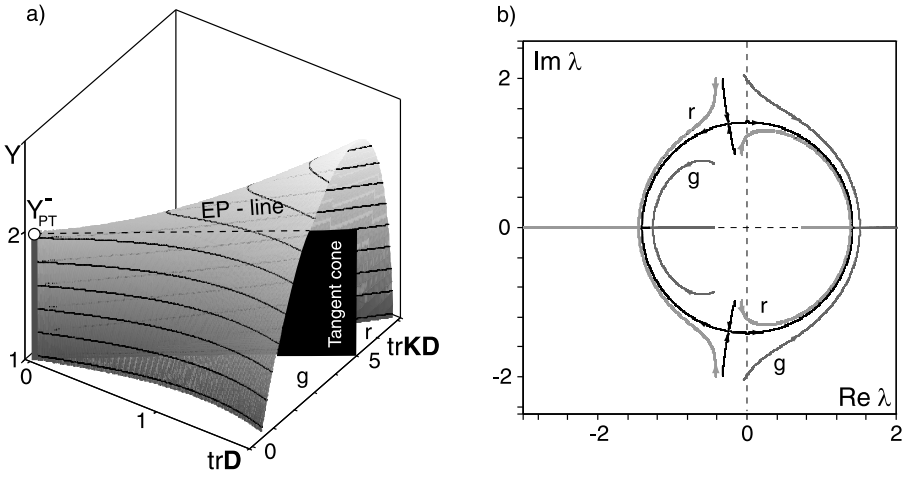

Figure 5.3. When $\kappa_1 = 1$ and $\kappa_2 = 4$: (a) In the half-space $\mathrm{tr}\mathbf{D} > 0$ of the $(\mathrm{tr}\mathbf{D}, \mathrm{tr}\mathbf{KD}, Y)$-space, where $Y = \delta_1 - \delta_2$, a part of the surface (5.31) with the Whitney umbrella singularity at the exceptional point $(0, 0, Y^-_{\mathcal{PT}})$ bounds the domain of asymptotic stability of the system (5.9) with $m = 2$ degrees of freedom. The tangent cone $\{\mathrm{tr}\mathbf{KD} = \mathrm{tr}\mathbf{D}(\mathrm{tr}\mathbf{K} - \sqrt{\det \mathbf{K}}),\ Y < Y^-_{\mathcal{PT}},\ \mathrm{tr}\mathbf{D} > 0\}$ to the stability domain at $(0, 0, Y^-_{\mathcal{PT}})$ is shown in black. At the points of the (dashed) EP-line $\{\mathrm{tr}\mathbf{KD} = \mathrm{tr}\mathbf{D}(\mathrm{tr}\mathbf{K} - \sqrt{\det \mathbf{K}}),\ Y = Y^-_{\mathcal{PT}}\}$ the eigenvalues of the indefinitely damped system are double nonsemisimple. (b) Movement of eigenvalues of the indefinitely damped system (5.9) when Y varies from 0 to 8 and (black) $\mathrm{tr}\mathbf{D} = 1$ and $\mathrm{tr}\mathbf{KD} = 3$, (dark gray, g) $\mathrm{tr}\mathbf{D} = 1$ and $\mathrm{tr}\mathbf{KD} = 1.1$, and (light gray, r) $\mathrm{tr}\mathbf{D} = 1$ and $\mathrm{tr}\mathbf{KD} = 3.5$. It illustrates how penetrating the tangent cone yields exchange of instability between modes.

circle (5.37) that is shown in black in Figure 5.3 (b). They merge at an EP into a double eigenvalue with negative real part when $Y = Y^-_{\mathcal{PT}}$. After its subsequent splitting, the newborn simple eigenvalues evolve along the circle (5.37) in opposite directions, Figure 5.3 (b). At the instability threshold (5.32) the eigenvalues are

$$\lambda = \pm\frac{i}{4}\sqrt{\left(Y^+_{\mathcal{PT}}\right)^2 - \left(Y^-_{\mathcal{PT}}\right)^2}, \quad \lambda = -\frac{1}{2}\mathrm{tr}\mathbf{D} \pm \frac{i}{4}\sqrt{\left(Y^+_{\mathcal{PT}}\right)^2 - \left(Y^-_{\mathcal{PT}}\right)^2 - 4\,(\mathrm{tr}\mathbf{D})^2}. \tag{5.38}$$

When Y exceeds the threshold (5.32), the first pair of eigenvalues moves in the complex plane to the right of the imaginary axis, causing instability.

Choosing the values of $\mathrm{tr}\mathbf{D}$ and $\mathrm{tr}\mathbf{KD}$ that do not belong to the tangent cone destroys the perfect collision of eigenvalues on the circle (5.37), as demonstrated by the dark gray (g) and light gray (r) eigencurves in Figure 5.3 (b) corresponding to the parameters taken, respectively, from the 'g' or 'r' compartment of the stability domain shown in Figure 5.3 (a). When the parameters are in the g-area selected by the condition $\mathrm{tr}\mathbf{KD} < \frac{\mathrm{tr}\mathbf{D}}{16}\left(3\left(Y^-_{\mathcal{PT}}\right)^2 + \left(Y^+_{\mathcal{PT}}\right)^2\right)$, the eigenvalues do not interact and pass in close vicinity of the EP in such a manner that the mode with the higher frequency destabilizes the system, Figure 5.3 (b). When $\mathrm{tr}\mathbf{KD} > \frac{\mathrm{tr}\mathbf{D}}{16}\left(3\left(Y^-_{\mathcal{PT}}\right)^2 + \left(Y^+_{\mathcal{PT}}\right)^2\right)$, the

black eigencurves unfold into two light gray ones. In this case the instability transfers to the mode with the lower frequency.

To illustrate our geometrical considerations, consider system (5.9) with $\mathbf{M} = \mathbf{I}$ and the following matrices of potential forces and indefinite damping

$$\mathbf{K} = \begin{pmatrix} 1 & 0 \\ 0 & 4 \end{pmatrix}, \qquad \mathbf{D}_\mathrm{b} = \frac{1}{3}\begin{pmatrix} 1 & \sqrt{11} \\ \sqrt{11} & 2 \end{pmatrix},$$
$$\mathbf{D}_\mathrm{r} = \frac{1}{6}\begin{pmatrix} 1 & \sqrt{41} \\ \sqrt{41} & 5 \end{pmatrix}, \quad \mathbf{D}_\mathrm{g} = \frac{1}{30}\begin{pmatrix} 29 & \sqrt{929} \\ \sqrt{929} & 1 \end{pmatrix}. \tag{5.39}$$

The eigenvalues of the matrix $\mathbf{K}$ are $\kappa_1 = 1$ and $\kappa_2 = 4$. The damping matrices are isospectral, i.e. all the three indefinite damping matrices have as eigenvalues

$$\delta_1 = \frac{1}{2}(1 - \sqrt{5}) < 0, \quad \delta_2 = \frac{1}{2}(1 + \sqrt{5}) > 0. \tag{5.40}$$

Then, $\mathrm{tr}\mathbf{D}_\mathrm{b} = \mathrm{tr}\mathbf{D}_\mathrm{g} = \mathrm{tr}\mathbf{D}_\mathrm{r} = 1$. However, $\mathrm{tr}\mathbf{K}\mathbf{D}_\mathrm{b} = 3$, $\mathrm{tr}\mathbf{K}\mathbf{D}_\mathrm{r} = 3.5$, and $\mathrm{tr}\mathbf{K}\mathbf{D}_\mathrm{g} = 1.1$. Therefore, $\mathbf{D}_\mathrm{b}$ corresponds to the black tangent cone in Figure 5.3 (a), $\mathbf{D}_\mathrm{g}$ to the g-compartment of the stability domain, and $\mathbf{D}_\mathrm{r}$ to the r-one.

Calculating the eigenvalues λ of the operator $\mathbf{I}\lambda^2 + \mathbf{D}\lambda + \mathbf{K}$ with the three damping matrices and the matrix $\mathbf{K}$ from equation (5.39), we find

$$\begin{aligned} \lambda_1^\mathrm{b} &= -\frac{1}{2} \pm i\frac{\sqrt{7}}{2}, \quad \lambda_2^\mathrm{b} = \pm i\sqrt{2}, \\ \lambda_1^\mathrm{g} &\approx -0.672 \pm i\,0.889, \quad \lambda_2^\mathrm{g} \approx 0.172 \pm i\,1.786, \\ \lambda_1^\mathrm{r} &\approx -0.548 \pm i\,1.489, \quad \lambda_2^\mathrm{r} \approx 0.048 \pm i\,1.260. \end{aligned} \tag{5.41}$$

Thus, the system (5.9) with the matrix $\mathbf{D}_\mathrm{b}$ is exactly at the stability boundary that according to equation (5.32) corresponds to $Y = \sqrt{5}$. At the same value $Y = \sqrt{5}$, the matrix $\mathbf{D}_\mathrm{g}$ destabilizes the mode with the higher frequency, whereas the matrix $\mathbf{D}_\mathrm{r}$ makes the mode with the lower frequency unstable, cf. Figure 5.3 (b).

Concluding, we quote from Freitas et al. [175] who noticed that the dependence of the spectrum of the indefinitely damped potential system on the spectra of $\mathbf{K}$ and $\mathbf{D}$ "is very nontrivial". We have just demonstrated that these peculiarities are essentially described by the properties of the stability boundary in the vicinity of the exceptional point and in particular by the tangent cone to the stability domain at the EP.

5.3 Undamped gyroscopic systems

Consider the undamped gyroscopic system (5.3) and assume that $\mathbf{M} > 0$. Theorems 3.8 and 3.12 imply that when $\nu(\mathbf{K})$ is odd, there exists a positive real eigenvalue (divergence instability). When $\nu(\mathbf{K})$ is even, the undamped gyroscopic system can be either stable (gyroscopic stabilization) or unstable [127,330,573,613]. In particular, if the $m \times m$ matrix $\mathbf{K}$ is negative definite, i.e. the potential energy has a maximum, then

for odd m the system (5.3) is unstable, while for even m the gyroscopic stabilization is possible [98]. Hence, when $\det \mathbf{K} < 0$, the system (5.3) is unstable; it is stable when $\mathbf{K} > 0$ [437].

5.3.1 Extension of Rayleigh's theorem

It follows from Theorem 3.9 that the gyroscopic system (5.3) with $\mathbf{M} > 0$ and $\mathbf{K}$ non-degenerate has $(s + \pi(\mathbf{K}))/2$ eigenfrequencies corresponding to pairs of complex-conjugate pure imaginary eigenvalues with positive Krein signature and $(s - \pi(\mathbf{K}))/2$ eigenfrequencies corresponding to pairs of complex-conjugate pure imaginary eigenvalues with negative Krein signature. According to equation (3.43) the former increase while the latter decrease when $\mathbf{M}$ decreases or $\mathbf{K}$ increases [613]. Thus Rayleigh's theorem (Theorem 5.2) can be extended to the gyroscopic system (5.3) only when the number of its frequencies is equal to the number of frequencies of the corresponding potential system when there are no gyroscopic forces acting [613]. This condition is certainly satisfied if the system is statically stable $\mathbf{K} > 0, s = \pi(\mathbf{K}) = m$ and also if the Poincaré instability degree is equal to one, i.e. if $\nu(\mathbf{K}) = 1$ and $s = \pi(\mathbf{K}) = m - 1$ [613].

Theorem 5.10 (V. F. Zhuravlev, 1976 [617]). *When the rigidity of the system* (5.3) *with* $\mathbf{M} > 0$ *and* $\mathbf{K} > 0$ *is increased, then all its natural frequencies can only increase.*

5.3.2 Criteria of gyroscopic stabilization

In the case when the gyroscopic stabilization is possible, it is practically important to determine the conditions for its onset in terms of the matrices of the gyroscopic system (5.3).

Theorem 5.11 (K. Huseyin, P. Hagedorn and W. Teschner, 1983 [98, 237, 325]). *If* $\mathbf{KG} = \mathbf{GK}$*, the gyroscopic system* (5.3) *with m even,* $\mathbf{M} = \mathbf{I}$*, and* $\mathbf{K} < 0$*, is stable if and only if* $4\mathbf{K} - \mathbf{G}^2 > 0$*. If* $4\mathbf{K} - \mathbf{G}^2 < 0$*, the system is unstable.*

Another relatively simple sufficient condition for the system (5.3) with m even, $\mathbf{M} = \mathbf{I}$, and $\mathbf{K} < 0$ to be gyroscopically stabilized is $2\mathbf{K} - \mathbf{G}^2 + 2\kappa\mathbf{I} > 0$, where κ is the smallest eigenvalue of the matrix $\mathbf{K}$ [98].

In rotor dynamics, a specific gyroscopic system frequently originates

$$\begin{pmatrix} \mathbf{M} & 0 \\ 0 & \mathbf{M} \end{pmatrix} \begin{pmatrix} \ddot{\mathbf{x}} \\ \ddot{\mathbf{y}} \end{pmatrix} + 2\Omega \begin{pmatrix} 0 & -\mathbf{M} \\ \mathbf{M} & 0 \end{pmatrix} \begin{pmatrix} \dot{\mathbf{x}} \\ \dot{\mathbf{y}} \end{pmatrix} + \begin{pmatrix} \mathbf{W}_{11} - \Omega^2\mathbf{M} & \mathbf{W}_{12} \\ \mathbf{W}_{12}^T & \mathbf{W}_{22} - \Omega^2\mathbf{M} \end{pmatrix} \begin{pmatrix} \mathbf{x} \\ \mathbf{y} \end{pmatrix} = 0, \tag{5.42}$$

where the real $\frac{m}{2} \times \frac{m}{2}$ matrix $\mathbf{M} = \mathbf{M}^T > 0$ and the real $m \times m$ matrix $\mathbf{W} = \begin{pmatrix} \mathbf{W}_{11} & \mathbf{W}_{12} \\ \mathbf{W}_{12}^T & \mathbf{W}_{22} \end{pmatrix}$ is symmetric but not necessarily positive definite; $\Omega \geq 0$ has the meaning of the rotation speed [238, 239, 582]. For example, the equations (1.1) of the Brouwer particle in a rotating vessel is a particular case of (5.42).

As it was established by Veselic [582], at large Ω the gyroscopic system (5.42) behaves like an axially symmetric system whose stiffness is obtained by an averaging of the original asymmetric stiffness around the rotation axis. The positive definiteness of the effective stiffness matrix

$$\mathbf{V} = \frac{1}{2}(\mathbf{W} - \mathbf{G}\mathbf{W}\mathbf{G}) \tag{5.43}$$

implies the Lyapunov stability of (5.42) for Ω large enough; indefiniteness of $\mathbf{V}$ yields the instability.

Theorem 5.12 (K. Veselic, 1995 [582]). *Let the effective stiffness matrix* (5.43) *be positive definite. Then, the system* (5.42) *is stable at* $\Omega > \Omega_0$, *where* $\Omega = \Omega_0$ *is the largest root of the equation*

$$\det\left(\mathbf{W} - \Omega^2 \begin{pmatrix} \mathbf{M} & 0 \\ 0 & \mathbf{M} \end{pmatrix}\right) = 0.$$

5.4 Damped gyroscopic systems

Assuming $\mathbf{N} = 0$ in equation (5.1) we arrive at the gyroscopic system with damping

$$\mathbf{M}\ddot{\mathbf{x}} + (\mathbf{D} + \mathbf{G})\dot{\mathbf{x}} + \mathbf{K}\mathbf{x} = 0. \tag{5.44}$$

With the block matrices

$$\mathbf{A} = \begin{pmatrix} 0 & \mathbf{I} \\ -\mathbf{M}^{-1}\mathbf{K} & -\mathbf{M}^{-1}(\mathbf{D} + \mathbf{G}) \end{pmatrix}, \quad \mathbf{Q} = \begin{pmatrix} 0 & 0 \\ 0 & \mathbf{D} \end{pmatrix} \tag{5.45}$$

and $\mathbf{L}(\lambda) = \mathbf{M}\lambda^2 + (\mathbf{D} + \mathbf{G})\lambda + \mathbf{K}$, the statement of Theorem 5.3 by Wimmer is valid for the damped gyroscopic system (5.44) [348, 525, 600]. In particular, if $\mathbf{D} > 0$ and

$\mathbf{M}$ and $\mathbf{K}$ nonsingular, then $\nu(\mathbf{L}(\lambda)) = \pi(\mathbf{M}) + \pi(\mathbf{K})$, and $\pi(\mathbf{L}(\lambda)) = \nu(\mathbf{M}) + \nu(\mathbf{K})$. This result contains several classical stability theorems associated with the names of Kelvin, Tait, Chetaev, and Zajac.

5.4.1 Kelvin–Tait–Chetaev theorem

Theorem 5.13 (W. Kelvin and P. G. Tait, 1879; N. G. Chetaev, 1961 [127, 573, 608]). *Stability of the solutions of equation* (5.44) *with* $\mathbf{M} > 0$, $\mathbf{D} > 0$ *and* $\mathbf{K}$ *nondegenerate is the same as the stability of the solutions of the corresponding undamped potential system* (5.2).

In particular, if all of the eigenvalues of the matrix $\mathbf{K}$ are positive (negative), the system (5.44) is asymptotically stable (unstable) [608].

Theorem 5.14 (E. E. Zajac, 1964 [525, 608]). *If* $\mathbf{M} > 0$ *and* $\mathbf{D} > 0$, *then the number of eigenvalues with positive real parts of the system* (5.44), *is equal to the number of negative eigenvalues of the matrix* $\mathbf{K}$.

For example, although the equilibrium of the potential system (5.2) with the even Poincaré instability degree $\nu(\mathbf{K})$ can be stabilized by the gyroscopic forces, this gyroscopic stabilization is destroyed when dissipative forces with full dissipation ($\mathbf{D} > 0$) are added, no matter how weak they are. This effect is a classical example of dissipation-induced instabilities [74, 333].

Following Zevin [613], let us consider a gyroscopic system with small dissipative perturbation, i.e.,

$$\mathbf{M}\ddot{\mathbf{x}} + (\varepsilon\mathbf{D} + \mathbf{G})\dot{\mathbf{x}} + \mathbf{K}\mathbf{x} = 0, \tag{5.46}$$

where $\mathbf{M} > 0$, $\mathbf{D} > 0$, and $\det \mathbf{K} \neq 0$ and $\varepsilon \geq 0$ is a small parameter. Let $\lambda = i\omega$ be a simple eigenvalue of the operator $\mathbf{M}\lambda^2 + \mathbf{G}\lambda + \mathbf{K}$ with the eigenvector $\mathbf{u}$. Let $\lambda(\varepsilon)$ be a perturbed eigenvalue such that $\lambda(0) = i\omega$. Then,

$$\left.\frac{d\lambda}{d\varepsilon}\right|_{\varepsilon=0} = -\omega^2 \frac{\overline{\mathbf{u}}^T \mathbf{D}\mathbf{u}}{\overline{\mathbf{u}}^T (\mathbf{M}\omega^2 + \mathbf{K})\mathbf{u}}, \tag{5.47}$$

see also [289, 291, 312]. The denominator in equation (5.47) is proportional to the energy of the mode with the frequency ω, the sign of which for $\omega > 0$ corresponds to the Krein signature of the eigenvalue $i\omega$ [613]. Therefore, the eigenvalues $i\omega$ with the positive Krein signature get negative real increments while those with the negative Krein signature move to the right half-plane of the complex plane [74, 391, 394, 613].

In the gyroscopically stabilized statically unstable system the number $\nu(\mathbf{K})$ is even and all eigenvalues are pure imaginary which implies the stability degree $s = m$. Let for simplicity all these eigenvalues be simple. Then, by Theorem 3.9, $(m + \pi(\mathbf{K}))/2$ positive pure imaginary eigenvalues (and their complex conjugates) have positive Krein signature while the remaining $(m - \pi(\mathbf{K}))/2 = \nu(\mathbf{K})/2$ positive pure imaginary eigenvalues (with their complex conjugates) have negative Krein signature. By formula (5.47), it is the $\nu(\mathbf{K})/2$ pairs of complex-conjugate pure imaginary eigenvalues with the negative Krein signature that are moved by the full dissipation to the open right half-plane of the complex plane and destroy the gyroscopic stabilization [613]. The total number of eigenvalues with the positive real parts is thus $\nu(\mathbf{K})/2+\nu(\mathbf{K})/2 = \nu(\mathbf{K})$ in agreement with Theorem 5.14.

5.5 Circulatory systems with and without velocity-dependent forces

Consider the circulatory system (5.4) and set $\mathbf{M} = \mathbf{I}$. After separating time with the substitution $\mathbf{x} = \mathbf{u}\exp(\lambda t)$ we come to the eigenvalue problem

$$(\lambda^2 + \mathbf{K} + \mathbf{N})\mathbf{u} = 0, \tag{5.48}$$

where the eigenvalues λ are the roots of the characteristic polynomial

$$p(\lambda) = \det(\lambda^2 + \mathbf{K} + \mathbf{N}) = a_0\lambda^{2m} + a_1\lambda^{2m-2} + a_2\lambda^{2m-4} + \dots. \tag{5.49}$$

Assuming $\mu = \lambda^2$ in equation (5.49) for the reduced polynomial $p(\mu)$ of order m, we write the $2m \times 2m$ *discriminant matrix* [187]

$$\begin{pmatrix}
a_0 & a_1 & a_2 & a_3 & \cdots & a_n & 0 & 0 & 0 \\
0 & ma_0 & (m-1)a_1 & (m-2)a_2 & \cdots & a_{m-1} & 0 & 0 & 0 \\
0 & a_0 & a_1 & a_2 & \cdots & a_{m-1} & a_m & 0 & 0 \\
0 & 0 & ma_0 & (m-1)a_1 & \cdots & 2a_{m-2} & a_{m-1} & 0 & 0 \\
\cdots & \cdots & \cdots & \cdots & \cdots & \cdots & \cdots & \cdots & \cdots \\
\cdots & \cdots & \cdots & \cdots & \cdots & \cdots & \cdots & \cdots & \cdots \\
0 & 0 & 0 & \cdots & 0 & a_0 & a_1 & \cdots & a_m \\
0 & 0 & 0 & \cdots & 0 & 0 & ma_0 & \cdots & a_{m-1}
\end{pmatrix}. \tag{5.50}$$

The sequence

$$\Delta_1, \Delta_2, \dots, \Delta_m, \tag{5.51}$$

where Δ_j is the determinant of the submatrix of the discriminant matrix (5.50) formed by the first $2j$ rows and $2j$ columns, is called a *discriminant sequence* of the polynomial $p(\mu)$.

It is well known that the real polynomial $p(\mu)$ has only real roots if and only if the elements of the discriminant sequence are all nonnegative: $\Delta_j \geq 0$, $j = 1, 2, \dots, m$

[187]. Otherwise, there exists μ with $\mathrm{Im}\,\mu \neq 0$ which yields the existence of a complex root λ of the polynomial (5.49) with $\mathrm{Re}\lambda > 0$ (flutter instability). Furthermore, if $p(\mu)$ has only real roots, then they are negative if and only if its coefficients are either all nonpositive or all nonnegative [187].

Theorem 5.15 (P. Gallina, 2003 [187]). *A necessary and sufficient condition for all the eigenvalues λ of the eigenvalue problem* (5.48) *of the undamped circulatory system* (5.4) *to be pure imaginary is that the elements of the discriminant sequence* (5.51) *corresponding to the discriminant matrix* (5.50) *are all nonnegative and that the coefficients of the polynomial* (5.49) *are either all nonpositive or all nonnegative.*

We remark that the *Gallina criterion* guarantees only spectral stability of the circulatory system but not the Lyapunov stability, because among the pure imaginary roots of the polynomial (5.49) there can be multiple ones that correspond to the multiple eigenvalues of the eigenvalue problem (5.48) with the nontrivial Jordan block. The latter means instability because of the secular terms in the solution with polynomial time dependence.

On the other hand, violation of the conditions of Theorem 5.15 guarantees instability, either flutter ($\Delta_s < 0$ for some $s \in \{1, 2, \ldots, m\}$) or divergence (all $\Delta_s \geq 0$ and $a_i a_j < 0$ for some $i \neq j$, $i, j \in \{1, 2, \ldots, m\}$) [187]. Note that these conclusions are valid in fact for any system with the real characteristic polynomial containing only even powers of the spectral parameter, including potential, undamped gyroscopic, and oscillatory damped systems, see e.g. [3].

5.5.1 Merkin's theorem and Bulatovic's flutter condition

Theorem 5.16 (D. R. Merkin, 1956 [422, 423]). *Perturbation by arbitrary linear circulatory forces of a stable pure potential system with eigenfrequencies coinciding into one with the algebraic multiplicity equal to the dimension of the system destroys the stability of the equilibrium regardless of the form of the nonlinear terms.*

We will prove Merkin's theorem for the linear circulatory system (5.4) with $\mathbf{M} = \mathbf{I}$. Expressing the coefficients of the polynomial (5.49) by means of the Leverrier–Barnett algorithm given by Theorem 5.1, we find

$$p(\lambda) = \lambda^{2m} + \mathrm{tr}\mathbf{K}\lambda^{2m-2} + \frac{1}{2}\left((\mathrm{tr}\mathbf{K})^2 - \mathrm{tr}\mathbf{K}^2 - \mathrm{tr}\mathbf{N}^2\right)\lambda^{2m-4} + \cdots . \qquad (5.52)$$

Checking the conditions of the Gallina criterion, we observe that the first element of the discriminant sequence is $\Delta_1 = m > 0$, whereas the second one gives the following sufficient condition for flutter instability

$$a_0^2((a_1^2 - 2a_2a_0)m - a_1^2) < 0. \tag{5.53}$$

Substituting the coefficients from (5.52) into the inequality (5.53), we get

$$\mathrm{tr}\mathbf{K}^2 + \mathrm{tr}\mathbf{N}^2 < \frac{1}{m}(\mathrm{tr}\mathbf{K})^2. \tag{5.54}$$

Recall that the Frobenius norm of a matrix is defined as $\|\mathbf{A}\|^2 = \mathrm{tr}(\mathbf{A}^T\mathbf{A})$ [548].

Theorem 5.17 (R. M. Bulatovic, 2011 [100]). *If*

$$\|\mathbf{N}\|^2 > \|\mathbf{K}\|^2 - \frac{1}{m}(\mathrm{tr}\mathbf{K})^2 \tag{5.55}$$

the circulatory system (5.4) *with* $\mathbf{M} = \mathbf{I}$ *is unstable by flutter.*

Note that for $m = 2$ this inequality is a necessary and sufficient condition for the onset of flutter instability [26, 290]. On the other hand, when the matrix $\mathbf{K} > 0$ has a single semisimple eigenvalue of algebraic multiplicity m, then the right side of the inequality (5.55) vanishes which means instability. This is a statement of Theorem 5.16 for a linear circulatory system. Other stability criteria for circulatory systems can be found in the articles [4, 5, 65, 257, 342, 575, 612] and monographs [239, 369, 423, 437].

5.5.2 Bottema–Lakhadanov–Karapetyan theorem

Consider a circulatory system with the gyroscopic forces

$$\ddot{\mathbf{x}} + \mathbf{G}\dot{\mathbf{x}} + (\mathbf{K} + \mathbf{N})\mathbf{x} = 0. \tag{5.56}$$

The following analogue of Merkin's theorem is known:

Theorem 5.18 (V. M. Lakhadanov, 1975 [342]). *If* $\mathbf{K} = \kappa\mathbf{I}$*, where* κ *is an arbitrary constant, and matrices* $\mathbf{G}$ *and* $\mathbf{N}$ *are commutative, then system* (5.56) *is unstable.*

With the use of the Leverrier–Barnett algorithm given by Theorem 5.1 we find that the coefficient of the characteristic polynomial of the system (5.56) at λ^{2m-1} is $\mathrm{tr}\mathbf{G} = 0$ while that at λ^{2m-3} is equal to $-\mathrm{tr}\mathbf{N}\mathbf{G}$ and in general does not vanish. This observation yields a sufficient condition for instability:

Theorem 5.19 (V. M. Lakhadanov, A. V. Karapetyan, 1975 [257,342]). *The system* (5.56) *is not asymptotically stable. It is unstable if*

$$\mathrm{tr}\mathbf{NG} \neq 0. \tag{5.57}$$

In the early work of Bottema [80] Theorem 5.19 was established in the particular cases of $m = 2$ and $m = 3$ degrees of freedom. Note that in the case of $m = 2$, the simultaneous action of circulatory and gyroscopic forces always destabilizes a potential system. If $m > 2$, the system (5.56) is generically unstable; it can be Lyapunov stable in the set of measure zero if $\mathrm{tr}\mathbf{NG} = 0$.

The system (5.56) can frequently be interpreted as a result of a small perturbation of a gyroscopic system (5.3) by circulatory forces. The Bottema–Lakhadanov–Karapetyan theorem demonstrates that, similar to the destabilizing effect of full dissipation on gyroscopic stabilization, the nonconservative positional forces generically destroy the marginal stability of gyroscopic systems. This conclusion is practically important in a number of engineering applications, such as the acoustics of friction [6,538,539], friction-induced instabilities in rotor dynamics [123,268,456,574,604], and electromagnetic tethered satellite systems [41,44], to name a few.

In this respect a natural question arises. From Section 5.4.1 we know that full dissipation shifts pure imaginary eigenvalues with the negative Krein signature of the gyroscopically stabilized system to the right in the complex plane. Does the Krein signature govern the destabilizing effect of circulatory forces? What will happen to the stability of the gyroscopically stabilized system when both full dissipation and circulatory forces are added? The answer to these intriguing questions will be found in Chapter 6.

5.5.3 Stabilizing and destabilizing damping configurations

In 1952 Ziegler [622] showed that full dissipation can destabilize the circulatory system (5.4). Indeed, in the equations of motion of Ziegler's pendulum

$$\begin{pmatrix} m_1l^2 + m_2l^2 & m_2l^2 \\ m_2l^2 & m_2l^2 \end{pmatrix}\begin{pmatrix} \ddot{\varphi}_1 \\ \ddot{\varphi}_2 \end{pmatrix} + \begin{pmatrix} d_1 + d_2 & -d_2 \\ -d_2 & d_2 \end{pmatrix}\begin{pmatrix} \dot{\varphi}_1 \\ \dot{\varphi}_2 \end{pmatrix} + \begin{pmatrix} -Pl + 2c & Pl - c \\ -c & c \end{pmatrix}\begin{pmatrix} \varphi_1 \\ \varphi_2 \end{pmatrix} = 0, \tag{5.58}$$

the damping matrix is positive definite if the coefficients of the viscous damping are positive: $d_1 > 0$ and $d_2 > 0$. When $d_1 = 0$ and $d_2 = 0$, the system (5.58) is marginally stable when $P < P_u$, where [302]

$$P_u := \frac{4m_2c_2 + \left(\sqrt{m_1c_2} - \sqrt{m_2c_1}\right)^2}{2lm_2} \geq \frac{2c_2}{l}. \tag{5.59}$$

With dissipation, asymptotic stability takes place when $P < P_d$, where [302]

$$P_d := \frac{4m_2^2(d_2^2c_1^2 + d_1^2c_2^2) + d_1d_2(8m_2(m_1+2m_2)c_2^2 + (c_1m_2 - m_1c_2)^2)}{2m_2l(4m_2d_2 + d_1m_2 + m_1d_2)(c_1d_2 + d_1c_2)} + \frac{1}{2}\frac{d_1d_2}{m_2l^3}. \tag{5.60}$$

For almost every ratio $\beta := d_1/d_2 = \tilde{d}_1/\tilde{d}_2$, we have

$$\lim_{\varepsilon\to 0} P_d(d_1 = \varepsilon\tilde{d}_1, d_2 = \varepsilon\tilde{d}_2) < P_u \tag{5.61}$$

with the exception of $\beta = \beta_0$, where

$$\beta_0 = \frac{c_1\sqrt{m_1m_2} - (m_1+4m_2)\sqrt{c_1c_2}}{m_2\sqrt{c_1c_2} - c_2\sqrt{m_1m_2}}. \tag{5.62}$$

When $d_1 = \beta_0 d_2$,

$$P_d = P_u + \frac{\beta_0}{2}\frac{d_2^2}{m_2l^3} \tag{5.63}$$

and P_d tends to P_u when $d_2 \to 0$.

The inequality (5.61) shows that the full dissipation of order $O(\varepsilon)$ generically makes the interval of marginal stability of Ziegler's pendulum smaller by the amount of order $O(1)$. This discontinuous drop of the stability threshold under the action of infinitesimally small dissipation is known as the Ziegler (or Ziegler–Bottema) destabilization paradox [312]. On the other hand, equation (5.63) indicates the existence of damping distributions that (if $\beta_0 > 0$) make the system stable at $P < P_u$ and asymptotically stable on a larger interval $P < P_d$. Furthermore, the latter tends to the former in the limit of vanishing dissipation.

In order to find the stabilizing damping configurations in the general case, we consider the system

$$\mathbf{M}\ddot{\mathbf{x}} + \varepsilon\mathbf{V}\dot{\mathbf{x}} + \mathbf{P}\mathbf{x} = 0, \tag{5.64}$$

where $\mathbf{M} = \mathbf{M}^T > 0$ is a real $m \times m$ matrix, $\mathbf{V} = \mathbf{G} + \mathbf{D}$ is a nonsymmetric matrix of velocity-dependent forces and $\mathbf{P} = \mathbf{K} + \mathbf{N}$ is a nonsymmetric matrix of positional forces [281].

Theorem 5.20 (J. A. Walker, 1973 [281, 589]). *Velocity-dependent forces with the matrix*

$$\mathbf{V} = \sum_{p=0}^{m-1} c_p\mathbf{M}(\mathbf{M}^{-1}\mathbf{P})^p, \quad c_p \geq 0 \tag{5.65}$$

make the circulatory system $\mathbf{M}\ddot{\mathbf{x}} + \mathbf{P}\mathbf{x} = 0$ *asymptotically stable at* $\varepsilon > 0$*, if at* $\varepsilon = 0$ *it is stable or situated on the boundary between stability and flutter domains.*

For example, for $m = 2$ the Walker matrices have the form $c_0\mathbf{M} + c_1\mathbf{P}$.

The Walker matrices (5.65) constitute a rather narrow subset of the set of all possible stabilizing velocity-dependent perturbations $\varepsilon\mathbf{V}$ that was found for the system (5.64) in the general case by Kirillov and Seyranian in [281].

To illustrate this, let us for simplicity set $m = 2$, assume that $\mathbf{M} > 0$, the matrices $\mathbf{P}$ and $\mathbf{V}$ are not degenerate, and introduce the adjugate matrices

$$\mathbf{V}^* := \mathrm{adj}\mathbf{V} = \mathbf{V}^{-1}\det\mathbf{V}, \quad \mathbf{P}^* := \mathrm{adj}\mathbf{P} = \mathbf{P}^{-1}\det\mathbf{P}.$$

Then, as was established in [281, 285, 286], the linear variations $\varepsilon\mathbf{V}$ are stabilizing, if $\mathbf{V}$ satisfies the conditions

$$\mathrm{tr}\mathbf{P}^*\mathbf{V} = \omega_0^2\mathrm{tr}\mathbf{V}^*\mathbf{M}, \quad \mathrm{tr}\mathbf{V}^*\mathbf{M} > 0, \quad \det\mathbf{V} > 0, \tag{5.66}$$

where $\omega_0^2 = (\mathrm{tr}\mathbf{M}\mathrm{tr}\mathbf{P} - \mathrm{tr}\mathbf{M}\mathbf{P})/(2\det\mathbf{M})$.

The conditions (5.66) define nothing else but the tangent cone to the asymptotic stability domain that is given by the Routh–Hurwitz criterion written for the characteristic polynomial of the system (5.64) with $\varepsilon = 1$:

$$\mathrm{tr}\mathbf{P}^*\mathbf{V}\mathrm{tr}\mathbf{V}^*\mathbf{M}\det\mathbf{V} > \det\mathbf{M}(\mathrm{tr}\mathbf{P}^*\mathbf{V} - \omega_0^2\mathrm{tr}\mathbf{V}^*\mathbf{M})^2, \quad \mathrm{tr}\mathbf{V}^*\mathbf{M} > 0, \quad \det\mathbf{V} > 0. \tag{5.67}$$

In the $(\mathrm{tr}\mathbf{V}^*\mathbf{M}, \mathrm{tr}\mathbf{P}^*\mathbf{V}, \det\mathbf{V}/\det\mathbf{M})$-space the domain of asymptotic stability has the Whitney umbrella singularity at the origin corresponding to the nonperturbed circulatory system that has a pair of double eigenvalues $i\omega_0$ with the Jordan block – the fact established by Bottema in 1956 [81]. The tangent cone (5.66) (hatched in Figure 5.4) contains all linear perturbations $\varepsilon\mathbf{V}$ leading to the asymptotic stability domain (5.67). On the other hand, if we look for a *symmetric* Walker matrix of velocity-dependent forces, it can only have the form $\mathbf{V} = c_0\mathbf{M}$. Such matrices satisfy the equation

$$\frac{\det\mathbf{V}}{\det\mathbf{M}} = \left(\frac{\mathrm{tr}\mathbf{V}^*\mathbf{M}}{2\det\mathbf{M}}\right)^2, \tag{5.68}$$

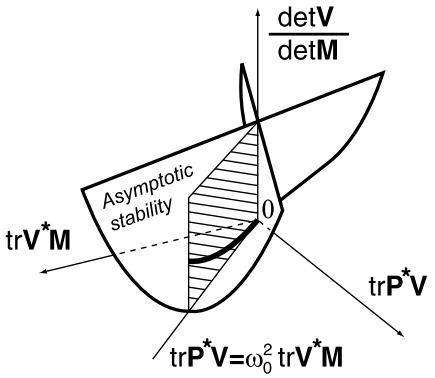

Figure 5.4. The asymptotic stability domain (5.67), (hatched) the tangent cone (5.66) at the Whitney umbrella singular point, and (red curve) the set (5.68) of symmetric Walker's matrices $\mathbf{V} = c_0\mathbf{M}$.

which defines a parabolic curve (shown in bold black in Figure 5.4) that belongs to the tangent cone (5.66). Note that Walker obtained his result with the use of the direct Lyapunov method, while the tangent cone to the domain of asymptotic stability was computed in [281] via perturbation of multiple eigenvalues.

Throughout this chapter, we have had the opportunity to ascertain that mechanisms of destabilization and stabilization of nonconservative systems involve both the singularities of the stability boundary and that of the bifurcation diagrams situated inside the domain of asymptotic stability. In the next chapter the perturbation theory of multiple eigenvalues will be used for uncovering the connections between the singularities of the stability boundary, bifurcation diagrams, Krein signature of eigenvalues, and dissipation-induced instabilities. [332, 333].

Chapter 6

Dissipation-induced instabilities

Unfortunately, it is quite common for an eigenvalue which is moving steadily towards a positive growth rate to suffer a sudden change of direction and subsequently fail to become unstable; similarly, it happens that modes which initially become more stable as [the Reynolds number] increases change direction and subsequently achieve instability. It is believed that these changes of direction are due to the nearby presence of multiple-eigenvalue points.

C. A. Jones [246]

6.1 Crandall's gyropendulum

Crandall's gyropendulum [139] is an axisymmetric rigid body pivoted at a point O on the symmetry axis as shown in Figure 6.1 (a). When the axial spin Ω is absent, the upright position is statically unstable. When $\Omega \neq 0$, the body becomes a *gyroscopic pendulum*. Its primary parameters are its mass m, the distance L between the mass center and the pivot point, the axial moment of inertia I_a, and the diametral moment of inertia I_d about the pivot point. The gravity acceleration is denoted by g.

It is assumed that a drag force proportional to the linear velocity of the center of mass of the gyropendulum acts at the center of mass to oppose that velocity (stationary damping with the coefficient b_s). Additionally, it is assumed that a rigid sphere concentric with the pendulum tip O, is attached to the pendulum and rubs against a fixed rub plate. The gyropendulum is supported without friction at O, while a viscous friction force acts between the larger sphere and the rub plate, being responsible for the rotating damping with the coefficient b_r. The linearized equations of motion for the gyropendulum in the vicinity of the vertical equilibrium position derived in [139] have the form of the general nonconservative system (5.1) with the matrices $\mathbf{G}$, $\mathbf{D}$, $\mathbf{K}$, and $\mathbf{N}$ specified by the expressions

$$\mathbf{G} = \begin{pmatrix} 0 & \eta\Omega \\ -\eta\Omega & 0 \end{pmatrix}, \quad \mathbf{D} = \begin{pmatrix} \sigma+\rho & 0 \\ 0 & \sigma+\rho \end{pmatrix},$$
$$\mathbf{K} = \begin{pmatrix} -\alpha^2 & 0 \\ 0 & -\alpha^2 \end{pmatrix}, \quad \mathbf{N} = \begin{pmatrix} 0 & \rho\Omega \\ -\rho\Omega & 0 \end{pmatrix}. \tag{6.1}$$

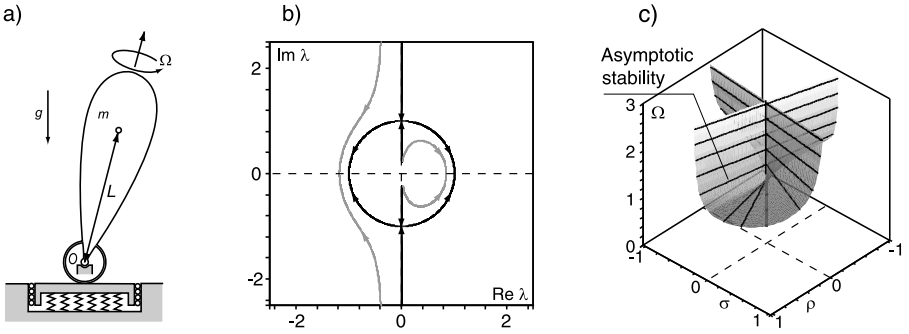

Figure 6.1. (a) Crandall's gyropendulum. For $\alpha = 1$ and $\eta = 1.5$ the panel (b) shows the movement of eigenvalues of the gyropendulum with $\rho = 0$ and (black lines) $\sigma = 0$ or (light gray lines) $\sigma = 1/3$ when the angular velocity decreases from $\Omega = 3$ to zero; the panel (c) shows in the (ρ, σ, Ω)-space the domain of gyroscopic stabilization with the Whitney umbrella singularity at $(0, 0, \Omega_2)$ where $\Omega_2 = 2\alpha/\eta$.

The system depends on the spin Ω and four parameters

$$\eta = \frac{I_a}{I_d}, \quad \sigma = \frac{b_s}{I_d}, \quad \rho = \frac{b_r}{I_d}, \quad \alpha^2 = \frac{mgL}{I_d}, \tag{6.2}$$

where α is the nonspinning pendulum frequency and η is responsible for the shape of the gyropendulum: for $\eta < 1$ the pendulum is prolate, and for $\eta > 1$ it is oblate. Parameters σ and ρ correspond to the stationary and rotating damping, respectively. We note that the stationary damping contributes only to the matrix $\mathbf{D}$ while the rotating damping is responsible also for the appearance of the nonconservative positional forces described by the skew-symmetric matrix $\mathbf{N}$. Thus, Crandall's gyropendulum can be treated as a conservative gyroscopic system perturbed by weak damping and circulatory forces.

6.1.1 Conservative gyroscopic stabilization and its destruction by stationary damping

Since the number of degrees of freedom of Crandall's gyropendulum is even ($m = 2$) and $\mathbf{K} < 0$, then it can be stabilized by the gyroscopic forces at sufficiently large absolute values of Ω when $\sigma = \rho = 0$. Indeed, the gyroscopic stabilization in the conservative case happens at $\Omega^2 > {\Omega_2}^2$, where

$$\Omega_2 = \frac{2\alpha}{\eta} \tag{6.3}$$

is higher for the prolate pendulum ($\eta < 1$) in comparison with the oblate one ($\eta > 1$) [508]. At the points of the stability boundary, the spectrum of the gyropendulum has a pair of double pure imaginary eigenvalues $\pm i\,\omega_0$ with the Jordan block, where $\omega_0 = \alpha$

[139,289]. When $\Omega \geq 0$ decreases, the pure imaginary eigenvalues move toward each other, collide at $\Omega = \Omega_2$ and then diverge in order to continue the motion along the circle

$$(\mathrm{Im}\lambda)^2 + (\mathrm{Re}\lambda)^2 = \alpha^2, \tag{6.4}$$

shown in black in Figure 6.1 (b). This linear Hamiltonian–Hopf bifurcation (Krein collision) accompanies the loss of the conservative gyroscopic stabilization.

In the case when only stationary damping is acting ($\rho = 0, \sigma \neq 0$), the dissipation is full. Then, in accordance with the Kelvin–Tait–Chetaev and Zajac theorems described in Section 5.4.1 the number of eigenvalues in the open right half-plane of the complex plane at any Ω is equal to the number of negative eigenvalues of the matrix $\mathbf{K}$, i.e. two. This implies that the Krein collision of the conservative case is replaced by an imperfect merging of modes [226] shown in light gray in Figure 6.1 (b). The eigenvalue paths are bent due to the nearby presence of the double eigenvalue $i\alpha$ that exists at $\sigma = 0$ and $\rho = 0$ at $\Omega = \Omega_2$.

Note that the full dissipation alone destabilizes the mode with the lower frequency and stabilizes that with the higher frequency. From the Hamiltonian representation of the gyroscopic system with the Hamiltonian (3.56) applied to the equations of Crandall's gyropendulum it follows that the eigenvalues $i\omega$ with the higher frequency ω have positive energy in the sense of the definition (3.57), while the energy of those with the lower frequency is negative. Therefore, it is the negative energy modes that are destabilized by the stationary damping, which agrees with the formula (5.47).

6.1.2 Singular threshold of the nonconservative gyroscopic stabilization

Writing the Liénard–Chipart conditions (2.59) for the characteristic polynomial of the gyropendulum when both the stationary and rotating damping forces are acting, we find the inequalities defining its asymptotic stability domain

$$\sigma + \rho > 0, \tag{6.5}$$

$$\eta^2\Omega^2 + (\sigma + \rho)^2 - 2\alpha^2 > 0, \tag{6.6}$$

$$\Omega^2 > \frac{(\sigma + \rho)^2\alpha^2}{\sigma\eta\rho + \eta\rho^2 - \rho^2}. \tag{6.7}$$

After transformation of its right-hand side, the inequality (6.7) yields

$$\Omega^2 > {\Omega_2}^2 + \frac{1}{\rho}\frac{\alpha^2}{\eta^2}\frac{(\sigma\eta + \rho(\eta - 2))^2}{\sigma\eta + \rho(\eta - 1)} \geq {\Omega_2}^2. \tag{6.8}$$

Hence, the asymptotic stability domain is completely determined by the conditions (6.5) and (6.7), which can be written in the form

$$\Omega > \Omega_{cr}^{+}(\rho, \sigma), \quad \Omega < \Omega_{cr}^{-}(\rho, \sigma), \quad \sigma + \rho > 0, \tag{6.9}$$

where the critical values of the spin Ω as a function of the two damping parameters are

$$\Omega_{cr}^{\pm}(\rho,\sigma) = \pm\frac{(\sigma+\rho)\alpha}{\sqrt{-\rho^2+\rho^2\eta+\rho\eta\sigma}}. \tag{6.10}$$

Equations (6.10) describe two surfaces in the space of the parameters ρ, σ, and Ω. Both surfaces have the Whitney umbrella singularity at the points $(0,0,\pm\Omega_2)$. The surface $\Omega_{cr}^{+}(\rho,\sigma)$ is shown in Figure 6.1 (a) for $\alpha = 1$ and $\eta = 1.5$. The inequality (6.5) selects the stable pocket of the Whitney umbrella.

As follows from the expressions (6.8) and (6.10), $\Omega_{cr}^{+} \geq \Omega_2$ and $\Omega_{cr}^{-} \leq -\Omega_2$, i.e. the damping and nonconservative positional forces generically increase the threshold of gyroscopic stabilization. The critical angular velocities coincide ($\Omega_{cr}^{\pm} = \pm\Omega_0^{+}$) only at the specific ratios of the coefficients of the stationary and rotating damping [139, 289]

$$\frac{b_s}{b_r} = \frac{\sigma}{\rho} = \frac{2-\eta}{\eta} = \frac{\Omega_2}{\omega_0} - 1. \tag{6.11}$$

It turns out that the rotating damping (and thus circulatory forces) can compensate the dissipation-induced instability caused by the stationary damping although this happens at the cost of generally higher angular velocities at the onset of the nonconservative gyroscopic stabilization.

6.1.3 Imperfect Krein collision and exchange of instability between negative and positive energy modes

How does the simultaneous action of both types of damping, i.e. that of full dissipation and circulatory forces, influence the pure imaginary eigenvalues of the conservative Crandall's gyropendulum in dependence on their Krein signature or the energy of the associated vibration mode? To clarify this issue, let us proceed similarly to as we did in Section 2.6.2 and find the set of double complex eigenvalues (EP-set) inside the domain of asymptotic stability:

$$\left\{\sigma = \frac{2-\eta}{\eta}\rho, \quad \Omega = \Omega_{EP} := \frac{2\sqrt{\alpha^2\eta^2+\rho^2}}{\eta^2}\right\}. \tag{6.12}$$

The EP-set belongs to the tangent cone to the asymptotic stability domain at the singular point $(0,0,\Omega_2)$

$$\left\{\sigma = \frac{2-\eta}{\eta}\rho, \quad \sigma+\rho>0, \quad \Omega>\Omega_2\right\}. \tag{6.13}$$

The double complex eigenvalues at the EP-set are

$$\lambda_{EP}^{\pm} = -\frac{\rho}{\eta} \pm i\sqrt{\alpha^2+\frac{\rho^2}{\eta^2}} \tag{6.14}$$

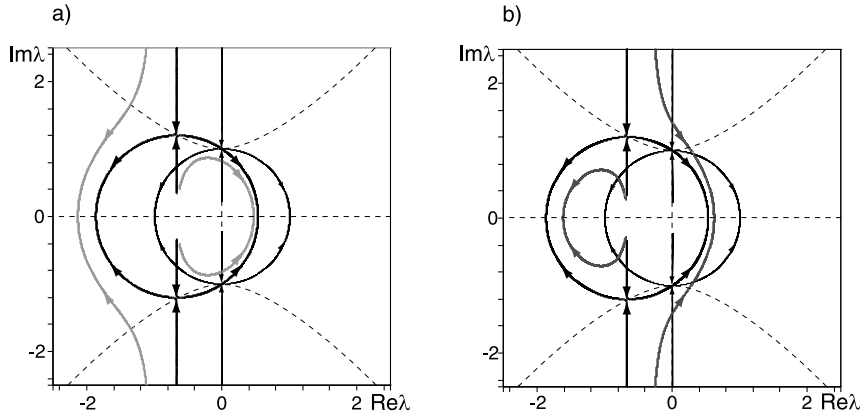

Figure 6.2. For $\alpha = 1$ and $\eta = 1.5$ the movement of eigenvalues in the complex plane for (thin black lines) $\rho = 0$ and $\sigma = 0$, (thick black lines) $\rho = 1$ and $\sigma = 1/3$, (light gray lines) $\rho = 1$ and $\sigma = 2/3$, and (dark gray lines) $\rho = 1$ and $\sigma = 0$ when the angular velocity decreases from $\Omega = 3$ to zero. (a) Destabilization of negative energy modes when $\sigma/\rho > (\eta - 2)/\eta$. (b) Destabilization of positive energy modes when $\sigma/\rho < (\eta - 2)/\eta$. Dashed line marks the hyperbola of double eigenvalues (6.15).

and they live in the complex plane on the hyperbola

$$(\mathrm{Im}\lambda)^2 - (\mathrm{Re}\lambda)^2 = \alpha^2, \tag{6.15}$$

shown by the dashed lines in Figure 6.2. When $\rho = 0$ and $\sigma = 0$, the hyperbola (6.15) and the circle (6.4) have two common points that correspond to the double eigenvalues $\pm i\alpha$.

Remarkably, when $\rho \neq 0$ and $\sigma \neq 0$ related as $\sigma = \frac{2-\eta}{\eta}\rho$ are fixed and thus Ω varies along a vertical line inside the tangent cone, the complex eigenvalues move in the complex plane along the line $\mathrm{Re}\lambda = -\rho/\eta$ when $\Omega > \Omega_{EP}$. At $\Omega = \Omega_{EP}$ they collide into the double complex eigenvalues $\lambda_{EP}^{\pm}$ that bifurcate with the further decrease in Ω into a quadruplet of simple eigenvalues that evolve along the circle

$$\mathrm{Im}\lambda^2 + \left(\mathrm{Re}\lambda + \frac{\rho}{\eta}\right)^2 = \alpha^2 + \frac{\rho^2}{\eta^2}, \tag{6.16}$$

shown by the thick black lines in Figure 6.2. The circle (6.16) and the hyperbola (6.15) intersect exactly at the double eigenvalues (6.14). The intersection points evolve along the hyperbola (6.15) when ρ and σ increase along the line $\sigma = \frac{2-\eta}{\eta}\rho$. However, the frequency of the unstable mode at the threshold of instability remains the same as in the conservative case: $\omega = \alpha$.

When $\sigma \neq \frac{2-\eta}{\eta}\rho$, then with the variation of Ω the eigenvalues in the complex plane pass in close vicinity of each other without merging. This avoided crossing happens

near the location of a double eigenvalue corresponding to parameters ρ, σ, and Ω from the EP-set (6.12). The pattern of the avoided crossing depends on the sign of the quantity $\sigma - \frac{2-\eta}{\eta}\rho$.

If $\sigma > \frac{2-\eta}{\eta}\rho$, then at the fixed σ and ρ the decrease in Ω is accompanied by the destabilization of the mode with the lower frequency ($\omega < \alpha$) and stabilization of the mode with the higher frequency ($\omega > \alpha$), Figure 6.2 (a). If $\sigma < \frac{2-\eta}{\eta}\rho$, then the higher mode is destabilized and the lower one is stabilized by the combined action of the stationary and rotating damping, Figure 6.2 (b).

The light gray and dark gray eigenvalue trajectories in Figure 6.2 can be interpreted as the locations of eigenvalues that at a given Ω are shifted from the imaginary axis by the dissipative and circulatory perturbation. Then, at $\sigma > \frac{2-\eta}{\eta}\rho$ and $\Omega > \Omega_{cr}^{+}(\rho,\sigma)$ both negative and positive energy modes are stabilized, whereas at $\Omega < \Omega_{cr}^{+}(\rho,\sigma)$ the negative energy modes are destabilized. On the other hand, at $\sigma < \frac{2-\eta}{\eta}\rho$ and $\Omega < \Omega_{cr}^{+}(\rho,\sigma)$ the positive energy modes are destabilized, while at $\Omega > \Omega_{cr}^{+}(\rho,\sigma)$ both negative and positive energy modes are stabilized.

Therefore, it is the penetration of the tangent cone to the domain of asymptotic stability at the Whitney umbrella singularity that governs the bifurcation of the pattern of imperfect merging of modes and thus the transfer of instability between the modes of negative and positive energy. Samantaray et al. pointed out in [508] that exactly at the stability boundary, the work done by the nonpotential positional forces coming from the rotating damping is equal to the energy loss due to full dissipation coming from both the stationary and the rotating damping. The negative energy mode corresponds to the *slow precession* and the positive energy mode is the *fast precession* of the gyropendulum. When the parameters leave the stability domain at $\sigma > \frac{2-\eta}{\eta}\rho$, the slow precession is destabilized by the full dissipation [552]. If the stability boundary is penetrated at $\sigma < \frac{2-\eta}{\eta}\rho$, the fast precession is destabilized by the rotating damping that imports energy from a hypothetical driving system that would maintain Ω constant at the threshold of the nonconservative gyroscopic stabilization [508]. *The distinction between the two physical mechanisms of stability loss has a clear geometrical meaning: the tangent cone to the domain of asymptotic stability at the singular point.*

6.2 Gyroscopic stabilization of nonconservative systems

We see that in the presence of circulatory forces the number of scenarios of dissipation-induced instabilities increases with respect to the classical Kelvin–Tait–Chetaev theorem discussed in Section 5.4.1. Not only negative energy modes can be destabilized but also the modes of positive energy that traditionally are considered to be not susceptible to dissipation-induced instabilities. That is why recently damping and circulatory forces were recognized as the two fundamental nonconservative forces [332].

We consider a linear mechanical system (5.1) with m degrees of freedom

$$\ddot{\mathbf{x}} + (\delta\mathbf{D} + \Omega\mathbf{G})\dot{\mathbf{x}} + (\mathbf{K} + \nu\mathbf{N})\mathbf{x} = 0, \tag{6.17}$$

that depends on the parameters δ, Ω, and ν, of the damping, gyroscopic and nonconservative positional forces. Recall that m is even and $\mathbf{K}<0$.

Seeking for the solutions to equation (6.17) in the form $\mathbf{x} \sim \mathbf{u}\exp(\lambda t)$, we arrive at the eigenvalue problem for a matrix polynomial

$$\mathbf{L}(\lambda)\mathbf{u} := (\lambda^2 + (\delta\mathbf{D} + \Omega\mathbf{G})\lambda + \mathbf{K} + \nu\mathbf{N})\mathbf{u} = 0. \tag{6.18}$$

Our goal is to confirm the observations made in the study of Crandall's gyropendulum in the case of the general nonconservative system (6.17).

When applied separately, dissipative and nonconservative positional forces destroy gyroscopic stabilization, see Theorems 5.13 and 5.19. However, a combination of these forces can make the system (6.17) asymptotically stable, as we have seen in the example of Crandall's gyropendulum. Below we will demonstrate that the peculiarities of the choice of such a combination are associated with the Whitney umbrella singularity existing on the boundary of the gyroscopic stabilization domain of the nonconservative system (6.17).

6.2.1 The case of $m = 2$ degrees of freedom

When $m = 2$, then without loss of generality we can take

$$\mathbf{G} = \mathbf{N} = \begin{pmatrix} 0 & -1 \\ 1 & 0 \end{pmatrix}. \tag{6.19}$$

Then, the Leverrier–Barnett algorithm [36] applied to $\mathbf{L}(\lambda)$ results in the characteristic polynomial $q(\lambda) = \lambda^4 + q_1\lambda^3 + q_2\lambda^2 + q_3\lambda + q_4$ with the coefficients

$$\begin{aligned} q_1 &= \delta\mathrm{tr}\mathbf{D}, & q_2 &= \mathrm{tr}\mathbf{K} + \delta^2 \det\mathbf{D} + \Omega^2, \\ q_3 &= \delta(\mathrm{tr}\mathbf{K}\mathrm{tr}\mathbf{D} - \mathrm{tr}\mathbf{K}\mathbf{D}) + 2\Omega\nu, & q_4 &= \det\mathbf{K} + \nu^2. \end{aligned} \tag{6.20}$$

When the damping and nonconservative positional forces are absent, i.e. $\delta = 0$ and $\nu = 0$, the equation (6.17) describes a conservative gyroscopic system. Then, equation (6.17) can be transformed to the form $\dot{\mathbf{z}} = \mathbf{A}\mathbf{z}$, where the matrix $\mathbf{A}$ obeys the Hamiltonian symmetry, $\mathbf{J}\mathbf{A}\mathbf{J} = \mathbf{A}^T$, and

$$\mathbf{A} = \begin{pmatrix} -\frac{1}{2}\Omega\mathbf{G} & \mathbf{I} \\ -\mathbf{K} - \frac{1}{4}\Omega^2\mathbf{I} & -\frac{1}{2}\Omega\mathbf{G} \end{pmatrix}, \ \mathbf{J} = \begin{pmatrix} 0 & -\mathbf{I} \\ \mathbf{I} & 0 \end{pmatrix}, \ \mathbf{z} = \begin{pmatrix} \mathbf{x} \\ \dot{\mathbf{x}} + \frac{1}{2}\Omega\mathbf{G}\mathbf{x} \end{pmatrix}; \tag{6.21}$$

$\mathbf{I}$ is a unit 2×2 matrix, see Section 3.3.7.

Resolving the equation $q(\lambda) = 0$ with respect to λ in the assumption that $\delta = 0$ and $\nu = 0$, we find that $\lambda = \pm i\omega_\pm(\Omega)$, where [290]

$$\omega_\pm(\Omega) = \sqrt{\omega_0^2 + \frac{\Omega_2}{2}\left(\sqrt{\Omega^2 - \Omega_2^2} \pm \sqrt{\Omega^2 - \Omega_1^2}\right)\sqrt{\frac{\Omega^2}{\Omega_2^2} - 1}}. \tag{6.22}$$

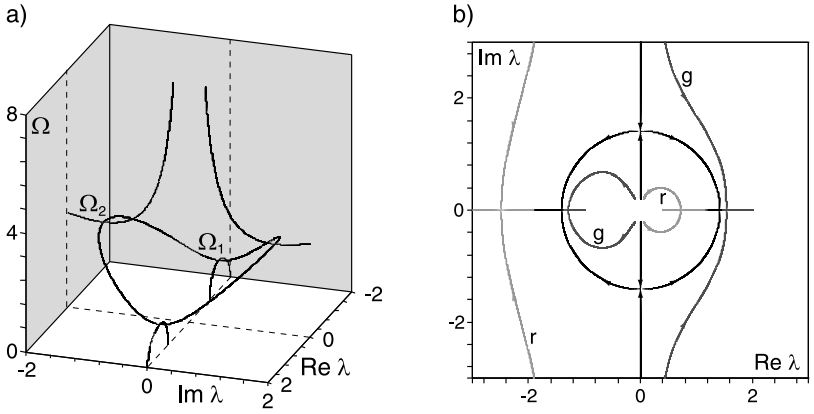

Figure 6.3. For $\kappa_1 = -1$, $\kappa_2 = -4$, tr$\mathbf{D} = 3$, tr$\mathbf{KD} = -6$, and det $\mathbf{D} = 1$: movement of eigenvalues (a) in the $(\mathrm{Re}\lambda, \mathrm{Im}\lambda, \Omega)$-space and (b) in the complex plane when Ω decreases from 10 to 0 and (black) $\delta = 0$ and $\nu = 0$, (light gray, r) $\delta = 1$ and $\nu = 0$, and (dark gray, g) $\delta = 0$ and $\nu = 1$ [305].

The frequency $\omega_0 = \frac{1}{2}\sqrt{\Omega_2^2 - \Omega_1^2}$ is defined via the critical values of the gyroscopic parameter, $\Omega_{1,2}$, such that

$$0 \le \sqrt{-\kappa_2} - \sqrt{-\kappa_1} =: \Omega_1 \le \Omega_2 := \sqrt{-\kappa_1} + \sqrt{-\kappa_2}, \tag{6.23}$$

where $\kappa_2 < \kappa_1 < 0$ are eigenvalues of the matrix of potential forces $\mathbf{K}$.

Since $\mathbf{K} < 0$, the potential system without gyroscopic forces ($\Omega = 0$) is statically unstable, which corresponds to the two real positive eigenvalues λ and to their negative counterparts. With the increase in Ω, the real eigenvalues of the same sign move along the real axis in the complex plane towards each other until they merge at the exceptional point at $\Omega = \Omega_1$ into the double real ones $\lambda = \pm\omega_0$. Increasing Ω further yields splitting of the double real eigenvalues into complex-conjugate pairs that start moving along the circle

$$(\mathrm{Re}\lambda)^2 + (\mathrm{Im}\lambda)^2 = \omega_0^2 \tag{6.24}$$

until they collide at $\Omega = \Omega_2$, see the black curves in Figure 6.3 (b). When $\Omega > \Omega_2 > 0$, the gyroscopic system without damping and nonconservative positional forces is stable with four simple pure imaginary eigenvalues $\lambda = \pm i\omega_\pm(\Omega)$, where the frequencies $0 < \omega_-(\Omega) < \omega_+(\Omega)$ are given by equation (6.22).

The Krein signature associated with each of the pure imaginary eigenvalues $\lambda = \pm i\omega_\pm(\Omega)$ of the conservative gyroscopically stabilized system is

$$\kappa(i\omega_\pm) := \mathrm{sign}\big(i\overline{\mathbf{w}}_\pm^T \mathbf{J}\mathbf{w}_\pm\big), \tag{6.25}$$

where $\mathbf{w}_\pm$ are the eigenvectors of the matrix $\mathbf{A}$ given by equation (6.21) at the eigenvalues $i\omega_\pm(\Omega)$. Calculating the eigenvectors and substituting them into equation (6.25),

we find

$$i\overline{\mathbf{w}}_{\pm}^{T}\mathbf{S}\mathbf{w}_{\pm} = \pm F^{\mp}(\Omega)\omega_{\pm}(\Omega)\sqrt{\Omega^2-\Omega_2^2}\sqrt{\Omega^2-\Omega_1^2}, \tag{6.26}$$

where [305]

$$F^{\mp}(\Omega) = \frac{4k_{11} - \left(\sqrt{\Omega^2-\Omega_1^2} \mp \sqrt{\Omega^2-\Omega_2^2}\right)^2}{2(\Omega^2 k_{11} + k_{12}^2)}, \tag{6.27}$$

and k_{11} and k_{12} are the entries of the matrix $\mathbf{K}$. When $\Omega > \Omega_2$, the sign of the right-hand side of equation (6.26) depends only on the sign of the functions $F^{+}(\Omega)$ and $F^{-}(\Omega)$. In the limit $\Omega \to \infty$ we have $F^{\mp}(\Omega) \sim \frac{2}{\Omega^2} > 0$ and thus $\kappa(i\omega_{\pm}) = \pm 1$ as $\Omega \to \infty$. Since the eigenvalues remain simple and pure imaginary on the whole interval $\Omega \in (\Omega_2, \infty)$ and the Krein signature is an invariant of an eigenvalue, we have $\kappa(i\omega_{\pm}(\Omega)) = \pm 1$ for all $\Omega \in (\Omega_2, \infty)$. Note that $\kappa(-i\omega_{\pm}) = -\kappa(i\omega_{\pm})$, since $\mathbf{w}_{\pm}(-i\omega_{\pm}) = \overline{\mathbf{w}}_{\pm}(i\omega_{\pm})$ [603].

Therefore, the lower eigenfrequency, ω_{-}, of the conservative gyroscopic system under study acquires negative Krein signature whereas the higher eigenfrequency, ω_{+}, has a positive Krein signature when Ω is within the interval of gyroscopic stabilization, $\Omega > \Omega_2 > 0$. According to equation (3.57) the signature coincides with the sign of the energy of a mode with a given eigenfrequency $\omega_{\pm} > 0$. Passing through a nonsemisimple $1:1$ resonance at $\Omega = \Omega_2$ when Ω is decreasing, is thus accompanied by the Krein collision of the two eigenvalues, one with positive and the other with negative energy sign (Krein signature), see black curves in Figure 6.3.

How do the damping and nonconservative positional forces affect the pure imaginary eigenvalues $i\omega_{\pm}(\Omega)$ of the gyroscopically stabilized conservative system? Does the Krein signature of the eigenvalues play a part?

The answer follows from the Taylor expansions of the eigenvalues of the perturbed gyroscopic system with respect to the parameters δ and ν. Indeed, if $i\omega_{\pm}(\Omega)$ is a simple root of the characteristic polynomial $q(\lambda)$ at $\delta = 0$ and $\nu = 0$, then the first order correction to this root is [292]

$$\lambda(\delta, \Omega, \nu) = i\omega_{\pm}(\Omega) - \delta\frac{\partial_{\delta} q(\Omega)}{\partial_{\lambda} q(\Omega)} - \nu\frac{\partial_{\nu} q(\Omega)}{\partial_{\lambda} q(\Omega)} + o(\delta, \nu), \tag{6.28}$$

where the derivatives are taken at $\delta = 0$ and $\nu = 0$. Taking into account that

$$2\omega_0^2 - 2\omega_{\pm}^2 + \Omega^2 - \Omega_2^2 = \mp\sqrt{\Omega^2-\Omega_2^2}\sqrt{\Omega^2-\Omega_1^2}, \tag{6.29}$$

from equation (6.28) we obtain in the linear approximation [305]

$$\lambda(\delta, \Omega, \nu) = i\omega_{\pm}(\Omega) \pm \nu\frac{\Omega}{\sqrt{\Omega^2-\Omega_2^2}\sqrt{\Omega^2-\Omega_1^2}} \mp \delta\frac{(\omega_{\pm}^2(\Omega) - \omega_0^2)\mathrm{tr}\mathbf{D} + 2\Omega_2\gamma_*}{2\sqrt{\Omega^2-\Omega_2^2}\sqrt{\Omega^2-\Omega_1^2}}, \tag{6.30}$$

where [290]

$$\gamma_* = \frac{\mathrm{tr}\mathbf{K}\mathbf{D} + \left(\Omega_2^2 - \omega_0^2\right)\mathrm{tr}\mathbf{D}}{2\Omega_2}. \tag{6.31}$$

Therefore, when $\Omega > \Omega_2 > 0$, the *nonconservative positional forces* with $\nu > 0$ *stabilize the negative energy mode*, $i\omega_-(\Omega)$, but *destabilize the mode with the positive Krein signature*, $i\omega_+(\Omega)$, see dark gray curves in Figure 6.3 (b).

The effect of damping forces depends on the structure of both the damping matrix $\mathbf{D}$ and the matrix $\mathbf{K}$ of potential forces.

When $\Omega > \Omega_2 > 0$, the *damping forces* with $\delta > 0$ *destabilize the negative energy mode*, $i\omega_-(\Omega)$, and *stabilize the positive energy mode*, $i\omega_+(\Omega)$, if

$$(A): \quad (\omega_\pm^2(\Omega) - \omega_0^2)\mathrm{tr}\mathbf{D} + 2\Omega_2\gamma_* > 0. \tag{6.32}$$

If

$$(B): \quad (\omega_\pm^2(\Omega) - \omega_0^2)\mathrm{tr}\mathbf{D} + 2\Omega_2\gamma_* < 0, \tag{6.33}$$

damping stabilizes the negative energy mode of the gyroscopically stabilized conservative system under study; *it can destabilize the positive energy mode* when $\Omega_2 < \Omega < \Omega_{cr} < \infty$.

An example of matrices $\mathbf{K}$ and $\mathbf{D}$ that fulfill the condition (6.32) is given by

$$\mathbf{K}_A = \begin{pmatrix} -1 & 0 \\ 0 & -4 \end{pmatrix}, \quad \mathbf{D}_{A_1} = \begin{pmatrix} 2 & 1 \\ 1 & 1 \end{pmatrix}. \tag{6.34}$$

Then, $\Omega_1 = 1$, $\Omega_2 = 3$, $\omega_0 = \sqrt{2}$, and $\gamma_* = 5/2$. The eigenvalues of the matrix $\mathbf{D}_{A_1}$ are $\delta_{1,2} = (3 \pm \sqrt{5})/2 > 0$. The light gray (r) curves in Figure 6.3 (b) show the effect of the full dissipation with the positive definite matrix $\mathbf{D}_{A_1}$.

The destabilizing effect of damping forces with full dissipation on the negative energy modes of a stable Hamiltonian system is well known [74, 391, 395, 613]. In hydrodynamics this phenomenon manifests itself in connection, e.g., with the Kelvin–Helmholtz instability [168, 462], stability of a boundary layer over a flexible surface [112, 349], and Benjamin–Feir instability [90].

An interesting fact following from equation (6.32) is that the same effect can be produced by indefinite damping too. Indeed, taking, e.g., $\mathbf{D} = \mathbf{D}_{A_2}$ with

$$\mathbf{D}_{A_2} = \begin{pmatrix} 1 & 2 \\ 2 & 1 \end{pmatrix} \tag{6.35}$$

and $\mathbf{K} = \mathbf{K}_A$ as in the above example, we find that the eigenvalues of $\mathbf{D}_{A_2}$ are $\delta_1 = -1$ and $\delta_2 = 3$, and $\gamma_* = 3/2$. Hence, with $\mathbf{K} = \mathbf{K}_A$ and $\mathbf{D} = \mathbf{D}_{A_2}$, the inequality (6.32) is fulfilled for all $\Omega > \Omega_2 = 3$. The light gray (r) curves in Figure 6.4 (a) show how the

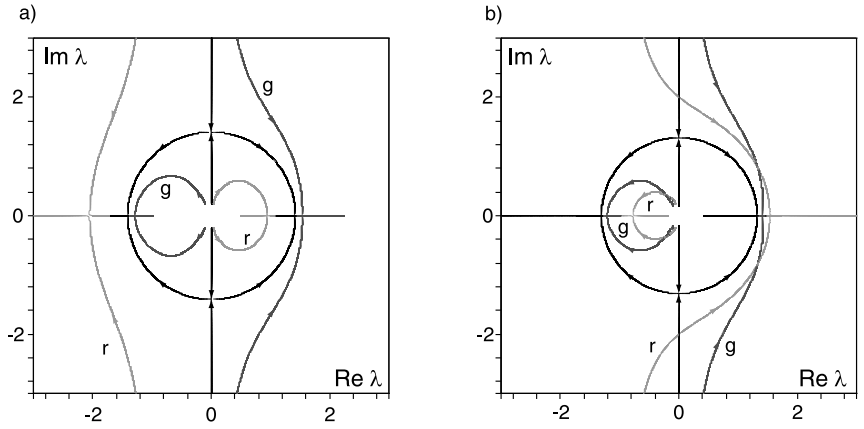

Figure 6.4. (a) For $\kappa_1 = -1$, $\kappa_2 = -4$, $\mathrm{tr}\mathbf{D} = 2$, $\mathrm{tr}\mathbf{KD} = -5$, and $\det \mathbf{D} = -3$ and (b) for $\kappa_1 = -1$, $\kappa_2 = -3$, $\mathrm{tr}\mathbf{D} = 2$, $\mathrm{tr}\mathbf{KD} = -16$, and $\det \mathbf{D} = -35$: movement of eigenvalues in the complex plane when Ω decreases from 10 to 0 and (black) $\delta = 0$ and $\nu = 0$, (light gray, r) $\delta = 1$ and $\nu = 0$, and (dark gray, g) $\delta = 0$ and $\nu = 1$.

positive energy modes are stabilized and the negative energy modes are destabilized by the indefinite damping matrix $\mathbf{D}_{A_2}$.

However, indefinite damping can act inversely in comparison with the just described effect, by stabilizing the negative energy mode and destabilizing the positive energy mode for Ω sufficiently close to Ω_2, see light gray (r) curves in Figure 6.4 (b). They are plotted for the matrices

$$\mathbf{K}_B = \begin{pmatrix} -2 & 1 \\ 1 & -2 \end{pmatrix}, \quad \mathbf{D}_B = \begin{pmatrix} 1 & -6 \\ -6 & 1 \end{pmatrix}, \tag{6.36}$$

with which the inequality (6.33) is satisfied in case of $\omega_-(\Omega)$ for all $\Omega > \Omega_2$ and in case of $\omega_+(\Omega)$ for $\Omega_2 < \Omega < \Omega_{cr} < \infty$.

As established in [293,294], destabilization of the positive energy modes of a Hamiltonian system by indefinite damping or nonconservative positional forces is a basic mechanism leading to the onset of oscillatory instabilities induced by friction applied to rotating or moving continua [340] such as the singing wine glass [6,541] or a squealing disk brake [268], see Chapter 10 in this book for more mechanical examples and Chapter 9 for an example of a similar effect in magnetohydrodynamics.

From equation (6.30) a linear approximation follows to the boundary of the domain of asymptotic stability in the (δ, ν, Ω)-space

$$\nu = \frac{\Omega_2}{\Omega}\left[\gamma_* + \frac{\mathrm{tr}\mathbf{D}}{2}\frac{(\omega_\pm^2(\Omega) - \omega_0^2)}{\Omega_2}\right]\delta. \tag{6.37}$$

In the vicinity of $\Omega = \Omega_2$, we have $\omega_\pm^2(\Omega) - \omega_0^2 \approx \pm\omega_0\sqrt{2\Omega_2(\Omega - \Omega_2)}$. Taking this into account in equation (6.37), we find a simple approximation to the gyroscopic

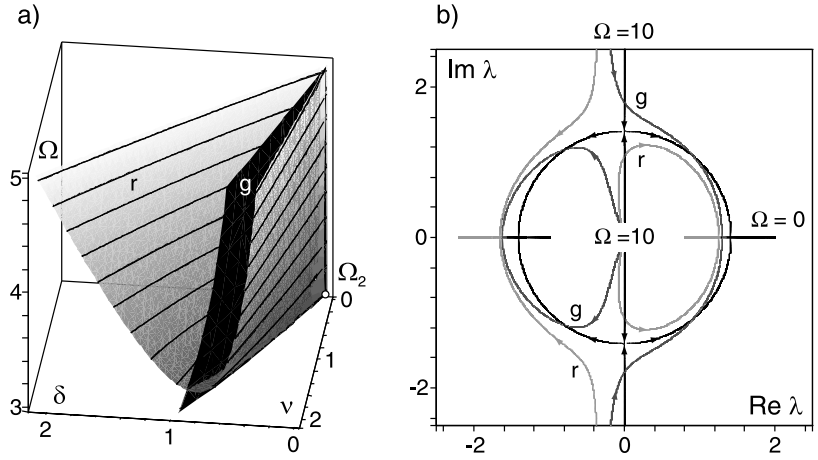

Figure 6.5. For $\kappa_1 = -1$, $\kappa_2 = -4$, $\mathrm{tr}\mathbf{D} = 3$, $\mathrm{tr}\mathbf{KD} = -6$, and $\det \mathbf{D} = 1$: (a) The boundary of the domain of asymptotic stability with the Whitney umbrella singularity at the exceptional point $(0, 0, \Omega_2 = 3)$ in the (δ, ν, Ω)-space and (black) the switching surface (6.44); (b) movement of eigenvalues in the complex plane when Ω decreases from 10 to 0 and (black) $\delta = 0$ and $\nu = 0$, (light gray, r) $\delta = 0.3$ and $\nu = 0.6$, and (dark gray, g) $\delta = 0.3$ and $\nu = 0.9$.

parameter Ω near the exceptional point $(0, 0, \Omega_2)$ at the threshold of the gyroscopic stabilization (for $\mathrm{tr}\mathbf{D} \neq 0$) [290, 291]

$$\Omega = \Omega_2 + \Omega_2 \frac{2}{(\omega_0 \mathrm{tr}\mathbf{D})^2} \left(\frac{\nu}{\delta} - \gamma_*\right)^2 + o\left(\left(\frac{\nu}{\delta} - \gamma_*\right)^2\right). \tag{6.38}$$

Again, we obtained an equation which is in the familiar canonical form for the Whitney umbrella surface: $Y = X^2/Z^2$. Hence, at the exceptional point $(0, 0, \Omega_2)$, the boundary of the domain of gyroscopic stabilization in the presence of damping and nonconservative forces has the Whitney umbrella singularity, see Figure 6.5 (a). In the first approximation with respect to δ and ν the stability boundary is a ruled surface, i.e. a set of points swept by moving straight lines given by equation (6.37) that all intersect orthogonally the Ω-axis. At $\Omega = \Omega_2$ the lines degenerate and merge into one

$$\nu = \gamma_* \delta. \tag{6.39}$$

In the (δ, ν, Ω)-space, a part of the plane (6.39) limited by the inequalities $\Omega > \Omega_2$ and $\delta > 0$ constitutes a tangent cone [375] to the domain of gyroscopic stabilization at the exceptional point $(0, 0, \Omega_2)$.

In the vicinity of the exceptional point, it is the tangent cone to the stability domain that determines the transfer of instability from the negative energy modes to the positive energy modes. Indeed, as was shown in [287, 288], perturbation of the double eigenvalue $i\omega_0$ at the EP yields the following approximation to the trajectories of the

perturbed simple eigenvalues in the complex plane

$$(\mathrm{Im}\lambda - \omega_0 - \mathrm{Re}\lambda - a/2)^2 - (\mathrm{Im}\lambda - \omega_0 + \mathrm{Re}\lambda + a/2)^2 = 2d, \tag{6.40}$$

where $a := -\omega_0\langle \mathbf{h}, \mathbf{p}\rangle$, $d := \omega_0\langle \mathbf{f}, \mathbf{p}\rangle$, the angular brackets denote the scalar product in $\mathbb{R}^2$ of the vector of parameters $\mathbf{p}^T = (\delta, \nu)$ and the real vectors $\mathbf{f}^T = (f_\delta, f_\nu)$ and $\mathbf{h}^T = (h_\delta, h_\nu)$ with the components that are expressed by means of the derivatives of the characteristic polynomial $q(\lambda)$ as [292]

$$f_s := \frac{2}{i\omega_0}\frac{\partial_{p_s} q}{\partial_\lambda^2 q}, \quad h_s := \frac{2}{\omega_0}\frac{2\alpha_0(i\omega_0)^{-1}\partial_{p_s} q - \partial^2_{\lambda,p_s} q}{\partial_\lambda^2 q}, \quad \alpha_0 = i\omega_0\frac{1}{3}\frac{\partial_\lambda^3 q}{\partial_\lambda^2 q} \tag{6.41}$$

and should be evaluated at the EP. Then,

$$\alpha_0 = 1, \;\; f_\delta = \frac{\Omega_2}{2\omega_0^2}\gamma_*, \;\; f_\nu = -\frac{\Omega_2}{2\omega_0^2}, \;\; h_\delta = \frac{\Omega_2\gamma_* - \omega_0^2 \mathrm{tr}\mathbf{D}}{2\omega_0^3}, \;\; h_\nu = -\frac{\Omega_2}{2\omega_0^3}, \tag{6.42}$$

and finally [305]

$$a = \frac{\mathrm{tr}\mathbf{D}}{2}\delta, \quad d = \frac{\Omega_2}{2\omega_0}(\gamma_*\delta - \nu). \tag{6.43}$$

Therefore, in close vicinity of the EP, the movement of the perturbed eigenvalues in the complex plane is well approximated by the branches of a hyperbola (6.40), which are shifted off the imaginary axis to the left by a quantity $\delta\mathrm{tr}\mathbf{D}/4$. It is clear that when $\gamma_*\delta - \nu > 0$, i.e. when 'dissipation prevails', the eigenvalue with the lower frequency (negative energy mode) becomes unstable, see the r-curves in Figure 6.5 (b). If $\gamma_*\delta - \nu < 0$, which happens either when 'nonconservative positional forces prevail' in the perturbation or when specific forms of indefinite damping are used, the instability transfers to the mode with the higher frequency (positive energy mode), see g-curves in Figure 6.5 (b). Hence, the tangent cone to the stability domain in the (δ, ν, Ω)-space at the EP gives a linear approximation to a surface (shown in black in Figure 6.5 (a)) that subdivides the stability domain into two compartments (marked by dark gray (g) and light gray (r) level curves in Figure 6.5 (a)) that correspond to destabilization of either negative energy modes (r) or positive energy modes (g) of the stable gyroscopic system,[1] Figure 6.5 (b).

The full stability boundary determined by the equation $q_1q_2q_3 - q_1^2q_4 - q_3^2 = 0$ following from the Routh–Hurwitz conditions applied to the polynomial $q(\lambda)$, is shown in Figure 6.5 (a). It is a quadratic equation in ν that yields two sheets of the stability boundary that are connected to each other when the discriminant of the quadratic equation vanishes. This yields an equation of the surface

$$\nu = \delta\Omega\frac{\delta^2\mathrm{tr}\mathbf{D}\det\mathbf{D} + 4\Omega_2\gamma_* + \mathrm{tr}\mathbf{D}(\Omega^2 - \Omega_2^2)}{\delta^2(\mathrm{tr}\mathbf{D})^2 + 4\Omega^2} \tag{6.44}$$

that is shown in black in Figure 6.5 (a). The linear approximation to this surface at the EP is the plane (6.39) that contains a tangent cone to the stability domain.

[1] Cf. the eigencurves of fast and slow precession of Crandall's gyropendulum in Fig 6.2.

When the parameters are in the g-compartment of the stability domain with respect to this surface, the eigenvalue with the higher frequency has a larger negative real part whereas inside the r-compartment it is the eigenvalue with the lower frequency that is less stable. Consequently, when parameters are varied in such a manner that the stability boundary is penetrated from the g-side, the higher frequency mode is unstable. If this happens from the r-side, then the lower frequency mode is destabilized.

Therefore, the Krein signature of pure imaginary eigenvalues of the stable gyroscopic (Hamiltonian) system manifests itself even inside the parameter region of the dissipative system. In the first approximation, it is the tangent cone to the stability boundary at the EP associated with the Whitney umbrella singularity that separates the parameter sets destabilizing either negative or positive energy modes. The former are made unstable either by full dissipation or by a specific indefinite damping prescribed by equation (6.32) while the latter needs either nonconservative positional forces or another specific type of indefinite damping determined by equation (6.33), in order to be unstable.

6.2.2 The case of arbitrary even *m*

Let in equation (6.17) m be an arbitrary even number. In the presence of only potential forces with the matrix $\mathbf{K} < 0$, the trivial solution to equation (6.17) is statically unstable. In the absence of nonconservative forces ($\delta = \nu = 0$) the statically unstable potential system becomes Lyapunov stable due to the action of gyroscopic forces provided that $\det \mathbf{G} \neq 0$ and the absolute value of the gyroscopic parameter is sufficiently large ($|\Omega| > \Omega_2 > 0$) [34, 325]. In the generic case, all the eigenvalues of the matrix polynomial $\mathbf{I}\lambda^2 + \lambda\Omega\mathbf{G} + \mathbf{K}$ are pure imaginary and simple. At $\Omega = \Omega_2$ there exists a pair of double pure imaginary eigenvalues $\lambda = \pm i\omega_0$ with the Jordan chain of length 2, while the remaining eigenvalues are simple and lie on the imaginary axis [34, 394]. For $m = 2$ the exact value of the gyroscopic parameter Ω_2 is given by equation (6.23). Determining Ω_2 at $m > 2$ is a more complicated problem [34, 326].

The Jordan chain at the eigenvalue $i\omega_0$ consists of the eigenvector $\mathbf{u}_0$ and an associated vector $\mathbf{u}_1$ that satisfy the equations [74, 291]

$$(-\mathbf{I}\omega_0^2 + i\omega_0\Omega_2\mathbf{G} + \mathbf{K})\mathbf{u}_0 = 0, \tag{6.45}$$

$$(-\mathbf{I}\omega_0^2 + i\omega_0\Omega_2\mathbf{G} + \mathbf{K})\mathbf{u}_1 = -(2i\omega_0\mathbf{I} + \Omega_2\mathbf{G})\mathbf{u}_0. \tag{6.46}$$

The eigenvector $\mathbf{u}_0$ satisfies the orthogonality condition

$$\overline{\mathbf{u}}_0^T(2i\omega_0\mathbf{I} + \Omega_2\mathbf{G})\mathbf{u}_0 = 0. \tag{6.47}$$

Equation (6.45) and the orthogonality condition (6.47) yield the *Rayleigh quotient* for the critical frequency:

$$\omega_0^2 = -\frac{\overline{\mathbf{u}}_0^T\mathbf{K}\mathbf{u}_0}{\overline{\mathbf{u}}_0^T\mathbf{u}_0} > 0. \tag{6.48}$$

In the neighborhood of $\Omega = \Omega_2$ the double eigenvalue and the corresponding eigenvector vary according to the formulas [291, 518]

$$i\omega(\Omega) = i\omega_0 \pm i\mu\sqrt{\Omega - \Omega_2} + O(\Omega - \Omega_2), \tag{6.49}$$

$$\mathbf{u}(\Omega) = \mathbf{u}_0 \pm i\mu\mathbf{u}_1\sqrt{\Omega - \Omega_2} + O(\Omega - \Omega_2), \tag{6.50}$$

where μ^2 is a real number given by

$$\mu^2 = -\frac{2\omega_0^2\overline{\mathbf{u}}_0^T\mathbf{u}_0}{\Omega_2(\omega_0^2\overline{\mathbf{u}}_1^T\mathbf{u}_1 - \overline{\mathbf{u}}_1^T\mathbf{K}\mathbf{u}_1 - i\omega_0\Omega_2\overline{\mathbf{u}}_1^T\mathbf{G}\mathbf{u}_1 - \overline{\mathbf{u}}_0^T\mathbf{u}_0)}. \tag{6.51}$$

For $m = 2$ and $\det\mathbf{G} = 1$ the double eigenvalue $i\omega_0 = i\sqrt[4]{\det\mathbf{K}}$ for $\Omega = \Omega_2$, defined by equation (6.23), has a Jordan chain consisting of an eigenvector $\mathbf{u}_0$ and an associated vector $\mathbf{u}_1$

$$\mathbf{u}_0 = C\begin{pmatrix} i\omega_0\Omega_2 + k_{12} \\ \omega_0^2 - k_{11} \end{pmatrix}, \quad \mathbf{u}_1 = \frac{C}{\omega_0^2 - k_{22}}\begin{pmatrix} 0 \\ i\omega_0(k_{22} - k_{11}) - \Omega_2 k_{12} \end{pmatrix}, \tag{6.52}$$

where C is an arbitrary constant. The vector $\mathbf{u}_1$ is defined up to a term proportional to $\mathbf{u}_0$. Substituting the eigen- and associated vectors into equation (6.51) and taking into account the orthogonality condition (6.47), we find

$$\mu^2 = \frac{\Omega_2}{2}\frac{(\omega_0^2 - k_{11})(\omega_0^2 - k_{22})}{\Omega_2^2\omega_0^2 + k_{12}^2} = \frac{\Omega_2}{2} > 0. \tag{6.53}$$

The coefficient $\mu = \sqrt{\Omega_2/2}$ is real-valued and, according to formula (6.49), for $\Omega > \Omega_2$ the double eigenvalue splits into two simple pure imaginary ones (gyroscopic stabilization). The gyroscopic stabilization of a statically unstable potential system for arbitrary even m follows the same scenario.

Let us study the influence of dissipative and nonconservative positional forces on gyroscopic stabilization. First, we note that in practice the most interesting situation is when these forces in the system (6.17) are small as compared with the gyroscopic ones: $\delta \sim \nu \ll \Omega \sim \Omega_2$. The critical gyroscopic parameter $\Omega_{cr}(\delta, \nu)$ on the boundary of the gyroscopic stabilization domain of the nonconservative system is a function of the parameters corresponding to the dissipative and circulatory forces and may differ significantly from Ω_2. Moreover, stability is sensitive to choice of perturbation, while the balance of forces leading to asymptotic stability is not obvious. This is why the effect of small dissipative and nonconservative positional forces on the stability of gyroscopic systems is considered paradoxical [139], although the destabilization paradox is also connected with physical paradoxes, such as the inversion of the tippe top equilibrium and the tendency of Jellet's egg to spin about its longest axis [83, 84].

To estimate $\Omega_{cr}(\delta, \nu)$, we note that, when the potential system gyroscopically stabilized for $\Omega > \Omega_2$ is perturbed by small dissipative and circulatory forces, a simple eigenvalue $i\omega(\Omega)$ with the eigenvector $\mathbf{u}(\Omega)$ takes the increment [291]:

$$\lambda = i\omega - \frac{\omega^2 \overline{\mathbf{u}}^T \mathbf{D}\mathbf{u}\delta - i\omega \overline{\mathbf{u}}^T \mathbf{N}\mathbf{u}\nu}{\overline{\mathbf{u}}^T \mathbf{K}\mathbf{u} + \omega^2 \overline{\mathbf{u}}^T \mathbf{u}} + o(\delta, \nu). \tag{6.54}$$

Since $\mathbf{D}$ and $\mathbf{K}$ are real symmetric matrices and $\mathbf{N}$ is skew-symmetric, this increment is real-valued. When $\nu = 0$, the formula (6.54) is reduced to equation (5.47), where $\mathbf{M}$ is the identity matrix. Taking into account that the denominator in equation (6.54) is $\overline{\mathbf{u}}^T \mathbf{K}\mathbf{u} + \omega^2 \overline{\mathbf{u}}^T \mathbf{u} = i\omega \overline{\mathbf{w}}^T \mathbf{J}\mathbf{w}$, where $\mathbf{w} = (\mathbf{u}^T, i\omega\mathbf{u}^T - \Omega\mathbf{u}^T\mathbf{G}/2)^T$ is an eigenvector of the matrix $\mathbf{A}$ of equation (6.21) at $i\omega$, we rewrite equation (6.54) as

$$\lambda = i\omega - \omega \frac{\overline{\mathbf{u}}^T \mathbf{D}\mathbf{u}}{i\overline{\mathbf{w}}^T \mathbf{J}\mathbf{w}}\delta + \omega \frac{i\overline{\mathbf{u}}^T \mathbf{N}\mathbf{u}}{i\overline{\mathbf{w}}^T \mathbf{J}\mathbf{w}}\nu + o(\delta, \nu). \tag{6.55}$$

The sign of the denominator in equation (6.55) is exactly the Krein signature of the eigenvalue $i\omega$ in the sense of Definition 3.5, whereas the sign of the denominator in equation (6.54) is the sign of energy, which coincides with the Krein signature if $\omega > 0$.

Therefore, full dissipation with $\mathbf{D} > 0$ destabilizes negative energy modes and stabilizes positive energy modes. If $i\overline{\mathbf{u}}^T \mathbf{N}\mathbf{u} > 0$, the negative energy modes are stabilized and positive energy modes are destabilized by the circulatory forces and vice-versa.

In the first approximation in δ and ν a simple eigenvalue $i\omega(\Omega)$ remains on the imaginary axis if

$$\nu = \gamma(\Omega)\delta, \tag{6.56}$$

where

$$\gamma(\Omega) = -i\omega(\Omega) \frac{\overline{\mathbf{u}}^T(\Omega)\mathbf{D}\mathbf{u}(\Omega)}{\overline{\mathbf{u}}^T(\Omega)\mathbf{N}\mathbf{u}(\Omega)}. \tag{6.57}$$

For a fixed $\Omega > \Omega_2$ expressions (6.56) and (6.57) define at the origin in the plane of δ and ν a tangent line to the boundary of the domain where the increment of $i\omega(\Omega)$ is negative. In the generic case, a linear approximation to the boundary of the intersection of all such domains corresponding to the various simple eigenvalues of the unperturbed gyroscopic system is specified by only two straight lines of the form (6.56).

It follows from expansions (6.49) and (6.50), that, in the neighborhood of $\Omega = \Omega_2$ all the simple eigenvalues $i\omega(\Omega)$, that remain simple at $\Omega = \Omega_2$, and also the corresponding eigenvectors $\mathbf{u}(\Omega)$ vary slowly with Ω in comparison with the pair of eigenvalues that coincide with each other at $\Omega = \Omega_2$. Clearly, the behavior of these two eigenvalues is also of key importance for the stability of the gyroscopic system under small nonconservative perturbations. For this reason, the critical gyroscopic parameter

on the boundary of the stability domain of the system (6.17), is estimated by plugging expansions (6.49) and (6.50) into formula (6.57), which yields:

$$\gamma(\Omega) = -(\omega_0 \pm \mu\sqrt{\Delta\Omega} + O(\Omega - \Omega_2))\frac{d_1 \mp \mu d_2\sqrt{\Delta\Omega} + O(\Delta\Omega)}{n_1 \pm \mu n_2\sqrt{\Delta\Omega} + O(\Delta\Omega)}, \tag{6.58}$$

where $\Delta\Omega = \Omega - \Omega_2$. The coefficients d_1, d_2, n_1, and n_2 are real:

$$\begin{aligned} d_1 &= \mathrm{Re}(\overline{\mathbf{u}}_0^T \mathbf{D}\mathbf{u}_0), \quad d_2 = \mathrm{Im}(\overline{\mathbf{u}}_0^T \mathbf{D}\mathbf{u}_1 - \overline{\mathbf{u}}_1^T \mathbf{D}\mathbf{u}_0), \\ n_1 &= \mathrm{Im}(\overline{\mathbf{u}}_0^T \mathbf{N}\mathbf{u}_0), \quad n_2 = \mathrm{Re}(\overline{\mathbf{u}}_0^T \mathbf{N}\mathbf{u}_1 - \overline{\mathbf{u}}_1^T \mathbf{N}\mathbf{u}_0). \end{aligned} \tag{6.59}$$

Formula (6.58) implies that, for $|\gamma - \gamma_*| \ll 1$, where

$$\gamma_* = \gamma(\Omega_2) = -i\omega_0 \frac{\overline{\mathbf{u}}_0^T \mathbf{D}\mathbf{u}_0}{\overline{\mathbf{u}}_0^T \mathbf{N}\mathbf{u}_0}, \tag{6.60}$$

the new critical value of the gyroscopic parameter is given by

$$\Omega_{cr}(\gamma) = \Omega_2 + \frac{n_1^2(\gamma - \gamma_*)^2}{\mu^2(\omega_0 d_2 - \gamma_* n_2 - d_1)^2},$$

which, after substituting $\gamma = \nu/\delta$ becomes

$$\Omega_{cr}(\delta, \nu) = \Omega_2 + \frac{n_1^2(\nu - \gamma_*\delta)^2}{\mu^2(\omega_0 d_2 - \gamma_* n_2 - d_1)^2\delta^2} \geq \Omega_2. \tag{6.61}$$

In the (δ, ν, Ω)-space the graph of $\Omega_{cr}(\delta, \nu)$ under the condition $(\mu/n_1)(\omega_0 d_2 - \gamma_* n_2 - d_1)\delta > 0$ encloses a domain where two eigenvalues of the unperturbed gyroscopic system that coincide at $\Omega = \Omega_2$ take a negative real increment due to a nonconservative perturbation. At $m = 2$, and for $m > 2$ under the assumption that, when parameters are chosen from this domain, the remaining pure imaginary eigenvalues of the unperturbed system are shifted to the left half of the complex plane, equation (6.61) is an approximation to the boundary of the asymptotic stability domain of the nonconservative gyroscopic system (6.17) in the neighborhood of $(0, 0, \Omega_2)$ in the parameter space. Moreover, formula (6.61) gives a simple estimate for $\Omega_{cr}(\delta, \nu)$.

Equation (6.61) has the form canonical for a surface with the Whitney umbrella singularity that typically arises on the boundary of the asymptotic stability domain of a three-parameter family of real matrices [17, 232, 354]. That is why $\Omega_{cr}(\delta, \nu)$ in equation (6.61) is not differentiable at zero and depends only on the ratio $\gamma = \nu/\delta$. Thus, the limit $\Omega_{cr}(\delta, \nu)$ at zero is indeterminate and depends on the direction specified by γ. For all directions $\gamma \neq \gamma_*$ the limiting value satisfies $\Omega_{cr}(\gamma) > \Omega_2$. This means that the critical gyroscopic parameter varies discontinuously under infinitesimal

variations in δ and ν which we know as the Ziegler–Bottema destabilization paradox that was observed in both gyroscopic systems with small dissipative and circulatory forces [139, 232] and in circulatory systems with small dissipative and gyroscopic forces [81, 622].

The formulas (6.60) and (6.61) can be reduced to the equations (6.31) and (6.38). Indeed, for $m = 2$ and $\det \mathbf{G} = 1$ the computation of γ_* by formula (6.60) with the use of the eigenvector (6.52) yields formula (6.31). Substituting the eigen- and associated vectors (6.52) into equations (6.59), yields

$$\begin{aligned} n_1 &= -2\Omega_2\omega_0(\omega_0^2 - k_{11}), \quad n_2 = -2\Omega_2\frac{\omega_0^2(k_{11} - k_{22}) + k_{12}^2}{\omega_0^2 - k_{22}}, \\ d_1 &= 2\Omega_2\gamma_*(\omega_0^2 - k_{11}), \\ \frac{d_2}{2\omega_0} &= \frac{(d_{12}k_{12} - d_{22}(\omega_0^2 - k_{11}))(k_{22} - k_{11}) + d_{12}k_{12}\Omega_2^2}{\omega_0^2 - k_{22}}. \end{aligned} \tag{6.62}$$

Taking into account $\Omega_2^2 = \mathrm{tr}\mathbf{K} + 2\omega_0^2$, and using relations (6.62), we calculate the expression in the denominator of equation (6.61)

$$\omega_0 d_2 - \gamma_* n_2 - d_1 = -2\omega_0^2(\omega_0^2 - k_{11})\mathrm{tr}\mathbf{D}. \tag{6.63}$$

Plugging equations (6.53), (6.62) and (6.63) into equation (6.61), we reproduce, for $\mathrm{tr}\mathbf{D} \neq 0$ the formula (6.38) where γ_* is given by equation (6.31). The condition $(\mu/n_1)(\omega_0 d_2 - \gamma_* n_2 - d_1)\delta = \delta\omega_0\mathrm{tr}\mathbf{D}/\sqrt{2\Omega_2} > 0$ singles out a stable pocket of the stability domain approximated by equation (6.38).

6.3 Near-Hamiltonian systems

Consider a system of differential equations of the form [125, 429]

$$\frac{d\mathbf{x}}{dt} = (\mathbf{J}^{-1} - \mathbf{D})\mathbf{H}\mathbf{x}, \tag{6.64}$$

where $\mathbf{x} \in \mathbb{R}^{2k}$, $\mathbf{J}$ is a canonical symplectic matrix (3.20), and $\mathbf{D}$ and $\mathbf{H}$ are real symmetric $2k \times 2k$ matrices. The matrix $\mathbf{D}$ is assumed to be positive semidefinite ($\mathbf{D} \geq 0$). When $\mathbf{D} = 0$, the system (6.64) is reduced to the Hamiltonian system (3.21). The system of the form (6.64)

$$\frac{d\mathbf{x}}{dt} = (\mathbf{J}^{-1} - \varepsilon\mathbf{D})\mathbf{H}\mathbf{x}, \tag{6.65}$$

where $\varepsilon \geq 0$ is a small parameter, is called the *near-Hamiltonian system* [74].

Theorem 6.1 (S.-J. Chern, 2002 [125]). *For the system* (6.64) *with* $\mathbf{D} \geq 0$

$$\nu\left((\mathbf{J}^{-1} - \mathbf{D})\mathbf{H}\right) \leq \pi(\mathbf{H}), \quad \pi\left((\mathbf{J}^{-1} - \mathbf{D})\mathbf{H}\right) \leq \nu(\mathbf{H}). \tag{6.66}$$

Furthermore, if $\delta\left((\mathbf{J}^{-1} - \mathbf{D})\mathbf{H}\right) = 0$, *then*

$$\nu\left((\mathbf{J}^{-1} - \mathbf{D})\mathbf{H}\right) = \pi(\mathbf{H}), \quad \pi\left((\mathbf{J}^{-1} - \mathbf{D})\mathbf{H}\right) = \nu(\mathbf{H}). \tag{6.67}$$

Let $\lambda(\varepsilon)$ be a simple eigenvalue of the operator $(\mathbf{J}^{-1} - \mathbf{D})\mathbf{H}$ and $\mathbf{u}(\varepsilon)$ its eigenvector such that $\lambda(0) = i\omega_0$ is a simple eigenvalue too with the eigenvector $\mathbf{u}(0) = \mathbf{u}_0$. Then [584],

$$\lambda(\varepsilon) = i\omega_0 + \varepsilon\frac{d\lambda(0)}{d\varepsilon} + o(\varepsilon),$$

where [125, 394]

$$\frac{d\lambda(0)}{d\varepsilon} = -\frac{\overline{\mathbf{u}}_0{}^T\mathbf{HDHu}_0}{\overline{\mathbf{u}}_0{}^T\mathbf{Hu}_0} = -\frac{1}{\omega_0}\frac{\overline{\mathbf{u}}_0{}^T\mathbf{HDHu}_0}{i\overline{\mathbf{u}}_0{}^T\mathbf{Ju}_0}. \tag{6.68}$$

Assuming that $\overline{\mathbf{u}}_0{}^T\mathbf{HDHu}_0 > 0$ (which happens, e.g., when $\mathbf{D} > 0$ [394]), we conclude that in the first-order in ε approximation the pure imaginary eigenvalue with $\omega_0 > 0$ and positive Krein signature $\kappa(i\omega_0) := \operatorname{sign}(i\overline{\mathbf{u}}_0{}^T\mathbf{Ju}_0)$ acquires a negative real increment (asymptotic stability). If $\kappa(i\omega_0) < 0$, the eigenvalue moves to the open right half-plane of the complex plane (instability). In [391] MacKay pointed out that $-\overline{\mathbf{u}}_0{}^T\mathbf{HDHu}_0$ in equation (6.68) is nothing other than one half of the rate of change of energy due to the perturbation, averaged over an oscillation cycle, whereas the denominator is the energy of the mode with the frequency ω_0, i.e.

$$\frac{d\lambda(0)}{d\varepsilon} = \frac{\langle\dot{\mathcal{E}}\rangle}{2\mathcal{E}} + O(\varepsilon^2). \tag{6.69}$$

Hence, if the energy is drained from the negative (positive) energy mode, it becomes unstable (stable). *MacKay's formula* (6.69) thus quantitatively supports the kinematics reasoning of Sturrock [552].

Maddocks and Overton [395] initiated the study of multiple eigenvalues of near-Hamiltonian systems and showed that for an appropriate class of dissipatively perturbed Hamiltonian systems, the number of unstable modes of the dynamics linearized at a nondegenerate equilibrium is determined solely by the index of the equilibrium regarded as a critical point of the Hamiltonian. They analyzed the movement of the eigenvalues in the limit of vanishing dissipation without direct application, however, to the destabilization paradox and approximation of the singular stability boundary. Some further developments of these ideas can be found in the recent work [231], where the stability domain near $1:1$ semisimple resonance of a dissipative system is investigated and its relation to the ruled surface known as the Plücker conoid of degree $n = 1$, is established. Bridges [89] raised a question on the effect of nonconservative perturbations

on positive energy modes of a Hamiltonian system. Therefore, a further development of the Maddocks and Overton theory in order to take into account non-Hamiltonian perturbations equivalent to the action of nonconservative positional forces is required. Important nonlinear and statistical mechanical aspects of the dissipation-induced instabilities in Hamiltonian systems are discussed in [74, 152], and [73].

6.4 Gyroscopic and circulatory systems as limits of dissipative systems

Finally, on the example of the general nonconservative system (6.17) with $m = 2$ degrees of freedom we would like to demonstrate how the stable 'ideal' gyroscopic and circulatory systems co-exist at different singularities of the same boundary of the domain of asymptotic stability of a dissipative system.

In the absence of damping and gyroscopic forces ($\delta = \Omega = 0$) the system (6.17) is circulatory, with the matrix $\mathbf{N}$ specified by equation (6.19), and its characteristic polynomial $q(\lambda)$ has four roots $\pm\lambda_+$, $\pm\lambda_-$, where

$$\lambda_\pm = \sqrt{-\frac{1}{2}\mathrm{tr}\mathbf{K} \pm \frac{1}{2}\sqrt{(\mathrm{tr}\mathbf{K})^2 - 4(\det\mathbf{K} + \nu^2)}}. \tag{6.70}$$

The eigenvalues (6.70) can be real, complex or pure imaginary implying instability or marginal stability in accordance with the following statement.

Theorem 6.2 (O. N. Kirillov, 2007 [290]). *If* $\mathrm{tr}\mathbf{K} > 0$ *and* $\det\mathbf{K} \le 0$*, the circulatory system with two degrees of freedom originated from equation* (6.17) *at* $\Omega = 0$ *and* $\delta = 0$ *is stable for* ${\nu_d}^2 < \nu^2 < {\nu_f}^2$*, unstable by divergence for* $\nu^2 \le {\nu_d}^2$*, and unstable by flutter for* $\nu^2 \ge {\nu_f}^2$*, where* ν_d *and* ν_f *are*

$$0 \le \sqrt{-\det\mathbf{K}} =: \nu_d \le \nu_f := \frac{1}{2}\sqrt{(\mathrm{tr}\mathbf{K})^2 - 4\det\mathbf{K}}. \tag{6.71}$$

If $\mathrm{tr}\mathbf{K} > 0$ *and* $\det\mathbf{K} > 0$*, the circulatory system is stable for* $\nu^2 < {\nu_f}^2$ *and unstable by flutter for* $\nu^2 \ge {\nu_f}^2$*. If* $\mathrm{tr}\mathbf{K} \le 0$*, the system is unstable.*

For $\mathbf{K}$, having two equal eigenvalues, $\nu_f = 0$ and the circulatory system is unstable in agreement with Merkin's theorem (Theorem 5.16).

Stability diagrams and motion of eigenvalues in the complex plane for ν increasing from zero are presented in Figure 6.6. When $\mathrm{tr}\mathbf{K} > 0$ and $\det\mathbf{K} < 0$ there are two real and two pure imaginary eigenvalues at $\nu = 0$, and the system is statically unstable, see Figure 6.6 (a). With the increase of ν both the imaginary and real eigenvalues are moving to the origin, until at $\nu = \nu_d$ the real pair merges and originates a double zero

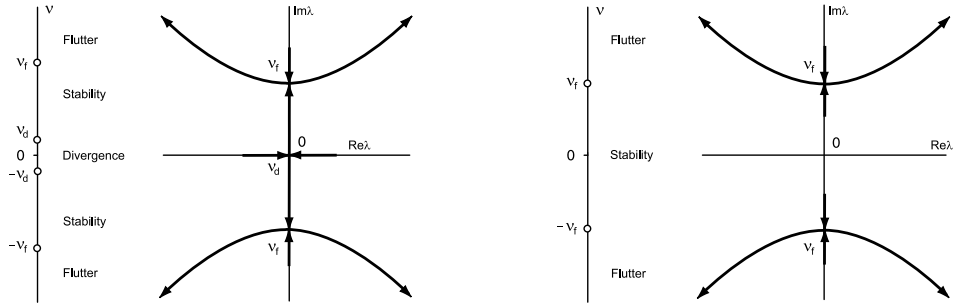

Figure 6.6. Stability diagrams and trajectories of eigenvalues for the increasing parameter $\nu > 0$ for the circulatory system originated from equation (6.17) at $\Omega = 0$ and $\delta = 0$ with (a) $\mathrm{tr}\mathbf{K} > 0$ and $\det \mathbf{K} < 0$ and (b) $\mathrm{tr}\mathbf{K} > 0$ and $\det \mathbf{K} > 0$ [290].

eigenvalue with the Jordan block. At $\nu = \nu_d$ the system is unstable due to linear time dependence of a solution corresponding to $\lambda = 0$. The further increase of ν yields splitting of the double zero eigenvalue into two pure imaginary ones. The imaginary eigenvalues of the same sign are then moving towards each other until at $\nu = \nu_f$ they originate a pair of double eigenvalues $\pm i\omega_f$ with the Jordan block, where

$$\omega_f = \sqrt{\frac{1}{2}\mathrm{tr}\mathbf{K}}. \tag{6.72}$$

At $\nu = \nu_f$ the system is unstable by flutter due to secular terms in its solutions. For $\nu > \nu_f$ the flutter instability is caused by two of the four complex eigenvalues lying on the branches of a hyperbolic curve

$$\mathrm{Im}\lambda^2 - \mathrm{Re}\lambda^2 = \omega_f^2. \tag{6.73}$$

The critical values ν_d and ν_f constitute the boundaries between the divergence and stability domains and between the stability and flutter domains respectively. For $\mathrm{tr}\mathbf{K} > 0$ and $\det \mathbf{K} = 0$ the divergence domain shrinks to a point $\nu_d = 0$, and for $\mathrm{tr}\mathbf{K} > 0$ and $\det \mathbf{K} > 0$ there exist only stability and flutter domains as shown in Figure 6.6 (b). For negative ν the boundaries of the divergence and flutter domains are $\nu = -\nu_d$ and $\nu = -\nu_f$.

In general, the Jordan chain for the eigenvalue $i\omega_f$ consists of an eigenvector $\mathbf{u}_0$ and an associated vector $\mathbf{u}_1$ that satisfy the equations [288]

$$(-\omega_f^2\mathbf{I} + \mathbf{K} + \nu_f\mathbf{N})\mathbf{u}_0 = 0, \quad (-\omega_f^2\mathbf{I} + \mathbf{K} + \nu_f\mathbf{N})\mathbf{u}_1 = -2i\omega_f\mathbf{u}_0. \tag{6.74}$$

Due to the nonself-adjointness of the matrix operator, the same eigenvalue possesses the left Jordan chain of generalized eigenvectors $\mathbf{v}_0$ and $\mathbf{v}_1$

$$\mathbf{v}_0^T(-\omega_f^2\mathbf{I} + \mathbf{K} + \nu_f\mathbf{N}) = 0, \quad \mathbf{v}_1^T(-\omega_f^2\mathbf{I} + \mathbf{K} + \nu_f\mathbf{N}) = -2i\omega_f\mathbf{v}_0^T. \tag{6.75}$$

The eigenvalues $\mathbf{u}_0$ and $\mathbf{v}_0$ are biorthogonal

$$\mathbf{v}_0^T \mathbf{u}_0 = 0. \tag{6.76}$$

In the neighborhood of $\nu = \nu_f$ the double eigenvalue and the corresponding eigenvectors vary according to the formulas [288, 296]

$$\begin{aligned}
\lambda(\nu) &= i\omega_f \pm \mu\sqrt{\nu - \nu_f} + o((\nu - \nu_f)^{\frac{1}{2}}),\\
\mathbf{u}(\nu) &= \mathbf{u}_0 \pm \mu\mathbf{u}_1\sqrt{\nu - \nu_f} + o((\nu - \nu_f)^{\frac{1}{2}}),\\
\mathbf{v}(\nu) &= \mathbf{v}_0 \pm \mu\mathbf{v}_1\sqrt{\nu - \nu_f} + o((\nu - \nu_f)^{\frac{1}{2}}),
\end{aligned} \tag{6.77}$$

where μ^2 is a real number given by

$$\mu^2 = -\frac{\mathbf{v}_0^T \mathbf{N}\mathbf{u}_0}{2i\omega_f \mathbf{v}_0^T \mathbf{u}_1}. \tag{6.78}$$

For $m = 2$ the generalized eigenvectors of the right and left Jordan chains at the eigenvalue $i\omega_f$, where the eigenfrequency is given by (6.72) and the critical value ν_f is defined by (6.71), are [281]

$$\mathbf{u}_0 = \begin{pmatrix} 2k_{12} + 2\nu_f \\ k_{22} - k_{11} \end{pmatrix}, \quad \mathbf{v}_0 = \begin{pmatrix} 2k_{12} - 2\nu_f \\ k_{22} - k_{11} \end{pmatrix}, \quad \mathbf{u}_1 = \mathbf{v}_1 = \begin{pmatrix} 0 \\ -4i\omega_f \end{pmatrix}. \tag{6.79}$$

Substituting (6.79) into equation (6.78) yields the expression

$$\mu^2 = -\frac{4\nu_f(k_{11} - k_{22})}{2i\omega_f \mathbf{v}_0^T \mathbf{u}_1} = \frac{\nu_f}{2\omega_f^2} > 0. \tag{6.80}$$

After plugging the real-valued coefficient μ into expansions (6.77) we obtain an approximation of order $|\nu - \nu_f|^{1/2}$ of the exact eigenvalues $\lambda = \lambda(\nu)$. This can be verified by the series expansions of (6.70) about $\nu = \nu_f$.

The one-dimensional domain of marginal stability of the circulatory system given by Theorem 6.2 blows up into a three-dimensional domain of asymptotic stability of the system (6.17) in the space of the parameters δ, Ω, and ν, which is described by the Routh and Hurwitz criterion for the polynomial $q(\lambda)$

$$\delta \mathrm{tr}\mathbf{D} > 0,\ \mathrm{tr}\mathbf{K} + \delta^2 \det \mathbf{D} + \Omega^2 > 0,\ \det \mathbf{K} + \nu^2 > 0,\ (\nu - \nu_{cr}^-)(\nu - \nu_{cr}^+) < 0, \tag{6.81}$$

where

$$\nu_{cr}^{\pm}(\delta, \Omega) = \frac{\Omega b \pm \sqrt{\Omega^2 b^2 + ac}}{a}\,\delta. \tag{6.82}$$

The coefficients a, b, and c are

$$\begin{aligned}
a(\delta, \Omega) &= 4\Omega^2 + \delta^2(\mathrm{tr}\mathbf{D})^2, \quad b(\delta, \Omega) = 4\nu_f\beta_* + (\delta^2 \det \mathbf{D} + \Omega^2)\mathrm{tr}\mathbf{D},\\
c(\delta, \Omega) &= \nu_f^2((\mathrm{tr}\mathbf{D})^2 - 4\beta_*^2) + (\omega_f^2 \mathrm{tr}\mathbf{D} - 2\nu_f\beta_*)(\delta^2 \det \mathbf{D} + \Omega^2)\mathrm{tr}\mathbf{D},
\end{aligned}$$

where

$$\beta_* := \frac{\mathrm{tr}(\mathbf{K} - \omega_f^2 \mathbf{I})\mathbf{D}}{2\nu_f}. \tag{6.83}$$

The first two of the conditions of asymptotic stability (6.81) restrict the region of variation of parameters δ and Ω either to a half-plane $\delta \mathrm{tr}\mathbf{D} > 0$, if $\det \mathbf{D} \geq 0$, or to a region between the line $\delta = 0$ and one of the branches of a hyperbola $|\det \mathbf{D}|\,\delta^2 - \Omega^2 = 2\omega_f^2$, if $\det \mathbf{D} < 0$. Provided that δ and Ω belong to the described domain, the asymptotic stability of system (6.17) is determined by the last two of the inequalities (6.81).

For $\det \mathbf{K} \leq 0$, the domain of asymptotic stability consists of two nonintersecting parts, bounded by the surfaces $\nu = \nu_{cr}^{\pm}(\delta, \Omega)$ and by the planes $\nu = \pm\nu_d$, separating it from the divergence domain. For $\det \mathbf{K} > 0$, inequality $\det \mathbf{K} + \nu^2 > 0$ is fulfilled, and the asymptotic stability domain is contained between the surfaces $\nu = \nu_{cr}^{+}(\delta, \Omega)$ and $\nu = \nu_{cr}^{-}(\delta, \Omega)$.

The functions $\nu_{cr}^{\pm}(\delta, \Omega)$ defined by expressions (6.82) are singular at the origin due to the vanishing denominator. Assuming $\Omega = \beta\delta$ and calculating a limit of these functions when δ tends to zero, we obtain

$$\nu_0^{\pm}(\beta) := \lim_{\delta \to 0} \nu_{cr}^{\pm} = \nu_f \frac{4\beta\beta_* \pm \mathrm{tr}\mathbf{D}\sqrt{(\mathrm{tr}\mathbf{D})^2 + 4(\beta^2 - \beta_*^2)}}{(\mathrm{tr}\mathbf{D})^2 + 4\beta^2}. \tag{6.84}$$

The functions $\nu_0^{\pm}(\beta)$ are real-valued if the radicand in (6.84) is nonnegative.

Theorem 6.3 (O. N. Kirillov, 2007 [290]). *Let* $\lambda_1(\mathbf{D})$ *and* $\lambda_2(\mathbf{D})$ *be eigenvalues of* $\mathbf{D}$. *Then,*

$$|\beta_*| \leq \frac{|\lambda_1(\mathbf{D}) - \lambda_2(\mathbf{D})|}{2}. \tag{6.85}$$

If $\mathbf{D}$ *is semidefinite* ($\det \mathbf{D} \geq 0$) *or indefinite with*

$$0 > \det \mathbf{D} \geq -\frac{(k_{12}(d_{22} - d_{11}) - d_{12}(k_{22} - k_{11}))^2}{4\nu_f^2}, \tag{6.86}$$

then

$$|\beta_*| \leq \frac{|\mathrm{tr}\mathbf{D}|}{2}, \tag{6.87}$$

and the limits $\nu_0^{\pm}(\beta)$ *are continuous real-valued functions of* β. *Otherwise, there exists an interval of discontinuity* $\beta^2 < \beta_*^2 - (\mathrm{tr}\mathbf{D})^2/4$.

Proof. With the use of the definition of β_*, (6.83), a series of transformations

$$\begin{aligned}\beta_*^2 - \frac{(\mathrm{tr}\mathbf{D})^2}{4} &= \frac{1}{4\nu_f^2}\left(\frac{(k_{11}-k_{22})(d_{11}-d_{22})}{2} + 2k_{12}d_{12}\right)^2 \\ &\quad - \frac{(d_{11}+d_{22})^2}{4}\,\frac{((k_{11}-k_{22})^2+4k_{12}^2)}{4\nu_f^2} \\ &= -\det\mathbf{D} - \frac{(k_{12}(d_{22}-d_{11}) - d_{12}(k_{22}-k_{11}))^2}{4\nu_f^2} \end{aligned} \tag{6.88}$$

yields the expression

$$\beta_*^2 = \frac{(\lambda_1(\mathbf{D}) - \lambda_2(\mathbf{D}))^2}{4} - \frac{(k_{12}(d_{22}-d_{11}) - d_{12}(k_{22}-k_{11}))^2}{4\nu_f^2}. \tag{6.89}$$

For real β_*, formula (6.88) implies inequality (6.86). The remaining part of the proposition follows from (6.89). □

Inequality (6.89) subdivides the set of indefinite damping matrices into two classes. We call a 2×2 real symmetric matrix $\mathbf{D}$ with $\det\mathbf{D} < 0$ *weakly indefinite* if $4\beta_*^2 < (\mathrm{tr}\mathbf{D})^2$, and *strongly indefinite* if $4\beta_*^2 > (\mathrm{tr}\mathbf{D})^2$.

The calculated $\nu_0^{\pm}(\beta)$ are bounded functions of β, nonexceeding the critical values $\pm\nu_f$ of the unperturbed circulatory system:

$$|\nu_0^{\pm}(\beta)| \le |\nu_0^{\pm}(\pm\beta_*)| = \nu_f. \tag{6.90}$$

Indeed, let us observe that $\mu_0^{\pm} := \nu_0^{\pm}/\nu_f$ are roots of the quadratic equation

$$\nu_f^2 a_\beta \mu^2 - 2\delta\Omega b_0 \nu_f \mu - \delta^2 c_0 = 0, \tag{6.91}$$

with $\delta^2 a_\beta := a(\delta, \beta\delta)$, $b_0 := b(0,0)$, $c_0 := c(0,0)$. According to the Schur criterion [62, 409] all the roots μ of equation (6.91) are inside the closed unit disk if

$$\begin{aligned} \delta^2 c_0 + \nu_f^2 a_\beta &= (\mathrm{tr}\mathbf{D})^2 + 4(\beta^2 - \beta_*^2) + (\mathrm{tr}\mathbf{D})^2 \ge 0, \\ 2\delta\Omega\nu_f b_0 + \nu_f^2 a_\beta - \delta^2 c_0 &= (\beta+\beta_*)^2 \ge 0, \\ -2\delta\Omega\nu_f b_0 + \nu_f^2 a_\beta - \delta^2 c_0 &= (\beta-\beta_*)^2 \ge 0. \end{aligned} \tag{6.92}$$

The first of conditions (6.92) is satisfied for real $\nu_0^{\pm}$, implying $|\mu_0^{\pm}(\beta)| \le 1$ with $|\mu_0^{+}(\beta_*)| = |\mu_0^{-}(-\beta_*)| = 1$.

The limits $\nu_0^{\pm}(\beta)$ of the critical values of the circulatory parameter $\nu_{cr}^{\pm}(\delta,\Omega)$, effectively depend only on the ratio $\beta = \Omega/\delta$, defining the direction of approaching zero in the (δ,Ω)-plane. Along the directions $\beta = \beta_*$ and $\beta = -\beta_*$, the limits coincide with the critical flutter loads of the unperturbed circulatory system in such a way that $\nu_0^{+}(\beta_*) = \nu_f$ and $\nu_0^{-}(-\beta_*) = -\nu_f$. According to equation (6.90), the limit of the

nonconservative positional force at the onset of flutter for system (6.17) with dissipative and gyroscopic forces tending to zero does not exceed the critical flutter load of the circulatory system, demonstrating a drop in the critical load.

Power series expansions of the functions $\nu_0^{\pm}(\beta)$ around $\beta = \pm\beta_*$ (with the radius of convergence not exceeding $|\mathrm{tr}\mathbf{D}|/2$) yield simple estimates of the drops in the critical load for the two-dimensional system (6.17)

$$\nu_f \mp \nu_0^{\pm}(\beta) = \nu_f \frac{2}{(\mathrm{tr}\mathbf{D})^2}(\beta \mp \beta_*)^2 + o((\beta \mp \beta_*)^2). \tag{6.93}$$

Leaving in expansions (6.93) only the second-order terms and then substituting $\beta = \Omega/\delta$, we get an approximation to the boundary of the asymptotic stability domain of the system (6.17) in the vicinity of the points $(0, 0, \pm\nu_f)$ in the (δ, Ω, ν)-space. An extension to the case when the system (6.17) has m degrees of freedom is given by the following statement.

Theorem 6.4. *Let the system* (6.17) *with m degrees of freedom be stable at* $\nu < \nu_f$ *and let at* $\nu = \nu_f$ *its spectrum contain a double eigenvalue* $i\omega_f$ *with the left and right Jordan chains of generalized eigenvectors* $\mathbf{u}_0$, $\mathbf{u}_1$ *and* $\mathbf{v}_0$, $\mathbf{v}_1$, *satisfying equations* (6.74) *and* (6.75). *Define the real quantities*

$$\begin{aligned} d_1 &= \mathrm{Re}(\mathbf{v}_0^T\mathbf{D}\mathbf{u}_0), \quad d_2 = \mathrm{Im}(\mathbf{v}_0^T\mathbf{D}\mathbf{u}_1 + \mathbf{v}_1^T\mathbf{D}\mathbf{u}_0), \\ g_1 &= \mathrm{Re}(\mathbf{v}_0^T\mathbf{G}\mathbf{u}_0), \quad g_2 = \mathrm{Im}(\mathbf{v}_0^T\mathbf{G}\mathbf{u}_1 + \mathbf{v}_1^T\mathbf{G}\mathbf{u}_0), \end{aligned} \tag{6.94}$$

and

$$\beta_* = -\frac{\mathbf{v}_0^T\mathbf{D}\mathbf{u}_0}{\mathbf{v}_0^T\mathbf{G}\mathbf{u}_0}. \tag{6.95}$$

Then, in the vicinity of $\beta := \Omega/\delta = \beta_*$ *the limit of the critical flutter load* ν_{cr}^+ *of the near-reversible system with m degrees of freedom as* $\delta \to 0$ *is*

$$\nu_0^+(\beta) = \nu_f - \frac{g_1^2(\beta - \beta_*)^2}{\mu^2(d_2 + \beta_* g_2)^2} + o((\beta - \beta_*)^2). \tag{6.96}$$

Proof. Perturbing a simple eigenvalue $i\omega(\nu)$ of the stable circulatory system at a fixed $\nu < \nu_f$ by small dissipative and gyroscopic forces yields the increment

$$\lambda = i\omega - \frac{\mathbf{v}^T\mathbf{D}\mathbf{u}}{2\mathbf{v}^T\mathbf{u}}\delta - \frac{\mathbf{v}^T\mathbf{G}\mathbf{u}}{2\mathbf{v}^T\mathbf{u}}\Omega + o(\delta, \Omega). \tag{6.97}$$

Since the eigenvectors $\mathbf{u}(\nu)$ and $\mathbf{v}(\nu)$ can be chosen real, the first-order increment is real-valued. Therefore, in the first approximation in δ and Ω, the simple eigenvalue

$i\omega(\nu)$ remains on the imaginary axis if $\Omega = \beta(\nu)\delta$, where

$$\beta(\nu) = -\frac{\mathbf{v}^T(\nu)\mathbf{D}\mathbf{u}(\nu)}{\mathbf{v}^T(\nu)\mathbf{G}\mathbf{u}(\nu)}. \tag{6.98}$$

Substituting expansions (6.77) into formula (6.98), we obtain

$$\beta(\nu) = -\frac{d_1 \pm d_2\mu\sqrt{\nu_f - \nu} + o\left(\sqrt{\nu_f - \nu}\right)}{g_1 \pm g_2\mu\sqrt{\nu_f - \nu} + o\left(\sqrt{\nu_f - \nu}\right)}, \tag{6.99}$$

wherefrom expression (6.96) follows, if $|\beta - \beta_*| \ll 1$. □

With $\beta = \Omega/\delta$ the formula (6.96) yields an approximation to the critical flutter load

$$\nu_{cr}^{+}(\delta, \Omega) = \nu_f - \frac{g_1^2(\Omega - \beta_*\delta)^2}{\mu^2(d_2 + \beta_* g_2)^2\delta^2}. \tag{6.100}$$

The coefficients (6.78) and (6.94) calculated with the use of vectors (6.79) are

$$\begin{aligned} d_1 &= 2(k_{22} - k_{11})\mathrm{tr}(\mathbf{K} - \omega_f^2\mathbf{I})\mathbf{D}, & g_1 &= 4(k_{11} - k_{22})\nu_f \\ d_2 &= -8\omega_f(2d_{12}k_{12} + d_{22}(k_{22} - k_{11})), & g_2 &= 16\omega_f\nu_f. \end{aligned} \tag{6.101}$$

With (6.101) expression (6.96) is reduced to (6.93).

Using exact expressions for the functions $\omega(\nu)$, $\mathbf{u}(\nu)$, and $\mathbf{v}(\nu)$, we obtain better estimates in the case when $m = 2$. Substituting the explicit expression for the eigenfrequency

$$\omega^2(\nu) = \omega_f^2 \pm \sqrt{\nu_f^2 - \nu^2}, \tag{6.102}$$

following from (6.70)–(6.72), into the equation (6.98), which now reads

$$\delta\left(2\nu_f\beta_* + \left(\omega^2(\nu) - \omega_f^2\right)\mathrm{tr}\mathbf{D}\right) - 2\Omega\nu = 0, \tag{6.103}$$

we obtain

$$\Omega = \frac{\nu_f}{\nu}\left[\beta_* \pm \frac{\mathrm{tr}\mathbf{D}}{2}\sqrt{1 - \frac{\nu^2}{\nu_f^2}}\right]\delta. \tag{6.104}$$

Equation (6.104) is simply formula (6.84) inverted with respect to $\beta = \Omega/\delta$.

We use the linear approximation (6.104) to study the asymptotic behavior of the stability domain of the two-dimensional system (6.17) in the vicinity of the origin in the (δ, Ω)-plane for various ν. It is enough to consider only the case when $\mathrm{tr}\mathbf{K} > 0$ and $\det\mathbf{K} > 0$, so that $-\nu_f < \nu < \nu_f$, because for $\det\mathbf{K} \le 0$ the region $\nu^2 < \nu_d^2 \le \nu_f^2$ is unstable and should be excluded.

For $\nu^2 < \nu_f^2$ the radicand in expression (6.104) is real and nonzero, so that in the first approximation the domain of asymptotic stability is contained between two lines intersecting at the origin, see Figure 6.7 (central column). When ν approaches the critical values $\pm\nu_f$, the angle becomes more acute until at $\nu = \nu_f$ or $\nu = -\nu_f$ it degenerates to a single line $\Omega = \delta\beta_*$ or $\Omega = -\delta\beta_*$ respectively. For $\beta_* \neq 0$ these

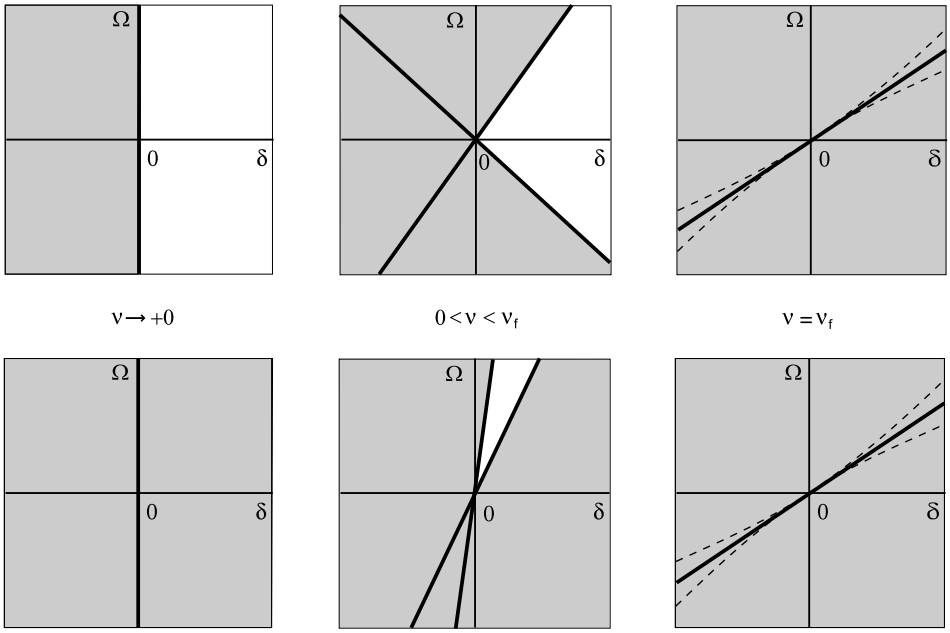

Figure 6.7. For various ν, bold lines show linear approximations to the boundary of the asymptotic stability domain (white) of the system (6.17) in the vicinity of the origin in the plane (δ, Ω), when $\mathrm{tr}\mathbf{K} > 0$ and $\det \mathbf{K} > 0$, and $4\beta_*^2 < (\mathrm{tr}\mathbf{D})^2$ (upper row) or $4\beta_*^2 > (\mathrm{tr}\mathbf{D})^2$ (lower row).

lines are not parallel to each other, and due to inequality (6.87) they are never vertical, see Figure 6.7 (right column). However, the degeneration can be lifted already in the second-order approximation in δ

$$\Omega = \pm\delta\beta_* \pm \frac{\omega_f \mathrm{tr}\mathbf{D}\sqrt{\det \mathbf{D} + \beta_*^2}}{2\nu_f}\delta^2 + O(\delta^3). \tag{6.105}$$

If the radicand is positive, equation (6.105) defines two curves touching each other at the origin, as shown in Figure 6.7 by dashed lines. Inside the cusps $|\nu_{cr}^{\pm}(\delta, \Omega)| \geq \nu_f$.

The evolution of the domain of asymptotic stability in the plane (δ, Ω), when ν goes from $\pm\nu_f$ to zero, depends on the structure of the matrix $\mathbf{D}$ and is governed by the sign of the expression $4\beta_*^2 - (\mathrm{tr}\mathbf{D})^2$. For the negative sign, the angle between the lines (6.104) is getting wider, tending to π as $\nu \to 0$, see Figure 6.7 (upper left). Otherwise, the angle reaches a maximum for some $\nu^2 < \nu_f^2$ and then shrinks to a single line $\delta = 0$ at $\nu = 0$, Figure 6.7 (lower left). At $\nu = 0$ the Ω-axis corresponds to a marginally stable gyroscopic system. Since the linear approximation to the asymptotic stability domain does not contain the Ω-axis at any $\nu \neq 0$, small gyroscopic forces cannot stabilize a circulatory system in the absence of damping forces ($\delta = 0$), which is in agreement with the Bottema–Lakhadanov–Karapetyan theorem (Theorem 5.19).

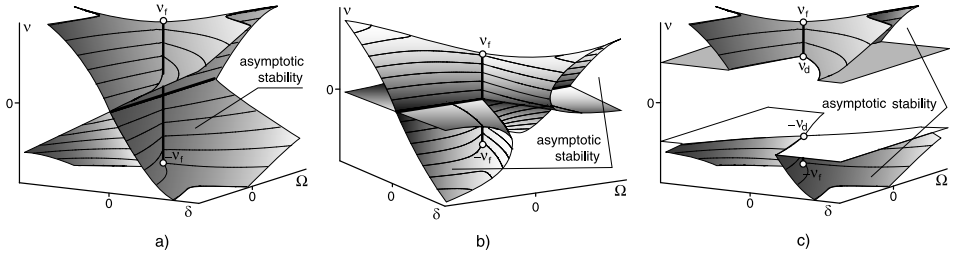

Figure 6.8. The domain of asymptotic stability of the dissipative system (6.17): (a) Plücker conoid of degree $n = 1$ when $\mathbf{K} > 0$ and $4\beta_*^2 < (\mathrm{tr}\mathbf{D})^2$; two disconnected pockets at (b) $\mathbf{K} > 0$ and $4\beta_*^2 > (\mathrm{tr}\mathbf{D})^2$ and (c) $\mathrm{tr}\mathbf{K} > 0$ and $\det\mathbf{K} < 0$.

Reconstructing with the use of the obtained results the asymptotic stability domain of system (6.17), we find that it has three typical configurations in the vicinity of the ν-axis in the (δ, Ω, ν)-space, see Figure 6.8. In the case of a positive-definite matrix $\mathbf{K}$ and a semidefinite or a weakly-indefinite matrix $\mathbf{D}$, the addition of small damping and gyroscopic forces blows the stability interval of a circulatory system $\nu^2 < \nu_f^2$ up to a three-dimensional region bounded by the parts of a singular surface $\nu = \nu_{cr}^{\pm}(\delta, \Omega)$, which belong to the half-space $\delta\mathrm{tr}\mathbf{D} > 0$, Figure 6.8 (a). The stability interval of a circulatory system forms an edge of a dihedral angle. At $\nu = 0$ the angle of the intersection reaches its maximum (π), creating another edge along the Ω-axis, which corresponds to a conservative statically stable gyroscopic system. While approaching the points $\pm\nu_f$, the angle of the sector becomes more acute and finally vanishes, Figure 6.8 (a). The whole surface that has two intervals of self-intersection and two Whitney umbrella points is known as the Plücker conoid of degree $n = 1$ [231]. It is remarkable that the vertical interval of self-intersection of the Plücker conoid corresponds to the 'ideal' circulatory system whereas the horizontal line of self-intersection corresponds to the conservative gyroscopic system. *We see that both the ideal systems co-exist at different singularities of one and the same boundary of the domain of asymptotic stability of a general nonconservative system* (6.17). Hence, by varying parameters of a dissipative system we can obtain in the limiting cases different 'ideal' systems such as gyroscopic, circulatory, or even $\mathcal{PT}$-symmetric [303, 305].

When the matrix $\mathbf{D}$ approaches the threshold $4\beta_*^2 = (\mathrm{tr}\mathbf{D})^2$, two smooth parts of the stability boundary corresponding to negative and positive ν come towards each other until they touch, when $\mathbf{D}$ is at the threshold. After $\mathbf{D}$ becomes strongly indefinite this temporary glued configuration collapses into two disconnected pockets of asymptotic stability, as shown in Figure 6.8 (b). Each of the two pockets has a deadlock of an edge as well as two edges which meet at the origin and form a singularity known as the break of an edge [17].

The configuration of the asymptotic stability domain, shown in Figure 6.8 (c), corresponds to an indefinite matrix $\mathbf{K}$ with $\mathrm{tr}\mathbf{K} > 0$ and $\det\mathbf{K} < 0$. In this case, the

condition $\nu^2 > \nu_d^2$ divides the domain of asymptotic stability into two parts, corresponding to positive and negative ν. The intervals of the ν-axis form edges of dihedral angles, which end up with the deadlocks at $\nu = \pm\nu_f$ and with the trihedral angles at $\nu = \pm\nu_d$, Figure 6.8 (c). Qualitatively, this configuration does not depend on the properties of the matrix $\mathbf{D}$.

Chapter 7

Nonself-adjoint boundary eigenvalue problems for differential operators and operator matrices dependent on parameters

Normally, the boundary conditions have great influence on the stability limits.
P. Pedersen [474]

Nonself-adjoint boundary eigenvalue problems for matrix differential operators describe distributed nonconservative systems with the coupled modes and appear in structural mechanics, fluid dynamics, magnetohydrodynamics, to name a few.

Practical needs for optimization and rational experiment planning in modern applications allow both the differential expression and the boundary conditions to depend analytically on the spectral parameter and smoothly on several physical parameters (which can be scalar or distributed) [85, 105, 106, 195, 307, 474].

According to the ideas going back to von Neumann and Wigner [587], in the multiparameter operator families, eigenvalues with various algebraic and geometric multiplicities can be generic [18, 130, 569]. In some applications additional symmetries [146, 147] yield the existence of *spectral meshes* [208] of eigencurves [63, 64] in the plane 'eigenvalue versus parameter' containing an infinite number of nodes with multiple eigenvalues. A classical example is the Campbell diagrams in rotor dynamics [109], see also [123, 245, 370, 583] and references therein.

As has been pointed out already by Rellich [495], sensitivity analysis of multiple eigenvalues is complicated by their nondifferentiability as functions of several parameters. Singularities corresponding to multiple eigenvalues [18] are related to such important effects as the destabilization paradox in near-Hamiltonian and near-reversible systems [81, 90, 232, 312, 333, 354], geometric phase [154, 397], transfer of instability between modes in dissipative problems of fluid mechanics [106, 246, 458], reversals of the geomagnetic field [195, 545], emission of sound by rotating continua interacting with the friction pads [123, 254, 294, 538, 604], material instabilities (flutter) in elastoplastic flows [59, 60], and other phenomena [518].

An increasing number of multiparameter nonself-adjoint boundary eigenvalue problems and the need for simple constructive estimates of critical parameters and eigenvalues as well as for verification of numerical codes and discretization schemes [75, 107, 249, 419] require development of applicable methods, allowing one to track relatively easily and conveniently the changes in simple and multiple eigenvalues and the corresponding eigenvectors due to variation of the differential expression and es-

pecially due to transition from one type of boundary condition to another without discretization of the original distributed problem, see e.g. [85, 195, 249, 307, 474, 604].

A systematical study of bifurcation of eigenvalues of a nonself-adjoint linear operator L_0 under the perturbation $L_0 + \varepsilon L_1$, where ε is a small parameter, dates back to at least the 1950s. Apparently, Krein was the first who derived a formula for the splitting of a double eigenvalue with the Jordan block at the Hamiltonian 1 : 1 resonance (the Krein collision [430]), which was expressed through the generalized eigenvectors of the double eigenvalue [336,337]. In the 1960s Vishik and Lyusternik [584] and Lidskii [379] created a perturbation theory for nonsymmetric matrices and nonself-adjoint differential operators allowing one to find the perturbation coefficients of eigenvalues and eigenfunctions in an explicit form by means of the eigenelements of the unperturbed operator [428]. Classical monographs by Rellich [496], Kato [258], and Baumgärtel [37], mostly focussing on the self-adjoint case, contain a detailed treatment of eigenvalue problems linearly or quadratically dependent on the spectral parameter.

Multiparameter perturbation theory for simple and multiple eigenvalues of matrices and generalized matrix eigenvalue problems initiated by Sun [560, 561] was continued, e.g., in recent works [270,517,518]. Gohberg, Lancaster and Rodman [201], Najman [441], Langer and Najman [352], Hryniv and Lancaster [233], Lancaster, Markus, and Zhou [347], and Kirillov [288] studied perturbation of eigenelements in one- and multiparameter families of analytic matrix functions. Recently, eigenvalue series of holomorphic matrix operators were derived by Chen et al. [124] to provide efficient computational solutions to a class of stability problems relevant to control systems with time delay. Explicit recursive formulas to compute all the Puiseux series coefficients for the perturbed multiple eigenvalues with the Jordan block from the derivatives of an analytic one-parameter matrix family were obtained by Welters [593]. Differential equations allowing for the individual tracking of an eigenvalue and eigenvector of a parameterized matrix family were derived by Kalaba et al. [251, 252]. Kollar developed a homotopy method for counting stable and unstable eigenvalues of nonlinear matrix pencils [318].

Sensitivity analysis of double semisimple and nonderogatory eigenvalues of differential operators dependent on parameters was used in 1984 by DiPrima and Hall [155] for the study of oscillatory and nonoscillatory instability in the cylindrical Couette–Taylor flow.[1] In 1986 Busse and Or perturbed a nonself-adjoint boundary eigenvalue problem to study the effect of the boundary conditions (the wall curvature) on the bifurcation of the basic mode of the thermal convection in a rotating annulus [106,458]. Sensitivity analysis of the critical parameters at the onset of flutter in nonconservative problems of solid mechanics was discussed in 1983 by Pedersen and Seyranian [473].

[1] More precisely, they showed the existence of complex higher eigenvalues in the spectrum of the cylindrical Couette–Taylor flow where the first unstable eigenvalue has imaginary part equal to zero. This is a weak form of the *principle of exchange of stabilities* [145, 183]. Its strong form requires that all nondecaying disturbances be nonoscillatory in time [223].

Recently, Kirillov and Seyranian derived explicit formulae for bifurcation of multiple eigenvalues and eigenvectors of two-point nonself-adjoint boundary eigenvalue problems with scalar differential expression and boundary conditions, which depend analytically on the spectral parameter and smoothly on a vector of physical parameters, and applied them to the sensitivity analysis of distributed nonconservative problems prone to dissipation-induced instabilities [273,277,280,282,284]. An extension to the case of intermediate boundary conditions with an application to the problem of the onset of friction-induced oscillations in the moving beam and rotating disk was considered in [538,539]. In [208,298,307] this technique was applied to the study of an MHD α^2-dynamo.

In this chapter following [298] we develop this approach further and consider boundary eigenvalue problems for linear nonself-adjoint m-th order $N \times N$ matrix differential operators on the interval $[0,1] \ni x$. The coefficient matrices in the differential expression and the matrix boundary conditions are assumed to depend analytically on the spectral parameter λ and on a vector of real physical parameters $\mathbf{p}$. The matrix formulation of the boundary conditions is chosen for the convenience of its implementation in computer algebra systems for an automatic derivation of the adjoint eigenvalue problem and perturbed eigenvalues and eigenvectors, which is especially helpful when the order of the derivatives in the differential expression is high, see e.g. [204].

Based on the eigenelements of the unperturbed problem, explicit formulae are derived describing bifurcation of the semisimple multiple eigenvalues (diabolical points) as well as nonderogatory eigenvalues (branch points, exceptional points) under small variation of the parameters both in the differential expression and in the boundary conditions. Finally, the general technique is applied to the investigation of the onset of the oscillatory instability in a rotating string as well as in an extended Beck's column with and without elastic foundation.

7.1 Adjoint boundary eigenvalue problems

Following [277, 280, 282, 284, 298, 421, 442] we consider the boundary eigenvalue problem

$$\mathbf{L}(\lambda,\mathbf{p})\mathbf{u} = 0, \quad \mathbf{U}_k(\lambda,\mathbf{p})\mathbf{u} = 0, \quad k = 1,\dots,m, \tag{7.1}$$

with $\mathbf{u}(x) \in \mathbb{C}^N \otimes C^{(m)}[0,1]$. The *differential expression* $\mathbf{Lu}$ of the operator is

$$\mathbf{Lu} = \sum_{j=0}^{m} \mathrm{l}_j(x)\partial_x^{m-j}\mathbf{u}, \quad \mathrm{l}_j(x) \in \mathbb{C}^{N\times N} \otimes C^{(m-j)}[0,1], \quad \det[\mathrm{l}_0(x)] \neq 0, \tag{7.2}$$

and the *boundary forms* $\mathbf{U}_k\mathbf{u}$ are

$$\mathbf{U}_k\mathbf{u} = \sum_{j=0}^{m-1} \mathbf{A}_{kj}\mathbf{u}_x^{(j)}(x=0) + \sum_{j=0}^{m-1} \mathbf{B}_{kj}\mathbf{u}_x^{(j)}(x=1), \quad \mathbf{A}_{kj}, \mathbf{B}_{kj} \in \mathbb{C}^{N\times N}. \tag{7.3}$$

Introducing the block matrix $\mathfrak{U} := [\mathfrak{A}, \mathfrak{B}] \in \mathbb{C}^{mN\times 2mN}$ and the vector

$$\mathfrak{u}^T := \left(\mathbf{u}^T(0), \mathbf{u}_x^{(1)T}(0), \ldots, \mathbf{u}_x^{(m-1)T}(0), \mathbf{u}^T(1), \mathbf{u}_x^{(1)T}(1), \ldots, \mathbf{u}_x^{(m-1)T}(1)\right) \in \mathbb{C}^{2mN} \tag{7.4}$$

the *boundary conditions* can be compactly rewritten as [280, 282, 298]

$$\mathfrak{U}\mathfrak{u} = [\mathfrak{A}, \mathfrak{B}]\mathfrak{u} = 0, \tag{7.5}$$

where $\mathfrak{A} = (\mathbf{A}_{kj})\big|_{x=0} \in \mathbb{C}^{mN\times mN}$ and $\mathfrak{B} = (\mathbf{B}_{kj})\big|_{x=1} \in \mathbb{C}^{mN\times mN}$. It is assumed that the matrices $\mathbf{l}_j$, $\mathfrak{A}$, and $\mathfrak{B}$ are analytic functions of the complex spectral parameter λ and of the real vector of physical parameters $\mathbf{p} \in \mathbb{R}^n$.

Given a vector $\mathbf{p} = \mathbf{p}_0$, the eigenvalue λ_0, to which the eigenvector $\mathbf{u}_0$ corresponds, is a root of the characteristic equation obtained after substitution of the general solution to equation $\mathbf{Lu} = 0$ into the boundary conditions (7.5) [442].

Let us introduce a scalar product $(\mathbf{u}, \mathbf{v}) := \int_0^1 \mathbf{v}^*\mathbf{u}dx$, where the asterisk denotes complex-conjugate transpose ($\mathbf{v}^* := \overline{\mathbf{v}}^T$) [442]. Taking the scalar product of $\mathbf{Lu}$ and a vector-function $\mathbf{v}$ and integrating it by parts yields the *Lagrange formula* for the case of operator matrices (cf. [298, 421, 442])

$$\Omega(\mathbf{u}, \mathbf{v}) := (\mathbf{Lu}, \mathbf{v}) - (\mathbf{u}, \mathbf{L}^\dagger\mathbf{v}) = \mathfrak{v}^*\mathfrak{L}\mathfrak{u}, \tag{7.6}$$

with the *adjoint differential expression* [421, 442]

$$\mathbf{L}^\dagger\mathbf{v} := \sum_{q=0}^{m}(-1)^{m-q}\partial_x^{m-q}\left(\mathbf{l}_q^*\mathbf{v}\right), \tag{7.7}$$

the vector $\mathfrak{v}$ that is defined as

$$\mathfrak{v}^T := \left(\mathbf{v}^T(0), \mathbf{v}_x^{(1)T}(0), \ldots, \mathbf{v}_x^{(m-1)T}(0), \mathbf{v}^T(1), \mathbf{v}_x^{(1)T}(1), \ldots, \mathbf{v}_x^{(m-1)T}(1)\right) \in \mathbb{C}^{2mN} \tag{7.8}$$

and the block matrix $\mathfrak{L} := (\mathbf{l}_{ij})$

$$\mathfrak{L} = \begin{pmatrix} -\mathfrak{L}(0) & 0 \\ 0 & \mathfrak{L}(1) \end{pmatrix}, \quad \mathfrak{L}(x) = \begin{pmatrix} \mathbf{l}_{00} & \mathbf{l}_{01} & \cdots & \mathbf{l}_{0\,m-2} & \mathbf{l}_{0\,m-1} \\ \mathbf{l}_{10} & \mathbf{l}_{11} & \cdots & \mathbf{l}_{1\,m-2} & 0 \\ \vdots & \vdots & \ddots & \vdots & \vdots \\ \mathbf{l}_{m-2\,0} & \mathbf{l}_{m-2\,1} & \cdots & 0 & 0 \\ \mathbf{l}_{m-1\,0} & 0 & \cdots & 0 & 0 \end{pmatrix}, \tag{7.9}$$

where the $N \times N$ matrices $\mathbf{l}_{ij}$ are [298, 421, 442]

$$\begin{aligned} \mathbf{l}_{ij} &:= \sum_{k=i}^{m-1-j}(-1)^k M_{ij}^k\,\partial_x^{k-i}\mathbf{l}_{m-1-j-k}, \\ M_{ij}^k &:= \begin{cases} \dfrac{k!}{(k-i)!\,i!}, & i+j \le m-1 \quad \cap \quad k \ge i \ge 0 \\ 0, & i+j > m-1 \quad \cup \quad k < i. \end{cases} \end{aligned} \tag{7.10}$$

Extend the original matrix $\mathfrak{U}$ (cf. equation (7.5)) to a square matrix $\mathcal{U}$, which is made nondegenerate in a neighborhood of the point $\mathbf{p} = \mathbf{p}_0$ and the eigenvalue $\lambda = \lambda_0$ by an appropriate choice of the auxiliary matrices $\widetilde{\mathfrak{A}}(\lambda, \mathbf{p})$ and $\widetilde{\mathfrak{B}}(\lambda, \mathbf{p})$

$$\mathfrak{U} = [\mathfrak{A}, \mathfrak{B}] \hookrightarrow \mathcal{U} := \begin{pmatrix} \mathfrak{A} & \mathfrak{B} \\ \widetilde{\mathfrak{A}} & \widetilde{\mathfrak{B}} \end{pmatrix} \in \mathbb{C}^{2mN \times 2mN}, \quad \widetilde{\mathfrak{U}} := [\widetilde{\mathfrak{A}}, \widetilde{\mathfrak{B}}], \quad \det(\mathcal{U}) \neq 0. \tag{7.11}$$

For the adjoint boundary conditions $\mathfrak{V}\mathfrak{v} = [\mathfrak{C}, \mathfrak{D}]\mathfrak{v} = 0$ a similar process yields

$$\mathfrak{V} := [\mathfrak{C}, \mathfrak{D}] \hookrightarrow \mathcal{V} := \begin{pmatrix} \mathfrak{C} & \mathfrak{D} \\ \widetilde{\mathfrak{C}} & \widetilde{\mathfrak{D}} \end{pmatrix} \in \mathbb{C}^{2mN \times 2mN}, \quad \widetilde{\mathfrak{V}} := [\widetilde{\mathfrak{C}}, \widetilde{\mathfrak{D}}], \quad \det(\mathcal{V}) \neq 0. \tag{7.12}$$

Then, the form $\Omega(\mathbf{u}, \mathbf{v})$ in equation (7.6) can be represented as [442]

$$\Omega(\mathbf{u}, \mathbf{v}) = (\mathfrak{V}\mathfrak{v})^* \widetilde{\mathfrak{U}}\mathfrak{u} - (\widetilde{\mathfrak{V}}\mathfrak{v})^* \mathfrak{U}\mathfrak{u}, \tag{7.13}$$

so that without loss in generality we can assume [280, 282, 298]

$$\mathfrak{L} = \mathfrak{V}^* \widetilde{\mathfrak{U}} - \widetilde{\mathfrak{V}}^* \mathfrak{U}. \tag{7.14}$$

Hence, we obtain the formula for calculation of the matrix $\mathfrak{V}$ of the *adjoint boundary conditions* and the auxiliary matrix $\widetilde{\mathfrak{V}}$

$$\begin{bmatrix} -\widetilde{\mathfrak{V}} \\ \mathfrak{V} \end{bmatrix}^* = \mathfrak{L}\mathcal{U}^{-1} = \begin{pmatrix} -\mathfrak{L}(0) & 0 \\ 0 & \mathfrak{L}(1) \end{pmatrix} \begin{pmatrix} \mathfrak{A} & \mathfrak{B} \\ \widetilde{\mathfrak{A}} & \widetilde{\mathfrak{B}} \end{pmatrix}^{-1}, \tag{7.15}$$

which exactly reproduces and extends the corresponding result of [280, 282, 298]. Differentiating the equation (7.14) we find

$$\partial_\lambda^r \mathfrak{L} = \sum_{k=0}^{r} \binom{r}{k} \left[\left(\partial_{\bar{\lambda}}^{r-k} \mathfrak{V} \right)^* \partial_\lambda^k \widetilde{\mathfrak{U}} - \left(\partial_{\bar{\lambda}}^{r-k} \widetilde{\mathfrak{V}} \right)^* \partial_\lambda^k \mathfrak{U} \right]. \tag{7.16}$$

The boundary eigenvalue problem

$$\mathbf{L}^\dagger(\overline{\lambda}, \mathbf{p})\mathbf{v} = 0, \quad \mathfrak{V}(\overline{\lambda}, \mathbf{p})\mathfrak{v} = 0 \tag{7.17}$$

is referred to as adjoint to the boundary eigenvalue problem (7.1). We say that (7.1) is a *self-adjoint* boundary eigenvalue problem if the problems given by equations (7.1) and (7.17) coincide, and *nonself-adjoint* otherwise [421, 442].

7.2 Perturbation of eigenvalues

Assume that in the neighborhood of the point $\mathbf{p} = \mathbf{p}_0$ the spectrum of the boundary eigenvalue problem (7.1) is discrete. Denote $\mathbf{L}_0 = \mathbf{L}(\lambda_0, \mathbf{p}_0)$ and $\mathfrak{U}_0 = \mathfrak{U}(\lambda_0, \mathbf{p}_0)$. Let

us consider an analytic perturbation of parameters in the form $\mathbf{p} = \mathbf{p}(\varepsilon)$ where $\mathbf{p}(0) = \mathbf{p}_0$ and ε is a small real number. Then, as in the case of analytic matrix functions [233, 288,347,352], the Taylor decomposition of the differential operator matrix $\mathbf{L}(\lambda, \mathbf{p}(\varepsilon))$ and the matrix of the boundary conditions $\mathfrak{U}(\lambda, \mathbf{p}(\varepsilon))$ are [277,280,282,298]

$$\mathbf{L}(\lambda, \mathbf{p}(\varepsilon)) = \sum_{r,s=0}^{\infty} \frac{(\lambda - \lambda_0)^r}{r!} \varepsilon^s \mathbf{L}_{rs}, \quad \mathfrak{U}(\lambda, \varepsilon) = \sum_{r,s=0}^{\infty} \frac{(\lambda - \lambda_0)^r}{r!} \varepsilon^s \mathfrak{U}_{rs}, \tag{7.18}$$

with $\mathbf{L}_{00} = \mathbf{L}_0$, $\mathfrak{U}_{00} = \mathfrak{U}_0$, and

$$\mathbf{L}_{r0} = \partial_\lambda^r \mathbf{L}, \quad \mathfrak{U}_{r0} = \partial_\lambda^r \mathfrak{U}; \quad \mathbf{L}_{r1} = \sum_{j=1}^{n} \frac{dp_j}{d\varepsilon} \partial_\lambda^r \partial_{p_j} \mathbf{L}, \quad \mathfrak{U}_{r1} = \sum_{j=1}^{n} \frac{dp_j}{d\varepsilon} \partial_\lambda^r \partial_{p_j} \mathfrak{U};$$

$$\mathbf{L}_{r2} = \frac{1}{2} \sum_{j=1}^{n} \frac{d^2 p_j}{d\varepsilon^2} \partial_\lambda^r \partial_{p_j} \mathbf{L} + \frac{1}{2} \sum_{j,t=1}^{n} \frac{dp_j}{d\varepsilon} \frac{dp_t}{d\varepsilon} \partial_\lambda^r \partial_{p_j} \partial_{p_t} \mathbf{L},$$

$$\mathfrak{U}_{r2} = \frac{1}{2} \sum_{j=1}^{n} \frac{d^2 p_j}{d\varepsilon^2} \partial_\lambda^r \partial_{p_j} \mathfrak{U} + \frac{1}{2} \sum_{j,t=1}^{n} \frac{dp_j}{d\varepsilon} \frac{dp_t}{d\varepsilon} \partial_\lambda^r \partial_{p_j} \partial_{p_t} \mathfrak{U}, \tag{7.19}$$

where the derivatives with respect to ε are evaluated at $\varepsilon = 0$ and partial derivatives are evaluated at $\mathbf{p}{=}\mathbf{p}_0$, $\lambda{=}\lambda_0$. We assume that the perturbation is *regular* in the sense that it does not contain derivatives higher than those in the differential expression and the boundary conditions of the unperturbed problem. Our aim is to derive explicit expressions for the leading terms in the expansions for multiple-semisimple and nonderogatory [428] eigenvalues and for the corresponding eigenvectors.

7.2.1 Semisimple eigenvalues

Let at the point $\mathbf{p} = \mathbf{p}_0$ the spectrum contain a semisimple μ-fold eigenvalue λ_0 with μ linearly independent eigenvectors $\mathbf{u}_0(x)$, $\mathbf{u}_1(x), \ldots, \mathbf{u}_{\mu-1}(x)$. Then, the perturbed eigenvalue $\lambda(\varepsilon)$ and the eigenvector $\mathbf{u}(\varepsilon)$ are represented as Taylor series in ε [155, 233,277,347,561,584]

$$\lambda = \lambda_0 + \varepsilon\lambda_1 + \varepsilon^2\lambda_2 + \cdots, \quad \mathbf{u} = \mathbf{b}_0 + \varepsilon\mathbf{b}_1 + \varepsilon^2\mathbf{b}_2 + \cdots. \tag{7.20}$$

For the sake of brevity we do not concern ourselves here with the existence and convergence of expansions (7.20) that can be treated by the methods described in, e.g. [584].

Substituting expansions (7.18) and (7.20) into equation (7.1) and collecting the terms with the same powers of ε we derive the boundary value problems

$$\mathbf{L}_0\mathbf{b}_0 = 0, \ \ \mathfrak{U}_0\mathfrak{b}_0 = 0, \tag{7.21}$$

$$\mathbf{L}_0\mathbf{b}_1 + (\lambda_1\mathbf{L}_{10} + \mathbf{L}_{01})\mathbf{b}_0 = 0, \ \ \mathfrak{U}_0\mathfrak{b}_1 + (\lambda_1\mathfrak{U}_{10} + \mathfrak{U}_{01})\mathfrak{b}_0 = 0, \tag{7.22}$$

The scalar product of (7.22) with the eigenvectors $\mathbf{v}_j$, $j = 0, 1, \ldots, \mu-1$ of the adjoint boundary eigenvalue problem

$$\mathbf{L}_0^{\dagger}\mathbf{v} = 0, \quad \mathfrak{V}_0 \mathfrak{v} = 0 \tag{7.23}$$

yields μ equations

$$(\mathbf{L}_0\mathbf{b}_1, \mathbf{v}_j) = -(\mathbf{L}_{01}\mathbf{b}_0, \mathbf{v}_j) - \lambda_1(\mathbf{L}_{10}\mathbf{b}_0, \mathbf{v}_j). \tag{7.24}$$

With the use of the Lagrange formula (7.6), (7.14) and the boundary conditions (7.22), the left-hand side of equation (7.24) takes the form

$$(\mathbf{L}_0\mathbf{b}_1, \mathbf{v}_j) = (\widetilde{\mathfrak{V}}_0\mathfrak{v}_j)^*(\mathfrak{U}_{01}\mathfrak{b}_0 + \lambda_1\mathfrak{U}_{10}\mathfrak{b}_0). \tag{7.25}$$

Together equations (7.24) and (7.25) result in the expression

$$\lambda_1\big((\mathbf{L}_{10}\,\mathbf{b}_0, \mathbf{v}_j) + (\widetilde{\mathfrak{V}}_0\mathfrak{v}_j)^*\mathfrak{U}_{10}\,\mathfrak{b}_0\big) = -(\mathbf{L}_{01}\mathbf{b}_0, \mathbf{v}_j) - (\widetilde{\mathfrak{V}}_0\mathfrak{v}_j)^*\mathfrak{U}_{01}\mathfrak{b}_0. \tag{7.26}$$

Assuming in the equations (7.26) the vector $\mathbf{b}_0(x)$ as a linear combination

$$\mathbf{b}_0(x) = c_0\mathbf{u}_0(x) + c_1\mathbf{u}_1(x) + \cdots + c_{\mu-1}\mathbf{u}_{\mu-1}(x), \tag{7.27}$$

and taking into account that

$$\mathfrak{b}_0 = c_0\mathfrak{u}_0 + c_1\mathfrak{u}_1 + \cdots + c_{\mu-1}\mathfrak{u}_{\mu-1}, \tag{7.28}$$

where $\mathbf{c}^T = (c_0, c_1, \ldots, c_{\mu-1})$, we arrive at the matrix eigenvalue problem (cf. [155, 347])

$$-\mathbf{F}\mathbf{c} = \lambda_1\mathbf{G}\mathbf{c}. \tag{7.29}$$

The entries of the $\mu \times \mu$ matrices $\mathbf{F}$ and $\mathbf{G}$ are defined by the expressions

$$F_{ij} = (\mathbf{L}_{01}\mathbf{u}_j, \mathbf{v}_i) + \mathfrak{v}_i^*\widetilde{\mathfrak{V}}_0^*\mathfrak{U}_{01}\mathfrak{u}_j, \quad G_{ij} = (\mathbf{L}_{10}\mathbf{u}_j, \mathbf{v}_i) + \mathfrak{v}_i^*\widetilde{\mathfrak{V}}_0^*\,\mathfrak{U}_{10}\,\mathfrak{u}_j. \tag{7.30}$$

Therefore, in the first approximation the splitting of the semisimple eigenvalue due to variation of parameters $\mathbf{p}(\varepsilon)$ is $\lambda = \lambda_0 + \varepsilon\lambda_1 + o(\varepsilon)$, where the coefficients λ_1 are generically μ distinct roots of the μ-th order polynomial

$$\det(\mathbf{F} + \lambda_1\mathbf{G}) = 0. \tag{7.31}$$

When $\mu = 1$ the equation (7.31) describes perturbation of a simple eigenvalue

$$\lambda = \lambda_0 - \varepsilon\frac{(\mathbf{L}_{01}\mathbf{u}_0, \mathbf{v}_0) + \mathfrak{v}_0^*\widetilde{\mathfrak{V}}_0^*\mathfrak{U}_{01}\mathfrak{u}_0}{(\mathbf{L}_{10}\mathbf{u}_0, \mathbf{v}_0) + \mathfrak{v}_0^*\widetilde{\mathfrak{V}}_0^*\,\mathfrak{U}_{10}\,\mathfrak{u}_0} + o(\varepsilon). \tag{7.32}$$

The formulas (7.30), (7.31), and (7.32) generalize the corresponding results of the works [155, 277, 347, 561] to the case of the multiparameter nonself-adjoint boundary eigenvalue problems for operator matrices.

7.2.2 Multiple eigenvalues with the Keldysh chain

Let at the point $\mathbf{p} = \mathbf{p}_0$ the spectrum contain a μ-fold eigenvalue λ_0 with the *Keldysh chain* of length μ, consisting of the eigenvector $\mathbf{u}_0(x)$ and the associated vectors $\mathbf{u}_1(x), \ldots, \mathbf{u}_{\mu-1}(x)$ that solve the boundary value problems [421, 442]

$$\mathbf{L}_0\mathbf{u}_0 = 0, \quad \mathfrak{U}_0\mathbf{u}_0 = 0, \tag{7.33}$$

$$\mathbf{L}_0\mathbf{u}_j = -\sum_{r=1}^{j}\frac{1}{r!}\partial_\lambda^r\mathbf{L}\mathbf{u}_{j-r}, \quad \mathfrak{U}_0\mathbf{u}_j = -\sum_{r=1}^{j}\frac{1}{r!}\partial_\lambda^r\mathfrak{U}\mathbf{u}_{j-r}. \tag{7.34}$$

The eigenvalue λ_0 is referred to as nonderogatory in [428].

Consider vector functions $\mathbf{v}_0(x), \mathbf{v}_1(x), \ldots, \mathbf{v}_{\mu-1}(x)$. Let us take the scalar product of the differential equation (7.33) and the vector function $\mathbf{v}_{\mu-1}(x)$. For each $j = 1, \ldots, \mu-2$ we take the scalar product of the equation (7.34) and the vector function $\mathbf{v}_{\mu-1-j}(x)$. Summation of the results yields the expression

$$\sum_{j=0}^{\mu-1}\sum_{r=0}^{j}\frac{1}{r!}(\partial_\lambda^r\mathbf{L}\mathbf{u}_{j-r}, \mathbf{v}_{\mu-1-j}) = 0. \tag{7.35}$$

Applying the Lagrange identity (7.6) and taking into account the relations (7.14) and (7.16), we transform equation (7.35) to the form

$$\sum_{j=0}^{\mu-1}\left(\mathbf{u}_{\mu-1-j}, \sum_{r=0}^{j}\frac{1}{r!}\partial_{\bar\lambda}^r\mathbf{L}^\dagger\mathbf{v}_{j-r}\right) + \sum_{k=0}^{\mu-1}\sum_{j=0}^{\mu-1-k}\left[\sum_{r=0}^{j}\left(\frac{1}{r!}\partial_{\bar\lambda}^r\mathfrak{V}\mathrm{v}_{j-r}\right)^*\right]\frac{\partial_\lambda^k\widetilde{\mathfrak{U}}}{k!}\mathrm{u}_{\mu-1-j-k} = 0. \tag{7.36}$$

Equation (7.36) is satisfied in the case when the vector functions $\mathbf{v}_0(x)$, $\mathbf{v}_1(x)$, …, $\mathbf{v}_{\mu-1}(x)$ originate the Keldysh chain of the adjoint boundary value problem, corresponding to the μ-fold eigenvalue $\bar\lambda_0$ [280, 282]

$$\mathbf{L}_0^\dagger\mathbf{v}_0 = 0, \quad \mathfrak{V}_0\mathrm{v}_0 = 0, \tag{7.37}$$

$$\mathbf{L}_0^\dagger\mathbf{v}_j = -\sum_{r=1}^{j}\frac{1}{r!}\partial_{\bar\lambda}^r\mathbf{L}^\dagger\mathbf{v}_{j-r}, \quad \mathfrak{V}_0\mathrm{v}_j = -\sum_{r=1}^{j}\frac{1}{r!}\partial_{\bar\lambda}^r\mathfrak{V}\mathrm{v}_{j-r}. \tag{7.38}$$

Taking the scalar product of equation (7.34) and the vector $\mathbf{v}_0$ and employing the expressions (7.6) and (7.14) we arrive at the orthogonality conditions

$$\sum_{r=1}^{j}\frac{1}{r!}\left[(\partial_\lambda^r\mathbf{L}\mathbf{u}_{j-r}, \mathbf{v}_0) + \mathrm{v}_0^*\widetilde{\mathfrak{V}}_0^*\partial_\lambda^r\mathfrak{U}\mathrm{u}_{j-r}\right] = 0, \quad j = 1, \ldots, \mu-1. \tag{7.39}$$

When $\mu = 2$, the conditions (7.39) are reduced to the unique one

$$(\partial_\lambda \mathbf{L}\mathbf{u}_0, \mathbf{v}_0) + \mathrm{v}_0^* \widetilde{\mathfrak{V}}_0^* \partial_\lambda \mathfrak{U} \mathrm{u}_0 = 0. \tag{7.40}$$

Since the double eigenvalues with the geometric multiplicity 1 frequently correspond to the threshold of oscillatory instability (flutter), the orthogonality condition (7.40) can serve as an indicator of the flutter boundary, e.g. in circulatory systems [277, 473, 474]. Such a *flutter condition*[2] that could be easily verified is especially important in aeroelasticity where this was first emphasized by Plaut [479] who, however, did not take into account a possibility of variation of the boundary conditions. Plaut's derivation was based on the idea that the first derivative of the nonconservative load with respect to the spectral parameter λ becomes zero at the onset of flutter. In our approach, the flutter condition (7.40) is just a consequence of the existence of the Keldysh chain of length 2 at a double eigenvalue λ_0. Hence, this condition is satisfied at the flutter boundary of a multiparameter circulatory system and applies to a much wider class of the nonself-adjoint boundary eigenvalue problems with the boundary conditions containing both the spectral parameter λ and the physical parameters $\mathbf{p}$, see e.g. [307, 473, 474, 604].

Substituting into equations (7.1) the *Newton–Puiseux series* for the perturbed eigenvalue $\lambda(\varepsilon)$ and eigenvector $\mathbf{u}(\varepsilon)$ [155, 277, 584]

$$\lambda = \lambda_0 + \lambda_1 \varepsilon^{1/\mu} + \cdots, \quad \mathbf{u} = \mathbf{w}_0 + \mathbf{w}_1 \varepsilon^{1/\mu} + \cdots, \tag{7.41}$$

where $\mathbf{w}_0 = \mathbf{u}_0$, taking into account expansions (7.18) and (7.41), and collecting terms with the same powers of ε, yields $\mu - 1$ boundary value problems serving for determining the functions $\mathbf{w}_r$, $r = 1, 2, \ldots, \mu - 1$

$$\mathbf{L}_0 \mathbf{w}_r = -\sum_{j=0}^{r-1} \Bigg(\sum_{\sigma=1}^{r-j} \frac{1}{\sigma!} \mathbf{L}_{\sigma 0} \sum_{|\alpha|_\sigma = r-j} \lambda_{\alpha_1} \cdots \lambda_{\alpha_\sigma} \Bigg) \mathbf{w}_j, \tag{7.42}$$

$$\mathfrak{U}_0 \mathrm{w}_r = -\sum_{j=0}^{r-1} \sum_{\sigma=1}^{r-j} \Bigg(\sum_{|\alpha|_\sigma = r-j} \lambda_{\alpha_1} \cdots \lambda_{\alpha_\sigma} \Bigg) \frac{1}{\sigma!} \mathfrak{U}_{\sigma 0} \mathrm{w}_j, \tag{7.43}$$

where $|\alpha|_\sigma = \alpha_1 + \ldots + \alpha_\sigma$ and $\alpha_1, \ldots, \alpha_{\mu-1}$ are positive integers. For the existence and convergence of expansions (7.41) one can consult the work [584].

The vector function $\mathbf{w}_\mu(x)$ is a solution of the boundary value problem

$$\mathbf{L}_0 \mathbf{w}_\mu = -\mathbf{L}_{01} \mathbf{w}_0 - \sum_{j=0}^{\mu-1} \Bigg(\sum_{\sigma=1}^{\mu-j} \frac{1}{\sigma!} \mathbf{L}_{\sigma 0} \sum_{|\alpha|_\sigma = \mu-j} \lambda_{\alpha_1} \cdots \lambda_{\alpha_\sigma} \Bigg) \mathbf{w}_j, \tag{7.44}$$

[2] An inverse to the quantity in the left-hand side of equation (7.40) is known also as a *condition number* of an eigenvalue [7].

$$\mathcal{U}_0 \mathrm{w}_\mu = -\mathcal{U}_{01}\mathrm{w}_0 - \sum_{j=0}^{\mu-1}\sum_{\sigma=1}^{\mu-j}\Bigg(\sum_{|\alpha|_\sigma=\mu-j}\lambda_{\alpha_1}\cdots\lambda_{\alpha_\sigma}\Bigg)\frac{1}{\sigma!}\mathcal{U}_{\sigma 0}\mathrm{w}_j. \tag{7.45}$$

Comparing equations (7.44) and (7.45) with the expressions (7.34) we find the first $\mu-1$ functions $\mathbf{w}_r$ in the expansions (7.41)

$$\mathbf{w}_r = \sum_{j=1}^{r}\mathbf{u}_j \sum_{|\alpha|_j=r}\lambda_{\alpha_1}\ldots\lambda_{\alpha_j}. \tag{7.46}$$

With the vectors (7.46) we transform the equations (7.44) and (7.45) into

$$\mathbf{L}_0\mathbf{w}_\mu = -\mathbf{L}_{01}\mathbf{u}_0 - \lambda_1^\mu\sum_{r=1}^{\mu}\frac{1}{r!}\partial_\lambda^r\mathbf{L}\mathbf{u}_{\mu-r} + \sum_{j=1}^{\mu-1}\mathbf{L}_0\mathbf{u}_j\sum_{|\alpha|_j=\mu}\lambda_{\alpha_1}\ldots\lambda_{\alpha_j}, \tag{7.47}$$

$$\mathcal{U}_0\mathrm{w}_\mu = -\mathcal{U}_1\mathrm{u}_0 - \lambda_1^\mu\sum_{r=1}^{\mu}\frac{1}{r!}\partial_\lambda^r\mathcal{U}\mathrm{u}_{\mu-r} + \sum_{j=1}^{\mu-1}\mathcal{U}_0\mathrm{u}_j\sum_{|\alpha|_j=\mu}\lambda_{\alpha_1}\ldots\lambda_{\alpha_j}. \tag{7.48}$$

Applying the expression following from the Lagrange formula

$$\begin{aligned}(\mathbf{L}_0\mathbf{w}_\mu,\mathbf{v}_0) = {}& \mathrm{v}_0^*\widetilde{\mathfrak{V}}_0^*\mathcal{U}_{01}\mathrm{u}_0 + \lambda_1^\mu\sum_{r=1}^{\mu}\frac{1}{r!}\mathrm{v}_0^*\widetilde{\mathfrak{V}}_0^*\mathcal{U}_{r0}\mathrm{u}_{\mu-r}\\ & - \sum_{j=1}^{\mu-1}\mathrm{v}_0^*\widetilde{\mathfrak{V}}_0^*\mathcal{U}_0\mathrm{u}_j\sum_{|\alpha|_j=\mu}\lambda_{\alpha_1}\ldots\lambda_{\alpha_j},\end{aligned} \tag{7.49}$$

and taking into account the equations for the adjoint Keldysh chain (7.37) and (7.38) yields the coefficient λ_1 in (7.41).

Hence, the splitting of the μ-fold nonderogatory eigenvalue λ_0 due to perturbation of the parameters $\mathbf{p} = \mathbf{p}(\varepsilon)$ is described by the following expression, generalizing the results of the works [155, 277, 280, 282]

$$\lambda = \lambda_0 + \sqrt[\mu]{-\varepsilon\frac{(\mathbf{L}_{01}\mathbf{u}_0,\mathbf{v}_0) + \mathrm{v}_0^*\widetilde{\mathfrak{V}}_0^*\mathcal{U}_{01}\mathrm{u}_0}{\sum_{r=1}^{\mu}\frac{1}{r!}\left((\mathbf{L}_{r0}\mathbf{u}_{\mu-r},\mathbf{v}_0) + \mathrm{v}_0^*\widetilde{\mathfrak{V}}_0^*\mathcal{U}_{r0}\mathrm{u}_{\mu-r}\right)}} + o(\varepsilon^{\frac{1}{\mu}}). \tag{7.50}$$

For $\mu = 1$ equation (7.50) is reduced to equation (7.32) for a simple eigenvalue.

7.2.3 Higher order perturbation terms for double nonderogatory eigenvalues

For a double ($\mu = 2$) nonderogatory eigenvalue we will derive the next order perturbation term with respect to that given by equation (7.50). With the expansions (7.18)

and (7.41) the eigenvalue problem (7.1) yields the following equations and boundary conditions for the functions $\mathbf{w}_1$, $\mathbf{w}_2$, and $\mathbf{w}_3$

$$\mathbf{L}_0\mathbf{w}_1 = -\lambda_1\mathbf{L}_{10}\mathbf{u}_0, \quad \mathfrak{U}_0\mathbf{w}_1 = -\lambda_1\mathfrak{U}_{10}u_0, \tag{7.51}$$

$$\begin{aligned}\mathbf{L}_0\mathbf{w}_2 &= -\lambda_1\mathbf{L}_{10}\mathbf{w}_1 - \lambda_2\mathbf{L}_{10}u_0 - \mathbf{L}_{01}\mathbf{u}_0 - \frac{\lambda_1^2}{2!}\mathbf{L}_{20}\mathbf{u}_0,\\ \mathfrak{U}_0\mathbf{w}_2 &= -\lambda_1\mathfrak{U}_{10}\mathbf{w}_1 - \lambda_2\mathfrak{U}_{10}u_0 - \mathfrak{U}_{01}u_0 - \frac{\lambda_1^2}{2!}\mathfrak{U}_{20}u_0,\end{aligned} \tag{7.52}$$

$$\begin{aligned}\mathbf{L}_0\mathbf{w}_3 &= -\lambda_1\mathbf{L}_{10}\mathbf{w}_2 - \left(\mathbf{L}_{01} + \lambda_2\mathbf{L}_{10} + \frac{\lambda_1^2}{2!}\mathbf{L}_{20}\right)\mathbf{w}_1\\ &\quad - \left(\lambda_1\mathbf{L}_{11} + \lambda_3\mathbf{L}_{10} + \lambda_1\lambda_2\mathbf{L}_{20} + \frac{\lambda_1^3}{3!}\mathbf{L}_{30}\right)\mathbf{u}_0,\\ \mathfrak{U}_0\mathbf{w}_3 &= -\lambda_1\mathfrak{U}_{10}\mathbf{w}_2 - \left(\mathfrak{U}_{01} + \lambda_2\mathfrak{U}_{10} + \frac{\lambda_1^2}{2!}\mathfrak{U}_{20}\right)\mathbf{w}_1\\ &\quad - \left(\lambda_1\mathfrak{U}_{11} + \lambda_3\mathfrak{U}_{10} + \lambda_1\lambda_2\mathfrak{U}_{20} + \frac{\lambda_1^3}{3!}\mathfrak{U}_{30}\right)u_0.\end{aligned} \tag{7.53}$$

From equations (7.51) it follows that the function $\mathbf{w}_1$ is

$$\mathbf{w}_1 = \lambda_1\mathbf{u}_1 + \gamma\mathbf{u}_0, \tag{7.54}$$

where γ is an arbitrary constant. The coefficient λ_1 follows from equation (7.50) as

$$\lambda_1^2 = -\frac{(\mathbf{L}_{01}\mathbf{u}_0, \mathbf{v}_0) + \ v_0^*\widetilde{\mathfrak{V}}_0^*\mathfrak{U}_{01}u_0}{\sum_{r=1}^{2}\frac{1}{r!}\left((\mathbf{L}_{r0}\mathbf{u}_{2-r}, \mathbf{v}_0) + \ v_0^*\widetilde{\mathfrak{V}}_0^*\mathfrak{U}_{r0}u_{2-r}\right)}. \tag{7.55}$$

Evaluating the scalar product of equation (7.53) and the vector $\mathbf{v}_0$ and then using the Lagrange formula (7.6) and the expression (7.54), we obtain

$$\begin{aligned}&\gamma\frac{\lambda_1^2}{2}\big((\mathbf{L}_{20}\mathbf{u}_0, \mathbf{v}_0) + (\widetilde{\mathfrak{V}}_0v_0)^*\mathfrak{U}_{20}u_0\big) + \lambda_1\big((\mathbf{L}_{10}\mathbf{w}_2, \mathbf{v}_0) + (\widetilde{\mathfrak{V}}_0v_0)^*\mathfrak{U}_{10}\mathbf{w}_2\big)\\ &\quad + \gamma\big((\mathbf{L}_{01}\mathbf{u}_0, \mathbf{v}_0) + (\widetilde{\mathfrak{V}}_0v_0)^*\mathfrak{U}_1u_0\big)\\ &\quad + \lambda_1\big((\mathbf{L}_{01}\mathbf{u}_1 + \mathbf{L}_{11}\mathbf{u}_0, \mathbf{v}_0) + (\widetilde{\mathfrak{V}}_0v_0)^*(\mathfrak{U}_{01}u_1 + \mathfrak{U}_{11}u_0)\big)\\ &\quad + \lambda_1^3\Big(\Big(\frac{1}{2!}\mathbf{L}_{20}\mathbf{u}_1 + \frac{1}{3!}\mathbf{L}_{30}\mathbf{u}_0, \mathbf{v}_0\Big) + (\widetilde{\mathfrak{V}}_0v_0)^*\Big(\frac{1}{2!}\mathfrak{U}_{20}u_1 + \frac{1}{3!}\mathfrak{U}_{30}u_0\Big)\Big)\\ &\quad + \lambda_1\lambda_2\big((\mathbf{L}_{10}\mathbf{u}_1 + \mathbf{L}_{20}\mathbf{u}_0, \mathbf{v}_0) + (\widetilde{\mathfrak{V}}_0v_0)^*(\mathfrak{U}_{10}u_1 + \mathfrak{U}_{20}u_0)\big) = 0.\end{aligned} \tag{7.56}$$

The scalar product of equation (7.52) and the vector $\mathbf{v}_1$ after taking into account the Lagrange formula (7.6) and expressions (7.14) and (7.16) yields

$$\begin{aligned}&(\mathbf{L}_{10}\mathbf{w}_2, \mathbf{v}_0) + (\widetilde{\mathfrak{V}}_0v_0)^*\mathfrak{U}_{10}\mathbf{w}_2 =\\ &\quad - (\widetilde{\mathfrak{V}}_0v_1 + \widetilde{\mathfrak{V}}_{\bar{\lambda}}^{(1)}v_0)^*\mathfrak{U}_0\mathbf{w}_2 + \lambda_1^2(\mathbf{L}_{10}\mathbf{u}_1, \mathbf{v}_1)\\ &\quad + \gamma\lambda_1(\mathbf{L}_{10}\mathbf{u}_0, \mathbf{v}_1) + (\mathbf{L}_{01}\mathbf{u}_0, \mathbf{v}_1) + \lambda_2(\mathbf{L}_{10}\mathbf{u}_0, \mathbf{v}_1) + \frac{\lambda_1^2}{2}(\mathbf{L}_{20}\mathbf{u}_0, \mathbf{v}_1).\end{aligned} \tag{7.57}$$

In addition, we have the identity

$$(\mathbf{L}_{10}\mathbf{u}_0, \mathbf{v}_1) + (\widetilde{\mathfrak{V}}_0 v_1 + \widetilde{\mathfrak{V}}^{(1)}_{\lambda} \mathbf{v}_0)^* \mathcal{U}_{10} u_0 = (\mathbf{L}_{10}\mathbf{u}_1, \mathbf{v}_0) + (\widetilde{\mathfrak{V}}_0 v_0)^* \mathcal{U}_{10} u_1 \quad (7.58)$$

that follows from equations (7.33) and (7.34) and equations (7.37) and (7.38).

Using relations (7.55), (7.57) and (7.58) we deduce from equation (7.56) that

$$\lambda_2 = -\frac{(\mathbf{L}_{01}\mathbf{u}_0, \mathbf{v}_1) + (\mathbf{L}_{01}\mathbf{u}_1, \mathbf{v}_0) + (\mathbf{L}_{11}\mathbf{u}_0, \mathbf{v}_0)}{2\sum_{r=1}^{2} \frac{1}{r!}\big((\mathbf{L}_{r0}\mathbf{u}_{2-r}, \mathbf{v}_0) + \ v_0^* \widetilde{\mathfrak{V}}_0^* \mathcal{U}_{r0} u_{2-r}\big)}$$

$$- \frac{v_1^* \widetilde{\mathfrak{V}}_0^* \mathcal{U}_{01} u_0 + v_0^* \widetilde{\mathfrak{V}}_0^* \mathcal{U}_{01} u_1 + v_0^* (\widetilde{\mathfrak{V}}^* \mathcal{U}_1)^{(1)}_{\lambda} u_0 + \lambda_1^2 Q}{2\sum_{r=1}^{2} \frac{1}{r!}\big((\mathbf{L}_{r0}\mathbf{u}_{2-r}, \mathbf{v}_0) + \ v_0^* \widetilde{\mathfrak{V}}_0^* \mathcal{U}_{r0} u_{2-r}\big)}, \quad (7.59)$$

where

$$Q = (\mathbf{L}_{10}\mathbf{u}_1, \mathbf{v}_1) + \frac{1}{2!}(\mathbf{L}_{20}\mathbf{u}_0, \mathbf{v}_1) + \frac{1}{2!}(\mathbf{L}_{20}\mathbf{u}_1, \mathbf{v}_0) + \frac{1}{3!}(\mathbf{L}_{30}\mathbf{u}_0, \mathbf{v}_0) \quad (7.60)$$
$$+ \Big(\widetilde{\mathfrak{V}}_0 v_1 + \widetilde{\mathfrak{V}}^{(1)}_{\lambda} v_0\Big)^* \Big(\mathcal{U}_{10} u_1 + \frac{1}{2!}\mathcal{U}_{20} u_0\Big) + (\widetilde{\mathfrak{V}}_0 v_0)^* \Big(\frac{1}{2!}\mathcal{U}_{20} u_1 + \frac{1}{3!}\mathcal{U}_{30} u_0\Big).$$

7.2.4 Degenerate splitting of double nonderogatory eigenvalues

Generally, bifurcation of an eigenvalue λ_0 with the algebraic multiplicity $\mu = 2$ and geometric multiplicity 1 is described by equation (7.50). Let us study the case when equation (7.50) degenerates, i.e. when

$$(\mathbf{L}_{01}\mathbf{u}_0, \mathbf{v}_0) + \ v_0^* \widetilde{\mathfrak{V}}_0^* \mathcal{U}_{01} u_0 = 0. \quad (7.61)$$

The degeneracy condition (7.61) is equivalent to the vanishing coefficient λ_1 in the expansions (7.41). Substituting them together with equations (7.18) into the eigenvalue problem (7.1) yields the boundary value problems

$$\mathbf{L}_0 \mathbf{w}_1 = 0, \ \ \mathcal{U}_0 w_1 = 0, \quad (7.62)$$

$$\mathbf{L}_0 \mathbf{w}_2 = -\lambda_2 \mathbf{L}_{10}\mathbf{u}_0 - \mathbf{L}_{01}\mathbf{u}_0, \ \ \mathcal{U}_0 w_2 = -\lambda_2 \mathcal{U}_{10} u_0 - \mathcal{U}_{01} u_0, \quad (7.63)$$

$$\mathbf{L}_0 \mathbf{w}_4 = -\lambda_3 \mathbf{L}_{10}\mathbf{w}_1 - \lambda_2 \mathbf{L}_{10}\mathbf{w}_2 - \mathbf{L}_{01}\mathbf{w}_2 - \lambda_2 \mathbf{L}_{11}\mathbf{u}_0 - \lambda_2^2 \frac{1}{2}\mathbf{L}_{20}\mathbf{u}_0 - \lambda_4 \mathbf{L}_{10}\mathbf{u}_0 - \mathbf{L}_{02}\mathbf{u}_0, \quad (7.64)$$

$$\mathcal{U}_0 w_4 = -\lambda_3 \mathcal{U}_{10} w_1 - \lambda_2 \mathcal{U}_{10} w_2 - \mathcal{U}_{01} w_2 - \lambda_2 \mathcal{U}_{11} u_0 - \lambda_2^2 \frac{1}{2}\mathcal{U}_{20} u_0 - \lambda_4 \mathcal{U}_{10} u_0 - \mathcal{U}_{02} u_0. \quad (7.65)$$

Solving equations (7.62) and (7.63), we obtain

$$\mathbf{w}_1 = \beta \mathbf{u}_0, \quad \mathbf{w}_2 = \lambda_2 \mathbf{u}_1 + \gamma \mathbf{u}_0 + \hat{\mathbf{w}}_2, \quad (7.66)$$

where β and γ are arbitrary constants, the function $\hat{\mathbf{w}}_2$ is a solution of the boundary value problem

$$\mathbf{L}_0 \hat{\mathbf{w}}_2 = -\mathbf{L}_{01}\mathbf{u}_0, \ \ \mathcal{U}_0 \hat{w}_2 = -\mathcal{U}_{01} u_0 \quad (7.67)$$

and $\hat{w}_2^T = (\hat{\mathbf{w}}_2^T(0), \hat{\mathbf{w}}_{2,x}^{(1)T}(0), \dots, \hat{\mathbf{w}}_{2,x}^{(m-1)T}(0), \hat{\mathbf{w}}_2^T(1), \hat{\mathbf{w}}_{2,x}^{(1)T}(1), \dots, \hat{\mathbf{w}}_{2,x}^{(m-1)T}(1))$.

The scalar product of equation (7.63) and the function $\mathbf{v}_1$ after taking into account the Lagrange formula (7.6) and expressions (7.14) and (10.19), yields

$$(\mathbf{L}_{10}\mathbf{w}_2, \mathbf{v}_0) + (\widetilde{\mathfrak{V}}_0\mathfrak{v}_0)^*\mathfrak{U}_{10}\mathfrak{w}_2 = -\left(\widetilde{\mathfrak{V}}_0\mathfrak{v}_1 + \widetilde{\mathfrak{V}}_{\tilde{\lambda}}^{(1)}\mathfrak{v}_0\right)^*\mathfrak{U}_0\mathfrak{w}_2 + \lambda_2(\mathbf{L}_{10}\mathbf{u}_0, \mathbf{v}_1) + (\mathbf{L}_{01}\mathbf{u}_0, \mathbf{v}_1). \tag{7.68}$$

Similarly, taking the scalar product of equation (7.64) and the function $\mathbf{v}_0$, then using the Lagrange formula (7.6), the orthogonality condition (7.40), the boundary conditions (7.65), and the expressions (7.37) and (7.66), we obtain

$$\begin{aligned}&\lambda_2\left((\mathbf{L}_{10}\mathbf{w}_2, \mathbf{v}_0) + (\widetilde{\mathfrak{V}}_0\mathfrak{v}_0)^*\mathfrak{U}_{10}\mathfrak{w}_2\right) + (\mathbf{L}_{01}\mathbf{w}_2, \mathbf{v}_0) + (\widetilde{\mathfrak{V}}_0\mathfrak{v}_0)^*\mathfrak{U}_{01}\mathfrak{w}_2 \\ &+(\mathbf{L}_{02}\mathbf{u}_0, \mathbf{v}_0) + (\widetilde{\mathfrak{V}}_0\mathfrak{v}_0)^*\mathfrak{U}_{02}\mathfrak{u}_0 + \lambda_2\left((\mathbf{L}_{11}\mathbf{u}_0, \mathbf{v}_0) + (\widetilde{\mathfrak{V}}_0\mathfrak{v}_0)^*\mathfrak{U}_{11}\mathfrak{u}_0\right) \\ &+\frac{1}{2}\lambda_2^2\left((\mathbf{L}_{20}\mathbf{u}_0, \mathbf{v}_0) + (\widetilde{\mathfrak{V}}_0\mathfrak{v}_0)^*\mathfrak{U}_{20}\mathfrak{u}_0\right) = 0.\end{aligned} \tag{7.69}$$

After substituting the expression (7.68) into equation (7.69) and using the identity (7.58) as well as the degeneration condition (7.61), the boundary conditions (7.63), and expressions (7.66), the equation (7.69) takes the form

$$\begin{aligned}&\lambda_2^2 + \lambda_2\frac{(\mathbf{L}_{01}\mathbf{u}_0, \mathbf{v}_1) + (\mathbf{L}_{01}\mathbf{u}_1, \mathbf{v}_0) + (\mathbf{L}_{11}\mathbf{u}_0, \mathbf{v}_0)}{\sum_{r=1}^{2}\frac{1}{r!}\left((\mathbf{L}_{r0}\mathbf{u}_{2-r}, \mathbf{v}_0) + \mathfrak{v}_0^*\widetilde{\mathfrak{V}}_0^*\mathfrak{U}_{r0}\mathfrak{u}_{2-r}\right)} \\ &+\lambda_2\frac{\mathfrak{v}_1^*\widetilde{\mathfrak{V}}_0^*\mathfrak{U}_{01}\mathfrak{u}_0 + \mathfrak{v}_0^*\widetilde{\mathfrak{V}}_0^*\mathfrak{U}_{01}\mathfrak{u}_1 + \mathfrak{v}_0^*\widetilde{\mathfrak{V}}_0^*\mathfrak{U}_{11}\mathfrak{u}_0 + \left(\widetilde{\mathfrak{V}}_{\tilde{\lambda}}^{(1)}\mathfrak{v}_0\right)^*\mathfrak{U}_{01}\mathfrak{u}_0}{\sum_{r=1}^{2}\frac{1}{r!}\left((\mathbf{L}_{r0}\mathbf{u}_{2-r}, \mathbf{v}_0) + \mathfrak{v}_0^*\widetilde{\mathfrak{V}}_0^*\mathfrak{U}_{r0}\mathfrak{u}_{2-r}\right)} \\ &+\frac{(\mathbf{L}_{02}\mathbf{u}_0, \mathbf{v}_0) + (\mathbf{L}_{01}\hat{\mathbf{w}}_2, \mathbf{v}_0) + (\widetilde{\mathfrak{V}}_0\mathfrak{v}_0)^*(\mathfrak{U}_{02}\mathfrak{u}_0 + \mathfrak{U}_{01}\hat{\mathfrak{w}}_2)}{\sum_{r=1}^{2}\frac{1}{r!}\left((\mathbf{L}_{r0}\mathbf{u}_{2-r}, \mathbf{v}_0) + \mathfrak{v}_0^*\widetilde{\mathfrak{V}}_0^*\mathfrak{U}_{r0}\mathfrak{u}_{2-r}\right)} = 0.\end{aligned} \tag{7.70}$$

When the boundary conditions do not depend on the parameters or the operator $\mathbf{L}$ is a matrix, the formula (7.70) is simplified [285, 288]

$$\lambda_2^2 + \lambda_2\frac{(\mathbf{L}_{01}\mathbf{u}_0, \mathbf{v}_1) + (\mathbf{L}_{01}\mathbf{u}_1, \mathbf{v}_0) + (\mathbf{L}_{11}\mathbf{u}_0, \mathbf{v}_0)}{(\mathbf{L}_{10}\mathbf{u}_1, \mathbf{v}_0) + \frac{1}{2}(\mathbf{L}_{20}\mathbf{u}_0, \mathbf{v}_0)} + \frac{(\mathbf{L}_2\mathbf{u}_0, \mathbf{v}_0) + (\mathbf{L}_{01}\hat{\mathbf{w}}_2, \mathbf{v}_0)}{(\mathbf{L}_{10}\mathbf{u}_1, \mathbf{v}_0) + \frac{1}{2}(\mathbf{L}_{20}\mathbf{u}_0, \mathbf{v}_0)} = 0. \tag{7.71}$$

Thus, the expansion $\lambda = \lambda_0 + \varepsilon\lambda_2 + o(\varepsilon)$ with the quadratic equation (7.70), generalizing the results of the works [277, 282], describes unfolding of the double eigenvalue in the degenerate case (7.61).

7.3 Example: a rotating circular string with an elastic restraint

Consider a circular string of displacement $W(\psi,\tau)$, radius r, and mass per unit length ρ that rotates with the speed γ and passes at $\psi = 0$ through a massless eyelet supported by the spring with the stiffness K, as shown in Figure 7.1 (a). Introducing the nondimensional variables and parameters

$$t = \frac{\tau}{r}\sqrt{\frac{P}{\rho}}, \quad w = \frac{W}{r}, \quad \Omega = \gamma r\sqrt{\frac{\rho}{P}}, \quad k = \frac{Kr}{P}, \quad \varphi = \frac{\psi}{2\pi}, \tag{7.72}$$

and assuming $w(\varphi,t) = u(\varphi)\exp(\lambda t)$ we arrive at the nonself-adjoint boundary eigenvalue problem for a matrix ($N = 2, m = 1$) differential operator [604]

$$\mathbf{Lu} := \mathbf{l}_0\partial_\varphi\mathbf{u} + \mathbf{l}_1\mathbf{u} = 0, \quad \mathfrak{U}u := [\mathfrak{A},\mathfrak{B}]u = 0, \tag{7.73}$$

where

$$\mathbf{l}_0 = \begin{pmatrix} 1 & 0 \\ 0 & 1-\Omega^2 \end{pmatrix}, \quad \mathbf{l}_1 = -\begin{pmatrix} 0 & 1 \\ 4\pi^2\lambda^2 & 4\pi\Omega\lambda \end{pmatrix}, \tag{7.74}$$

$$\mathfrak{A} = \begin{pmatrix} 1 & 0 \\ \frac{2\pi k}{\Omega^2-1} & 1 \end{pmatrix}, \quad \mathfrak{B} = -\begin{pmatrix} 1 & 0 \\ 0 & 1 \end{pmatrix}. \tag{7.75}$$

The parameters Ω and k expressing the speed of rotation and the stiffness coefficient of the support of the eyelet are contained both in the differential expression and in the boundary conditions.

With $\mathbf{u} = C_1(1, \frac{2\pi\lambda}{1-\Omega})^T \exp(\frac{2\pi\varphi\lambda}{1-\Omega}) + C_2(1, -\frac{2\pi\lambda}{1+\Omega})^T \exp(-\frac{2\pi\varphi\lambda}{1+\Omega})$ assumed as a solution to the equation $\mathbf{Lu} = 0$, the characteristic equation follows from the boundary conditions $[\mathfrak{A},\mathfrak{B}]u = 0$

$$k\sinh\frac{2\pi\lambda}{1-\Omega^2} - 4\lambda\sin\frac{\pi\lambda}{i(1-\Omega)}\sin\frac{\pi\lambda}{i(1+\Omega)} = 0, \tag{7.76}$$

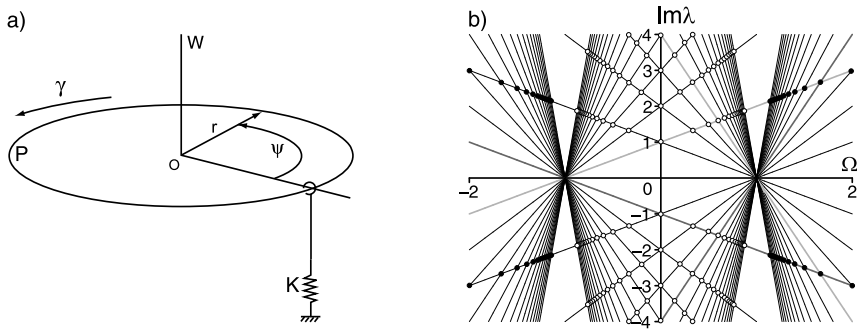

Figure 7.1. (a) A rotating circular string passing through an elastically supported eyelet and (b) first 30 modes of its spectral mesh [293, 298].

and the relation between the coefficients C_1 and C_2 of the eigenvector $\mathbf{u}$

$$(1 - e^{-\frac{2\lambda\pi}{\Omega-1}})C_1 + (1 - e^{-\frac{2\lambda\pi}{\Omega+1}})C_2 = 0. \tag{7.77}$$

For the unconstrained rotating string with $k = 0$, the eigenvectors $\mathbf{v}$ and $\mathbf{u}$ of the adjoint problems corresponding to purely imaginary eigenvalue λ and $\bar{\lambda}$ coincide. The eigenvalues $\lambda_n^{\pm} = in(1 \pm \Omega)$, $n \in \mathbb{Z}$, form the spectral mesh in the plane $(\Omega, \mathrm{Im}\lambda)$, see Figure 7.1 (b) and Figure 7.2 (a). The lines

$$\lambda_n^{\varepsilon} = in(1 + \varepsilon\Omega), \quad \lambda_m^{\delta} = im(1 + \delta\Omega), \tag{7.78}$$

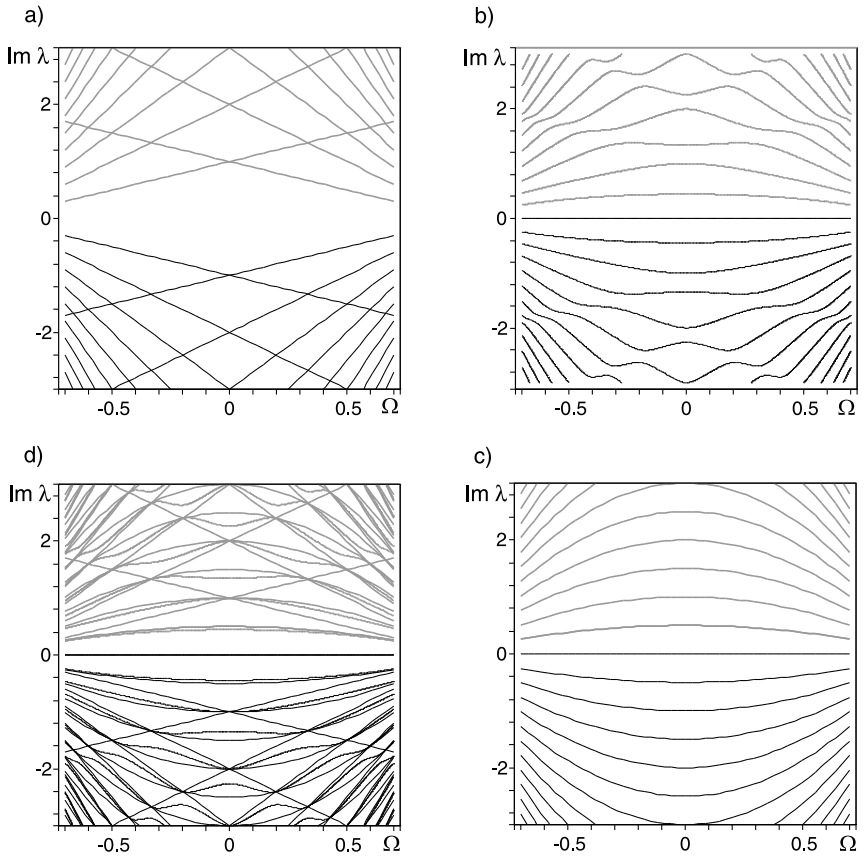

Figure 7.2. In the subcritical range $|\Omega| < 1$ the eigencurves of the rotating circular string form (a) a spectral mesh when the stiffness constraint is absent ($k = 0$). (b) The mesh deforms into separated eigencurves when $k \neq 0$ ($k = 5$). (c) The eigencurves tend to the parabolas (7.81) when the eyelet is rigid ($k \to \infty$). (d) Combined view.

where $\varepsilon, \delta = \pm$, intersect each other at the node $(\Omega_{nm}^{\varepsilon\delta}, \lambda_{nm}^{\varepsilon\delta})$ with[3]

$$\Omega_{nm}^{\varepsilon\delta} = \frac{n-m}{m\delta - n\varepsilon}, \quad \lambda_{nm}^{\varepsilon\delta} = \frac{inm(\delta 1 - \varepsilon 1)}{m\delta - n\varepsilon}, \tag{7.79}$$

where the double eigenvalue $\lambda_{nm}^{\varepsilon\delta}$ has two orthogonal eigenvectors

$$\mathbf{u}_n^{\varepsilon} = \begin{pmatrix} 1 \\ -i\varepsilon 2\pi n \end{pmatrix} e^{-i\varepsilon 2\pi n\varphi}, \quad \mathbf{u}_m^{\delta} = \begin{pmatrix} 1 \\ -i\delta 2\pi m \end{pmatrix} e^{-i\delta 2\pi m\varphi}. \tag{7.80}$$

For a rigid eyelet $k \to \infty$ and the roots of equation (7.76) determine parabolic eigencurves [476]

$$\lambda_n(\Omega) = in\frac{1-\Omega^2}{2}, \quad n \in \mathbb{Z} \tag{7.81}$$

that are presented in Figure 7.2 (c). When $k \in [0, \infty)$ interpolates between the two limiting cases, the spectral mesh in the subcritical speed range is deformed into parabolas (7.81) in such a manner that at every k the eigencurves pass through the loci of the nodes of the spectral mesh,[4] see Figure 7.2 (b, d).

Using the formulas (7.30) and (7.31) for semisimple eigenvalues with the eigenelements (7.79) and (7.80) we find an asymptotic expression for the eigenvalues originated after the splitting of the double eigenvalues $\lambda_{nm}^{\varepsilon\delta}$ at the nodes of the spectral mesh in the subcritical region $|\Omega| < 1$ ($\varepsilon = -$, $\delta = +$, and $m > n > 0$, i.e. at the light gray–light gray or dark gray–dark gray crossings marked by white circles in Figure 7.1 (b)) due to interaction of the rotating string with the external spring

$$\lambda = \lambda_{nm}^{\varepsilon\delta} + i\frac{m-n}{2}\Delta\Omega + i\frac{n+m}{8\pi nm}k \pm i\sqrt{\frac{k^2}{16\pi^2 nm} + \left(\frac{m-n}{8\pi mn}k - \frac{m+n}{2}\Delta\Omega\right)^2}. \tag{7.82}$$

In the supercritical region $|\Omega| > 1$ ($\varepsilon = -$, $\delta = +$, and $m > 0$, $n < 0$, i.e. at the light gray–dark gray crossings marked by the black circles in Figure 7.1 (b)), we have

$$\lambda = \lambda_{nm}^{\varepsilon\delta} + i\frac{m+|n|}{2}\Delta\Omega + i\frac{|n|-m}{8\pi|n|m}k \pm \sqrt{\frac{k^2}{16\pi^2|n|m} - \left(\frac{|n|-m}{2}\Delta\Omega - \frac{m+|n|}{8\pi m|n|}k\right)^2}. \tag{7.83}$$

Therefore, at $|\Omega| < 1$ the spectral mesh collapses into separated eigencurves demonstrating avoided crossings; for $|\Omega| > 1$ the eigenvalue branches overlap forming the bubbles of instability with eigenvalues having positive real parts, see Figure 7.3 (a).

[3] When $|m| \neq |n|$ the first of equalities (7.79) is, in fact, a necessary condition for a *combination parametric resonance* of either summation or difference type [110]. Note that in case of a rotating string the former could happen only in the supercritical speed range $|\Omega| > 1$ while the latter only when $|\Omega| < 1$; $|\Omega| = 1$ corresponds therefore to the *principal parametric resonance* [110].

[4] Similar homotopic deformation of eigencurves when boundary conditions are varied demonstrates the model of MHD kinematic mean field α^2-dynamo [208, 209, 298]; see Chapter 9.

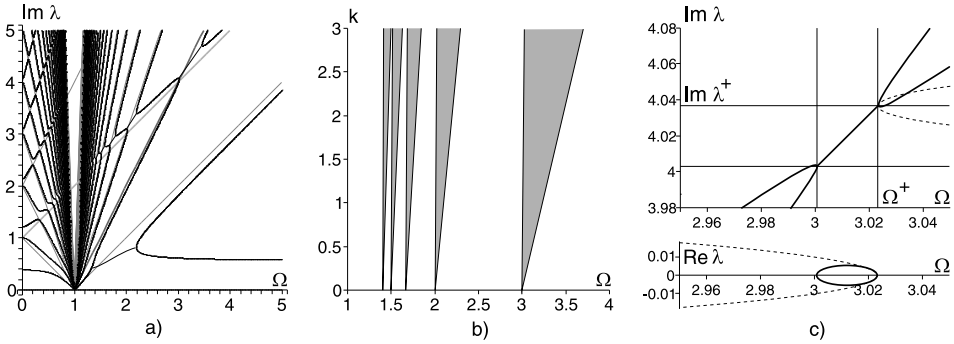

Figure 7.3. (a) Deformation of the spectral mesh (gray lines) of the rotating string interacting with the external spring with $k = 2$; (b) linear approximation to the corresponding tongues of the oscillatory instability (or, equivalently, summation type combination resonance [110]); (c) comparing numerically calculated eigenvalue curves (full lines) with the approximation (7.87) (dashed lines) for $k = 0.1$ [298].

From equation (7.83) a linear approximation follows to the boundary of the domains of supercritical flutter instability in the plane (Ω, k) (gray resonance tongues in Figure 7.3 (b)):

$$k = \frac{4\pi|n|m(|n|-m)}{(\sqrt{|n|} \pm \sqrt{m})^2}\left(\Omega - \frac{|n|+m}{|n|-m}\right). \tag{7.84}$$

The (conical, cf. Section 3.3.3) stability boundary consists of exceptional points (EPs) at which there exist double purely imaginary eigenvalues with the Keldysh chain. Their approximate locations in the $(\Omega, \mathrm{Im}\lambda)$-plane follow from the expressions (7.83) and (7.84). For the resonance tongue, originated at the diabolical point $(\Omega = 3, \mathrm{Im}\lambda = 4)$, the approximation to the loci of the EPs are

$$\Omega^{\pm} = 3 + \frac{3 \pm 2\sqrt{2}}{8\pi}k, \quad \lambda^{\pm} = i\left(4 + \frac{5 \pm 3\sqrt{2}}{8\pi}k\right). \tag{7.85}$$

For small values of k the coordinates (7.85) are very close to those found from the numerical solution of the characteristic equation (7.76), as is illustrated by Figure 7.3 (c).

The double eigenvalue λ^+ at $\Omega = \Omega^+$ has an eigenvector $\mathbf{u}_0 = (u_{01}, u_{02})^T$ and an associated vector $\mathbf{u}_1 = (u_{11}, u_{12})^T$. Given k, the eigenvalue λ^+ splits with the variation of Ω in accordance with equation (7.50), which now reads as

$$\lambda = \lambda^+ \pm \sqrt{\frac{(1-\Omega^{+2})\int_0^1 \bar{v}_{02}(\Omega^+\partial_\varphi u_{02} + 2\pi\lambda^+ u_{02})d\varphi + 2\pi k\Omega^+\bar{v}_{02}(0)u_{01}(0)}{-2\pi(1-\Omega^{+2})\int_0^1 \bar{v}_{02}(2\pi\lambda^+ u_{11} + \Omega^+ u_{12} + \pi u_{01})d\varphi}(\Omega - \Omega^+)}. \tag{7.86}$$

With the vectors $\mathbf{u}_0$ and $\mathbf{u}_1$ and the left eigenvector $\mathbf{v}_0 = (v_{01}, v_{02})^T$ evaluated at $k = 0.1$ at the EP $(\Omega^+, \mathrm{Im}\lambda^+)$, the formula (7.86) yields

$$\lambda = \lambda^+ \pm \sqrt{-0.004349(\Omega - \Omega^+)}. \tag{7.87}$$

In Figure 7.3 (c) the dashed lines correspond to approximation (7.87) and the full lines show the numerical solution of equation (7.76) which on this scale is undistinguishable from the approximation (7.83). The deformation patterns of the spectral mesh and first-order approximations of the instability tongues obtained by the perturbation technique are in good qualitative and quantitative agreement with the numerical calculations of Yang and Hutton [604].

7.4 Example: the Herrmann–Smith paradox

In 1958, a problem was posed by Dzhanelidze [163] on the stability of a cantilever column compressed at the free end by a force inclined at a certain angle to the tangent of the elastic line (a partially follower force). It was shown that, depending on the values of the problem's parameters, this nonconservative system is prone to both nonoscillatory (divergence) and oscillatory (flutter) instability. Kordas and Zyczkowski [321] have thoroughly analyzed the boundaries of stability and instability domains in this problem. Furthermore, Smith and Herrmann [535] have generalized the problem by assuming the column to be attached to the *Winkler elastic foundation*. They found that the critical load causing flutter does not depend on the magnitude of the modulus of the uniform elastic foundation. This effect, known as the *Herrmann–Smith paradox*, has stimulated considerable interest among researchers in applied mechanics, see e.g. [40, 550] and references therein.

7.4.1 Formulation of the problem

Following [276] we consider a uniform elastic cantilever column of length L attached to a Winkler elastic foundation having a constant modulus of elasticity χ as shown in Figure 7.4 (a). It is assumed that the free end of the column is loaded by a nonconservative force P whose direction is determined by the parameter η. The case $\eta = 1$ implies that the column is loaded by a purely tangential follower force (*Beck's problem* [39, 113]). If $\eta = 0$, then the force P is potential (conservative).

Small transverse in-plane vibrations of the column are described by the partial differential equation with the boundary conditions

$$\partial_x^4 y(x,\tau) + q\partial_x^2 y(x,\tau) + \kappa y(x,\tau) + \partial_\tau^2 y(x,\tau) = 0 \tag{7.88}$$

$$y(0,\tau) = 0,\ \ y_x^{(1)}(0,\tau) = 0,\ \ y_x^{(2)}(1,\tau) = 0,\ \ y_x^{(3)}(1,\tau) + (1-\eta)q y_x^{(1)}(1,\tau) = 0,$$

where the dimensionless variables and parameters are

$$x = \frac{X}{L},\ \ y = \frac{Y}{L},\ \ \tau = t\sqrt{\frac{EI}{\rho A L^4}},\ \ q = \frac{PL^2}{EI},\ \ \kappa = \frac{\chi L^4}{EI}, \tag{7.89}$$

and t denotes time, ρ the material density, A the cross-sectional area, E the Young modulus, and I the moment of inertia of the cross-section.

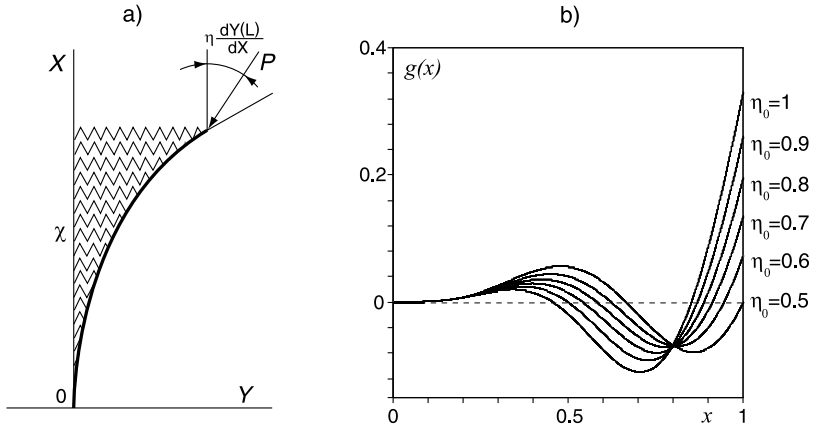

Figure 7.4. (a) A cantilevered column on a Winkler elastic foundation that is loaded by a partially follower force at the free end. (b) The gradient $g(x)$ of the critical flutter load with respect to the distributed modulus of the elastic foundation $\kappa(x)$ [276].

Isolating time by $y(x,\tau) = u(x)\exp(i\sqrt{\lambda}\tau)$ yields the eigenvalue problem for a scalar ($N = 1$) differential operator of order $m = 4$

$$Lu := l_0\partial_x^4 u + l_1\partial_x^3 u + l_2\partial_x^2 u + l_3\partial_x u + l_4 u = 0, \quad \mathfrak{U}\mathfrak{u} := [\mathfrak{A},\mathfrak{B}]\mathfrak{u} = 0, \tag{7.90}$$

where $l_0 = 1, l_1 = 0, l_2 = q, l_3 = 0, l_4 = \kappa - \lambda$, and

$$\mathfrak{A} = \begin{pmatrix} 1 & 0 & 0 & 0 \\ 0 & 1 & 0 & 0 \\ 0 & 0 & 0 & 0 \\ 0 & 0 & 0 & 0 \end{pmatrix}, \quad \mathfrak{B} = \begin{pmatrix} 0 & 0 & 0 & 0 \\ 0 & 0 & 0 & 0 \\ 0 & 0 & 1 & 0 \\ 0 & (1-\eta)q & 0 & 1 \end{pmatrix} \tag{7.91}$$

with $\mathfrak{u}^T = (u(0), u_x^{(1)}(0), u_x^{(2)}(0), u_x^{(3)}(0), u(1), u_x^{(1)}(1), u_x^{(2)}(1), u_x^{(3)}(1))$. Then, according to equation (7.9)

$$\mathfrak{L}(x) = \begin{pmatrix} 0 & q & 0 & 1 \\ -q & 0 & -1 & 0 \\ 0 & 1 & 0 & 0 \\ -1 & 0 & 0 & 0 \end{pmatrix}. \tag{7.92}$$

Choosing

$$\widetilde{\mathfrak{A}} = \begin{pmatrix} 0 & 0 & 1 & 0 \\ 0 & 0 & 0 & 1 \\ 0 & 0 & 0 & 0 \\ 0 & 0 & 0 & 0 \end{pmatrix}, \quad \widetilde{\mathfrak{B}} = \begin{pmatrix} 0 & 0 & 0 & 0 \\ 0 & 0 & 0 & 0 \\ 1 & 0 & 0 & 0 \\ 0 & 1 & 0 & 0 \end{pmatrix} \tag{7.93}$$

and then using the formula (7.15), we find that

$$\mathfrak{V} = \begin{pmatrix} 0 & 1 & 0 & 0 & 0 & 0 & 0 & 0 \\ -1 & 0 & 0 & 0 & 0 & 0 & 0 & 0 \\ 0 & 0 & 0 & 0 & 0 & -q & 0 & -1 \\ 0 & 0 & 0 & 0 & q\eta & 0 & 1 & 0 \end{pmatrix},$$

$$\widetilde{\mathfrak{V}} = \begin{pmatrix} 0 & -q & 0 & -1 & 0 & 0 & 0 & 0 \\ q & 0 & 1 & 0 & 0 & 0 & 0 & 0 \\ 0 & 0 & 0 & 0 & 0 & 1 & 0 & 0 \\ 0 & 0 & 0 & 0 & -1 & 0 & 0 & 0 \end{pmatrix}. \tag{7.94}$$

Then, according to equations (7.17) the adjoint eigenvalue problem is

$$\partial_x^4 v + q\partial_x^2 v + \kappa v = \overline{\lambda} v, \tag{7.95}$$

$$v(0) = 0, \;\; v_x^{(1)}(0) = 0, \;\; v_x^{(2)}(1) + \eta q v(1) = 0, \;\; v_x^{(3)}(1) + q v_x^{(1)} = 0. \tag{7.96}$$

Substituting the general solution of the differential equation (7.90)

$$u(x) = C_1 \cosh(ax) + C_2 \sinh(ax) + C_3 \cos(bx) + C_4 \sin(bx), \tag{7.97}$$

with

$$a = \sqrt{-\frac{q}{2} + \sqrt{\frac{q^2}{4} + \lambda - \kappa}}, \quad b = \sqrt{\frac{q}{2} + \sqrt{\frac{q^2}{4} + \lambda - \kappa}}, \quad \kappa \neq \lambda + \frac{q^2}{4}, \tag{7.98}$$

into the boundary conditions (7.90), we obtain the condition for the existence of a nontrivial solution $u(x)$ to the eigenvalue problem (7.90)

$$\Delta(\lambda - \kappa, \eta, q) = 0, \tag{7.99}$$

where [273, 276]

$$\Delta := (2(\lambda - \kappa) + (1 - \eta)q^2)(1 + \cosh(a)\cos(b)) + q(2\eta - 1)(q + ab\sinh(a)\sin(b)). \tag{7.100}$$

Eigenvalues λ are the roots of the characteristic equation (7.99). The eigenfunction at the eigenvalue $\lambda = \lambda_0$ and the corresponding eigenfunction of the adjoint problem are, respectively

$$u_0(x) = \cosh(ax) - \cos(bx) + F(a\sin(bx) - b\sinh(ax)), \tag{7.101}$$

$$v_0(x) = \cosh(ax) - \cos(bx) + G(a\sin(bx) - b\sinh(ax)), \tag{7.102}$$

where the coefficients F and G depend on the parameters η and q [276]

$$F = \frac{a^2\cosh(a) + b^2\cos(b)}{ab(a\sinh(a) + b\sin(b))}, \quad G = \frac{(a^2 + \eta q)\cosh(a) + (b^2 - \eta q)\cos(b)}{b(a^2 + \eta q)\sinh(a) + a(b^2 - \eta q)\sin(b)}. \tag{7.103}$$

Solution to the boundary value problem (7.88) is marginally stable if and only if all the eigenvalues λ of the eigenvalue problem (7.90) are positive and semisimple. If for all $\lambda \in \mathbb{R}$ some of them are negative, then the system is statically unstable (divergence). The existence of at least one $\lambda \in \mathbb{C}$ implies flutter [277].

Given $\eta = \eta_0$ and $q = q_0$ and in the assumption that $\lambda \in \mathbb{R}$, the zeros of the function $\Delta(\lambda - \kappa)$ differ from the zeros of $\Delta(\lambda)$ by the quantity κ only, whereas their multiplicities do not change. Since the flutter boundary is defined by the multiple real-valued eigenvalues, the point (κ, η_0, q_0) belongs to the flutter boundary for arbitrary κ, if $(0, \eta_0, q_0)$ is located at this boundary. In contrast, the boundary between the stability and divergence domains determined by zero eigenvalues has to change when $\kappa \neq 0$ because the eigenvalue $\lambda_0 = 0$ takes a nonzero increment equal to κ.

7.4.2 Stationary flutter domain and mobile divergence region

Putting $\lambda = 0$ into equation (7.99), we find the divergence boundary

$$\eta(q, \kappa) = \frac{r_2 q - r_1(q^2 - 2\kappa)}{2r_2 q - r_1 q^2}, \tag{7.104}$$

where $r_1 = 1 + \cosh(a)\cos(b)$ and $r_2 = q + ab\sinh(a)\sin(b)$.

The function $\eta(q, 0)$ attains its maximum $\eta_* = 1/2$ at $q_* = (2j + 1)^2\pi^2$ when $j = 0, 1, \ldots$, whereas $\eta(q, 0) \to -\infty$ at the points $q_{**} = (2j)^2\pi^2$. For arbitrary $\kappa > 0$, the function $\eta(q)$, $(q > 0)$ defined in (7.104) represents a smooth curve of zero eigenvalues in the (η, q)-plane. The maximum, η_*, and its coordinate, q_*, therefore depend on κ.

Numerical solution to the equation $\frac{d\eta}{dq} = 0$ at different values of κ yields the function $q_*(\kappa)$ and by equation (7.104) the function $\eta_*(\kappa)$. These functions determine the trajectory of the point $\mathbf{p}_* = (\eta_*, q_*)$ corresponding to each maximum of the function $\eta(q)$ in the (η, q)-plane when κ varies. It can be shown that all these trajectories belong to the half-plane $\eta \leq 1/2$. Therefore, when $\eta > 1/2$, the divergence instability is impossible for any $\kappa \geq 0$ [276].

In Figure 7.5 stability diagrams are plotted when $\eta \in [0, 1]$ and $q \in [0, 150]$. Within this range of parameters, there exist two curves corresponding to the double real-valued eigenvalues. These curves bounding the flutter domain are invariable with respect to the change of κ.

At relatively small κ, there also exist two curves of zero eigenvalues. The part of the lower curve corresponding to the vanishing first eigenvalue forms the boundary between the stability and divergence domains, see Figure 7.5.

At $\kappa = 0$ there exists a point $\mathbf{p}_0 \approx (0.354313302, 17.06957477)$ where the spectrum of the column has the double zero eigenvalue (0^2 in the notation proposed by Arnold [17]). At $\mathbf{p}_0$ the divergence and flutter boundaries have a common tangent, Figure 7.5. With κ increasing, the flutter boundary preserves its form whereas the double real-valued eigenvalues linearly change. As a consequence, the singular point 0^2

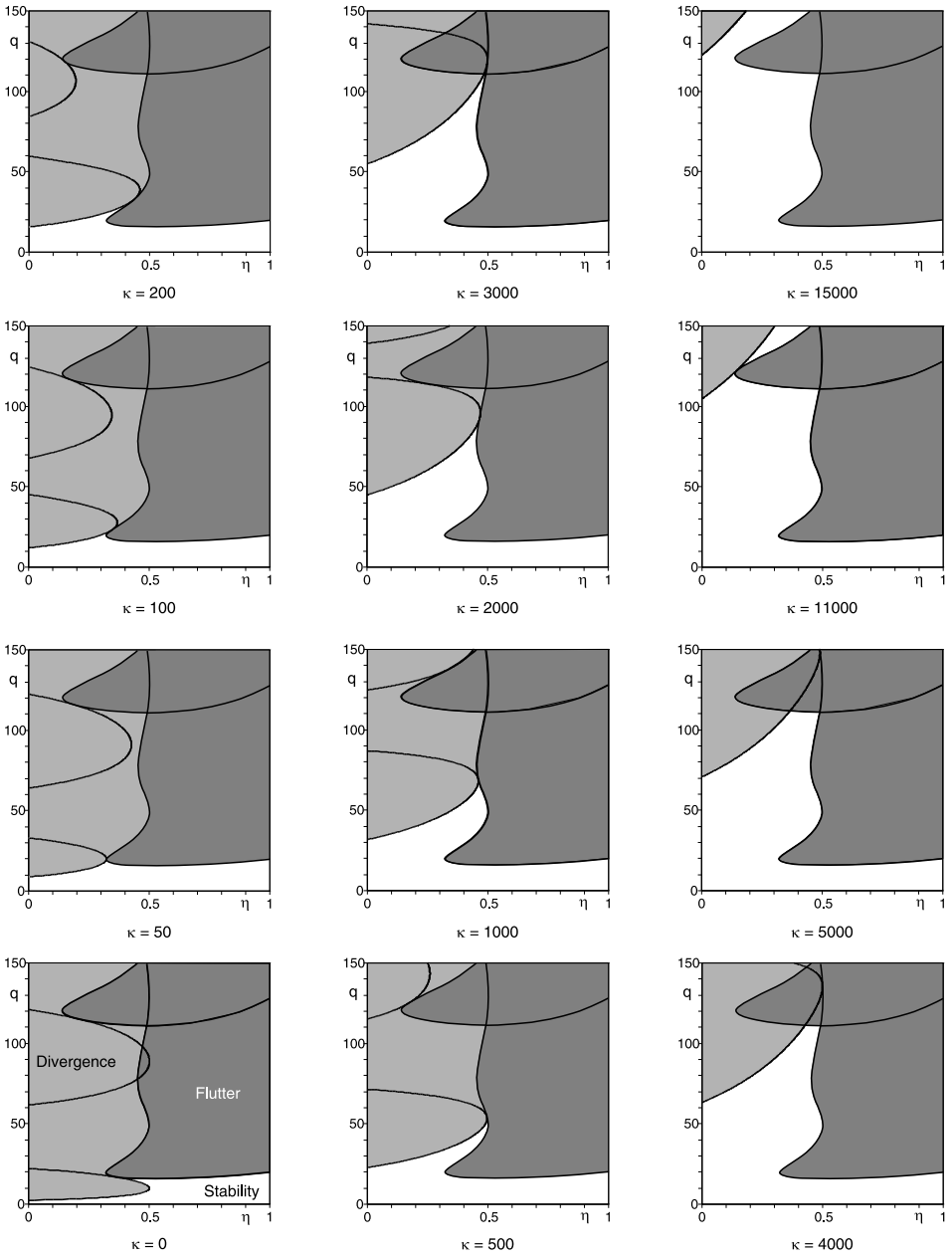

Figure 7.5. Stability diagrams in the (η, q)-plane when the elasticity modulus of the foundation κ takes values from (the lower left corner) 0 to (the upper right corner) 15000. The divergence domain (light gray) is shifted up with the increase in κ in such a way that the line of simple zero eigenvalues that separates stability and divergence domains has always a tangent point with the stationary flutter boundary [276].

moves up the stationary flutter boundary, carrying the curves of zero eigenvalues and the divergence domain itself along with it. The described process is shown in Figure 7.5 for $\kappa \in [0, 15000]$. When $\kappa > 3000$, only the lowest curve of zero eigenvalues remains within the range $\eta \in [0, 1]$ and $q \in [0, 150]$. At $\kappa = 15000$, the divergence domain almost completely disappears, opening a vast stability domain in the (η, q)-plane, Figure 7.5.

7.4.3 Sensitivity of the critical flutter load to the redistribution of the elasticity modulus

When the modulus of the elastic foundation is uniformly distributed along the column, then $\kappa = \text{const}$. The results of the numerical calculations shown in Figure 7.5 evidence that increasing or decreasing κ does not affect the flutter domain. Nevertheless, this situation can be changed when the modulus $\kappa = \kappa(x)$ is distributed along the column nonuniformly.

Let us introduce a small inhomogeneity into the uniform distribution of the elasticity modulus as

$$\kappa(x) = \kappa_0 + \delta\kappa(x), \tag{7.105}$$

where $\kappa_0 = \text{const}$, $\delta\kappa(x) = \varepsilon e_\kappa(x)$ and $\varepsilon \geq 0$ is a small parameter. Then the critical parameters η_0 and q_0 at the flutter boundary take the increments

$$\eta = \eta_0 + \varepsilon e_\eta + o(\varepsilon), \quad q = q_0 + \varepsilon e_q + o(\varepsilon). \tag{7.106}$$

At the flutter threshold the double real eigenvalue λ_0 exists with the Keldysh chain of length 2. The chain consists of the eigenfunction u_0 and the associated function u_1. The functions u_0 and u_1 as well as the corresponding eigenfunction v_0 and associated function v_1 of the adjoint problem can be chosen real-valued. The eigenfunctions u_0 and v_0 are orthogonal: $(u_0, v_0) = \int_0^1 u_0 \overline{v}_0 dx = 0$.

With the variations (7.105) and (7.106), the differential expression (7.90), and the matrices of the boundary conditions (7.91) and (7.94), the formula (7.50) describing splitting of the eigenvalue λ_0 with the algebraic multiplicity $\mu = 2$ takes the form

$$\lambda = \lambda_0 \pm \sqrt{\frac{(\delta\kappa(x)u_0, v_0)}{(u_1, v_0)} + \frac{q_0 u_0'(1)\overline{v}_0(1)}{(u_1, v_0)}\Delta\eta + \frac{(u_0'', v_0) - (1-\eta_0)u_0'(1)\overline{v}_0(1)}{(u_1, v_0)}\Delta q}, \tag{7.107}$$

where $\Delta\eta = \eta - \eta_0$, $\Delta q = q - q_0$ and $' = \partial_x$.

According to equation (7.107), the splitting yields either two simple eigenvalues (stability or divergence depending on the sign of λ_0), if the radicand in equation (7.107) is positive, or the complex-conjugate pair (flutter) if the radicand is negative. The vanishing radicand in equation (7.107) determines a linear approximation to the flutter boundary

$$\Delta q = -\frac{(\delta\kappa(x)u_0, v_0) + q_0 u_0'(1)\overline{v}_0(1)\Delta\eta}{(u_0'', v_0) - (1-\eta_0)u_0'(1)\overline{v}_0(1)}. \tag{7.108}$$

On the other hand, equation (7.108) is a linear part of the increment of the critical flutter load q_0 when η is changed and the elasticity modulus $\kappa(x)$ is re-arranged along the column. Note that when the modulus is changed uniformly ($\delta\kappa = const$), then by the orthogonality condition $(u_0, v_0) = 0$ we have $(\delta\kappa u_0, v_0) = \delta\kappa(u_0, v_0) = 0$. Consequently, the flutter load indeed does not depend on the modulus κ of the uniform elastic foundation [535].

Introducing the function of the gradient of the critical flutter load with respect to the distribution of the modulus $\kappa(x)$

$$g(x) = \frac{-u_0(x)\overline{v}_0(x)}{(u_0'', v_0) - (1-\eta_0)u_0'(1)\overline{v}_0(1)}, \tag{7.109}$$

we finally express equation (7.108) as

$$\Delta q = \int_0^1 g(x)\delta\kappa(x)dx + \frac{\partial q}{\partial \eta}\Delta\eta, \tag{7.110}$$

where

$$\frac{\partial q}{\partial \eta} = \frac{-q_0 u_0'(1)\overline{v}_0(1)}{(u_0'', v_0) - (1-\eta_0)u_0'(1)\overline{v}_0(1)}. \tag{7.111}$$

Let $\kappa_0 = \text{const}$, $\eta_0 = 1$, and $q_0 \approx 20.05095361$. This choice corresponds to the column loaded by a purely tangential follower force at the flutter threshold [113]. Substituting into equation (7.109) the eigenfunctions (7.101) and (7.102) evaluated at these values of the parameters, we find the gradient function $g(x)$. In Figure 7.4 (b) it is seen that the gradient is an oscillating function. In particular, at $\eta_0 = 1$, the column's free end is the most sensitive part with respect to re-distribution of the modulus κ [474].

When $\Delta\eta = 0$ and the modulus κ is distributed in the gradient direction, i.e. $\delta\kappa(x) = \gamma g(x)$, equation (7.110) yields [276]

$$q = q_0 + \gamma \int_0^1 g^2(x)dx \approx q_0 + \gamma \cdot 0.007085923. \tag{7.112}$$

Therefore, already a small inhomogeneity in the distribution of the modulus of the elastic foundation along the column can both increase ($\gamma > 0$) and decrease ($\gamma < 0$) the critical flutter load, which resolves the Herrmann–Smith paradox.

7.5 Example: Beck's column loaded by a partially follower force

In the absence of the Winkler elastic foundation, i.e. when $\kappa = 0$, the Herrmann–Smith problem is reduced to the question of stability of the cantilevered column under the action of a partially follower force, which is frequently referred to as the extended Beck's problem [163, 321]. Recall that the parameter $\eta \in [0, 1]$ measures the degree

of the nonconservativeness of the load. If $\eta = 0$, then the force P is potential (conservative). The case $\eta = 1$ corresponding to the purely tangential follower force is known as Beck's problem [113], see Figure 7.4 (a). Note that the force P can be realized experimentally to good approximation as the jet thrust of a small, powerful solid propellant rocket motor mounted at the free end of the column [556]. Experiments on the stability of such columns were carried out by Sugiyama et al. [356, 554, 557–559].

The numerically calculated stability diagram of the extended Beck's problem is shown in Figure 7.6 (a) and in another scale in the lower left panel of Figure 7.5. At $\kappa = 0$ the expression for the line of zero eigenvalues (7.104) is simplified to

$$\eta(q) = \frac{\cos(\sqrt{q})}{\cos(\sqrt{q}) - 1}. \tag{7.113}$$

A part of the curve (7.113) forms the boundary between the stability and divergence domains in the (η, q)-plane. The smooth parts of the flutter boundary consist of such points (η, q) that $\lambda(\eta, q)$ is a double real eigenvalue with the Keldysh chain. Calculation of the roots λ of the characteristic equation $\delta(\eta, q, \lambda) = 0$, where Δ is given by equation (7.100) for different values of the load parameter q (at a fixed value of the parameter η) gives approximately the point where two simple eigenvalues form a double one. Finding such points for different values of the parameter η we get the curve of double real eigenvalues.

The curves found subdivide the plane of the parameters (η, q) into stability, flutter, and divergence domains, Figure 7.6 (a). Note that the boundary of the stability domain has a singular point B. The divergence boundary has a point A with the vertical tangent. The point C in Figure 7.6 (a) corresponds to the pure tangential follower force $(\eta = 1)$.

In the following we will study sensitivity of the eigenvalues at the points A, B, and C. The coordinates of the first point $(\eta_0 = 0.5, q_0 = \pi^2)$ follow from equation (7.113). To find the point B, we solve numerically the system of equations $\Delta(\kappa = 0, \eta, q, \lambda = 0) = 0$ and $\partial_\lambda \Delta(\kappa = 0, \eta, q, \lambda = 0) = 0$ that locate a double zero root of the characteristic equation. In order to find the coordinates of the point C at $\eta = 1$, we use the fact that the divergence boundary of the Herrmann–Smith problem has a common point with the flutter boundary at every κ; see Figure 7.5. Then we solve numerically a system consisting of the equation $\eta(q, \kappa) = 1$, where the function $\eta(q, \kappa)$ is defined by equation (7.104), and the equation $\partial_\lambda \Delta(\eta = \eta(q, \kappa), q, \kappa, \lambda = 0) = 0$; the result is a value of q at the point C and the value of $\kappa = -\lambda$, where λ is the double eigenvalue at C. Finally,

$$\begin{array}{lllll} A\colon & \eta_0 = 0.5, & q_0 = \pi^2 \approx 9.869604401, & \lambda_0 = 0 \\ B\colon & \eta_0 \approx 0.354313302, & q_0 \approx 17.06957477, & \lambda_0 = 0 \\ C\colon & \eta_0 = 1, & q_0 \approx 20.05095361, & \lambda_0 \approx 121.3425101. \end{array} \tag{7.114}$$

7.5.1 The stability-divergence boundary (point A)

At the point A on the boundary between the stability and divergence domains the spectrum of the extended Beck's problem contains a simple eigenvalue $\lambda_0 = 0$. Due to variation of parameters, a simple eigenvalue changes according to equation (7.32). With the differential expression (7.90) (where $\kappa = 0$) and the matrices of the boundary conditions (7.91) and (7.94) the equation (7.32) can be written as $\lambda = \lambda_0 + \varepsilon\langle \mathbf{g}, \mathbf{e}\rangle + o(\varepsilon)$, where

$$\mathbf{g}^T = \left(\frac{q_0 u_0'(1)\overline{v}_0(1)}{\int_0^1 u_0 \overline{v}_0 dx}, \frac{\int_0^1 u_0''\overline{v}_0 dx - (1-\eta_0)u_0'(1)\overline{v}_0(1)}{\int_0^1 u_0 \overline{v}_0 dx} \right), \tag{7.115}$$

the angular brackets denote scalar product of real vectors in $\mathbb{R}^2$, and $\mathbf{e}^T = (e_\eta, e_q)$ with $e_\eta = \frac{d\eta}{d\varepsilon}(0)$ and $e_q = \frac{dq}{d\varepsilon}(0)$. The eigenfunctions u_0 and v_0 at the simple zero eigenvalue are [277]

$$u_0 = \sin(b) - xb\cos(b) - \sin(b)\cos(bx) + \cos(b)\sin(bx), \tag{7.116}$$

$$v_0 = 1 - \cos(bx), \quad b = \sqrt{q_0}. \tag{7.117}$$

These eigenfunctions evaluated at the point A with the coordinates $\eta_0 = 0.5$ and $q_0 = \pi^2$ are presented in Figure 7.6 (b). Substituting them into equation (7.115), we get the normal vector to the divergence boundary

$$\mathbf{g}^T \approx (78.95683520, 0).$$

Hence, the divergence boundary has the vertical tangent at the point A, Figure 7.6 (a). Indeed, variation of the parameters $\Delta\mathbf{p} = (\eta - \eta_0, 0)$ changes the zero eigenvalue in

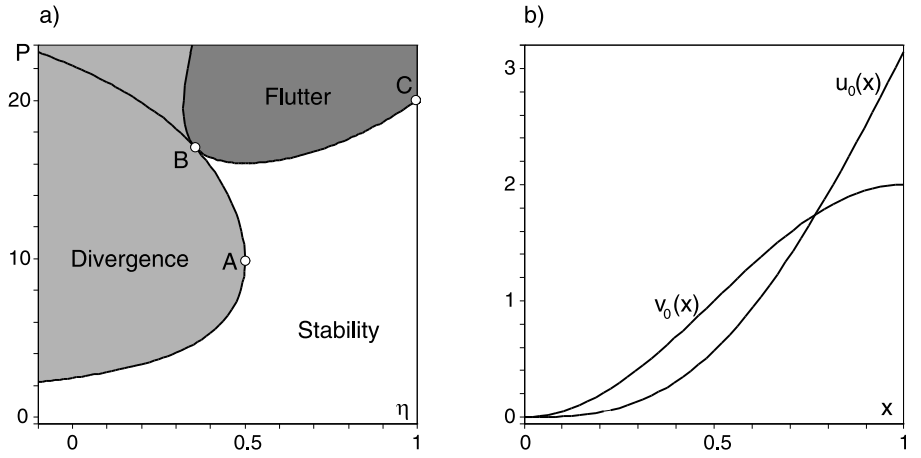

Figure 7.6. (a) Stability diagram of the extended Beck's problem. (b) The eigenfunctions (7.116) and (7.117) of the simple eigenvalue $\lambda_0 = 0$ at the point A [277].

the first-order approximation as

$$\lambda \approx 78.95683520(\eta - \eta_0). \tag{7.118}$$

For $\eta - \eta_0 < 0$ the eigenvalue $\lambda_0 = 0$ becomes negative. Therefore, the point $\mathbf{p}_0 + \Delta\mathbf{p}$ is inside the divergence domain, Figure 7.6 (a). If $\eta - \eta_0 > 0$ we come to the stability domain, see Table 7.1. Therefore, the equation $\eta = \eta_0 = 0.5$ is a linear approximation of the boundary between the stability and divergence domains at the point A.

Table 7.1. Variation of the simple zero eigenvalue near the point A (up to the 10th digit).

$(\Delta\eta, \Delta q)$	λ: equation (7.118)	λ: equation (7.99)
$(10^{-4}, 0)$	0.007895683	0.007894976
$(-10^{-4}, 0)$	−0.007895683	−0.007896390

7.5.2 The flutter threshold of Beck's column (point C)

Consider a point $\mathbf{p}_0 = (\eta_0, q_0)$ of the flutter boundary, where the spectrum of the extended Beck's problem contains a double eigenvalue λ_0 with the Keldysh chain of length 2. Bifurcation of this eigenvalue is described by equation (7.50).

Substituting the differential expression (7.90) and the matrices of the boundary conditions (7.91) and (7.94) into equation (7.50), we write it as $\lambda = \lambda_0 \pm \sqrt{\varepsilon\langle \mathbf{f}, \mathbf{e}\rangle} + o(\varepsilon^{1/2})$, where

$$\mathbf{f}^T = \left(\frac{q_0 u_0'(1)\overline{v}_0(1)}{\int_0^1 u_1 \overline{v}_0 dx}, \frac{\int_0^1 u_0'' \overline{v}_0 dx - (1-\eta_0) u_0'(1)\overline{v}_0(1)}{\int_0^1 u_1 \overline{v}_0 dx} \right). \tag{7.119}$$

To evaluate the vector $\mathbf{f}$ it is essential to know the eigenfunctions u_0, v_0 as well as the associated functions u_1, v_1 at the double eigenvalue λ_0. The first pair of functions is given by the equations (7.101) and (7.102). The associated function u_1 is a solution of the boundary value problem (7.34), where we should put $\mu = 2$ and $j = 1$ and take into account the differential expression (7.90) and the matrices of the boundary conditions (7.91) and (7.94).

A particular solution of the ordinary linear differential equation with constant coefficients $\partial_x^4 u_1 + q_0 \partial_x^2 u_1 - \lambda_0 u_1 = u_0$, where the right-hand side is the linear combination of trigonometric and hyperbolic functions (7.101), has the form

$$\hat{u}_1 = x(C_1 \sin(bx) + C_2 \cos(bx) + C_3 \sinh(ax) + C_4 \cosh(ax)).$$

Substitution of $\hat{u}_1$ into the equation of the Keldysh chain (7.34) allows one to determine the coefficients $C_1, \ldots, C_4$. After these coefficients are found, one tries solution of the boundary value problem (7.34) in the form

$$u_1 = \hat{u}_1 + D_1 \sin(bx) + D_2 \cos(bx) + D_3 \sinh(ax) + D_4 \cosh(ax).$$

The unknown constants $D_1, \ldots, D_4$ can be found from the boundary conditions (7.34), which yield the associated function u_1

$$u_1(x) = \frac{a\sin(bx) + b\sinh(ax) + F(a^2\cos(bx) - b^2\cosh(ax))}{2ab(a^2+b^2)}x + \frac{A_1\sinh(ax) - B_1\sin(bx)}{2ab(a^2+b^2)(a\sinh(a) + b\sin(b))^2}, \tag{7.120}$$

where F is determined by equation (7.103) while the coefficients A_1 and B_1 are

$$\begin{aligned} A_1 &= \frac{q}{a^2}\left(\sin(b)(b^2\cos(b) - a^2\cosh(a)) + 2ab\cos(b)\sinh(a)\right) + bT, \\ B_1 &= \frac{q}{b^2}\left(\sinh(a)(b^2\cos(b) - a^2\cosh(a)) - 2ab\cosh(a)\sin(b)\right) + aT, \\ T &= (a^2+b^2)(1+\cosh(a)\cos(b)). \end{aligned} \tag{7.121}$$

Similarly, solving the boundary value problem (7.37), (7.38) with the differential expression (7.90) and the matrices (7.94) yields

$$v_1(x) = \frac{a\sin(bx) + b\sinh(ax) + G(a^2\cos(bx) - b^2\cosh(ax))}{2ab(a^2+b^2)}x + \frac{A_2\sinh(ax) - B_2\sin(bx)}{2ab(a^2+b^2)(b(a^2+\eta q)\sinh(a) + a(b^2-\eta q)\sin(b))^2}, \tag{7.122}$$

where the coefficient G is defined in equation (7.103) and the coefficients A_2, B_2 are

$$\begin{aligned} A_2 &= q\sin(b)[[-a^2b^2 + \eta((a^2+b^2)^2 - \eta q^2)]\cosh(a) + \cos(b)(b^2-\eta q)^2] \\ &\quad + b(a^2+b^2)[a^2b^2 + \eta^2q^2 + (a^2b^2 + \eta(1-\eta)q^2)\cos(b)\cosh(a)] \\ &\quad + 2qab^3(1-2\eta)\sinh(a)\cos(b), \\ B_2 &= q\sinh(a)[[a^2b^2 - \eta((a^2+b^2)^2 - \eta q^2)]\cos(b) - \cosh(a)(a^2+\eta q)^2] \\ &\quad + a(a^2+b^2)[a^2b^2 + \eta^2q^2 + (a^2b^2 + \eta(1-\eta)q^2)\cos(b)\cosh(a)] \\ &\quad - 2qba^3(1-2\eta)\sin(b)\cosh(a). \end{aligned} \tag{7.123}$$

Note that despite the eigenfunctions u_0, v_0 being defined up to arbitrary multipliers and associated functions u_1, v_1 being defined up to the addends C_1u_0 and C_2v_0, respectively, the vector $\mathbf{f}$ does not depend on these uncertainties [277].

Let $\mathbf{p}_0$ be the point C in Figure 7.6 (a), corresponding to the double eigenvalue $\lambda_0 \approx 121.3425101$. This point is known as a flutter threshold for a column subjected to a purely tangential follower force [39, 113]. Substituting the values of λ_0, η_0 and q_0 given by equation (7.114) into equations (7.120)–(7.123) we obtain the functions[5] u_0, v_0, u_1, v_1 shown in Figure 7.7 (a).

[5] Notice that at $\eta = 1$ the eigenfunction v_0 is the vibrational mode at the flutter threshold of a column loaded by a force with a fixed line of action (Reut's column), see [75, 287, 361] for the theory and [356, 555] for the experiments.

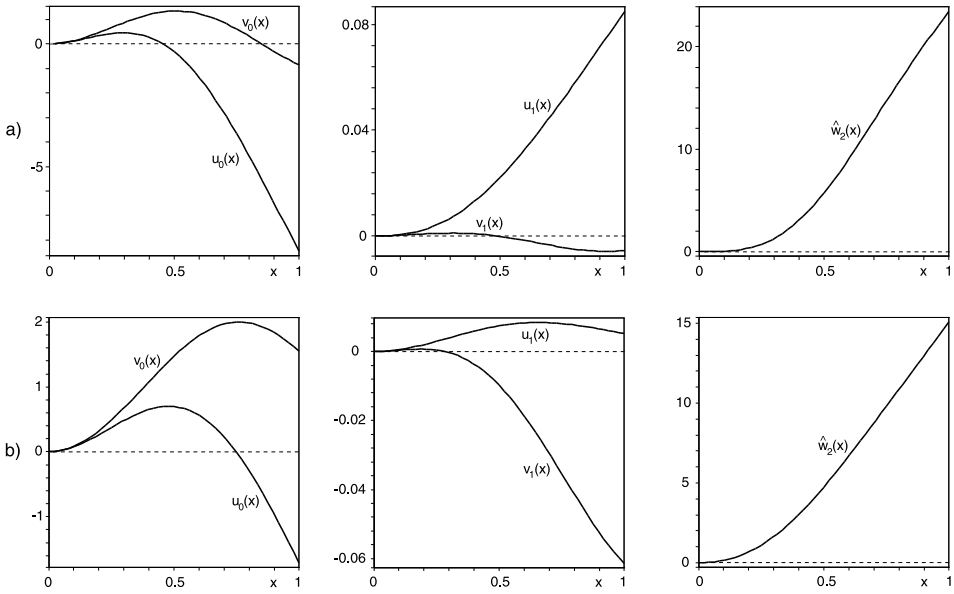

Figure 7.7. The eigenfunctions, associated functions and functions $\hat{w}_2(x)$ at the point C (row (a)) and B (row (b)) [277].

With the use of these functions the equation (7.119) gives the normal vector to the flutter boundary at the point C

$$\mathbf{f}^T \approx (35450.7004, -2295.669253).$$

Let us look at the splitting of the double eigenvalue λ_0 due to change of the parameters in a direction $\mathbf{e}$ in the (η, q)-plane. Consider for example the vertical direction: $\mathbf{e} = (0, 1)$. Thus, when $\Delta\mathbf{p}^T = (0, q - q_0)$, equation (7.50) yields

$$\lambda \approx 121.3425101 \pm 47.91314280\sqrt{q_0 - q}. \tag{7.124}$$

For the variation $\Delta\mathbf{p}^T = (\eta - \eta_0, 0)$ corresponding to $\mathbf{e} = (1, 0)$ we have

$$\lambda \approx 121.3425101 \pm 188.2835638\sqrt{\eta - \eta_0}. \tag{7.125}$$

The results of probing a small neighborhood of the point C in different directions are summarized in Table 7.2. Thus, for example, for $q = q_0 + 0.00002$, i.e. when the new point is situated above the initial point $\mathbf{p}_0$, the splitting yields $\lambda \approx 121.3425101 \pm i0.214274088$, and thus the point $\mathbf{p}_0 + \Delta\mathbf{p}$ belongs to the flutter domain, Figure 7.6 (a). The characteristic equation (7.99) gives for the same values of parameters two complex-conjugate eigenvalues, which differ from those found with the use of (7.124) only in the sixth digit, Table 7.2.

Table 7.2. Splitting of the double eigenvalue near the point C (up to the 10th digit).

$(\Delta\eta, \Delta q)$	λ: equations (7.124), (7.125), (7.130).	λ: equation (7.99)
$(0,\ \ 2{\cdot}10^{-5})$	$121.3425101 \pm i\,0.214274088$	$121.3423790 \pm i\,0.214274069$
$(0, -2{\cdot}10^{-5})$	121.1282360 121.5567842	121.1283671 121.5569153
$(\ 2{\cdot}10^{-5}, 0)$	122.1845398 120.5004804	122.1885157 120.5044440
$(-2{\cdot}10^{-5}, 0)$	$121.3425101 \pm i\,0.842029695$	$121.3385403 \pm i\,0.842023527$
$2{\cdot}10^{-3}\mathbf{e}_*$	120.7553885 121.5408235	120.7576667 121.5385351

The degeneration condition (7.61) defines the vector $\mathbf{e}_* \approx (-1, -15.44242506)$ tangent to the flutter boundary at the point C. The double eigenvalue λ_0 splits in the tangent direction in accordance with equation (7.70) as

$$\lambda = \lambda_0 - \frac{a_1}{2}\varepsilon \pm \frac{\varepsilon}{2}\sqrt{a_1^2 - 4a_2} + o(\varepsilon), \tag{7.126}$$

where

$$a_1 = \frac{e_2^* \int_0^1 (u_0'\overline{v}_1' + \overline{v}_0' u_1')dx - (e_2^*\eta_0 + e_1^* q_0)(\overline{v}_1(1)u_0'(1) + \overline{v}_0(1)u_1'(1))}{\int_0^1 u_0\overline{v}_1 dx},$$

$$a_2 = \frac{e_2^* \int_0^1 \overline{v}_0'\hat{w}_2' dx - (e_2^*\eta_0 + e_1^* q_0)\overline{v}_0(1)\hat{w}_2'(1) - e_1^* e_2^* \overline{v}_0(1)u_0'(1)}{\int_0^1 u_0\overline{v}_1 dx}, \tag{7.127}$$

and $' = \partial_x$. The functions u_0, v_0, u_1, v_1 are determined by the equations (7.101), (7.102) and (7.120), (7.122). The function $\hat{w}_2(x)$, Figure 7.7 (a), is a solution to the boundary value problem (7.67)

$$\hat{w}_2(x) = \frac{b\sin(bx) - a\sinh(ax) + Fab(\cos(bx) + \cosh(ax))}{2(a^2 + b^2)} e_2^* x$$
$$+ \frac{A_3\sin(bx) - B_3\sinh(ax)}{2ab(a^2 + b^2)(b\sin(b) + a\sinh(a))^2} e_2^*. \tag{7.128}$$

The coefficient F is determined by equation (7.103). For A_3 and B_3 we have

$$\begin{aligned} A_3 &= -a(a^2 + b^2)(q + ab\sin(b)\sinh(a)) - 2a^3\cosh(a)(a\sinh(a) + b\sin(b)) \\ &\quad + 2a^2 b(b\sinh(a)\cos(b) - a\cosh(a)\sin(b)), \\ B_3 &= -b(a^2 + b^2)(q + ab\sin(b)\sinh(a)) + 2b^3\cos(b)(a\sinh(a) + b\sin(b)) \\ &\quad + 2b^2 a(b\sinh(a)\cos(b) - a\cosh(a)\sin(b)). \end{aligned} \tag{7.129}$$

With the use of the eigenfunctions, associated functions and the function $\hat{w}_2$, we find from equations (7.127) the coefficients $a_1 \approx 194.5367520$ and $a_2 \approx -28627.5496$.

With these coefficients equation (7.126) yields approximate expressions for the two simple eigenvalues which originate from the splitting of the double λ_0 in the tangent direction to the stability boundary

$$\lambda_1 \approx 121.3425101 - 292.4316068\varepsilon, \quad \lambda_2 \approx 121.3425101 + 97.89485480\varepsilon. \quad (7.130)$$

For example, take $\varepsilon = 0.002$; then the double eigenvalue λ_0 splits into two positive eigenvalues, Tab. 7.2. This means that the tangent vector $\mathbf{e}_* \approx (-1, -15.44242506)$ lies in the stability domain, whence it follows that the flutter domain is convex at the point C, see Figure 7.6 (a). At the same values of the parameters the characteristic equation has very close solutions (Tab. 7.2) showing thereby that the equations (7.130) well approximate the numerically computed eigenvalues.

7.5.3 The singularity 0^2 on the stability boundary (point B)

Recall that at the points of the boundary between the flutter and stability domains the spectrum of the extended Beck's problem contains positive double eigenvalues while at the points of the boundary between the flutter and divergence domains double eigenvalues are negative. Thus, the double eigenvalue becomes double zero at such a point of the flutter boundary that at the same time belongs to the curve of zero eigenvalues (7.113). Since the orthogonality condition $\int_0^1 u_0 \overline{v}_0 dx = 0$ must be true at the points of the flutter boundary, this integral evaluated at the points of the curve (7.113) vanishes only at the point B, corresponding to the double zero eigenvalue. Following Arnold [17] we denote this singularity by the symbol 0^2, where the upper index means the length of the Keldysh chain corresponding to the double zero eigenvalue.

Integrating the product of the eigenfunctions given by equations (7.116) and (7.117) over the range $[0, 1]$ we come to the transcendental equation for the critical load q_0 at the point B

$$q_0 = (\sqrt{q_0} - 2\sin(\sqrt{q_0}))(\sqrt{q_0}(1 + 2\cos(\sqrt{q_0})) - 4\sin(\sqrt{q_0})). \quad (7.131)$$

The minimal element of the set of solutions of equation (7.131) at $q_0 > 0$ is $q_0 \approx 17.06957477$. Substituting this solution into equation (7.113), we find the corresponding value of the second parameter $\eta_0 \approx 0.354313302$ [277, 321].

Solving the boundary value problem (7.34) at $\mu = 2$, $j = 1$, and $\lambda_0 = 0$, we find the associated functions of the Keldysh chain at the double zero eigenvalue

$$u_1 = -\frac{\cot(b)}{6b}x^3 + \frac{1}{2b^2}x^2 + \frac{\cot(b)(\cos(bx) - 1) + \sin(bx)}{2b^3}x + \frac{(bx - \sin(bx))(b + 2b\cos(b) - 2\sin(b))}{2b^4 \sin^2(b)}, \quad (7.132)$$

$$v_1 = \frac{x + x^2}{2b^2} + \frac{x - 1}{2b^3}\sin(bx) + \frac{b^2\cos(b) - \sin^2(b)}{b^4(b\cos(b) - \sin(b))}(\sin(bx) - bx),$$

where $b = \sqrt{q_0}$.

Table 7.3. Splitting of the double zero near the singular point B (up to the 10th digit).

$(\Delta\eta, \Delta q)$	λ: equations (7.134),(7.135)	λ: equation (7.99)
$(0,\ \ 10^{-4})$	$\pm i\,0.320078036$	$-0.001511883 \pm i\,0.320075851$
$(0, -10^{-4})$	0.320078036 -0.320078036	0.321592103 -0.318568338
$(\ 10^{-4}, 0)$	$\pm i\,1.558486892$	$0.026687442 \pm i\,1.558232905$
$(-10^{-4}, 0)$	1.558486892 -1.558486892	1.532051701 -1.585430038
$-10^{-5}\mathbf{e}_*$	-0.012075314 -0.000431083	-0.012075428 -0.000431085
$10^{-5}\mathbf{e}_*$	0.012075314 0.000431083	0.012075200 0.000431081

Substituting eigenfunctions (7.116), (7.117) and the associated functions (7.132) into expression (7.119), we find the normal vector to the flutter boundary at the singular point B

$$\mathbf{f}^T \approx (-24288.81395, -1024.499494). \tag{7.133}$$

Knowing the normal vector allows us to study the neighborhood of the point B in any direction $\mathbf{e}$ such that $\langle \mathbf{f}, \mathbf{e} \rangle \neq 0$. In particular, for two orthogonal directions $\mathbf{e} = (1, 0)$ and $\mathbf{e} = (0, 1)$, we find, respectively

$$\lambda \approx \pm 155.8486892\sqrt{\eta_0 - \eta}, \quad \lambda \approx \pm 32.00780364\sqrt{q_0 - q}. \tag{7.134}$$

In the typical situation, the double zero eigenvalue splits either into a complex-conjugate pair or into two real eigenvalues, one of which is negative, Table 7.3. Thus, the normal vector $\mathbf{f}$ at the point B is directed into the divergence domain. The inequality $\langle \mathbf{f}, \mathbf{e} \rangle > 0$ defines the tangent cone to this domain, and $\langle \mathbf{f}, \mathbf{e} \rangle < 0$ defines the tangent cone to the flutter domain, Figure 7.6 (a). Only the curves emitted in the tangent direction to the boundary can reach the stability domain from the singular point B (0^2).

Using the degeneration condition $\langle \mathbf{f}, \mathbf{e}_* \rangle = 0$ we find the tangent vector $\mathbf{e}_*^T \approx (1, -23.70798041)$. To examine whether this vector points to the stability domain we should consider bifurcation of a double zero eigenvalue in the degenerate case. Substituting into equation (7.127) the eigenfunctions (7.116) and (7.117), associated functions (7.132) and the function $\hat{w}_2$ (7.128) that at $\lambda_0 = 0$ reduces to

$$\hat{w}_2 = e_2^* x \frac{\cot(b)(\cos(bx) - 1) + \sin(bx)}{2b} + e_2^* \frac{bx - \sin(bx)}{2b \sin^2(b)}, \quad b = \sqrt{q_0},$$

we find the coefficients of the equation (7.126)

$$a_1 \approx 1250.639809, \quad a_2 \approx 52054.68890,$$

which yields

$$\lambda_1 \approx 1207.531459\varepsilon, \quad \lambda_2 \approx 43.10835008\varepsilon. \tag{7.135}$$

Equation (7.135) implies that the double zero eigenvalue splits into two positive simple eigenvalues (stability) only if the parameters change in the direction specified by the vector $\mathbf{e}_*^T \approx (1, -23.70798041)$, Table 7.3. Changing the parameters in the opposite direction leads to the splitting of the double zero eigenvalue into two negative simple ones, which means static instability (divergence). Note that the approximate expressions for the eigenvalues are in good agreement with the solutions of the characteristic equation (7.99), see Table 7.3.

The examples considered demonstrate that the developed perturbative approach to multiparameter nonself-adjoint boundary eigenvalue problems for operator matrices is convenient for implementation in computer algebra systems for an automatic calculation of the adjoint differential expression and boundary conditions as well as the coefficients in the perturbation series for simple and multiple eigenvalues and their eigenvectors. The approach is efficient in applications requiring frequent switches from one set of boundary conditions to another. In the next section we will demonstrate this by applying the developed method to a difficult problem of the analytical description of the influence of small dissipation on the stability of Beck's column and its generalization to a wide class of continuous nonconservative systems with damping.

Chapter 8

The destabilization paradox in continuous circulatory systems

The greatest theoretical interest is evidently centered in the unique effect of damping in the presence of pseudo-gyroscopic forces, and in particular, in the differences in the results for systems with slight damping which then becomes zero and systems in which damping is absent from the start ... These interesting aspects require further study ... for obtaining further, more definite, results.

V. V. Bolotin [75]

In 1952, Ziegler [622] when investigating the stability of a double pendulum subjected to a follower load, reached the unexpected conclusion that the flutter threshold of the nonconservative system with negligibly small damping is significantly lower than it is in the ideal (undamped) case. In 1956, Bottema [81] was the first who understood the Ziegler effect as a *structural instability* (in the sense of dynamical systems theory) by linking it to the Whitney umbrella singularity that (as was established in 1971 by Arnold [17]) generically exists on the boundary of the domain of the asymptotic stability of a general finite-dimensional dissipative system depending on at least three parameters.

This phenomenon, which we now know as the Ziegler–Bottema destabilization paradox, was subsequently observed in many nonconservative systems of solid and fluid mechanics, both finite-dimensional and continuous [312]. The well-known examples of the destabilization paradox in continuous systems of fluid dynamics are the enlargement of the domain of *baroclinic instability* due to friction in the Ekman boundary layer observed by Holopainen in 1961 and described by Romea in 1977 [228,334,501,563], and the enhancement of the *modulational instability* of the Stokes waves with dissipation found by Bridges and Dias in 2007 [90,303]. The destabilizing effect of damping is important in nonconservative problems of fluid-structure interaction such as *aircraft flutter* [452] and stability of pipes conveying fluids [85,513,556], as well as in solid mechanics, e.g., in the dynamics of large space structures [224] and in the optimization of slender structures with respect to stability criteria [355].

The analytical description of the destabilization paradox was recognized as one of the main theoretical challenges in nonconservative stability theory [75]. However, de-

spite the large number of publications, the problems arising from the destabilization paradox still await a general solution.[1]

As a canonical example of a continuous circulatory system possessing the destabilization paradox, let us consider transverse vibrations of a uniform Beck's column with internal (Kelvin–Voigt type) and external (viscous) damping [14, 77, 556]. In dimensionless variables (7.89), the equation of motion and the boundary conditions for small amplitude vibrations of the column that is clamped at $x = 0$ and free at $x = 1$ (Figure 7.4 (a)) are

$$\begin{gathered}\partial_x^4 y + q\partial_x^2 y + k_1\partial_x^4\partial_\tau y + k_2\partial_\tau y + \partial_\tau^2 y = 0,\\ y(0,\tau) = 0, \quad \partial_x y(0,\tau) = 0,\\ \partial_x^2 y(1,\tau) + k_1\partial_x^2\partial_\tau y(1,\tau) = 0, \quad \partial_x^3 y(1,\tau) + k_1\partial_x^3\partial_\tau y(1,\tau) = 0. \end{gathered} \tag{8.1}$$

The coefficient of internal damping $k_1 = \frac{c_1}{EL^2}\sqrt{\frac{EI}{\rho A}}$ characterizes the viscoelastic properties of the material whereas the coefficient of external damping $k_2 = \frac{c_2 L^2}{\sqrt{EI\rho A}}$ represents the resistance of the medium [76, 77]. Remember that ρ is the material density of the column, A the cross-sectional area, E the Young modulus, I the moment of inertia of the cross-section, L the length of the column, c_1 the coefficient of dynamic viscoelastic resistance, and c_2 the coefficient of external viscous damping [556].

Assuming $y(x,\tau) = u(x)\exp\lambda\tau$, we arrive at the eigenvalue problem

$$\begin{gathered}(1 + \lambda k_1)\partial_x^4 u + q\partial_x^2 u + (\lambda^2 + \lambda k_2)u = 0,\\ u(0) = 0, \quad u_x^{(1)}(0) = 0, \quad u_x^{(2)}(1) = 0, \quad u_x^{(3)}(1) = 0, \end{gathered} \tag{8.2}$$

where λ is an eigenvalue, $u(x)$ is an eigenfunction, and $x \in [0,1]$.

The trivial solution to the system (8.1) is asymptotically stable if all the eigenvalues λ of the nonself-adjoint boundary eigenvalue problem (8.2) have negative real parts. It is unstable if there is at least one eigenvalue in the right half of the complex plane ($\mathrm{Re}\lambda > 0$) or a multiple pure imaginary eigenvalue with the Keldysh chain. The critical load $q_{cr}(k_1, k_2)$, characterizing the transition from the asymptotic stability to

[1] It is worth noticing that in his book [75] Bolotin states: "We have here a situation which is very similar to that in the theory of stability of laminar flow (the paradoxical difference between the parameters of "viscous" and "nonviscous" instability)." However, as was correctly remarked by Swaters [563] with respect to baroclinic instability: "It is important to appreciate that the discontinuous behavior of the zero dissipation limit of the marginal stability boundary when an Ekman layer is present cannot be dismissed as akin to the well-known property that solutions to the Orr–Sommerfeld equation need not necessarily reduce to solutions to the Rayleigh stability equation in the infinite Reynolds number limit" [162, 388]. The point is that [334, 563] "the infinite Reynolds number limit of the Orr–Sommerfeld equation is singular in the sense that the order of the differential equation changes from fourth order to second order so that the mathematical properties of the allowed solutions cannot be expected to depend continuously as the Reynolds number increases without limit." This is not the case for either the problems of solid mechanics discussed by Bolotin or for baroclinic instability and modulational instability because the zero dissipation limit does not reduce the order of derivatives in the differential expression or boundary conditions.

instability is determined by the condition that the real part of one or more eigenvalues should vanish ($\mathrm{Re}\lambda = 0$) while the remaining eigenvalues have negative real parts ($\mathrm{Re}\lambda < 0$).

If the damping parameters in equation (8.1) are equated to zero, a circulatory system results. A circulatory system is marginally stable if all its eigenvalues are pure imaginary and semisimple, i.e. the algebraic multiplicity of each eigenvalue is identical with the number of its eigenfunctions [280,284,521]. Consequently, as the load parameter q is increased from zero, the eigenvalues of the ideal (undamped) Beck's column move along the imaginary axis (marginal stability) and at some value of $q = q_0$ two of them merge into a double eigenvalue $i\omega_0$, which then splits into a pair of complex-conjugate eigenvalues (flutter) [77]. The double eigenvalue $i\omega_0$ has a Keldysh chain of length 2, consisting of the eigenfunction u_0 and associated function u_1. The functions of the Keldysh chain are solutions to the following boundary value problems [14]

$$\begin{gathered}
\partial_x^4 u_0 + q_0 \partial_x^2 u_0 - \omega_0^2 u_0 = 0, \\
u_0(0) = 0, \quad u_{0x}^{(1)}(0) = 0, \quad u_{0x}^{(2)}(1) = 0, \quad u_{0x}^{(3)}(1) = 0; \\
\partial_x^4 u_1 + q_0 \partial_x^2 u_1 - \omega_0^2 u_1 = -2i\omega_0 u_0, \\
u_1(0) = 0, \quad u_{1x}^{(1)}(0) = 0, \quad u_{1x}^{(2)}(1) = 0, \quad u_{1x}^{(3)}(1) = 0.
\end{gathered} \tag{8.3}$$

At $q = q_0$ only one eigenfunction corresponds to the algebraically double eigenvalue $\lambda_0 = i\omega_0$, which yields a secular term of the form $(u_1(x) + tu_0(x))e^{i\omega_0 \tau}$ in the general solution to the boundary value problem (8.1). If at $q = q_0$ all other eigenvalues are pure imaginary and semisimple, then this value of the load parameter is the boundary between the domains of stability and oscillatory instability [280, 284, 521].

The vertical equilibrium position of the Beck's column considered without damping ($k_1 = 0, k_2 = 0$) is marginally stable for $0 \le q < q_0 \approx 20.05$ [113]. If allowance is made for arbitrary small internal damping ($k_1 \to +0, k_2 = 0$) the interval of the asymptotic stability shrinks to $0 \le q < q_{cr} \approx 10.94 < q_0$. This is a manifestation of the Ziegler–Bottema destabilization paradox: in the limit of vanishing internal damping the critical load falls abruptly. Similarly, there is a drop in the frequency of the unstable mode at the flutter threshold from $\omega_0 \approx 11.02$ to $\omega_{cr} \approx 5.40$. These effects are shown in Figure 8.1 for $k_1 \neq 0$ and $k_2 = 0$. The external damping ($k_2 > 0$) that is proportional to the mass distribution, which is uniform in the Beck's column, inhibits the destabilizing effect of the internal damping [14, 76, 77]. Other forms of external damping that are not proportional to the mass distribution of the structure can also have a destabilizing effect in the Beck's problem [466, 615].

The fact that different models of damping could lead either to a collapse of the marginal stability boundary associated with the zero dissipation limit of a dissipative system to the instability threshold of the undamped system or to a discontinuous change of the stability boundary was observed in fluid mechanics too [90, 563]. This raises a question, which limiting scenario is generic? For example, "the answer would seem to be that the generic situation is that the stability boundary associated with the

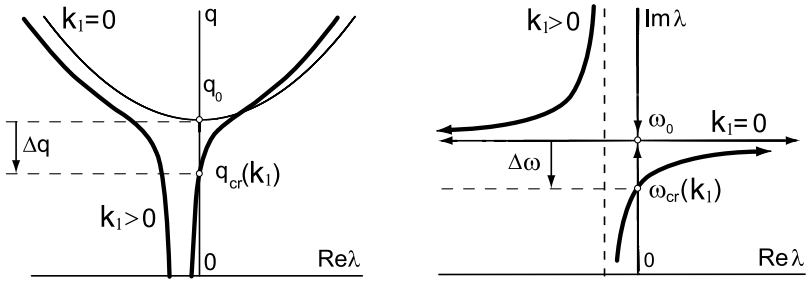

Figure 8.1. Schematic movement of eigenvalues (thin lines) of the ideal Beck's column and (bold lines) of Beck's column in the presence of the internal damping ($k_1 > 0$) that illustrates the destabilization paradox: (a) growth rates as functions of the load parameter q and the drop in the critical flutter load; (b) movement of eigenvalues in the complex plane and the drop in the frequency of the unstable mode.

zero dissipation limit of a dissipative baroclinic instability theory does not collapse to the inviscid result" [563]. This general question applies to continuous nonconservative problems of solid mechanics, e.g. to the damped Beck's column, as well.

We note that typically the destabilization paradox was studied only in particular continuous nonconservative systems of solid and fluid mechanics with the use of numerical and semianalytical methods. In the following, we investigate the effect of small dissipation on the stability of a rather broad class of continuous circulatory systems that includes the problem (8.1) as a special case. Using the perturbation theory developed in Chapter 7 we will find an explicit analytical approximation both to the eigencurves and to the critical flutter load as a function of damping parameters and give a geometrical interpretation to the destabilization paradox that generalizes the result of Bottema [81] to the infinite-dimensional case. Finally, we will re-consider the dissipation-induced destabilization of Beck's column under different forms of dissipative perturbations.

8.1 Movement of eigenvalues under a velocity-dependent perturbation

Stability analysis of continuous circulatory systems with dissipation in many cases is reduced to the study of a nonconservative system, described by a linear partial differential equation with the boundary conditions

$$M\partial_t^2 y(x,t) + D\partial_t y(x,t) + Py(x,t) = 0,$$
$$U_M^k \partial_t^2 y + U_D^k \partial_t y + U_P^k y = 0, \tag{8.4}$$

where

$$My = \sum_{j=0}^{m} l_j^M(x)\partial_x^{m-j} y, \quad Dy = \sum_{j=0}^{m} l_j^D(x)\partial_x^{m-j} y, \quad Py = \sum_{j=0}^{m} l_j^P(x)\partial_x^{m-j} y, \tag{8.5}$$

and

$$\begin{aligned} U_M^k y &= \sum_{j=0}^{m-1} A_{kj}^M y_x^{(j)}(x=0) + \sum_{j=0}^{m-1} B_{kj}^M y_x^{(j)}(x=1), \\ U_D^k y &= \sum_{j=0}^{m-1} A_{kj}^D y_x^{(j)}(x=0) + \sum_{j=0}^{m-1} B_{kj}^D y_x^{(j)}(x=1), \\ U_P^k y &= \sum_{j=0}^{m-1} A_{kj}^P y_x^{(j)}(x=0) + \sum_{j=0}^{m-1} B_{kj}^P y_x^{(j)}(x=1). \end{aligned} \tag{8.6}$$

8.1.1 Generalized boundary eigenvalue problem

Separating time with the substitution $y(x,t) = u(x)e^{\lambda t}$, we arrive at the boundary eigenvalue problem (7.1) for a scalar ($N = 1$) differential operator of order m, which takes the form[2] [280, 282]

$$\begin{aligned} &L(\lambda, q, \mathbf{k})u := P(q)u + \lambda D(\mathbf{k})u + \lambda^2 M u = 0, \\ &\mathfrak{U}(\lambda, q, \mathbf{k})\mathfrak{u} := \mathfrak{U}_P(q)\mathfrak{u} + \lambda \mathfrak{U}_D(\mathbf{k})\mathfrak{u} + \lambda^2 \mathfrak{U}_M \mathfrak{u} = 0. \end{aligned} \tag{8.7}$$

The coefficients of the differential operators P, D, and M of order m and the elements of the $m \times 2m$ matrices $\mathfrak{U}_P$, $\mathfrak{U}_D$, and $\mathfrak{U}_M$ are assumed to be real.

Let $\mathbf{p}^T = (\mathbf{k}^T, q)$ be an n-dimensional vector of real parameters. The operator $P(q)$ and the matrix $\mathfrak{U}_P(q)$ are smooth functions of the real 'loading' parameter $q \geq 0$. The elements of the differential operator $D(\mathbf{k})$ and the matrix $\mathfrak{U}_D(\mathbf{k})$, containing derivatives of the order of at most m and $m-1$, respectively, are smooth functions of the vector of real 'dissipation' parameters $\mathbf{k}^T = (k_1, \ldots, k_{n-1})$. Moreover, it is assumed that if $\mathbf{k} = 0$ then $D(0) = 0$ and $\mathfrak{U}_D(0) = 0$. The operator M and the matrix $\mathfrak{U}_M$ are parameter independent. Thus, the perturbation of the system by small dissipative forces ($\|\mathbf{k}\| \ll 1$) is *regular* [584].

It is assumed that the unperturbed 'ideal' boundary eigenvalue problem

$$P(q)u + \lambda^2 M u = 0, \quad \mathfrak{U}_P(q)\mathfrak{u} + \lambda^2 \mathfrak{U}_M \mathfrak{u} = 0 \tag{8.8}$$

[2] Higher than second-order operator polynomials in the spectral parameter λ can also appear in nonconservative dissipative stability problems, e.g. in aeroelasticity, where hereditary damping is described by means of fractional derivatives with respect to time [317]. Although the methods of Chapter 7 allow efficient treatment of such generalized eigenvalue problems, here we restrict our consideration to the quadratic operator polynomials in λ.

considered over an interval $0 \le q < q_0$ has a discrete spectrum consisting of simple pure imaginary eigenvalues $\lambda = i\omega$, and consequently the trivial solution to the system (8.4) is marginally stable when $\mathbf{k} = 0$.

We further assume that at $q = q_0$ there exists a pair of double eigenvalues $\pm i\omega_0$, $\omega_0 > 0$ with a Keldysh chain of length 2 whereas other eigenvalues $\pm i\omega_{0,j}$, $\omega_{0,j} > 0$ are pure imaginary and simple, which implies instability because of the secular terms in the solution of the undamped system (8.4) corresponding to the double eigenvalue. Consequently, at $q = q_0$ when there are no velocity-dependent forces ($\mathbf{k}$=0), the nonconservative system is on the boundary between the domains of stability and flutter [273, 277, 298].

The eigenfunction u_0 and the associated eigenfunction u_1 at $i\omega_0$ satisfy equations (7.33) and (7.34), which are now

$$\begin{aligned} L_0 u_0 &:= P(q_0)u_0 - \omega_0^2 M u_0 = 0, \quad \mathfrak{U}_0 \mathfrak{u}_0 := \mathfrak{U}_P(q_0)\mathfrak{u}_0 - \omega_0^2 \mathfrak{U}_M \mathfrak{u}_0 = 0; \\ P(q_0)u_1 - \omega_0^2 M u_1 &= -2i\omega_0 M u_0, \quad \mathfrak{U}_P(q_0)\mathfrak{u}_1 - \omega_0^2 \mathfrak{U}_M \mathfrak{u}_1 = -2i\omega_0 \mathfrak{U}_M \mathfrak{u}_0. \end{aligned} \tag{8.9}$$

The reality of the coefficients of the differential expressions and matrices of the boundary conditions in equations (8.9) implies that the eigenfunction u_0 can be chosen real. Then the associated eigenfunction u_1 will be pure imaginary.

Since the differential expression Lu is a polynomial in the spectral parameter λ, the matrix $\mathfrak{L}(x)$, defined by the formula (7.9), has the form

$$\mathfrak{L}(x) = \lambda^2 \mathfrak{M}(x) + \lambda \mathfrak{D}(x, \mathbf{k}) + \mathfrak{P}(x, q). \tag{8.10}$$

The components of the matrices $\mathfrak{M}$, $\mathfrak{D}$, and $\mathfrak{P}$ consist of the coefficients of the operators M, D and P and their derivatives with respect to x, respectively. Choosing a real matrix $\widetilde{\mathfrak{U}}$ of order $m \times 2m$, we use the equation (7.15) to find matrices $\mathfrak{V}$ and $\widetilde{\mathfrak{V}}$ of order $m \times 2m$, defining the boundary conditions of the adjoint eigenvalue problem.

The eigenfunction v_0 and associated eigenfunction v_1 of the complex-conjugate eigenvalue $-i\omega_0$ satisfy the equations and boundary conditions that follow from equations (7.37) and (7.38)

$$\begin{aligned} P^\dagger(q_0)v_0 - \omega_0^2 M^\dagger v_0 &= 0, \quad \mathfrak{V}_0 \mathfrak{v}_0 = 0, \\ P^\dagger(q_0)v_1 - \omega_0^2 M^\dagger v_1 &= 2i\omega_0 M^\dagger v_0, \quad \mathfrak{V}_0 \mathfrak{v}_1 = -\frac{\partial \mathfrak{V}}{\partial \bar{\lambda}} \mathfrak{v}_0. \end{aligned} \tag{8.11}$$

Since the matrices $\mathfrak{U}_0$ and $\widetilde{\mathfrak{U}}_0$ are real and the matrix polynomial $\mathfrak{L}(x)$, defined by equation (8.10) has real coefficients, it follows by formula (7.15) that the matrices $\mathfrak{V}_0$ and $\widetilde{\mathfrak{V}}_0$ are also real, and the matrices $\frac{\partial \mathfrak{V}}{\partial \lambda}(\bar{\lambda}_0, \mathbf{p}_0)$ and $\frac{\partial \widetilde{\mathfrak{V}}}{\partial \lambda}(\bar{\lambda}_0, \mathbf{p}_0)$, where $\mathbf{p}_0^T = (0, \ldots, 0, q_0)$, are pure imaginary. Consequently, the function v_0 may be assumed to be real and v_1 may be assumed to be pure imaginary.

Since the functions u_0, v_0 are defined up to arbitrary factors, and u_1 and v_1 up to the terms $C_1 u_0$ and $C_2 v_0$, respectively, where C_1 and C_2 are arbitrary constants, we can

choose real functions u_0 and v_0 and pure imaginary functions u_1 and v_1 that satisfy the normalization and orthogonality conditions [280, 282]

$$
\begin{aligned}
&2i\omega_0\left((Mu_1, v_0) + \mathfrak{v}_0^*\widetilde{\mathfrak{V}}_0^*\mathfrak{U}_M\mathfrak{u}_1\right) = 1,\\
&2i\omega_0(Mu_1, v_1) + (Mu_0, v_1) + (Mu_1, v_0)\\
&\quad + \left(\widetilde{\mathfrak{V}}_0\mathfrak{v}_1 + \widetilde{V}_{\tilde{\lambda}}^{(1)}\mathfrak{v}_0\right)^* (2i\omega_0\mathfrak{U}_M\mathfrak{u}_1 + \mathfrak{U}_M\mathfrak{u}_0) + \mathfrak{v}_0^*\widetilde{\mathfrak{V}}_0^*\mathfrak{U}_M\mathfrak{u}_1 = 0.
\end{aligned}
\tag{8.12}
$$

8.1.2 Variation of parameters that is transversal to the stability boundary

Let us vary the parameters in the $(k_1, \ldots, k_n - 1, q)$-space along a smooth curve $\mathbf{p}(\varepsilon)$ that is issued from the point $\mathbf{p}_0^T = (0, \ldots, 0, q_0)$. In the case of the general position, the perturbed double nonsemisimple eigenvalue is determined by the Newton–Puiseux series (7.41) with $k = 2$.

Substituting the operator L, defined by equation (8.7) into equations (7.55) and (7.59) and using the conditions (8.12), we obtain the coefficients λ_1 and λ_2

$$
\lambda_1^2 = -i\omega_0\left\langle \mathbf{f}, \frac{d\mathbf{k}}{d\varepsilon}\right\rangle - \widetilde{f}\frac{dq}{d\varepsilon}, \quad 2\lambda_2 = -\left\langle \mathbf{f} - \omega_0\mathbf{h}, \frac{d\mathbf{k}}{d\varepsilon}\right\rangle - i\widetilde{h}\frac{dq}{d\varepsilon},
\tag{8.13}
$$

where the derivatives are evaluated at $\varepsilon = 0$ and the angular brackets denote the scalar product of real vectors in $\mathbb{R}^{n-1}$. The components of the vector $\mathbf{f} \in \mathbb{R}^{n-1}$ and the real scalar $\widetilde{f}$ are

$$
\begin{aligned}
f_r &= \left(\partial_{k_r} Du_0, v_0\right) + \mathfrak{v}_0^*\widetilde{\mathfrak{V}}_0^*\partial_{k_r}\mathfrak{U}_D\mathfrak{u}_0,\\
\widetilde{f} &= \left(\partial_q Pu_0, v_0\right) + \mathfrak{v}_0^*\widetilde{\mathfrak{V}}_0^*\partial_q\mathfrak{U}_P\mathfrak{u}_0,
\end{aligned}
\tag{8.14}
$$

whereas the components of the vector $\mathbf{h} \in \mathbb{R}^{n-1}$ and the real scalar $\widetilde{h}$ are

$$
\begin{aligned}
ih_r &= \left(\partial_{k_r} Du_1, v_0\right) + \left(\partial_{k_r} Du_0, v_1\right)\\
&\quad + \mathfrak{v}_1^*\widetilde{\mathfrak{V}}_0^*\partial_{k_r}\mathfrak{U}_D\mathfrak{u}_0 + \mathfrak{v}_0^*\widetilde{\mathfrak{V}}_0^*\partial_{k_r}\mathfrak{U}_D\mathfrak{u}_1 + \mathfrak{v}_0^*\left(\widetilde{\mathfrak{V}}_{\tilde{\lambda}}^{(1)}\right)^*\partial_{k_r}\mathfrak{U}_D\mathfrak{u}_0,\\
i\widetilde{h} &= \left(\partial_q Pu_1, v_0\right) + \left(\partial_q Pu_0, v_1\right)\\
&\quad + \mathfrak{v}_1^*\widetilde{\mathfrak{V}}_0^*\partial_q\mathfrak{U}_P\mathfrak{u}_0 + \mathfrak{v}_0^*\widetilde{\mathfrak{V}}_0^*\partial_q\mathfrak{U}_P\mathfrak{u}_1 + \mathfrak{v}_0^*\left(\widetilde{\mathfrak{V}}_{\tilde{\lambda}}^{(1)}\right)^*\partial_q\mathfrak{U}_P\mathfrak{u}_0.
\end{aligned}
\tag{8.15}
$$

Consequently, the splitting of the double eigenvalue $i\omega_0$ due to variation of the parameters $\mathbf{k} = (k_1, \ldots, k_{n-1})$ and q is described by the formula

$$
\lambda = i\omega_0 \pm \sqrt{-i\omega_0\langle \mathbf{f}, \mathbf{k}\rangle - \widetilde{f}(q - q_0)} - \frac{1}{2}\left(\langle \mathbf{f} - \omega_0\mathbf{h}, \mathbf{k}\rangle + i\widetilde{h}(q - q_0)\right) + o\left(|\mathbf{p} - \mathbf{p}_0|\right),
\tag{8.16}
$$

which is valid when the radicand does not vanish [282, 285, 288].

If $\mathbf{k} = 0$, the double eigenvalue splits into two simple pure imaginary eigenvalues (stability), provided that $\widetilde{f}(q - q_0) > 0$. Hence, from the assumption that the system

is stable at $q < q_0$, and unstable at $q > q_0$ it follows that $\widetilde{f} < 0$. The case $\widetilde{f}=0$ is degenerate and will not be considered here.

For a sufficiently small variation of the parameters $\mathbf{k}$ and q, the double eigenvalue $i\omega_0$ generally splits into a complex-conjugate pair of eigenvalues, one of which has a positive real part (flutter). Nevertheless, if $\langle \mathbf{f}, \mathbf{k}\rangle = 0$ and $\langle \mathbf{h}, \mathbf{k}\rangle < 0$, then at $q < q_0$ the square root in equation (8.16) is pure imaginary and the double eigenvalue $i\omega_0$ (and also $-i\omega_0$) splits into two simple eigenvalues with negative real parts (asymptotic stability).

Asymptotic stability of the system (8.4) under perturbation of parameters also depends on the behavior of simple pure imaginary eigenvalues $\pm i\omega_{0,s}$. Choosing the real eigenfunctions $u_{0,s}$, and $v_{0,s}$ of the eigenvalue $i\omega_{0,s}$ that satisfy the normalization conditions

$$2\omega_{0,s}\big((M u_{0,s}, v_{0,s}) + \mathfrak{v}^*_{0,s}\widetilde{\mathfrak{V}}^*_0 \mathfrak{U}_M \mathfrak{u}_{0,s}\big) = 1, \tag{8.17}$$

by equation (7.32), we find the increments to simple eigenvalues

$$\lambda = \pm i\omega_{0,s} \mp i\widetilde{g}_s(q - q_0) - \omega_{0,s}\langle \mathbf{g}_s, \mathbf{k}\rangle + o(|\mathbf{p} - \mathbf{p}_0|^2), \quad s = 1, 2 \ldots \tag{8.18}$$

The real quantity $\widetilde{g}_s$ and the components of the real vector $\mathbf{g}_s \in \mathbb{R}^{n-1}$ are

$$\begin{aligned} \widetilde{g}_s &= (\partial_q P u_{0,s}, v_{0,s}) + \mathfrak{v}^*_{0,s}\widetilde{\mathfrak{V}}^*_0 \partial_q \mathfrak{U}_P \mathfrak{u}_{0,s}, \\ g_{s,r} &= (\partial_{k_r} D u_{0,s}, v_{0,s}) + \mathfrak{v}^*_{0,s}\widetilde{\mathfrak{V}}^*_0 \partial_{k_r} \mathfrak{U}_D \mathfrak{u}_{0,s}. \end{aligned} \tag{8.19}$$

Therefore $\mathrm{Re}\lambda_s < 0$, if $\langle \mathbf{g}_s, \mathbf{k}\rangle > 0$.

We see from equations (8.16) and (8.18) that the system (8.4) is asymptotically stable for sufficiently small *linear* variations of the parameters $\mathbf{k}$, and q, provided the following conditions hold simultaneously

$$\langle \mathbf{f}, \mathbf{k}\rangle = 0, \quad q < q_0, \quad \langle \mathbf{h}, \mathbf{k}\rangle < 0, \quad \langle \mathbf{g}_s, \mathbf{k}\rangle > 0, \quad s = 1, 2, \ldots \tag{8.20}$$

The set determined by equation (8.20) is tangent to the boundary of asymptotic stability. The variations of the parameters such that $\langle \mathbf{f}, \mathbf{k}\rangle \neq 0$ are *transversal* to the stability boundary at the point $\mathbf{p} = \mathbf{p}_0$. According to equation (8.16) they lead to the flutter domain.

8.1.3 Variation of parameters that is tangential to the stability boundary

The conditions (8.20) demonstrate that the set of directions leading from the point $\mathbf{p}_0$ to the domain of asymptotic stability is of dimension $n - 1$ in the $(k_1, \ldots, k_{n-1}, q)$-space of parameters. This set forms a (degenerate) tangent cone [374, 375, 518] to the domain of asymptotic stability at $\mathbf{p}_0$. Thus, starting from the point $\mathbf{p}_0$, one can reach other points of the asymptotic stability domain only along the curves that are tangent to the plane $\langle \mathbf{f}, \mathbf{k}\rangle = 0$ at $\mathbf{p}_0$:

$$\mathbf{p}(\varepsilon) = \begin{pmatrix} 0 \\ q_0 \end{pmatrix} + \varepsilon \begin{pmatrix} d\mathbf{k}/d\varepsilon \\ 0 \end{pmatrix} + \frac{\varepsilon^2}{2} \begin{pmatrix} d^2\mathbf{k}/d\varepsilon^2 \\ d^2q/d\varepsilon^2 \end{pmatrix} + o(\varepsilon^2) \tag{8.21}$$

where

$$\left\langle \mathbf{f}, \frac{d\mathbf{k}}{d\varepsilon} \right\rangle = 0. \tag{8.22}$$

The curve (8.21) is orthogonal to the q axis in the $(k_1, \ldots, k_{n-1}, q)$-space because of the assumption that $dq/d\varepsilon \equiv 0$. Therefore, the coefficient λ_1 determined by the first of equations (8.13) vanishes along the curve.

Consequently, the double eigenvalue $i\omega_0$ in this degenerate case splits into two simple eigenvalues that depend linearly on ε [584]

$$\lambda = i\omega_0 + \lambda_2 \varepsilon + o(\varepsilon), \tag{8.23}$$

where λ_2 is a root of the quadratic equation (7.70), which, for an operator L with boundary conditions given by (8.7) and eigenfunctions and associated eigenfunctions satisfying equations (8.9), (8.11), and (8.12), takes the form[3]

$$\lambda_2^2 - \lambda_2 \omega_0 \left\langle \mathbf{h}, \frac{d\mathbf{k}}{d\varepsilon} \right\rangle + \left(\frac{1}{2} \widetilde{f} \frac{d^2 q}{d\varepsilon^2} + \omega_0^2 \left\langle \mathbf{G} \frac{d\mathbf{k}}{d\varepsilon}, \frac{d\mathbf{k}}{d\varepsilon} \right\rangle \right) + i\omega_0 \left(\frac{1}{2} \left\langle \mathbf{f}, \frac{d^2 \mathbf{k}}{d\varepsilon^2} \right\rangle + \left\langle \mathbf{H} \frac{d\mathbf{k}}{d\varepsilon}, \frac{d\mathbf{k}}{d\varepsilon} \right\rangle \right) = 0. \tag{8.24}$$

The real vectors $\mathbf{f}$, $\mathbf{h}$ and the coefficient $\widetilde{f}$ in equation (8.24) are defined by equations (8.14) and (8.15), the real matrix $\mathbf{H}$ has the components

$$H_{r\sigma} = \frac{1}{2} \left(\partial_{k_r} \partial_{k_\sigma} D u_0, v_0 \right) + \frac{1}{2} v_0^* \widetilde{\mathfrak{V}}_0^* \partial_{k_r} \partial_{k_\sigma} \mathfrak{U}_D \mathfrak{u}_0, \tag{8.25}$$

and the real matrix $\mathbf{G}$ is defined by the expression

$$\left\langle \mathbf{G} \frac{d\mathbf{k}}{d\varepsilon}, \frac{d\mathbf{k}}{d\varepsilon} \right\rangle = \sum_{r=1}^{n-1} \frac{dk_r}{d\varepsilon} \left((\partial_{k_r} D \hat{w}_2, v_0) + v_0^* \widetilde{\mathfrak{V}}_0^* \partial_{k_r} \mathfrak{U}_D \hat{\mathfrak{w}}_2 \right), \tag{8.26}$$

where $\hat{w}_2$ is a solution to the boundary value problem

$$\begin{aligned} P(q_0)\hat{w}_2 - \omega_0^2 M \hat{w}_2 &= \sum_{r=1}^{n-1} \frac{dk_r}{d\varepsilon} \partial_{k_r} D u_0, \\ \mathfrak{U}_P(q_0)\hat{\mathfrak{w}}_2 - \omega_0^2 \mathfrak{U}_M \hat{\mathfrak{w}}_2 &= \sum_{r=1}^{n-1} \frac{dk_r}{d\varepsilon} \partial_{k_r} \mathfrak{U}_D \mathfrak{u}_0 \end{aligned} \tag{8.27}$$

that exists owing to the validity of the solvability condition (8.22).

[3] Note that a similar equation was obtained in 1989 by Banichuk et al. [32, 33] who were apparently the first to propose probing the parameter space along the curves tangent to the stability boundary for a quantitative description of the Ziegler–Bottema destabilization paradox in one-parameter finite-dimensional circulatory systems.

8.1.4 Transfer of instability between modes

With expressions (8.21)–(8.23), the quadratic equation (8.24) transforms into

$$(\lambda - i\omega_0)^2 - \omega_0\langle \mathbf{h}, \mathbf{k}\rangle(\lambda - i\omega_0) + \widetilde{f}(q - q_0) + \omega_0^2\langle \mathbf{Gk}, \mathbf{k}\rangle + i\omega_0\left(\langle \mathbf{f}, \mathbf{k}\rangle + \langle \mathbf{Hk}, \mathbf{k}\rangle\right) = 0 \tag{8.28}$$

Assuming $\lambda = \mathrm{Re}\lambda + i\,\mathrm{Im}\lambda$ in equation (8.28) and separating the real and imaginary parts, we find the following expressions [282, 285, 288]

$$(\mathrm{Im}\lambda - \omega_0 + \mathrm{Re}\lambda + c/2)^2 - (\mathrm{Im}\lambda - \omega_0 - \mathrm{Re}\lambda - c/2)^2 = -2e, \tag{8.29}$$

$$\left(\mathrm{Re}\lambda + \frac{c}{2}\right)^4 + \left(d - \frac{c^2}{4}\right)\left(\mathrm{Re}\lambda + \frac{c}{2}\right)^2 = \frac{e^2}{4}, \tag{8.30}$$

$$(\mathrm{Im}\lambda - \omega_0)^4 - \left(d - \frac{c^2}{4}\right)(\mathrm{Im}\lambda - \omega_0)^2 = \frac{e^2}{4}, \tag{8.31}$$

where

$$c = -\omega_0\langle \mathbf{h}, \mathbf{k}\rangle, \quad d = \widetilde{f}(q - q_0) + \omega_0^2\langle \mathbf{Gk}, \mathbf{k}\rangle, \quad e = \omega_0\left(\langle \mathbf{f}, \mathbf{k}\rangle + \langle \mathbf{Hk}, \mathbf{k}\rangle\right). \tag{8.32}$$

Let $\mathbf{k} = 0$, i.e. the system (8.4), be circulatory. Then, by equation (8.32), we have $c = 0$, $d = \widetilde{f}(q - q_0)$, $e = 0$. Hence, equations (8.30) and (8.31) become

$$q \le q_0\colon\ \mathrm{Re}\lambda = 0, \quad \mathrm{Im}\lambda = \omega_0 \pm \sqrt{\widetilde{f}(q - q_0)}, \tag{8.33}$$

$$q \ge q_0\colon\ \mathrm{Re}\lambda = \pm\sqrt{-\widetilde{f}(q - q_0)}, \quad \mathrm{Im}\lambda = \omega_0. \tag{8.34}$$

Since we assumed that $\widetilde{f} < 0$, as the load parameter q is increased, the two pure imaginary eigenvalues move along the imaginary axis, coalesce at $q = q_0$ and form a pair of double eigenvalues (flutter boundary). Then the double eigenvalue splits into two simple ones that move apart in directions perpendicular to the imaginary axis. The trajectories of the eigenvalues of the circulatory system that pass through the 1:1 nonsemisimple resonance as the parameter q varies, are shown in Figure 8.2 by thin lines.

If $\mathbf{k}\neq 0$ and $e\neq 0$, the velocity-dependent forces [459, 460] disturb the coalescent at the 1:1 resonance modes by displacing and splitting the trajectories of the eigenvalues, as shown in Figure 8.2 (a) by the bold black lines. This qualitative effect (the *imperfect merging of modes* [226]), known in the literature only from numerical solutions of particular problems, see e.g. [14, 75–77, 501], is described here analytically by equations (8.29)–(8.31) for a sufficiently broad class of continuous nonconservative systems described by equation (8.4).

Indeed, given the vector $\mathbf{k} \neq 0$ such that $c \neq 0$ and $e \neq 0$, as the parameter q varies, the perturbed eigenvalues move in the complex plane along the branches of the

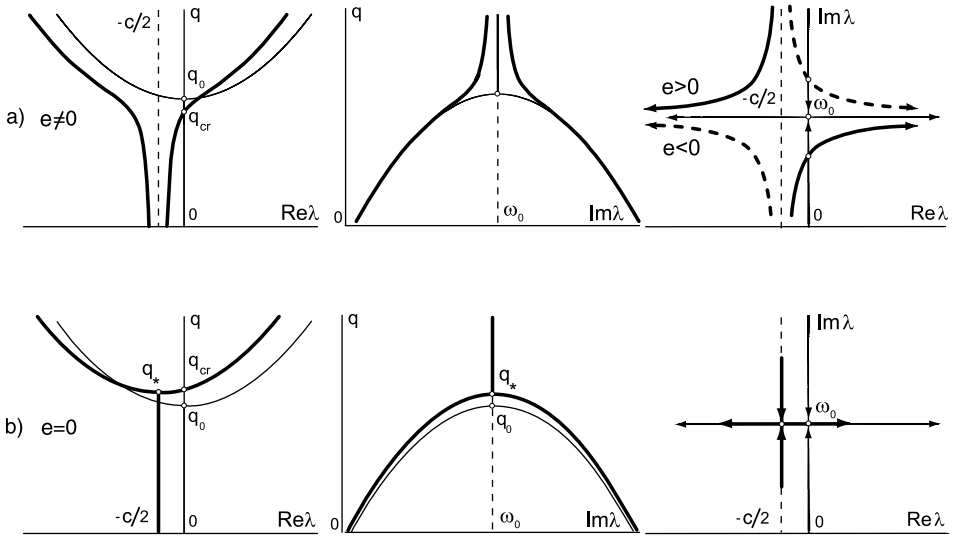

Figure 8.2. The eigenvalues in the 1 : 1 nonsemisimple resonance (thin lines) and its dissipative unfolding (bold lines) when (a) $e := \omega_0 (\langle \mathbf{f}, \mathbf{k} \rangle + \langle \mathbf{Hk}, \mathbf{k} \rangle) \neq 0$ and (b) when $e = 0$. In the former case, the sign of e determines which of the two modes involved in the resonance becomes unstable in the presence of the velocity-dependent perturbation (transfer of instability between modes).

hyperbola (8.29) that has two asymptotes, $\mathrm{Re}\lambda = -c/2$ and $\mathrm{Im}\lambda = \omega_0$, where c and e are defined by equation (8.32). If $c > 0$, then one of the two eigenvalues remains in the left half of the complex plane, whereas the other crosses the imaginary axis and enters the right half at $q = q_{cr}(\mathbf{k})$ becoming $\lambda = \lambda_{cr}$, where

$$\mathrm{Re}\lambda_{cr} = 0, \quad \mathrm{Im}\lambda_{cr} = \omega_0 - \frac{e}{c}. \tag{8.35}$$

Therefore, when $e > 0$ the mode with the frequency that is lower than ω_0 is unstable by flutter (cf. the solid black line in the far right panel of Figure 8.2 (a)) whereas for $e < 0$ the unstable mode is that whose frequency exceeds ω_0 (shown by the dashed black line in the far right panel of Figure 8.2 (a)). The quantity e thus governs the *transfer of instability between modes* that frequently occurs in nonconservative systems with dissipation [75, 157, 246, 518].

8.1.5 Drop in the critical frequency

Taking into account equation (8.32) we write an explicit expression for the critical frequency at the flutter threshold as a function of the parameters of dissipation

$$\omega_{cr}(\mathbf{k}) := \mathrm{Im}\lambda_{cr}(\mathbf{k}) = \omega_0 + \frac{\langle \mathbf{f}, \mathbf{k} \rangle + \langle \mathbf{Hk}, \mathbf{k} \rangle}{\langle \mathbf{h}, \mathbf{k} \rangle}. \tag{8.36}$$

Assuming $\mathbf{k} = \epsilon\widetilde{\mathbf{k}}$, where the vector $\widetilde{\mathbf{k}}$ is fixed and $\epsilon > 0$ is a small parameter, we find that the critical frequency exhibits a finite drop/jump when $\epsilon \to 0$:

$$\Delta\omega := \omega_0 - \lim_{\epsilon\to 0} \omega_{cr}(\epsilon\widetilde{\mathbf{k}}) = -\frac{\langle \mathbf{f}, \widetilde{\mathbf{k}}\rangle}{\langle \mathbf{h}, \widetilde{\mathbf{k}}\rangle} \tag{8.37}$$

this does not happen only if $e = 0$. In this case, by equations (8.30) and (8.31)

$$q \le q_*: \qquad \mathrm{Re}\lambda = \omega_0 \frac{\langle \mathbf{h}, \mathbf{k}\rangle}{2}, \ \ \mathrm{Im}\lambda = \omega_0 \pm \sqrt{\widetilde{f}(q - q_*)}, \tag{8.38}$$

$$q \ge q_*: \qquad \mathrm{Re}\lambda = \omega_0 \frac{\langle \mathbf{h}, \mathbf{k}\rangle}{2} \pm \sqrt{-\widetilde{f}(q - q_*)}, \ \ \mathrm{Im}\lambda = \omega_0, \tag{8.39}$$

meaning that the complex eigenvalues λ with $\mathrm{Re}\lambda = -c/2$ merge at $q = q_*$,

$$q_* = q_0 + \omega_0^2 \frac{\langle \mathbf{h}, \mathbf{k}\rangle^2 - 4\langle \mathbf{G}\mathbf{k}, \mathbf{k}\rangle}{4\widetilde{f}}, \tag{8.40}$$

see Figure 8.2 (b). When the parameter q is increased further, the double complex eigenvalue $\lambda_* = -c/2 + i\omega_0$ splits into two simple eigenvalues, one of which crosses the imaginary axis at $q = q_{cr}(\mathbf{k})$, where

$$q_{cr}(\mathbf{k}) = q_0 - \frac{\omega_0^2}{\widetilde{f}} \langle \mathbf{G}\mathbf{k}, \mathbf{k}\rangle. \tag{8.41}$$

Thus, we arrive at the conclusion that in the case when $e = 0$, small velocity-dependent forces only displace the picture of bifurcation of eigenvalues at the 1:1 nonsemisimple resonance from the imaginary axis, as shown in Figure 8.2 (b) for $c > 0$. As in the case $e \neq 0$, both eigenvalues are in the left half-plane if

$$q < q_{cr}(\mathbf{k}), \quad \langle \mathbf{h}, \mathbf{k}\rangle < 0. \tag{8.42}$$

The critical load (8.41) smoothly depends on the vector $\mathbf{k}$ and tends to q_0 when $\mathbf{k}$ vanishes. Depending on the sign of the quadratic form $\langle \mathbf{G}\mathbf{k}, \mathbf{k}\rangle$, the critical load can both increase or decrease with the increase in the magnitude of the velocity-dependent (damping) forces, when $e = 0$.

8.2 Singular threshold of the flutter instability

In general, the value of the parameter q, at which one of the eigenvalues of the perturbed 1:1 resonance crosses the imaginary axis, is obtained from equation (8.30) by assuming that $\mathrm{Re}\lambda = 0$. This yields a relation $dc^2 = e^2$, which, given the explicit

expressions (8.32) for c, d, and e, becomes [278, 280, 285, 288]

$$q_{cr}(\mathbf{k}) = q_0 + \frac{(\langle \mathbf{f},\mathbf{k}\rangle + \langle \mathbf{Hk},\mathbf{k}\rangle)^2}{\widetilde{f}\,\langle \mathbf{h},\mathbf{k}\rangle^2} - \frac{\omega_0^2}{\widetilde{f}}\langle \mathbf{Gk},\mathbf{k}\rangle. \tag{8.43}$$

Thus, both perturbed eigenvalues are situated in the left half of the complex plane when the conditions (8.42) are fulfilled.[4]

Since by assumption $\widetilde{f} < 0$, it follows from equation (8.43) that the critical load of the system perturbed by the velocity-dependent forces is such that $q_{cr}(\mathbf{k}) < q_0$, provided that $\langle \mathbf{Gk},\mathbf{k}\rangle < 0$. However, if $\langle \mathbf{Gk},\mathbf{k}\rangle > 0$ there is a region of the parameter space in which, given a variation of the parameter vector $\mathbf{k}$, defined by the second inequality of (8.42) and the condition

$$(\langle \mathbf{f},\mathbf{k}\rangle + \langle \mathbf{Hk},\mathbf{k}\rangle)^2 - \omega_0^2\langle \mathbf{Gk},\mathbf{k}\rangle\langle \mathbf{h},\mathbf{k}\rangle^2 < 0, \tag{8.44}$$

the critical load of the perturbed system exceeds that of the ideal one: $q_{cr}(\mathbf{k}) > q_0$.

8.2.1 Drop in the critical flutter load

Let us confine ourselves to the case when

$$\{\mathbf{k} : \langle \mathbf{f},\mathbf{k}\rangle = 0, \langle \mathbf{h},\mathbf{k}\rangle < 0\} \subset \{\mathbf{k} : \langle \mathbf{g}_s,\mathbf{k}\rangle > 0, s = 1,2,\ldots\}, \tag{8.45}$$

implying that all simple eigenvalues $\pm i\omega_{0,s}$ for a small perturbation of the parameters q and $\mathbf{k}$ move into the left half of the complex plane. Therefore, the stability of the system (8.4) depends only on the behavior of the double eigenvalues $\pm i\omega_0$ under the perturbation. Consequently, the surface $q_{cr}(k_1,\ldots,k_{n-1})$, which is approximated by equation (8.43) under the restriction imposed by the second inequality of equation (8.42), is the boundary of the asymptotic stability domain in a small neighborhood of the point $\mathbf{p}_0^T = (0,\ldots,0,q_0)$.

The function $q_{cr}(\mathbf{k})$, defined by equation (8.43), is the sum of rational and polynomial parts. Both the numerator and denominator of the rational part contain linear forms in the vector $\mathbf{k}$. Thus, the function $q_{cr}(\mathbf{k})$ has a singularity at the point $\mathbf{k} = 0$, and the critical load, as a function of $n-1$ variables, does not have a limit as $\mathbf{k}^T = (k_1,\ldots,k_{n-1}) \to 0$. This fact was known for the critical load of Ziegler's pendulum [615] and has proved to be valid for arbitrary linear nonconservative systems with a finite number of degrees of freedom in [285, 287, 288].

Nevertheless, the homogeneity of the numerator and denominator of the rational part of $q_{cr}(\mathbf{k})$ guarantees the existence of a limit $\lim_{\epsilon\to 0} q_{cr}(\epsilon\widetilde{\mathbf{k}})$ for any direction $\widetilde{\mathbf{k}}$, such that

[4] The necessary and sufficient conditions (8.42) and (8.43) for all roots of the complex polynomial (8.28) to have negative real parts may also be obtained from Bilharz's criterion [62], which is an analogue for the Routh–Hurwitz criterion for complex polynomials.

$\langle \mathbf{h}, \widetilde{\mathbf{k}} \rangle \neq 0$. Substituting $\mathbf{k} = \epsilon \widetilde{\mathbf{k}}$ in equation (8.43), we obtain an explicit expression approximating the drop in the critical flutter load caused by the infinitesimally small velocity-dependent (e.g. damping) forces [278]:

$$\Delta q := q_0 - \lim_{\epsilon \to 0} q_{cr}(\epsilon \widetilde{\mathbf{k}}) = -\frac{1}{\widetilde{f}} \frac{\langle \mathbf{f}, \widetilde{\mathbf{k}} \rangle^2}{\langle \mathbf{h}, \widetilde{\mathbf{k}} \rangle^2}. \tag{8.46}$$

This formula gives a constructive answer to Swaters' question [563]: the drop in the flutter threshold in a zero dissipation limit is a generic phenomenon because it takes place for almost every combination of damping parameters specified by the vector $\widetilde{\mathbf{k}}$.

8.2.2 The "no drop" condition and the tangent cone to the domain of asymptotic stability

The finite drop in the critical load (8.43) does not occur ($\Delta q = 0$) in the degenerate case: $\langle \mathbf{f}, \widetilde{\mathbf{k}} \rangle = 0$. For a two-dimensional vector $\mathbf{k}^T = (k_1, k_2)$ this condition yields the following ratio of the parameters k_1 and k_2

$$\frac{k_i}{k_j} = -\frac{f_j}{f_i}, \quad i, j = 1, 2, \tag{8.47}$$

at which small velocity-dependent forces do not reduce the critical flutter load. The quantities f_1 and f_2 are defined by the first of equations (8.14). Note that the strong dependence of the critical flutter load on the ratio of the damping parameters was observed already by Smith [534] in rotor dynamics and then by Bolotin in structural mechanics [75].

The function $q_{cr}(\mathbf{k})$, defined by equation (8.43) under the constraint (8.42), defines the boundary between the domains of the asymptotic stability and flutter of the system (8.4) in the n-dimensional space of the parameters $\mathbf{k}$ and q. The level sets of the function $q_{cr}(\mathbf{k})$ are the boundaries of the stability domain in the $(k_1, \ldots, k_{n-1})$-space. The level set $q_{cr} = q_0$, where q_0 is the critical value of the parameter q in the ideal system, is given by the equation

$$\langle \mathbf{f}, \mathbf{k} \rangle = \pm \omega_0 \langle \mathbf{h}, \mathbf{k} \rangle \sqrt{\langle \mathbf{G}\mathbf{k}, \mathbf{k} \rangle} - \langle \mathbf{H}\mathbf{k}, \mathbf{k} \rangle. \tag{8.48}$$

This equation has real solutions if $\langle \mathbf{G}\mathbf{k}, \mathbf{k} \rangle \geq 0$. In that case the set (8.48) bounds the domain of variation of the vector of parameters $\mathbf{k}$, in which $q_{cr}(\mathbf{k}) > q_0$. If the matrix $\mathbf{G}$ is negative-definite, then $\langle \mathbf{G}\mathbf{k}, \mathbf{k} \rangle < 0$, and equation (8.48) has a unique real solution $\mathbf{k} = 0$, implying a decrease in the critical flutter load (destabilization) for any small $\mathbf{k} \neq 0$.

Let $\mathbf{k}^T = (k_1, k_2)$. Then the boundary of the stability domain, described by the function $q_{cr}(k_1, k_2)$, is a surface in the three-dimensional (k_1, k_2, q)-space. To understand

the structure of this surface, we shall find asymptotic formulae for the level curves of the function $q_{cr}(k_1, k_2)$ in the neighborhood of the origin in the (k_1, k_2)-plane for q_{cr}, close to q_0.

We first approximate the level curves when $q_{cr} < q_0$. Assuming $k_i = \beta_j k_j + o(k_j)$, where β_j is an unknown coefficient, we find from equation (8.43) that

$$k_i = -\frac{f_j \pm h_j \sqrt{\widetilde{f}\,(q_{cr} - q_0)}}{f_i \pm h_i \sqrt{\widetilde{f}\,(q_{cr} - q_0)}} k_j + o(k_j), \quad i, j = 1, 2. \tag{8.49}$$

Since by assumption $\widetilde{f} < 0$, at $q_{cr} < q_0$ the boundary of the asymptotic stability domain in the (k_1, k_2)-plane is approximated by the two straight lines intersecting at the origin, as shown in Figure 8.3 (a). Note that only the parts of the lines that belong to the half-plane $\langle \mathbf{h}, \mathbf{k} \rangle < 0$, bound the domain of the asymptotic stability (hatched).

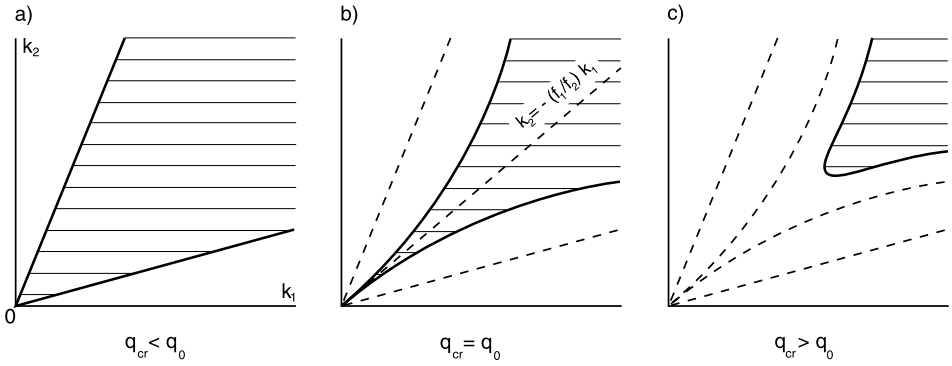

Figure 8.3. Cross-sections of the singular surface (8.43) in the vicinity of the origin at different levels of q_{cr} in the (k_1, k_2)-plane. The diagonal dashed line in the panel (b) marks the projection of the tangent cone to the three-dimensional domain of the asymptotic stability at its singular point.

It follows from equation (8.49) that, as q_{cr} increases, the angle between the lines bounding the asymptotic stability domain decreases, vanishing at $q_{cr} = q_0$. In that case the equations of the first-order approximation (8.49) define only the ratio of the parameters k_1 and k_2, as in equation (8.47). Substituting $k_i = -(f_j/f_i)k_j + \gamma_j k_j^2 + o(k_j^2)$, where γ_j is an unknown coefficient, into equation (8.48) and collecting terms with the similar powers of k_j, we find a second-order approximation to the level curve $q_{cr} = q_0$:

$$k_i = -\frac{f_j}{f_i} k_j - \frac{\mathbf{f}^T \hat{\mathbf{H}} \mathbf{f} \pm \omega_0 (h_i f_j - h_j f_i) \sqrt{\mathbf{f}^T \hat{\mathbf{G}} \mathbf{f}}}{f_i^3} k_j^2 + o(k_j^2), \tag{8.50}$$

where

$$\hat{\mathbf{H}} = \begin{pmatrix} H_{22} & -H_{12} \\ -H_{21} & H_{11} \end{pmatrix}, \quad \hat{\mathbf{G}} = \begin{pmatrix} G_{22} & -G_{12} \\ -G_{21} & G_{11} \end{pmatrix},$$

and H_{rs}, G_{rs} $(r, s = 1, 2)$ are the components of the matrices $\mathbf{H}$ and $\mathbf{G}$, determined by equations (8.25) and (8.26).

Equation (8.50) describes two curves that touch each other at the origin in the (k_1, k_2)-plane, forming a degenerate singularity known as a cuspidal point [17]. Generally, the straight line $k_i = -(f_j/f_i)k_j$ is not always situated within the stability domain. However, in the case when the operator $D(\mathbf{k})$ and the matrix $\mathfrak{U}_D(\mathbf{k})$ is a linear function of the parameters, it will always be in the asymptotic stability domain, see Figure 8.3 (b), because the matrix $\mathbf{H}$, whose elements are the second derivatives of $D(\mathbf{k})$ and $\mathfrak{U}_D(\mathbf{k})$ with respect to the parameters k_1 and k_2, vanishes.

To study the level curves at $q_{cr} > q_0$, we rewrite equation (8.43) as follows:

$$\langle \mathbf{f}, \mathbf{k} \rangle + \langle \mathbf{Hk}, \mathbf{k} \rangle = \pm \langle \mathbf{h}, \mathbf{k} \rangle \sqrt{\widetilde{f}(q_{cr} - q_0) + \omega_0^2 \langle \mathbf{Gk}, \mathbf{k} \rangle} \tag{8.51}$$

If $\langle \mathbf{Gk}, \mathbf{k} \rangle > 0$, the real solutions of equation (8.51) exist provided that

$$\|\mathbf{k}\| := \sqrt{\langle \mathbf{k}, \mathbf{k} \rangle} > \sqrt{\frac{-\widetilde{f}(q_{cr} - q_0)}{\omega_0^2 \langle \mathbf{Ge}, \mathbf{e} \rangle}} > 0, \tag{8.52}$$

where $\mathbf{e} = \mathbf{k}/\|\mathbf{k}\|$. The condition (8.52) means that the level curves $q_{cr} > q_0$ do not pass through the origin, as shown in Figure 8.3 (c).

Thus, having analyzed the level curves of the function $q_{cr}(k_1, k_2)$, one can state that the boundary of the asymptotic stability domain given by equation (8.43), in the neighborhood of the point $(0, 0, q_0)$ in the (k_1, k_2, q)-space is a surface with self-intersection along the q-axis and a singular point at $q = q_0$ and $k_{1,2} = 0$. This is the Whitney umbrella singularity, because equation (8.43) is equivalent to $cd^2 = e^2$, i.e. to the defining equation for the Whitney umbrella surface [17, 231]. The second condition of (8.42) cuts off half of the umbrella. The remaining pocket bounds the asymptotic stability domain.

We know that the Whitney umbrella is a singularity of general position of the boundary of the domain of asymptotic stability of three-parameter finite-dimensional dissipative nonconservative systems, corresponding to a pure imaginary eigenvalue with algebraic multiplicity 2 and geometric multiplicity 1 [17]. In mechanical applications, this singularity was first found in 1956 on the stability boundary of Ziegler's pendulum by Bottema [80, 81]. We have established that the Whitney umbrella is also a generic singularity of the boundary of the asymptotic stability domain in continuous nonconservative systems of type (8.4) that depend on three parameters. The set $\{\mathbf{k} : \langle \mathbf{f}, \mathbf{k} \rangle = 0, \ \langle \mathbf{h}, \mathbf{k} \rangle < 0, \ q < q_0\}$ is thus a tangent cone to the singular domain of asymptotic stability at the exceptional point $(0, 0, q_0)$. According to equation (8.29), at small k_1 and k_2, it is the penetration of the plane (8.47) that yields transition of instability between modes shown in Figure 8.2 (a).

Therefore, by means of approximations (8.29)–(8.31) and (8.43), we have established a direct link between the singular geometry of the domain of asymptotic sta-

bility and the peculiar movement of eigenvalues of a circulatory system perturbed by small velocity-dependent forces.

8.3 Example: dissipation-induced instability of Beck's column

Let us return to the problem (8.1) of transverse vibrations in a viscous medium of a cantilever rod made of a viscoelastic Kelvin–Voigt material, loaded at its free end by a tangential follower force q [14,77]. In dimensionless variables, the stability problem reduces to investigation of the eigenvalue problem (8.2), which can be represented in the form (8.7) with the operators

$$P := \partial_x^4 + q\partial_x^2, \quad D := k_1\partial_x^4 + k_2, \quad M := 1 \tag{8.53}$$

and the matrix of the boundary conditions

$$\mathfrak{U} = \mathfrak{U}_P := \begin{pmatrix} 1 & 0 & 0 & 0 & 0 & 0 & 0 & 0 \\ 0 & 1 & 0 & 0 & 0 & 0 & 0 & 0 \\ 0 & 0 & 0 & 0 & 0 & 0 & 1 & 0 \\ 0 & 0 & 0 & 0 & 0 & 0 & 0 & 1 \end{pmatrix}. \tag{8.54}$$

By formula (7.9), we have $\mathfrak{L}(x) = \mathfrak{L}_P(x) + \lambda\mathfrak{L}_D(x)$, where

$$\mathfrak{L}_P(x) = \begin{pmatrix} 0 & q & 0 & 1 \\ -q & 0 & -1 & 0 \\ 0 & 1 & 0 & 0 \\ -1 & 0 & 0 & 0 \end{pmatrix}, \quad \mathfrak{L}_D(x) = \begin{pmatrix} 0 & 0 & 0 & k_1 \\ 0 & 0 & -k_1 & 0 \\ 0 & k_1 & 0 & 0 \\ -k_1 & 0 & 0 & 0 \end{pmatrix}. \tag{8.55}$$

Then, choosing the matrix $\widetilde{\mathfrak{U}}$ in the form

$$\widetilde{\mathfrak{U}} = \begin{pmatrix} 0 & 0 & 0 & 0 & 1 & 0 & 0 & 0 \\ 0 & 0 & 0 & 0 & 0 & 1 & 0 & 0 \\ 0 & 0 & 1 & 0 & 0 & 0 & 0 & 0 \\ 0 & 0 & 0 & 1 & 0 & 0 & 0 & 0 \end{pmatrix} \tag{8.56}$$

from equation (7.15) we obtain

$$\mathfrak{V} = \begin{pmatrix} 0 & 0 & 0 & 0 & 0 & -q & 0 & -1-k_1\overline{\lambda} \\ 0 & 0 & 0 & 0 & q & 0 & 1+k_1\overline{\lambda} & 0 \\ 0 & 1+k_1\overline{\lambda} & 0 & 0 & 0 & 0 & 0 & 0 \\ -1-k_1\overline{\lambda} & 0 & 0 & 0 & 0 & 0 & 0 & 0 \end{pmatrix},$$

$$\widetilde{\mathfrak{V}} = \begin{pmatrix} 0 & -q & 0 & -1-k_1\overline{\lambda} & 0 & 0 & 0 & 0 \\ q & 0 & 1+k_1\overline{\lambda} & 0 & 0 & 0 & 0 & 0 \\ 0 & 0 & 0 & 0 & 0 & 1+k_1\overline{\lambda} & 0 & 0 \\ 0 & 0 & 0 & 0 & -1-k_1\overline{\lambda} & 0 & 0 & 0 \end{pmatrix}. \tag{8.57}$$

Hence, by equation (7.17) the eigenvalue problem that is adjoint to (8.2) is

$$\begin{gathered}(1+k_1\overline{\lambda})\partial_x^4 v + q\partial_x^2 v + (\overline{\lambda}^2 + k_2\overline{\lambda})v = 0, \\ v(0) = 0, \quad v_x^{(1)}(0) = 0, \\ (1+k_1\overline{\lambda})v_x^{(2)}(1) + qv(1) = 0, \quad (1+k_1\overline{\lambda})v_x^{(3)}(1) + qv_x^{(1)} = 0.\end{gathered} \tag{8.58}$$

8.3.1 Beck's column without damping

When there is no damping, i.e. $k_1 = 0$ and $k_2 = 0$, the natural frequencies, ω, of the system (8.2), are defined by the characteristic equation (7.99) where one should put $\kappa = 0$, $\eta = 1$ and $\lambda = \omega^2$. It is well known that the undamped Beck's column is marginally stable at the magnitudes of the follower force in the interval $0 \le q < q_0$, where $q_0 \approx 20.05095361$ [39, 113].

When $q = q_0$, the spectrum of the undamped Beck's column is discrete [14]. It consists of a pair of double pure imaginary eigenvalues $\pm i\omega_0$ ($\omega_0 \approx 11.01555764$) and simple pure imaginary eigenvalues $\pm i\omega_{0,s}$, $s = 1, 2, \ldots$, the sequence of simple frequencies being

$$\begin{aligned}\omega_{0,1} &\approx 53.70722261, \\ \omega_{0,2} &\approx 112.3934991, \\ \omega_{0,3} &\approx 191.0562906, \\ &\cdots \\ \omega_{0,s\to\infty} &\sim \pi^2 s^2 + O(s).\end{aligned} \tag{8.59}$$

The asymptotic behavior of the eigenvalues (8.59) was obtained in [14].

The double eigenvalue $i\omega_0$ has a Keldysh chain of length 2, consisting of the eigenfunction u_0 and associated eigenfunction u_1, which satisfy the equations with boundary conditions (8.3). The eigenfunction and associated function of the complex-conjugate eigenvalue $-i\omega_0$ are solutions to the equations and boundary conditions obtained from equations (8.11) and (8.58):

$$\begin{gathered}\partial_x^4 v_0 + q_0\partial_x^2 v_0 - \omega_0^2 v_0 = 0, \\ v_0(0) = 0, \quad v_{0x}^{(1)}(0) = 0, \quad v_{0x}^{(2)}(1) + q_0 v_0(1) = 0, \quad v_{0x}^{(3)}(1) + q_0 v_{0x}^{(1)}(1) = 0, \\ \partial_x^4 v_1 + q_0\partial_x^2 v_1 - \omega_0^2 v_1 = 2i\omega_0 v_0, \\ v_1(0) = 0, \quad v_{1x}^{(1)}(0) = 0, \quad v_{1x}^{(2)}(1) + q_0 v_1(1) = 0, \quad v_{1x}^{(3)}(1) + q_0 v_{1x}^{(1)}(1) = 0.\end{gathered} \tag{8.60}$$

The eigenfunctions u_0, v_0 are defined by equations (7.101)–(7.103) and (7.98), where one should put $\kappa = 0$ and $\lambda = \omega_0^2$.

Solving the second boundary value problem (8.3) we find the associated function u_1

$$u_1(x) = -2i\omega_0 \frac{a\sin(bx) + b\sinh(ax) + F(a^2\cos(bx) - b^2\cosh(ax))}{2ab(a^2+b^2)}x$$
$$- 2i\omega_0 \frac{A_1\sinh(ax) - B_1\sin(bx)}{2ab(a^2+b^2)(a\sinh(a) + b\sin(b))^2}. \tag{8.61}$$

The second boundary value problem (8.60) yields the associated function v_1

$$v_1(x) = 2i\omega_0 \frac{a\sin(bx) + b\sinh(ax) + G(a^2\cos(bx) - b^2\cosh(ax))}{2ab(a^2+b^2)}x$$
$$+ 2i\omega_0 \frac{A_2\sinh(ax) - B_2\sin(bx)}{2ab(a^2+b^2)(b^3\sinh(a) + a^3\sin(b))^2}. \tag{8.62}$$

The coefficients A_1, B_1 and A_2, B_2 are defined by equations (7.121) and (7.123), and the quantities a and b by equation (7.98) where $\kappa = 0$, $\eta = 1$, and $\lambda = \omega_0^2$.

In the following we will use the eigenfunctions and associated functions that are evaluated at $k_1 = 0$, $k_2 = 0$, and $q = q_0$ to derive an approximation to the boundary of the asymptotic stability domain of the dissipatively perturbed Beck's column, i.e. when $k_1 \neq 0$ and $k_2 \neq 0$.

8.3.2 Beck's column with Kelvin–Voigt and viscous damping

We first investigate the effect of small internal damping ($k_1 \neq 0$) and external damping ($k_2 \neq 0$) on the simple eigenvalues $\pm i\omega_{0,s}$ ($s = 1, 2, \ldots$). The behavior of the simple eigenvalues as the parameters are varied[5] is described by equations (8.18). The increment in the real part of the perturbed pure imaginary simple eigenvalues $\pm i\omega_{0,s}$ is determined by the vectors $\mathbf{g}_s$ defined by equation (8.19). Subjecting the eigenfunctions of the simple eigenvalues to the normalization conditions (8.17) that with the operators (8.53) and the matrices (8.54) and (8.57) take the form

$$2\omega_{0,s}(Mu_{0,s}, v_{0,s}) = 2\omega_{0,s}(u_{0,s}, v_{0,s}) = 1, \tag{8.63}$$

we find that

$$g_{s,1} := \left(\partial_{k_1} Du_{0,s}, v_{0,s}\right) = (u_{0,s}{}_x^{(4)}, v_{0,s}), \quad g_{s,2} := \left(\partial_{k_2} Du_{0,s}, v_{0,s}\right) = (u_{0,s}, v_{0,s}), \tag{8.64}$$

and, consequently

$$\mathbf{g}_s^T = \left((u_{0,s}{}_x^{(4)}, v_{0,s}),\ \frac{1}{2\omega_{0,s}}\right). \tag{8.65}$$

[5] Similar formulas for the dissipative perturbation of simple eigenvalues of a pipe conveying fluid were derived in [85].

As $s \to \infty$ the eigenfrequencies $\omega_{0,s}$ have the asymptotic behavior expressed by equation (8.59), which yields the following asymptotic formulas for the corresponding eigenfunctions [14]:

$$u_{0,s} \sim \frac{\sin(s\pi x)}{s\pi} + O(s^{-2}), \quad v_{0,s} \sim \frac{\sin(s\pi x)}{s\pi} + O(s^{-2}). \tag{8.66}$$

Using the eigenfrequencies (8.59) and eigenfunctions (7.101)–(7.103) and (8.66), we evaluate the vectors $\mathbf{g}_s$ given by equation (8.65)

$$\begin{aligned}
\mathbf{g}_1^T &\approx (35.44204292, 0.009309734),\\
\mathbf{g}_2^T &\approx (65.03341903, 0.004448655),\\
\mathbf{g}_3^T &\approx (104.5361973, 0.002617029),\\
&\cdots\\
\mathbf{g}_s^T &\sim \frac{1}{2}\left(s^2\pi^2 + o(s^2),\ s^{-2}\pi^{-2} + o(s^{-2})\right), \quad s \to \infty.
\end{aligned} \tag{8.67}$$

By conditions (8.20), all the simple eigenvalues are displaced under the action of small damping into the left half-plane of the complex plane, if all the scalar products $\langle \mathbf{g}_s, \mathbf{k}\rangle > 0$ $(s = 1, 2, \ldots)$, where $\mathbf{k}^T = (k_1, k_2)$. The first five boundaries determined by this infinite set of inequalities are shown in Figure 8.4 (a). With the increase of the mode number, s, the boundaries tend to the vertical k_2-axis, confirming the asymptotic law (8.67). Therefore, the intersection of the infinite number of the half-planes $\langle \mathbf{g}_s, \mathbf{k}\rangle > 0$ is determined by the vector $\mathbf{g}_1$ and the limit $\mathbf{g}_{s\to\infty}$ only, i.e. just by the two conditions

$$k_2 \gtrapprox -3806.987379 k_1, \quad k_1 > 0. \tag{8.68}$$

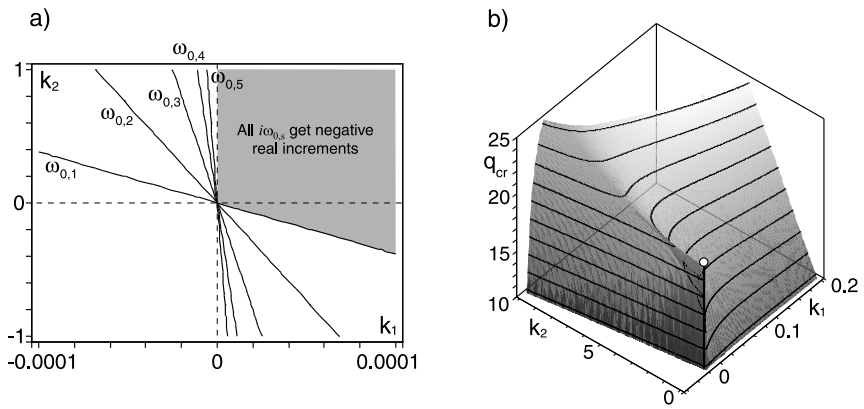

Figure 8.4. (a) Linear approximations to stability boundaries corresponding to simple eigenvalues $\pm i\,\omega_{0,s}$ tend to the k_2 axis in the (k_1, k_2)-plane as $s \to \infty$. (b) Approximation (8.76) in the (k_1, k_2, q)-space to the singular surface determining the stability boundary associated with the splitting of the double nonderogatory eigenvalues $\pm i\,\omega_0$. At the point $(0, 0, q_0)$ the surface possesses the Whitney umbrella singularity.

Further limitations on the variation of parameters follow from the behavior of the double eigenvalue $i\omega_0$. Subjecting the eigenfunctions and associated functions of the double eigenvalue to orthogonality and normalization conditions (8.12) that simplify to the following form

$$2i\omega_0(u_1, v_1) + (u_1, v_0) + (u_0, v_1) = 0, \quad 2i\omega_0(u_1, v_0) = 1, \tag{8.69}$$

and then substituting the differential operators (8.53) and the matrices (8.54) and (8.57) into equations (8.14) and (8.15), we obtain

$$\begin{aligned}
&f_1 := \left(\partial_{k_1} D u_0, v_0\right) = (u_{0x}^{(4)}, v_0), \quad f_2 := \left(\partial_{k_2} D u_0, v_0\right) = (u_0, v_0) = 0,\\
&\widetilde{f} := \left(\partial_q P u_0, v_0\right) = (u_{0x}^{(2)}, v_0),\\
&h_1 := -i\left(\partial_{k_1} D u_1, v_0\right) - i\left(\partial_{k_1} D u_0, v_1\right) = -i(u_{1x}^{(4)}, v_0) - i(u_{0x}^{(4)}, v_1),\\
&h_2 := -i\left(\partial_{k_2} D u_1, v_0\right) - i\left(\partial_{k_2} D u_0, v_1\right) = -2i\,(u_1, v_0) = -\omega_0^{-1},\\
&\widetilde{h} := -i\left(\partial_q P u_1, v_0\right) - i\left(\partial_q P u_0, v_1\right) = -i(u_{1x}^{(2)}, v_0) - i(u_{0x}^{(2)}, v_1).
\end{aligned} \tag{8.70}$$

Consequently,

$$\mathbf{f}^T = \left((u_{0x}^{(4)}, v_0), 0\right), \quad \mathbf{h}^T = -\left(i(u_{0x}^{(4)}, v_1) + i(u_{1x}^{(4)}, v_0), \omega_0^{-1}\right). \tag{8.71}$$

From the last formula of (8.71) and from the expressions (8.29) and (8.32) it immediately follows that the contribution of a small external damping with the coefficient k_2 to the increment of the real part of the perturbed double eigenvalue is exactly $-k_2/2$, in agreement with [77].

Evaluating the scalar products in equation (8.71) at $q = q_0$ and $\omega = \omega_0$, we finally obtain

$$\widetilde{f} \approx -4.729730023, \quad \mathbf{f} \approx \begin{pmatrix} 94.83559733 \\ 0 \end{pmatrix}, \quad \mathbf{h} \approx -\begin{pmatrix} 14.33730669 \\ 0.090780696 \end{pmatrix}. \tag{8.72}$$

The matrix $\mathbf{H} \equiv 0$ according to equation (8.25), because the operators defined by equation (8.53) depend linearly on the parameters. To evaluate the matrix $\mathbf{G}$ with the help of equation (8.26), one has to solve the boundary value problem (8.27), which now has the form

$$\begin{gathered}
\partial_x^4 \hat{w}_2 + q_0 \partial_x^2 \hat{w}_2 - \omega_0^2 \hat{w}_2 = \tfrac{dk_2}{d\varepsilon} u_0,\\
\hat{w}_2(0) = 0, \quad \hat{w}_{2x}^{(1)}(0) = 0, \quad \hat{w}_{2x}^{(2)}(1) = 0, \quad \hat{w}_{2x}^{(3)}(1) = 0.
\end{gathered} \tag{8.73}$$

Comparing the boundary value problems (8.73) and (8.3), we deduce that $\hat{w}_2 = -\frac{dk_2}{d\varepsilon}\frac{u_1}{2i\omega_0}$. Taking this expression into consideration in equation (8.26), we obtain

$$\mathbf{G} = \frac{i}{4\omega_0}\begin{pmatrix} 0 & (u_{1x}^{(4)}, v_0) \\ (u_{1x}^{(4)}, v_0) & 2(u_1, v_0) \end{pmatrix} = \frac{i}{4\omega_0}\begin{pmatrix} 0 & (u_{1x}^{(4)}, v_0) \\ (u_{1x}^{(4)}, v_0) & -i\omega_0^{-1} \end{pmatrix}. \tag{8.74}$$

After evaluation of the scalar products, equation (8.74) gives

$$\mathbf{G} \approx \begin{pmatrix} 0 & 0.247048251 \\ 0.247048251 & 0.002060283 \end{pmatrix}. \tag{8.75}$$

With the quantities (8.72) and (8.75), the formula (8.43) yields an approximation to the critical flutter load as a function of the dissipation parameters

$$q_{cr}(k_1, k_2) \approx q_0 - \frac{1901.544163k_1^2}{(14.33730669k_1 + 0.090780696k_2)^2} + 12.67618014k_1k_2 + 0.052857139k_2^2. \tag{8.76}$$

The necessary condition for stability $\langle \mathbf{h}, \mathbf{k} \rangle < 0$ now becomes

$$k_2 \gtrapprox -157.9334283k_1. \tag{8.77}$$

The part of the critical surface (8.76) selected by the condition (8.77) is plotted in Figure 8.4 (b).

Combining the stability conditions corresponding to both simple and double eigenvalues, we conclude that the viscoelastic Beck's column in a viscous medium is asymptotically stable in the neighborhood of the point

$$k_1 = 0, \quad k_2 = 0, \quad q = q_0,$$

provided that the following three conditions hold

$$q < q_{cr}(k_1, k_2), \quad k_1 > 0, \quad k_2 \gtrapprox -157.9334283k_1. \tag{8.78}$$

Gray areas in Figure 8.5 show sections of the asymptotic stability domain (8.78) in the (k_1, k_2)-plane of the damping parameters at different levels of q_{cr}.

It is clear from Figures 8.4 and 8.5 that there is an asymptotic stability domain in the (k_1, k_2, q)-space with the Whitney umbrella singularity at the point $(0, 0, q_0)$. When

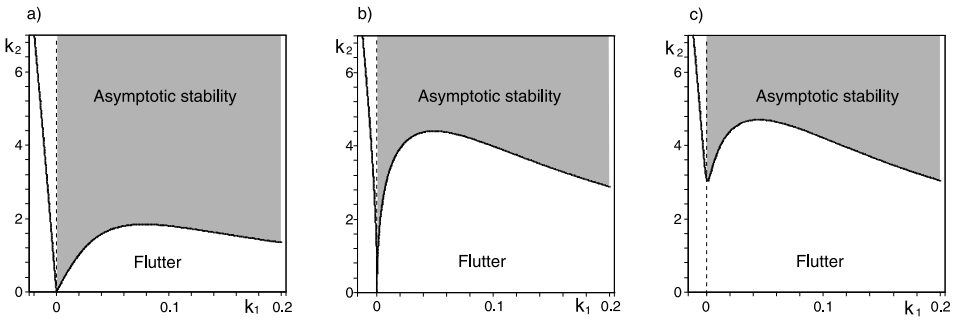

Figure 8.5. (Black solid lines) cross-sections of the surface (8.76) and (gray areas) the approximation (8.78) to the domain of asymptotic stability in the (k_1, k_2)-plane corresponding to (a) $q_{cr} = q_0 - 5$, (b) $q_{cr} = q_0$, and (c) $q_{cr} = q_0 + 0.5$.

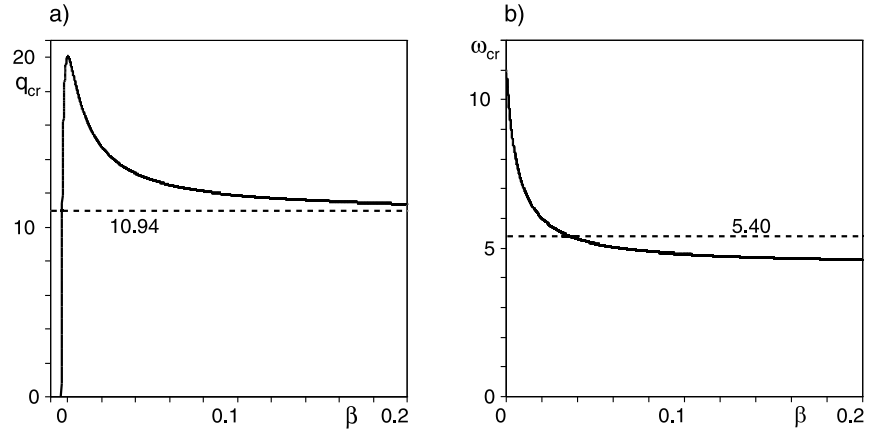

Figure 8.6. Drop in (a) the critical flutter load and (b) frequency in the limit of vanishing dissipation when $\beta = k_1/k_2$ is maintained constant, as a function of β [282].

q_{cr} is close to q_0, this domain is strongly stretched along the axis, corresponding to the coefficient of external damping k_2. Moreover, given any small amount of internal damping k_1, the coefficient of external damping k_2 exists for which $q_{cr}(k_1, k_2) > q_0$ and the system with damping is asymptotically stable, cf. e.g. the stability diagram of the finite dimensional analogue of the Beck's problem with damping studied by Plaut [312, 480].

Expressions approximating the drop in the critical flutter load and frequency follow from equations (8.37), (8.46), and (8.72)

$$\Delta q \approx \frac{1901.544163\beta^2}{(14.33730669\beta + 0.090780696)^2}, \quad \Delta\omega \approx \frac{94.83559733\beta}{14.33730669\beta + 0.090780696}, \tag{8.79}$$

where $\beta = k_1/k_2$. The solid curves in Figure 8.6 represent the limiting values of the critical flutter load and frequency as functions of the ratio β, as evaluated from formulae (8.79). The results are in good agreement with the previous, numerically evaluated, data [14]. The accuracy of the approximations (8.79) is best in the neighborhood of $\beta = 0$. Nevertheless, the limits of the critical load and frequency at $k_2 = 0$ and $k_1 \to 0$ are $q_{cr} \approx 10.80032458$ and $\omega_{cr} \approx 4.400954260$, respectively, which are close to the values $q_{cr} \approx 10.94$ and $\omega_{cr} \approx 5.40$, obtained numerically in [14].

8.3.3 Viscoelastic Beck's column with a dash-pot

In 1987, Panovko and Sorokin [466] and then in 1994 Zhinzher [615] considered a Beck's column made of viscoelastic Kelvin–Voigt material with the damping coefficient k_1. They neglected the damping due to resistance of the medium ($k_2 = 0$) and assumed that instead a dash-pot with the damping coefficient k_3 is attached to the

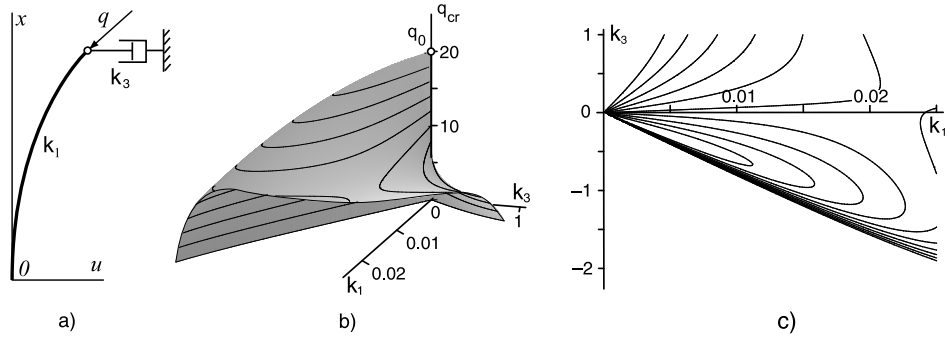

Figure 8.7. (a) The viscoelastic Beck's column with the dash-pot [466, 615]. (b) Approximation (8.93) in the (k_1, k_3, q)-space to the singular surface determining the stability boundary associated with the splitting of the double nonderogatory eigenvalues $\pm i\omega_0$. At the point $(0, 0, q_0)$ the surface possesses the Whitney umbrella singularity [278, 279]. (c) Cross-sections of the approximation (8.93) showing that the 'petal' of asymptotic stability shrinks to a point at the origin when $q_{cr} \to q_0$.

free end of the column, Figure 8.7 (a). This results in the following nonself-adjoint boundary eigenvalue problem

$$(1 + k_1\lambda)\partial_x^4 u + q\partial_x^2 u + \lambda^2 u = 0, \tag{8.80}$$
$$u(0) = 0, \quad u_x^{(1)}(0) = 0, \quad u_x^{(2)}(1) = 0, \quad (1 + k_1\lambda)u_x^{(3)}(1) - k_3\lambda u(1) = 0.$$

We denote $\mathbf{k}^T = (k_1, k_3)$. In the problem (8.80) the physical ($\mathbf{k}$) and spectral (λ) parameters are both in the differential expression and in the boundary conditions. We will show that our perturbation theory can be efficiently applied to treat this complication.

First we note that the problem (8.80) is of the form (8.7), where the operators P, D, and M are given by equation (8.53) with $k_2 = 0$, the matrix $\mathfrak{U}_M = 0$, $\mathfrak{U}_P$ is determined by equation (8.54), and

$$\mathfrak{U}_D = \begin{pmatrix} 0 & 0 & 0 & 0 & 0 & 0 & 0 & 0 \\ 0 & 0 & 0 & 0 & 0 & 0 & 0 & 0 \\ 0 & 0 & 0 & 0 & 0 & 0 & 0 & 0 \\ 0 & 0 & 0 & 0 & -k_3 & 0 & 0 & k_1 \end{pmatrix}. \tag{8.81}$$

With the matrices (8.55) and (8.56) by formula (7.15), we find

$$\mathfrak{V} = \begin{pmatrix} 0 & 0 & 0 & 0 & k_3\overline{\lambda} & -q & 0 & -1 - k_1\overline{\lambda} \\ 0 & 0 & 0 & 0 & q & 0 & 1 + k_1\overline{\lambda} & 0 \\ 0 & 1 + k_1\overline{\lambda} & 0 & 0 & 0 & 0 & 0 & 0 \\ -1 - k_1\overline{\lambda} & 0 & 0 & 0 & 0 & 0 & 0 & 0 \end{pmatrix},$$

$$\widetilde{\mathfrak{B}} = \begin{pmatrix} 0 & -q & 0 & -1-k_1\overline{\lambda} & 0 & 0 & 0 & 0 \\ q & 0 & 1+k_1\overline{\lambda} & 0 & 0 & 0 & 0 & 0 \\ 0 & 0 & 0 & 0 & 0 & 1+k_1\overline{\lambda} & 0 & 0 \\ 0 & 0 & 0 & 0 & -1 & 0 & 0 & 0 \end{pmatrix}. \tag{8.82}$$

With the eigenfunctions (7.101) and (7.102) at the simple eigenvalues of the ideal (undamped) Beck's problem that satisfy the orthogonality and normalization conditions (8.63), we find the vector $\mathbf{g}_s$ determining the linear approximation to the domain where a simple eigenvalue $i\omega_{0,s}$ acquires negative real part:

$$\mathbf{g}_s = \begin{pmatrix} (u_{0,s}{}_x^{(4)}, v_{0,s}) \\ u_{0,s}(1)\overline{v}_{0,s}(1) \end{pmatrix}. \tag{8.83}$$

Evaluating at $q = q_0 \approx 20.05095361$ the vectors (8.83) corresponding to the eigenvalues (8.59) yields

$$\begin{aligned} \mathbf{g}_1^T &\approx (35.44204292,\ \ 0.043193894)\,, \\ \mathbf{g}_2^T &\approx (65.03341903,\ \ 0.019193683)\,, \\ \mathbf{g}_3^T &\approx (104.5361973,\ \ 0.010961677)\,, \\ &\cdots \\ \mathbf{g}_s^T &\sim \frac{1}{2}\left(s^2\pi^2 + o(s^{-2}),\ \ o(s^{-2})\right). \end{aligned} \tag{8.84}$$

Therefore, linear approximation to the domain in the (k_1, k_3)-plane, where all simple pure imaginary eigenvalues of the ideal Beck's problem have negative real part under the dissipative perturbation, is

$$k_1 > 0, \quad k_3 \gtrapprox -820.5336357 k_1. \tag{8.85}$$

On the other hand, with the eigenvectors and associated vectors of the double eigenvalue $i\omega_0$ of the ideal problem that satisfy the conditions (8.69), we find the vectors $\mathbf{f}$, $\mathbf{g}$, and the coefficient $\widetilde{f}$ determined by equations (8.14) and (8.15):

$$\begin{aligned} \mathbf{h} &= -\begin{pmatrix} i(u_{1x}^{(4)}, v_0) + i(u_{0x}^{(4)}, v_1) \\ iu_1(1)\overline{v}_0(1) + iu_0(1)\overline{v}_1(1) \end{pmatrix} \approx \begin{pmatrix} -14.33730669 \\ -0.134073064 \end{pmatrix}, \\ \mathbf{f} &= \begin{pmatrix} (u_{0x}^{(4)}, v_0) \\ u_0(1)\overline{v}_0(1) \end{pmatrix} \approx \begin{pmatrix} 94.83559733 \\ 1.563105909 \end{pmatrix}, \\ \widetilde{f} &= (u_{0x}^{(2)}, v_0) \approx -4.729730023. \end{aligned} \tag{8.86}$$

The matrix $\mathbf{H} \equiv 0$ according to equation (8.25), because the operators defined by equations (8.53), (8.54), and (8.81) depend linearly on the parameters. The function $\hat{w}_2$ determining the matrix $\mathbf{G}$ in equation (8.26) follows from the boundary value problem (8.27) that in case of the dash-pot damping takes the form

$$\begin{gathered} \partial_x^4\hat{w}_2 + q_0\partial_x^2\hat{w}_2 - \omega_0^2\hat{w}_2 = \tfrac{dk_1}{d\varepsilon}\partial_x^4 u_0, \\ \hat{w}_2(0) = 0, \quad \hat{w}_{2x}^{(1)}(0) = 0, \quad \hat{w}_{2x}^{(2)}(1) = 0, \quad \hat{w}_{2x}^{(3)}(1) = -\tfrac{dk_3}{d\varepsilon}u_0(1). \end{gathered} \tag{8.87}$$

Then,

$$\left\langle \mathbf{G}\frac{d\mathbf{k}}{d\varepsilon}, \frac{d\mathbf{k}}{d\varepsilon}\right\rangle = \frac{dk_1}{d\varepsilon}\left((\partial_x^4\hat{w}_2, v_0) - \hat{w}_{2x}^{(3)}(1)v_0(1)\right) + \frac{dk_3}{d\varepsilon}\hat{w}_2(1)v_0(1). \tag{8.88}$$

Solution to the boundary value problem (8.87) exists because of the solvability condition $(u_{0x}^{(4)}, v_0)\frac{dk_1}{d\varepsilon} + u_0(1)\overline{v}_0(1)\frac{dk_3}{d\varepsilon} = 0$, and has the form

$$\hat{w}_2(x) = \frac{dk_1}{d\varepsilon}\frac{Fab(b^2\cos(bx) - a^2\cosh(ax)) + b^3\sin(bx) + a^3\sinh(ax)}{2(a^2+b^2)}x \tag{8.89}$$
$$+ \frac{dk_1}{d\varepsilon}\frac{(a^2-b^2)Fb\sinh(ax)}{2(a^2+b^2)} - \frac{dk_1}{d\varepsilon}\frac{A_3(\cos(bx)-\cosh(ax))}{2(a^2+b^2)(a^2\cosh(a)+b^2\cos(b))},$$

where the coefficients F, a, and b are determined by the equations (7.103) and (7.98) with $\eta = 1$, $\kappa = 0$, $\lambda = \omega_0^2$, and $q = q_0$. The coefficient A_3 is

$$A_3 = Fab(2b^3\sin(b) + a(a^2+b^2)\sinh(a) + b^4\cos(b) + a^4\cosh(a))$$
$$- 2b^4\cos(b) - 2a^4\cosh(a) + b^5\sin(b) - a^5\sinh(a). \tag{8.90}$$

Therefore, the matrix $\mathbf{G}$ evaluated at $q = q_0$, is

$$\mathbf{G} \approx \begin{pmatrix} -53.33393310 & 4.848259906 \\ 4.848259906 & 0 \end{pmatrix}. \tag{8.91}$$

Proceeding as in the previous example we conclude that the domain of asymptotic stability of the viscoelastic Beck's column with the dash-pot is described by the conditions

$$k_1 > 0, \quad k_3 \gtrapprox -106.9365181k_1, \quad q < q_{cr}(k_1, k_3), \tag{8.92}$$

where the critical flutter load is approximated by the expression [278, 279]

$$q_{cr}(k_1, k_3) \approx q_0 - \frac{(43.60669860k_1 + 0.718737375k_3)^2}{(14.33730669k_1 + 0.134073064k_3)^2}$$
$$- 1368.296559k_1^2 + 248.7668530k_1k_3. \tag{8.93}$$

The stability domain described by conditions (8.92) is shown in Figure 8.7 (b). The critical load as a function of damping parameters has the Whitney umbrella singularity at the origin. According to equation (8.93) the critical load decreases for any combination of damping parameters k_1 and k_3 in the vicinity of the origin, contrary to the resistance of a medium (k_2) that can increase the critical load, no matter how small k_2 is. When $q_{cr} < q_0$ is close to q_0, the asymptotic stability is confined inside a closed 'petal' in the (k_1, k_3)-plane as Figure 8.7 (c) demonstrates. It grows with the decrease of q_{cr}. When $q_{cr} \to q_0$, the petal shrinks to a point in the (k_1, k_3)-plane. A further increase in the critical load yields an unstable region surrounding the origin. Note that the same qualitative behavior is demonstrated by the flutter threshold in the two-degrees-of-freedom models of the analogous physical systems: Ziegler's pendulum with a dash-pot [615] and Reut's pendulum with a dash-pot [553, 555].

8.3.4 Ziegler's pendulum with a dash-pot

Consider, for example, stability of the vertical equilibrium position of the two-link pendulum that is connected to a firm basement by a revolute joint and is loaded at its free end by a follower force, P, Figure 8.8 (a). The links have equal length, l. A mass, m, is attached to the free end of the pendulum. Another mass, $2m$, is concentrated at the joint, connecting the two links. At both joints the elastic torques are acting with the stiffness coefficient, c. The coefficient of viscous damping is b_1 at the lower joint and b_4 at the upper one. This is the classical Ziegler's pendulum [622]. In addition, a dash-pot with the damping coefficient, b_3, is attached to the pendulum at its free end [615], see Figure 8.8 (a).

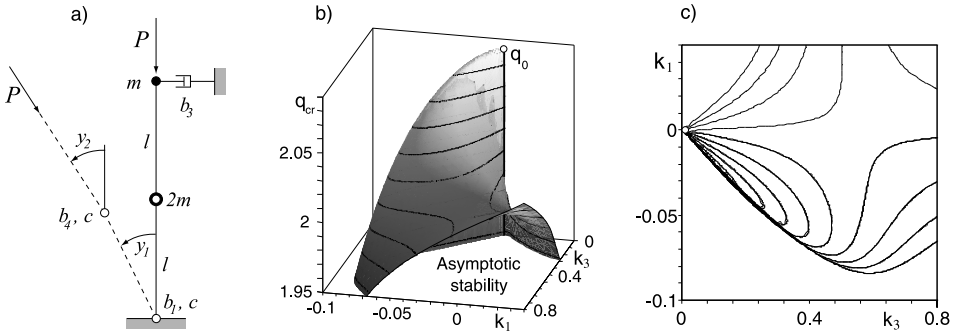

Figure 8.8. (a) Ziegler's pendulum with a dash-pot [615]. (b) Singular boundary of the domain of asymptotic stability. (c) Contours of the stability boundary shrinking to a point when $q_{cr} \to q_0 = \frac{7}{2} - \sqrt{2}$.

Small oscillations of the pendulum about the equilibrium are described by the linear equation

$$\mathbf{M}\frac{d^2\mathbf{y}}{dt^2} + \mathbf{D}\frac{d\mathbf{y}}{dt} + \mathbf{P}\mathbf{y} = 0. \tag{8.94}$$

After introduction of dimensionless parameters and separation of time, $\mathbf{y} = \mathbf{u}\exp(\lambda\tau)$, equation (8.94) yields the eigenvalue problem for a matrix polynomial

$$(\lambda^2\mathbf{M} + \lambda\mathbf{D} + \mathbf{P})\mathbf{u} = 0, \tag{8.95}$$

where the mass, damping, and stiffness matrices have the form [615, 622]

$$\mathbf{M} = \begin{pmatrix} 3 & 1 \\ 1 & 1 \end{pmatrix}, \quad \mathbf{D} = \begin{pmatrix} k_3 + k_1 + k_4 & k_3 - k_1 \\ k_3 - k_1 & k_3 + k_1 \end{pmatrix}, \quad \mathbf{P} = \begin{pmatrix} 2 - q & q - 1 \\ -1 & 1 \end{pmatrix}, \tag{8.96}$$

and

$$q = \frac{Pl}{c}, \quad k_{1,3,4} = \frac{b_{1,3,4}}{l\sqrt{cm}}, \quad \tau = \frac{t}{l}\sqrt{\frac{c}{m}}. \tag{8.97}$$

Assuming here that $k_4 = k_1$, we find from the Routh–Hurwitz stability conditions that Ziegler's pendulum with the dash-pot is asymptotically stable if and only if $7k_1 + 2k_3 > 0$ and $q < q_{cr}(k_1, k_3)$, where

$$q_{cr}(k_1,k_3) = \frac{37}{28}k_3k_1 + \frac{5}{14}k_3^2 + \frac{1}{2}\frac{k_1}{k_3} + \frac{1}{7}\frac{k_3}{k_1} + \frac{20}{7} + \frac{1}{4}k_1^2 \qquad (8.98)$$
$$\pm \frac{7k_1+2k_3}{28}\sqrt{k_1^2-\frac{4k_1}{k_3}+10k_3k_1-16+\frac{4}{k_3^2}+25k_3^2+\frac{20k_3}{k_1}+\frac{20}{k_3k_1}+\frac{4}{k_1^2}}.$$

The domain of asymptotic stability bounded by the surface $q = q_{cr}(k_1, k_3)$ is shown in Figure 8.8 (b). One can see that the critical flutter value attains its maximum $q = q_0 = 7/2 - \sqrt{2}$ at $k_1 = 0$ and $k_3 = 0$, which corresponds to the ideal (undamped) system.

The critical load (8.98) is a strictly decreasing function of the damping parameters in a neighborhood of the origin. This means that in this domain small damping always destabilizes the pendulum, whatever the combination of the damping parameters is. The level curves of the surface (8.98) shown for different $q_{cr} < q_0$ in Figure 8.8 (c) evidence that for q_{cr} tending to q_0, the domain of asymptotic stability, confined in the petal-like regions in the (k_1, k_3)-plane, shrinks to the exceptional point $(0, 0, q_0)$ in the (k_1, k_3, q)-space.

Comparing the approximation to the stability domain of Beck's column with the dash-pot shown in Figure 8.7 (b, c) with the exact stability domain of Ziegler's pendulum presented in Figure 8.8 (b, c), we see that both the continuous and finite-dimensional models possess qualitatively the same destabilizing effect of external damping in the dash-pot. In the next section we will demonstrate that the method developed for the analysis of the dissipation-induced instabilities in continuous systems is directly applicable to finite-dimensional systems.

8.4 Application to finite-dimensional systems

All the results of this chapter remain valid in the case when the operator L in the eigenvalue problem (8.7) is a matrix polynomial, such as (8.95) that corresponds to the equation (8.94), where the matrices can be of arbitrary dimension, say m. In this case, one should simply omit the terms describing the contribution of the boundary conditions in the perturbation formulas for eigenvalues and eigenvectors and understand the scalar product $(.,.)$ as that in the complex vector space.

Let us calculate, for example, the approximation to the drop in the critical flutter load in the finite-dimensional circulatory system

$$\frac{d^2\mathbf{y}}{dt^2} + k\mathbf{D}\frac{d\mathbf{y}}{dt} + \mathbf{P}(q)\mathbf{y} = 0 \qquad (8.99)$$

in the classical formulation, when $\mathbf{M}$ is the identity matrix, the operator of velocity-dependent forces has the form $k\mathbf{D}$, k is a scalar parameter and $\mathbf{D}$ is a constant matrix [75, 159, 369, 589].

Calculating the vectors $\mathbf{f}$, $\mathbf{h}$, and the scalar $\widetilde{f}$ by equations (8.14) and (8.15), we derive from equation (8.46) that [288]

$$\Delta q := q_0 - \lim_{k\to 0} q_{cr}(k) = \frac{1}{(\mathbf{P}_1\mathbf{u}_0, \mathbf{v}_0)} \left(\frac{(\mathbf{D}\mathbf{u}_0, \mathbf{v}_0)}{(\mathbf{D}\mathbf{u}_1, \mathbf{v}_0) + (\mathbf{D}\mathbf{u}_0, \mathbf{v}_1)} \right)^2, \qquad (8.100)$$

where $\mathbf{P}_1 = d\mathbf{P}/dq$, and the derivative is evaluated at $q{=}q_0$.

In a particular case when system (8.99) has $m = 2$ degrees of freedom, the eigenvectors and associated vectors of the double eigenvalue $i\omega_0$ in equation (8.100) can be expressed in terms of the entries p_{ij}, $i, j = 1, 2$, of the matrix $\mathbf{P}_0 = \mathbf{P}(q_0)$:

$$\mathbf{u}_0 = \frac{1}{4p_{12}\mathrm{tr}\mathbf{P}_0} \begin{pmatrix} 2p_{12} \\ p_{22} - p_{11} \end{pmatrix}, \quad \mathbf{v}_0 = \frac{1}{2} \begin{pmatrix} p_{11} - p_{22} \\ 2p_{12} \end{pmatrix},$$
$$\mathbf{u}_1 = \frac{-i\sqrt{2\mathrm{tr}\mathbf{P}_0}}{4p_{12}(\mathrm{tr}\mathbf{P}_0)^2} \begin{pmatrix} -2p_{12} \\ 3p_{11}{+}p_{22} \end{pmatrix}, \quad \mathbf{v}_1 = -i\sqrt{2\mathrm{tr}\mathbf{P}_0} \begin{pmatrix} 1 \\ 0 \end{pmatrix}, \qquad (8.101)$$

where $\mathrm{tr}\mathbf{P}_0 = 2\omega_0^2$ and $p_{12} \neq 0$. Then,[6]

$$(\mathbf{P}_1\mathbf{u}_0, \mathbf{v}_0) = \tfrac{2\mathrm{tr}\mathbf{P}_0\mathbf{P}_1 - \mathrm{tr}\mathbf{P}_0\mathrm{tr}\mathbf{P}_1}{4\mathrm{tr}\mathbf{P}_0}, \quad (\mathbf{D}\mathbf{u}_0, \mathbf{v}_0) = \tfrac{2\mathrm{tr}\mathbf{P}_0\mathbf{D} - \mathrm{tr}\mathbf{P}_0\mathrm{tr}\mathbf{D}}{4\mathrm{tr}\mathbf{P}_0},$$
$$(\mathbf{D}\mathbf{u}_1, \mathbf{v}_0) + (\mathbf{D}\mathbf{u}_0, \mathbf{v}_1) = i\,\tfrac{2\mathrm{tr}\mathbf{P}_0\mathbf{D} - 3\mathrm{tr}\mathbf{P}_0\mathrm{tr}\mathbf{D}}{4(\mathrm{tr}\mathbf{P}_0)^2}\sqrt{2\mathrm{tr}\mathbf{P}_0}. \qquad (8.102)$$

With the quantities (8.102), equation (8.100) yields [286]

$$\Delta q = \frac{-2(\mathrm{tr}\mathbf{P}_0)^2}{2\mathrm{tr}\mathbf{P}_0\mathbf{P}_1 - \mathrm{tr}\mathbf{P}_0\mathrm{tr}\mathbf{P}_1} \left(\frac{2\mathrm{tr}\mathbf{P}_0\mathbf{D} - \mathrm{tr}\mathbf{P}_0\mathrm{tr}\mathbf{D}}{2\mathrm{tr}\mathbf{P}_0\mathbf{D} - 3\mathrm{tr}\mathbf{P}_0\mathrm{tr}\mathbf{D}} \right)^2, \qquad (8.103)$$

where $\mathbf{P}_0 = \mathbf{P}(q_0)$, $\mathbf{P}_1 = d\mathbf{P}/dq|_{q=q_0}$. According to equation (8.103), $\Delta q = 0$ for the matrices $\mathbf{D}$ satisfying the condition $\mathrm{tr}\mathbf{P}_0\mathbf{D} = \omega_0^2\mathrm{tr}\mathbf{D}$. In the vicinity of this set we can simplify the denominator of equation (8.103) to obtain [296, 312]

$$\Delta q = \frac{-1}{\mathrm{tr}\mathbf{P}_0\mathbf{P}_1 - \omega_0^2\mathrm{tr}\mathbf{P}_1} \left(\frac{\mathrm{tr}\mathbf{P}_0\mathbf{D} - \omega_0^2\mathrm{tr}\mathbf{D}}{\mathrm{tr}\mathbf{D}} \right)^2, \quad \mathrm{tr}\mathbf{D} \neq 0. \qquad (8.104)$$

8.4.1 The destabilization paradox in Ziegler's pendulum

Consider Ziegler's pendulum without a dash-pot but with different coefficients of viscous damping in the joints [622]. Its small oscillations about the vertical equilibrium position are described by equation (8.94) with the matrices (8.96), where $k_3 = 0$ and $k_4 \neq k_1$.

[6] The case $p_{12} = 0$ is considered in the same way and gives the same results.

If the damping is absent ($k_{1,4} = 0$), the system is marginally stable at $q < q_0$, where the critical load q_0 corresponds to the double eigenvalues $\pm i\,\omega_0$, and [622]

$$\omega_0 = 2^{-1/4}, \quad q_0 = \frac{7}{2} - \sqrt{2}. \tag{8.105}$$

The dissipative system ($k_{1,4} \neq 0$) is asymptotically stable if and only if

$$q < q_{cr}(k_1, k_4), \;\; k_1 > -k_4, \tag{8.106}$$

where [222]

$$q_{cr}(k_1, k_4) = q_0 - \frac{(3-2\sqrt{2})}{2} \frac{(k_1-(4+5\sqrt{2})k_4)^2}{(k_1+k_4)(k_1+6k_4)} + \frac{1}{2}k_1 k_4. \tag{8.107}$$

The domain of asymptotic stability determined by equations (8.106) and (8.107) is shown in Figure 8.9 (a). It appeared first in the work [520].

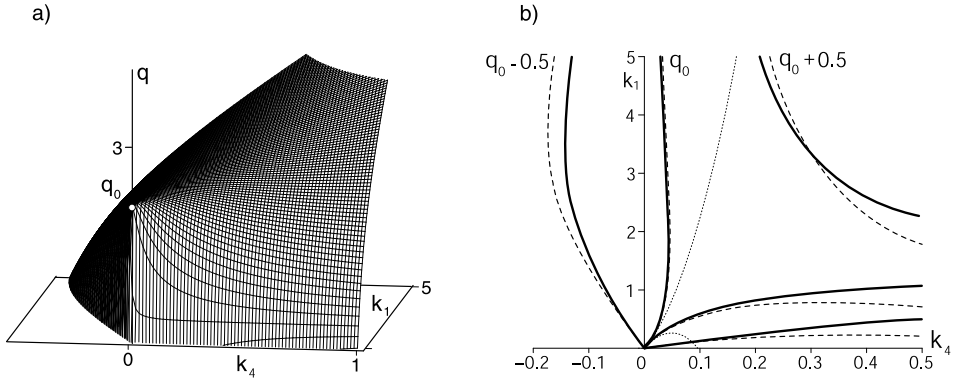

Figure 8.9. (a) The domain of asymptotic stability (8.106), (8.107) of Ziegler's pendulum. (b, c) The level curves of the function $q_{cr}(k_1, k_4)$: (solid lines) exact solution (8.107), (dashed lines) approximation (8.110), (dotted lines) equation (8.112) [288].

If we assume $k_1 = k_4$ in equation (8.107) and consider a limit of $q_{cr}(k_4)$ as k_4 goes to zero, then we obtain

$$\widetilde{q}_{cr} \equiv \lim_{k_4 \to 0} q_{cr}(k_4) = \frac{41}{28} \approx 1.46 < q_0 = \frac{7}{2} - \sqrt{2} \approx 2.09. \tag{8.108}$$

Inequality (8.108) established by Ziegler in 1952 shows that the critical load of the pendulum with equal damping coefficients decreases in a discontinuous manner due to infinitesimally small dissipation. This inequality constitutes the Ziegler–Bottema destabilization paradox [81, 312, 622].

Now we apply the theory developed in this chapter to approximate the stability domain. First, we find the right and left Keldysh chains of the double eigenvalue $\lambda_0 =$

$i\omega_0$ at the critical load q_0:

$$\mathbf{u}_0 = \begin{pmatrix} 5\sqrt{2}-6 \\ 3\sqrt{2}+2 \end{pmatrix}, \quad \mathbf{u}_1 = 8i\omega_0 \begin{pmatrix} 5\sqrt{2}-6 \\ 0 \end{pmatrix},$$
$$\mathbf{v}_0 = \frac{-1}{112} \begin{pmatrix} \sqrt{2}+4 \\ -7 \end{pmatrix}, \quad \mathbf{v}_1 = \frac{i\omega_0}{112} \begin{pmatrix} 10-8\sqrt{2} \\ 19\sqrt{2}-36 \end{pmatrix}. \tag{8.109}$$

The vectors satisfy conditions (8.12). Then, from equations (8.14), (8.15), and (8.26), we find that $\mathbf{H}\equiv 0$, $\widetilde{f} = -1/4$, and [288]

$$\mathbf{f} = \frac{1}{8} \begin{pmatrix} 1-\sqrt{2} \\ 6-\sqrt{2} \end{pmatrix}, \ \mathbf{h} = \frac{-1}{8\omega_0} \begin{pmatrix} 1+\sqrt{2} \\ 6+\sqrt{2} \end{pmatrix}, \ \mathbf{G} = \frac{1}{8} \begin{pmatrix} 0 & 2-\sqrt{2} \\ 2-\sqrt{2} & 14-8\sqrt{2} \end{pmatrix}.$$

With these vectors and matrices, the approximation of the function $q_{cr}(k_1, k_2)$ (8.43) and of the second of inequalities (8.42), takes the form

$$q_{cr}(k_1, k_4) = q_0 - 2\sqrt{2}(3-2\sqrt{2})^2 \frac{(k_1-(4+5\sqrt{2})k_4)^2}{(k_1-(4-5\sqrt{2})k_4)^2}$$
$$+ 2\sqrt{2}\left(\left(\frac{7}{4}-\sqrt{2}\right)k_4^2 + \left(\frac{1}{2}-\frac{1}{4}\sqrt{2}\right)k_1k_4\right), \tag{8.110}$$

$$k_1 > (4-5\sqrt{2})k_4. \tag{8.111}$$

Equation (8.110) and inequality (8.111) approximate the boundary of the asymptotic stability domain given by equations (8.106) and (8.107) in the vicinity of the point $(k_1 = 0, k_4 = 0, q = q_0)$. The level curves of this boundary in the plane of the damping parameters k_1 and k_4 given by equations (8.107) and (8.110) are shown in Figure 8.9 (b, c) by solid and dashed lines, respectively. Figure 8.9 (b) demonstrates that both the exact function $q_{cr}(k_1, k_4)$ and its approximation are symmetrical with respect to the origin of the (k_1, k_4)-plane. Inequalities (8.106) and (8.110) determine which half of the surface $q_{cr}(k_1, k_4)$ bounds the domain of asymptotic stability. We see that equation (8.110) approximates the exact stability boundary (8.107) with good accuracy even when the variation of the parameters k_1, k_4, and q is large.

The level curves corresponding to $q_{cr} = q_0$ can be approximated as well by formula (8.50):

$$k_1 = k_4(4+5\sqrt{2}) \pm k_4^2\sqrt{50(133+94\sqrt{2})} + O(k_4^3). \tag{8.112}$$

Approximation (8.112) is shown in Figure 8.9 (c) by the dotted lines. We see that equation (8.110) gives a more accurate approximation of the level curve at $q_{cr} = q_0$ than equation (8.112) because the latter contains only second-order terms with respect to k_4. Note that asymptotic expression (8.112) appeared first in [520] from the analysis of the Routh–Hurwitz inequalities. We obtained exactly the same result analyzing splitting of the double eigenvalue of the circulatory system under dissipative perturbation.

Let us now find how the critical load of Ziegler's pendulum drops at various ratios of the damping coefficients. Assume $k_1 = \delta\cos\alpha$, $k_4 = \delta\sin\alpha$ in equations (8.107)

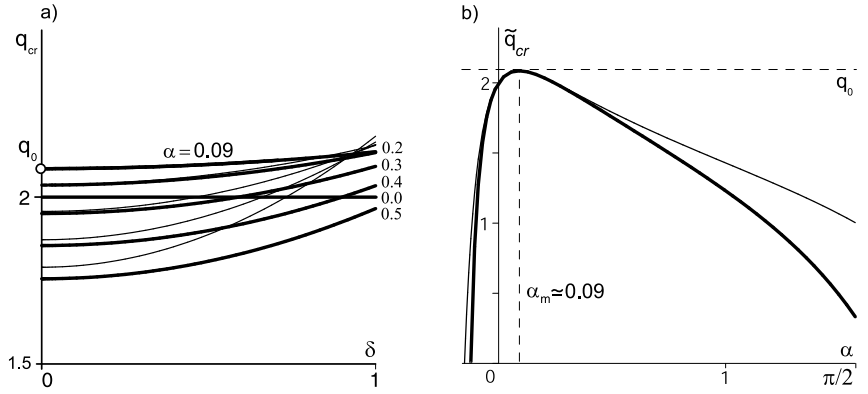

Figure 8.10. The critical load $q_{cr}(\delta\cos\alpha, \delta\sin\alpha)$ and its limit as $\delta\to 0$ for Ziegler's pendulum: Bold lines – exact solutions, thin lines – the approximations [288].

and (8.110) and plot the critical value $q_{cr}(\delta)$ and its approximation as functions of the parameter δ for different values of the parameter α, as shown in Figure 8.10 (a). Consider a limit of $q_{cr}(\delta\cos\alpha, \delta\sin\alpha)$ as δ goes to zero:

$$\widetilde{q}_{cr}(\alpha) = q_0 - \frac{(3-2\sqrt{2})}{2}\frac{(\cos\alpha-(4+5\sqrt{2})\sin\alpha)^2}{(\cos\alpha+\sin\alpha)(\cos\alpha+6\sin\alpha)}. \tag{8.113}$$

Transforming equation (8.110) in the same way, we get

$$\widetilde{q}_{cr}(\alpha) = q_0 - 2\sqrt{2}(3-2\sqrt{2})^2\left(\frac{\cos\alpha-(4+5\sqrt{2})\sin\alpha}{\cos\alpha-(4-5\sqrt{2})\sin\alpha}\right)^2. \tag{8.114}$$

The function (8.113) and its approximation (8.114) are shown in Figure 8.10 (b). Note that the limit of the critical load smoothly depends on the direction in the plane of the damping parameters determined by the angle α and never exceeds q_0: $\widetilde{q}_{cr}(\alpha) \le q_0$. Therefore, the limit of the function $q_{cr}(k_1, k_4)$ when k_1 and k_4 tend to zero is not defined, as was first noted in [615].

Therefore, an infinitesimally small dissipation generically destabilizes the circulatory system, and $\Delta q := q_0 - \widetilde{q}_{cr}(\alpha)$ measures a drop in the critical flutter load for the different directions α. Only for a unique combination of the damping parameters, $k_1 = (4+5\sqrt{2})k_4$ (corresponding to $\alpha \approx 0.09$), does a small dissipation stabilize the pendulum. In this case, the exact equation (8.113) as well as its approximation (8.114) take the form

$$q_{cr}(k_4) = q_0 + \frac{k_4^2}{2}(4+5\sqrt{2}). \tag{8.115}$$

Therefore, while tending the damping parameters to zero one can reach q_0 only by maintaining the ratio $k_1/k_4 = (4+5\sqrt{2})$.

Finally, we obtain the approximate expressions describing the trajectories of the eigenvalues of Ziegler's pendulum and compare the approximations with the numerical solution of the characteristic equation. Substituting the vectors and matrices given

by equation (8.110) into expressions (8.32), we find

$$c = \frac{\sqrt{2}+1}{8}(k_1 - k_4(4-5\sqrt{2})),$$
$$d = \frac{1}{4}(q_0 - q) + \omega_0^2\left(\left(\frac{7}{4}-\sqrt{2}\right)k_4^2 + \left(\frac{1}{2}-\frac{1}{4}\sqrt{2}\right)k_1 k_4\right),$$
$$e = \omega_0\frac{1-\sqrt{2}}{8}(k_1 - k_4(4+5\sqrt{2})). \tag{8.116}$$

The real and imaginary parts of the eigenvalues as functions of parameters are determined by equations (8.30) and (8.31) with the coefficients c, d, and e given by equation (8.116). The function $\mathrm{Re}\lambda(q)$ is shown in Figure 8.11 (a) at different values of k_1 under the assumption that $k_4 = k_1$. Since $k_1 \neq (4+5\sqrt{2})k_4$ the small damping destabilizes the pendulum. In this case the eigenvalues move in the complex plane along the branches of the hyperbola given by equation (8.29), which takes here the form

$$(\mathrm{Im}\lambda - \omega_0 + \mathrm{Re}\lambda + \frac{\sqrt{2}+1}{16}(k_1 - k_4(4-5\sqrt{2})))^2$$
$$- (\mathrm{Im}\lambda - \omega_0 - \mathrm{Re}\lambda - \frac{\sqrt{2}+1}{16}(k_1 - k_4(4-5\sqrt{2})))^2$$
$$= \omega_0\frac{\sqrt{2}-1}{4}(k_1 - k_4(4+5\sqrt{2})). \tag{8.117}$$

The approximations of the eigenvalue trajectories shown in Figure 8.11 by the dashed lines give a correct qualitative picture of the behavior of the eigenvalues in good agreement with the exact solutions of the characteristic equation for small variations of the parameters. However, the critical load $q_{cr}(k_1, k_4)$ is approximated with good accuracy even for large deviations of the damping parameters.

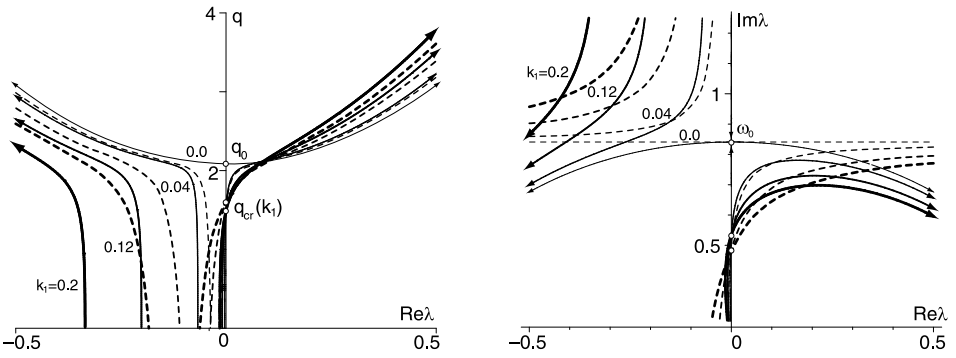

Figure 8.11. Movement of eigenvalues of the Ziegler's pendulum calculated numerically (solid lines) and their approximations by equations (8.30), (8.116), and (8.117) (dashed lines) for $k_4/k_1 = 1$ [288].

Chapter 9

The MHD kinematic mean field α^2-dynamo

Although eigencurves have been used in a variety of ways for about a century, they seem comparatively underdeveloped in their own right.

P. Binding and H. Volkmer [64]

Motions of an electrically conducting medium (plasma or liquid metal) can produce a magnetic field. Electric currents and fields that are generated by the moving fluid amplify the existing magnetic field and maintain it against resistive decay. The process of conversion of mechanical energy into magnetic energy is called *dynamo*. The magnetohydrodynamics (MHD) dynamo is the main mechanism that creates magnetic fields of stars and planets [199, 359].

9.1 Eigenvalue problem for α^2-dynamo

The motion of a conducting fluid in a magnetic field is described by the MHD equations that basically couple the Navier–Stokes equations of a viscous fluid to the induction equation for a magnetic field [199]. This set of nonlinear partial differential equations with boundary conditions requires as a rule computationally expensive numerical simulations [197, 198]. Nevertheless, the dynamo action can be understood already by means of simplified models of the *kinematic dynamo* theory based on the assumption that the velocity field of the fluid, $\mathbf{v}$, is prescribed and not affected by the magnetic field, $\mathbf{B}$.

In the kinematic regime, the time evolution of the magnetic field is reduced to the linear induction equation

$$\partial_t \mathbf{B} = \nabla \times (\mathbf{v} \times \mathbf{B}) + \eta \nabla^2 \mathbf{B}, \tag{9.1}$$

where $\nabla \cdot \mathbf{B} = 0$ and $\eta = (\mu_0 \sigma)^{-1}$ is the magnetic diffusivity, $\sigma = \text{const}$ the electrical conductivity of the fluid, and μ_0 the magnetic permeability of free space. Although a number of flows are known that make the kinematic dynamo (9.1) work, see e.g. [188], it is a hard problem to find such a flow configuration [247].

In 1966, in order to further simplify the model (9.1), Steenbeck,[1] Krause, and Rädler [331, 543] proposed to split the magnetic field and the flow as

$$\mathbf{B} = \overline{\mathbf{B}} + \mathbf{B}', \quad \mathbf{v} = \overline{\mathbf{v}} + \mathbf{v}' \tag{9.2}$$

into mean and fluctuating components, respectively. Then, averaging the induction equation (9.1) by applying the Reynolds averaging rules yields

$$\partial_t \overline{\mathbf{B}} = \nabla \times (\overline{\mathbf{v}} \times \overline{\mathbf{B}}) + \nabla \times \mathcal{E} + \eta \nabla^2 \overline{\mathbf{B}}, \tag{9.3}$$

where $\mathcal{E} = \overline{\mathbf{v}' \times \mathbf{B}'}$ is the mean electromotive force due to fluctuations [247]. For its occurrence, known as the α-effect, the small scale (convective or turbulent) motions of the fluid must on average be nonmirrorsymmetric, e.g. helical. Such a *chirality* of the medium naturally occurs due to Coriolis force when it moves in a rotating body [489] or can be created artificially by impellers [545].

Subtracting the mean field equation (9.3) from the original one (9.1) gives an equation for the evolution of $\mathbf{B}'$ that suggests that this field is generated by the interaction of the turbulent $\mathbf{v}'$ with the mean magnetic field $\overline{\mathbf{B}}$. Therefore,

$$\mathcal{E}_i = a_{ij} \overline{B_j} + \beta_{ijk} \partial_{x_k} \overline{B_j} + \cdots, \tag{9.4}$$

where the tensors a_{ij} and b_{ijk} depend on the velocity fields $\mathbf{v}'$ and $\overline{\mathbf{v}}$. Assuming further that a_{ij} and b_{ijk} are isotropic, i.e. $a_{ij} = \alpha(\mathbf{r})\delta_{ij}$ and $b_{ijk} = -\beta\epsilon_{ijk}$, where $\beta = const$, and that the mean flow is vanishing ($\overline{\mathbf{v}} = 0$), we arrive at the equations of the MHD kinematic mean field α^2-dynamo

$$\partial_t \overline{\mathbf{B}} = \nabla \times \alpha \overline{\mathbf{B}} + \eta_T \nabla^2 \overline{\mathbf{B}}, \tag{9.5}$$

where $\eta_T = \beta + \eta$ is the turbulent diffusivity [195, 247, 489].

In spherical geometry (r, θ, ϕ), we can specify $\overline{\mathbf{B}}$ by two independent scalar fields – toroidal (T) and poloidal (P) as [247]

$$\overline{\mathbf{B}} = \mathbf{B}_T + \mathbf{B}_P, \quad \mathbf{B}_T = \nabla \times T\mathbf{r}, \quad \mathbf{B}_P = \nabla \times \nabla \times P\mathbf{r}. \tag{9.6}$$

Then, assuming that $\alpha = \alpha(r)$ is a smooth function of the radial coordinate only, from equation (9.5), we obtain [207, 331]

$$\begin{aligned} \partial_t P &= \alpha T + \eta_T \nabla^2 P, \\ \partial_t T &= -\alpha \nabla^2 P - \frac{1}{r}(\partial_r \alpha)(\partial_r r P) + \eta_T \nabla^2 T. \end{aligned} \tag{9.7}$$

Thus, the distributed spherically symmetric helicity parameter $\alpha(r)$ couples the evolution equations for the poloidal ($\sim$ axial) and toroidal ($\sim$ azimuthal) components of

[1] Max Steenbeck (1904–1981) – a German physicist, one of the inventors of the betatron [489], in which electrons are accelerated by the electric *curl forces* (circulatory forces) [55] generated by a time-dependent magnetic field.

the field which can yield their mutual amplification. This *double* α-effect is reflected in the name of α^2-dynamo [247].

Expanding the poloidal and toroidal components in spherical harmonics as $P \sim e^{\lambda_{l,n}t} P^{(l,m,n)}(r) Y_l^m(\theta,\phi)$ and $T \sim e^{\lambda_{l,n}t} T^{(l,m,n)}(r) Y_l^m(\theta,\phi)$, finally yields the system of equations [207, 211]

$$\begin{pmatrix} \partial_r^2 - \frac{l(l+1)}{r^2} & \alpha(r) \\ -\partial_r \alpha(r) \partial_r + \alpha(r) \frac{l(l+1)}{r^2} & \partial_r^2 - \frac{l(l+1)}{r^2} \end{pmatrix} \begin{pmatrix} u_1 \\ u_2 \end{pmatrix} = \lambda \begin{pmatrix} u_1 \\ u_2 \end{pmatrix}, \tag{9.8}$$

where $u_1 = rP^{(l,m,n)}$, $u_2 = rT^{(l,m,n)}$, $\lambda = \lambda_{l,n}$, and the variables r and t are re-scaled so that $\eta_T = 1$ and $r \in (0, 1]$. The equations (9.8) are equipped with the boundary conditions [307]

$$(\beta l + 1 - \beta) u_1(1) + \beta u_1{}_r^{(1)}(1) = 0, \quad u_2(1) = 0. \tag{9.9}$$

The homotopy parameter $\beta \in [0, 1]$ interpolates between the Dirichlet ($\beta = 0$) boundary conditions, corresponding to an infinitely conducting exterior, and Robin-type ($\beta = 1$) boundary conditions, corresponding to a nonconducting exterior of the dynamo region [331]. Although the latter are more relevant for the use in applications [195], the former allow for an almost completely analytical treatment of the problem and in this way provide immediate deep insights into underlying structures and effects [208].

The eigenvalues, λ, of the problem (9.8) with the boundary conditions (9.9) indicate stability or instability that is determined by the result of a competition between the resistive dissipation and the α-effect due to vortical motions of the fluid, i.e. in fact by the spatial profile of $\alpha(r)$. Existence of at least one eigenvalue with $\mathrm{Re}\lambda > 0$ means instability, i.e. dynamo, which can be either oscillatory ($\mathrm{Im}\lambda \neq 0$) or nonoscillatory ($\mathrm{Im}\lambda = 0$).

It is known that when spatial distribution of the helicity parameter is uniform, i.e. $\alpha(r) = \alpha_0 = const$, the principle of exchange of stabilities [145, 183] holds: at some threshold value $\alpha_0 > 0$ the first unstable eigenvalue has imaginary part equal to zero. Hence, the α^2-dynamo is nonoscillatory when $\nabla\alpha \equiv 0$ [331]. Some nonuniformly distributed helicity parameters can, however, produce complex eigenvalues with positive real part and, in particular, make the leading unstable mode oscillatory, see e.g. [195,211] where successful helicity distributions were suggested by numerical optimization to have the form

$$\alpha(r) = \alpha_0 f(r) \tag{9.10}$$

with $\alpha_0 = const$ and $f(r)$ the algebraic or trigonometric polynomial.

With the distributions (9.10) the following situation typically occurs that is schematically illustrated by Figure 9.1 (a). For a given $f(r) = f_A(r)$ the growth rates $\mathrm{Re}\lambda_{1,2}(\alpha_0)$ of the two lowest eigenvalues, which are real, meet at some value of α_0 (exceptional point) where a double real eigenvalue with the Keldysh chain of length 2

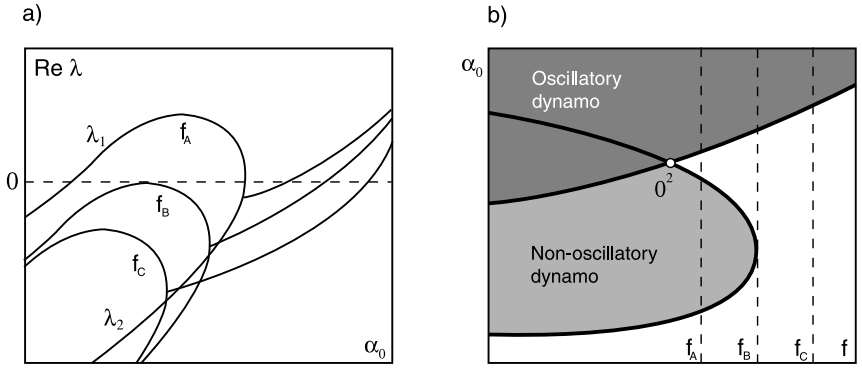

Figure 9.1. (a) Typical behavior of the growth rates of the eigenmodes of the α^2-dynamo with the nonuniform profile of $\alpha(r)$ [195, 547]. (b) A scheme of the corresponding stability diagram with the 0^2 singularity, with white color encoding the asymptotic stability, dark gray the oscillatory dynamo (flutter), and light gray the nonoscillatory dynamo (divergence).

is originated. The double eigenvalue splits into two complex eigenvalues with the further increase of α_0. The eigencurve $\mathrm{Re}\lambda_1(\alpha_0)$ has a maximum as a function of α_0 when $\lambda_1 > 0$. The dynamo is nonoscillatory. Slightly changing $f(r)$ one obtains $f(r) = f_B(r)$ such that the eigencurves behave similar to the case A except that the maximum is associated now with the simple eigenvalue $\lambda_1 = 0$ and the instability threshold jumps to the oscillating branch. When $f(r) = f_C(r)$, the maximum corresponds to a simple real eigenvalue $\lambda_1 < 0$ so that the first unstable eigenvalue is of an oscillatory mode.

In the (f, α_0)-space the described behavior of the growth rates suggests the stability diagram that is schematically shown as a planar one in Figure 9.1 (b). It consists of two sheets, one corresponding to the spectra where the first eigenvalue is simple and vanishing ($\lambda = 0$) and another one corresponding to the spectra where the first eigenvalue is pure imaginary ($\lambda = \pm i\omega$). The two sheets transversally intersect at a set that corresponds to a spectrum with the double zero eigenvalue with the Keldysh chain of length 2 (0^2 in terminology of Arnold [17]). The first sheet separates the domains of asymptotic stability and nonoscillatory dynamo (divergence). It is curved in such a manner that it has a vertical tangent at $f = f_B$. The second sheet separates the domains of asymptotic stability and oscillatory dynamo (flutter). Note that in finite-dimensional dissipative systems depending on at least two scalar parameters, the 0^2 singularity is generic [17, 518].

The parameter regimes near the 0^2 singularity shown in Figure 9.1 (b) were employed by Stefani and Gerbeth [547] in order to construct a nonlinear model based on the kinematic α^2-dynamo equations, demonstrating reversals of polarity[2] of the dipole

[2] Polarity reversals of the Earth's magnetic field have fascinated geophysicists since their discovery about a century ago. While the last reversal occurred approximately 780 000 years ago, the mean

component of the magnetic field generated by the α^2-dynamo. The singular geometry of the stability boundary appears to be responsible for the self-tuning mechanism of field reversals discussed in [547]. The importance of the specific interplay between oscillatory and nonoscillatory modes for the reversal mechanism had been emphasized by Sarson and Jones [509]. A particular problem of this nonlinear model in which exceptional points are involved, is how to describe a class of functions $\alpha(r)$ that robustly produce either oscillatory or nonoscillatory dynamos. The problem is complicated by strong sensitivity of the destabilizing properties of $\alpha(r)$ to the choice of boundary conditions.

In this context it is worthwhile to note that important features of dynamos are most easily understandable when treated with idealized (i.e. perfectly conducting) boundary conditions. This was the case for explaining the famous eigenvalue symmetry between dipole and quadrupole modes as was done by Proctor in 1977 [487]. Standing in this tradition, in the present chapter we obtain analytically the destabilizing spatial profiles $\alpha(r)$ in case of physically realistic boundary conditions ($\beta = 1$) via a homotopic deformation of eigencurves of the problem with idealistic boundary conditions ($\beta = 0$) [208, 307].

9.2 Uniform α-profiles generate only nonoscillatory dynamos

We rewrite the boundary eigenvalue problem of the α^2-dynamo given by equations (9.8) and (9.9) in the matrix form (7.1) with $N = 2$ and $m = 2$, convenient for the implementation of the perturbation theory developed in Chapter 7:

$$\mathbf{Lu} := \mathrm{l}_0\partial_x^2\mathbf{u} + \mathrm{l}_1\partial_x\mathbf{u} + \mathrm{l}_2\mathbf{u} = 0, \quad \mathfrak{U}\mathrm{u} := [\mathfrak{A}, \mathfrak{B}]\mathrm{u} = 0. \tag{9.11}$$

The matrices in the differential expression $\mathbf{L}$ are

$$\mathrm{l}_0 = \begin{pmatrix} 1 & 0 \\ -\alpha(x) & 1 \end{pmatrix}, \quad \mathrm{l}_1 = \partial_x\mathrm{l}_0,$$
$$\mathrm{l}_2 = \begin{pmatrix} -\frac{l(l+1)}{x^2} - \lambda & \alpha(x) \\ \alpha(x)\frac{l(l+1)}{x^2} & -\frac{l(l+1)}{x^2} - \lambda \end{pmatrix}, \tag{9.12}$$

reversal rate is about 4 per Myr [307]. The nature of reversals is quite complex and there is little hope to understand all their details within a simple model. Recent computer simulations of the geodynamo have progressed much since the first fully coupled 3D simulations of a reversal by Glatzmaier and Roberts in 1995 [198]. Polarity reversals were observed in one of the recent liquid sodium dynamo experiments [545]. Nevertheless, apparently only kinematic mean field dynamo models are so far available to provide detailed matches with observations of at least solar magnetism.

and $\mathfrak{U} := [\mathfrak{A}, \mathfrak{B}] \in \mathbb{C}^{4\times 8}$ in the boundary conditions, consists of the blocks

$$\mathfrak{A} = \begin{pmatrix} 1 & 0 & 0 & 0 \\ 0 & 1 & 0 & 0 \\ 0 & 0 & 0 & 0 \\ 0 & 0 & 0 & 0 \end{pmatrix}, \quad \mathfrak{B} = \begin{pmatrix} 0 & 0 & 0 & 0 \\ 0 & 0 & 0 & 0 \\ \beta l + 1 - \beta & 0 & \beta & 0 \\ 0 & 1 & 0 & 0 \end{pmatrix}. \tag{9.13}$$

The vector function $\mathbf{u} \in \tilde{\mathcal{H}} = L_2(0,1) \oplus L_2(0,1)$ lives in the Hilbert space $(\tilde{\mathcal{H}}, (.,.))$ with inner product $(\mathbf{u}, \mathbf{v}) = \int_0^1 \overline{\mathbf{v}}^T \mathbf{u}\, dx$, where the overbar denotes complex conjugation, and the boundary vector $\mathfrak{u}$ is given as

$$\mathfrak{u}^T := \left(\mathbf{u}^T(0), \partial_x \mathbf{u}^T(0), \mathbf{u}^T(1), \partial_x \mathbf{u}^T(1)\right) \in \mathbb{C}^8. \tag{9.14}$$

We assume that $\alpha(x) := \alpha_0 + \gamma \Delta\alpha(x)$, where $\alpha_0 = const$, γ is a scalar parameter, and $\Delta\alpha(x)$ is a smooth real function $C^2(0,1) \ni \Delta\alpha(x) : (0,1) \to \mathbb{R}$. The helicity parameter can also be represented in the form (9.10) as $\alpha(x) = \alpha_0 f(x)$ with $f(x) = 1 + \frac{\gamma}{\alpha_0}\Delta\alpha(x)$. For a fixed $\Delta\alpha(x)$ the differential expression $\mathbf{L}$ depends on the parameters α_0 and γ, while β interpolates between idealized ($\beta = 0$) boundary conditions, corresponding to an infinitely conducting exterior, and physically realistic ones ($\beta = 1$) corresponding to a nonconducting exterior of the dynamo region [307].

9.2.1 Conducting exterior: self-adjointness in a Krein space

The spectral problem (9.11) is not self-adjoint in a Hilbert space, but in the case of idealized boundary conditions ($\beta = 0$) the fundamental symmetry of the differential expression [207, 208]

$$\mathbf{L}_0 := \mathbf{L}(\lambda = 0) = \mathbf{J}\mathbf{L}_0^\dagger \mathbf{J}, \quad \mathbf{J} = \begin{pmatrix} 0 & 1 \\ 1 & 0 \end{pmatrix}, \tag{9.15}$$

makes $\mathbf{L}_0$ self-adjoint in a *Krein space* $(\mathcal{K}, [.,.])$ [202, 203] with *indefinite inner product* $[.,.] = (\mathbf{J}.,.)$:

$$[\mathbf{L}_0\mathbf{u}, \mathbf{v}] = [\mathbf{u}, \mathbf{L}_0\mathbf{v}], \quad \mathbf{u}, \mathbf{v} \in \mathcal{K}\,. \tag{9.16}$$

For $\beta \neq 0$ the operator $\mathbf{L}_0$ is not self-adjoint even in a Krein space. The matrix $\mathfrak{V}$ of the boundary conditions and auxiliary matrix $\widetilde{\mathfrak{V}}$ for the adjoint differential expression $\mathbf{L}^\dagger\mathbf{v} = \mathbf{l}_0^* \partial_x^2 \mathbf{v} - \mathbf{l}_1^* \partial_x \mathbf{v} + \mathbf{l}_2^* \mathbf{v}$ follow from the formula (7.15) where the 4×4 matrices $\widetilde{\mathfrak{A}}$ and $\widetilde{\mathfrak{B}}$ are chosen as

$$\widetilde{\mathfrak{A}} = \begin{pmatrix} 0 & \mathbf{I} \\ 0 & 0 \end{pmatrix}, \quad \widetilde{\mathfrak{B}} = \begin{pmatrix} 0 & 0 \\ 0 & \mathbf{I} \end{pmatrix}, \quad \mathbf{I} = \begin{pmatrix} 1 & 0 \\ 0 & 1 \end{pmatrix}. \tag{9.17}$$

9.2.2 Basis properties of eigenfunctions

For constant $\alpha-$profiles $\alpha(x) \equiv \alpha_0 = const,\ x \in [0,1)$, the operator matrix $\mathbf{L}_0$ takes the simpler form [208]

$$\mathbf{L}_0^{\alpha_0} = \begin{pmatrix} -1 & 0 \\ \alpha_0 & -1 \end{pmatrix} \otimes A_l + \begin{pmatrix} 0 & \alpha_0 \\ 0 & 0 \end{pmatrix} \otimes I, \tag{9.18}$$

where I is the identity and

$$A_l := -\partial_x^2 + \frac{l(l+1)}{x^2}. \tag{9.19}$$

Then, the two-component eigenfunctions $\mathbf{u}(x)$ can be derived in the form [208]

$$\mathbf{u}_n(x) = \begin{pmatrix} C_1 \\ C_2 \end{pmatrix} \otimes u_n(x) \in \mathbb{C}^2 \otimes L_2(0,1)\,, \tag{9.20}$$

where $C_1, C_2 \in \mathbb{C}$ are constants to be determined and u_n are the eigenfunctions of the operator A_l

$$A_l u_n = \rho_n u_n, \quad u(x \searrow 0) = u(x=1) = 0\,. \tag{9.21}$$

These eigenfunctions u_n are Riccati–Bessel functions [208]

$$u_n(x) = N_n x^{1/2} J_{l+\frac{1}{2}}(\sqrt{\rho_n}x), \quad N_n := \frac{\sqrt{2}}{|J_{l+\frac{3}{2}}(\sqrt{\rho_n})|} \tag{9.22}$$

that are orthonormalized as

$$(u_m, u_n) = \delta_{mn}, \qquad \|u_n\| = 1\,. \tag{9.23}$$

Hence, the spectrum of the operator A_l consists of simple real eigenvalues $\rho_n > 0$ – the squares of Bessel function zeros

$$J_{l+\frac{1}{2}}(\sqrt{\rho_n}) = 0, \qquad 0 < \sqrt{\rho_1} < \sqrt{\rho_2} < \cdots\,. \tag{9.24}$$

Spectrum and eigenvectors of $\mathbf{L}_0^{\alpha_0}$ follow from equations (9.18) and (9.20) as

$$\lambda_n^{\pm} = \lambda_n^{\pm}(\alpha_0) = -\rho_n \pm \alpha_0\sqrt{\rho_n} \in \mathbb{R}, \quad n \in \mathbb{Z}^+ \tag{9.25}$$

and

$$\mathbf{u}_n^{\pm} = \begin{pmatrix} 1 \\ \pm\sqrt{\rho_n} \end{pmatrix} u_n \in \mathbb{R}^2 \otimes L_2(0,1)\,, \tag{9.26}$$

and correspond to Krein space states of *positive* and *negative* type

$$[\mathbf{u}_m^{\pm}, \mathbf{u}_n^{\pm}] = \pm 2\sqrt{\rho_n}\delta_{mn}, \qquad [\mathbf{u}_m^{\pm}, \mathbf{u}_n^{\mp}] = 0, \qquad \mathbf{u}_n^{\pm} \in \mathcal{K}_{\pm} \subset \mathcal{K}\,. \tag{9.27}$$

9.2.3 Spectral mesh of eigencurves

The branches $\lambda_n^{\pm}$ of the spectrum (9.25) are real-valued linear functions of the parameter α_0 with signature-defined slopes $\pm\sqrt{\rho_n}$ and form for all $l = 0, 1, 2, \ldots$ a mesh-like structure in the $(\alpha_0, \mathrm{Re}\lambda)$-plane, as depicted in Figure 9.2 (a).

In order to calculate the intersection points of the spectral branches (the nodes of the spectral mesh), we introduce the following convenient notation

$$\begin{aligned} \lambda_n^{\varepsilon} &= -\rho_n + \varepsilon\alpha_0\sqrt{\rho_n}\,, \qquad \varepsilon = \pm \\ \mathbf{u}_n^{\varepsilon} &= \begin{pmatrix} 1 \\ \varepsilon\sqrt{\rho_n} \end{pmatrix} u_n\,, \end{aligned} \tag{9.28}$$

which allows us to treat in a unified way positive and negative Krein space states, marked in Figure 9.2 (a) by light and dark gray colors, respectively.

Two branches $\lambda_m^{\delta}, \lambda_n^{\varepsilon}$ with $n \neq m$ intersect at a point $(\alpha_0^{\nu}, \lambda_0^{\nu})$ when

$$\begin{aligned} \lambda_n^{\varepsilon} &= \lambda_m^{\delta} \\ -\rho_n + \varepsilon\alpha_0\sqrt{\rho_n} &= -\rho_m + \delta\alpha_0\sqrt{\rho_m} \\ \alpha_0 &= \frac{\rho_n - \rho_m}{\varepsilon\sqrt{\rho_n} - \delta\sqrt{\rho_m}} \\ \alpha_0^{\nu} := \alpha_0 &= \varepsilon\sqrt{\rho_n} + \delta\sqrt{\rho_m} \end{aligned} \tag{9.29}$$

and hence

$$\lambda_n^{\varepsilon} = \lambda_m^{\delta} = \lambda_0^{\nu} := \varepsilon\delta\sqrt{\rho_n\rho_m}\,. \tag{9.30}$$

equations (9.29) and (9.30) imply that spectral branches of different type $\delta \neq \varepsilon$ intersect for both signs of α_0 at $\lambda_0^{\nu} < 0$. In contrast, intersections at $\lambda_0^{\nu} > 0$ are induced by

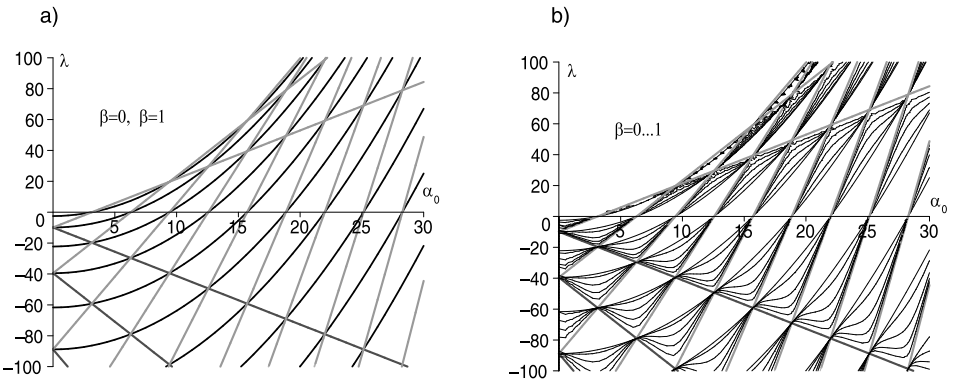

Figure 9.2. For $\alpha(x) = \alpha_0 = const$ and $l = 0$: (a) Eigencurves of the eigenvalue problem (9.11), corresponding to the perfectly conducting surrounding ($\beta = 0$, spectral mesh of light and dark gray straight lines) and to the insulating surrounding ($\beta = 1$, separated black parabolic branches). (b) Numerically calculated homotopic deformation of the spectral mesh into the parabolic eigencurves for $\beta \in [0, 1]$ [209].

spectral branches of positive type (light gray lines in Figure 9.2 (a)) when $\alpha_0 > 0$, and by spectral branches of negative type (dark gray lines in Figure 9.2 (a)) when $\alpha_0 < 0$.

According to equation (9.26) the double eigenvalue λ_0^ν possesses the two distinct eigenvectors $\mathbf{u}_n^\varepsilon$ and $\mathbf{u}_m^\delta$:

$$\mathbf{u}_n^\varepsilon = \begin{pmatrix} 1 \\ \varepsilon\sqrt{\rho_n} \end{pmatrix} u_n, \qquad \mathbf{u}_m^\delta = \begin{pmatrix} 1 \\ \delta\sqrt{\rho_m} \end{pmatrix} u_m\,. \tag{9.31}$$

Consequently, the intersection points given by equation (9.29) correspond to double eigenvalues (9.30) with two linearly independent eigenvectors (9.31), i.e. they are semisimple eigenvalues (diabolical points, DPs, [270]) of algebraic and geometric multiplicity two [155, 298, 428].

Spectral meshes for neighboring mode numbers l and $l+1$ have only slightly different slopes of their branches and behave qualitatively similar under perturbations, cf. Figure 9.2 (a) and Figure 9.3 (a). Therefore, basic spectral structures for $l = 1, 2$ dipole and quadrupole modes can be illustrated by the simpler but less physical $l = 0$ monopole modes given by trigonometric functions.

9.2.4 Deformation of the spectral mesh via transition from conducting to insulating surrounding

When $l = 0$, the eigenelements (9.28) of the spectral mesh simplify [208]

$$\lambda_n^\varepsilon = -(\pi n)^2 + \varepsilon\alpha_0\pi n, \quad \lambda_m^\delta = -(\pi m)^2 + \delta\alpha_0\pi m, \quad \varepsilon, \delta = \pm, \tag{9.32}$$

$$\mathbf{u}_n^\varepsilon = \begin{pmatrix} 1 \\ \varepsilon\pi n \end{pmatrix} \sin(n\pi x), \quad \mathbf{u}_m^\delta = \begin{pmatrix} 1 \\ \delta\pi m \end{pmatrix} \sin(m\pi x). \tag{9.33}$$

The eigencurves (9.32) intersect and originate a double semisimple eigenvalue with two linearly independent eigenvectors (9.33) at the node $(\alpha_0^\nu, \lambda_0^\nu)$, where

$$\lambda_0^\nu = \varepsilon\delta\pi^2 nm, \quad \alpha_0^\nu = \varepsilon\pi n + \delta\pi m. \tag{9.34}$$

For the $(l = 0)-$mesh, depicted as dark and light gray lines in Figure 9.2, the diabolical crossings of the (εn)-th and $(\varepsilon n + j)$-th modes with the same fixed $|j| \in \mathbb{Z}^+$ are located on a parabolic curve [208]

$$\lambda(\alpha_0) = \frac{1}{4}\left(\alpha_0^2 - \pi^2 j^2\right) \tag{9.35}$$

where $\alpha_0 = \alpha_0^\nu = \pi(2n\varepsilon + j)$ and $\lambda_0^\nu = \lambda(\alpha_0^\nu) = \pi^2 n(n + \varepsilon j)$.

Eigencurves of different Krein signature $\delta \neq \varepsilon$ intersect for both signs of α_0 at $\lambda_0^\nu < 0$ (the resulting Krein signature of the double eigenvalue is thus mixed [390, 603]), whereas intersections at $\lambda_0^\nu > 0$ are induced by spectral branches of coinciding signatures: for $\varepsilon = \delta = +$ at $\alpha_0 > 0$, and for $\varepsilon = \delta = -$ at $\alpha_0 < 0$ (λ_0^ν has definite Krein signature [390, 603]).

For constant $\alpha(x) = \alpha_0$, the spectrum remains purely real on the full homotopic family $\beta \in [0, 1]$ and passes smoothly in the $(\alpha_0, \mathrm{Re}\lambda)$-plane from the spectral mesh at $\beta = 0$ to nonintersecting branches of simple real eigenvalues at $\beta = 1$, see Figure 9.2 (b). In the monopole case $l = 0$ the full spectral homotopy is described by the characteristic equation [209]

$$(1-\beta)\sqrt{\alpha_0^2 - 4\lambda}\left[\cos\left(\sqrt{\alpha_0^2 - 4\lambda}\right) - \cos(\alpha_0)\right] + 2\beta\lambda \sin\left(\sqrt{\alpha_0^2 - 4\lambda}\right) = 0. \quad (9.36)$$

For the idealized boundary conditions ($\beta = 0$) equation (9.36) yields the spectral mesh (9.32) whereas for physically realistic boundary conditions ($\beta = 1$) it leads to a spectrum consisting of the countably infinite set of parabolas

$$\lambda_s(\alpha_0) = \frac{1}{4}(\alpha_0^2 - \pi^2 s^2), \quad (9.37)$$

which are shown as black curves in Figure 9.2 (a). The parabolic eigencurve (9.37) passes exactly through the nodes of the spectral mesh (9.32), located on the curve (9.35) with $j = s$. Moreover, when β takes values between $\beta = 0$ and $\beta = 1$, the spectral mesh unfolds into eigencurves that always pass through the loci of the diabolical points at the intersections of the spectral mesh at $\beta = 0$, see Figure 9.2 (b). The loci of the DPs are fixed points of the homotopy $\forall \beta \in [0, 1]$, which indicates that they are 'deeply imprinted' in the boundary eigenvalue problem[3] (9.11).

It is remarkable that for any $\beta \in [0, 1]$, all the eigenvalues are real and negative until at $\alpha_0^{cr} = \pi n$ the first ($n = 1$) eigenvalue vanishes, becoming positive with the further increase of α_0. We see that at $\alpha_0 < \alpha_0^{cr}$ the α^2-dynamo is a *heavily damped* [34,99] dissipative system that is unstable by divergence at $\alpha_0 > \alpha_0^{cr}$ when the α-effect produced by the vortical motions of the electrically conducting fluid is intense enough. Thus, when $\alpha(x)$ is a uniformly distributed helicity parameter, the eigenvalues remain real under variation of the parameter β in the boundary conditions, and the monopole ($l = 0$) modes of the α^2-dynamo are always nonoscillatory. This result persists at $l \neq 0$ too [331].

9.3 Nonhomogeneous α-profiles and the conducting exterior

Complex eigenvalues in the eigenvalue problem (9.11) can be produced by nonuniform spatial distributions of the helicity parameter $\alpha(x) = \alpha_0 + \gamma\Delta\alpha(x)$, as Figure 9.3 (b) demonstrates for the dipole mode $l = 1$ and $\alpha(x) = \alpha_0 + 2.5\cos(6\pi x)$ when the exterior is conducting ($\beta = 0$). We see that in the spectral mesh shown in Figure 9.3 (a) for $\alpha(x) = \alpha_0 = const$ the nodes unfold under the cosine perturbation either into rings of complex eigenvalues (black lines in Figure 9.3 (b)) when $\lambda_0^{\nu} < 0$,

[3] Cf. the same homotopic deformation effect in the eigenvalue problem associated with the rotating circular string with an elastic restraint [476,510] discussed in Section 7.3.

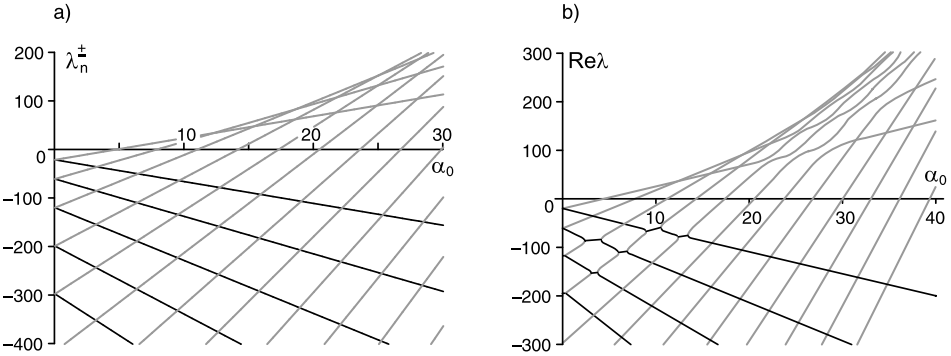

Figure 9.3. For $l = 1$ and $\beta = 0$: (a) Eigencurves $\lambda_n^{\pm}(\alpha_0 \geq 0)$ are straight lines intersecting at semisimple degeneration points (diabolical points) of algebraic and geometric multiplicity two. (b) Numerically calculated deformation of the spectral mesh with unfolding of diabolical points for the nonuniformly distributed helicity parameter $\alpha(x) = \alpha_0 + 2.5\cos(6\pi x)$ [208].

or veer away forming avoided crossings when $\lambda_0^{\nu} > 0$. Note that the deformations of the mesh spread over a broad parabola-like region with the pronounced maximum of the effect localized along one of the parabolic curves (9.35). With distance from such a resonant parabola the effect of the nonuniform perturbation of the α-profile vanishes.

Another important observation is that complex eigenvalues are produced only by eigencurve crossings with the mixed Krein signature ($\varepsilon \neq \delta$). The eigencurve crossings with the definite Krein signature yield real eigenvalues, Figure 9.3 (b). This happens in the situation when the α-profile loses its uniformity but the boundary conditions are not perturbed ($\beta = 0$), i.e. when the operator $\mathbf{L}_0$ of the α^2-dynamo remains self-adjoint in a Krein space under perturbation of α-profile, cf. equation (9.15). In the following, we will demonstrate this explicitly by means of the sensitivity analysis of Chapter 7.

9.3.1 $l \geq 0$: definite Krein signature prohibits formation of complex eigenvalues

Let us assume that the operator $\mathbf{L}_0^{\alpha_0}$ in equation (9.18) has at $\alpha_0 = \alpha_0^{\nu}$ a semisimple double eigenvalue λ_0^{ν} with eigenvectors $\mathbf{u}_n^{\varepsilon}$ and $\mathbf{u}_m^{\delta}$ determined by equations (9.30) and (9.31). Consider a perturbation of the α-profile of the form

$$\alpha(x) = \alpha_0^{\nu} + \gamma\Delta\alpha(x). \tag{9.38}$$

Then, the perturbed operator is given by

$$\mathbf{L}_0^{\alpha} = \mathbf{L}_0^{\alpha_0} + \gamma \begin{pmatrix} 0 & \Delta\alpha(x) \\ \Delta\alpha(x)A_l - \Delta\alpha'(x)\partial_x & 0 \end{pmatrix} =: \mathbf{L}_0^{\alpha_0} + \gamma\mathbf{L}_1 \tag{9.39}$$

and the eigenvalue problem (9.11) can be expanded in terms of the small parameter γ as [155, 208, 298]

$$(\mathbf{L}_0^{\alpha_0} + \gamma \mathbf{L}_1)(\mathbf{u}_0^\nu + \gamma \mathbf{u}_1 + \ldots) = (\lambda_0^\nu + \gamma\lambda_1 + \ldots)(\mathbf{u}_0^\nu + \gamma \mathbf{u}_1 + \ldots)\,. \tag{9.40}$$

Here, $\mathbf{u}_0^\nu$ is an eigenvector of the unperturbed operator $\mathbf{L}_0^{\alpha_0}$ at the eigenvalue λ_0^ν and, hence, has to be a linear combination of $\mathbf{u}_n^\varepsilon$ and $\mathbf{u}_m^\delta$

$$\mathbf{u}_0^\nu = c_1 \mathbf{u}_n^\varepsilon + c_2 \mathbf{u}_m^\delta \in \mathrm{span}\Big(\mathbf{u}_n^\varepsilon, \mathbf{u}_m^\delta\Big) \subset \mathcal{K}\,. \tag{9.41}$$

Comparing the coefficients at the same powers of γ yields up to first order in γ

$$\mathbf{L}_0^{\alpha_0}\mathbf{u}_0^\nu = \lambda_0^\nu \mathbf{u}_0^\nu\,, \tag{9.42}$$

$$\mathbf{L}_0^{\alpha_0}\mathbf{u}_1 + \mathbf{L}_1\mathbf{u}_0^\nu = \lambda_0^\nu \mathbf{u}_1 + \lambda_1 \mathbf{u}_0^\nu\,. \tag{9.43}$$

The first of these equations is satisfied identically, whereas the second one can be most conveniently analyzed by projecting it with the help of the Krein space inner product $[.,.]$ onto the two-dimensional subspace[4] $\mathrm{span}\Big(\mathbf{u}_n^\varepsilon, \mathbf{u}_m^\delta\Big) \subset \mathcal{K}$

$$[\mathbf{L}_1\mathbf{u}_0^\nu, \mathbf{u}_n^\varepsilon] = \lambda_1[\mathbf{u}_0^\nu, \mathbf{u}_n^\varepsilon], \quad [\mathbf{L}_1\mathbf{u}_0^\nu, \mathbf{u}_m^\delta] = \lambda_1[\mathbf{u}_0^\nu, \mathbf{u}_m^\delta]\,. \tag{9.44}$$

Using (9.41) in (9.44) yields a closed system of defining equations for the first-order spectral perturbation λ_1 and the coefficients c_1 and c_2 [155, 208]

$$\begin{pmatrix} [\mathbf{L}_1\mathbf{u}_n^\varepsilon, \mathbf{u}_n^\varepsilon] - \lambda_1[\mathbf{u}_n^\varepsilon, \mathbf{u}_n^\varepsilon] & [\mathbf{L}_1\mathbf{u}_m^\delta, \mathbf{u}_n^\varepsilon] \\ [\mathbf{L}_1\mathbf{u}_n^\varepsilon, \mathbf{u}_m^\delta] & [\mathbf{L}_1\mathbf{u}_m^\delta, \mathbf{u}_m^\delta] - \lambda_1[\mathbf{u}_m^\delta, \mathbf{u}_m^\delta] \end{pmatrix} \begin{pmatrix} c_1 \\ c_2 \end{pmatrix} = 0, \tag{9.45}$$

i.e. in first-order approximation the perturbation $\gamma\mathbf{L}_1$ defines the spectral shift λ_1 and lifts the directional degeneration (9.41) of the zeroth order eigenvectors $\mathbf{u}_0^\nu$ by fixing two rays in the subspace $\mathrm{span}(\mathbf{u}_n^\varepsilon, \mathbf{u}_m^\delta) \subset \mathcal{K}$, see e.g. [270, 517].

In our subsequent considerations of the system (9.45) we will need different explicit representations of the matrix elements containing $\mathbf{L}_1$. Partial integration and substitution of the relation $\partial_x^2 u_n = [-\rho_n + l(l+1)/x^2]u_n$ give these representations as [208]

$$[\mathbf{L}_1\mathbf{u}_m^\delta, \mathbf{u}_n^\varepsilon] = \int_0^1 \Delta\alpha \left[(\rho_m + \varepsilon\delta\sqrt{\rho_n\rho_m})u_m u_n + u_m'' u_n + u_m' u_n'\right] dx \tag{9.46}$$

$$= \int_0^1 \Delta\alpha \left[\left(\varepsilon\delta\sqrt{\rho_n\rho_m} + \frac{l(l+1)}{x^2}\right) u_m u_n + u_m' u_n'\right] dx \tag{9.47}$$

$$= 2(\rho_m\rho_n)^{1/4} \int_0^1 \Delta\alpha(x) g_{mn}^l(x) dx, \quad m, n \in \mathbb{Z}^+, \tag{9.48}$$

[4] The terms containing $\mathbf{u}_1$ cancel due to the self-adjointness (9.15) of the operator $\mathbf{L}_0^{\alpha_0}$ and equations (9.41), (9.42).

where the functions $g^l_{mn}(x)$ can be naturally interpreted as components of a perturbation gradient in the Krein space $\mathcal{K}$

$$\begin{aligned} g^l_{mn}(x) = {} & \frac{(\varepsilon_n\varepsilon_m\sqrt{\rho_n\rho_m}x^2 + l^2 + l)J_{l+1/2}(x\sqrt{\rho_m})J_{l+1/2}(x\sqrt{\rho_n})}{x(\rho_n\rho_m)^{1/4}J_{l-1/2}(\sqrt{\rho_n})J_{l-1/2}(\sqrt{\rho_m})} \\ & + \frac{x\sqrt{\rho_m}J_{l-1/2}(x\sqrt{\rho_m}) - lJ_{l+1/2}(x\sqrt{\rho_m})}{x(\rho_n\rho_m)^{1/4}J_{l-1/2}(\sqrt{\rho_n})J_{l-1/2}(\sqrt{\rho_m})} \\ & \times \left(x\sqrt{\rho_n}J_{l-1/2}(x\sqrt{\rho_n}) - lJ_{l+1/2}(x\sqrt{\rho_n})\right). \end{aligned} \tag{9.49}$$

We note that they are symmetric $g^l_{mn} = g^l_{nm}$. Representation (9.48) may prove especially useful for the *optimization* of α-profiles with respect to given constraints or experimental requirements [195]. The symmetry properties of equation (9.47) and its implication

$$[\mathbf{L}_1\mathbf{u}^\delta_m, \mathbf{u}^\varepsilon_n] = [\mathbf{L}_1\mathbf{u}^\varepsilon_n, \mathbf{u}^\delta_m] \tag{9.50}$$

are a natural consequence of the Krein space self-adjointness of the perturbation operator $\mathbf{L}_1$ and the real-valuedness of the eigenvectors $\mathbf{u}^\varepsilon_n$, $\mathbf{u}^\delta_m$.

From (9.45) and (9.50) we obtain the following defining equation for λ_1

$$\lambda_1^2 - \lambda_1\left(\frac{[\mathbf{L}_1\mathbf{u}^\varepsilon_n, \mathbf{u}^\varepsilon_n]}{[\mathbf{u}^\varepsilon_n, \mathbf{u}^\varepsilon_n]} + \frac{[\mathbf{L}_1\mathbf{u}^\delta_m, \mathbf{u}^\delta_m]}{[\mathbf{u}^\delta_m, \mathbf{u}^\delta_m]}\right) + \frac{[\mathbf{L}_1\mathbf{u}^\varepsilon_n, \mathbf{u}^\varepsilon_n][\mathbf{L}_1\mathbf{u}^\delta_m, \mathbf{u}^\delta_m] - [\mathbf{L}_1\mathbf{u}^\varepsilon_n, \mathbf{u}^\delta_m]^2}{[\mathbf{u}^\varepsilon_n, \mathbf{u}^\varepsilon_n][\mathbf{u}^\delta_m, \mathbf{u}^\delta_m]} = 0, \tag{9.51}$$

which with the Krein space norm (9.27) reduces to

$$\lambda_1^2 - \lambda_1\left(\frac{[\mathbf{L}_1\mathbf{u}^\varepsilon_n, \mathbf{u}^\varepsilon_n]}{2\varepsilon\sqrt{\rho_n}} + \frac{[\mathbf{L}_1\mathbf{u}^\delta_m, \mathbf{u}^\delta_m]}{2\delta\sqrt{\rho_m}}\right) + \frac{[\mathbf{L}_1\mathbf{u}^\varepsilon_n, \mathbf{u}^\varepsilon_n][\mathbf{L}_1\mathbf{u}^\delta_m, \mathbf{u}^\delta_m] - [\mathbf{L}_1\mathbf{u}^\varepsilon_n, \mathbf{u}^\delta_m]^2}{4\varepsilon\delta\sqrt{\rho_n\rho_m}} = 0. \tag{9.52}$$

The unfolding of the diabolical points is accompanied by a fixing of the directions of the zeroth order eigenvectors $\mathbf{u}^\nu_0 \in \mathrm{span}(\mathbf{u}^\varepsilon_n, \mathbf{u}^\delta_m) \subset \mathcal{K}$ [270]. Using $\lambda_{1,\pm}$ in (9.45) one finds these directions as rays $\mathbf{u}^\nu_{0,\pm} = c_{1,\pm}\mathbf{u}^\varepsilon_n + c_{2,\pm}\mathbf{u}^\delta_m$, where

$$\frac{c_{1,\pm}}{c_{2,\pm}} = -\frac{[\mathbf{L}_1\mathbf{u}^\delta_m, \mathbf{u}^\varepsilon_n]}{[\mathbf{L}_1\mathbf{u}^\varepsilon_n, \mathbf{u}^\varepsilon_n] - [\mathbf{u}^\varepsilon_n, \mathbf{u}^\varepsilon_n]\lambda_{1,\pm}} = -\frac{[\mathbf{L}_1\mathbf{u}^\delta_m, \mathbf{u}^\delta_m] - [\mathbf{u}^\delta_m, \mathbf{u}^\delta_m]\lambda_{1,\pm}}{[\mathbf{L}_1\mathbf{u}^\varepsilon_n, \mathbf{u}^\delta_m]}. \tag{9.53}$$

The quadratic equation (9.52) is of the type $\lambda_1^2 - \lambda_1(a_1 + a_2) + a_1a_2 - \varepsilon\delta b^2/4 = 0$, $a_1, a_2, b \in \mathbb{R}$, and its solutions $\lambda_{1,\pm} = (a_1 + a_2 \pm \sqrt{(a_1 - a_2)^2 + \varepsilon\delta b^2})/2$ are real-valued for $\varepsilon = \delta$ and complex for $\varepsilon \neq \delta \cap (a_1 - a_2)^2 < b^2$. We see that they show the typical Krein space behavior [390]: Intersections of eigencurves corresponding to Krein-space states of the same type ($\varepsilon = \delta$) induce no real-to-complex transitions in the spectrum (veering or avoided crossing [370, 583]). In contrast, intersections of spectral branches corresponding to states of different types ($\varepsilon \neq \delta$) may in general be accompanied by real-to-complex transitions (bubbles of instability [390, 392]).

In terms of the gradient functions $g^l_{mn}(x)$ the defining equation (9.52) for the first-order spectral perturbations λ_1 reduces to

$$\lambda_1^2 - \lambda_1 \int_0^1 \Delta\alpha \left(\varepsilon g^l_{nn} + \delta g^l_{mm}\right) dx + \varepsilon\delta \left[\left(\int_0^1 \Delta\alpha g^l_{nn} dx\right)\left(\int_0^1 \Delta\alpha g^l_{mm} dx\right) - \left(\int_0^1 \Delta\alpha g^l_{mn} dx\right)^2\right] = 0 \qquad (9.54)$$

with solutions

$$\lambda_{1,\pm} = \frac{1}{2}\int_0^1 \Delta\alpha\left(\varepsilon g^l_{nn} + \delta g^l_{mm}\right) dx \pm \frac{1}{2}\sqrt{\left[\int_0^1 \Delta\alpha \left(\varepsilon g^l_{nn} - \delta g^l_{mm}\right) dx\right]^2 + 4\varepsilon\delta\left[\int_0^1 \Delta\alpha g^l_{mn} dx\right]^2}. \qquad (9.55)$$

From equation (9.55) we see that when $\varepsilon\delta < 0$ the 'diagonal' terms

$$\int_0^1 \Delta\alpha\left(g^l_{nn} + g^l_{mm}\right) dx \qquad (9.56)$$

prevent the imaginary offset of an eigenvalue whereas the 'off-diagonal' terms

$$\left[\int_0^1 \Delta\alpha g^l_{mn} dx\right]^2 \qquad (9.57)$$

enhance possible transitions to complex eigenvalues, which thus occur for

$$\varepsilon \neq \delta \quad \cap \quad \left(\frac{1}{2}\int_0^1 \left(g^l_{nn} + g^l_{mm}\right)\Delta\alpha dx\right)^2 < \left(\int_0^1 g^l_{mn}\Delta\alpha dx\right)^2. \qquad (9.58)$$

Condition (9.58) yields an explicit classification criterion for $\alpha-$profile perturbations with respect to their capability to induce complex eigenvalues. It is an efficient search tool for concrete $\alpha(x)$-profiles – and transforms in this way some general observations made in [207] into a technique of direct applicability.

The functions $g^l_{nm}(x)$ for $l = 1$ and different values of n, m and $\varepsilon\delta$ are shown in Figure 9.4. The 'diagonal' functions with $m = n$ are always nonnegative and the graphs of any two of them, $g^1_{nn}(x)$, $g^1_{mm}(x)$ with $m \neq n$ intersect only marginally, Figure 9.4 (c). Their differences $g^1_{nn}(x) - g^1_{mm}(x)$ are oscillating but mainly sign-preserving functions so that they act as an averaging integration kernel, Figure 9.4 (d). In contrast, the 'off-diagonal' functions $g^1_{nm}(x)$ with $m \neq n$ show strong sign changes and in this way they act as filter kernel, Figure 9.4 (a, b). The subtle interplay of the 'offset' and 'oscillation filter' functions is crucial for the α-profile to act as a generator of complex eigenvalues [208].

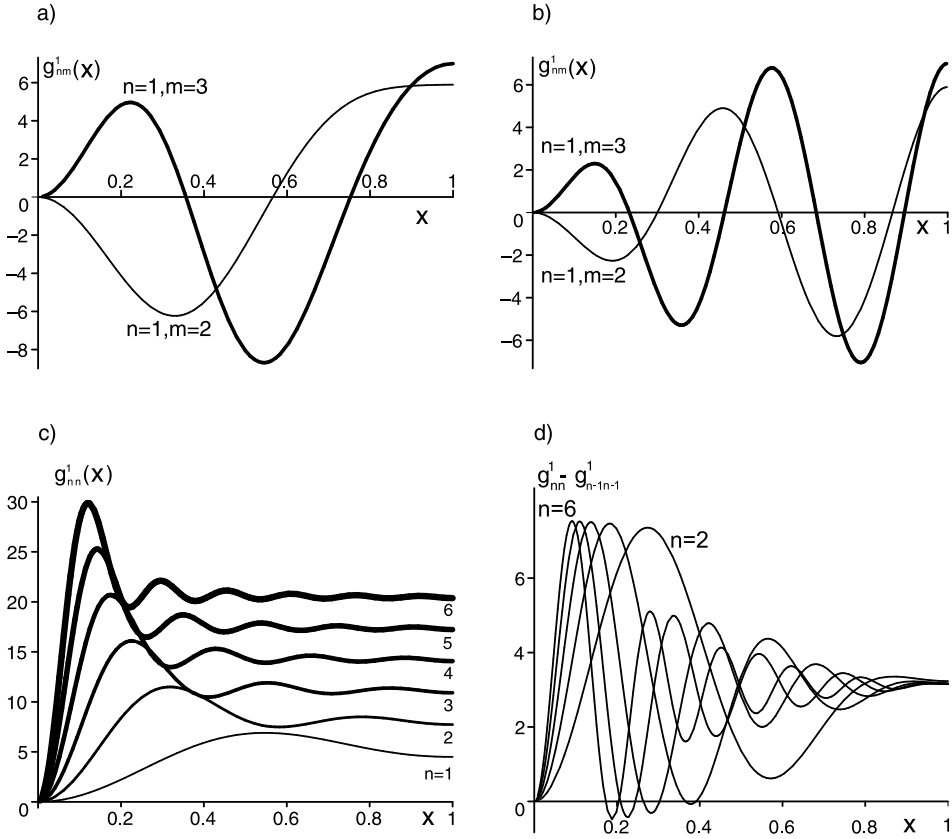

Figure 9.4. Functions $g^l_{nm}(x)$ for $l = 1$ and (a, b) $n = 1$, $m = 2, 3$ in the cases (a) $\varepsilon\delta = 1$ and (b) $\varepsilon\delta = -1$ and (c) for $l = 1$ and $n = m$. (d) Gradient function differences $g^1_{nn}(x) - g^1_{n-1n-1}(x)$ for $n = 2, \ldots, 6$ [208].

9.3.2 $l = 0$: oscillating solutions from the repeated decaying modes with mixed Krein signature

In this section, following the work [208] we consider the rather idealized case of zero spherical harmonics, $l = 0$, which in analogy to quantum scattering theory can be interpreted as s-wave sector. Due to its symmetry contents, this sector does not play a significant role in physical dynamos [207, 331]. Nevertheless, the study of such idealized models will turn out very instructive from a technical point of view. Due to their simpler structure they will allow for a detailed analytical handling and a transparent demonstration of some of the essential mathematical features of the dynamo models. In this way, they will provide some basic intuitive insight into the dynamo-related specifics of the unfolding of diabolical points. In the more realistic ($l \geq 1$)-sectors, these specifics re-appear in a similar but more complicated way. Subsequently, we

perform an analytical study of the local unfolding of the diabolical points (along the lines of Section 9.3.1) that we supplement by numerical results on the deformation of the spectral mesh.

Let $l = 0$. Then the differential expression of the operator $A_{l=0}$ reads simply $A_{l=0} = -\partial_x^2$ and $A_{l=0}$ has orthonormalized eigenfunctions $u_n(x)$, $u_n(0) = u_n(1) = 0$ and eigenvalues ρ_n

$$u_n = \sqrt{2}\sin(n\pi x), \qquad \rho_n = (\pi n)^2 . \tag{9.59}$$

The eigenvalues of the matrix differential operator $\mathbf{L}_0^{\alpha_0}$ are given by equation (9.32) and the corresponding eigenvectors (9.33) yield Krein space inner products

$$[\mathbf{u}_n^\varepsilon, \mathbf{u}_m^\delta] = \varepsilon 2\pi n \delta_{\varepsilon\delta}\delta_{mn} \tag{9.60}$$

and perturbation terms

$$[\mathbf{L}_1\mathbf{u}_m^\delta, \mathbf{u}_n^\varepsilon] = 2\pi^2 mn \int_0^1 \Delta\alpha(x)\cos\left[(\delta m - \varepsilon n)\pi x\right] dx. \tag{9.61}$$

According to equations (9.30), the diabolical points are located at points

$$\alpha_0^\nu = \pi(\varepsilon n + \delta m) =: \pi M, \quad \lambda_0^\nu = \varepsilon\delta\pi^2 mn \tag{9.62}$$

and form a periodic vertical line structure in the $(\alpha_0, \mathrm{Re}\lambda)$-plane. Note that in the $(l \geq 1)$-sectors (for fixed $l \geq 1$), this line structure is approached asymptotically in the $|m|, |n| \to \infty$ limit [208].

In order to simplify notations, we pass from double-indexed eigenvalues λ_n^ε and states $\mathbf{u}_n^\varepsilon \in \mathcal{K}_\varepsilon \subset \mathcal{K}_+ \oplus \mathcal{K}_- \subset \mathcal{K}$ with $(n, \varepsilon) \in \mathbb{Z}^+ \times \mathbb{Z}_2 \sim \mathbb{Z}^* = \mathbb{Z} - \{0\}$ to eigenvalues λ_n and normalized states $\mathbf{v}_n$ depending only on the single state number $n \in \mathbb{Z}$:

$$\lambda_n = \begin{cases} \lambda_n^+ & \text{for } n \in \mathbb{Z}^+ \\ \lambda_{|n|}^- & \text{for } n \in \mathbb{Z}^- \end{cases}, \quad 2^{1/2}\rho_n^{1/4}\mathbf{v}_n = \begin{cases} \mathbf{u}_n^+ \in \mathcal{K}_+ & \text{for } n \in \mathbb{Z}^+ \\ \mathbf{u}_{|n|}^- \in \mathcal{K}_- & \text{for } n \in \mathbb{Z}^- \end{cases} \tag{9.63}$$

with obvious implication

$$[\mathbf{v}_n, \mathbf{v}_m] = \varepsilon_n\, \delta_{nm}, \quad \varepsilon_n := \mathrm{sign}\,(n)\,. \tag{9.64}$$

Inspection of the defining equation (9.51) for the first-order spectral perturbations λ_1 shows that this equation is invariant with respect to a re-scaling of $\mathbf{u}_n^\varepsilon, \mathbf{u}_m^\delta$. Passing to the single-index notation (9.63) yields

$$\lambda_n = -(\pi n)^2 + \alpha_0\pi n, \quad \mathbf{v}_n(x) = \frac{1}{\sqrt{\pi|n|}}\begin{pmatrix} 1 \\ \pi n \end{pmatrix}\sin(\pi|n|x), \quad n \in \mathbb{Z}^* \tag{9.65}$$

with the following convenient representation of the perturbation terms (9.61)

$$[\mathbf{L}_1\mathbf{v}_{n+j}, \mathbf{v}_n] = \pi\sqrt{|n(n+j)|}\int_0^1 \Delta\alpha(x)\cos(j\pi x)dx\,. \tag{9.66}$$

This reduces the defining equation (9.52) for the spectral perturbation at the $(n, n+j)$ node of the spectral mesh (the intersection point of the λ_n and λ_{n+j} branches of the spectrum) with coordinates

$$\alpha_0^{\nu} = \pi(2n+j) =: \pi M, \quad \lambda_0^{\nu} = \pi^2 n(n+j) \tag{9.67}$$

to

$$\begin{aligned} &\lambda_1^2 - \lambda_1 \pi(2n+j) \int_0^1 \Delta\alpha(x)dx \\ &\quad + \pi^2 n(n+j)\left[\left(\int_0^1 \Delta\alpha(x)dx\right)^2 - \left(\int_0^1 \Delta\alpha(x)\cos(j\pi x)dx\right)^2\right] = 0 \end{aligned} \tag{9.68}$$

with solutions

$$\begin{aligned} \lambda_{1,\pm} = &\frac{\pi}{2}(2n+j)\int_0^1 \Delta\alpha(x)dx \\ &\pm \frac{\pi}{2}\sqrt{j^2\left(\int_0^1 \Delta\alpha(x)dx\right)^2 + 4n(n+j)\left(\int_0^1 \Delta\alpha(x)\cos(j\pi x)dx\right)^2}. \end{aligned} \tag{9.69}$$

We observe that the strength of the complex-valued unfolding of a diabolical point at a node with $n(n+j) < 0$ is defined by the relation between its $\cos(j\pi x)$-filtered perturbation $\int_0^1 \Delta\alpha(x)\cos(j\pi x)dx$ (cf. gradient function in Figure (9.4) (b)) and its average perturbation $\int_0^1 \Delta\alpha(x)dx$ (cf. gradient function in Figure (9.4) (c)). A deeper insight into this peculiar feature of the unfolding process can be gained by expanding the perturbation $\Delta\alpha(x)$ in Fourier components over the interval $[0, 1]$

$$\Delta\alpha(x) = \frac{a_0}{2} + \sum_{k=1}^{\infty}\left[a_k \cos(2\pi kx) + b_k \sin(2\pi kx)\right] \tag{9.70}$$

with coefficients given as $a_0 = 2\int_0^1 \Delta\alpha(x)dx$, $a_k = 2\int_0^1 \Delta\alpha(x)\cos(2\pi kx)dx$, $b_k = 2\int_0^1 \Delta\alpha(x)\sin(2\pi kx)dx$. In this way, the integral $\int_0^1 \Delta\alpha(x)\cos(j\pi x)dx$ in (9.66) reduces to components of the type

$$\begin{aligned} \int_0^1 \cos(j\pi x)dx &= \delta_{j,0}\,, \\ \int_0^1 \cos(2\pi kx)\cos(j\pi x)dx &= \frac{1}{2}\left(\delta_{j,2k} + \delta_{-j,2k}\right), \\ \int_0^1 \sin(2\pi kx)\cos(j\pi x)dx &= \begin{cases} 0 & \text{for } \; j = \pm 2k \\ \dfrac{1-(-1)^j}{\pi}\dfrac{2k}{4k^2-j^2} & \text{for } \; j \neq \pm 2k \end{cases} \end{aligned} \tag{9.71}$$

and we obtain the perturbation terms (9.66) as

$$[\mathbf{L}_1 \mathbf{v}_{n+j}, \mathbf{v}_n] = \frac{\pi}{2}\sqrt{|n(n+j)|}\, Q_j\,, \tag{9.72}$$

$$Q_j := a_0\delta_{j,0} + \sum_{k=1}^{\infty}\left[a_k\left(\delta_{j,2k} + \delta_{-j,2k}\right) + \frac{1-(-1)^j}{\pi}\frac{4b_k k}{4k^2 - j^2}\right]. \tag{9.73}$$

The defining equation for the spectral perturbation λ_1 now takes the form

$$\lambda_1^2 - \lambda_1\frac{\pi}{2}(2n+j)a_0 + \frac{\pi^2}{4}n(n+j)(a_0^2 - Q_j^2) = 0 \tag{9.74}$$

and leads to the following very instructive representation for its solutions

$$\lambda_{1,\pm} = \frac{\pi}{4}\left[(2n+j)a_0 \pm \sqrt{j^2 a_0^2 + 4n(n+j)Q_j^2}\right]. \tag{9.75}$$

The structure of these solutions shows that the unfolding of the diabolical points is controlled by several, partially competing, effects. Apart from the above mentioned Krein space related feature of unfolding into real eigenvalues for states of the same Krein space type ($n(n+j) > 0$), and the possibility for unfolding into pairwise complex-conjugate eigenvalues in case of states of opposite type ($n(n+j) < 0$), a competition occurs between oscillating perturbations ($a_{k\neq 0}, b_k$) and homogeneous offset-shifts a_0. In the case of vanishing offset-shifts (mean perturbations), $a_0 = 0$, any inhomogeneous perturbation with $a_k, b_k \neq 0$ for some $k \geq 1$ leads for two branches with $n(n+j) < 0$ to a complex unfolding of the diabolical point. The strength of this complex directed unfolding becomes weaker when the homogeneous offset perturbation is switched on ($a_0 \neq 0$). There exists a critical offset

$$a_{0(c)}^2 := -\frac{4n(n+j)}{j^2}Q_j^2 \tag{9.76}$$

which separates the regions of real-valued and complex-valued unfoldings[5] (in the present first-order approximation).

For $a_0^2 < a_{0(c)}^2 \cap n(n+j) < 0$ a complex-valued unfolding occurs, whereas for $a_0^2 > a_{0(c)}^2 \cap n(n+j) < 0$ the diabolical point unfolds real-valued. The special case of a critical (balanced) perturbation $a_0^2 = a_{0(c)}^2 \cap n(n+j) < 0$ corresponds to an eigenvalue degeneration $\lambda_{1,+} = \lambda_{1,-} =: \lambda_{1(c)}$ which, because of equations (9.53) and (9.63) and $c_{1,+}/c_{2,+} = c_{1,-}/c_{2,-}$, has coinciding zeroth order rays so that via appropriate normalization the corresponding vectors $\mathbf{v}_{0,+}^{\nu}$ and $\mathbf{v}_{0,-}^{\nu}$ can be made coinciding $\mathbf{v}_{0,+}^{\nu} = \mathbf{v}_{0,-}^{\nu} =: \mathbf{v}_{0(c)}^{\nu}$. This means that the original diabolical point splits into a pair of exceptional (branch) points at perturbation configurations $a_0 = \pm|a_{0(c)}|$ with a Jordan (Keldysh) chain consisting of the single (geometric) eigenvector (ray) $\mathbf{v}_{0(c)}^{\nu}$

[5] We note that for intersecting spectral branches it necessarily holds that $j \neq 0$ so that the offset term $a_0\delta_{j,0}$ in Q_j cancels and the definition (9.76) of the critical offset $a_{0(c)}^2$ is justified.

supplemented by an associated vector (algebraic eigenvector). This is in agreement with the unfolding scenario of diabolical points of general-type complex matrices described in [270].

Finally, the special case of $j = -2n$ is of interest. It corresponds to the intersection points located on the $(\alpha_0 = 0)$-axis of the $(\alpha_0, \mathrm{Re}\lambda)$-plane, where the operator matrix is not only self-adjoint in the Krein space $\mathcal{K}$, but also in the Hilbert space $\tilde{\mathcal{H}}$. Due to the vanishing factor $2n + j$, these diabolical points unfold via perturbations with $\lambda_1 = \pm(\pi/2)|n|\sqrt{a_0^2 - a_{|n|}^2}$.

9.3.3 $l = 0$: Fourier components of $\alpha(x)$ determine the unfolding pattern of the spectral mesh.

Let us now consider the strength of the unfolding contributions induced by certain Fourier components. For this purpose, we remember that the diabolical points at nodes $(n, n + j)$ with the same absolute value of the index j are located on a parabolic curve

$$\lambda_0^{\nu} = \frac{1}{4}(\alpha_0^{\nu 2} - \pi^2 j^2) = \frac{\pi^2}{4}(M^2 - j^2). \tag{9.77}$$

Due to its special role, we will refer to $j \in \mathbb{Z}$ as parabola index ($M \in \mathbb{Z}$ is the index of the vertical line in the $(\alpha_0, \mathrm{Re}\lambda)$-plane defined in equations (9.62) and (9.67)). The explicit structure of Q_j following from equation (9.73)

$$Q_j = \begin{cases} \frac{8}{\pi}\sum_{k=1}^{\infty} b_k \frac{k}{4k^2 - j^2}, & j = \pm 1, \pm 3, \ldots \\ a_k(\delta_{j,2k} + \delta_{-j,2k}), & j = \pm 2, \pm 4, \ldots \end{cases} \tag{9.78}$$

shows that cosine and sine components of a similar order $|a_k| \sim |b_k|$ contribute differently at different nodes of the spectral mesh. It is remarkable that for all DPs with the same *even* $|j|$ (parabolas consisting of black points in Figure 9.5 (a)), the splitting of the corresponding double eigenvalues depends (modulo the pre-factors $4n(n + j)$, j^2) only on the mean value a_0 of the perturbation $\Delta\alpha(x)$ and its $|j/2|$-th cosine component $a_{|j/2|}$. For $n(n + j) < 0$ these contributions are competing, whereas for a strictly real-valued unfolding $n(n + j) > 0$ they enhance each other, see Figure 9.5 (b). Furthermore, we find from $M := 2n + j$ that the even/odd mode properties of j imply the same properties for M: even (odd) modes affect the unfolding of diabolical points at even (odd) M only. This is also clearly visible in Figure 9.5 (a).

In the more complicated case of *odd* parabola indices $|j|$ the splitting of the diabolical points on the parabola (9.77) (in Figure 9.5 (a) they are marked as points of the same shape) is governed by the competition between a_0 and the complete set of sine components b_k of the perturbation $\Delta\alpha(x)$. According to equation (9.78), a dominant role is played by sine harmonics with $j^2 \approx 4k^2$, i.e. with $k_{\pm} = (|j| \pm 1)/2$, such that a clear resonance pattern occurs, see Figure 9.5 (c). Sine components with

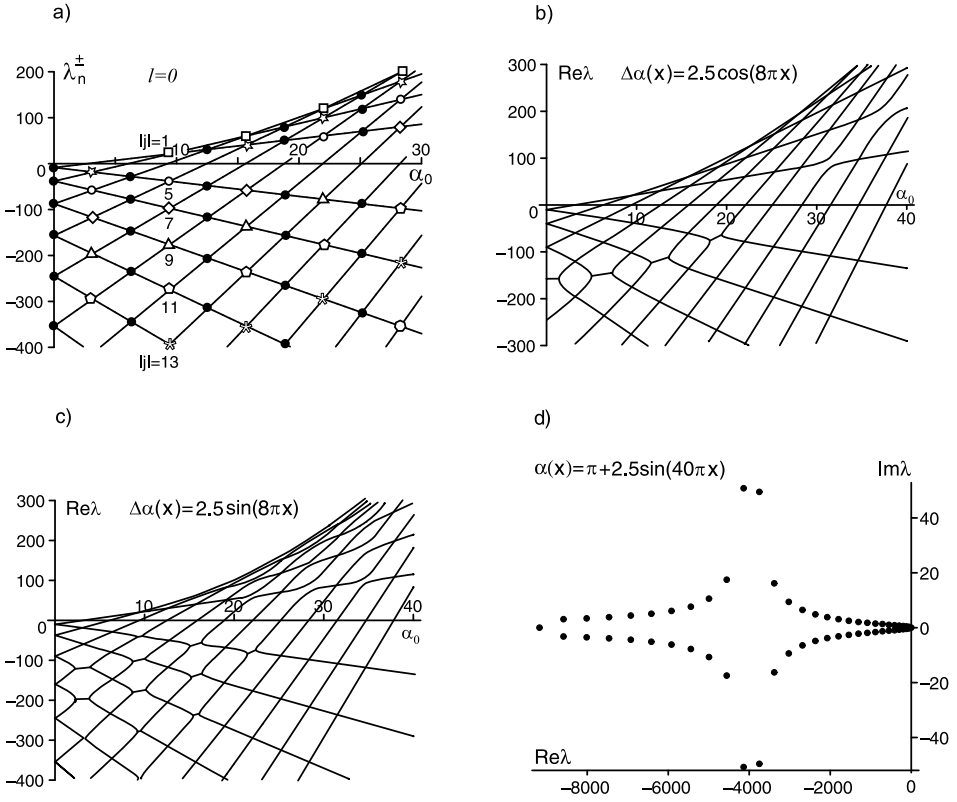

Figure 9.5. (a) Odd harmonics of $\alpha(x)$ define the unfolding properties only of the white diabolical points (equally shaped DPs correspond to the same value of $|j|$), whereas even harmonics affect only the black DPs. Selective deformation of the spectral mesh with resonant unfolding of diabolical points due to perturbation by pure harmonics for $\gamma = 5/2$ and (b) $\Delta\alpha(x) = \cos(8\pi x)$, (c) $\Delta\alpha(x) = \sin(8\pi x)$. (d) The resonant unfolding under $\alpha(x) = \pi + 2.5\sin(40\pi x)$ in the complex plane [208, 306].

$j^2 \approx 4k^2$ are highly enhanced by a small denominator over the other sine components and the corresponding harmonics can be regarded as resonant ones. In contrast, sine contributions with modes away from the resonant $k_\pm = (|j| \pm 1)/2$ are strongly inhibited by the denominator $4k^2 - j^2$ and tend asymptotically to zero for $j^2 \to \infty$, as Figure 9.5 (d) illustrates.

A first-order approximation based insight into this asymptotical behavior can be gained from the positions of the exceptional points (EPs) in the $(\alpha_0, \mathrm{Re}\lambda)$-plane (the points where real-to-complex transitions occur). For this purpose, we use a 1D-lattice type parameterization for α_0 in form of $\alpha_0 = \alpha_0^\nu + \Delta\alpha_0 = \pi M + \Delta\alpha_0$, $M \in \mathbb{Z}$, and switch to a setting with $\gamma = 1$. Interpreting $\Delta\alpha_0$ as perturbation of a configuration with $\alpha_0^\nu = \pi M$ allows us to relate $\Delta\alpha_0$ to the Fourier coefficient $a_0 = 2\Delta\alpha_0$ and to estimate

the α_0-positions of the EPs $\Delta\alpha_e(M, j)$ relative to their corresponding diabolical points located on the line $\alpha_0^v = \pi M$. Via equation (9.76) and $n = (M - j)/2$ we get for given Q_j

$$[\Delta\alpha_e(M, j)]^2 = -\frac{n(n + j)}{j^2} Q_j^2 = \frac{1}{4}\left(1 - \frac{M^2}{j^2}\right) Q_j^2. \tag{9.79}$$

For diabolical points in the lower $(\alpha_0, \mathrm{Re}\lambda)$-half-plane, it holds that $|j| \geq |M| + 2$ and expression (9.79) is well-defined. In the case of cosine perturbations $a_k \cos(2\pi k x)$, equation (9.78) implies that only a single diabolical point per $M = 0, \pm 2, \pm 4, \ldots$ unfolds, Figure 9.5 (b), whereas for sine perturbations $b_k \sin(2\pi k x)$ it leads to a countably infinite number of unfolding diabolical points per $M = \pm 1, \pm 3, \pm 5, \ldots$, see Figure 9.5 (c, d).

Substituting equation (9.78) into equation (9.79) one obtains the $M^2, k^2 \ll j^2 \to \infty$ asymptotics of the EP positions as

$$|\Delta\alpha_e(M, j)| \approx \frac{4|b_k|k}{\pi j^2}, \tag{9.80}$$

i.e. for increasing j^2 the distance of the EPs from the DPs tends to zero, see Figure 9.5 (c). Conversely, equation (9.80) may be used to give an estimate for the number of complex eigenvalues for a given $\alpha_0 = \pi M + \Delta\alpha_0$ close to a diabolical point line at $\alpha_0 \approx \pi M$, $|\Delta\alpha_0| \ll \pi : |j| \approx 2[k|b_k|/(\pi|\Delta\alpha_0|)]^{1/2}$, see Figure 9.5 (d).

We arrive at the conclusion that both types of $|j|$-nodes (even ones and odd ones) show a similar collective behavior along the parabolic curves (9.77) of fixed j^2, responding on some specific α-perturbation harmonics in a resonant way. Hence, a specific α-resonance pattern is imprinted in the spectral unfolding picture of the diabolical points.[6]

For example, we find for *cosine* perturbations (depicted in Figure 9.5 (b)) that the harmonic $k = 4$ induces a visible unfolding effect only for diabolical points located strictly on the associated parabola with index $j = 2k$. This corresponds to the prediction of first-order perturbation theory. However, when the amplitude of the perturbation, γ, is big enough, the unfolding of other DPs becomes visible too, see Figure 9.6 (a), which is not caught by the first-order perturbation formulas.

The effect of *sine* perturbations with mode numbers $k = 4, 20$ is shown in Figure 9.5 (c, d). As predicted by the resonant condition (9.78), we find a strongly pronounced unfolding of diabolical points located on the parabolas with $|j| = 2k \pm 1$, that is for $|j| = 7$ and $|j| = 9$ (Figure 9.5 (c)) and for $|j| = 39$ and $|j| = 41$ (Figure 9.5 (d)). The DPs with $|j| = 2k \pm m, m > 1$ are less affected and the strength of the unfolding quickly decreases with increasing distance m to the resonant parabolas in good coincidence with the analytically predicted α-resonance pattern and in accordance with the estimate (9.79) and (9.80).

[6] Similar resonant unfolding demonstrates the spectral mesh of a rotating circular string on a partial elastic foundation when the stiffness distribution of the foundation is varied with the angular coordinate, see e.g. [602].

With the increase of the strength of the pure harmonic perturbations, the regions with complex-conjugate spectral contributions grow and shift into the upper $(\alpha_0, \mathrm{Re}\lambda)$-plane leading to overcritical oscillatory dynamo regimes ($\mathrm{Re}\lambda > 0, \mathrm{Im}\lambda \neq 0$). An estimate of critical α-profiles, for which such a transition to the upper $(\alpha_0, \mathrm{Re}\lambda)$-half-plane starts to occur, can be given within a first-order (linear) perturbative approximation by assuming $\mathrm{Re}\lambda(\alpha_0) = 0$ for the exceptional point closest to the $(\mathrm{Re}\lambda = 0)$-line. Relations (9.77) and (9.79) and $\mathrm{Re}\lambda = \lambda_0^{\nu} + \mathrm{Re}\lambda_1 = \lambda_0^{\nu} + \pi M a_0/4$ yield this condition in terms of the Fourier components (Q_j) of such a critical α-profile as

$$\mathrm{Re}\lambda = \frac{\pi^2}{4}(M^2 - j^2) + \frac{\pi}{4} M \left(1 - \frac{M^2}{j^2}\right)^{1/2} |Q_j| = 0. \tag{9.81}$$

This relation may be used for testing α-profiles on their capability to produce complex eigenvalues in the right spectral half-plane ($\mathrm{Re}\lambda > 0, \mathrm{Im}\lambda \neq 0$).

Explicit analytical considerations of the spectrum in the $(l > 0)$-sector are obstructed by the lack of simple transformation rules between Riccati–Bessel functions. Nevertheless, the strong similarity between the spectral behavior of the s-wave sector and the $(l > 0)$-sector suggests to use $(l = 0)$-mode models as analytic testing ground for a deeper understanding of structural subtleties of dynamo models – in a similar way as the spherically symmetric α^2-dynamo is a mathematical idealization compared to more realistic setups [208].

9.4 Insulating boundary conditions induce unstable oscillations

We have established that since in the case of conducting boundary conditions ($\beta = 0$) the operator $\mathbf{L}_0$ is self-adjoint in a Krein space both for the uniform and nonuniform α-profiles, the perturbation $\alpha(x) = \alpha_0 + \gamma\Delta\alpha(x)$ induces complex unfolding only of negative real double eigenvalues at the diabolical points of the spectral mesh. Such oscillatory modes are decaying, if γ is not large, see Figure 9.5 and Figure 9.6 (a). In order to break this restriction imposed by the Krein space structure of the boundary eigenvalue problem (9.11) with the Dirichlet boundary conditions and to force the complex splitting of the growing repeated modes, we need to depart from these boundary conditions by assuming that $\beta \neq 0$.

Figure 9.6 (a) shows in the (α_0, γ)-plane the zones of the oscillating solutions of the dynamo problem (9.11) found numerically for $\beta = 0$ and $\Delta\alpha(x) = \cos(2\pi k x)$. We see the regular structure of the tongue-shaped regions shown in dark gray that stem from the points on the α_0-axis with the coordinates $\alpha_0 = \pm 2\pi s$, $s = 0, 1, \ldots$. At small γ the tongues are associated with the decaying oscillations of the magnetic field. The tongues with the index $s = 0, 1, \ldots, k-1$ are angle-shaped and thus should be well described by the linear approximation following from the first-order perturbation formulas (9.69). The tongues with $s \geq k$ are degenerate and require taking into account

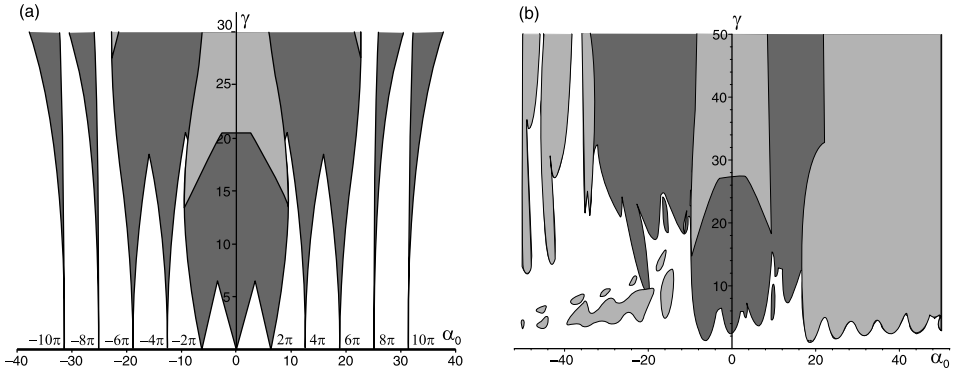

Figure 9.6. $l = 0$, $\alpha(x) = \alpha_0 + \gamma\cos(4\pi x)$: (a) Numerically calculated tongue-shaped regions in (α_0, γ)-plane corresponding to the decaying (dark gray) and growing (light gray) oscillations of the magnetic field for (a) $\beta = 0$ and (b) $\beta = 0.2$ [210].

higher-order perturbation terms describing splitting of the negative double eigenvalues at the nodes of the spectral mesh.

Numerical calculations with $\beta \neq 0$ evidence that the dark gray tongues lose their sharpness and depart from the α_0-axis, Figure 9.6 (b). Surprisingly, in addition a large domain of growing oscillatory solutions (shown in light gray in Figure 9.6 (b)) originates without any evident connection to the case $\beta = 0$. However, a look at the numerically found deformation pattern of eigencurves shown in Figure 9.7 under variation of the constant α-profile into an inhomogeneous one, $\alpha(x) = \alpha_0 + \gamma\Delta\alpha(x)$, with simultaneous variation of the boundary conditions demonstrates that the process of creation of the eigenvalue branches with $\mathrm{Re}\lambda > 0, \mathrm{Im}\lambda \neq 0$ (important for the magnetic field reversal mechanism [547]) is governed by a strong resonant correlation between the Fourier mode number of the inhomogeneous $\Delta\alpha(x)$ and the index (j) of the parabola (9.77).

Indeed, in Figure 9.7 the perturbation of the α-profile $\Delta\alpha(x) = \cos(2\pi k x)$ highly selectively induces complex eigenvalue segments in the vicinity of DPs (dark and light gray circles) located on the parabola (9.35) with index $j = 2k$. We see that in contrast to the case $\beta = 0$, simultaneous variation of the α-profile and the boundary parameter β produces the bubbles of instability not only from the crossings with mixed Krein signature (dark gray circles) but also from those with definite Krein signature (light gray circles).

The underlying influence of 'hidden' DPs on real-to-complex transitions of the spectral branches can be made transparent by analyzing the unfolding of the DPs [277,298] at the mesh-nodes $(\alpha_0^\nu, \lambda_0^\nu)$ under variation of the parameters α_0, β, and γ, with the use of the perturbation theory in Chapter 7.

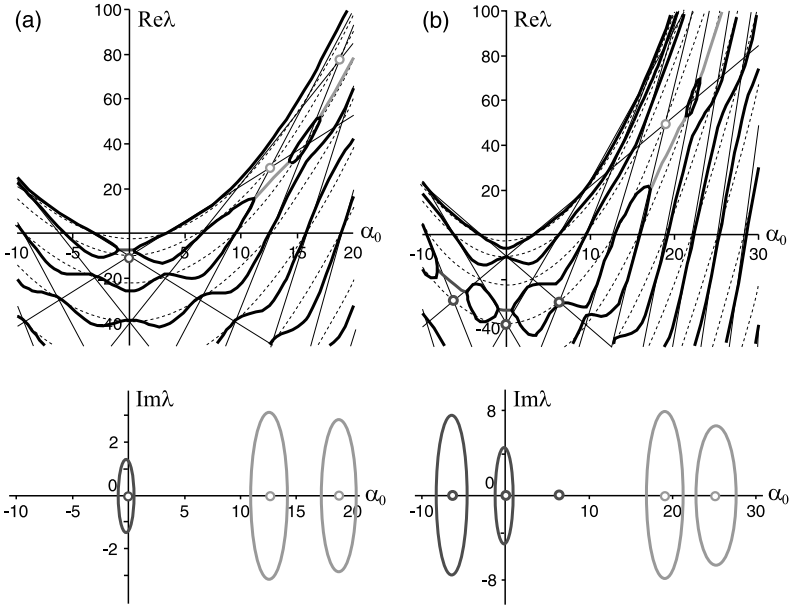

Figure 9.7. $l = 0$: (thin lines) spectral mesh (9.32) for $\gamma = 0$, $\beta = 0$; (dashed) eigenvalue parabolas (9.35) for $\gamma = 0$, $\beta = 1$; (bold black) eigenvalue branches for $\beta = 0.3$, $\Delta\alpha(x) = \cos(2\pi k x)$, and (a) $k = 1$, $\gamma = 2.5$, (b) $k = 2$, $\gamma = 3$, with resonant overlaps near the locations of the diabolically crossed modes having (light gray) definite and (dark gray) mixed Krein signature [307].

9.4.1 $l = 0$: complex unfolding of double eigenvalues with definite Krein signature

Taking into account that the components of the eigenfunction $\mathbf{u}^T = (u_1, u_2)$ of the eigenvalue problem (9.11) and $\mathbf{v}^T = (v_1, v_2)$ of its adjoint are related as $\bar{v}_2 = u_1$ and $\bar{v}_1 = u_2$, where the overbar denotes complex conjugation, we find from equations (7.30) and (7.31) the asymptotic formula for the perturbed eigenvalues, originating after the splitting of the double semisimple eigenvalues at the node $(\alpha_0^\nu, \lambda_0^\nu)$ of the spectral mesh, by deforming the constant α-profile into an inhomogeneous one, $\alpha(x) = \alpha_0 + \Delta\alpha_0 + \gamma\Delta\alpha(x)$, $\int_0^1 \Delta\alpha(x) = 0$, with simultaneous variation of the parameter β in boundary conditions. For the $(l = 0)$-model this formula reads [298,307]

$$\lambda = \lambda_0^\nu - \lambda_0^\nu\beta + \frac{\alpha_0^\nu}{2}\Delta\alpha_0 \pm \frac{\pi}{2}\sqrt{D}, \tag{9.82}$$

where $\Delta\alpha_0 := \alpha_0 - \alpha_0^\nu$, $\alpha_0^\nu = \pi(\varepsilon n + \delta m)$, $\lambda_0^\nu = \varepsilon\delta\pi^2 mn$,

$$\begin{aligned} D := {} & ((\varepsilon n - \delta m)\Delta\alpha_0)^2 + mn\left((\varepsilon 1 + \delta 1)\gamma A - (-1)^{n+m}(n+m)\beta\pi\right)^2 \\ & - mn\left((\varepsilon 1 - \delta 1)\gamma A - (-1)^{n-m}(n-m)\beta\pi\right)^2, \end{aligned} \tag{9.83}$$

and $A := \int_0^1 \Delta\alpha(x)\cos((\varepsilon n - \delta m)\pi x)dx$.

For $\gamma = 0$ it holds that $D \geq 0$, confirming that the eigenvalues remain real under variation of the parameters α_0 and β only. If, additionally, $\alpha_0 = \alpha_0^\nu$, then one of the two simple eigenvalues (9.82) remains fixed under first-order perturbations with respect to β: $\lambda = \lambda_0^\nu$ in full accordance with the fixed point nature of the DP loci under the β-homotopy shown in Figure 9.2 (b). The sign of the first-order increment of the other eigenvalue $\lambda = \lambda_0^\nu - 2\lambda_0^\nu\beta$ depends on the sign of λ_0^ν and, therefore, directly on the Krein signature of the modes involved in the crossing $(\alpha_0^\nu, \lambda_0^\nu)$. This is in full agreement with the numerically computed roots of the characteristic equation (9.36) for the problem (9.11) with $\alpha(x) = \alpha_0 = const$ and $l = 0$, shown in Figure 9.2 (b). Therefore, to create complex eigenvalues an additional parameter, γ, is necessary.

Equation (9.82) implies that in first-order approximation the domain of oscillatory solutions with $\mathrm{Re}\lambda \neq 0$ and $\mathrm{Im}\lambda \neq 0$ in the $(\alpha_0, \beta, \gamma)$-space is bounded by the conical surfaces $D = 0$ with apexes at the DPs $(\alpha_0^\nu, 0, 0)$, as shown in Figure 9.8 (a). At the boundary $D = 0$ the eigenvalues are twofold degenerate and nonderogatory, that is they have Jordan (Keldysh) chains consisting of an eigenvector and an associated vector. Thus, DPs in the $(\alpha_0, \beta, \gamma)$-space unfold into 3D conical surfaces consisting of exceptional points (EPs).

The inequality $D < 0$ defines the inner part of the cone $D = 0$ in the $(\alpha_0, \beta, \gamma)$-space. The part of the cone corresponding to $\mathrm{Re}\lambda > 0$ (oscillatory dynamo) is selected by the condition $2\lambda_0^\nu(1-\beta) + \alpha_0^\nu\Delta\alpha_0 > 0$. The conical zones develop according to resonance selection rules similar to those given by equation (9.78) for the case $\beta = 0$. For example, if $\Delta\alpha(x) = \cos(2\pi kx)$, $k \in \mathbb{Z}$, then

$$A = \int_0^1 \cos(2\pi kx)\cos((\varepsilon n - \delta m)\pi x)dx = \begin{cases} 1/2, & 2k = \pm(\varepsilon n - \delta m) \\ 0, & 2k \neq \pm(\varepsilon n - \delta m) \end{cases} \quad (9.84)$$

so that in first-order approximation only DPs located on the $(j = 2|k|)$-parabola (9.35) show a DP-EP unfolding (cf. numerical results in Figure 9.7). The cone apexes correspond to $2|k| - 1$ DPs with mixed Krein signature $(\varepsilon\delta = -)$ and countably infinite DPs with definite Krein signature $(\varepsilon\delta = +)$. The two groups are shown in Figure 9.8(b) in dark and light gray, respectively.

The real parts of the perturbed complex eigenvalues are given by $\mathrm{Re}\lambda = \lambda_0^\nu(1-\beta) + \alpha_0^\nu\left(\alpha_0 - \alpha_0^\nu\right)/2$ and for fixed α_0 and increasing β they are shifted (for both groups) away from the original DP positions toward the $(\mathrm{Re}\lambda = 0)$-axis (cf. the numerical results in Figure 9.7) – an effect which is similar to the self-tuning mechanism of field-reversals uncovered in [547].

Apart from this similarity, the eigenvalues of the two cone groups show significant differences. The $2|k| - 1$ cones of the first group have a nontrivial intersection with the plane $\beta = 0$. In this (α_0, γ)-plane the zones of decaying oscillatory modes are $\gamma \rightleftharpoons -\gamma$ symmetric and defined by the inequality [307]

$$(\alpha_0 \pm 2\pi(n - |k|))^2 < \frac{\gamma^2}{4}\left[1 - \left(\frac{n - |k|}{|k|}\right)^2\right], \quad (9.85)$$

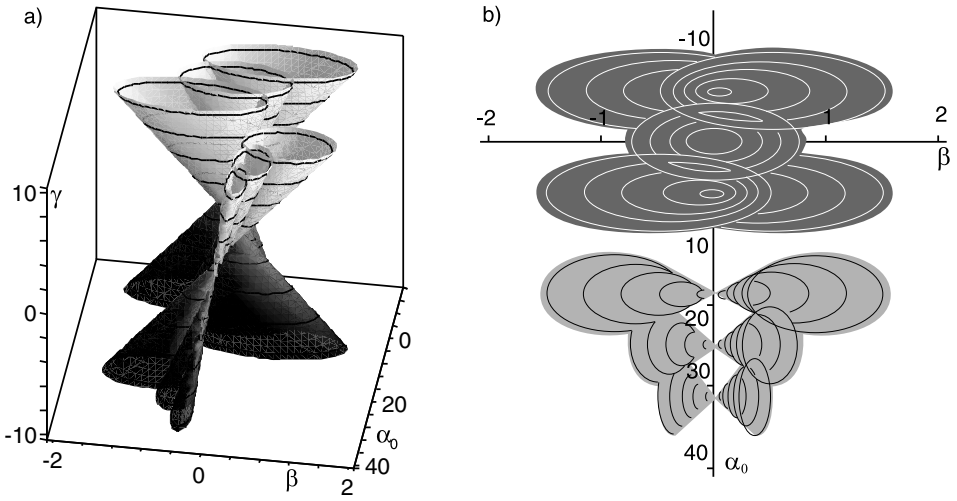

Figure 9.8. $l = 0$, $\Delta\alpha(x) = \cos(4\pi x)$: (a) linear approximation of the 3D zones of oscillatory solutions (9.86) and (9.87) and (b) their projection onto the (α_0, β)-plane indicating the influence of the Krein signature of the double eigenvalues at the apexes on the inclination of the cones [307].

where $n = 1, 2, \ldots, |k|$. For $k = 2$ there are three primary tongues: $4\alpha_0^2 < \gamma^2$ and $16\,(\alpha_0 \pm 2\pi)^2 < 3\gamma^2$, in agreement with the numerically found primary zones shown in Figure 9.6 (a).

The cones of the second group meet the plane $\beta = 0$ only at the apexes, having their skirts located in the sectors $[\beta > 0, \gamma \text{ sign } (\alpha_0) > 0]$ and $[\beta < 0, \gamma \text{ sign } (\alpha_0) < 0]$ (cf. Figure 9.8 (b)). Therefore, in models with $\beta = 0$ complex eigenvalues occur only in zones (9.85) in the (α_0, γ)-plane.

The different oscillatory behavior induced by the two cone groups has its origin in the different Krein-signature defined inclination of the $(D < 0)$-cones with respect to the $(\beta = 0)$-plane.

Passing from $\beta = 0$ to a parallel $(\beta \neq 0)$-plane, the $(D < 0)$-tongues (9.85), corresponding to $\lambda_0^\nu < 0$ deform into cross-sections bounded by hyperbolic curves (black dashed lines in Figure 9.9 (a))

$$-4k^2(\alpha_0 \pm 2\pi(n-|k|))^2 + n(2|k|-n)(\gamma \pm 2\pi(n-|k|)\beta)^2 > n(2|k|-n)4\pi^2\beta^2k^2, \tag{9.86}$$

with $n = 1, 2, \ldots, |k|$. Since $n \leq |k|$, the lines $\gamma = \pm 2\pi n\beta$ and $\gamma = \pm 2\pi(n-2|k|)\beta$, bounding the cross-sections of the 3D cones by the plane $\alpha_0^\nu = \pm 2\pi(n-|k|)$, always have slopes of different sign. This allows decaying oscillatory modes for $\beta = 0$ due to variation of γ only.

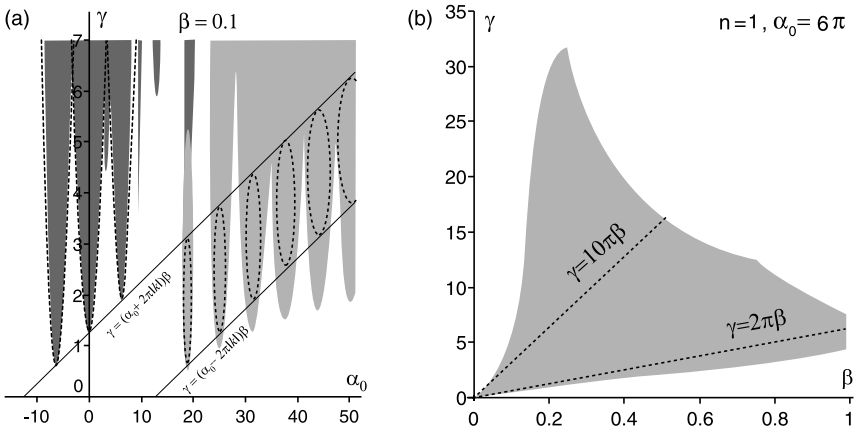

Figure 9.9. $l = 0$: Numerically found tongue-shaped zones of oscillatory solutions for $\Delta\alpha(x) = \cos(2\pi kx)$, $k = 2$, and $\lambda_0^\nu < 0$ (dark gray) or $\lambda_0^\nu > 0$ (light gray) and their approximations (9.86) and (9.87) (dashed lines) (a) in the (α_0, γ)-plane and (b) the (β, γ)-plane [307].

The $(\beta \neq 0)$-cross-sections of the cones with $(\lambda_0^\nu > 0)$-apexes have the form of ellipses (white dashed lines in Figure 9.9 (a))

$$4k^2\left(\alpha_0 \pm 2\pi(n+|k|)\right)^2 + n(2|k|+n)\left(\gamma \pm 2\pi(n+|k|)\beta\right)^2 < n(2|k|+n)4\pi^2\beta^2k^2, \tag{9.87}$$

where $n = 1, 2, \ldots$. In the $(\beta \neq 0)$-plane the ellipses are located inside the stripe with boundaries $\gamma = (\alpha_0 \pm 2\pi|k|)\beta$ (thin lines in Figure 9.9 (a)), while the hyperbolas lie outside this stripe. Moreover, since in the plane $\alpha_0^\nu = \pm 2\pi(n + |k|)$ the boundary lines $\gamma = \pm 2\pi n\beta$ and $\gamma = \pm 2\pi(n + 2|k|)\beta$ have slopes of the same sign, the γ-axis does not belong to the instability domains, showing that for growing oscillatory modes the parameters β and γ have to be taken in a prescribed proportion, see Figure 9.9 (b).

The amplitude γ of the inhomogeneous perturbation of the α-profile $\gamma\Delta\alpha(x)$ is limited both from below and from above in the vicinity of the DPs with the definite Krein signature. However, numerical calculations indicate that this property can persist on the whole interval $\beta \in [0, 1]$, see Figure 9.9 (b), in agreement with the numerical simulations of the earlier work [545].

Therefore, using a homotopic family of boundary eigenvalue problems for the mean field α^2-dynamo with helical turbulence parameter $\alpha(x) = \alpha_0 + \gamma\Delta\alpha(x)$ and homotopy parameter $\beta \in [0, 1]$, we have shown that the underlying network of diabolical points for Dirichlet (idealized, $\beta = 0$) boundary conditions substantially determines the choreography of eigenvalues and thus the character of the dynamo instability for Robin (physically realistic, $\beta = 1$) boundary conditions. In the $(\alpha_0, \beta, \gamma)$-space, the tongue-shaped zones of oscillatory solutions at $\beta = 1$ end up at the diabolical points for $\beta = 0$. In the vicinity of the diabolical points, the space orientation of the 3D

tongues, which are cones in first-order approximation, is determined by the Krein signature of the modes involved in the diabolical crossings at the apexes of the cones. The Krein space induced geometry of the resonance zones explains the subtleties in finding α-profiles leading to spectral exceptional points, which are important ingredients in recent theories of polarity reversals of the geomagnetic field. Although this has been exemplified for the unphysical monopole ($l = 0$) mode of a simplified spherically symmetric α^2-dynamo model, the general idea is well generalizable to physical modes and to more realistic dynamo models.

In the next chapter, we will further explore implications of self-adjointness of governing operators in a Krein space as well as of breaking this fundamental symmetry for stability properties and behavior of eigencurves with the example of nonconservative gyroscopic systems originated in rotor dynamics.

Chapter 10

Campbell diagrams of gyroscopic continua and subcritical friction-induced flutter

The ringing of a wine glass by a wetted finger is due to the fall in [the coefficient of friction] with increasing velocity which occurs at low sliding speeds before full hydrodynamic lubrication sets in.

R. T. Spurr [541]

10.1 Friction-induced vibrations and sound generation

In 1638 Galileo Galilei remarked that "a glass of water may be made to emit a tone merely by the friction of the finger-tip upon the rim of the glass" [184]. In 1761 Benjamin Franklin designed an "armonica", where sound was radiated due to vibration of rotating glass bowls in frictional contact with the moistened fingers of a performer [502]. Shortly after Rayleigh [493] qualitatively described the onset of bending waves in the singing wine glass by friction applied in the circumferential direction and pointed out the proximity of the main audible frequency of the glass to the one of the spectrum of its free vibrations, a disk brake had been invented [268]. Nowadays, the automotive car brake squeal due to vibrations of a rotating annular plate in contact with the friction pads – in general, a sound with one dominant frequency – is one of the primary subjects of investigation in the *acoustics of friction* [6, 268, 433, 463] because its "reliable reproduction or even prediction … is still not possible" [461]. The attempts to design a silent brake are still extensively based on the 'trial-and-error' method [461]. Among other examples of such audible friction-induced oscillations we mention high-frequency self-excitation in paper calenders that yields emission of sound and a wear pattern known as the calender barring [92, 537] and squeaking occurring in ceramic-on-ceramic hip arthroplasty [255].

The author of one of the first theories of brake squeal, Spurr [542], experimentally observed that a rotating wine glass sang when the dynamic friction coefficient was a decreasing function of the velocity [541]. Linearizing the system with the negative friction-velocity gradient produces an eigenvalue problem with an *indefinite* matrix of damping forces. Effectively, negatively damped vibration modes may lead to complex eigenvalues with positive real parts and cause flutter instability [174, 175, 303, 314].

The growth in amplitude will be limited in practice by some nonlinearity. Since the engineering design is often more concerned with if a brake may squeal and less

with how loud the brake may squeal, a complex eigenvalue analysis offers a pragmatic approach used currently by most production work in industry [463].

The fall in the dynamic friction coefficient with increasing velocity is among the main empirical reasons for disk brake squeal, categorized by Kinkaid et al. [268]. One more is nonconservative positional (or circulatory) forces [623], which first appeared in the model by North [454]. The binary flutter in such models happens through the coalescence of two modes according to the reversible Hopf bifurcation scenario [263, 340, 531, 588]. Inclusion of damping leads to the imperfect merging of modes [226, 288,292] and to the flutter through the dissipative Hopf bifurcation, which is connected to the reversible one by means of the Whitney umbrella singularity [81, 312, 354].

The nonconservative positional forces in the models of frictional contact between a rotating disk and the brake pads were frequently interpreted as tangential follower forces [268, 454, 604]. Despite the existing discussion of the very possibility of realization of the pure follower force in practice [167,557,558], its main role is in bringing the nonpotential terms, which can also be of other origin [588], into the equations of motion of brake components. The destabilizing role of circulatory forces in gyroscopic systems, well-known since the works of Bottema [80], Lakhadanov [342], and Karapetyan [257], was emphasized recently by Krechetnikov and Marsden [332, 333], see also [84, 289–291, 539].

Historically, in the studies of brake squeal, the rotational symmetry of the disk as well as the gyroscopic effects were frequently ignored. The latter in the assumption that the low rotor speed range in which squeal tends to occur does not warrant this complication [463]. However, as in the case of a singing wine glass, experiments revealed the proximity of the squealing frequency and mode shape of brake's rotor for low rotational speeds to a natural frequency and corresponding mode shape of a stationary rotor [268,415,433,463]. Since an axially symmetric rotor possesses pairs of identical frequencies, Chan et al. [118] proposed another mechanism of squeal in the classification of Kinkaid et al. [268] based on the splitting of a double eigenfrequency of a symmetric disk when a friction force was applied. The splitting of a repeated eigenvalue of a potential system by circulatory forces could lead to flutter (recall (Merkin) Theorem 5.16), equated to brake squeal.

Rotation also causes double eigenfrequencies to split [96]. The newborn pair of simple eigenvalues corresponds to the forward and backward traveling waves, which propagate along the circumferential direction [96,248,433,523]. Viewed from the stationary frame, the frequency of the forward traveling wave appears to increase and that of the backward traveling wave appears to decrease, as the spin increases [109, 433]. Double eigenvalues thus originate again at nonzero angular velocities, forming nodes of the spectral mesh [208] of the crossed eigencurves in the plane 'eigenfrequency' versus 'angular velocity' known in rotor dynamics since 1924 as the *Campbell diagram* [109]. Spectral meshes are characteristic for many rotating symmetric continua of solid mechanics such as circular strings [510, 604], disks [123, 242, 433, 538], rings and cylindrical and hemispherical shells [96, 110, 248, 523]. A similar mesh-like struc-

ture of eigencurves can be encountered within studies of vortex rings and tubes [180] and, as we have seen in Chapter 9, in some models of the MHD dynamo[1] [208].

The lowest angular velocity at which the frequency of a backward traveling wave vanishes to zero, so that the wave remains stationary in the nonrotating frame, is called *critical* [242,433]. When the speed of rotation exceeds the critical speed, the backward wave travels slower than the disk rotation speed and in the stationary frame appears to be traveling forward (reflected wave [242, 433, 552]). The effective energy of the reflected wave is negative and that of the forward and backward traveling waves is positive [390, 392, 552]. Therefore, in the *subcritical* speed region all the crossings of the eigencurves correspond to the forward and backward modes of the same Krein signature, while in the *supercritical* speed region there exist crossings that are formed by the modes of opposite Krein signature. According to MacKay's theory [390], exploiting the properties of operators that are self-adjoint in a Krein space, the crossings in the subcritical region veer away into avoided crossings (marginal stability) under Hamiltonian perturbations like mass and stiffness constraints [242]. In contrast, in the supercritical region the crossings of the modes of opposite signature turn into the rings of complex eigenvalues – bubbles of instability [390] – leading to flutter and divergence known also as the 'mass and stiffness instabilities' [242].

A *supercritical flutter* frequently occurs in high speed applications like turbines, circular saws, and computer storage devices, while the *subcritical flutter* – either desirable as a source of instability at low speeds as in the case of musical instruments like the singing wine glass and a glass harmonica, or undesirable as in the case of the squealing disk and drum brakes – is an elusive phenomenon. Being prohibited by the limitations imposed on the eigenvalue movement by the Krein space (symplectic) structure, characteristic of Hamiltonian systems, subcritical flutter can occur, however, due to non-Hamiltonian perturbations [123, 456]. Subcritical flutter was detected by numerical approaches in modern models of disk brakes that incorporate gyroscopic and centripetal effects and accommodate more than one squeal mechanism through splitting the doublet modes of a disk by dissipative and circulatory perturbations coming from the negative friction-velocity gradient and frictional follower load. The models include both the case when the pointwise or distributed friction pads are rotated around a stationary disk, affecting a point or a sector of it, and when the disk rotates past the stationary friction pads, see [118,268,293,294,463,538], and references therein.

In the following, using perturbation theory of multiple eigenvalues of non-self-adjoint operators from Chapter 7, we show that even if the eigencurves in the subcritical region are well separated at the avoided crossings, created by the stiffness

[1] Note that in the case of an MHD α^2-dynamo with constant α-profile we have a spectral mesh of *growth rates* because the eigenvalues of a heavily damped system are pure real [34, 100]. In contrast, in the discussed case of conservative gyroscopic systems with rotational symmetry, the pure imaginary eigenvalues originate a spectral mesh of *eigenfrequencies*.

variation, they can be forced to bend into arches of complex eigenvalues with positive real parts by indefinite damping and circulatory forces.

Instead of deriving particular operators of dissipative and circulatory forces by accurate modeling the frictional contact and then studying their effect on the spectrum and stability as was done, e.g. in [538, 539], we solve an inverse problem. Assuming *a priori* only the existence of distinct squeal frequencies close to the double eigenfrequencies of the Campbell diagram of a gyroscopic continuum, we find the structure of the dissipative and circulatory operators that cause flutter in the subcritical region near the nodes of the spectral mesh. We describe analytically the movement of eigenvalues and the deformation of the spectral mesh. Using this data, we find explicit analytic approximations to the domain of subcritical flutter in the space of a system's parameters.

Finally, we reveal that unfolding the Campbell diagrams is determined by a limited number of local scenarios for eigenvalues as a function of parameters, which form stratified manifolds with the shape determined by the Krein signature of eigenvalues of the unperturbed system [293,294]. This result generalizes the theory of MacKay [390] to the case of dissipative and circulatory perturbations of a gyroscopic system in the semisimple $1:1$ resonance.

10.2 Example. Subcritical flutter of a rotating circular string

We start with a nonconservative version of the problem of stability of a rotating string that was discussed in Section 7.3.

Recall that a circular string of displacement $W(\varphi, \tau)$, radius r, and mass per unit length ρ, rotates with the speed γ and passes at $\varphi = 0$ through a massless eyelet generating now a constant frictional follower force F on the string, as shown in Figure 10.1 (a). The circumferential tension P in the string is assumed to be constant; the stiffness of the spring supporting the eyelet is K and the damping coefficient of the viscous damper is D; the velocity of the string in the φ-direction has constant value γr [604].

This somewhat artificial system contains, however, the fundamental physics of interest, i.e. the interaction of rotating flexible medium with a stationary constraint in which the inertial, gyroscopic, and centripetal acceleration effects, together with the stiffness effects of the medium, are in dynamic equilibrium with the (in general, nonconservative) forces generated by the constraint. Moreover, we note that in the modeling of the friction-induced instabilities in brakes various simplified models are widely used, e.g. Heilig and Wauer approximated the rotating brake disk by a rotating *ring* [217].

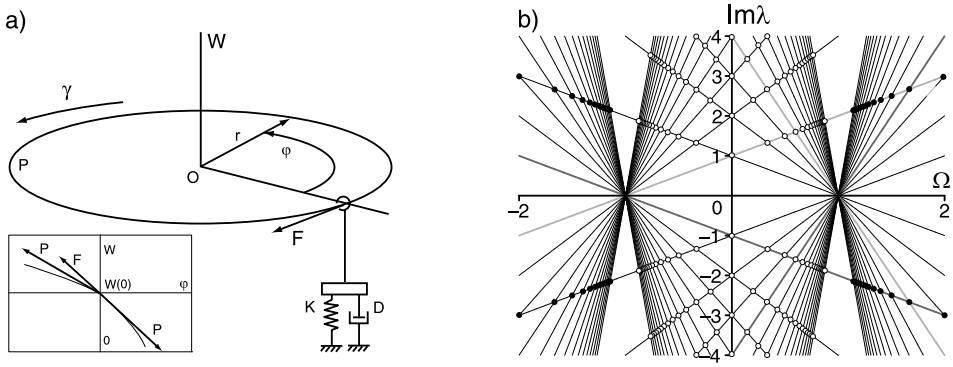

Figure 10.1. A rotating circular string and its Campbell diagram constituted by eigencurves intersecting at the marked by white and black nodes of the spectral mesh. The critical speed is $|\Omega| = 1$. Eigencurves corresponding to eigenvalues of positive (light gray) and negative (dark gray) Krein signature intersect in supercritical speed range $|\Omega| > 1$. At $|\Omega| < 1$ the double eigenvalues at the crossings have definite Krein signature [298].

With the nondimensional variables and parameters

$$t = \frac{\tau}{r}\sqrt{\frac{P}{\rho}}, \quad w = \frac{W}{r}, \quad \Omega = \gamma r\sqrt{\frac{\rho}{P}}, \quad k = \frac{Kr}{P}, \quad \mu = \frac{F}{P}, \quad d = \frac{D}{\sqrt{\rho P}} \tag{10.1}$$

the substitution of $w(\varphi, t) = u(\varphi)\exp(\lambda t)$ into the governing equation and boundary conditions yields the boundary eigenvalue problem [604]

$$Lu = \lambda^2 u + 2\Omega\lambda u' - (1-\Omega^2)u'' = 0, \tag{10.2}$$

$$u(0) - u(2\pi) = 0, \quad u'(0) - u'(2\pi) = \frac{\lambda d + k}{1-\Omega^2}u(0) + \frac{\mu}{1-\Omega^2}u'(0), \tag{10.3}$$

where $' = \partial_\varphi$. The nonself-adjoint boundary eigenvalue problem (10.2) and (10.3) depends on the speed of rotation (Ω) and damping (d), stiffness (k), and friction (μ) coefficients of the constraint.

With the use of the Galerkin method, the boundary eigenvalue problem (10.2) and (10.3) can be approximated by the $2N+1$-dimensional system of ordinary differential equations [604], that has the following form

$$(\mathbf{I}\lambda^2 + (2\Omega\mathbf{G} + \delta\mathbf{D})\lambda + \mathbf{P} + \Omega^2\mathbf{G}^2 + \kappa\mathbf{K} + \nu\mathbf{N})\mathbf{u} = 0, \tag{10.4}$$

where $\mathbf{I}$ is the identity, $\mathbf{u} \in \mathbb{C}^{2N+1}$ and $\delta = d/\pi$, $\kappa = k/\pi$, and $\nu = \mu/\pi$. The damping matrix $\mathbf{D} = \mathbf{K}$, where a real $(2N+1) \times (2N+1)$ stiffness matrix $\mathbf{K}$ is

$$\mathbf{K} = \begin{pmatrix} \frac{1}{2} & \frac{\sqrt{2}}{2} & 0 & \cdots & \frac{\sqrt{2}}{2} & 0 \\ \frac{\sqrt{2}}{2} & 1 & 0 & \cdots & 1 & 0 \\ 0 & 0 & 0 & \cdots & 0 & 0 \\ \vdots & \vdots & \vdots & \ddots & \vdots & \vdots \\ \frac{\sqrt{2}}{2} & 1 & 0 & \cdots & 1 & 0 \\ 0 & 0 & 0 & \cdots & 0 & 0 \end{pmatrix}, \tag{10.5}$$

the matrix of potential forces $\mathbf{P} = \operatorname{diag}(0, 1, 1, 4, 4, \ldots, N^2, N^2)$, and real matrices of nonconservative positional and gyroscopic forces, $\mathbf{N}$ and $\mathbf{G}$, are

$$\mathbf{N} = \begin{pmatrix} 0 & 0 & \frac{\sqrt{2}}{2} & \cdots & 0 & N\frac{\sqrt{2}}{2} \\ 0 & 0 & 1 & \cdots & 0 & N \\ 0 & 0 & 0 & \cdots & 0 & 0 \\ \vdots & \vdots & \vdots & \ddots & \vdots & \vdots \\ 0 & 0 & 1 & \cdots & 0 & N \\ 0 & 0 & 0 & \cdots & 0 & 0 \end{pmatrix}, \quad \mathbf{G} = \begin{pmatrix} 0 & 0 & 0 & \cdots & 0 & 0 \\ 0 & 0 & 1 & \cdots & 0 & 0 \\ 0 & -1 & 0 & \cdots & 0 & 0 \\ \vdots & \vdots & \vdots & \ddots & \vdots & \vdots \\ 0 & 0 & 0 & \cdots & 0 & N \\ 0 & 0 & 0 & \cdots & -N & 0 \end{pmatrix}. \tag{10.6}$$

Both the discrete and continuous eigenvalue problem give the same eigencurves of the unconstrained string ($k = 0, d = 0, \mu = 0$) as a set of straight lines (7.78) intersecting each other at the points (7.79). The only eigencurve that does not have crossing points is that of zero eigenvalue (it has zero slope).

The spectral mesh (7.78) in the plane $(\Omega, \operatorname{Im}\lambda)$ is shown in Figure 10.1 (b). Intersections (7.79), corresponding to the forward and backward traveling waves, occur in the subcritical region ($|\Omega| < 1$) and are marked in Figure 10.1 (b) by white dots. The black dots indicate the intersections of the forward and reflected waves taking place in the supercritical region ($|\Omega| > 1$).

Perturbing the string by an additional stiffness constraint ($k \neq 0$) when damping and circulatory forces are vanishing yields avoided crossings (marginal stability) in the subcritical speed range, see Figure 7.2 and Figure 7.3 (a). What is the effect of dissipation or friction on the spectral mesh and stability? Figure 10.2 based on the Galerkin approximation (10.4) with $N = 2$ gives an idea.

It is not surprising that at $|\Omega| < 1$ damping shifts pure imaginary eigenvalues to the left in the complex plane.[2] Quite unexpectedly, the stabilizing effect is not uniform with regard to Ω! In fact, it is inhibited near the locations of the crossings of the spectral mesh, where growth rate plots have an elliptical or bell-like shape, Figure 10.2 (a). These bubbles or peaks of complex eigenvalues submerged under the line $\operatorname{Re}\lambda = 0$ look like latent sources of instability waiting until other forces activate them.

[2] In view of the result that full dissipation shifts simple eigenvalues of a Hamiltonian system corresponding to the modes with positive energy to the left in the complex plane [74, 90, 127, 391].

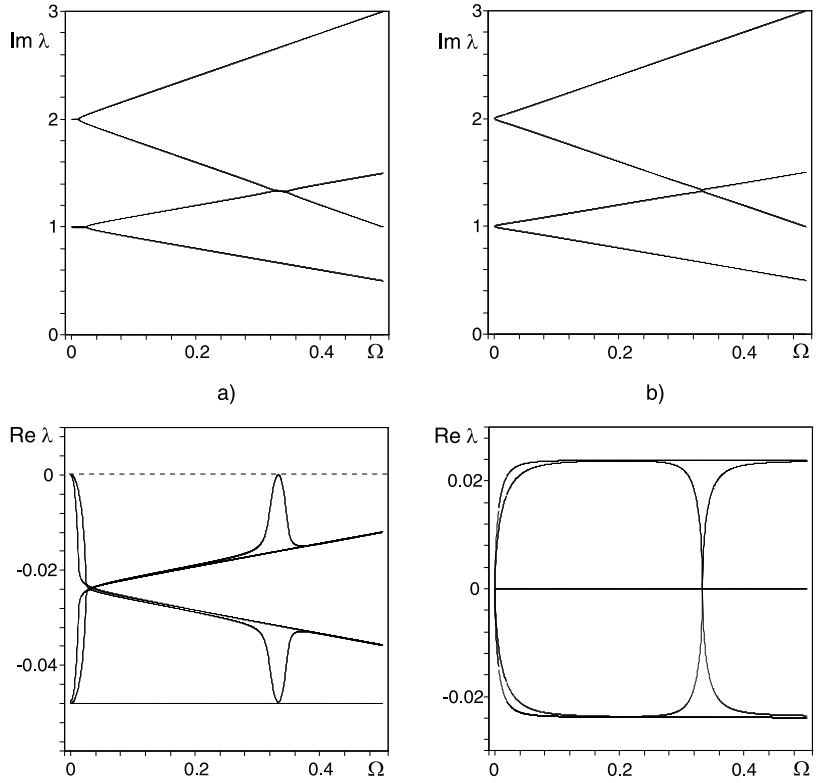

Figure 10.2. Frequencies and growth rates of eigenvalues according to $N = 2$ - Galerkin approximation (10.4) of the boundary eigenvalue problem (10.2) and (10.3) (a) when $k = 0$, $d = 0.3$, and $\mu = 0$; (b) when $k = 0$, $d = 0$, and $\mu = 0.3$.

Circulatory forces due to friction in the eyelet ($\mu \neq 0$) act in accordance with the Bottema–Lakhadanov–Karapetyan theorem [80, 257, 342], by destabilizing the string at almost all Ω, Figure 10.2 (b). By this theorem (see Theorem 5.19), it is sufficient for the undamped system corresponding to the eigenvalue problem (10.4) to be unstable that $\mathrm{tr}(\Omega\nu\mathbf{G}(\mathbf{N} - \mathbf{N}^T)) \neq 0$. Since

$$\mathrm{tr}(\Omega\nu\mathbf{G}(\mathbf{N} - \mathbf{N}^T)) = -\frac{2\Omega\mu}{\pi}\sum_{s=1}^{N} s^2,$$

at $\mu \neq 0$ the system can be stable only when $\Omega = 0$, in full agreement with Figure 10.2 (b). Again, the effect of friction is nonuniform with respect to Ω. It vanishes for all modes at $\Omega = 0$ and for some modes at the locations of the crossings of the spectral mesh at $\Omega \neq 0$, Figure 10.2 (b).

Could the results of the low-order Galerkin numerical predictions be believed? The resonant reaction of the growth rates of the modes to the proximity to the loci of the

diabolical points of the spectral mesh suggests perturbative treating of the unfolding of the double eigenvalues at the 1 : 1 semisimple resonance.

Applying the perturbation theory of Chapter 7 to the boundary eigenvalue problem (10.2) and (10.3), we find an asymptotic formula for the eigenvalues originated after the splitting of the double semisimple eigenvalue $\lambda_{nm}^{\varepsilon\sigma}$ at the crossing (7.79) of two eigencurves (7.78) due to interaction of the rotating string with the external loading system [293, 294]:

$$\lambda = \lambda_{nm}^{\varepsilon\sigma} - \frac{f_{nn}^{\varepsilon\varepsilon} + f_{mm}^{\sigma\sigma}}{2} - \frac{\epsilon_{nn}^{\varepsilon\varepsilon} + \epsilon_{mm}^{\sigma\sigma}}{2} \pm \sqrt{\frac{\left(f_{nn}^{\varepsilon\varepsilon} - f_{mm}^{\sigma\sigma} + \epsilon_{nn}^{\varepsilon\varepsilon} - \epsilon_{mm}^{\sigma\sigma}\right)^2}{4} - (f_{nm}^{\varepsilon\sigma} + \epsilon_{nm}^{\varepsilon\sigma})(f_{mn}^{\sigma\varepsilon} + \epsilon_{mn}^{\sigma\varepsilon})}, \quad (10.7)$$

where $\varepsilon, \sigma = \pm$ and $m, n \in \mathbb{Z} - \{0\}$. The coefficients $f_{nm}^{\varepsilon\sigma}$ are

$$f_{nm}^{\varepsilon\sigma} = \frac{2\lambda_{nm}^{\varepsilon\sigma} \int_0^{2\pi} u_n^{\varepsilon\prime} \bar{u}_m^{\sigma} d\varphi + 2\Omega_{nm}^{\varepsilon\sigma} \int_0^{2\pi} u_n^{\varepsilon\prime\prime} \bar{u}_m^{\sigma} d\varphi}{2\sqrt{\int_0^{2\pi} (\lambda_{nm}^{\varepsilon\sigma} u_n^{\varepsilon} + \Omega_{nm}^{\varepsilon\sigma} u_n^{\varepsilon\prime}) \bar{u}_n^{\varepsilon} d\varphi \int_0^{2\pi} (\lambda_{nm}^{\varepsilon\sigma} u_m^{\sigma} + \Omega_{nm}^{\varepsilon\sigma} u_m^{\sigma\prime}) \bar{u}_m^{\sigma} d\varphi}} \Delta\Omega, \quad (10.8)$$

while the quantities $\epsilon_{nm}^{\varepsilon\sigma}$ have the form

$$\epsilon_{nm}^{\varepsilon\sigma} = \frac{(d\lambda_{nm}^{\varepsilon\sigma} + k) u_n^{\varepsilon}(0) \bar{u}_m^{\sigma}(0) + \mu u_n^{\varepsilon\prime}(0) \bar{u}_m^{\sigma}(0)}{2\sqrt{\int_0^{2\pi} (\lambda_{nm}^{\varepsilon\sigma} u_n^{\varepsilon} + \Omega_{nm}^{\varepsilon\sigma} u_n^{\varepsilon\prime}) \bar{u}_n^{\varepsilon} d\varphi \int_0^{2\pi} (\lambda_{nm}^{\varepsilon\sigma} u_m^{\sigma} + \Omega_{nm}^{\varepsilon\sigma} u_m^{\sigma\prime}) \bar{u}_m^{\sigma} d\varphi}} \quad (10.9)$$

with $\Delta\Omega = \Omega - \Omega_{nm}^{\varepsilon\sigma}$ and

$$u_n^{\varepsilon} = \cos(n\varphi) - \varepsilon i \sin(n\varphi), \quad u_m^{\sigma} = \cos(m\varphi) - \sigma i \sin(m\varphi). \quad (10.10)$$

Taking into account expressions (7.79) and (10.10) yields

$$\lambda = \lambda_{nm}^{\varepsilon\sigma} + i\frac{\varepsilon n + \sigma m}{2}\Delta\Omega + i\frac{n+m}{8\pi nm}(d\lambda_{nm}^{\varepsilon\sigma} + k) + \frac{\varepsilon 1 + \sigma 1}{8\pi}\mu \pm i\sqrt{c}, \quad (10.11)$$

where

$$c = \left(\frac{\varepsilon n - \sigma m}{2}\Delta\Omega + \frac{m-n}{8\pi mn}(d\lambda_{nm}^{\varepsilon\sigma} + k) - i\mu\frac{\varepsilon 1 - \sigma 1}{8\pi}\right)^2 + \frac{(d\lambda_{nm}^{\varepsilon\sigma} + k - i\varepsilon n\mu)(d\lambda_{nm}^{\varepsilon\sigma} + k - i\sigma m\mu)}{16\pi^2 nm}. \quad (10.12)$$

Formula (10.11) is applicable to any node of the spectral mesh.

For example, at $\Omega = 0$ we have $m = n$ and $\varepsilon = -\sigma$, and deduce that the double eigenvalue in splits due to action of gyroscopic forces and an external spring as

$$\lambda = in + i\frac{k}{4\pi n} \pm i\sqrt{n^2\Omega^2 + \frac{k^2}{16\pi^2 n^2}}. \quad (10.13)$$

Similarly, the effect of damping and gyroscopic forces yields

$$\left(\mathrm{Re}\lambda + \frac{d}{4\pi}\right)^2 + n^2\Omega^2 = \frac{d^2}{16\pi^2}, \quad \mathrm{Im}\lambda = n, \tag{10.14}$$

$$n^2\Omega^2 - (\mathrm{Im}\lambda - n)^2 = \frac{d^2}{16\pi^2}, \quad \mathrm{Re}\lambda = -\frac{d}{4\pi}, \tag{10.15}$$

while circulatory and gyroscopic forces lead to the perturbed eigenvalues with

$$\mathrm{Im}\lambda = n \pm \frac{1}{2\pi}\sqrt{2\pi^2 n^2\Omega^2 \pm \pi n\Omega\sqrt{4\pi^2 n^2\Omega^2 + \mu^2}}, \tag{10.16}$$

$$\mathrm{Re}\lambda = \pm\frac{1}{2\pi}\sqrt{-2\pi^2 n^2\Omega^2 \pm \pi n\Omega\sqrt{4\pi^2 n^2\Omega^2 + \mu^2}}. \tag{10.17}$$

The lower branch of the hyperbola (10.13) passes through the location of the node at $\Omega = 0$ and $\mathrm{Im}\lambda = n$, while the upper one intersects the axis $\Omega = 0$ at $\mathrm{Im}\lambda = n + \frac{k}{2\pi n}$ in the plane $(\Omega, \mathrm{Im}\lambda)$, see Figure 10.3 (a).

The external damper creates a latent source of subcritical flutter instability exactly as it is shown in Figure 10.2 (a). Indeed, the bubble of complex eigenvalues (10.14)

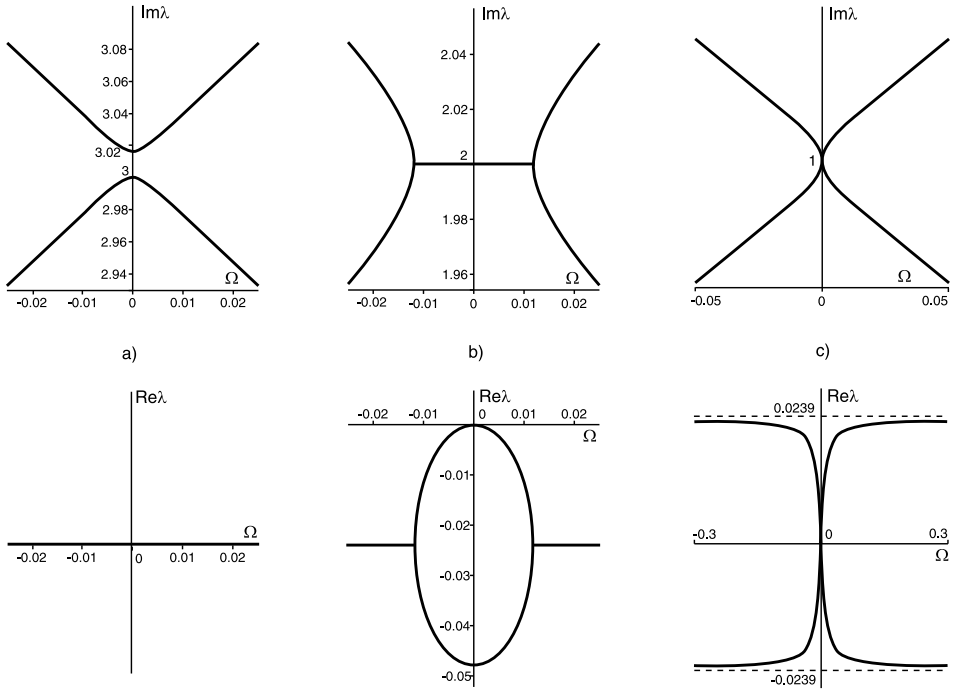

Figure 10.3. Deformation of the spectral mesh of the rotating string near the nodes $(0, 3)$, $(0, 2)$, and $(0, 1)$ in the $(\Omega, \mathrm{Im}\lambda)$-plane caused by the action of the external spring with $k = 0.3$ (a), damper with $d = 0.3$ (b), and friction with $\mu = 0.3$ (c), respectively.

together with the adjacent hyperbola (10.15) is under the plane $\mathrm{Re}\lambda = 0$, touching it at the origin, see Figure 10.3 (b).

The action of gyroscopic forces and external friction deforms the spectral mesh exactly as the $N = 2$-Galerkin approximation shows in Figure 10.2 (b). Formal expansion of equation (10.17) at $\Omega \to \infty$ shows that the real parts of the perturbed eigenvalues

$$\mathrm{Re}\lambda = \pm\frac{\mu}{4\pi} \mp \frac{\mu^3}{128\pi^3 n^2 \Omega^2} + o(\Omega^{-2}), \tag{10.18}$$

are close to the lines $\pm\mu/(4\pi)$, except for the vicinity of the node of the spectral mesh at $\Omega = 0$, where the real parts rapidly tend to zero as

$$\mathrm{Re}\lambda = \pm\frac{1}{2\pi}\sqrt{\pi n \mu|\Omega|} + O(\Omega^{3/2}), \tag{10.19}$$

demonstrating the inhibition of the destabilization effect registered in Figure 10.3 (c).

Expanding expression (10.16) in the vicinity of $\Omega = 0$, we find that

$$\mathrm{Im}\lambda = n \pm \frac{1}{2\pi}\sqrt{\pi n \mu|\Omega|} + O(\Omega^{3/2}). \tag{10.20}$$

For $\Omega \to \infty$ the imaginary parts tend to $n(1 \pm \Omega)$. Thus, at $\Omega = 0$ the double eigenvalue $i\,n$ does not split (marginal stability) due to perturbation by friction from the eyelet so that both the real and imaginary parts of the perturbed eigenvalue branches show a degenerate crossing,[3] touching at the node $(0, n)$, see Figure 10.3 (c).

The competing nonhomogeneous with respect to Ω effects of damping and nonconservative positional forces lead us to a conclusion that their combination may choose the parameters k and Ω that are prone to subcritical flutter, very selectively. Indeed, numerically calculated growth rates of the eigenvalues of the rotating string perturbed by damping, potential, and nonconservative positional forces, which are shown in Figure 10.4 (b, e), are positive in the vicinity of the loci of the crossings of the spectral mesh of the unperturbed string, Figure 10.4 (a, d). Moreover, the corresponding regions of flutter instability in the subcritical speed range ($|\Omega| < 1$) in the (Ω, k)-plane stem exactly from the points $(0, 0)$ and $(\frac{1}{3}, 0)$ corresponding to the nodes (7.79) of the spectral mesh (7.78) with the eigenvalues $\lambda_{11}^{+-} = i$, $\lambda_{22}^{+-} = 2i$ and $\lambda_{12}^{+-} = \frac{4}{3}i$, respectively.

From the growth rates of perturbed eigenvalues (10.11) found by means of the perturbation theory of Chapter 7, applied directly to the boundary eigenvalue problem (10.2) and (10.3) without its preliminary discretization, it follows that in the first-order approximation the domain of subcritical flutter originating due to splitting of the double eigenvalue $\lambda_{nm}^{\varepsilon\sigma} = i\,\omega_{nm}^{\varepsilon\sigma}$ at $\Omega = \Omega_{nm}^{\varepsilon\sigma}$, is

$$\Omega_{nm}^{\varepsilon\sigma} + k\frac{\omega_{nm}^{\varepsilon\sigma}(n+m)\mu d}{4\pi n^2 m^2\left(\mu - \frac{(1-\varepsilon\sigma 1)m}{n\varepsilon - m\sigma}d\right)\left(\mu + \frac{(1-\varepsilon\sigma 1)n}{n\varepsilon - m\sigma}d\right)} < \Omega < \Omega_{nm}^{\varepsilon\sigma}. \tag{10.21}$$

[3] Cf. energy and width plots of the resonances in open quantum systems discussed in [166].

According to equations (7.79),

$$\omega_{nm}^{\varepsilon\sigma} = \frac{nm(\sigma 1 - \varepsilon 1)}{m\sigma - n\varepsilon}, \quad \Omega_{nm}^{\varepsilon\sigma} = \frac{n-m}{m\sigma - n\varepsilon}, \quad \varepsilon, \sigma = \pm, \quad \varepsilon \neq \sigma. \tag{10.22}$$

Equation (10.21) gives a linear approximation to the boundaries of the regions of subcritical flutter that exactly coincides with that following from the Galerkin system (10.4), as Figure 10.4 (c, f) demonstrates. Formula (10.21) is valid at any node of the spectral mesh. When $\sigma = -\varepsilon$, it simplifies to

$$\Omega_{nm}^{\varepsilon\sigma} + \frac{k\mu d}{2\pi(\mu n - \varepsilon\omega_{nm}^{\varepsilon\sigma} d)(\mu m + \varepsilon\omega_{nm}^{\varepsilon\sigma} d)} < \Omega < \Omega_{nm}^{\varepsilon\sigma}. \tag{10.23}$$

Therefore, tongues of flutter instability in the (Ω, k)-plane in the subcritical speed range ($|\Omega| < 1$) indeed exist. According to equation (10.23) subcritical flutter depends, in particular, on the product of the coefficients of stiffness (k), friction (μ), and damping (d) so that simultaneous presence of all three of these factors is necessary for the instability tongues to originate![4] Remarkably, the tongues grow exactly from the locations of the crossings of the spectral mesh of the nonperturbed string, which implies combination resonance [110, 118] conditions (10.22) between the eigenfrequencies of the nonrotating string and the angular velocity.

We see that the main reason for subcritical flutter instabilities to occur is that non-Hamiltonian perturbation (equivalently, perturbation breaking self-adjointness of an operator in a Krein space) yields unstable unfolding of double eigenvalues with the definite Krein signature – an effect similar to that which we observed already in Chapter 9 in the model of an MHD α^2-dynamo when boundary conditions were changing from conducting to insulating. In the following, we will explore this instability mechanism in greater detail by using one of the standard general models of rotor dynamics [238].

10.3 Axially symmetric rotor with anisotropic stator

Linear stability analysis is widely used to predict possible instabilities in the dynamics of rotor systems to which the disk brake can be attributed. The presence of imperfections in rotor and stator makes the operator of the linearized equations of motion nonself-adjoint with time-dependent coefficients. The latter considerably complicates the stability analysis. Nevertheless, an axially symmetric rotor with an anisotropic stator as well as an asymmetric rotor with an isotropic stator can easily be described as an autonomous nonconservative gyroscopic system [194]. Unless the vented disk or

[4] Remember that for a wine glass to sing it is necessary to move along its rim a moistened (d) finger with some pressure (k), which creates a friction force (μ).

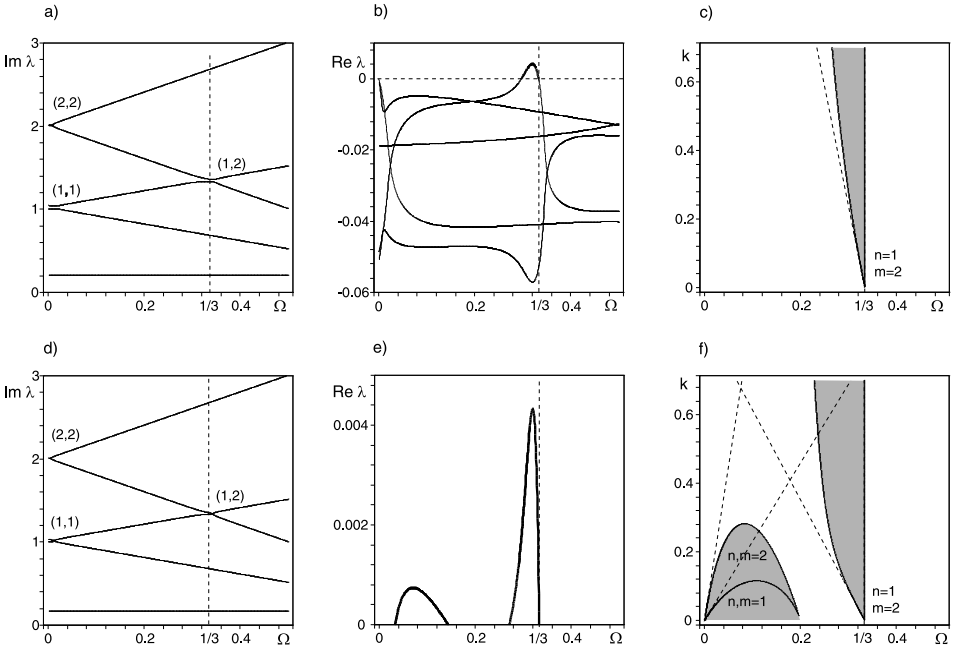

Figure 10.4. $N = 2$-Galerkin approximation (10.4) when (a–c) $d = 0.3$ and $\mu = 0.3$ and (a, b), additionally, $k = 0.3$; (d–f) when $d = 0.25$ and $\mu = 0.3$ and (d, e), additionally, $k = 0.2$. The bold black curves mark the excess of the growth rate over the ($\mathrm{Re}\lambda = 0$)-line that yields subcritical flutter instability in the vicinity of the ($n = 1, m = 1$), ($n = 2, m = 2$), and ($n = 1, m = 2$) nodes of the spectral mesh with $\varepsilon = +$ and $\sigma = -$. (c, f) Regions of subcritical flutter instability (or, equivalently, difference type combination resonance [110, 118]) according to (gray) $N = 2$-Galerkin approximation and (dashed lines) perturbation formula (10.21).

the disk with specially manufactured symmetry-breaking pattern [169] is considered, the model of an axially symmetric rotor with an anisotropic stator is reasonable for the description of the disk brake as well as other sound-radiating rotating elastic solids of revolution in frictional contact such as the glass harmonica.

When the stator (brake pad) does not interact with the rotor, the unperturbed system is assumed to be isotropic with the constant speed of the rotor, Ω. It is described by the equations of a standard nondimensional form [194]

$$\ddot{\mathbf{z}} + 2\Omega \begin{pmatrix} \mathbf{0} & -\widetilde{\mathbf{G}} \\ \widetilde{\mathbf{G}} & \mathbf{0} \end{pmatrix} \dot{\mathbf{z}} + \left[\begin{pmatrix} \widetilde{\mathbf{P}} & \mathbf{0} \\ \mathbf{0} & \widetilde{\mathbf{P}} \end{pmatrix} + \Omega^2 \begin{pmatrix} \widetilde{\mathbf{G}}^2 + \widetilde{\mathbf{C}} & \mathbf{0} \\ \mathbf{0} & \widetilde{\mathbf{G}}^2 + \widetilde{\mathbf{C}} \end{pmatrix} \right] \mathbf{z} = 0, \quad (10.24)$$

where $\mathbf{z} \in \mathbb{R}^{2n}$ and we assume $\widetilde{\mathbf{G}} = \mathrm{diag}(1, 2, \ldots, n)$, $\widetilde{\mathbf{P}} = \mathrm{diag}(\omega_1^2, \omega_2^2, \ldots, \omega_n^2)$, and $\widetilde{\mathbf{C}} = \mathrm{diag}(c_1^2, c_2^2, \ldots, c_n^2)$.

The spectrum of a perfect rotationally symmetric rotor at standstill has infinitely many double semisimple eigenvalues $\pm i\omega_s$, $\omega_s > 0$, with two linearly independent

eigenvectors. Indeed, e.g. for

$$\mathbb{R}^{2\times 2} \ni \mathbf{A} = \mathrm{diag}(\omega_1^2, \omega_2^2) \quad \text{and} \quad \mathbf{R} = \begin{pmatrix} \cos\theta & \sin\theta \\ -\sin\theta & \cos\theta \end{pmatrix}$$

the restriction $\mathbf{R}^T\mathbf{A}\mathbf{R} = \mathbf{A}$ imposed by equivariance of the equations of motion with respect to the action of the circle group implies $\omega_1^2 = \omega_2^2$, see e.g. [146, 440]. The distribution of the double eigenfrequencies ω_s as a function of the integer index s differs for various solids of revolution.[5]

In the following, we prefer to consider equation (10.24) in the equivalent form that shows the double eigenvalues explicitly [238]

$$\ddot{\mathbf{x}} + 2\Omega\mathbf{G}\dot{\mathbf{x}} + (\mathbf{P} + \Omega^2(\mathbf{G}^2 + \mathbf{C}))\mathbf{x} = 0, \tag{10.25}$$

where $\mathbf{x} \in \mathbb{R}^{2n}$, $\mathbf{P} = \mathrm{diag}(\omega_1^2, \omega_1^2, \omega_2^2, \omega_2^2, \ldots, \omega_n^2, \omega_n^2) = \mathbf{P}^T$ is the stiffness matrix of the rotor, $\mathbf{C} = \mathrm{diag}(c_1^2, c_1^2, c_2^2, c_2^2, \ldots, c_n^2, c_n^2)$ is the matrix of the centrifugal stiffness, and $\mathbf{G} = -\mathbf{G}^T$ is the matrix of gyroscopic forces defined as

$$\mathbf{G} = \mathrm{blockdiag}(\mathbf{J}, 2\mathbf{J}, \ldots, n\mathbf{J}), \quad \mathbf{J} = \begin{pmatrix} 0 & -1 \\ 1 & 0 \end{pmatrix}. \tag{10.26}$$

Equations of motion of the symmetric rotor interacting with the anisotropic stator can be considered as a perturbation of the system (10.25) by elastic, dissipative, and nonconservative positional (circulatory) forces

$$\ddot{\mathbf{x}} + (2\Omega\mathbf{G} + \delta\mathbf{D})\dot{\mathbf{x}} + (\mathbf{P} + \Omega^2(\mathbf{G}^2 + \mathbf{C}) + \kappa\mathbf{K} + \nu\mathbf{N})\mathbf{x} = 0. \tag{10.27}$$

The matrices of the non-Hamiltonian perturbation corresponding to velocity-dependent dissipative forces, $\mathbf{D} = \mathbf{D}^T$, and nonconservative positional forces, $\mathbf{N} = -\mathbf{N}^T$, as well as the matrix $\mathbf{K} = \mathbf{K}^T$ of the Hamiltonian perturbation that breaks the rotational symmetry, could, in general, depend on the rotational speed Ω, although in the applications considered in this chapter they are always Ω-independent. The intensity of the perturbation is controlled by the factors δ, κ, and ν. For a given structure of the matrices, stability is determined by a combination of the parameters. When the intensities δ, κ, and ν are fixed, one effects the eigenvalue assignment by modifying the structure of the corresponding matrices.

[5] For example, $\omega_s = s$ corresponds to the doubly degenerate natural frequency $f_s = \frac{s}{2\pi r}\sqrt{\frac{P}{\rho}}$ of a circular string of radius r, circumferential tension P, and mass density ρ per unit length [604]. On the other hand, $\omega_s = \frac{s(s^2-1)}{\sqrt{1+s^2}}$ is related to the double natural frequency $f_s = \frac{\omega_s}{2\pi r^2}\sqrt{\frac{EI}{A\rho}}$ of a circular ring of mean radius r, density ρ, Young's modulus E, uniform cross-section of area A, and moment of inertia of the cross-section I [110]. The natural frequency, $f_s = \frac{\omega_s^2 h}{2\pi a^2}\sqrt{\frac{E}{12\rho(1-\nu^2)}}$, of a doubly repeated mode with one nodal circle and s nodal diameters of the clamped-free annular disk of thickness h, inner radius b, outer radius a, mass per unit volume ρ, Poisson's ratio ν, and elastic modulus E corresponds to the nondimensional eigenvalue constant ω_s, which can be found numerically for a given Poisson ratio and radius ratio b/a. For $\nu = 0.3$ and $b/a = 0.1$ the first two constants are $\omega_1 \approx 5.2605$, and $\omega_2 \approx 6.0779$ [181]. Notice that in experiments squeal noise often associates with the rotor vibrating modes with nonzero number of nodal diameters [295].

Neglecting without loss of generality the centrifugal stiffness ($\mathbf{C} = 0$) and separating time by the substitution $\mathbf{x} = \mathbf{u}\exp(\lambda t)$ into equation (10.25), we arrive at the eigenvalue problem for the matrix operator $\mathbf{L}_0$

$$\mathbf{L}_0(\Omega)\mathbf{u} := (\mathbf{I}\lambda^2 + 2\Omega\mathbf{G}\lambda + \mathbf{P} + \Omega^2\mathbf{G}^2)\mathbf{u} = 0. \tag{10.28}$$

The eigenvalues of the operator $\mathbf{L}_0$ are found in the explicit form

$$\begin{aligned} \lambda_s^+ &= i\omega_s + is\Omega, \quad \overline{\lambda_s^-} = -i\omega_s + is\Omega, \\ \lambda_s^- &= i\omega_s - is\Omega, \quad \overline{\lambda_s^+} = -i\omega_s - is\Omega, \end{aligned} \tag{10.29}$$

with the overbar denoting complex conjugate. The eigenvectors at λ_s^+ and $\overline{\lambda_s^-}$ are

$$\mathbf{u}_1^+ = (-i, 1, 0, 0, \ldots, 0, 0)^T, \ \ldots, \ \mathbf{u}_n^+ = (0, 0, \ldots, 0, 0, -i, 1)^T, \tag{10.30}$$

where the imaginary unit holds the $(2s-1)$-st position in the vector $\mathbf{u}_s^+$. The eigenvectors, corresponding to the eigenvalues λ_s^- and $\overline{\lambda_s^+}$, are simply $\mathbf{u}_s^- = \overline{\mathbf{u}_s^+}$

For $\Omega > 0$, simple eigenvalues λ_s^+ and λ_s^- correspond to the forward and backward traveling waves, respectively, that propagate in the circumferential direction of the rotor. At the angular velocity $\Omega_s^{cr} = \omega_s/s$ the frequency of the s-th backward traveling wave vanishes to zero, so that the wave remains stationary in the nonrotating frame. We assume further in the text that the sequence of the double eigenvalues $i\omega_s$ has the property $\omega_{s+1} - \omega_s \geq \Omega_s^{cr}$, which implies the existence of the minimal critical speed $\Omega_{cr} = \Omega_1^{cr} = \omega_1$. When the speed of rotation exceeds the critical speed, some backward waves, corresponding to the eigenvalues $\overline{\lambda_s^-}$, travel slower than the disk rotation speed and appear to be traveling forward (reflected waves).

10.3.1 Sensitivity analysis of the Campbell diagram

Introducing the indices $\alpha, \beta, \varepsilon, \sigma = \pm$, we find that the eigencurves $\lambda_s^\varepsilon = i\alpha\omega_s + i\varepsilon s\Omega$ and $\lambda_t^\sigma = i\beta\omega_t + i\sigma t\Omega$ of the Campbell diagram cross each other at $\Omega = \Omega_{st}^{\varepsilon\sigma}$ with the origination of the double eigenvalue $\lambda_{st}^{\varepsilon\sigma} = i\omega_{st}^{\varepsilon\sigma}$ with two linearly independent eigenvectors $\mathbf{u}_s^\varepsilon$ and $\mathbf{u}_t^\sigma$, where

$$\Omega_{st}^{\varepsilon\sigma} = \frac{\alpha\omega_s - \beta\omega_t}{\sigma t - \varepsilon s}, \quad \omega_{st}^{\varepsilon\sigma} = \frac{\alpha\sigma\omega_s t - \beta\varepsilon\omega_t s}{\sigma t - \varepsilon s}. \tag{10.31}$$

Let $\mathbf{M}$ be one of the matrices $\mathbf{D}$, $\mathbf{K}$, or $\mathbf{N}$ in equation (10.27). In the following, we decompose the matrix $\mathbf{M} \in \mathbb{R}^{2n\times 2n}$ into n^2 blocks $\mathbf{M}_{st} \in \mathbb{R}^{2\times 2}$ [294]

$$\mathbf{M} = \begin{pmatrix} * & * & * & * & * \\ * & \mathbf{M}_{ss} & \cdots & \mathbf{M}_{st} & * \\ * & \vdots & \ddots & \vdots & * \\ * & \mathbf{M}_{ts} & \cdots & \mathbf{M}_{tt} & * \\ * & * & * & * & * \end{pmatrix}, \quad \mathbf{M}_{st} = \begin{pmatrix} m_{2s-1,2t-1} & m_{2s-1,2t} \\ m_{2s,2t-1} & m_{2s,2t} \end{pmatrix}. \tag{10.32}$$

Note that $\mathbf{D}_{st} = \mathbf{D}_{ts}^T$, $\mathbf{K}_{st} = \mathbf{K}_{ts}^T$, and $\mathbf{N}_{st} = -\mathbf{N}_{ts}^T$, where $s, t = 1, 2, \ldots, n$.

Consider a general perturbation of the matrix operator of the isotropic rotor $\mathbf{L}_0(\Omega)+\Delta\mathbf{L}(\Omega)$, where $\Delta\mathbf{L}(\Omega)=\delta\lambda\mathbf{D}+\kappa\mathbf{K}+\nu\mathbf{N}$. This yields an eigenvalue problem of the form (10.4). When the size of the perturbation $\Delta\mathbf{L}(\Omega)\sim\|\Delta\mathbf{L}(\Omega_{st}^{\varepsilon\sigma})\|$ and the variation $\Delta\Omega=|\Omega-\Omega_{st}^{\varepsilon\sigma}|$ are small, the increment to the eigenvalue $\lambda_{st}^{\varepsilon\sigma}=i\omega_{st}^{\varepsilon\sigma}$ with the eigenvectors $\mathbf{u}_s^{\varepsilon}$ and $\mathbf{u}_t^{\sigma}$, is given by the formula $\det(\mathbf{R}+(\lambda-\lambda_{st}^{\varepsilon\sigma})\mathbf{Q})=0$, where the entries of the 2×2 matrices $\mathbf{Q}$ and $\mathbf{R}$ are

$$Q_{ab}^{\varepsilon\sigma}=2i\omega_{st}^{\varepsilon\sigma}(\bar{\mathbf{u}}_a^{\varepsilon})^T\mathbf{u}_b^{\sigma}+2\Omega_{st}^{\varepsilon\sigma}(\bar{\mathbf{u}}_a^{\varepsilon})^T\mathbf{G}\mathbf{u}_b^{\sigma}, \tag{10.33}$$

$$\begin{aligned}R_{ab}^{\varepsilon\sigma}=&\left[2i\omega_{st}^{\varepsilon\sigma}(\bar{\mathbf{u}}_a^{\varepsilon})^T\mathbf{G}\mathbf{u}_b^{\sigma}+2\Omega_{st}^{\varepsilon\sigma}(\bar{\mathbf{u}}_a^{\varepsilon})^T\mathbf{G}^2\mathbf{u}_b^{\sigma}\right](\Omega-\Omega_{st}^{\varepsilon\sigma})\\&+i\omega_{st}^{\varepsilon\sigma}(\bar{\mathbf{u}}_a^{\varepsilon})^T\mathbf{D}\mathbf{u}_b^{\sigma}\delta+(\bar{\mathbf{u}}_a^{\varepsilon})^T\mathbf{K}\mathbf{u}_b^{\sigma}\kappa+(\bar{\mathbf{u}}_a^{\varepsilon})^T\mathbf{N}\mathbf{u}_b^{\sigma}\nu,\end{aligned} \tag{10.34}$$

where $a,b=s,t$. Calculating the coefficients (10.33) and (10.34) with the eigenvectors (10.30), we find the real and imaginary parts of the sensitivity of the doublet $\lambda_{st}^{\varepsilon\sigma}=i\omega_{st}^{\varepsilon\sigma}$ at the crossing (10.31)

$$\mathrm{Re}\lambda=-\frac{1}{8}\left(\frac{\mathrm{Im}A_1}{\alpha\omega_s}+\frac{\mathrm{Im}B_1}{\beta\omega_t}\right)\pm\sqrt{\frac{|c|-\mathrm{Re}c}{2}}, \tag{10.35}$$

$$\mathrm{Im}\lambda=\omega_{st}^{\varepsilon\sigma}+\frac{\Delta\Omega}{2}(s\varepsilon+t\sigma)+\frac{\kappa}{8}\left(\frac{\mathrm{tr}\mathbf{K}_{ss}}{\alpha\omega_s}+\frac{\mathrm{tr}\mathbf{K}_{tt}}{\beta\omega_t}\right)\pm\sqrt{\frac{|c|+\mathrm{Re}c}{2}}, \tag{10.36}$$

where $c=\mathrm{Re}c+i\,\mathrm{Im}c$ with [294, 295]

$$\begin{aligned}\mathrm{Im}c=&\frac{\alpha\omega_t\mathrm{Im}A_1-\beta\omega_s\mathrm{Im}B_1}{8\omega_s\omega_t}(s\varepsilon-t\sigma)\Delta\Omega\\&+\kappa\frac{(\alpha\omega_s\mathrm{tr}\mathbf{K}_{tt}-\beta\omega_t\mathrm{tr}\mathbf{K}_{ss})(\alpha\omega_s\mathrm{Im}B_1-\beta\omega_t\mathrm{Im}A_1)}{32\omega_s^2\omega_t^2}\\&-\alpha\beta\kappa\frac{\mathrm{Re}A_2\mathrm{tr}\mathbf{K}_{st}\mathbf{J}_{\varepsilon\sigma}-\mathrm{Re}B_2\mathrm{tr}\mathbf{K}_{st}\mathbf{I}_{\varepsilon\sigma}}{8\omega_s\omega_t},\end{aligned} \tag{10.37}$$

$$\begin{aligned}\mathrm{Re}c=&\left(\frac{t\sigma-s\varepsilon}{2}\Delta\Omega+\kappa\frac{\beta\omega_s\mathrm{tr}\mathbf{K}_{tt}-\alpha\omega_t\mathrm{tr}\mathbf{K}_{ss}}{8\omega_s\omega_t}\right)^2\\&+\alpha\beta\frac{(\mathrm{tr}\mathbf{K}_{st}\mathbf{J}_{\varepsilon\sigma})^2+(\mathrm{tr}\mathbf{K}_{st}\mathbf{I}_{\varepsilon\sigma})^2}{16\omega_s\omega_t}\kappa^2\\&-\frac{(\alpha\omega_s\mathrm{Im}B_1-\beta\omega_t\mathrm{Im}A_1)^2+4\alpha\beta\omega_s\omega_t((\mathrm{Re}A_2)^2+(\mathrm{Re}B_2)^2)}{64\omega_s^2\omega_t^2}.\end{aligned} \tag{10.38}$$

The coefficients A_1, A_2 and B_1, B_2 depend only on those entries of $\mathbf{D}$, $\mathbf{K}$, and $\mathbf{N}$ that belong to the four 2×2 blocks (10.32) with the indices s and t

$$\begin{aligned}A_1&=\delta\lambda_{st}^{\varepsilon\sigma}\mathrm{tr}\mathbf{D}_{ss}+\kappa\mathrm{tr}\mathbf{K}_{ss}+\varepsilon 2i\nu n_{2s-1,2s},\\A_2&=\sigma\nu\mathrm{tr}\mathbf{N}_{st}\mathbf{I}_{\varepsilon\sigma}+i(\delta\lambda_{st}^{\varepsilon\sigma}\mathrm{tr}\mathbf{D}_{st}\mathbf{J}_{\varepsilon\sigma}+\kappa\mathrm{tr}\mathbf{K}_{st}\mathbf{J}_{\varepsilon\sigma}),\\B_1&=\delta\lambda_{st}^{\varepsilon\sigma}\mathrm{tr}\mathbf{D}_{tt}+\kappa\mathrm{tr}\mathbf{K}_{tt}+\sigma 2i\nu n_{2t-1,2t},\\B_2&=\sigma\nu\mathrm{tr}\mathbf{N}_{st}\mathbf{J}_{\varepsilon\sigma}-i(\delta\lambda_{st}^{\varepsilon\sigma}\mathrm{tr}\mathbf{D}_{st}\mathbf{I}_{\varepsilon\sigma}+\kappa\mathrm{tr}\mathbf{K}_{st}\mathbf{I}_{\varepsilon\sigma}),\end{aligned} \tag{10.39}$$

where

$$\mathbf{I}_{\varepsilon\sigma} = \begin{pmatrix} \varepsilon & 0 \\ 0 & \sigma \end{pmatrix}, \quad \mathbf{J}_{\varepsilon\sigma} = \begin{pmatrix} 0 & -\sigma \\ \varepsilon & 0 \end{pmatrix}. \tag{10.40}$$

When $\alpha = \beta = +$, $t = s$, and $\sigma = -\varepsilon = -$, then $\omega_{st}^{\varepsilon\sigma} = \omega_s$ and $\Omega_{st}^{\varepsilon\sigma} = 0$, so that equations (10.35) and (10.36) are simplified to [293, 295]

$$\mathrm{Re}\lambda = -\frac{\mathrm{tr}\mathbf{D}_{ss}}{4}\delta \pm \sqrt{\frac{|c| - \mathrm{Re}c}{2}}, \quad \mathrm{Im}\lambda = \omega_s + \frac{\mathrm{tr}\mathbf{K}_{ss}}{4\omega_s}\kappa \pm \sqrt{\frac{|c| + \mathrm{Re}c}{2}}, \tag{10.41}$$

with

$$\begin{aligned} \mathrm{Re}c &= -\frac{(\mu_1 - \mu_2)^2}{16}\delta^2 + \frac{(\rho_1 - \rho_2)^2}{16\omega_s^2}\kappa^2 + s^2\Omega^2 - \nu^2\frac{n_{2s-1,2s}^2}{4\omega_s^2}, \\ \mathrm{Im}c &= \Omega\nu\frac{sn_{2s-1,2s}}{\omega_s} + \delta\kappa\frac{2\mathrm{tr}\mathbf{K}_{ss}\mathbf{D}_{ss} - \mathrm{tr}\mathbf{K}_{ss}\mathrm{tr}\mathbf{D}_{ss}}{8\omega_s}, \end{aligned} \tag{10.42}$$

where $\mu_{1,2}$ and $\rho_{1,2}$ are eigenvalues of matrices $\mathbf{D}_{ss}$ and $\mathbf{K}_{ss}$, respectively.

Therefore, we have identified the elements of the perturbing matrices that control practically important *eigenvalue assignment* near every particular node $(\Omega_{st}^{\varepsilon\sigma}, \omega_{st}^{\varepsilon\sigma})$ of the spectral mesh.

10.3.2 MacKay's eigenvalue cones and instability bubbles

Modification of the stiffness matrix induced by the elastic support interacting with the rotating continua is typical in models of rotating shafts [524], computer disk drives [123, 456], circular saws [574, 602, 604], car brakes [268, 433, 463], planetary gears [110], and turbine wheels [109, 194].

Assuming $\delta = 0$ and $\nu = 0$ in (10.35) and (10.36) we find that the eigenvalues of the system (10.27) with $\mathbf{C} = 0$ and the stiffness modification $\kappa\mathbf{K}$ either are pure imaginary ($\mathrm{Re}\lambda = 0$) and form a conical surface in the $(\Omega, \kappa, \mathrm{Im}\lambda)$-space with the apex at the point $(\Omega_{st}^{\varepsilon\sigma}, 0, \omega_{st}^{\varepsilon\sigma})$

$$\left(\mathrm{Im}\lambda - \omega_{st}^{\varepsilon\sigma} - \frac{\kappa}{8}\left(\frac{\mathrm{tr}\mathbf{K}_{ss}}{\alpha\omega_s} + \frac{\mathrm{tr}\mathbf{K}_{tt}}{\beta\omega_t}\right) - \frac{\Omega - \Omega_{st}^{\varepsilon\sigma}}{2}(s\varepsilon + t\sigma)\right)^2 = \mathrm{Re}c, \tag{10.43}$$

see Figure 10.5 (a), or they are complex and in the $(\Omega, \kappa, \mathrm{Re}\lambda)$-space their real parts originate a cone $(\mathrm{Re}\lambda)^2 = -\mathrm{Re}c$ with the apex at the point $(\Omega_{st}^{\varepsilon\sigma}, 0, 0)$, Figure 10.5 (c). In the $(\Omega, \kappa, \mathrm{Im}\lambda)$-space the corresponding imaginary parts belong to the plane

$$\mathrm{Im}\lambda = \omega_{st}^{\varepsilon\sigma} + \frac{\kappa}{8}\left(\frac{\mathrm{tr}\mathbf{K}_{ss}}{\alpha\omega_s} + \frac{\mathrm{tr}\mathbf{K}_{tt}}{\beta\omega_t}\right) + \frac{\Omega - \Omega_{st}^{\varepsilon\sigma}}{2}(s\varepsilon + t\sigma), \tag{10.44}$$

which is attached to the cone (10.43) as shown in Figure 10.5 (b).

The existence of eigenvalues with $\mathrm{Re}\lambda \neq 0$ depends on the sign of $\alpha\beta$. It is negative only if the crossing in the Campbell diagram is formed by the eigencurve of the reflected wave and by that of either the forward or backward traveling wave. Otherwise,

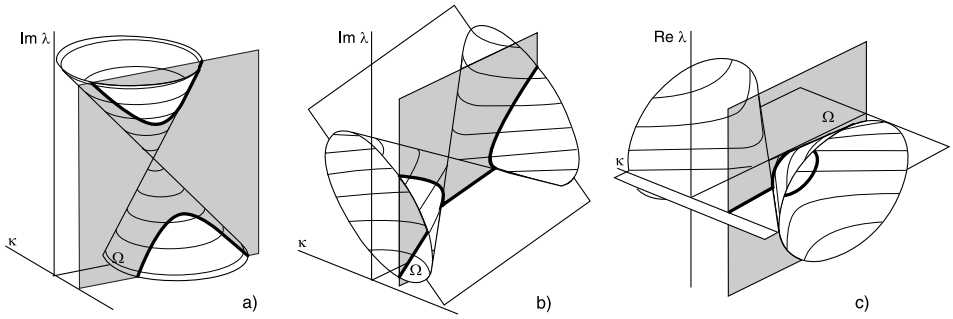

Figure 10.5. MacKay's eigenvalue cones [390] and (bold lines) their cross-sections in the plane $\kappa = const$ (gray): (a) a near-vertically oriented cone $\mathrm{Im}\lambda(\Omega,\kappa)$ in the subcritical range ($\mathrm{Re}\lambda = 0$); (b) imaginary parts forming a near-horizontally oriented cone (10.43) with the attached membrane (10.44) and (c) the real parts forming a near-horizontally oriented cone $(\mathrm{Re}\lambda)^2 = -\mathrm{Re}c$ with the attached membrane $\mathrm{Re}\lambda = 0$ in the supercritical range [294], see also Section 3.3.3.

$\alpha\beta = +$. Due to the property $\omega_{s+1} - \omega_s \geq \Omega_s^{cr}$ the crossings of the reflected wave with the forward and backward traveling waves occur only in the supercritical speed range $|\Omega| \geq \Omega_{cr}$. The crossings with $\alpha\beta = +$ are situated in both the super- and subcritical ($|\Omega| < \Omega_{cr}$) ranges. Therefore, the eigenvalues with $\mathrm{Re}\lambda \neq 0$ originate only near the supercritical crossings of the eigencurves λ_s^{ε} and λ_t^{σ} with $\alpha\beta = -$, when the parameters in the (Ω,κ)-plane are in the sector $\mathrm{Re}c < 0$ bounded by the straight lines $\mathrm{Re}c = 0$:

$$\kappa = \frac{4(s\varepsilon - t\sigma)(\Omega - \Omega_{st}^{\varepsilon\sigma})}{\frac{k_{2t-1,2t-1}+k_{2t,2t}}{\beta\omega_t} - \frac{k_{2s-1,2s-1}+k_{2s,2s}}{\alpha\omega_s} \pm 2\sqrt{\frac{(\varepsilon k_{2s-1,2t-1}+\sigma k_{2s,2t})^2+(\varepsilon k_{2s-1,2t}-\sigma k_{2s,2t-1})^2}{-\alpha\beta\omega_s\omega_t}}}. \tag{10.45}$$

Note that applying equation (10.45) to the Galerkin approximation (10.4) of the boundary eigenvalue problem for a rotating string, where the matrices $\mathbf{P}$, $\mathbf{G}$, and $\mathbf{K}$ are extended by an extra row of zeros from above and an extra column of zeros from the left, we exactly reproduce equation (7.84).

Since for $\alpha\beta = -$ the cones of the real parts $(\mathrm{Re}\lambda)^2 = -\mathrm{Re}c$ are near-horizontally oriented and extended along the κ-axis in the $(\Omega,\kappa,\mathrm{Re}\lambda)$-space, their cross-sections by the planes $\kappa = \mathrm{const}$ are ellipses, as shown in Figure 10.5 (c). As a part of the ellipse corresponds to the eigenvalues with positive real parts, the ellipse was called the bubble of instability by MacKay [390, 392].

Equation (10.45) is, therefore, a linear approximation to the boundary of the domain of supercritical instability, which is divergence (or principal parametric resonance) for $\Omega_{st}^{\varepsilon\sigma} = \Omega_s^{cr}$ and flutter (or combination parametric resonance) otherwise[6]. The near-

[6] By transition to the frame that rotates with speed Ω one can transform the *autonomous* system (10.27) to a $\pi\Omega^{-1}$-*periodic* system [110, 118, 297, 304, 325, 522].

horizontal orientation of the corresponding cones of imaginary parts (10.43) in the $(\Omega, \kappa, \mathrm{Im}\lambda)$-space explains deformation in the presence of the perturbation $\kappa\mathbf{K}$ of the crossings with $\alpha\beta = -$ into the branches of a hyperbola connected by a straight line in the Campbell diagram, see Figure 10.5 (b).

Near the crossings with $\alpha\beta = +$ the perturbed eigenvalues are pure imaginary (stability). The corresponding cones of imaginary parts (10.43) are near-vertically oriented in the $(\Omega, \kappa, \mathrm{Im}\lambda)$-space, Figure 10.5 (a). In the plane $\kappa = const$ this yields the avoided crossing [390, 392], which is approximated by a hyperbola shown by the bold lines in Figure 10.5 (a).

The conical singularities of the eigenvalue surfaces in the Hamiltonian systems are traced back to the works of Hamilton himself, who predicted the effect of conical refraction of light in birefringent crystals [53, 78, 189]. Later on, the conical singularities of eigenvalue surfaces were found in atomic, nuclear, and molecular physics [426, 568, 587] as well as in the material instability problems of continuum mechanics [59, 60]. Nowadays they bear the name of Hamilton's *diabolical points* [53, 56]. The existence of two different orientations of eigenvalue cones in the Hamiltonian systems was established by MacKay in [390]. His result is based on the works of Williamson [597, 598] and Krein [337], who introduced the signature of eigenvalues known as the symplectic signature in Hamiltonian mechanics [393] and as the Krein signature in a broader context of the theory of Krein spaces [202, 307].

To evaluate the signatures, we reduce equation (10.25) (with $\mathbf{C} = 0$) to $\dot{\mathbf{y}} = \mathbf{A}\mathbf{y}$, where

$$\mathbf{A} = \begin{pmatrix} -\Omega\mathbf{G} & \mathbf{I}_n \\ -\mathbf{P} & -\Omega\mathbf{G} \end{pmatrix} = \mathbf{J}_{2n}\mathbf{A}^T\mathbf{J}_{2n},$$

$$\mathbf{J}_{2n} = \begin{pmatrix} 0 & -\mathbf{I}_n \\ \mathbf{I}_n & 0 \end{pmatrix}, \quad \mathbf{y} = \begin{pmatrix} \mathbf{x} \\ \dot{\mathbf{x}} + \Omega\mathbf{G}\mathbf{x} \end{pmatrix}. \tag{10.46}$$

The Hamiltonian symmetry of $\mathbf{A}$ implies its self-adjointness in a Krein space with the indefinite inner product $[\mathbf{a}, \mathbf{b}] = i\overline{\mathbf{b}}^T\mathbf{J}_{2n}\mathbf{a}$, $\mathbf{a}, \mathbf{b} \in \mathbb{C}^{2n}$. The matrix $\mathbf{A}$ has the eigenvalues $\lambda_s^{\pm}$ given by equations (10.29) with the eigenvectors

$$\mathbf{a}_s^{++} = \begin{pmatrix} \mathbf{u}_s^+ \\ \lambda_s^+\mathbf{u}_s^+ + \Omega\mathbf{G}\mathbf{u}_s^+ \end{pmatrix}, \quad \mathbf{a}_s^{+-} = \begin{pmatrix} \mathbf{u}_s^- \\ \lambda_s^-\mathbf{u}_s^- + \Omega\mathbf{G}\mathbf{u}_s^- \end{pmatrix}, \tag{10.47}$$

where the vectors $\mathbf{u}_s^{\pm}$ are determined by expressions (10.30). Since $[\mathbf{a}_s^{++}, \mathbf{a}_s^{++}] = 4\omega_s > 0$ and $[\mathbf{a}_s^{+-}, \mathbf{a}_s^{+-}] = 4\omega_s > 0$, the eigenvalues λ_s^+ and λ_s^- of the forward and backward traveling waves acquire positive Krein signature [431]. The eigenvalues λ_s^+ and $\overline{\lambda_s^-}$ of the reflected waves with $[\mathbf{a}_s^{-+}, \mathbf{a}_s^{-+}] = -4\omega_s < 0$ and $[\mathbf{a}_s^{--}, \mathbf{a}_s^{--}] = -4\omega_s < 0$, have the opposite, negative Krein signature [390, 393]. The signature of an eigenvalue in the Campbell diagram coincides with the sign of the double eigenvalue at $\Omega = 0$, from which it is branched, and does not change with the variation of Ω. This implies $\alpha\beta = +$ and near-vertically oriented cones of imaginary parts (10.43) at the crossings of eigenvalue branches with the double eigenvalues having definite

signature, and $\alpha\beta = -$ and near-horizontally oriented cones of imaginary parts (10.43) at the crossings with the double eigenvalues having mixed signature [390, 603].

The Krein signature coincides with the sign of the second derivative of the energy, which is a nondegenerate definite quadratic form on the real invariant space associated to a complex-conjugate pair of simple pure imaginary nonzero eigenvalues [390]. Interaction of waves with positive and negative energy is a well-known mechanism of instability in fluids, plasmas, and spatio-temporal composites (*dynamic materials*) [90,108,111,112,115,168,386,390,430,551]; in rotor dynamics this yields flutter and divergence in the supercritical speed range [433].

Therefore, in the case when anisotropy of the stator is caused by stiffness modification only, the unfolding of the Campbell diagram is completely described by one-parameter slices of the two-parameter MacKay eigenvalue cones. Since there are only two possible spatial orientations of the cones, corresponding to either definite or mixed Krein signatures, all one has to do to predict the unfolding of the Campbell diagram into avoided crossings or into bubbles of instability is to calculate the signatures of the appropriate eigenvalues of the isotropic rotor [390]. In the following, we develop MacKay's theory further and show that even in the presence of non-Hamiltonian perturbations, many of the observed peculiarities of the perturbed Campbell diagrams and growth rate plots are in fact one-parameter slices of eigenvalue surfaces near a limited number of other singularities whose type is dictated by the definiteness or indefiniteness of the Krein signature of the double semisimple eigenvalues at the crossings of the unperturbed Campbell diagram.

10.3.3 Double-coffee-filter singularity near the crossings with definite Krein signature

Understanding general rules of unfolding Campbell diagrams of weakly anisotropic rotor systems in the presence of dissipative and nonconservative perturbations is important for linear stability analysis and for interpretation of numerical data in both low- and high-speed applications [194]. In the latter, supercritical flutter and divergence instabilities are easily excited near the crossings with the mixed Krein signature just by Hamiltonian perturbations like stiffness modification. In low-speed applications, unfolding the Campbell diagram is directly related to the onset of friction-induced oscillations in brakes, clutches, paper calenders, and even in musical instruments like the glass harmonica [6,92,123,502,537,538,541]. In contrast to the supercritical instabilities, excitation of the subcritical flutter near the crossings with definite Krein signature by Hamiltonian perturbations only, is impossible. In this case the non-Hamiltonian dissipative and circulatory forces are necessary for destabilization.

In general, dissipative, $\delta\mathbf{D}$, and nonconservative positional, $\nu\mathbf{N}$, perturbations unfold MacKay's eigenvalue cones (10.43) and $(\mathrm{Re}\lambda)^2 = -\mathrm{Re}c$ into the surfaces $\mathrm{Im}\lambda(\Omega,\kappa)$ and $\mathrm{Re}\lambda(\Omega,\kappa)$ described by formulas (10.35) and (10.36). The new eigenvalue surfaces have singularities at the *exceptional points* [52, 260]. The latter corre-

spond to the double eigenvalues with the Jordan chain born from the parent semisimple double eigenvalue $i\omega_{st}^{\varepsilon\sigma}$ at $\Omega = \Omega_{st}^{\varepsilon\sigma}$. In some works, numerical methods were developed to find the coordinates of these singularities [243, 246]. Perturbing Hamilton's diabolical points is another efficient way to locate the exceptional points [270]. Indeed, condition $c = 0$ yields their approximate loci in the (Ω, κ)-plane

$$\Omega_{EP}^{\pm} = \Omega_{st}^{\varepsilon\sigma} \pm \frac{4\omega_s\omega_t U - \beta\omega_s \mathrm{tr}\mathbf{K}_{tt} + \alpha\omega_t \mathrm{tr}\mathbf{K}_{ss}}{4\omega_s\omega_t(t\sigma - s\varepsilon)}\sqrt{\frac{N}{D}}, \quad \kappa_{EP}^{\pm} = \pm\sqrt{\frac{N}{D}}, \quad (10.48)$$

where [294]

$$\begin{aligned} U &= \frac{\mathrm{Re}A_2 \mathrm{tr}\mathbf{K}_{st}\mathbf{J}_{\varepsilon\sigma} - \mathrm{Re}B_2 \mathrm{tr}\mathbf{K}_{st}\mathbf{I}_{\varepsilon\sigma}}{\alpha\omega_s \mathrm{Im}B_1 - \beta\omega_t \mathrm{Im}A_1}, \qquad (10.49)\\ D &= U^2 + \alpha\beta\left[\left(\frac{\mathrm{tr}\mathbf{K}_{st}\mathbf{J}_{\varepsilon\sigma}}{2\sqrt{\omega_s\omega_t}}\right)^2 + \left(\frac{\mathrm{tr}\mathbf{K}_{st}\mathbf{I}_{\varepsilon\sigma}}{2\sqrt{\omega_s\omega_t}}\right)^2\right],\\ N &= \left(\frac{\alpha\omega_s \mathrm{Im}B_1 - \beta\omega_t \mathrm{Im}A_1}{4\omega_s\omega_t}\right)^2 + \alpha\beta\left[\left(\frac{\mathrm{Re}A_2}{2\sqrt{\omega_s\omega_t}}\right)^2 + \left(\frac{\mathrm{Re}B_2}{2\sqrt{\omega_s\omega_t}}\right)^2\right]. \end{aligned}$$

The crossings with definite Krein signature ($\alpha\beta = +$) always produce a pair of exceptional points. For example, for pure circulatory ($\delta = 0$) and pure dissipative ($\nu = 0$) perturbation of the doublets at $\Omega = \Omega_{ss}^{+-} = 0$, formulas (10.48) read (cf. equation (10.42))

$$\begin{aligned} &\Omega_{EP,n}^{\pm} = 0, \quad \kappa_{EP,n}^{\pm} = \pm\frac{2\nu n_{2s-1,2s}}{\rho_1(\mathbf{K}_{ss}) - \rho_2(\mathbf{K}_{ss})};\\ &\Omega_{EP,d}^{\pm} = \pm\delta\frac{\mu_1(\mathbf{D}_{ss}) - \mu_2(\mathbf{D}_{ss})}{4s}, \quad \kappa_{EP,d}^{\pm} = 0, \qquad (10.50) \end{aligned}$$

where $\rho_{1,2}(\mathbf{K}_{ss})$ are the eigenvalues of the block $\mathbf{K}_{ss}$ of the matrix $\mathbf{K}$ and $\mu_{1,2}(\mathbf{D}_{ss})$ are those of the block $\mathbf{D}_{ss}$ of $\mathbf{D}$. In the case of the mixed Krein signature ($\alpha\beta = -$), two exceptional points exist when $N/D > 0$ and do not exist otherwise.

The strong influence of exceptional points on stability and their relation to the Ziegler–Bottema destabilization paradox due to small damping is well recognized [81, 232,312,354,518]. In numerous applications in rotor dynamics [123,294,456,538,604] as well as in hydrodynamics [458], the theory of absolute and convective instability [235, 506], crystal optics [52], acoustics [527], and microwave physics [154], the generalized crossing scenario in the vicinity of the exceptional points has been observed (visible also in Figure 10.2) when at the same values of the parameters the imaginary parts of the eigenvalues cross, whereas the real parts do not and vice-versa. In our setting, the conditions for coincidence of imaginary parts of the eigenvalues (10.35) and (10.36) are $\mathrm{Im}c = 0$ and $\mathrm{Re}c \le 0$ and those for coincidence of the real parts are $\mathrm{Im}c = 0$ and $\mathrm{Re}c \ge 0$. Both real and imaginary parts of the eigenvalues coincide only at the two exceptional points $(\Omega_{EP}^{+}, \kappa_{EP}^{+})$ and $(\Omega_{EP}^{-}, \kappa_{EP}^{-})$. The segment of the line $\mathrm{Im}c = 0$ connecting the exceptional points is the projection of the

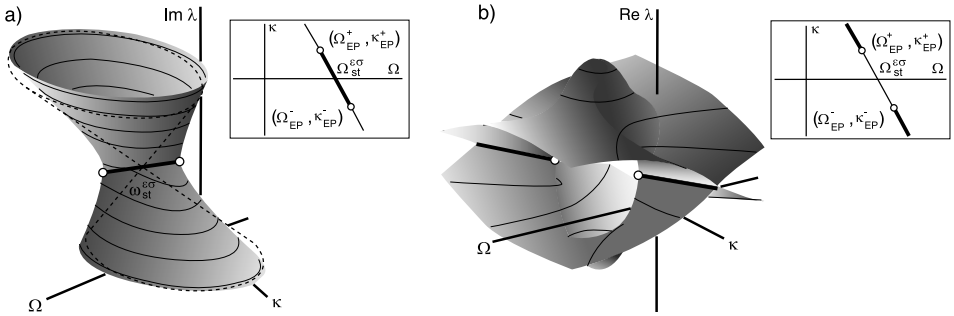

Figure 10.6. (a) The 'double-coffee-filter' surface $\mathrm{Im}\lambda(\Omega,\kappa)$ with the exceptional points (open circles) and branch cut (bold lines) originated from MacKay's cone (dashed lines) due to mixed dissipative and circulatory perturbation at any crossing with definite Krein signature; (b) the corresponding 'viaduct' $\mathrm{Re}\lambda(\Omega,\kappa)$ [294].

branch cut of a singular eigenvalue surface $\mathrm{Im}\lambda(\Omega,\kappa)$. The adjacent parts of the line correspond to the branch cuts of the singular eigenvalue surface $\mathrm{Re}\lambda(\Omega,\kappa)$. Since simultaneous intersection of the different segments of the line $\mathrm{Im}c = 0$ in the (Ω,κ)-plane is not possible, one observes the generalized crossing scenario [260, 270] in the planes $(\Omega,\mathrm{Im}\lambda)$ and $(\Omega,\mathrm{Re}\lambda)$ or $(\kappa,\mathrm{Im}\lambda)$ and $(\kappa,\mathrm{Re}\lambda)$.

For example, in the case of pure circulatory perturbation the real parts of the eigenvalues developing near the doublet modes at $\Omega = \Omega_{ss}^{+-} = 0$ cross each other in the $(\Omega,\mathrm{Re}\lambda)$-plane at the points of the branch cuts $\kappa^2 > (\kappa_{EP,n}^{\pm})^2$

$$\mathrm{Re}\lambda = \pm\frac{2\nu s n_{2s-1,2s}}{(\rho_1(\mathbf{K}_{ss}) - \rho_2(\mathbf{K}_{ss}))\sqrt{\kappa^2 - (\kappa_{EP,n}^{\pm})^2}}\Omega + O(\Omega^3), \tag{10.51}$$

whereas for $\kappa^2 < (\kappa_{EP,n}^{\pm})^2$ they avoid crossing

$$\mathrm{Re}\lambda = \pm\frac{\rho_1(\mathbf{K}_{ss}) - \rho_2(\mathbf{K}_{ss})}{4\omega_s}\sqrt{(\kappa_{EP,n}^{\pm})^2 - \kappa^2} + O(\Omega^2). \tag{10.52}$$

At the exceptional points $\kappa = \kappa_{EP,n}^{\pm}$ the eigenvalue branches touch each other

$$\mathrm{Re}\lambda = \pm\frac{1}{2}\sqrt{\frac{2\nu s n_{2s-1,2s}}{\omega_s}}\Omega + O(\Omega^{3/2}). \tag{10.53}$$

The degenerate crossing (10.53) of the real parts has been observed in the model of a rotating circular string, cf. equation (10.19).

Pure dissipative perturbation of the doublets at $\Omega = \Omega_{ss}^{+-} = 0$ yields crossings of the real parts at the branch cuts $\Omega^2 > (\Omega_{EP,d}^{\pm})^2$ in the $(\mathrm{Re}\lambda,\kappa)$-plane and veering of

the imaginary parts

$$\begin{aligned}
\mathrm{Im}\lambda &= \omega_s \pm s\sqrt{\Omega^2 - (\Omega^{\pm}_{EP,d})^2} + O(\kappa),\\
\mathrm{Re}\lambda &= -\frac{\delta \mathrm{tr}\mathbf{D}_{ss}}{4} \pm \frac{\gamma}{16 s\omega_s \sqrt{\Omega^2 - (\Omega^{\pm}_{EP,d})^2}}\delta\kappa + O(\kappa^3),
\end{aligned} \tag{10.54}$$

where $\gamma = 2\mathrm{tr}\mathbf{K}_{ss}\mathbf{D}_{ss} - \mathrm{tr}\mathbf{K}_{ss}\mathrm{tr}\mathbf{D}_{ss}$. At the branch cut $\Omega^2 < (\Omega^{\pm}_{EP,d})^2$ the imaginary parts cross and the real parts avoid crossing

$$\begin{aligned}
\mathrm{Im}\lambda &= \omega_s + \frac{\mathrm{tr}\mathbf{K}_{ss}}{4\omega_s}\kappa \pm \frac{\gamma}{16 s\omega_s \sqrt{(\Omega^{\pm}_{EP,d})^2 - \Omega^2}}\delta\kappa + O(\kappa^2),\\
\mathrm{Re}\lambda &= -\frac{\delta \mathrm{tr}\mathbf{D}_{ss}}{4} \pm s\sqrt{(\Omega^{\pm}_{EP,d})^2 - \Omega^2} + O(\kappa^2).
\end{aligned} \tag{10.55}$$

At $\Omega = \Omega^{\pm}_{EP,d}$ the crossings of both real and imaginary parts are degenerate

$$\begin{aligned}
\mathrm{Re}\lambda &= -\frac{\delta \mathrm{tr}\mathbf{D}_{ss}}{4} \pm \frac{1}{4}\sqrt{-\delta\kappa\frac{\gamma}{\omega_s}} + O(\kappa^{3/2}),\\
\mathrm{Im}\lambda &= \omega_s \pm \frac{1}{4}\sqrt{-\delta\kappa\frac{\gamma}{\omega_s}} + \frac{\mathrm{tr}\mathbf{K}_{ss}}{4\omega_s}\kappa + O(\kappa^{3/2}).
\end{aligned} \tag{10.56}$$

The evolving eigenvalue branches reconstruct the eigenvalue surfaces shown in Figure 10.6. In the one-parameter slices of the surfaces the transformation of the eigenvalue branches from the crossing to the avoided crossing due to variation of parameters Ω and κ occurs after the passage through the exceptional points, where the branches touch each other and the eigenvalue surfaces have the Whitney umbrella singularities. The surface of the imaginary parts shown in Figure 10.6 (a) is formed by two Whitney umbrellas with the handles (branch cuts) glued together when they are oriented toward each other. This singular surface is known in the physical literature on wave propagation in *absorptive* and *chiral* media as the *double-coffee-filter* [52, 260]. The *viaduct* [294] singular surface of the real parts results from gluing the roofs of two Whitney's umbrellas when their handles are oriented outwards, Figure 10.6 (b). The double-coffee-filter singularity is a result of the deformation of MacKay's eigenvalue cone (shown by the dashed lines in Figure 10.6 (a)) by dissipative and nonconservative positional perturbations. The perturbations foliate the plane $\mathrm{Re}\lambda = 0$ into the viaduct which has self-intersections along two branch cuts and an ellipse-shaped arch between the two exceptional points, Figure 10.6 (b). Both types of singular surfaces appear when non-Hermitian perturbation of Hermitian matrices is considered [270].

Therefore, in a weakly non-Hamiltonian system (10.27) *the fundamental qualitative effect of the splitting of the doublets with definite Krein signature is the origination of the double-coffee-filter of the imaginary parts and the viaduct of the real parts. Structural modification of the matrices of dissipative and nonconservative positional forces generically does not change the type of the surfaces, preserving the exceptional points and the branch cuts.*

10.3.4 Unfolding MacKay's cones with mixed Krein signature

The definite Krein signature ($\alpha\beta = +$) implies $D > 0$ and $N > 0$ and thus uniquely determines the type of singular surface for the real and imaginary parts of the perturbed eigenvalues. The case of the mixed Krein signature ($\alpha\beta = -$) possesses several scenarios for the unfolding of MacKay's cones by non-Hamiltonian perturbation, because D and N can have different signs.

When $D > 0$ and $N > 0$, the imaginary parts of the eigenvalues form the double-coffee-filter singular surface whereas the real parts originate the viaduct; see Figure 10.6. For negative D and negative N, the type of surfaces is interchanged: the imaginary parts form the viaduct and the real parts originate the double-coffee-filter singular surface; see Figure 10.7 (a).

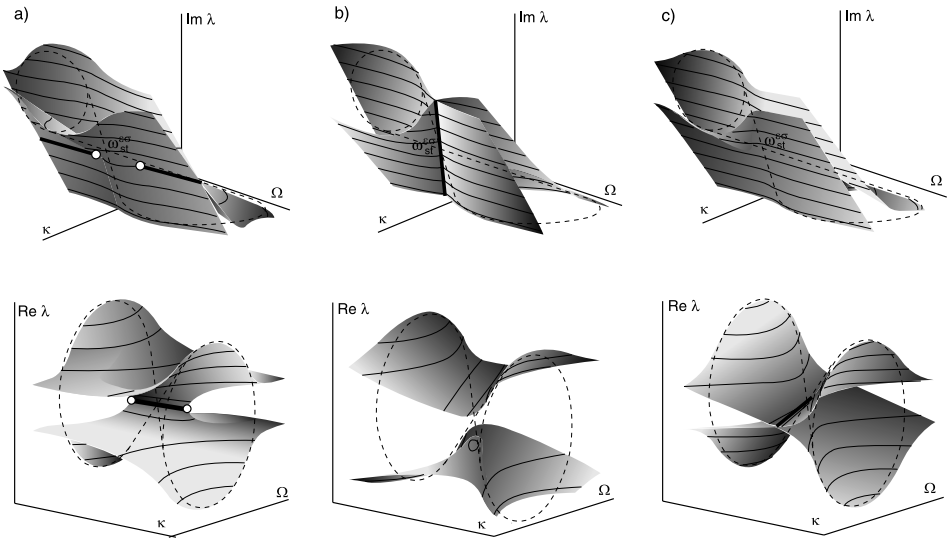

Figure 10.7. Mixed Krein signature ($\alpha\beta = -$): (a) The viaduct $\mathrm{Im}\lambda(\Omega, \kappa)$ and the double-coffee-filter $\mathrm{Re}\lambda(\Omega, \kappa)$ for $D < 0$ and $N < 0$; (b) the surfaces $\mathrm{Im}\lambda(\Omega, \kappa)$ crossed along the branch cut (bold line) and the separated surfaces $\mathrm{Re}\lambda(\Omega, \kappa)$ for $D < 0$, $N > 0$; (c) separated surfaces of imaginary parts and crossed surfaces of real parts for $D > 0$, $N < 0$ [294].

Exceptional points are not created for negative values of N/D. In this case the eigenvalue surfaces either intersect each other along the branch cut, which projects into the line $\mathrm{Im}c = 0$ in the (Ω, κ)-plane, or do not cross at all. When $N > 0$, the surfaces of the imaginary parts $\mathrm{Im}\lambda(\Omega, \kappa)$ cross and the surfaces $\mathrm{Re}\lambda(\Omega, \kappa)$ avoid crossing, Figure 10.7 (b). For $N < 0$ the surfaces of the imaginary parts are separated and that of the real parts cross, Figure 10.7 (c).

10.3.5 Indefinite damping as a reason for subcritical flutter

When typical unfolding of MacKay's cones and thus the singular geometry of the surfaces of the growth rates is established, we can determine the typical configuration of stability diagrams associated with the splitting of a given double eigenvalue of the Campbell diagram. For brevity we focus our efforts on the crossings at $\Omega = 0$, using the expressions (10.41) and (10.42).

Stability conditions, following from equations (10.41) and (10.42) under the requirement $\mathrm{Re}\lambda < 0$, are $\delta \mathrm{tr}\mathbf{D}_{ss} > 0$ and $B > 0$, where

$$\begin{aligned} B = {} & (2\Omega s(\delta^2\omega_s^2(\mathrm{tr}\mathbf{D}_{ss})^2 - 4\nu^2 n_{2s-1,2s}^2) + 4\beta_\circ(\rho_1(\mathbf{K}_{ss}) - \rho_2(\mathbf{K}_{ss}))\delta\kappa\nu n_{2s-1,2s})^2 \\ & - \delta^2(\mathrm{tr}\mathbf{D}_{ss})^2(\delta^2\omega_s^2(\mathrm{tr}\mathbf{D}_{ss})^2 - 4\nu^2 n_{2s-1,2s}^2)(\nu^2 n_{2s-1,2s}^2 - \delta^2\omega_s^2 \det \mathbf{D}_{ss}) \\ & + \delta^2(\mathrm{tr}\mathbf{D}_{ss})^2(A\delta^2\omega_s^2 - \nu^2 n_{2s-1,2s}^2(\rho_1(\mathbf{K}_{ss}) - \rho_2(\mathbf{K}_{ss}))^2)\kappa^2. \end{aligned} \tag{10.57}$$

The coefficient A can be represented in the two equivalent forms:

$$\begin{aligned} A = {} & \det \mathbf{D}_{ss}(\rho_1(\mathbf{K}_{ss}) - \rho_2(\mathbf{K}_{ss}))^2 \\ & + (d_{2s-1,2s}(k_{2s-1,2s-1} - k_{2s,2s}) - k_{2s-1,2s}(d_{2s-1,2s-1} - d_{2s,2s}))^2 \\ = {} & \frac{((\mathrm{tr}\mathbf{D}_{ss})^2 - 16\beta_\circ^2)(\rho_1(\mathbf{K}_{ss}) - \rho_2(\mathbf{K}_{ss}))^2}{4}, \end{aligned} \tag{10.58}$$

where

$$\beta_\circ = \frac{2\mathrm{tr}\mathbf{K}_{ss}\mathbf{D}_{ss} - \mathrm{tr}\mathbf{K}_{ss}\mathrm{tr}\mathbf{D}_{ss}}{4(\rho_1(\mathbf{K}_{ss}) - \rho_2(\mathbf{K}_{ss}))}. \tag{10.59}$$

Assuming $\nu = 0$, the expression $B = 0$ is simplified to

$$\kappa^2 A + s^2\Omega^2(2\omega_s \mathrm{tr}\mathbf{D}_{ss})^2 = -\det \mathbf{D}_{ss}(\omega_s \mathrm{tr}\mathbf{D}_{ss})^2\delta^2. \tag{10.60}$$

For the definite submatrix $\mathbf{D}_{ss}$ we have $A > 0$ because $\det \mathbf{D}_{ss} > 0$. Consequently, for $\delta\mathbf{D}_{ss} > 0$ the stability conditions

$$\delta \mathrm{tr}\mathbf{D}_{ss} > 0, \quad \kappa^2 A + s^2\Omega^2(2\omega_s \mathrm{tr}\mathbf{D}_{ss})^2 > -\det \mathbf{D}_{ss}(\omega_s \mathrm{tr}\mathbf{D}_{ss})^2\delta^2 \tag{10.61}$$

are always fulfilled, which means that both eigenvalues born in the unfolding of the diabolical point have negative real parts, implying asymptotic stability of the corresponding modes.

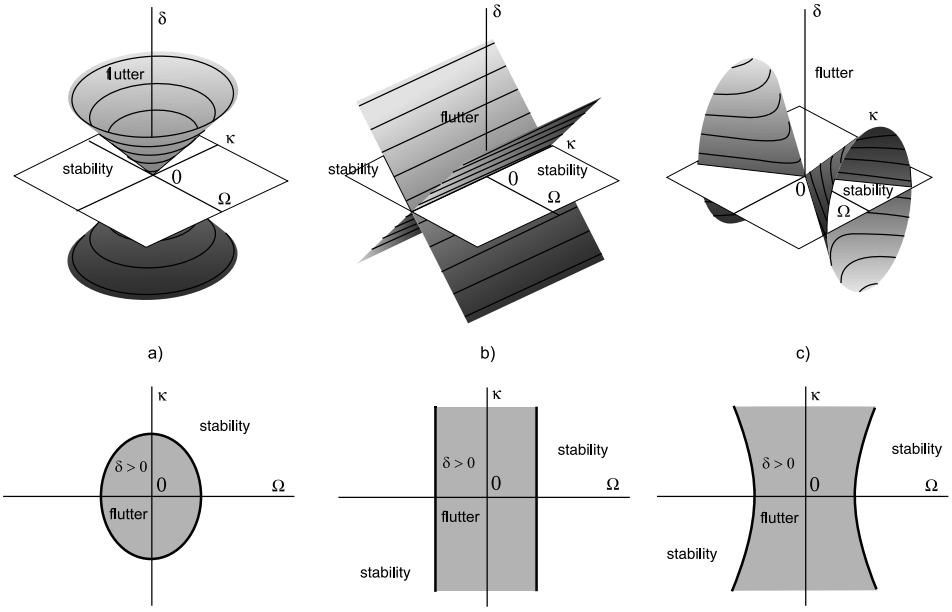

Figure 10.8. Domain of subcritical flutter associated with the double eigenvalue $i\omega_s$ at $\Omega = 0$ for the indefinite submatrix $\mathbf{D}_{ss}$ in the absence of circulatory forces when (a) $A > 0$, (b) $A = 0$, and (c) $A < 0$ [297].

However, an *indefinite* submatrix $\mathbf{D}_{ss}$ of the damping matrix $\mathbf{D}$ has $\det \mathbf{D}_{ss} < 0$. In this case, the inequalities (10.61) indicate that in the (Ω, κ, δ)-space the flutter instability domain is inside the conical surface extended (when $A > 0$) along the δ-axis. The stability domain is adjacent to the cone's skirt selected by the condition $\delta \mathrm{tr}\mathbf{D}_{ss} > 0$, see Figure 10.8 (a). The conical domain is stretched along the κ-axis when A tends to zero and is transformed into a dihedral angle when $A = 0$, as shown in Figure 10.8 (b).

With the further decrease in A, the dihedral angle is again wrapped into the conical surface which is then extended along the Ω-axis, Figure 10.8 (c). The domain of asymptotic stability is inside the half of the cone selected by the inequality $\delta \mathrm{tr}\mathbf{D}_{ss} > 0$. Note that the threshold $A = 0$, separating the indefinite damping matrices, coincides with that found in [290] from the criteria of Routh and Hurwitz for a general two-dimensional nonconservative gyroscopic system with dissipation.

In the (Ω, κ)-plane for a fixed $\delta > 0$ the instability domain has, respectively, the form of an ellipse, Figure 10.8 (a), a stripe, Figure 10.8 (b), or a region contained between the branches of a hyperbola, Figure 10.8 (c). The latter picture shows that even considerable stiffness modification separating the eigenvalue branches of the undamped system cannot always prevent the development of flutter instability in the presence of indefinite damping (Figure 10.9 (a, b)), which originates, e.g., at the frictional contact when the friction-velocity gradient is negative [340, 541].

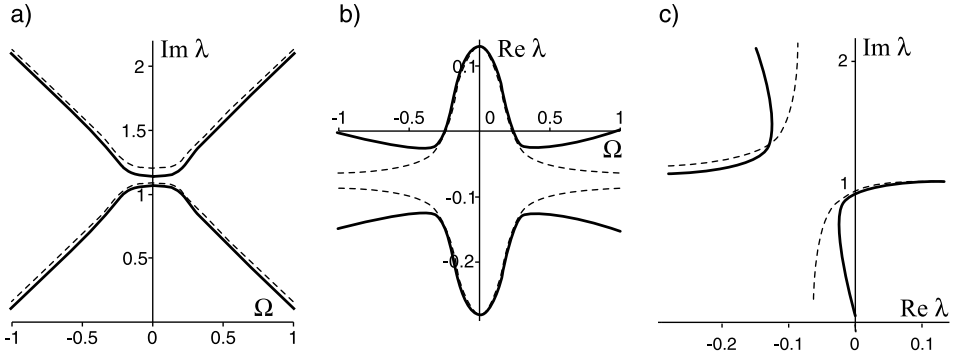

Figure 10.9. Numerically calculated eigencurves (bold lines) and their approximations (10.41) and (10.42) (dashed lines) for an indefinite damping matrix $\mathbf{D}_{ss}$ with $d_{2s-1,2s-1} = -1$, $d_{2s,2s} = 2$, and $d_{2s-1,2s} = 0$ when $\omega_s = 1$, $k_{2s-1,2s-1} = 1$, $k_{2s,2s} = 2$, $k_{2s-1,2s} = 1$ (i.e. $A = -1$) and $\nu = 0$, $\kappa = 0.2$, and $\delta = 0.3$.

Indeed, with the variation of the speed Ω, the eigenvalues (10.41) move along the branches of the hyperbola in the complex plane (see Figure 10.9 (c))

$$\left(\mathrm{Re}\lambda + \frac{\mathrm{tr}\mathbf{D}_{ss}}{4}\delta\right)\left(\mathrm{Im}\lambda - \omega_s - \frac{\mathrm{tr}\mathbf{K}_{ss}}{4\omega_s}\kappa\right) = -\frac{\mathrm{Im}c}{2}. \tag{10.62}$$

When $\mathrm{Im}c \equiv 0$ strong modal resonance occurs with the coupling of eigenvalues at $\mathrm{Re}\lambda = -\frac{\mathrm{tr}\mathbf{D}_{ss}}{4}\delta$ and $\mathrm{Im}\lambda = \omega_s + \frac{\mathrm{tr}\mathbf{K}_{ss}}{4\omega_s}\kappa$. This new double eigenvalue has only one eigenvector and strongly influences the eigenvalue trajectories for small values of κ and δ when $\mathrm{Im}c \neq 0$ and is known to be a precursor to flutter instability, e.g., in hydrodynamics [246] and in electrical circuits [157].

The branch crossing the imaginary axis from left to right is determined by the sign of $\mathrm{Im}c$. Assuming $\mathrm{Re}\lambda = 0$ in equation (10.62), we find the eigenfrequency of the mode at the onset of self-excited vibrations to be close to ω_s

$$\omega_{cr} = \omega_s + \kappa\frac{\mathrm{tr}\mathbf{K}_{ss}\mathrm{tr}\mathbf{D}_{ss} - \mathrm{tr}\mathbf{K}_{ss}\mathbf{D}_{ss}}{2\omega_s\mathrm{tr}\mathbf{D}_{ss}}. \tag{10.63}$$

Bifurcation of the stability diagrams with the change of entries to matrices $\mathbf{D}$ and $\mathbf{K}$ shows a way to explain the famous unsatisfactory reproducibility of experiments with the squealing disk brakes [461]. Indeed, some parameters like rotational speed and pressure on the brake pads can be regulated precisely, while the topography of the pads' surface as well as the material properties of the pads unavoidably undergo uncontrollable changes from one run of the experiment to the next. As a consequence, the very same values of stiffness parameter κ and rotational speed Ω, which yield flutter instability (squeal) for $A < 0$, Figure 10.8 (c), make the system stable (brake quiet) for $A > 0$ owing to the qualitative change of the stability diagram with the change in the structure of matrices $\mathbf{D}$ and $\mathbf{K}$, Figure 10.8 (a). This effect becomes even

more pronounced in the presence of nonconservative positional forces, because, as we show in the following, the conical stability boundaries are not structurally stable under small circulatory perturbation, $\nu\mathbf{N}$.

10.3.6 Destabilizing role of circulatory forces

For the fixed parameters $\delta \neq 0$ and $\nu \neq 0$ the equation $B = 0$ generically describes either an ellipse or a hyperbola in the (Ω, κ)-plane, Figure 10.10 (b, d).

In the case of indefinite damping matrix $\mathbf{D}_{ss}$ with $A > 0$ and δ large enough, the domain of subcritical flutter is inside the ellipse $B = 0$, and the domain of asymptotic stability is outside the ellipse similarly to the system without nonconservative

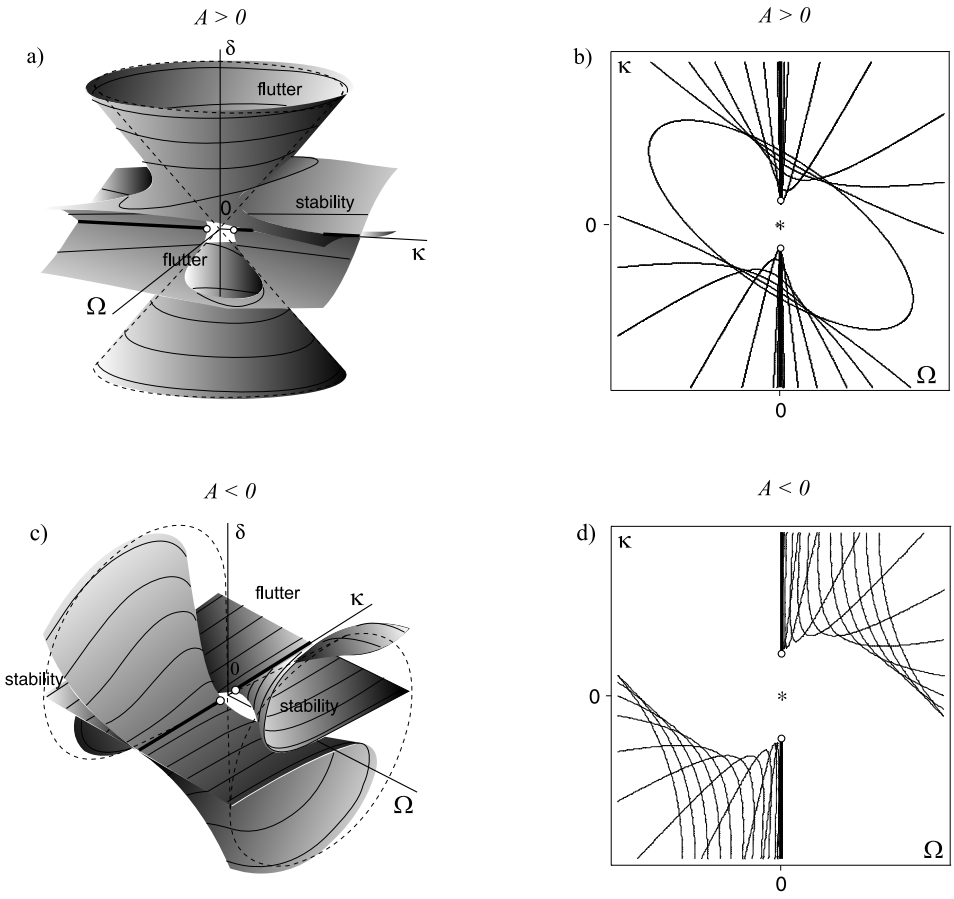

Figure 10.10. Unfolding the conical boundary of subcritical flutter created by the indefinite matrix $\mathbf{D}_{ss}$ (dashed lines) by the perturbation $\nu\mathbf{N}$ into a couple of Whitney's umbrellas with their level curves at $\delta > 0$ when (a, b) $A > 0$ and (c, d) $A < 0$.

positional forces, whose stability diagram is shown in Figure 10.8 (a). With the decrease in δ at the fixed $\nu \neq 0$ the ellipse is rotating around the origin in the (Ω, κ)-plane and simultaneously it is stretching along one of its main axes. At the threshold $A\delta^2\omega_s^2 = \nu^2 n_{2s-1,2s}^2(\rho_1(\mathbf{K}_{ss}) - \rho_2(\mathbf{K}_{ss}))^2$ the ellipse is transformed into two parallel lines, which with the further decrease in δ are bent into two branches of hyperbola $B = 0$. Then, the flutter instability domain lies between the two branches, Figure 10.10 (b). When δ tends to zero, the hyperbolic branches are shrunk to the union of the intervals $(-\infty, \kappa_{EP,n}^-] \bigcup [\kappa_{EP,n}^+, \infty)$ of the κ-axis, where the critical values $\kappa_{EP,n}^{\pm}$ are defined by equation (10.50). The exceptional points $(\Omega = 0, \kappa = \kappa_{EP,n}^{\pm}, \delta = 0)$ are shown as open circles in Figure 10.10.

In the vicinity of the EPs, the expression $B = 0$ yields a linear approximation to the stability boundary

$$\Omega = \frac{4\beta_\circ \kappa \pm \mathrm{tr}\mathbf{D}_{ss}\sqrt{\kappa^2 - (\kappa_{EP,n}^{\pm})^2}}{4\kappa_{EP,n}^{\pm}}\delta + o(\delta). \tag{10.64}$$

Thus, in the (Ω, δ)-plane the domain of asymptotic stability is bounded in the first-order approximation by the two straight lines (10.64). When κ goes to $\kappa_{EP,n}^{\pm}$, the slopes of both lines Ω/δ tend to the value $\Omega/\delta = \pm\beta_\circ$, where $\beta_\circ$ is defined by equation (10.59). Extracting κ from the equation (10.64) we find another representation for the stability boundary near exceptional points

$$\begin{aligned}\kappa = \kappa_{EP,n}^{\pm} &\frac{4(\Omega/\delta)\beta_\circ \pm \mathrm{tr}\mathbf{D}_{ss}\sqrt{(\Omega/\delta)^2 - \beta_\circ^2 + \left(\frac{\mathrm{tr}\mathbf{D}_{ss}}{4}\right)^2}}{4\beta_\circ^2 - \left(\frac{\mathrm{tr}\mathbf{D}_{ss}}{2}\right)^2} \\ &\approx \kappa_{EP,n}^{\pm}\left[1 + 8\left(\frac{\Omega/\delta \mp \beta_\circ}{\mathrm{tr}\mathbf{D}_{ss}}\right)^2\right],\end{aligned} \tag{10.65}$$

which has a canonical form for Whitney's umbrella $Z = X^2/Y^2$ [17].

Therefore, we explicitly demonstrated that the conical boundary of the domain of subcritical flutter, existing for indefinite $\mathbf{D}_{ss}$ and $A > 0$ (Figure 10.8 (a)), is structurally unstable under the circulatory perturbation, $\nu\mathbf{N}$.

With increasing ν from zero, the cone opens up and simultaneously the plane $\delta = 0$ foliates into two sheets intersecting along the branch cuts $\left(\pm\infty, \kappa_{EP,n}^{\pm}\right]$ on the κ-axis, which are marked by bold lines in Figure 10.10. The new surface has a couple of Whitney's umbrella singularities at the exceptional points $(0, \kappa_{EP,n}^{\pm}, 0)$.

The domain of asymptotic stability, which for $\nu = 0$ was adjacent to the conical domain of subcritical flutter, is now wrapped into the pockets of the two Whitney's umbrellas, selected by the inequality $\delta \mathrm{tr}\mathbf{D}_{ss} > 0$.

With the increase in δ the stability boundary gradually tends to the conical surface with the flutter instability inside it, Figure 10.10 (a).

Inclusion of the nonconservative forces qualitatively changes the stability diagram in the (Ω, κ)-plane transforming the elliptic flutter domain to a larger one located between the hyperbolic branches, Figure 10.10 (b). For $\nu = 0$ and $\delta = 0$ the (Ω, κ)-plane is stable, while for $\nu \neq 0$ and $\delta \to 0$ the stability domain dramatically shrinks to the branch cuts $(\pm\infty, \kappa^{\pm}_{EP,n}]$. Consequently, under small perturbation $\nu\mathbf{N}$ a point in the (Ω, κ)-plane, which was in the stability domain for $\nu = 0$, can suddenly find itself in the instability region when $\nu \neq 0$, similarly to the scenario described in the previous section.

When $\mathbf{D}_{ss}$ is indefinite and $A < 0$, the conical stability boundary of Figure 10.8 (c) unfolds into two surfaces with Whitney's umbrella singularities at the exceptional points $(0, \kappa^{\pm}_{EP,n}, 0)$ as shown in Figure 10.10 (c). The local approximations to the surfaces near the singularities are given by the same equation (10.64), where $\beta_\circ$ has a value different from the case when $A > 0$. For $\nu = 0$ and $\delta \neq 0$, the stability domain in the (Ω, κ)-plane is inside the two hyperbolic regions extended along the Ω-axis, as shown in Figure 10.8 (c). When $\nu \neq 0$, with the decrease of δ the stability domain rotates around the origin until it is completely reoriented and shrunk into the branch cuts $(\pm\infty, \kappa^{\pm}_{EP,n}]$ extended along the κ-axis, Figure 10.10 (d). Due to such a reorientation one can again observe sudden stabilization/destabilization at the very same values of Ω and κ when ν is slightly changed.

In the absence of damping ($\delta = 0$) the gyroscopic system with the potential and nonconservative positional forces cannot be asymptotically stable in accordance with the Bottema–Lakhadanov–Karapetyan theorem [80, 257, 342]. It is unstable almost everywhere in the space of the parameters and can be only marginally stable at the points of the branch cut, which is a set of measure zero. Introduction of damping into the gyroscopic system with nonconservative positional forces leads to the origination of zones of asymptotic stability, either intersecting with the κ-axis, Figure 10.10 (b), or not, Figure 10.10 (d).

Finally, it is instructive to find the stability diagram in the case when the damping submatrix $\mathbf{D}_{ss}$ is positive definite and $\nu \neq 0$. The result is presented in Figure 10.11 (a). In contrast to the case when $\mathbf{D}_{ss}$ is indefinite, at $\nu = 0$ and $\delta \geq 0$ the eigenvalues born in the unfolding of the diabolical point have nonpositive real parts, hence the points of the (Ω, κ)-plane in the (Ω, κ, δ)-space correspond to marginal stability. When, however, we put additionally $\nu \neq 0$, the (Ω, κ)-plane in the vicinity of the origin foliates into the viaduct singular surface, Figure 10.11 (a). Its part, selected by the constraint $\delta > 0$ separates the regions of subcritical flutter and asymptotic stability. Unlike the case of indefinite $\mathbf{D}_{ss}$, there is an upper bound for the variation of δ, above which both eigenvalues have negative real parts. In the vicinity of the exceptional points the stability diagram has a typical form for a circulatory system perturbed by dissipative and gyroscopic forces with the Whitney umbrella singularity [288].

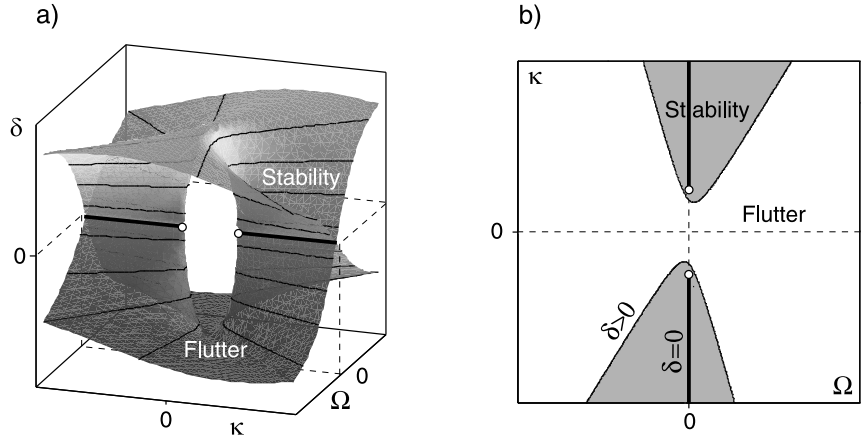

Figure 10.11. When $\nu \neq 0$, $\mathbf{D}_{ss} > 0$ and thus $A > 0$, the boundary between the domains of subcritical flutter and asymptotic stability is a part of the viaduct surface selected by the condition $\delta > 0$. In contrast to the case when $\mathbf{D}_{ss}$ is indefinite, a system unstable at small κ and Ω can be stabilized by large enough values of δ.

10.4 Example: eigenvalue surfaces of the rotating circular string

We return to the problem of stability of a rotating circular string that is loaded by potential, damping, and nonconservative forces at a point in space, through which it passes, see Figure 10.1 (a).

Recall that for $d = 0$, $k = 0$, and $\mu = 0$ the eigenvalue problem (10.2), (10.3) has the eigenvalues $\lambda_n^{\varepsilon} = in(1 + \varepsilon\Omega)$, $\lambda_m^{\delta} = im(1 + \delta\Omega)$, where $\varepsilon, \delta = \pm$ and $n, m \in \mathbb{Z} - \{0\}$. In the $(\Omega, \mathrm{Im}\lambda)$-plane the branches intersect at the nodes $(\Omega_{nm}^{\varepsilon\sigma}, \omega_{nm}^{\varepsilon\sigma})$ with $\Omega_{nm}^{\varepsilon\sigma}$ and $\omega_{nm}^{\varepsilon\sigma}$ defined by equation (7.79) Intersections of the eigencurve with $n = 1$ and $\varepsilon = +$ and those with $m > 0$ and $\delta = -$ in the subcritical range ($|\Omega| < 1$) are marked in Figure 10.12 (a) by black filled circles.

Taking into account that $\sigma = -\varepsilon$ at all the crossings, excluding $(\Omega_{n,-n}^{\varepsilon\varepsilon} = \pm 1, \omega_{n,-n}^{\varepsilon\varepsilon} = 0)$ where $\sigma = \varepsilon$, from equations (10.11) and (10.12) we find approximation to the real and imaginary parts of the perturbed nonzero double eigenvalues [293, 294]

$$\mathrm{Re}\lambda = -d\frac{n+m}{8\pi nm}\omega_{nm}^{\varepsilon\sigma} \pm \sqrt{\frac{|c| - \mathrm{Re}c}{2}},$$
$$\mathrm{Im}\lambda = \omega_{nm}^{\varepsilon\sigma} + \varepsilon\frac{n-m}{2}\Delta\Omega + \frac{n+m}{8\pi nm}k \pm \sqrt{\frac{|c| + \mathrm{Re}c}{2}}, \qquad (10.66)$$

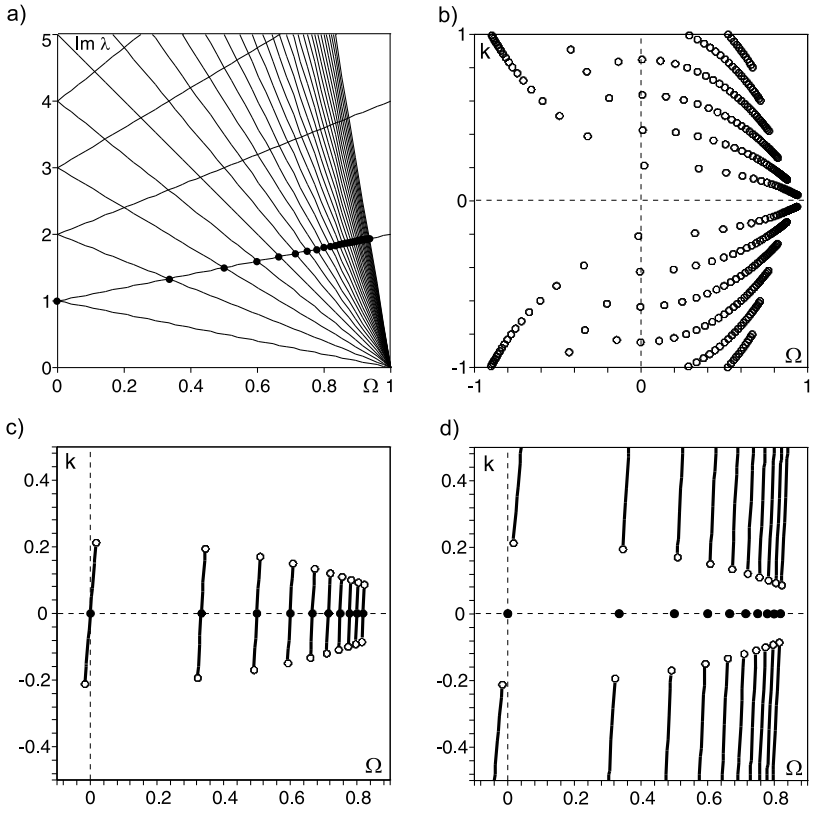

Figure 10.12. (a) The Campbell diagram of the unperturbed rotating string with the filled circles marking the nodes with $n = 1$; (b) distribution (10.69) of the exceptional points (open circles) in the subcritical speed range in the (Ω, k)-plane when $\mu = 0.3$ and $d = 0.3$; (c) projections of the branch cuts (10.70) of the double-coffee-filters $\mathrm{Im}\lambda(\Omega, k)$ and the exceptional points for $n = 1$; (d) projections of the branch cuts (10.70) of the viaducts $\mathrm{Re}\lambda(\Omega, k)$ and the exceptional points for $n = 1$. Black filled circles show locations of the diabolical points.

where $\Delta\Omega = \Omega - \Omega_{nm}^{\varepsilon\sigma}$, and for the complex coefficient c we have

$$\mathrm{Im}c = k\frac{2d\omega_{nm}^{\varepsilon\sigma} - \varepsilon\mu(n-m)}{16\pi^2 nm} - 2\left(\varepsilon\frac{n+m}{2}\Delta\Omega + \frac{m-n}{8\pi nm}k\right)\left(\frac{\varepsilon}{4\pi}\mu - d\frac{m-n}{8\pi nm}\omega_{nm}^{\varepsilon\sigma}\right), \quad (10.67)$$

and

$$\mathrm{Re}c = \left(\frac{\varepsilon n - \sigma m}{2}\Delta\Omega + \frac{m-n}{8\pi nm}k\right)^2 + \frac{k^2}{16\pi^2 nm} - \frac{\left[d(m+n)\omega_{nm}^{\varepsilon\sigma}\right]^2}{64\pi^2 n^2 m^2}. \quad (10.68)$$

Setting $\mathrm{Re}c = 0$ and $\mathrm{Im}c = 0$ we find the coordinates of the projections of the exceptional points of the surfaces $\mathrm{Re}\lambda(\Omega, k)$ and $\mathrm{Im}\lambda(\Omega, k)$ onto the (Ω, k)-plane

$$\Omega_{EP} = \Omega_{nm}^{\varepsilon\sigma} \pm \frac{\varepsilon}{8\pi nm} \frac{(m+n)d^2{\omega_{nm}^{\varepsilon\sigma}}^2}{\sqrt{nm(\mu^2 nm + d^2{\omega_{nm}^{\varepsilon\sigma}}^2)}},$$
$$k_{EP} = \pm \frac{d\omega_{nm}^{\varepsilon\sigma}(2\varepsilon\mu nm - d(m-n)\omega_{nm}^{\varepsilon\sigma})}{2\sqrt{nm(\mu^2 nm + d^2{\omega_{nm}^{\varepsilon\sigma}}^2)}}. \tag{10.69}$$

As in equations (10.48), the existence of the exceptional points (10.69) depends on the Krein signature of the intersecting branches, i.e. on the sign of nm, where $n, m \in \mathbb{Z} - \{0\}$. In the case of the rotating string, all the crossings in the subcritical speed range ($|\Omega| < 1$) have definite Krein signature ($nm > 0$). For those in the supercritical speed range ($|\Omega| > 1$) it is mixed with $nm < 0$. In the (Ω, κ)-plane the exceptional points are situated on the lines $\mathrm{Im}c = 0$:

$$k = 2\pi\varepsilon(n+m)\frac{2\varepsilon nm\mu - d\omega_{nm}^{\varepsilon\sigma}(m-n)}{d\omega_{nm}^{\varepsilon\sigma}(m^2+n^2)}\Delta\Omega. \tag{10.70}$$

Note that only exceptional points originated after the perturbation of the doublets with $\Omega_{nn}^{+-} = 0$ by pure damping ($\mu = 0$) are situated on the Ω-axis because $k_{EP} = 0$. That is why damping creates a perfect bubble of instability in the $(\Omega, \mathrm{Re}\lambda)$-plane for the double eigenvalues with $m = n$ and imperfect bell-shaped ones for those with $m \neq n$ [293, 604].

In Figure 10.12 (b) we show the exceptional points (10.69) of the string passing through the eyelet with the damping coefficient $d = 0.3$ and the friction coefficient $\mu = 0.3$. The exceptional points in the (Ω, κ)-plane are distributed over a large area, which preserves its form independently of the number of points involved. In comparison with numerical methods, our perturbation approach gives efficient explicit and interpretable expressions for the distribution of exceptional points, for the branch cuts, and for the very eigenvalue surfaces.

In Figure 10.12 (c) we plot the exceptional points originated after the splitting of the diabolical points with $n = 1$ and $\varepsilon = 1$ together with the projections of the branch cuts (10.70) of the double-coffee-filters $\mathrm{Im}\lambda(\Omega, k)$, which are shown by the bold lines. The corresponding projections of the branch cuts (10.70) of the viaducts $\mathrm{Re}\lambda(\Omega, k)$ are presented in Figure 10.12 (d).

Approximations (10.66) to the eigenvalue surfaces of a string with $\mu = 0.3$ and $d = 0.3$ are presented in Figure 10.13 for $n = 1$, $m = 2$, $\varepsilon = +$, and $\delta = -$. Since the corresponding diabolical point is in the subcritical range, the Krein signature of the double semisimple eigenvalue is definite. Then, the eigenfrequencies of the perturbed string originated after the splitting of the double eigenvalue λ_{12}^{+-} form the double-coffee-filter singular surface, Figure 10.13 (a). The corresponding growth rates constitute the viaduct singular surface that is almost completely submerged under the $(\mathrm{Re}\lambda = 0)$-plane (shown in black in Figure 10.13 (b)). The excess of the surface of the

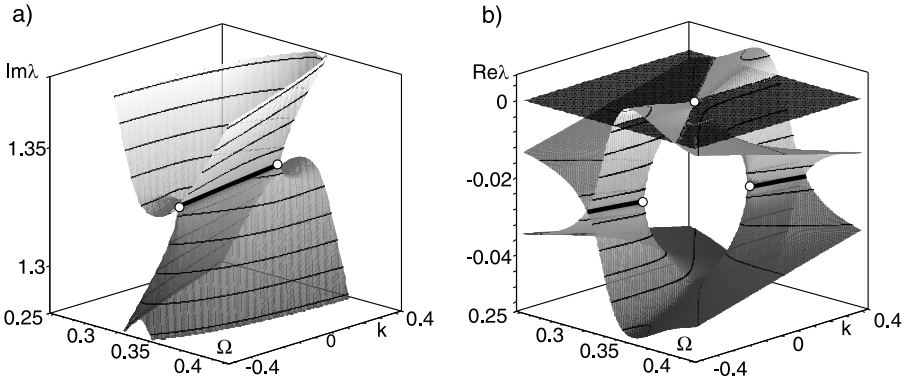

Figure 10.13. For $d = 0.3$ and $\mu = 0.3$: (a) the double-coffee-filter $\mathrm{Im}\lambda(\Omega, k)$ in the vicinity of the crossing $(n = 1, m = 2)$; (b) the corresponding viaduct $\mathrm{Re}\lambda(\Omega, k)$.

growth rates above the $(\mathrm{Re}\lambda = 0)$-plane means flutter in the subcritical speed range. The cross-section of the viaduct by this plane yields the linear approximation (10.21) to the instability tongue, cf. Figure 10.4 (c) and Figure 10.13 (b).

In Figure 10.14 we show in the complex plane the parent diabolical points (open boxes) and the corresponding exceptional points (open circles) whose locations are

$$\mathrm{Re}\lambda_{EP} = -\frac{d}{4\pi}, \quad \mathrm{Im}\lambda_{EP} = \frac{2nm}{n+m} \pm \frac{d}{4\pi}\frac{(m+n)\mu + 2d\varepsilon(n-m)}{\sqrt{\mu^2(m+n)^2 + 4d^2nm}}. \tag{10.71}$$

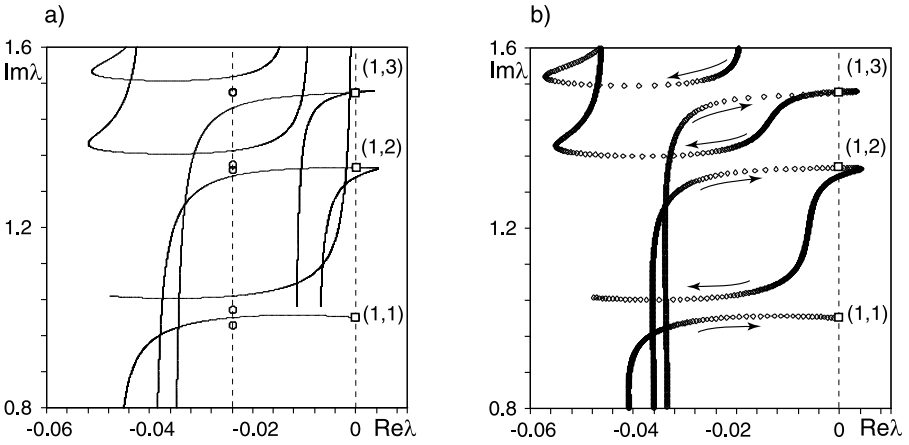

Figure 10.14. Exceptional points (open circles) with the parent diabolical points (open boxes) with $n = 1$, $\varepsilon = 1$ and $m = 1, 2, 3$, $\delta = -1$ in the complex plane when $d = 0.3$, $\mu = 0.3$, and $k = 0.3$. The trajectories $\lambda(\Omega)$ when Ω decreases from 1 to 0, calculated (a) by formula (10.66) and (b) by $N = 3$-Galerkin approximation (10.4). Growth rates are positive (flutter) near the double eigenfrequencies ω_{12}^{+-} and ω_{13}^{+-} of the string at rest.

In the engineering literature it was observed that the spectral exceptional points (strong modal resonances [157]) in the left half of the complex plane are precursors to flutter instability because of their strong influence on the movement of eigenvalues in the complex plane, see also [530]. In hydrodynamics it is believed that the sudden changes of direction of the movement of eigenvalues are "due to the nearby presence of multiple-eigenvalue points" [246]. Similar effects were observed in magnetohydrodynamics [309] and laser physics [380].

Figure 10.14 demonstrates the approximation of the 'dynamics' of eigenvalues in the vicinity of exceptional points, calculated by the formulas (10.66), which is in good qualitative and quantitative agreement with the numerical calculations based on the $N = 3$-Galerkin approximation (10.4). When Ω decreases from 1 to 0, the eigenvalues move in the left part of the complex plane until they pass nearby the locations of the exceptional points originated after the splitting of the double semisimple eigenvalues $i\omega_{11}^{+-}$, $i\omega_{12}^{+-}$, and $i\omega_{13}^{+-}$. Then, in each pair of interacting eigenvalues one suddenly turns to the right and approaches the imaginary axis in the vicinity of the frequencies ω_{11}^{+-}, ω_{12}^{+-}, or ω_{13}^{+-}, respectively, of the string at rest, Figure 10.14. More precisely, according to the formulas (10.66), the critical frequency at the onset ($\mathrm{Re}\lambda = 0$) of subcritical flutter instability of the rotating string is either $\omega_{cr,1} = \omega_{nm}^{\varepsilon\sigma}$ or

$$\omega_{cr,2} = \omega_{nm}^{\varepsilon\sigma} + k\frac{m+n}{4\pi}\frac{\mu(\mu - 2\varepsilon\Omega_{nm}^{\varepsilon\sigma}d)}{(\mu n - \varepsilon\omega_{nm}^{\varepsilon\sigma}d)(\mu m + \varepsilon\omega_{nm}^{\varepsilon\sigma}d)}. \tag{10.72}$$

Formula (10.72) explicitly confirms the proximity of the audible frequency of friction-induced vibrations to the frequency of free vibrations of a solid of revolution observed in experiments. The critical frequency $\omega_{cr,2}$ can acquire both higher and lower values than $\omega_{nm}^{\varepsilon\sigma}$, being however close to it when k is small. On the contrary, since the nonconservative parameters μ and d are both in the numerator and denominator of the formula (10.72), their ratio can take large values even when these parameters are vanishing, which may enhance the deviation of the unstable frequency from $\omega_{nm}^{\varepsilon\sigma}$.

10.5 How to play a disk brake?

Supporting an attractive thesis by Mottershead and Chan [432] that subcritical "flutter instabilities in brake systems occur primarily as a result of symmetry [breaking]; the frictional mechanism which has been the subject of much research over the past forty years is of secondary importance," the sensitivity analysis of the present chapter demonstrates how the nodes of the spectral mesh, situated in the subcritical range, may serve as a 'keyboard' of a rotating elastic solid of revolution.

Frictional contact is a source of non-Hamiltonian and symmetry-breaking perturbations. In the vicinity of the 'keys' of the 'keyboard' damping creates eigenvalue bubbles, which are dangerous by virtue of their ability to get positive real parts in the presence of nonconservative positional forces, or even without them if the damping matrix is indefinite. The activated bubbles of instability cause subcritical flutter of a rotating structure, forcing it to vibrate at a frequency close to the double frequency of the node and at the angular velocity close to that of the node.

Selection of the unstable modes that cause self-excited vibrations in the subcritical speed range is governed by the exceptional points at the corners of the singular eigenvalue surfaces, 'double-coffee-filter' and 'viaduct', that are sharply associated with the crossings of the unperturbed Campbell diagram with definite Krein signature.

Generically, the structure of the perturbing matrices determines only the details of the geometry of the surfaces, such as the coordinates of the exceptional points and the spacial orientation of the branch cuts. It does not yield the qualitative changes irrespective of whether dissipative and circulatory perturbations are applied separately or in a mixture. The two eigenvalue surfaces found unite seemingly different problems on friction-induced instabilities in rotating elastic continua, because their existence does not depend on the specific model of the rotor-stator interaction and is dictated by the Krein signature of the eigenvalues of the isotropic rotor and by the nonconservative nature of the forces originated at the frictional contact.

The double-coffee-filter singularity and its viaduct companion are true symbols of instabilities causing the wine glass to sing and the brake to squeal that connect these phenomena of wave propagation in rotating continua with the physics of non-Hermitian singularities associated with wave propagation in stationary absorptive and chiral media [52], which we will consider in detail in the next chapter.

Chapter 11

Non-Hermitian perturbation of Hermitian matrices with physical applications

> *By the various sections of this solid, in several positions ... divers new lines must arise, in a great variety, different from those arising from the section of a cone. Some of which ... might be of good use in the building of ships.*
>
> John Wallis, *Cono-cuneus* [591]

In 1662 Peter Pett (1610–1672), Commissioner of the Navy and son of a King's Master Shipwright, in an attempt to produce ship hulls of least resistance, visited a famous Oxford mathematician John Wallis[1] (1616–1703). Wallis was asked for help with respect to a specific geometric solid that Pett intended to use in shaping a new shipwright's tool for laying off vessels [402]. The so-called *shipwright's circular wedge* was thought to consist of progressively curved strips of wood, which could then be disassembled, much like a half hull. What mathematical law should determine the variation of the curvature?

Wallis proposed to model ship hulls using a universal ruled surface generated by a line (imagine a plank of wood) moving on two directors, one of which is rectilinear and perpendicular to all generators (imagine a bow of a ship as a simple upright line meeting a level keel at the bottom in a right angle), and the other (situated midship) is a circle perpendicular to the plane which contains its center and the other director, Figure 11.1 (left). Extending the basic conoid shape through the vertical (bow) line into its reflection [402], Wallis found the equation of the surface to be

$$c^2x^2 = y^2(a^2 - z^2), \tag{11.1}$$

where a is the radius of the circular director and c the distance of its center on the y-axis from the origin in the (x, y, z)-space. The rectilinear director on the z-axis, and the line at infinity perpendicular to the latter are self-intersections of the surface, Figure 11.1 (right). In the 21st century, 'a great variety of lines' in the cross-sections of the *conical wedge of Wallis*[2] determine peculiar crossings and avoided crossings of eigenvalues in non-Hermitian problems of fluid dynamics [246,458], optics [52,154], and atomic physics [260,365,426], to name a few.

[1] We recall for example the *Wallis product* (1655): $\frac{2}{1} \cdot \frac{2}{3} \cdot \frac{4}{3} \cdot \frac{4}{5} \cdot \frac{6}{5} \cdots = \frac{\pi}{2}$.

[2] The coffee-shop culture of our days quickly associated it with the 'double'-coffee-filter [260].

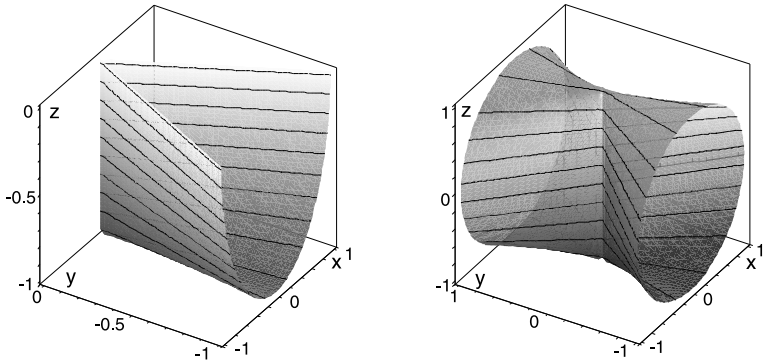

Figure 11.1. The conical wedge of Wallis (1684) with $a = 1$ and $c = 1$: (left) its quarter part, which is one of the classical shapes in naval architecture and (right) the full surface given by equation (11.1) known also as the double-coffee-filter [260].

Non-Hermitian Hamiltonians and matrices usually appear in physics when dissipative and other nonconservative effects are taken into account. For example, in hydrodynamics in buoyancy-driven thermal Rossby waves that commonly occur in geophysical flows, a phase shift in the periodic direction between the temperature and the velocity eddies produces a non-Hermitian governing operator [105, 106, 458]. Other known examples are complex refractive indices in optics and complex potentials describing scattering of electrons, X-rays or microwaves [154]. Non-Hermitian operators, which can be viewed as a perturbation of Hermitian ones, generate new physical effects, especially in the case of coalescence (coupling) of eigenvalues [51, 426].

Since the papers by von Neumann and Wigner (1929) [587] and Teller (1937) [568] it is known that the energy surfaces in quantum physics may cross, forming two sheets of a double cone resembling a children's toy 'diabolo' [426]. The vertex of the cone is therefore a *diabolical point* (DP) [56]. This kind of crossing is typical in systems described by real symmetric Hamiltonians with at least two parameters and Hermitian Hamiltonians depending on three or more parameters [130, 569]. DP corresponds to a double semisimple eigenvalue [270].

Historically, the first nontrivial physical effect associated with DPs is *Hamilton's conical refraction* in birefringent crystals [53]. Within such crystals of the lowest possible optical symmetry, two light waves of different polarization propagate in almost every direction with different phase velocities, which yields an easily observable *double refraction* [78]. In 1832 Hamilton discovered a limited number of directions of wave propagation where the velocities coincide.

The phase velocities and polarizations are associated with the eigenvalues and eigenvectors of a real symmetric matrix depending on the components of the wave vector. The coincidence of the phase velocities occurs exactly at a diabolical point where the eigenvalue is double-semisimple with two linearly independent eigenvectors. Then,

any linear combination of these eigenvectors (polarizations) is an eigenvector of the doublet too [270]. An immediate consequence of this freedom is that the light rays associated with one of the wave vectors (*optic axes*) specified by Hamilton are infinite in number and travel in all of the directions of a cone.

Compared to double refraction, conical refraction is a rare (nongeneric) phenomenon. It is not surprising then, that the latter appeared first as a theoretical prediction. Imagine how fascinating for the contemporaries it was that soon thereafter Lloyd[3] managed to observe the effect in a series of refined experiments [53,78]. As an example we quote the reaction of Plücker to *internal conical refraction* documented in 1839 [189]:

> No experiment in physics has made such an impression on my spirit as that of conical refraction. A ray of light entering a crystal and emerging in the shape of a cone of light: something fabulous without precedent. Mr. Hamilton announced it in the form of a wave which was the result of long and abstract calculations. I confess that I thought it impossible to see verified by experiment such an extraordinary result preceded only by a theory recently created by the genius of Mr. Fresnel. But since Mr. Lloyd has demonstrated that the experiments are in full concordance with the predictions by Mr. Hamilton, all prejudice against a theory so marvelously confirmed must vanish.

Later on, conical refraction was found in hydromagnetics [385, 578] and discussed together with diabolical points in the more general context of geometrical optics approximation of solutions of hyperbolic partial differential equations, see e.g. [104, 130, 189].

In modern non-Hermitian problems of quantum physics, crystal optics, physical chemistry, acoustics, hydro- and magnetohydrodynamics it is important to know how diabolical points of a Hermitian Hamiltonian unfold under arbitrary complex perturbation forming topological singularities of eigenvalue surfaces such as a double-coffee-filter with two *exceptional points* (EP), where both a pair of eigenvalues and their eigenvectors coalesce forming a double eigenvalue with the Jordan block [51, 52, 154, 155, 235, 246, 260, 426, 506, 527]. Both the DP and EP cases were observed in experiments, related in particular to the topics of the geometrical phase and $\mathcal{PT}$-symmetry, see for instance [154, 418, 426, 507, 511] and references therein.

Motivated by these applications, we start this chapter with the study of coupling of eigenvalues of complex matrices of arbitrary dimension in the general setting of the work [517]. We describe typical (generic) movements of eigenvalues and eigencurves as cross-sections of eigensurfaces.

Then, following the theory developed in [269,270], we consider a complex perturbation of multiparameter families of real symmetric and Hermitian matrices. In the case of real symmetric matrices we study unfolding of the conical singularities of eigensurfaces at a diabolical point under real and complex perturbations into new singular surfaces such as the conical wedge of Wallis.

[3] Humphrey Lloyd (1800–1881) – an Irish physicist.

As a physical application, singularities of the dispersion surfaces in crystal optics are studied. Asymptotic formulas for the metamorphoses of these surfaces depending on properties of a crystal are established and discussed in detail. Singular axes for general crystals with weak absorption and chirality are found. An explicit condition distinguishing the absorbtion-dominated and chirality-dominated crystals is established in terms of components of the inverse dielectric tensor. Numerical examples illustrate the general theory.

Finally, we turn to the question of approximate computation of the geometric phase along a path surrounding either DP or EP-set in the parameter space by means of the perturbation of eigenvectors at the degeneracies. In contrast to many existing studies of the Berry phase, we present a formalism suitable for the complex matrix families of arbitrary dimension and with arbitrary number of parameters [397, 398]. Recent experiments with dissipative microwave cavities are discussed that have confirmed some of the predictions of the theory [154].

11.1 Eigenvalue movement through a 1 : 1 resonance in complex matrices

Following [517] let us consider the eigenvalue problem

$$\mathbf{A}\mathbf{u} = \lambda\mathbf{u} \tag{11.2}$$

for an $m \times m$ complex matrix $\mathbf{A}(\mathbf{p})$ smoothly depending on a vector of real parameters $\mathbf{p}^T = (p_1, \ldots, p_n)$. Assume that, at $\mathbf{p} = \mathbf{p}_0$, a 1 : 1 resonance occurs, i.e. the matrix $\mathbf{A}_0 = \mathbf{A}(\mathbf{p}_0)$ has an eigenvalue λ_0 of multiplicity 2 as a root of the characteristic equation $\det(\mathbf{A}_0 - \lambda_0\mathbf{I}) = 0$; $\mathbf{I}$ is the identity matrix. The doublet has either one or two linearly independent eigenvectors $\mathbf{u}$, determining its geometric multiplicity. The eigenvalue problem adjoint to (11.2) is

$$\mathbf{A}^\dagger\mathbf{v} = \eta\mathbf{v}, \tag{11.3}$$

where $\mathbf{A}^\dagger = \overline{\mathbf{A}}^T$ is the adjoint matrix operator (Hermitian transpose) with the spectral parameter $\eta = \overline{\lambda}$.

Consider a smooth perturbation of parameters in the form $\mathbf{p} = \mathbf{p}(\varepsilon)$, where $\mathbf{p}(0) = \mathbf{p}_0$ and ε is a small real number [517]. Then,

$$\mathbf{A}(\mathbf{p}(\varepsilon)) = \mathbf{A}_0 + \varepsilon\mathbf{A}_1 + \frac{1}{2}\varepsilon^2\mathbf{A}_2 + o(\varepsilon^2), \quad \mathbf{A}_0 = \mathbf{A}(\mathbf{p}_0),$$
$$\mathbf{A}_1 = \sum_{i=1}^{n} \frac{\partial\mathbf{A}}{\partial p_i}\frac{dp_i}{d\varepsilon}, \quad \mathbf{A}_2 = \sum_{i=1}^{n} \frac{\partial\mathbf{A}}{\partial p_i}\frac{d^2p_i}{d\varepsilon^2} + \sum_{i,j=1}^{n} \frac{\partial^2\mathbf{A}}{\partial p_i\partial p_j}\frac{dp_i}{d\varepsilon}\frac{dp_j}{d\varepsilon}. \tag{11.4}$$

Generally, the perturbation transforms the doublet λ_0 into a pair of simple eigenvalues. A concrete scenario of such a transition depends on the geometric multiplicity of λ_0 [258, 428, 548, 584].

11.1.1 Diabolical point (DP): passing of eigenvalues

Let λ_0 have two linearly independent eigenvectors $\mathbf{u}_1$ and $\mathbf{u}_2$. The semisimple $1:1$ resonance is frequently called the diabolical point [56]. Let $\mathbf{v}_1$ and $\mathbf{v}_2$ be the eigenvectors of the eigenvalue $\eta = \overline{\lambda}$ of the adjoint problem (11.3) and satisfy the normalization conditions

$$(\mathbf{u}_1, \mathbf{v}_1) = (\mathbf{u}_2, \mathbf{v}_2) = 1, \quad (\mathbf{u}_1, \mathbf{v}_2) = (\mathbf{u}_2, \mathbf{v}_1) = 0, \tag{11.5}$$

where $(\mathbf{u}, \mathbf{v}) = \sum_{i=1}^{n} u_i \overline{v}_i$ denotes the Hermitian inner product. Conditions (11.5) define the unique vectors $\mathbf{v}_1$ and $\mathbf{v}_2$ for given $\mathbf{u}_1$ and $\mathbf{u}_2$ [155,517].

For nonzero small ε, the two eigenvalues λ_+ and λ_- resulting from the bifurcation of λ_0 and the corresponding eigenvectors $\mathbf{u}_\pm$ are given by

$$\lambda_\pm = \lambda_0 + \mu_\pm \varepsilon + o(\varepsilon), \quad \mathbf{u}_\pm = \alpha_\pm \mathbf{u}_1 + \beta_\pm \mathbf{u}_2 + o(1). \tag{11.6}$$

The coefficients $\mu_\pm$, $\alpha_\pm$, and $\beta_\pm$ are found from the eigenvalue problem for a 2×2 nonsymmetric matrix similar to that derived in 1984 by DiPrima and Hall in their study of stability of the Couette–Taylor flow [155]

$$\begin{pmatrix} (\mathbf{A}_1\mathbf{u}_1, \mathbf{v}_1) & (\mathbf{A}_1\mathbf{u}_2, \mathbf{v}_1) \\ (\mathbf{A}_1\mathbf{u}_1, \mathbf{v}_2) & (\mathbf{A}_1\mathbf{u}_2, \mathbf{v}_2) \end{pmatrix} \begin{pmatrix} \alpha_\pm \\ \beta_\pm \end{pmatrix} = \mu_\pm \begin{pmatrix} \alpha_\pm \\ \beta_\pm \end{pmatrix}. \tag{11.7}$$

Solving the characteristic equation for (11.7), we find [517]

$$\mu_\pm = \frac{(\mathbf{A}_1\mathbf{u}_1, \mathbf{v}_1) + (\mathbf{A}_1\mathbf{u}_2, \mathbf{v}_2)}{2} \pm \sqrt{\frac{((\mathbf{A}_1\mathbf{u}_1, \mathbf{v}_1) - (\mathbf{A}_1\mathbf{u}_2, \mathbf{v}_2))^2}{4} + (\mathbf{A}_1\mathbf{u}_1, \mathbf{v}_2)(\mathbf{A}_1\mathbf{u}_2, \mathbf{v}_1)}. \tag{11.8}$$

As the parameter vector passes the diabolical point $\mathbf{p}_0$ along the curve $\mathbf{p}(\varepsilon)$ in parameter space, the eigenvalues λ_+ and λ_- change smoothly and pass through each other at λ_0 in such a manner that their eigencurves touch the same plane at the DP, see Figure 11.2 (a). The corresponding eigenvectors $\mathbf{u}_+$ and $\mathbf{u}_-$ remain different (linearly independent) at all values of ε including the point $\mathbf{p}_0$. By means of eigenvectors, the eigenvalues $\lambda_\pm$ are well distinguished during passing through the semisimple $1:1$ resonance. The eigenvalues $\lambda_\pm$ and the eigenvectors $\mathbf{u}_\pm$ are however nondifferentiable functions of multiple parameters at $\mathbf{p}_0$ in the sense of Frechét [258,548].

Introducing a complex vector $\mathbf{f}_{ij} = (f_{ij}^1, \ldots, f_{ij}^n)$ with the components

$$f_{ij}^k = \left(\frac{\partial \mathbf{A}}{\partial p_k} \mathbf{u}_i, \mathbf{v}_j \right), \tag{11.9}$$

where the derivative is taken at $\mathbf{p}_0$, from equation (11.8) we find

$$\operatorname{Re} \lambda_\pm = \operatorname{Re} \lambda_0 + \operatorname{Re} \langle \mathbf{f}_{11} + \mathbf{f}_{22}, \Delta\mathbf{p} \rangle / 2 \pm \sqrt{(|c| + \operatorname{Re} c)/2}, \tag{11.10}$$

$$\operatorname{Im} \lambda_\pm = \operatorname{Im} \lambda_0 + \operatorname{Im} \langle \mathbf{f}_{11} + \mathbf{f}_{22}, \Delta\mathbf{p} \rangle / 2 \pm \sqrt{(|c| - \operatorname{Re} c)/2}, \tag{11.11}$$

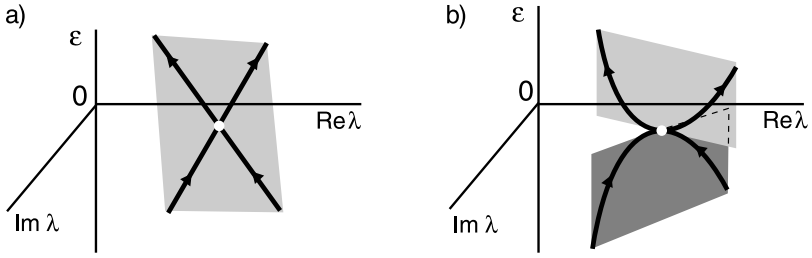

Figure 11.2. Eigenvalue movement of a complex matrix through a 1 : 1 resonance which is (a) semisimple (passing, DP), (b) nonsemisimple (splitting, EP) [146].

with $\Delta\mathbf{p} = \mathbf{p} - \mathbf{p}_0$, and

$$c = \langle \mathbf{f}_{11} - \mathbf{f}_{22}, \Delta\mathbf{p}\rangle^2/4 + \langle \mathbf{f}_{12}, \Delta\mathbf{p}\rangle\langle \mathbf{f}_{21}, \Delta\mathbf{p}\rangle. \tag{11.12}$$

The inner products of vectors here are given by $\langle \mathbf{a}, \mathbf{b}\rangle = \sum_{i=1}^{n} a_i \overline{b}_i$. Note that we use different notation for the inner product to distinguish between the linear complex space $\mathbb{C}^m$ (round brackets) and linear real space $\mathbb{R}^n$ (angular brackets). In expressions (11.10) and (11.11) the higher order terms $o(\|\Delta\mathbf{p}\|)$ and $o(\|\Delta\mathbf{p}\|^2)$ are omitted before and under the square root.

In order that λ_0 be algebraically double under perturbation of parameters, i.e. $\lambda_+ = \lambda_-$, the two independent equations must simultaneously be fulfilled

$$\operatorname{Re} c = 0, \quad \operatorname{Im} c = 0. \tag{11.13}$$

Generally this double eigenvalue $\lambda_+ = \lambda_-$ possesses a single eigenvector $\mathbf{u}_+ = \mathbf{u}_-$, i.e. the 1 : 1 resonance is no longer semisimple.

The doublet that survived perturbation has two eigenvectors only when the matrix in the left-hand side of the system (11.7) is proportional to the identity matrix. This yields the four constraints

$$\langle \mathbf{f}_{11}, \Delta\mathbf{p}\rangle = \langle \mathbf{f}_{22}, \Delta\mathbf{p}\rangle, \quad \langle \mathbf{f}_{12}, \Delta\mathbf{p}\rangle = \langle \mathbf{f}_{21}, \Delta\mathbf{p}\rangle = 0, \tag{11.14}$$

which imply (11.13) and represent six independent equations taken for real and imaginary parts. Thus, a semisimple 1 : 1 resonance is a rare phenomenon of codimension 6 in systems described by general complex matrices, which requires six parameters for complete qualitative description [517].

11.1.2 Exceptional point (EP): splitting of eigenvalues

Let at $\mathbf{p}_0$ a double eigenvalue λ_0 possess a single eigenvector $\mathbf{u}_0$. This nonsemisimple 1 : 1 resonance corresponds to the exceptional point. The second vector of the invariant subspace corresponding to λ_0 is a generalized eigenvector $\mathbf{u}_1$ determined by the equation

$$\mathbf{A}_0\mathbf{u}_1 = \lambda_0\mathbf{u}_1 + \mathbf{u}_0. \tag{11.15}$$

An eigenvector $\mathbf{v}_0$ and an associated vector $\mathbf{v}_1$ of $\mathbf{A}^\dagger$ are determined by

$$\mathbf{A}_0^\dagger \mathbf{v}_0 = \overline{\lambda}_0 \mathbf{v}_0, \quad \mathbf{A}_0^\dagger \mathbf{v}_1 = \overline{\lambda}_0 \mathbf{v}_1 + \mathbf{v}_0, \quad (\mathbf{u}_1, \mathbf{v}_0) = 1, \quad (\mathbf{u}_1, \mathbf{v}_1) = 0, \tag{11.16}$$

where the normalization conditions determine $\mathbf{v}_0$ and $\mathbf{v}_1$ uniquely for a given $\mathbf{u}_1$. The double eigenvalue λ_0 splits into two eigenvalues $\lambda_\pm$ with the eigenvectors $\mathbf{u}_\pm$

$$\begin{aligned} &\lambda_\pm = \lambda_0 \pm \sqrt{\mu_1 \varepsilon} + \mu_2 \varepsilon + o(\varepsilon), \\ &\mathbf{u}_\pm = \mathbf{u}_0 \pm \mathbf{u}_1 \sqrt{\mu_1 \varepsilon} + (\mu_2 \mathbf{u}_1 + \mathbf{G}^{-1}(\mu_1 \mathbf{u}_1 - \mathbf{A}_1 \mathbf{u}_0))\varepsilon + o(\varepsilon), \end{aligned} \tag{11.17}$$

where $\mathbf{G} = \mathbf{A}_0 - \lambda_0 \mathbf{I} + \mathbf{v}_0 \mathbf{v}_1^\dagger$ and the coefficients μ_1 and μ_2 are [517]

$$\mu_1 = (\mathbf{A}_1 \mathbf{u}_0, \mathbf{v}_0), \quad 2\mu_2 = (\mathbf{A}_1 \mathbf{u}_0, \mathbf{v}_1) + (\mathbf{A}_1 \mathbf{u}_1, \mathbf{v}_0). \tag{11.18}$$

With a variation of ε from negative to positive values, the two eigenvalues $\lambda_\pm$ approach, collide with infinite speed (the derivative with respect to ε tends to infinity [458]) at λ_0, and diverge in the perpendicular direction, see Figure 11.2 (b). The eigenvectors interact too. At $\varepsilon = 0$, they merge to $\mathbf{u}_0$ up to a scalar complex factor. Since the condition $\mu_1 = 0$ leads to degeneration of both the eigenvalues and the eigenvectors at the EP, this degeneracy has codimension 2 for general complex matrices.

An exciting feature of the movement of eigenvalues through the nonsemisimple $1:1$ resonance is that the two eigenvalues cannot be distinguished after the interaction. Indeed, there is no natural rule telling how the eigenvalues before coupling correspond to those after coupling [517].

11.2 Eigensurfaces associated with DPs

Although diabolical points in general families of complex matrices have codimension 6, additional symmetries or degeneracies may force them to take place in systems dependent on a smaller number of parameters [147]. Already in 1929, von Neumann and Wigner demonstrated that the codimension of the semisimple $1:1$ resonance decreases to 3 in the case of Hermitian matrices and to 2 in the real symmetric case [587].

A family of Hermitian matrices $\mathbf{A}(\mathbf{p})$ has real eigenvalues that are either simple or semisimple. If λ_0 is a double eigenvalue of $\mathbf{A}_0 = \mathbf{A}(\mathbf{p}_0)$ at some point $\mathbf{p}_0$, one should take $\mathbf{v}_1 = \mathbf{u}_1$ and $\mathbf{v}_2 = \mathbf{u}_2$ in equation (11.7), where the eigenvectors $\mathbf{u}_1$ and $\mathbf{u}_2$ of λ_0 at $\mathbf{p}_0$ satisfy the normalization conditions

$$(\mathbf{u}_1, \mathbf{u}_1) = (\mathbf{u}_2, \mathbf{u}_2) = 1, \quad (\mathbf{u}_1, \mathbf{u}_2) = 0. \tag{11.19}$$

Since the matrix $\mathbf{A}$ is Hermitian, the vectors $\mathbf{f}_{11}$ and $\mathbf{f}_{22}$ are real and the vectors $\mathbf{f}_{12} = \overline{\mathbf{f}}_{21}$ are complex conjugate in the asymptotic formulas (11.10) and (11.11) for

$\lambda_\pm$. In the case of real symmetric matrices $\mathbf{A} = \mathbf{A}^T$, the vectors $\mathbf{f}_{11}$, $\mathbf{f}_{22}$, and $\mathbf{f}_{12} = \mathbf{f}_{21}$ are real. The asymptotic expression for the eigenvectors corresponding to $\lambda_\pm$ takes the form [269, 270]

$$\mathbf{u}_\pm = \alpha_\pm \mathbf{u}_1 + \beta_\pm \mathbf{u}_2, \quad \frac{\alpha_\pm}{\beta_\pm} = \frac{\langle \mathbf{f}_{12}, \Delta\mathbf{p}\rangle}{\lambda_\pm - \lambda_0 - \langle \mathbf{f}_{11}, \Delta\mathbf{p}\rangle} = \frac{\lambda_\pm - \lambda_0 - \langle \mathbf{f}_{22}, \Delta\mathbf{p}\rangle}{\langle \mathbf{f}_{21}, \Delta\mathbf{p}\rangle}. \tag{11.20}$$

Expressions (11.20) provide zero order terms for the eigenvectors $\mathbf{u}_\pm$ under perturbation of the parameter vector in the Hermitian matrix family $\mathbf{A}(\mathbf{p})$.

11.2.1 Complex perturbation of a Hermitian matrix family

Now, consider an arbitrary complex perturbation of the Hermitian family: $\mathbf{A}(\mathbf{p}) + \Delta\mathbf{A}(\mathbf{p})$, see e.g. Kahan [250]. Such perturbations appear due to nonconservative effects breaking symmetry of the initial system [52]. We assume that the size of the non-Hermitian perturbation $\Delta\mathbf{A}(\mathbf{p}) \sim \varepsilon$ is small, where $\varepsilon = \|\Delta\mathbf{A}(\mathbf{p}_0)\|$ is the Frobenius norm of the perturbation at the diabolic point. The eigenvalues $\lambda_\pm$ for small $\Delta\mathbf{p}$ and small ε are described by the asymptotic formula [269, 270]

$$\lambda_\pm = \lambda_0 + \frac{\langle \mathbf{f}_{11} + \mathbf{f}_{22}, \Delta\mathbf{p}\rangle}{2} + \frac{\varepsilon_{11} + \varepsilon_{22}}{2} \pm \sqrt{\frac{(\langle \mathbf{f}_{11} - \mathbf{f}_{22}, \Delta\mathbf{p}\rangle + \varepsilon_{11} - \varepsilon_{22})^2}{4} + (\langle \mathbf{f}_{12}, \Delta\mathbf{p}\rangle + \varepsilon_{12})(\langle \mathbf{f}_{21}, \Delta\mathbf{p}\rangle + \varepsilon_{21})}. \tag{11.21}$$

The quantities ε_{ij} are small complex numbers of order ε given by the expression

$$\varepsilon_{ij} = \left(\Delta\mathbf{A}(\mathbf{p}_0)\mathbf{u}_i, \mathbf{u}_j\right). \tag{11.22}$$

A small variation of the matrix family leads to the following correction of the asymptotic expression for the eigenvectors

$$\mathbf{u}_\pm = \alpha^\varepsilon_\pm \mathbf{u}_1 + \beta^\varepsilon_\pm \mathbf{u}_2,$$
$$\frac{\alpha^\varepsilon_\pm}{\beta^\varepsilon_\pm} = \frac{\langle \mathbf{f}_{12}, \Delta\mathbf{p}\rangle + \varepsilon_{12}}{\lambda_\pm - \lambda_0 - \langle \mathbf{f}_{11}, \Delta\mathbf{p}\rangle - \varepsilon_{11}} = \frac{\lambda_\pm - \lambda_0 - \langle \mathbf{f}_{22}, \Delta\mathbf{p}\rangle - \varepsilon_{22}}{\langle \mathbf{f}_{21}, \Delta\mathbf{p}\rangle + \varepsilon_{21}}. \tag{11.23}$$

The ratios $\alpha^\varepsilon_+/\beta^\varepsilon_+ = \alpha^\varepsilon_-/\beta^\varepsilon_-$ at the point of coincident eigenvalues $\lambda_+ = \lambda_-$. Hence, the eigenvectors $\mathbf{u}_+ = \mathbf{u}_-$ coincide, and the point of eigenvalue coupling of the perturbed system becomes an exceptional point. For some specific perturbations $\Delta\mathbf{A}(\mathbf{p})$, the coupling point may remain diabolic under the conditions

$$\langle \mathbf{f}_{12}, \Delta\mathbf{p}\rangle + \varepsilon_{12} = 0, \quad \langle \mathbf{f}_{21}, \Delta\mathbf{p}\rangle + \varepsilon_{21} = 0, \quad \langle \mathbf{f}_{11} - \mathbf{f}_{22}, \Delta\mathbf{p}\rangle + \varepsilon_{11} - \varepsilon_{22} = 0, \tag{11.24}$$

when both ratios in (11.23) become undetermined.

The asymptotic description of unfolding the diabolical point by perturbing the Hermitian family requires only the value of $\Delta\mathbf{A}(\mathbf{p})$ taken at the coupling point $\mathbf{p}_0$. Dependence of the perturbation $\Delta\mathbf{A}$ on the vector $\mathbf{p}$ near the point $\mathbf{p}_0$ is not so important, since it influences higher order terms.

11.2.2 DP in the spectrum of real symmetric matrices

When $\mathbf{A}(\mathbf{p})$ is a family of real symmetric matrices, the asymptotic formula (11.10) describes a surface in $(p_1, p_2, \ldots, p_n, \lambda)$-space, consisting of two sheets $\lambda_+(\mathbf{p})$ and $\lambda_-(\mathbf{p})$ connected at the points specified by the equations

$$\lambda_\pm = \lambda_0 + \frac{1}{2}\langle \mathbf{f}_{11} + \mathbf{f}_{22}, \Delta\mathbf{p}\rangle, \;\; \langle \mathbf{f}_{11} - \mathbf{f}_{22}, \Delta\mathbf{p}\rangle = 0, \;\; \langle \mathbf{f}_{12}, \Delta\mathbf{p}\rangle = 0, \qquad (11.25)$$

where $\lambda_+ = \lambda_-$. In the $\mathbf{p}$ space the last two of equations (11.25) define a plane of dimension $n-2$. Thus, a double semisimple eigenvalue has codimension 2 in an n-parameter family of real symmetric matrices [587].

For the two-parameter matrix $\mathbf{A}(p_1, p_2)$ equation (11.10) defines a cone with the vertex at the diabolical point $(\mathbf{p}_0, \lambda_0)$ in (p_1, p_2, λ)-space, Figure 11.3.

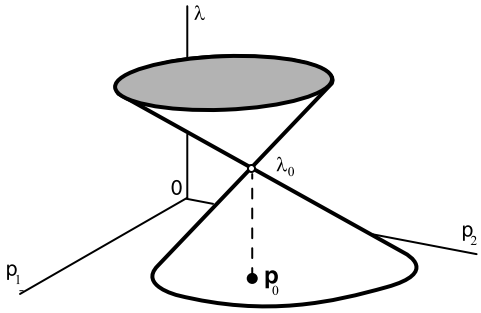

Figure 11.3. DP in a two-parameter family of real symmetric matrices [270].

11.2.3 How a DP unfolds into the conical wedge of Wallis

Let us consider a perturbation $\mathbf{A}(\mathbf{p}) + \Delta\mathbf{A}(\mathbf{p})$ of the real symmetric family $\mathbf{A}(\mathbf{p})$ in the vicinity of the diabolical point $\mathbf{p}_0$, where $\Delta\mathbf{A}(\mathbf{p})$ is a complex matrix with the small norm $\varepsilon = \|\Delta\mathbf{A}(\mathbf{p}_0)\|$. Splitting of the double eigenvalue λ_0 due to a change of the vector of parameters $\Delta\mathbf{p}$ and a small complex perturbation $\Delta\mathbf{A}$ is described by equation (11.21), which acquires the form

$$\lambda_\pm = \lambda_0' + \mu \pm \sqrt{c}, \;\; c = (x+\xi)^2 + (y+\eta)^2 - \zeta^2. \qquad (11.26)$$

In equation (11.26) the quantities λ_0', x, and y are real:

$$\lambda_0' = \lambda_0 + \frac{1}{2}\langle \mathbf{f}_{11} + \mathbf{f}_{22}, \Delta\mathbf{p}\rangle, \;\; x = \frac{1}{2}\langle \mathbf{f}_{11} - \mathbf{f}_{22}, \Delta\mathbf{p}\rangle, \;\; y = \langle \mathbf{f}_{12}, \Delta\mathbf{p}\rangle, \qquad (11.27)$$

while the small coefficients μ, ξ, η, and ζ are complex:

$$\mu = \frac{1}{2}(\varepsilon_{11}+\varepsilon_{22}), \;\; \xi = \frac{1}{2}(\varepsilon_{11}-\varepsilon_{22}), \;\; \eta = \frac{1}{2}(\varepsilon_{12}+\varepsilon_{21}), \;\; \zeta = \frac{1}{2}(\varepsilon_{12}-\varepsilon_{21}). \qquad (11.28)$$

Separating real and imaginary parts in equation (11.26), we find

$$\begin{aligned} \mathrm{Re}^2(\lambda-\lambda_0'-\mu)-\mathrm{Im}^2(\lambda-\lambda_0'-\mu)&=\mathrm{Re}c,\\ 2\mathrm{Re}(\lambda-\lambda_0'-\mu)\mathrm{Im}(\lambda-\lambda_0'-\mu)&=\mathrm{Im}c, \end{aligned} \tag{11.29}$$

where

$$\mathrm{Re}c=(\mathrm{Im}^2\zeta-\mathrm{Im}^2\xi-\mathrm{Im}^2\eta-\mathrm{Re}^2\zeta)+(x+\mathrm{Re}\xi)^2+(y+\mathrm{Re}\eta)^2, \tag{11.30}$$

$$\mathrm{Im}c=2((x+\mathrm{Re}\xi)\mathrm{Im}\xi+(y+\mathrm{Re}\eta)\mathrm{Im}\eta-\mathrm{Re}\zeta\mathrm{Im}\zeta). \tag{11.31}$$

equations (11.29) yield the real and imaginary parts of the perturbed eigenvalues

$$\mathrm{Re}\lambda_\pm=\lambda_0'+\mathrm{Re}\mu\pm\sqrt{\left(\mathrm{Re}c+\sqrt{\mathrm{Re}^2c+\mathrm{Im}^2c}\right)/2}, \tag{11.32}$$

$$\mathrm{Im}\lambda_\pm=\mathrm{Im}\mu\pm\sqrt{\left(-\mathrm{Re}c+\sqrt{\mathrm{Re}^2c+\mathrm{Im}^2c}\right)/2}, \tag{11.33}$$

which are hypersurfaces in $(p_1,p_2,\ldots,p_n,\mathrm{Re}\lambda)$ and $(p_1,p_2,\ldots,p_n,\mathrm{Im}\lambda)$-spaces. Two sheets of the surface (11.32) are connected (i.e. $\mathrm{Re}\lambda_+=\mathrm{Re}\lambda_-$) when

$$\mathrm{Re}c\le 0,\ \ \mathrm{Im}c=0,\ \ \mathrm{Re}\lambda_\pm=\lambda_0'+\mathrm{Re}\mu, \tag{11.34}$$

while the sheets $\mathrm{Im}\lambda_+(\mathbf{p})$ and $\mathrm{Im}\lambda_-(\mathbf{p})$ are glued at the set of points satisfying

$$\mathrm{Re}c\ge 0,\ \ \mathrm{Im}c=0,\ \ \mathrm{Im}\lambda_\pm=\mathrm{Im}\mu. \tag{11.35}$$

Near the intersections (11.34) and (11.35) the approximations are valid

$$\begin{aligned} \mathrm{Re}\lambda_\pm&=\lambda_0'+\mathrm{Re}\mu\pm\frac{\mathrm{Im}c}{2}\sqrt{\frac{-1}{\mathrm{Re}c}},\ \ \mathrm{Re}c<0,\\ \mathrm{Im}\lambda_\pm&=\mathrm{Im}\mu\pm\frac{\mathrm{Im}c}{2}\sqrt{\frac{1}{\mathrm{Re}c}},\qquad \mathrm{Re}c>0. \end{aligned} \tag{11.36}$$

The eigenvalue remains double under the perturbation of parameters when $c=0$, which yields two equations $\mathrm{Re}c=0$ and $\mathrm{Im}c=0$. Two cases are distinguished according to the sign of the quantity

$$D=\mathrm{Im}^2\xi+\mathrm{Im}^2\eta-\mathrm{Im}^2\zeta. \tag{11.37}$$

If $D>0$, then the equations $\mathrm{Re}c=0$ and $\mathrm{Im}c=0$ with expressions (11.30), (11.31) yield two solutions (x_a,y_a) and (x_b,y_b), where

$$x_{a,b}=\frac{\mathrm{Im}\xi\mathrm{Re}\zeta\mathrm{Im}\zeta\pm\mathrm{Im}\eta\sqrt{(\mathrm{Im}^2\xi+\mathrm{Im}^2\eta+\mathrm{Re}^2\zeta)D}}{\mathrm{Im}^2\xi+\mathrm{Im}^2\eta}-\mathrm{Re}\xi, \tag{11.38}$$

$$y_{a,b}=\frac{\mathrm{Im}\eta\mathrm{Re}\zeta\mathrm{Im}\zeta\mp\mathrm{Im}\xi\sqrt{(\mathrm{Im}^2\xi+\mathrm{Im}^2\eta+\mathrm{Re}^2\zeta)D}}{\mathrm{Im}^2\xi+\mathrm{Im}^2\eta}-\mathrm{Re}\eta. \tag{11.39}$$

These two solutions determine the points in parameter space where double eigenvalues appear. When $D = 0$, the two solutions coincide. For $D < 0$, the equations $\mathrm{Re}c = 0$ and $\mathrm{Im}c = 0$ have no real solutions. In the latter case, the eigenvalues λ_+ and λ_- separate for all $\Delta\mathbf{p}$.

Note that the quantities $\mathrm{Im}\xi$ and $\mathrm{Im}\eta$ are expressed by means of the anti-Hermitian part $\Delta\mathbf{A}_N = (\Delta\mathbf{A} - \overline{\Delta\mathbf{A}}^T)/2$ of the matrix $\Delta\mathbf{A}$ as

$$\mathrm{Im}\xi = \frac{(\Delta\mathbf{A}_N(\mathbf{p}_0)\mathbf{u}_1, \mathbf{u}_1) - (\Delta\mathbf{A}_N(\mathbf{p}_0)\mathbf{u}_2, \mathbf{u}_2)}{2i}, \tag{11.40}$$

$$\mathrm{Im}\eta = \frac{(\Delta\mathbf{A}_N(\mathbf{p}_0)\mathbf{u}_1, \mathbf{u}_2) + (\Delta\mathbf{A}_N(\mathbf{p}_0)\mathbf{u}_2, \mathbf{u}_1)}{2i}, \tag{11.41}$$

while $\mathrm{Im}\zeta$ depends on the Hermitian part $\Delta\mathbf{A}_H = (\Delta\mathbf{A} + \overline{\Delta\mathbf{A}}^T)/2$ as

$$\mathrm{Im}\zeta = \frac{(\Delta\mathbf{A}_H(\mathbf{p}_0)\mathbf{u}_1, \mathbf{u}_2) - (\Delta\mathbf{A}_H(\mathbf{p}_0)\mathbf{u}_2, \mathbf{u}_1)}{2i}. \tag{11.42}$$

If $D > 0$, one can say that the influence of the anti-Hermitian part of the perturbation $\Delta\mathbf{A}$ is stronger than that of the Hermitian part. If the Hermitian part prevails in the perturbation $\Delta\mathbf{A}$, we have $D < 0$. In particular, $D = -\mathrm{Im}^2\zeta < 0$ for a purely Hermitian perturbation $\Delta\mathbf{A}$.

Let $\mathbf{p}^T = (p_1, p_2)$ and $D < 0$. Then, the eigensheets $\mathrm{Re}\lambda_+(\mathbf{p})$ and $\mathrm{Re}\lambda_-(\mathbf{p})$ are separate, see Figure 11.4 (a). Indeed, for $D \le -\mathrm{Re}^2\zeta$ the inequality $\mathrm{Re}c \ge 0$ holds for all variations of parameters, see equation (11.30). When $-\mathrm{Re}^2\zeta < D < 0$ the equation $\mathrm{Re}c = 0$ with expressions (11.27) define an ellipse in the plane of parameters (p_1, p_2). Inside the ellipse we have $\mathrm{Re}c < 0$ and outside $\mathrm{Re}c > 0$. Equation $\mathrm{Im}c = 0$ defines a line in the same plane. The line and the ellipse have no common points for $D < 0$ since there are no real solutions of the equation $c = 0$. Hence, for $D < 0$ conditions (11.34) are not fulfilled and the real parts of the eigenvalues avoid crossing. As the size of the complex perturbation decreases ($\varepsilon \to 0$), the two sheets come closer and touch each other at the point $(\mathbf{p}_0, \lambda_0)$ for $\varepsilon = 0$ forming the diabolic singularity. The sheets $\mathrm{Im}\lambda_+(\mathbf{p})$ and $\mathrm{Im}\lambda_-(\mathbf{p})$ of the surface (11.33) intersect along the line

$$\mathrm{Im}c/2 = (x + \mathrm{Re}\xi)\mathrm{Im}\xi + (y + \mathrm{Re}\eta)\mathrm{Im}\eta - \mathrm{Re}\zeta\mathrm{Im}\zeta = 0, \;\; \mathrm{Im}\lambda_\pm = \mathrm{Im}\mu, \tag{11.43}$$

that follows from equations (11.35). According to equations (11.36) the angle of intersection of the imaginary eigensheets is small of order ε and vanishes as $\varepsilon \to 0$.

In the case when $D > 0$, the line $\mathrm{Im}c = 0$ and the ellipse $\mathrm{Re}c = 0$ have common points $\mathbf{p}_a$ and $\mathbf{p}_b$ where the eigenvalues couple. Coordinates of these points found from the equations (11.27) are

$$\mathbf{p}_{a,b}^T = \mathbf{p}_0^T + \left(\frac{-2f_{12}^2 x_{a,b} + (f_{11}^2 - f_{22}^2) y_{a,b}}{f_{12}^1(f_{11}^2 - f_{22}^2) - f_{12}^2(f_{11}^1 - f_{22}^1)}, \;\; \frac{2f_{12}^1 x_{a,b} - (f_{11}^1 - f_{22}^1) y_{a,b}}{f_{12}^1(f_{11}^2 - f_{22}^2) - f_{12}^2(f_{11}^1 - f_{22}^1)} \right), \tag{11.44}$$

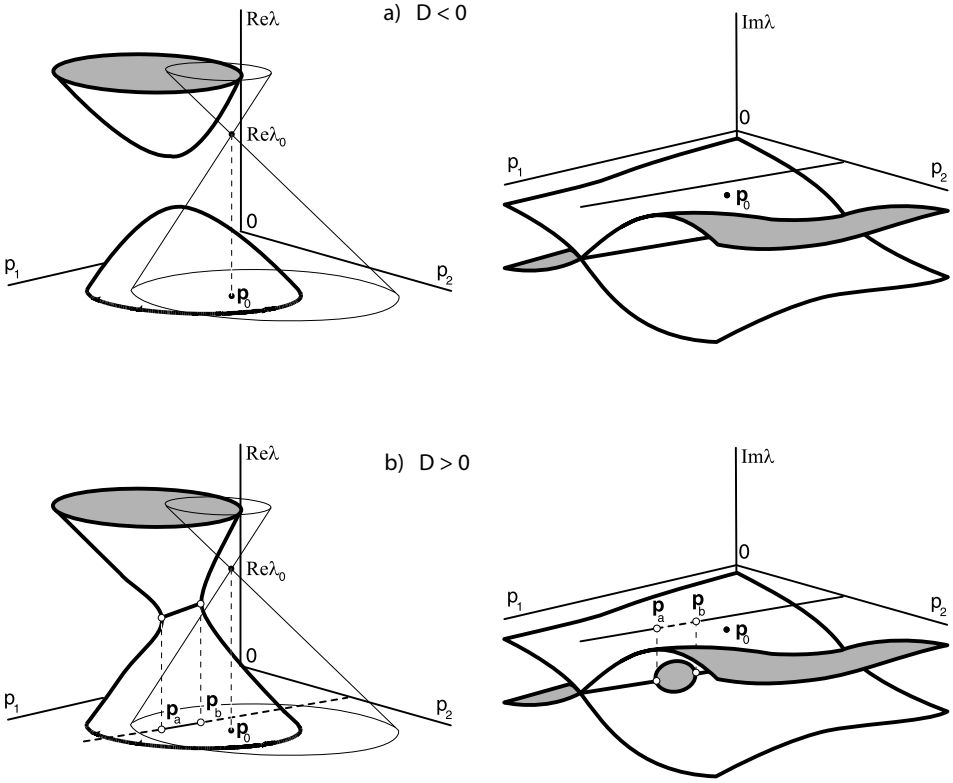

Figure 11.4. Unfolding the diabolical singularity in the case when in the complex perturbation (a) the Hermitian part prevails (separated eigensurfaces for the real parts and intersecting ones for the imaginary parts of the perturbed eigenvalues) and (b) the anti-Hermitian part prevails (the double-coffee-filter [260] for the real parts and the viaduct [294, 506] for the imaginary parts) [270].

where $x_{a,b}$ and $y_{a,b}$ are defined by expressions (11.38) and (11.39). Here we have assumed that the vectors $\mathbf{f}_{11} - \mathbf{f}_{22}$ and $\mathbf{f}_{12}$ are linearly independent. The points $\mathbf{p}_a$ and $\mathbf{p}_b$ coincide at $D = 0$. According to conditions (11.34) the real eigensheets $\mathrm{Re}\lambda_+(\mathbf{p})$ and $\mathrm{Re}\lambda_-(\mathbf{p})$ are glued in the interval $[\mathbf{p}_a, \mathbf{p}_b]$ of the line

$$\mathrm{Im}c/2 = (x+\mathrm{Re}\xi)\mathrm{Im}\xi+(y+\mathrm{Re}\eta)\mathrm{Im}\eta-\mathrm{Re}\zeta\mathrm{Im}\zeta = 0,\ \mathrm{Re}\lambda_\pm = \lambda_0'+\mathrm{Re}\mu. \quad (11.45)$$

The surface of real eigenvalues (11.32) easily reduces to the canonical form (11.1) of the conical wedge of Wallis, cf. Figure 11.1 and Figure 11.4 (b). In modern physical language, however, the term double-coffee-filter is more popular [260].

From conditions (11.35) it follows that the imaginary eigensheets $\mathrm{Im}\lambda_+(\mathbf{p})$ and $\mathrm{Im}\lambda_-(\mathbf{p})$ are connected along the straight line (11.43) where the interval $[\mathbf{p}_a, \mathbf{p}_b]$ is excluded, forming the viaduct singular surface [294,506], see Figure 11.4 (b). Accord-

ing to equations (11.36), the angle of intersection of the imaginary eigensheets tends to π as the points $\mathbf{p}_a$ and $\mathbf{p}_b$ are approached, since Rec goes to zero. At far distances from the interval $[\mathbf{p}_a, \mathbf{p}_b]$ this angle becomes small of order ε. With the decrease of the size of complex perturbation ε the interval shrinks and the angle of intersection goes to zero. At $\varepsilon = 0$ the imaginary parts of the eigenvalues coincide: $\mathrm{Im}\lambda_+ = \mathrm{Im}\lambda_- = 0$. Note that in crystal optics and acoustics the interval $[\mathbf{p}_a, \mathbf{p}_b]$ is referred to as a branch cut, and the points $\mathbf{p}_a$, $\mathbf{p}_b$ are called *singular axes*, see [52, 527]. According to equation (11.23), the double eigenvalues at $\mathbf{p}_a$ and $\mathbf{p}_b$ possess only one eigenvector and, hence, they are exceptional points (EPs).

11.2.4 Inflating the diabolical point into an exceptional ring

Let $\Delta\mathbf{A}(\mathbf{p})$ be a real nonsymmetric matrix. Then μ, ξ, η, ζ, and hence,

$$c = (x + \xi)^2 + (y + \eta)^2 - \zeta^2 \tag{11.46}$$

are real too. According to equation (11.26), the eigenvalues $\lambda_\pm$ are complex conjugate if $c < 0$ and real if $c > 0$. The eigenvalues couple for $c = 0$ forming a set consisting of exceptional points with double real eigenvalues.

Consider a system depending on a vector of two parameters $\mathbf{p} = (p_1, p_2)^T$. Then equation $c = 0$ with expressions (11.27) and (11.46) define an ellipse in parameter plane; $c < 0$ inside the ellipse and $c > 0$ outside. Real parts of the eigenvalues are given by the equations

$$c \geq 0 : (\mathrm{Re}\lambda - \lambda_0' - \mu)^2 - (x + \xi)^2 - (y + \eta)^2 = -\zeta^2, \tag{11.47}$$

$$c \leq 0 : \mathrm{Re}\lambda = \lambda_0' + \mu. \tag{11.48}$$

Equation (11.47) defines a hyperboloid in the space $(p_1, p_2, \mathrm{Re}\lambda)$. Real parts of the eigenvalues $\lambda_\pm$ coincide at the disk determined by equation (11.48), see Figure 11.5

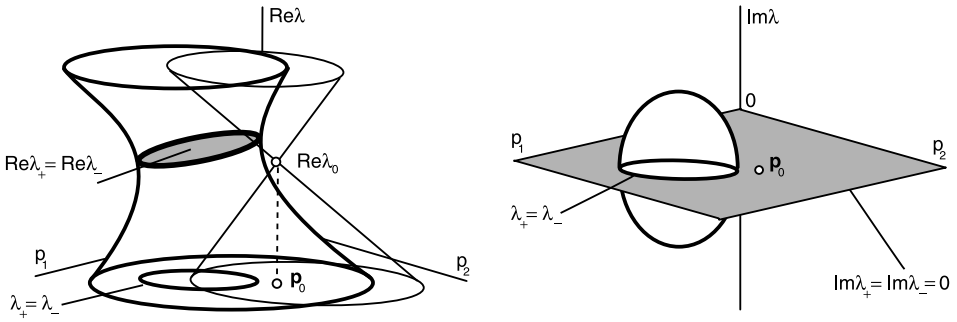

Figure 11.5. A real nonsymmetric perturbation of the diabolical point [270].

(left). Imaginary parts of the eigenvalues are

$$c \geq 0 : \mathrm{Im}\lambda = 0, \tag{11.49}$$

$$c \leq 0 : \mathrm{Im}^2\lambda + (x+\xi)^2 + (y+\eta)^2 = \zeta^2. \tag{11.50}$$

The imaginary parts are both zero at the points of the plane (11.49) surrounding the ellipsoid (11.50) ('a bubble') in the space $(p_1, p_2, \mathrm{Im}\lambda)$, see Figure 11.5 (right). The eigenvalues couple at the points of the elliptic ring

$$\lambda_\pm = \lambda_0' + \mu, \;\; (x+\xi)^2 + (y+\eta)^2 = \zeta^2, \tag{11.51}$$

consisting of exceptional points (shown by a bold black line in Figure 11.5). When $\Delta\mathbf{A}$ is a real symmetric matrix, the radius of the exceptional ring $\zeta = 0$. Similar inflation of the diabolical point into an *exceptional ring* generically happens when a Hermitian matrix is perturbed by a complex one, for details see [269, 270].

Finally, we describe deformation of the surfaces (11.47), (11.48) and (11.49), (11.50) as the real perturbation becomes complex. If $\mathrm{Im}\Delta\mathbf{A}$ is such that $D < 0$, the parts of the hyperboloid (11.47) connected by the disk (11.48) are separated into the two smooth surfaces described by the equation (11.32). On the other hand, the ellipsoid (11.50) surrounded by the plane (11.49) is foliated into two sheets crossing each other along the line $\mathrm{Im}c = 0$, see Figure 11.4 (a). Recall that the line $\mathrm{Im}c = 0$ does not intersect the ellipse $\mathrm{Re}c = 0$. When $D > 0$, the disk (11.48) foliates into two sheets crossing along the interval $[\mathbf{p}_a, \mathbf{p}_b]$, where the points $\mathbf{p}_a$ and $\mathbf{p}_b$ are given by expression (11.44). As $\mathrm{Im}\Delta\mathbf{A}$ increases, the angle of intersection of real eigensheets grows. In this manner the purely imaginary perturbation deforms the hyperboloid (11.47) into the double-coffee-filter (11.32), see Figure 11.4 (b). The ellipsoid (11.50) surrounded by the plane (11.49) is transformed into two smooth sheets intersecting along the line $\mathrm{Im}c = 0$, where the interval $[\mathbf{p}_a, \mathbf{p}_b]$ is excluded. The angle of intersection grows as the size of $\mathrm{Im}\Delta\mathbf{A}$ increases.

11.2.5 Example: flutter instability in granular flow

The unfolding of the conical eigenvalue surface shown in Figure 11.5 naturally arises in the problem of the flutter instability (*flutter ill-posedness*) in *granular flow* that was modeled by An and Schaeffer [9] as an *elastoplastic continuum* in two space dimensions. Writing the governing partial differential equations for the density, velocity, and the Cauchy stress tensor, supplementing them with an elastoplastic constitutive law in the assumption of the associative flow rule, objective stress rate, and a smooth, isotropic yield surface, and considering the anisotropic hardening as small perturbation, yields a quasilinear system of six equations for six scalar unknowns. Looking for a solution to the governing PDEs as a plane wave with the wavevector $\mathbf{k} = (k_1, k_2)^T$ and the frequency ω yields an eigenvalue problem for the *acoustic*

tensor $\mathbf{A}(s, \mathbf{k}, \varepsilon, \beta, \tau) = \mathbf{A}_0 + \varepsilon \mathbf{A}_1$, where

$$\mathbf{A}_0 = \begin{pmatrix} \left(2 - s\frac{(1-\beta)^2}{1+\beta^2}\right)k_1^2 + (1+\tau)k_2^2 & \left(1 + s\frac{1-\beta^2}{1+\beta^2} - \tau\right)k_1 k_2 \\ \left(1 + s\frac{1-\beta^2}{1+\beta^2} + \tau\right)k_1 k_2 & \left(2 - s\frac{(1+\beta)^2}{1+\beta^2}\right)k_2^2 + (1-\tau)k_1^2 \end{pmatrix},$$

$$\mathbf{A}_1 = -\frac{s}{1+\beta^2}\begin{pmatrix} 2(1-\beta)k_1 k_2 & (1-\beta)k_1^2 - (1+\beta)k_2^2 \\ (1-\beta)k_1^2 - (1+\beta)k_2^2 & -2(1+\beta)k_1 k_2 \end{pmatrix}, \quad (11.52)$$

ε is a small parameter, 2τ the difference between the principal stresses, s the inverse hardening modulus with $s = 0$ and $s = 1$ corresponding to the elastic and plastic limits, respectively, and the parameter $\beta \in (0, 1)$ specifies the angle of internal friction [9]. Eigenvalues of the acoustic tensor are squared eigenfrequencies ω^2. When $\varepsilon = 0$, $\tau = 0$, and $s \in [0, 1]$, the acoustic tensor is a real symmetric matrix with the real nonnegative eigenvalues [9]. Nonzero parameters ε and τ introduce a real non-symmetric perturbation to the real symmetric matrix family.

In the assumption that $k_1 = k \cos\theta$ and $k_2 = k \sin\theta$ and at the fixed parameters τ, β, k, and ε the acoustic tensor is a function of the softening s and the propagation angle θ only: $\mathbf{A} = \mathbf{A}(s, \theta)$. The eigenvalues of the two-parameter matrix family normalized by k^2 can thus be plotted in the three dimensional space. Figure 11.6(a) demonstrates the typical conical intersection at $\varepsilon = 0$ that unfolds into a hyperboloid of one sheet at $\varepsilon = 0.2$ shown in Figure 11.6(b). The top view of the hyperboloid in Figure 11.6(c) makes visible its central opening corresponding to a region of complex wave speeds (flutter), cf. Figure 11.5.

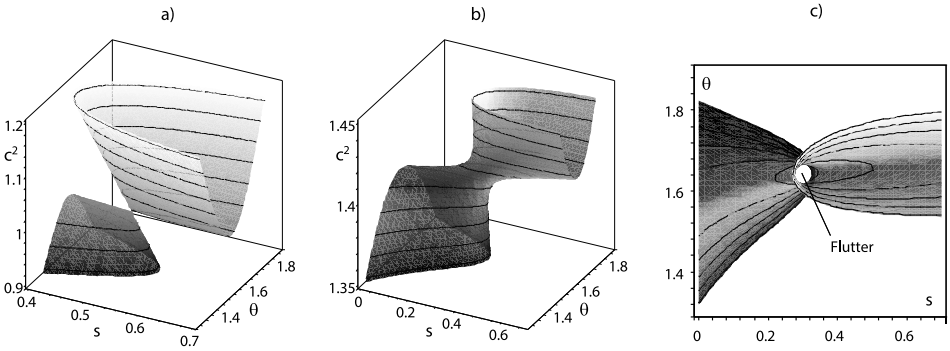

Figure 11.6. Squared wave speed $c := \omega/k$ at $k = 1$, $\beta = 0.7$, $\tau = 0.4$ as functions of the softening s and the angle of propagation θ when (a) $\varepsilon = 0$ (conical intersection) and (b,c) $\varepsilon = 0.2$ (a hyperboloid of one sheet and its top view).

11.3 Unfolding conical singularities in crystal optics

Following Berry and Dennis [52], we consider propagation of light in a nonmagnetic dichroic chiral anisotropic crystal. The optical properties of this dissipative medium are characterized by the inverse dielectric tensor $\boldsymbol{\eta}$, which relates the vectors of electric field $\mathbf{E}$ and displacement $\mathbf{D}$ as

$$\mathbf{E} = \boldsymbol{\eta}\mathbf{D}. \tag{11.53}$$

A monochromatic plane wave of frequency ω propagating in a direction specified by the real unit vector $\mathbf{s} = (s_1, s_2, s_3)$ has the form [78]

$$\mathbf{D}(\mathbf{r}, t) = \mathbf{D}(\mathbf{s}) \exp i\omega\left(\frac{n(\mathbf{s})}{c}\mathbf{s}^T\mathbf{r} - t\right), \tag{11.54}$$

where c is light's velocity in vacuum, n a refractive index (so that $v_p = cn^{-1}$ is the phase velocity), and $\mathbf{r}$ a real vector of spatial coordinates. With wave (11.54) and constitutive relation (11.53), Maxwell's equations yield

$$\boldsymbol{\eta}\mathbf{D}(\mathbf{s}) - \mathbf{s}\mathbf{s}^T\boldsymbol{\eta}\mathbf{D}(\mathbf{s}) = \frac{1}{n^2(\mathbf{s})}\mathbf{D}(\mathbf{s}). \tag{11.55}$$

Multiplying equation (11.55) by the vector $\mathbf{s}^T$ from the left, we find that for plane waves the vector $\mathbf{D}$ is always orthogonal to the direction $\mathbf{s}$, i.e. $\mathbf{s}^T\mathbf{D}(\mathbf{s}) = 0$. This constraint transforms (11.55) into the eigenvalue problem [270]

$$\left[(\mathbf{I} - \mathbf{s}\mathbf{s}^T)\boldsymbol{\eta}(\mathbf{I} - \mathbf{s}\mathbf{s}^T)\right]\mathbf{u} = \lambda\mathbf{u}, \tag{11.56}$$

where $\lambda = n^{-2}$, $\mathbf{u} = \mathbf{D}$, and $\mathbf{I}$ is the identity matrix. Since $\mathbf{I} - \mathbf{s}\mathbf{s}^T$ is a singular matrix, one of the eigenvalues λ is always zero. We denote the other two eigenvalues by λ_+ and λ_-. These eigenvalues determine refractive indices n. The corresponding eigenvectors yield polarizations.

The inverse dielectric tensor is a complex non-Hermitian matrix $\boldsymbol{\eta} = \boldsymbol{\eta}_{\text{transp}} + \boldsymbol{\eta}_{\text{dichroic}} + \boldsymbol{\eta}_{\text{chiral}}$. The symmetric part of $\boldsymbol{\eta}$ consists of the real matrix $\boldsymbol{\eta}_{\text{transp}}$ and the matrix $\boldsymbol{\eta}_{\text{dichroic}}$ with pure imaginary entries. It constitutes the anisotropy tensor, describing the birefringence of the crystal. For a transparent crystal, the anisotropy tensor is real and is represented only by the matrix $\boldsymbol{\eta}_{\text{transp}}$; for a crystal with linear dichroism it is complex. Choosing a basis along the principal axes of $\boldsymbol{\eta}_{\text{transp}}$, we have $\boldsymbol{\eta}_{\text{transp}} = \text{diag}\,(\eta_1, \eta_2, \eta_3)$.

The matrices

$$\boldsymbol{\eta}_{\text{dichroic}} = i\begin{pmatrix} \eta^d_{11} & \eta^d_{12} & \eta^d_{13} \\ \eta^d_{12} & \eta^d_{22} & \eta^d_{23} \\ \eta^d_{13} & \eta^d_{23} & \eta^d_{33} \end{pmatrix}, \quad \boldsymbol{\eta}_{\text{chiral}} = i\begin{pmatrix} 0 & -g_3 & g_2 \\ g_3 & 0 & -g_1 \\ -g_2 & g_1 & 0 \end{pmatrix}, \tag{11.57}$$

describe linear dichroism (absorption) and chirality (optical activity) of the crystal, respectively. The matrix $\boldsymbol{\eta}_{\text{chiral}}$ is determined by the optical activity vector $\mathbf{g} =$

(g_1, g_2, g_3) that linearly depends on s as

$$\mathbf{g} = \boldsymbol{\gamma}\mathbf{s} = \begin{pmatrix} \gamma_{11} & \gamma_{12} & \gamma_{13} \\ \gamma_{12} & \gamma_{22} & \gamma_{23} \\ \gamma_{13} & \gamma_{23} & \gamma_{33} \end{pmatrix} \begin{pmatrix} s_1 \\ s_2 \\ s_3 \end{pmatrix}, \tag{11.58}$$

where $\boldsymbol{\gamma}$ is a symmetric optical activity tensor; this tensor has an imaginary part for a material with circular dichroism [52]. Note that in [482, 533], the effective macroscopic dielectric tensor of anisotropic crystals with absorption and chirality has been instructively obtained on the basis of the most general Tellegen constitutive relations [567] in the long-wavelength limit of the Bloch waves representing the full solution of Maxwell's equations in periodic media.

11.3.1 DPs in Hamilton's conical refraction

In a transparent nonchiral crystal $\boldsymbol{\eta}_{\text{dichroic}} = 0$ and $\boldsymbol{\gamma} = 0$. Then the matrix

$$\mathbf{A}(\mathbf{p}) = (\mathbf{I} - \mathbf{s}\mathbf{s}^T)\boldsymbol{\eta}_{\text{transp}}(\mathbf{I} - \mathbf{s}\mathbf{s}^T) \tag{11.59}$$

is real symmetric and depends on a vector of two parameters $\mathbf{p} = (s_1, s_2)^T$. The third component of the direction vector s is found as $s_3 = \pm\sqrt{1 - s_1^2 - s_2^2}$. In biaxial anisotropic crystals the dielectric constants are different: $\eta_1 > \eta_2 > \eta_3$.

Nonzero eigenvalues $\lambda_\pm$ of $\mathbf{A}(\mathbf{p})$ follow from Lewin's formula (2.47) as

$$\lambda_\pm = \frac{\operatorname{tr}\mathbf{A}}{2} \pm \frac{1}{2}\sqrt{2\operatorname{tr}(\mathbf{A}^2) - (\operatorname{tr}\mathbf{A})^2}. \tag{11.60}$$

The eigenvalues $\lambda_\pm$ are the same for opposite directions s and −s. Taking into account that $\boldsymbol{\eta}_{\text{transp}} = \operatorname{diag}(\eta_1, \eta_2, \eta_3)$ and substituting equation (11.59) into equation (11.60), we find that λ_+ and λ_- are in 1 : 1 semisimple resonance at

$$\begin{aligned} &\mathbf{s}_0^T = (S_1, S_2, S_3), \quad \lambda_0 = \eta_2; \\ &S_1 = \pm\sqrt{(\eta_1 - \eta_2)/(\eta_1 - \eta_3)},\ S_2 = 0,\ S_3 = \pm\sqrt{1 - S_1^2}. \end{aligned} \tag{11.61}$$

The characteristic equation of the matrix (11.59) can be written in the form

$$\sum_{i=1}^{3} \frac{s_i^2}{\lambda - \eta_i} = 0 \tag{11.62}$$

that yields *Fresnel's equation of wave normals* after expressing $\lambda = v_p^2 c^{-2}$ and introducing the principle velocities of propagation $v_i = c\sqrt{\eta_i}$. The eigenvalues (11.60), i.e. the roots of equation (11.62) where the relation $s_3 = \pm\sqrt{1 - s_1^2 - s_2^2}$ is taken into account, define generically two phase velocities for every pair (s_1, s_2). Equations (11.61) determine four (for two signs of S_1 and S_3) directions along which there is only one velocity of propagation, i.e. the *optic axes* of wave normals [78]. They correspond to the diabolical points in Figure 11.7 (a).

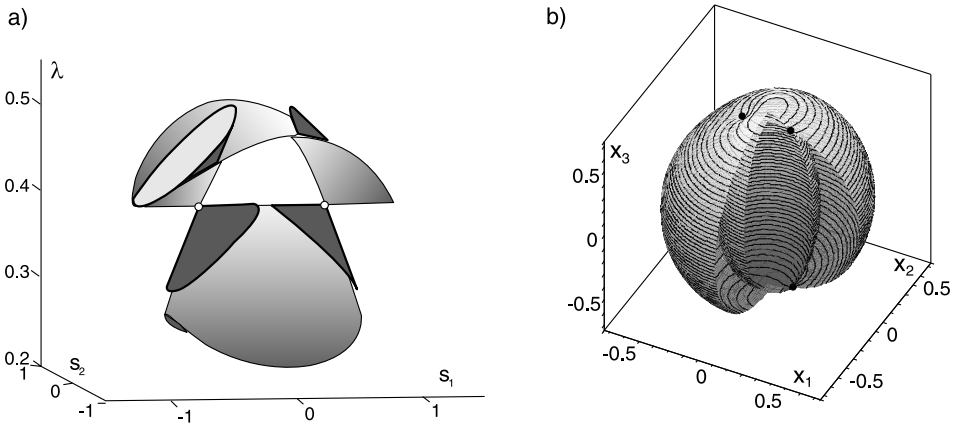

Figure 11.7. A biaxial crystal with $\eta_1 = 0.5$, $\eta_2 = 0.4$, $\eta_3 = 0.1$. (a) Two sheets (11.60) of the eigensurface determined by the dispersion relation (11.62) connected through the diabolical singularities at the optic axes with $s_1 = S_1 = \pm 0.5$ and $s_2 = S_2 = 0$ and the approximation of the cones (11.68) [270]; (b) the two-sheeted Fresnel wave surface (11.65) with the conical singularities at biradials $\mathbf{x}_0^T = (S_1\sqrt{\eta_3}, 0, S_3\sqrt{\eta_1})$.

With the *slowness vector* $\boldsymbol{\xi} = (c\sqrt{\lambda})^{-1}\mathrm{s}$, equation (11.62) determines the locus of points $v_p^{-1}\mathrm{s}$, i.e. the *slowness surface* of the crystal [104, 189]

$$\sum_{i=1}^{3} \frac{(c\xi_i)^2}{1 - \eta_i \|c\boldsymbol{\xi}\|^2} = 0. \tag{11.63}$$

Denoting $\mathbf{z} = c\boldsymbol{\xi}$, we arrive at the equivalent form of the slowness surface

$$\eta_1\eta_2\eta_3\|\mathbf{z}\|^2 \sum_{i=1}^{3} \frac{z_i^2}{\eta_i} - \sum z_1^2\eta_1(\eta_2 + \eta_3) + 1 = 0, \tag{11.64}$$

where the second sum is cyclic. The quartic (11.64) in $\mathbf{z}$ space consists of two sheets connected through the four conical points located at $\mathbf{z}_0 = c\xi_0 = \lambda_0^{-1/2}\mathrm{s}_0$, where s_0 is one of the four optic axes (*binormals*) specified by equation (11.61).

A reciprocal to the slowness surface is *Fresnel's wave surface* [104, 189]

$$\|\mathbf{x}\|^2 \sum_{i=1}^{3} \eta_i x_i^2 - \sum x_1^2\eta_1(\eta_2 + \eta_3) + \eta_1\eta_2\eta_3 = 0, \tag{11.65}$$

where, again, the second sum is cyclic. In the $\mathbf{x}$ space the two-sheeted wave surface has four conical self-intersections at the points $\mathbf{x}_0^T = (S_1\sqrt{\eta_3}, 0, S_3\sqrt{\eta_1})$ specifying the *biradial lines*. Four special planes are tangent to the surface (11.65) along the contours surrounding the biradials $\mathbf{x}_0$. These contours are reciprocal to the conical points of the slowness surface, $\mathbf{z}_0$ [104, 189]. The cones of the internal conical refraction predicted by Hamilton have their vertices at the origin of the $\mathbf{x}$ space and pass through the

contours on the wave surface that is plotted in Figure 11.7 (b). When a beam of light propagates through the crystal along a biradial line, rather than a binormal, it produces a diverging hollow cone of light outside the crystal (*external conical refraction*). Both types of conical refraction were observed already in Lloyd's experiments [78].

11.3.2 Approximation of the dispersion surface near a DP

The double eigenvalue $\lambda_0 = \eta_2$ of the matrix $\mathbf{A}_0 = \mathbf{A}(\mathbf{p}_0)$, $\mathbf{p}_0^T = (S_1, 0)$ possesses two linearly independent eigenvectors

$$\mathbf{u}_1^T = (0, 1, 0), \quad \mathbf{u}_2^T = (S_3, 0, -S_1), \tag{11.66}$$

satisfying normalization conditions (11.19). Then, at the diabolical points (11.61) the vectors $\mathbf{f}_{ij}$ with components (11.9) are

$$\mathbf{f}_{11}^T = (0, 0), \quad \mathbf{f}_{22}^T = (2(\eta_3 - \eta_1)S_1, 0), \quad \mathbf{f}_{12}^T = \mathbf{f}_{21}^T = (0, (\eta_3 - \eta_1)S_1S_3). \tag{11.67}$$

With the coordinates (11.61) and vectors (11.67), equation (11.10) yields an approximation of the dispersion surface in the (s_1, s_2, λ)-space near DPs

$$(\lambda - \eta_2 - (\eta_3 - \eta_1)S_1(s_1 - S_1))^2 = (\eta_3 - \eta_1)^2 S_1^2((s_1 - S_1)^2 + S_3^2 s_2^2). \tag{11.68}$$

Equation (11.68) is valid for each of the four optic axes (11.61).

As an example, consider the case of $\eta_1 = 0.5$, $\eta_2 = 0.4$, $\eta_3 = 0.1$. Conical surfaces (11.68) are shown in Figure 11.7 (a) together with the exact eigenvalue surfaces (11.60). The two optic axes presented in Figure 11.7 (a) are $\mathrm{s}_0 = (\pm 1/2, 0, \sqrt{3}/2)^T$ with the double eigenvalue $\lambda_0 = 2/5$; the eigenvalue surfaces for the opposite directions $\mathrm{s}_0 = (\pm 1/2, 0, -\sqrt{3}/2)^T$ are exactly the same.

11.3.3 Eigensurfaces of absorption- and chirality-dominated crystals

If the crystal possesses absorption and chirality, the matrix family (11.59) takes a complex increment $\mathbf{A}(\mathbf{p}) + \Delta\mathbf{A}(\mathbf{p})$, where

$$\Delta\mathbf{A}(\mathbf{p}) = (\mathbf{I} - \mathrm{ss}^T)(\boldsymbol{\eta}_{\text{dichroic}} + \boldsymbol{\eta}_{\text{chiral}})(\mathbf{I} - \mathrm{ss}^T). \tag{11.69}$$

In the case when the absorption and chirality are weak, i.e. $\varepsilon = \|\boldsymbol{\eta}_{\text{dichroic}}\| + \|\boldsymbol{\eta}_{\text{chiral}}\|$ is small, the perturbation theory presented above describes unfolding the diabolic singularities accurately enough. We need to know only the perturbation $\Delta\mathbf{A}$ at the optic axes of the transparent nonchiral crystal s_0.

Indeed, with the matrix (11.69) evaluated at (11.61), expression (11.22) yields

$$\begin{aligned}
&\varepsilon_{11} = i\eta_{22}^d, \quad \varepsilon_{22} = i\eta_{11}^d S_3^2 - 2i\eta_{13}^d S_1 S_3 + i\eta_{33}^d S_1^2,\\
&\varepsilon_{12} = -i(\eta_{23}^d + \gamma_{11}S_1 + \gamma_{13}S_3)S_1 + i(\eta_{12}^d - \gamma_{13}S_1 - \gamma_{33}S_3)S_3,\\
&\varepsilon_{21} = -i(\eta_{23}^d - \gamma_{11}S_1 - \gamma_{13}S_3)S_1 + i(\eta_{12}^d + \gamma_{13}S_1 + \gamma_{33}S_3)S_3.
\end{aligned} \tag{11.70}$$

Then, according to (11.15), we find

$$\begin{aligned}
\mu &= i\,(\eta^d_{22} + \eta^d_{11}S_3^2 - 2\eta^d_{13}S_1S_3 + \eta^d_{33}S_1^2)/2,\\
\xi &= i\,(\eta^d_{22} - \eta^d_{11}S_3^2 + 2\eta^d_{13}S_1S_3 - \eta^d_{33}S_1^2)/2,\\
\eta &= i\,(\eta^d_{12}S_3 - \eta^d_{23}S_1),\\
\zeta &= -i\,\left(\gamma_{11}S_1^2 + 2\gamma_{13}S_1S_3 + \gamma_{33}S_3^2\right).
\end{aligned} \tag{11.71}$$

Since ξ and η depend only on all the components of the tensor $\boldsymbol{\eta}_{\text{dichroic}}$ (absorption), whereas ζ depends only on the components of the optical activity tensor $\boldsymbol{\gamma}$ (chirality), the parameter $D = \mathrm{Im}^2\xi + \mathrm{Im}^2\eta - \mathrm{Im}^2\zeta$ can serve as an indicator of relative strength of dichroism and chirality.

Indeed, in [52] it was shown that the double-coffee-filter singularity arises in absorption-dominated crystals, and the sheets of real parts of eigenvalues are separated in chirality-dominated crystals. According to the general formulas (11.38) and (11.39), these two cases are explicitly determined by the conditions $D > 0$ and $D < 0$, respectively.

There are four optic axes (11.61), which determine two pairs of opposite space directions $\pm\mathbf{s}_0$. The unfolding conditions coincide for the optic axes given by opposite directions, while these conditions are different for different pairs of optic axes. In the absorption-dominated case, when diabolic singularities unfold into coffee filters near two opposite optic axes $\pm\mathbf{s}_0 = \pm(S_1, 0, S_3)^T$, the four exceptional points of eigenvalue coupling $\pm\mathbf{s}_a$ and $\pm\mathbf{s}_b$ (singular axes [52]) appear. By using (11.67) in (11.27), we obtain the asymptotic formulae

$$s_1^{a,b} = S_1 + \frac{x_{a,b}}{(\eta_1 - \eta_3)S_1}, \quad s_2^{a,b} = \frac{y_{a,b}}{(\eta_3 - \eta_1)S_1S_3}, \quad s_3^{a,b} = \sqrt{1 - \left(s_1^{a,b}\right)^2 - \left(s_2^{a,b}\right)^2}, \tag{11.72}$$

for the components of the vectors $\mathbf{s}_{a,b}$, where $x_{a,b}$ and $y_{a,b}$ are found by using expressions (11.38), (11.39), and (11.71).

Equation $\mathrm{Im}\,c = 0$ determines a line of singularities in the plane of the components of the vector $\mathbf{p} = (s_1, s_2)^T$. By using expressions (11.67) and (11.71) in equations (11.27) and (11.31), we find this line in the form

$$(s_1 - S_1)S_1(\eta_1 - \eta_3)\mathrm{Im}\,\xi - s_2S_1S_3(\eta_1 - \eta_3)\,\mathrm{Im}\,\eta - \mathrm{Re}\,\zeta\,\mathrm{Im}\,\zeta = 0. \tag{11.73}$$

In the *absorption-dominated crystal*, the line (11.73) contains two exceptional points $\mathbf{p}_{a,b} = (s_1^{a,b}, s_2^{a,b})^T$ corresponding to the singular axes $\mathbf{s}_{a,b}$. A segment between the points $\mathbf{p}_a$ and $\mathbf{p}_b$ corresponds to the coincidence of real parts of the eigenvalues $\mathrm{Re}\,\lambda_+ = \mathrm{Re}\,\lambda_-$, while imaginary parts of the eigenvalues $\mathrm{Im}\,\lambda_+ = \mathrm{Im}\,\lambda_-$ merge at points of line (11.73) outside this segment, see Figure 11.8 (b).

In the *chirality-dominated crystal*, when singular axes do not appear, imaginary parts of the eigenvalues $\mathrm{Im}\,\lambda_+ = \mathrm{Im}\,\lambda_-$ coincide at points of the whole line (11.73), see Figure 11.8 (a). If the optical activity tensor $\boldsymbol{\gamma}$ is real or purely imaginary, then the

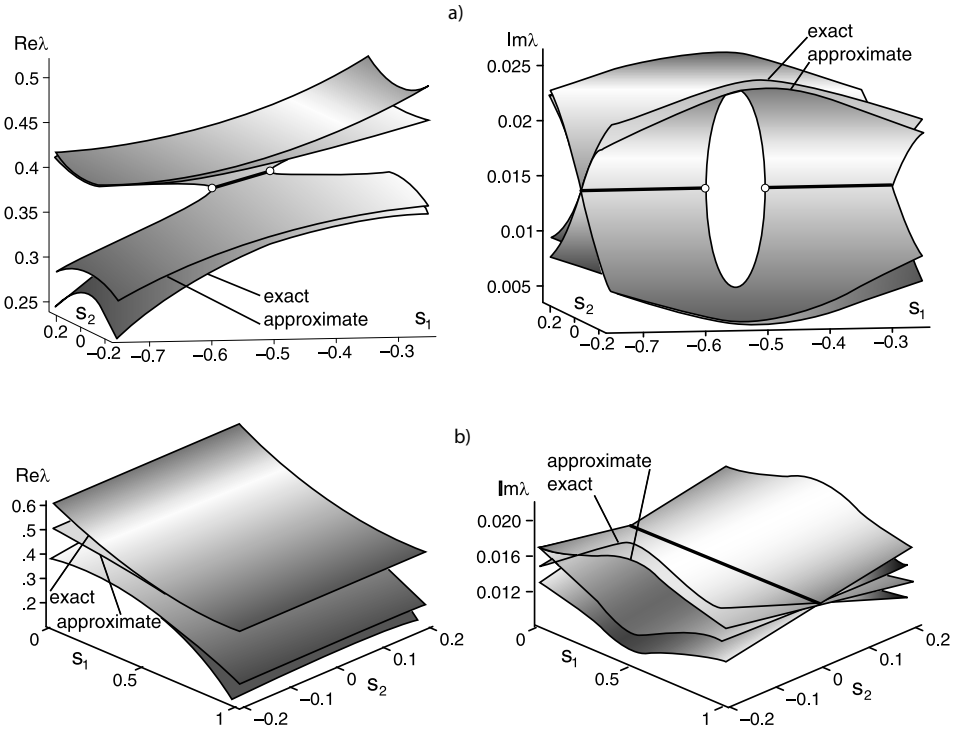

Figure 11.8. Eigensurfaces in (a) absorption-dominated case (the double-coffee-filter [260] and the viaduct [294, 506]) and (b) chirality-dominated case [270].

line of singularities (11.73) passes through the diabolic point $\mathbf{p}_0$, and the position of this line does not depend on $\boldsymbol{\gamma}$.

As a numerical example, let us consider a crystal possessing weak absorption and chirality described by the tensors (11.57), (11.58) with

$$\boldsymbol{\eta}_{\text{dichroic}} = \frac{i}{200}\begin{pmatrix} 3 & 2 & 0 \\ 2 & 3 & 1 \\ 0 & 1 & 3 \end{pmatrix}, \quad \boldsymbol{\gamma} = \frac{1}{200}\begin{pmatrix} 3 & 1 & 2 \\ 1 & 3 & 1 \\ 2 & 1 & 3 \end{pmatrix}. \tag{11.74}$$

A corresponding transparent nonchiral crystal is characterized by $\eta_1 = 0.5$, $\eta_2 = 0.4$, $\eta_3 = 0.1$, and its eigenvalue surfaces with two optic axes are presented in Figure 11.7. By using (11.74) in (11.71), we find that the condition $D = \frac{7}{160000}(4\sqrt{3} - 5) > 0$ is satisfied for the left optic axis $\mathbf{s}_0 = (-1/2,\ 0,\ \sqrt{3}/2)^T$. Hence, the diabolic singularity bifurcates into a double-coffee-filter with two exceptional points whose coordinates according to expressions (11.72) are

$$\mathbf{p}_a = \left(-\frac{1}{2} - \frac{1}{80}\sqrt{-35 + 28\sqrt{3}}, 0\right)^T, \quad \mathbf{p}_b = \left(-\frac{1}{2} + \frac{1}{80}\sqrt{-35 + 28\sqrt{3}}, 0\right)^T. \tag{11.75}$$

Local approximations of the eigensurfaces give equations (11.32) and (11.33), where

$$\mathrm{Re}\, c = \frac{35-28\sqrt{3}}{160000} + \frac{1}{25}(s_1+1/2)^2 + \frac{3}{100}s_2^2, \;\; \mathrm{Im}\, c = -\frac{6+\sqrt{3}}{2000}\, s_2. \quad (11.76)$$

Figure 11.8 (a) shows these local approximations compared with the exact eigenvalue surfaces given by (11.60). For the right optic axis $\mathbf{s}_0 = (1/2,\, 0,\, \sqrt{3}/2)^T$, the condition $D = -\frac{7}{160000}(4\sqrt{3}+5) < 0$ is satisfied. Hence, the eigenvalue sheets (for real parts) separate under the bifurcation of the right diabolic singularity. Approximate and exact eigenvalue surfaces are shown in Figure 11.8 (b). The approximations follow from equations (11.32) and (11.33), where

$$\mathrm{Re}\, c = \frac{35+28\sqrt{3}}{160000} + \frac{1}{25}(s_1-1/2)^2 + \frac{3}{100}s_2^2, \;\; \mathrm{Im}\, c = -\frac{6-\sqrt{3}}{2000}\, s_2. \quad (11.77)$$

11.4 Eigensurfaces associated with EPs

Let $\mathbf{p}_0$ be an exceptional point where the spectrum of the complex matrix family $\mathbf{A}(\mathbf{p})$ has a double complex eigenvalue λ_0 with an eigenvector $\mathbf{u}_0$ and an associated vector $\mathbf{u}_1$. Introducing real n-vectors $\mathbf{f}, \mathbf{g}, \mathbf{h}, \mathbf{r}$ with the components

$$f_s = \mathrm{Re}\left(\frac{\partial \mathbf{A}}{\partial p_s}\mathbf{u}_0, \mathbf{v}_0\right), \;\; g_s = \mathrm{Im}\left(\frac{\partial \mathbf{A}}{\partial p_s}\mathbf{u}_0, \mathbf{v}_0\right), \quad (11.78)$$

$$h_s = \mathrm{Re}\left(\frac{\partial \mathbf{A}}{\partial p_s}\mathbf{u}_0, \mathbf{v}_1\right) + \mathrm{Re}\left(\frac{\partial \mathbf{A}}{\partial p_s}\mathbf{u}_1, \mathbf{v}_0\right), \;\; r_s = \mathrm{Im}\left(\frac{\partial \mathbf{A}}{\partial p_s}\mathbf{u}_0, \mathbf{v}_1\right) + \mathrm{Im}\left(\frac{\partial \mathbf{A}}{\partial p_s}\mathbf{u}_1, \mathbf{v}_0\right)$$

and neglecting higher order terms, from (11.17) we obtain

$$\mathrm{Re}\Delta\lambda + i\,\mathrm{Im}\Delta\lambda = \pm\sqrt{\langle \mathbf{f}, \Delta\mathbf{p}\rangle + i\,\langle \mathbf{g}, \Delta\mathbf{p}\rangle} + \frac{1}{2}(\langle \mathbf{h}, \Delta\mathbf{p}\rangle + i\,\langle \mathbf{r}, \Delta\mathbf{p}\rangle), \quad (11.79)$$

where $\Delta\lambda = \lambda_\pm - \lambda_0$, $\Delta\mathbf{p} = \mathbf{p} - \mathbf{p}_0$, and angular brackets denote inner product of real vectors: $\langle \mathbf{a}, \mathbf{b}\rangle = \sum_{s=1}^{n} a_s b_s$. The perturbed eigenvalue remains double in the first approximation when the following two equations are satisfied

$$\langle \mathbf{f}, \Delta\mathbf{p}\rangle = 0, \;\; \langle \mathbf{g}, \Delta\mathbf{p}\rangle = 0. \quad (11.80)$$

Hence, codimension of the EP is 2 and the double complex eigenvalue corresponds to an isolated point in the plane of two parameters. In the three-parameter space the double eigenvalues form a curve, cf. Figure 11.5. Equations (11.80) define a tangent line to this curve at the point $\mathbf{p}_0$.

Taking the square of (11.79), where the terms linear with respect to the increment of parameters are neglected, and separating real and imaginary parts, we find

$$(\mathrm{Re}\Delta\lambda)^2 - (\mathrm{Im}\Delta\lambda)^2 = \langle \mathbf{f}, \Delta\mathbf{p}\rangle, \;\; 2\mathrm{Re}\Delta\lambda\,\mathrm{Im}\Delta\lambda = \langle \mathbf{g}, \Delta\mathbf{p}\rangle. \quad (11.81)$$

Isolating Δp_1 in one of the equations (11.81) and substituting it into the other yields

$$g_1(\mathrm{Re}\Delta\lambda)^2 - 2f_1\mathrm{Re}\Delta\lambda\mathrm{Im}\Delta\lambda - g_1(\mathrm{Im}\Delta\lambda)^2 = \gamma, \tag{11.82}$$

where γ is a small real constant

$$\gamma = \sum_{s=2}^{n}(f_s g_1 - f_1 g_s)\Delta p_s. \tag{11.83}$$

In equation (11.83) we assume $f_1^2 + g_1^2 \neq 0$. Equation (11.82) describes hyperbolic trajectories of the eigenvalues $\lambda_\pm$ in the complex plane when only Δp_1 is changed and the increments $\Delta p_2, \ldots, \Delta p_n$ are fixed. Of course, any component of the vector $\Delta\mathbf{p}$ can be chosen instead of Δp_1.

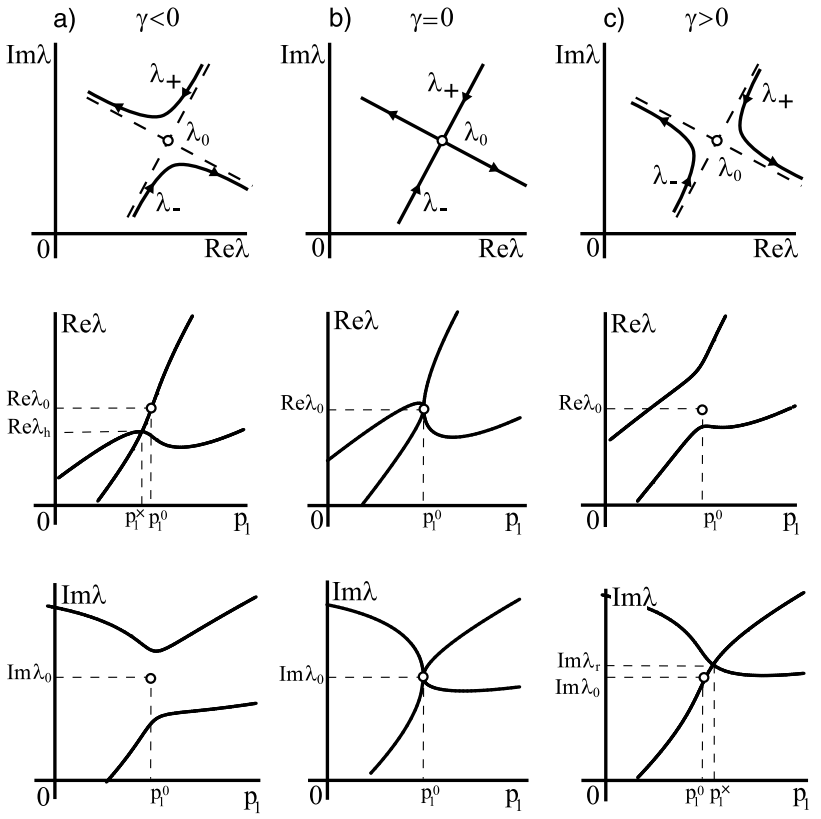

Figure 11.9. Crossing and avoided crossings of eigenvalues near an EP [458, 517] that represent, in particular, the 'great variety of new lines, different from those arising from the section of a cone' [591] in the cross-sections of the conical wedge of Wallis.

If $\Delta p_j = 0$, $j = 2, \ldots, n$, or if $\gamma = 0$, then equation (11.82) yields two perpendicular lines that for $g_1 \neq 0$ are described by the expression

$$g_1 \mathrm{Re}(\lambda - \lambda_0) - \left(f_1 \pm \sqrt{f_1^2 + g_1^2}\right) \mathrm{Im}(\lambda - \lambda_0) = 0. \tag{11.84}$$

These lines intersect at the point λ_0 of the complex plane. Due to variation of the parameter p_1 two eigenvalues $\lambda_\pm$ approach along one of the lines (11.84), merge to λ_0 at $\Delta p_1 = 0$, and then diverge along the other line (11.84), perpendicular to the line of approach; see Figure 11.9 (b), where the arrows show motion of eigenvalues with a monotonous change of p_1. The eigenvalues originated after the coupling cannot be identified with those before coupling.

If $\gamma \neq 0$, then equation (11.82) defines a hyperbola in the complex plane

$$(g_1 \mathrm{Re}(\lambda - \lambda_0) - f_1 \mathrm{Im}(\lambda - \lambda_0))^2 - (\mathrm{Im}(\lambda - \lambda_0))^2 (f_1^2 + g_1^2) = \gamma g_1, \tag{11.85}$$

where $g_1 \neq 0$. Its asymptotes are described by equation (11.84). As Δp_1 changes monotonously, two eigenvalues λ_+ and λ_- moving each along its own branch of hyperbola come closer, turn and diverge; see Figure 11.9 (a, c). Note that for a small γ the eigenvalues $\lambda_\pm$ come arbitrarily close to each other without coupling (*imperfect merging* [226]). When γ changes sign, the quadrants containing hyperbola branches are changed to the adjacent.

From the equations (11.81), it follows

$$\mathrm{Re}\lambda_\pm = \lambda_0 + \frac{1}{2}\langle \mathbf{h}, \Delta\mathbf{p}\rangle \pm \sqrt{\frac{1}{2}\left(\langle \mathbf{f}, \Delta\mathbf{p}\rangle + \sqrt{\langle \mathbf{f}, \Delta\mathbf{p}\rangle^2 + \langle \mathbf{g}, \Delta\mathbf{p}\rangle^2}\right)}, \tag{11.86}$$

$$\mathrm{Im}\lambda_\pm = \lambda_0 + \frac{1}{2}\langle \mathbf{r}, \Delta\mathbf{p}\rangle \pm \sqrt{\frac{1}{2}\left(-\langle \mathbf{f}, \Delta\mathbf{p}\rangle + \sqrt{\langle \mathbf{f}, \Delta\mathbf{p}\rangle^2 + \langle \mathbf{g}, \Delta\mathbf{p}\rangle^2}\right)}. \tag{11.87}$$

Equations (11.86) and (11.87) define hypersurfaces in the spaces $(p_1, p_2, \ldots, p_n, \mathrm{Re}\lambda)$ and $(p_1, p_2, \ldots, p_n, \mathrm{Im}\lambda)$, see Figure 11.10. The sheets $\mathrm{Re}\lambda_+(\mathbf{p})$ and $\mathrm{Re}\lambda_-(\mathbf{p})$ of the eigensurface (11.86) are connected at the points of the set

$$\mathrm{Re}\Delta\lambda = \frac{1}{2}\langle \mathbf{h}, \Delta\mathbf{p}\rangle, \quad \langle \mathbf{g}, \Delta\mathbf{p}\rangle = 0, \quad \langle \mathbf{f}, \Delta\mathbf{p}\rangle \leq 0, \tag{11.88}$$

where the real parts of the eigenvalues $\lambda_\pm$ coincide: $\mathrm{Re}\lambda_- = \mathrm{Re}\lambda_+$. The set

$$\mathrm{Im}\Delta\lambda = \frac{1}{2}\langle \mathbf{r}, \Delta\mathbf{p}\rangle, \quad \langle \mathbf{g}, \Delta\mathbf{p}\rangle = 0, \quad \langle \mathbf{f}, \Delta\mathbf{p}\rangle \geq 0, \tag{11.89}$$

glues the sheets $\mathrm{Im}\lambda_+(\mathbf{p})$ and $\mathrm{Im}\lambda_-(\mathbf{p})$ of the eigensurface (11.87).

Consider now the functions $\mathrm{Re}\lambda(p_1)$ and $\mathrm{Im}\lambda(p_1)$ at fixed values of the other parameters $p_2, p_3, \ldots, p_n$. When $\Delta p_s = 0$, $s = 2, 3, \ldots, n$, both the real and imaginary parts of the eigenvalues $\lambda_\pm$ cross at $p_1 = p_1^0$, see Figure 11.9 (b). The crossings are

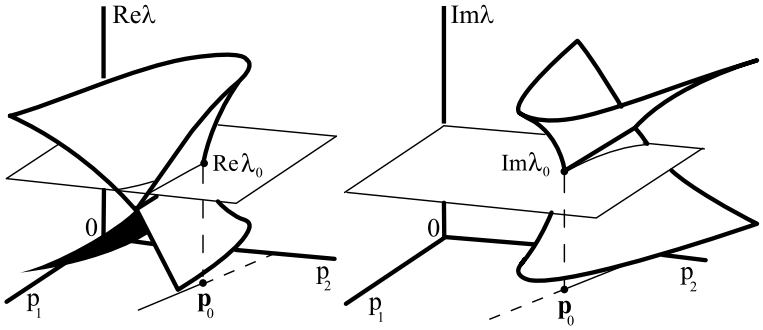

Figure 11.10. Eigenvalue surfaces in the vicinity of an exceptional point [517].

the double cusps which are approximated by the equations

$$\mathrm{Re}\Delta\lambda = \pm\sqrt{\frac{f_1 \pm \sqrt{f_1^2+g_1^2}}{2}\Delta p_1} + \frac{h_1}{2}\Delta p_1,$$
$$\mathrm{Im}\Delta\lambda = \pm\sqrt{\frac{-f_1 \pm \sqrt{f_1^2+g_1^2}}{2}\Delta p_1} + \frac{r_1}{2}\Delta p_1 \qquad (11.90)$$

that follow from equations (11.86) and (11.87).

Given $\Delta p_s \neq 0$, $s = 2, 3, \ldots, n$, either real parts of the eigenvalues $\lambda_\pm$ cross due to variation of p_1 whereas the imaginary parts avoid crossing or vice-versa, see Figure 11.9 (a, c). The crossings occur at $p_1^\times = p_1^0 - \sum_{s=2}^n (g_s/g_1)\Delta p_s$ and

$$\mathrm{Re}\lambda_h = \mathrm{Re}\lambda_0 - \frac{1}{2g_1}\sum_{s=2}^{n}(h_1 g_s - g_1 h_s)\Delta p_s,\ \ \mathrm{Im}\lambda_r = \mathrm{Im}\lambda_0 - \frac{1}{2g_1}\sum_{s=2}^{n}(r_1 g_s - g_1 r_s)\Delta p_s. \qquad (11.91)$$

Near these crossings the tangents to the curves (11.86) and (11.87) are

$$\mathrm{Re}\lambda = \mathrm{Re}\lambda_h + \left(\frac{h_1}{2} \pm \frac{g_1}{2}\sqrt{\frac{g_1}{\gamma}}\right)(p_1 - p_1^\times), \qquad (11.92)$$

$$\mathrm{Im}\lambda = \mathrm{Im}\lambda_r + \left(\frac{r_1}{2} \pm \frac{g_1}{2}\sqrt{-\frac{g_1}{\gamma}}\right)(p_1 - p_1^\times), \qquad (11.93)$$

where the coefficient γ is defined by equation (11.83). Lines (11.92) and (11.93) tend to the vertical position as $\gamma \to 0$ and coincide at $\gamma = 0$. The avoided crossings are governed by the equations (11.86) and (11.87).

If the vector of parameters consists of only two components $\mathbf{p} = (p_1, p_2)^T$, then in the vicinity of the EP the eigensurfaces (11.86) and (11.87) have the form of the Whitney umbrella, see Figure 11.10. The sheets of the eigensurfaces are connected along the rays (11.88) and (11.89). These rays are inclined with respect to the plane of the parameters p_1, p_2. The cross-sections of the eigensurfaces by the planes orthogonal

to the axis p_2, described by the equations (11.90)–(11.93), are shown in Figure 11.9. Note that the rays (11.88), (11.89) and the exceptional point $\mathbf{p}_0$ are known in crystal optics as branch cuts and singular axis, respectively [52]. In hydrodynamics, the crossings and avoided crossings of eigenvalues near EPs similar to those shown in Figure 11.9 appeared already in 1980s in the problem of excitation of thermal Rossby waves in a rotating cylindrical annulus with variable curvature [106, 458].

Finally, we look at the movement of eigenvalues in the complex plane near the point $\mathbf{p}_0$ due to cyclic variation of the parameters p_1 and p_2 of the form $\Delta p_1 = a + r\cos\varphi$ and $\Delta p_2 = b + r\sin\varphi$, where a, b, and r are small parameters of the same order. From equations (11.81) we derive

$$\begin{aligned}&(g_1\mathrm{Re}\Delta\lambda^2 - 2f_1\mathrm{Re}\Delta\lambda\mathrm{Im}\Delta\lambda - g_1\mathrm{Im}\Delta\lambda^2 - b(f_2g_1 - f_1g_2))^2 + \\ &(g_2\mathrm{Re}\Delta\lambda^2 - 2f_2\mathrm{Re}\Delta\lambda\mathrm{Im}\Delta\lambda - g_2\mathrm{Im}\Delta\lambda^2 - a(f_1g_2 - g_1f_2))^2 = (f_2g_1 - f_1g_2)^2r^2.\end{aligned} \tag{11.94}$$

If the contour encircles the EP, then the eigenvalues move along the curve (11.94) around the double eigenvalue λ_0 in the complex plane, Figure 11.11 (c), as happens, e.g. in the model of a laser induced photo-dissociation of molecules [365]. In this case $a^2 + b^2 < r^2$ and the loop (11.94) always crosses the lines $\mathrm{Re}\lambda = \mathrm{Re}\lambda_0$ and $\mathrm{Im}\lambda = \mathrm{Im}\lambda_0$ at the four points given by the equations

$$(\mathrm{Re}\Delta\lambda)^2 = \frac{(f_2g_1 - f_1g_2)\left(g_1b - g_2a \pm \sqrt{(g_1b - g_2a)^2 + (r^2 - a^2 - b^2)(g_1^2 + g_2^2)}\right)}{g_1^2 + g_2^2}, \tag{11.95}$$

$$(\mathrm{Im}\Delta\lambda)^2 = \frac{(f_2g_1 - f_1g_2)\left(g_2a - g_1b \pm \sqrt{(g_2a - g_1b)^2 + (r^2 - a^2 - b^2)(g_1^2 + g_2^2)}\right)}{g_1^2 + g_2^2}. \tag{11.96}$$

When $a^2 + b^2 = r^2$ the loop intersects itself at the double eigenvalue and its form depends on the sign of the quantity $\delta = (f_2g_1 - f_1g_2)(g_1b - g_2a)$. If $\delta < 0$ the eigenvalues cross the line $\mathrm{Re}\lambda = \mathrm{Re}\lambda_0$, Figure 11.11 (b), otherwise they cross the line $\mathrm{Im}\lambda = \mathrm{Im}\lambda_0$, Figure 11.11 (d). Eigenvalues pass through the nonsemisimple $1:1$ resonance at λ_0 in the complex plane.

When $a^2 + b^2 > r^2$, the circuit in the parameter plane does not contain the point $\mathbf{p}_0$ and the eigenvalues move in the complex plane along the two different closed paths,

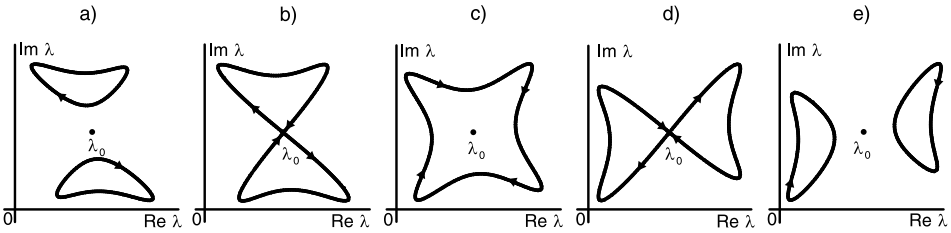

Figure 11.11. Eigenvalue paths when parameters experience a cyclic evolution.

kidneys [19], see Figure 11.11 (a, e). Each eigenvalue crosses the line $\mathrm{Re}\lambda = \mathrm{Re}\lambda_0$ twice for $\delta < 0$, Figure 11.11 (a), and for $\delta > 0$ they cross the axis $\mathrm{Im}\lambda = \mathrm{Im}\lambda_0$, Figure 11.11 (d). In a recent work [148] the 'kidneys' in the complex plane were observed in the case of an EP corresponding to a triple eigenvalue.

11.5 Perturbation of eigenvectors and Berry phase

Let the complex matrix $\mathbf{A}(\mathbf{p})$ be a Hamiltonian of a 'quantum' system [20, 398]

$$\frac{d\,\mathbf{q}}{d\,\tau} = i\,\mathbf{A}\mathbf{q}. \tag{11.97}$$

Assuming $\mathbf{q} = \mathbf{u}\exp i\lambda\tau$ yields the eigenvalue problem (11.2). In this section, we present an approach developed in [397, 398] that quite in the spirit of the work [20] uses the perturbation of eigenvectors at the diabolical and exceptional points for approximate computation of a geometric phase integral along a closed loop in the parameter space around the degeneracies. Indeed, knowing explicitly how the double eigenvalues split we can track the perturbed eigenvalues and eigenvectors with reasonable accuracy when the size of the loop is small. For alternative techniques of tracking the eigenvectors and eigenvalues of parameterized matrices we refer to the works [25, 251, 252].

11.5.1 Hermitian case: geometric phase around a DP

If $\mathbf{A}(\mathbf{p})$ is Hermitian, its eigenvector, $\mathbf{u}_s$, corresponds to a bounded state of the system (11.97) with the energy level $\lambda_s(\mathbf{p})$, where s is the level index. Assume that the eigenvectors corresponding to nondegenerate energy levels are chosen uniquely and depend smoothly on the parameters.

Consider the evolution of the system as the parameter vector $\mathbf{p}(t)$ undergoes an adiabatic cyclic variation, i.e. $\mathbf{p}(0) = \mathbf{p}(T)$. Denote by $C = \{\mathbf{p}(t) : 0 \le t \le T\}$ the parameter variation trajectory, which is an oriented cycle. At the initial time $t = 0$, let the system be at the nondegenerate discrete level $\lambda_s = \lambda_s(\mathbf{p}(0))$, i.e. the wave function $\mathbf{U}(t)$ at $t = 0$ be $\mathbf{U}(0) = \mathbf{u}_s(\mathbf{p}(0))$.

As a result of the cyclic variation of the parameters, the system returns to the initial position (in the adiabatic approximation), acquiring a phase factor consisting of the dynamic phase $\delta_s \sim -\int_0^T \lambda_s(t)dt$ and the geometric (Berry) phase γ_s: $\mathbf{U}(T) = e^{i(\delta_s+\gamma_s)}\mathbf{U}(0)$. The Berry phase is determined by the following integral along C in the parameter space [49]

$$\gamma_s = i\oint_C \frac{(d\,\mathbf{u}_s(\mathbf{p}), \mathbf{u}_s(\mathbf{p}))}{(\mathbf{u}_s(\mathbf{p}), \mathbf{u}_s(\mathbf{p}))}. \tag{11.98}$$

Formula (11.98) simplifies after applying the normalization $(\mathbf{u}_s(\mathbf{p}), \mathbf{u}_s(\mathbf{p})) = 1$. Note that γ_s is a real number for Hermitian Hamiltonians.

Let $\mathbf{p}_0$ be a diabolical point in the parameter space that corresponds to the double semisimple eigenvalue $\lambda_0 = \lambda_s(\mathbf{p}_0) = \lambda_{s+1}(\mathbf{p}_0)$. The eigenvectors $\mathbf{u}_1 = \mathbf{u}_s(\mathbf{p}_0)$ and $\mathbf{u}_2 = \mathbf{u}_{s+1}(\mathbf{p}_0)$ at the diabolic point are chosen so that they satisfy the orthogonality and normalization conditions (11.19).

Consider a cycle $C = \{\mathbf{p}(t) = \mathbf{p}_0 + \varepsilon\widehat{\mathbf{p}}(t) : 0 \le t \le T\}$ around $\mathbf{p}_0$, where $\widehat{\mathbf{p}}(T) = \widehat{\mathbf{p}}(0)$ and $\varepsilon > 0$ is a small parameter. We use the asymptotic formulas (11.6) and (11.7) for the eigenvalues and eigenvectors, where $\varepsilon\mathbf{A}_1$ is the linear part of the parameter dependence of the Hamiltonian at $\mathbf{p}_0$

$$\mathbf{A}_1(\mathbf{p}(t)) = \sum_{k=1}^{m} \frac{\partial \mathbf{A}}{\partial p_k}\bigg|_{\mathbf{p}=\mathbf{p}_0} \widehat{\mathbf{p}}_k(t). \tag{11.99}$$

Introducing real variables x, y, z, linearly related to the parameter vector $\mathbf{p}$ as

$$x + i\,y = (\mathbf{A}_1\mathbf{u}_1, \mathbf{u}_2), \quad 2z = (\mathbf{A}_1\mathbf{u}_1, \mathbf{u}_1) - (\mathbf{A}_1\mathbf{u}_2, \mathbf{u}_2), \tag{11.100}$$

we find from equation (11.8) the energy levels around the degeneracy [398]

$$\lambda_{s,s+1} = \lambda_0 + \varepsilon\left(\frac{(\mathbf{A}_1\mathbf{u}_1, \mathbf{u}_1) + (\mathbf{A}_1\mathbf{u}_2, \mathbf{u}_2)}{2} \pm \sqrt{x^2 + y^2 + z^2}\right) + o(\varepsilon). \tag{11.101}$$

If $\lambda_s \le \lambda_{s+1}$, the minus and plus signs correspond to the indices s and $s+1$ respectively. Thus, x, y and z are effective parameters responsible for the unfolding of the diabolical degeneracy.

By using asymptotic formulas (11.6), (11.7) and (11.101) in equation (11.98) and switching to the spherical coordinates $x = r\sin\theta\cos\varphi$, $y = r\sin\theta\sin\varphi$, $z = r\cos\theta$, we find an asymptotic expression for the Berry phase of the s-th and $(s+1)$-st states [398]

$$\gamma_{s,s+1} = -\frac{1}{2}\oint_C (1 \mp \cos\theta)d\varphi + o(1) = \mp\,\Omega/2 + o(1) \pmod{2\pi}, \tag{11.102}$$

where the upper and lower signs correspond to γ_s and γ_{s+1}, respectively. Here, the integral is evaluated along the cycle in the space of x, y, z, that is the image of C under linear transformation (11.100), and Ω is the solid angle subtended by C on the unit sphere in the space of x, y, z, (see Figure 11.12 (a) which shows a positively oriented cycle and a diabolical point at the origin). In the zeroth approximation with respect to ε the phases γ_s and γ_{s+1} have opposite signs. The general expression (11.102) for the Berry phase agrees with the results obtained for particular physical systems and for Hamiltonians approximable by 2×2 matrices [12, 20, 22, 49, 153, 411].

For time reversal invariant systems, the Hamiltonian $\mathbf{A}(\mathbf{p})$ is a real symmetric matrix [158, 595] and the codimension of a double degeneracy is two. In this case, the eigenvectors $\mathbf{u}_1$ and $\mathbf{u}_2$ can be chosen to be real. Therefore, $y \equiv 0$ and the image of C in the space of x, y, z lies in the plane x, z. As a result, we obtain the well-known

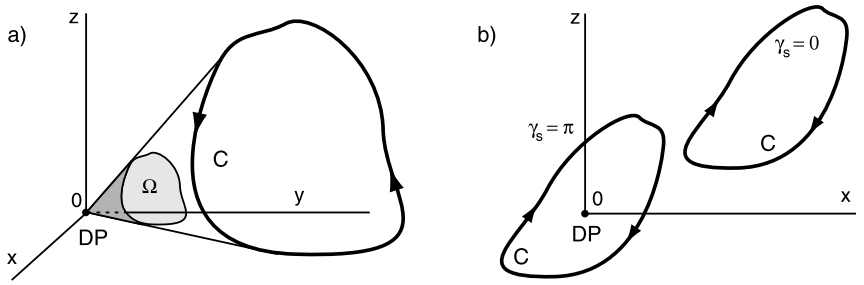

Figure 11.12. Berry phase for a cycle around a diabolic point for (a) Hermitian and (b) real symmetric Hamiltonians.

expressions for the phase: $\gamma_{s,s+1} = \pi$, if C makes a single turn around the diabolic point ($\Omega = 2\pi$), and $\gamma_{s,s+1} = 0$, if the DP lies outside the cycle ($\Omega = 0$), see Figure 11.12 (b). This result does not contain the small component $o(1)$, since the Berry phase for time reversal invariant systems depends only on the topology of the cycle with respect to the degeneracies [49, 398]. Indeed, in this case the integral (11.98) transforms into

$$\gamma_s = \frac{i}{2} \oint_C d \ln(\mathbf{u}_s(\mathbf{p}), \overline{\mathbf{u}_s(\mathbf{p})}),$$

which confirms that the phase is *topological* in contrast to the *geometric* one in irreversible systems with the Hermitian Hamiltonian. Note that the real eigenvector $\mathbf{u}_s(\mathbf{p})$ reverses its sign while going around a degeneracy [20]. Thus, for the eigenvector to be uniquely determined on the cycle, a complex factor has to be introduced that varies from 1 to -1 over a single turn around $\mathbf{p}_0$.

11.5.2 Non-Hermitian case: geometric phase around an EP

Quasi-stationary (metastable) states of a quantum system arise as the eigenvectors $\mathbf{u}_s(\mathbf{p})$ of a non-Hermitian Hamiltonian ($\mathbf{A}^\dagger \neq \mathbf{A}$) that correspond to complex eigenvalues $\lambda_s(\mathbf{p})$ [426]. The real part of an eigenvalue determines the mean energy of a state, and the imaginary part determines the characteristic life time of the state [154]. Generally, the Hamiltonian becomes non-Hermitian due to the boundary condition on the wave function, which requires that the wave be divergent at infinity (instead of vanishing as in the classical condition). Unstable states are frequently called *Gamow states* [362]. Non-Hermitian terms also arise in effective Hamiltonians in scattering theory [426].

As we know, the degenerate states $\lambda_s = \lambda_{s+1}$ of non-Hermitian Hamiltonians have a remarkable property: in contrast to stationary states, their eigenvectors can coincide: $\mathbf{u}_s = \mathbf{u}_{s+1}$. As a result, a double eigenvalue forms a Jordan block, a phenomenon possible only in non-Hermitian systems. The codimension of this exceptional point in the parameter space is two. Remember that non-Hermitian systems can involve

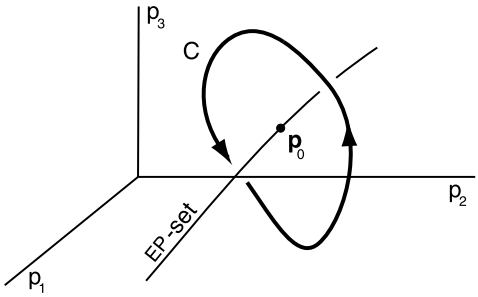

Figure 11.13. A cycle around an EP-set in the parameter space.

degeneracies without forming a Jordan block, but their codimension is much higher [517].

Let $\mathbf{p}_0$ be an exceptional point that corresponds to the double degeneracy $\lambda_0 = \lambda_s(\mathbf{p}_0) = \lambda_{s+1}(\mathbf{p}_0)$. The eigenvalue λ_0 corresponds to a single eigenvector $\mathbf{u}_0 = \mathbf{u}_s(\mathbf{p}_0) = \mathbf{u}_{s+1}(\mathbf{p}_0)$ and an associated vector $\mathbf{u}_1$ that satisfy the equations

$$\mathbf{A}(\mathbf{p}_0)\mathbf{u}_0 = \lambda_0\mathbf{u}_0, \quad \mathbf{A}(\mathbf{p}_0)\mathbf{u}_1 = \lambda_0\mathbf{u}_1 + \mathbf{u}_0. \tag{11.103}$$

The left eigen- and associated vectors $\mathbf{v}_0$ and $\mathbf{v}_1$ of the adjoint operator $\mathbf{A}^\dagger(\mathbf{p}_0)$ are defined in a similar fashion by equations (11.16). The eigenvectors possess the orthogonality property $(\mathbf{u}_0, \mathbf{v}_0) = 0$.

Consider the evolution of the system as its parameters adiabatically traverse a small single cycle $C = \{\mathbf{p}(t) = \mathbf{p}_0 + \varepsilon\widehat{\mathbf{p}}(t) : 0 \le t \le T\}$, around the set of exceptional points Figure 11.13. Let the system be initially at a quasi-stationary state $\mathbf{u}_s(\mathbf{p}(0))$. (Here, the adiabatic condition is supplemented with the requirement that the cycle period T be small compared with the life time of the unstable state.) While traversing the cycle in the parameter space, the system arrives at the second interacting state $\mathbf{u}_{s+1}(\mathbf{p}(0))$ (up to a complex factor) and returns to the initial state only after making the second cycle [418]. After making two cycles, the wave function acquires a dynamic phase and a geometric phase both of which are generally complex [68, 154, 190]. For the double cycle (denoted as $2C$), the Berry phase is defined as [190]

$$\gamma_s = \gamma_{s+1} = i\oint_{2C} \frac{(d\,\mathbf{u}_s(\mathbf{p}), \mathbf{v}_s(\mathbf{p}))}{(\mathbf{u}_s(\mathbf{p}), \mathbf{v}_s(\mathbf{p}))}, \tag{11.104}$$

where $\mathbf{v}_s(\mathbf{p})$ is the left eigenvector corresponding to $\lambda_s(\mathbf{p})$. Since the interacting states interchange after a single cycle, the Berry phases for these states are equal to each other ($\gamma_s = \gamma_{s+1}$). Note that the denominator in equation (11.104) vanishes at the EP.

According to equation (11.17), in the neighborhood of $\mathbf{p}_0$ the eigenvectors are

$$\mathbf{u}_{s,s+1}(\mathbf{p}) = \mathbf{u}_0 \pm \sqrt{\mu\varepsilon}\,\mathbf{u}_1 + o(\varepsilon^{1/2}), \;\; \mathbf{v}_{s,s+1}(\mathbf{p}) = \mathbf{v}_0 \pm \sqrt{\mu\varepsilon}\,\mathbf{v}_1 + o(\varepsilon^{1/2}), \tag{11.105}$$

where

$$\mu(\mathbf{p}) = (\mathbf{A}_1\mathbf{u}_0, \mathbf{v}_0), \quad \mathbf{A}_1(\mathbf{p}) = \sum_{k=1}^{m} \left.\frac{\partial \mathbf{A}}{\partial p_k}\right|_{\mathbf{p}=\mathbf{p}_0} \widehat{p}_k. \tag{11.106}$$

Substituting (11.105) and (11.106) into (11.104) and using the orthogonality and normalization conditions for $\mathbf{v}_{0,1}$ and $\mathbf{u}_{0,1}$, we find [397, 398]

$$\gamma_s = \frac{i}{4}\oint_{2C} d\ln\mu + o(1) = \pi + o(1) \pmod{2\pi}. \tag{11.107}$$

The last equality follows from the logarithm rule, since the complex value μ goes around zero as the parameter vector makes a turn around the EP.

For reversible systems, the Hamiltonian satisfies the condition $\mathbf{A}^\dagger = \overline{\mathbf{A}}$, where $\overline{\mathbf{A}}$ is the complex-conjugate operator [212]. Then the left eigenvectors are equal to the complex-conjugate right eigenvectors: $\mathbf{v}_s = \overline{\mathbf{u}_s}$. In this case

$$\gamma_s = \frac{i}{2}\oint_{2C} d\ln(\mathbf{u}_s(\mathbf{p}), \overline{\mathbf{u}_s(\mathbf{p})}),$$

i.e. it is determined only by the topology of the cycle relative to the degeneracies. Thus, expression (11.107) is exact: $\gamma_s = \pi \pmod{2\pi}$. This situation differs from the case of real Hermitian Hamiltonians only in that the cycle C has to be traversed twice. Therefore, for reversible systems represented by complex symmetric Hamiltonians, the Berry phase around an EP is topological.

In the general case of irreversible non-Hermitian systems ($\mathbf{A}^\dagger \neq \overline{\mathbf{A}}$ and $\mathbf{A} \neq \mathbf{A}^\dagger$) the Berry phase depends on the cycle, i.e. it is geometrical. To find the leading asymptotic term of this dependence, we represent the eigenvectors as

$$\begin{aligned} \mathbf{u}_{s,s+1}(\mathbf{p}) &= \widetilde{\mathbf{u}}_0(\mathbf{p}) \pm \sqrt{\sigma(\mathbf{p})}\widetilde{\mathbf{u}}_1(\mathbf{p}), \\ \mathbf{v}_{s,s+1}(\mathbf{p}) &= \widetilde{\mathbf{v}}_0(\mathbf{p}) \pm \sqrt{\sigma(\mathbf{p})}\widetilde{\mathbf{v}}_1(\mathbf{p}). \end{aligned} \tag{11.108}$$

Here, $\sigma(\mathbf{p}) = \varepsilon\mu(\mathbf{p}) + o(\varepsilon)$ is a smooth function of $\mathbf{p}$. The vectors $\widetilde{\mathbf{u}}_{0,1}(\mathbf{p})$ and $\widetilde{\mathbf{v}}_{0,1}(\mathbf{p})$ are smooth functions of $\mathbf{p}$ and satisfy the conditions [398]

$$\begin{gathered} \widetilde{\mathbf{u}}_{0,1}(\mathbf{p}_0) = \mathbf{u}_{0,1}, \quad \widetilde{\mathbf{v}}_{0,1}(\mathbf{p}_0) = \mathbf{v}_{0,1}, \\ (\widetilde{\mathbf{u}}_0(\mathbf{p}), \widetilde{\mathbf{v}}_0(\mathbf{p})) = (\widetilde{\mathbf{u}}_1(\mathbf{p}), \widetilde{\mathbf{v}}_1(\mathbf{p})) = 0, \ \ (\widetilde{\mathbf{u}}_0(\mathbf{p}), \widetilde{\mathbf{v}}_1(\mathbf{p})) = (\widetilde{\mathbf{u}}_1(\mathbf{p}), \widetilde{\mathbf{v}}_0(\mathbf{p})) = 1. \end{gathered} \tag{11.109}$$

Formulas for the derivatives of $\widetilde{\mathbf{u}}_{0,1}(\mathbf{p})$ and $\widetilde{\mathbf{v}}_{0,1}(\mathbf{p})$ with respect to the parameters at the point $\mathbf{p}_0$ can be found by applying the theory of versal deformations [17, 518]. As a result, combining (11.108) and (11.109) with (11.104), we find

$$\gamma_s = \pm\pi + ia\varepsilon^2 + o(\varepsilon^2), \tag{11.110}$$

where a is the constant defined by [397, 398]

$$a = \sum_{k \neq s,s+1} \oint_C \left(2 \frac{(\mathbf{A}_1 \mathbf{u}_k^{EP}, \mathbf{v}_0)(d\mathbf{A}_1 \mathbf{u}_0, \mathbf{v}_k^{EP})}{(\lambda_k^{EP} - \lambda_0)^3} + \right. \tag{11.111}$$

$$\left. + \frac{(\mathbf{A}_1 \mathbf{u}_k^{EP}, \mathbf{v}_1)(d\mathbf{A}_1 \mathbf{u}_0, \mathbf{v}_k^{EP}) + (\mathbf{A}_1 \mathbf{u}_k^{EP}, \mathbf{v}_0)(d\mathbf{A}_1 \mathbf{u}_1, \mathbf{v}_k^{EP})}{(\lambda_k^{EP} - \lambda_0)^2} \right).$$

Here, $d\mathbf{A}_1 = \sum_{k=1}^{m} \frac{\partial \mathbf{A}}{\partial p_k}\Big|_{\mathbf{p}=\mathbf{p}_0} d\widehat{p}_k$ and $\lambda_k^{EP} = \lambda_k(\mathbf{p}_0)$, $\mathbf{u}_k^{EP} = \mathbf{u}_k(\mathbf{p}_0)$ and $\mathbf{v}_k^{EP} = \mathbf{v}_k(\mathbf{p}_0)$. The right and left eigenvectors are assumed to be normalized: $(\mathbf{u}_k^{EP}, \mathbf{v}_k^{EP}) = 1$. Note that for $k \neq k'$

$$(\mathbf{u}_{0,1}, \mathbf{v}_k^{EP}) = (\mathbf{u}_k^{EP}, \mathbf{v}_{0,1}) = (\mathbf{u}_k^{EP}, \mathbf{v}_{k'}^{EP}) = 0.$$

The quantity $ia\varepsilon^2$ in the formula (11.111) determines the leading term in the dependence of the Berry phase on the size and shape of C only by the information on the system at the exceptional point $\mathbf{p}_0$.

In the expression (11.111), the terms $(\mathbf{A}_1 \mathbf{u}_k^{EP}, \mathbf{v}_{0,1})$ and $(d\mathbf{A}_1 \mathbf{u}_{0,1}, \mathbf{v}_k^{EP})$ describe the interaction of the degenerate level λ_0 with the other levels λ_k, where $k \neq s, s+1$. Thus, the change in the Berry phase with cycle variations in the parameter space is due to the influence of the energy levels not involved in the EP degeneracy.

If the difference $\lambda_k^{EP} - \lambda_0$ is large, the influence of λ_k is proportional to $(\lambda_k^{EP} - \lambda_0)^{-2}$, and can be neglected. However, if $\lambda_k^{EP} - \lambda_0$ is small, the change in the Berry phase due to the interaction with λ_k increases proportionally to $(\lambda_k^{EP} - \lambda_0)^{-3}$ and may be large. In the case $\lambda_k^{EP} - \lambda_0 \to 0$, i.e. near the triple degeneracy $\lambda_s = \lambda_{s+1} = \lambda_k$, we have $a \to \infty$. Thus, triple degeneracies require special analysis, see e.g. [148].

For Hamiltonians represented by 2×2 matrices, we have $a = 0$, since the sum in (11.111) does not contain any term. In this case, $\gamma_n = \pi$ irrespective of the shape or size of C [397, 426]. We have shown above that in the general case the phase is geometrical and deviates from π since the system is multidimensional, see also [418]. This deviation cannot be captured within the framework of two-dimensional approximations.

The derived general asymptotic formulas for the Berry phase around double stationary and quasi-stationary degeneracies can be applied to the analysis of the geometric phase in various physical systems where geometric phases defined in the form of integrals (11.98) and (11.104) arise [154, 351, 365].

11.5.3 Geometric phase around an EP in a microwave cavity

The first experimental evidence of exceptional points came from flat microwave cavities (resonators), which are analogues of quantum billiards [149, 477]. Subsequently

EPs were observed in coupled electronic circuits and recently in chaotic microcavities and atom-cavity quantum composites, for references see e.g. [154, 426, 511].

The microwave resonator used in the experiments [149, 154] consists of three 5 mm thick copper plates, sandwiched on top of each other. The center plate has a hole with the shape of two half circles of 250 mm in diameter, separated by a 10 mm bar of copper except for an opening of 80 mm length. The opening allows a coupling of the electric field modes excited in each half circle, which is varied with a movable gate of copper of length $80\,mm$ and width $3\,mm$ inserted through a small slit in the top plate and operated by a micrometer stepper motor. Its lifting s defines one parameter with 0 mm (no coupling) $\leq s \leq$ 9 mm (full coupling). One half of the cavity contains a movable semicircular Teflon piece with diameter 60 mm and height 5 mm operated by another stepper motor. Its displacement with respect to the center of the cavity defines the second parameter δ. Additionally, a cylindrical ferrite of diameter 4 mm and height 5 mm is put in the right part of the cavity and magnetized by two permanent magnets, which are mounted above and below the cavity. Magnetic field strengths $0\,mT \leq B \leq 90\,mT$ are obtained by varying their distance [154].

A pointlike dipole antenna intrudes into each half of the cavity. A vectorial network analyzer couples microwaves into the cavity through one antenna and measures amplitude and phase of the signal received at the same or the other antenna relative to the input signal. In this way the complex elements of the scattering matrix are determined yielding an effective 2×2 Hamiltonian for two resonances that are well separated from the others [154].

For a nondissipative system with broken time reversal invariance ($B \neq 0$), the Hamiltonian is Hermitian. For a dissipative system, the energy is not conserved such that for $B = 0$ it is described by a complex symmetric Hamiltonian. This case is referred to as the time reversal invariant one. In the general situation, the Hamiltonian comprises both dissipation in the resonator walls and the ferrite and time reversal invariance violation and thus is neither Hermitian nor symmetric complex 2×2 matrix [154].

To realize a coalescence of a pair of eigenmodes at an EP, in the experiment two parameters s and δ are varied with the resolution of 0.01 mm. Figure 11.14 (a) shows at $B = 53\,mT$ around an EP the differences of the real (frequency) and imaginary (width) parts of the complex eigenvalues (resonances), $f_{1,2}$ and $\Gamma_{1,2}$, respectively. The darker the color, the smaller the respective difference is. The darkest color visualizes the branch cut along which it vanishes. That the branch cuts all extend from one common point into opposite directions proves that this is an EP.

For systems with time reversal invariance violation the geometric phase gathered by the eigenvectors around an EP is predicted to be complex [68, 190]. For dissipative time reversal invariant systems it is topological and equal to π after two subsequent encirclings of the EP along even not-coinciding contours [149, 397, 418]. In the irreversible systems, the phase depends on the contour and this dependence is more pronounced if either the other resonances are close to the EP [397, 398], or the con-

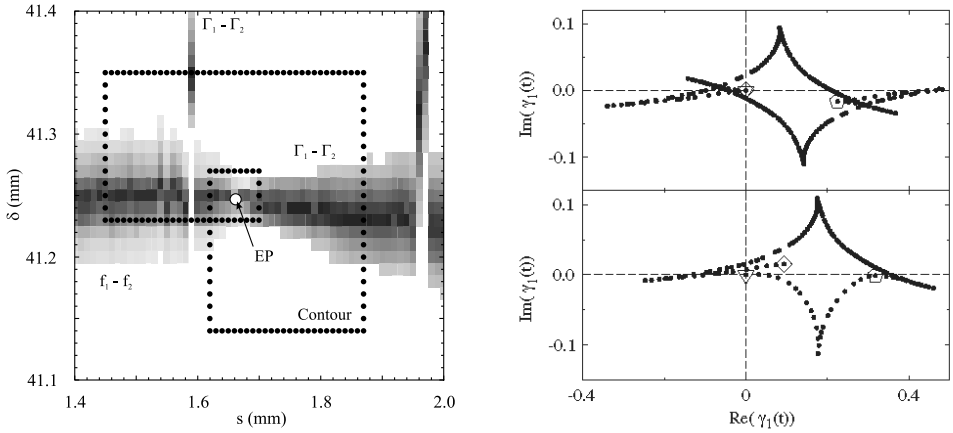

Figure 11.14. (a) In the (s, δ)-plane the gray points show the difference between the frequencies (f) and widths (Γ) of the resonances measured at $B = 53mT$: the darkest gray color indicates two branch cuts meeting at $s_{EP} \approx 1.66\,\text{mm}$ and $\delta_{EP} \approx 41.25\,\text{mm}$ corresponding to the doublet with $f_{1,2} \approx 2.7\,\text{GHz}$ and width $\Gamma_{1,2} \approx 2.0\,\text{MHz}$; black dots mark the double contour proposed in [418]. (b) In the complex plane the evolution of the essential geometric phase is shown in the irreversible case with $B = 53mT$ when (upper panel) the outer loop of the double contour is encircled twice or (lower panel) first the inner and then the outer loop is encircled [154].

tours during the first and second encircling do not coincide [418]. Since the doublets are well separated from neighboring resonances in the experiment [154], the contours around the EP are chosen consisting of two different loops as proposed in [418], see Figure 11.14 (a). The path is parameterized by a real variable t with initial value $t = 0$ at their intersection. After the first encircling $t = t_1$; after the second $t = t_2$ [154].

At every point of the contour the experimental output yields the effective Hamiltonian. Its right eigenvectors can be represented in the form

$$\mathbf{u}_1(t) = \begin{pmatrix} e^{-i\tau/2}\cos\theta \\ e^{i\tau/2}\sin\theta \end{pmatrix}, \quad \mathbf{u}_2(t) = \begin{pmatrix} -e^{-i\tau/2}\sin\theta \\ e^{i\tau/2}\cos\theta \end{pmatrix},$$

where the parameter of time reversal invariance violation, τ, and parameter θ are expressed via the components of the measured Hamiltonian. A reversible system has $\tau = 0$ [154].

The parameter τ is not constant along the contour, even though the magnetic field is fixed. In fact, it varies with the opening s between both parts of the resonator, because the ferrite is positioned in one of them. The position of the EP does not depend on τ. Thus, the space curve $(s(t), \delta(t), \tau(t))$ winds around the line $(s_{EP}, \delta_{EP}, \tau)$ similarly to as shown in Figure 11.13. Since τ has no singular points in the parameter plane considered, it returns to its initial value after each encircling of the EP. A single encircling of the EP changes θ to $\theta \pm \pi/2$.

The biorthonormality condition defines the right eigenvectors up to the phase factor $e^{i\gamma_{1,2}(t)}$. The essential geometric phases $\gamma_{1,2}$ are fixed by the condition of parallel transport $(d\,\mathbf{u}, \mathbf{v}) = 0$ [190]. The initial value of the phases is chosen as $\gamma_{1,2}(t = 0) = 0$. For the time reversal invariant case $\gamma_{1,2}(t) \equiv 0$ which yields

$$\mathbf{u}_1(t_1) = \mathbf{u}_2(0), \quad \mathbf{u}_2(t_1) = -\mathbf{u}_1(0), \quad \mathbf{u}_{1,2}(t_2) = -\mathbf{u}_{1,2}(0)$$

so that the total geometric phase after two encirclings is π [149].

In the lower (upper) panel of Figure 11.14 (b) is plotted the essential phase $\gamma_1(t)$ corresponding to the right eigenvector when encircling the EP along the contour in Figure 11.14 (a) twice (along its outer loop). The orientation is such that the EP is always to the left. The cusps occur at $\frac{d\tau}{dt} = 0$. In each panel the triangle marks the starting point, the pentagon t_1, and the diamond t_2. If the EP is encircled twice along the same loop, we obtain $\gamma_{1,2}(t_2) = 0$ within 10^{-7} and the total phase change is thus π within the same precision as it should be when the EP is well separated from the other levels, see equation (11.110) and equation (11.111).

In contrast, when the loops are different, γ_1 does not return to its initial value, $\gamma_1(t_2) = 0.0931 + i0.0152 \neq 0$, as seen in the lower panel of Figure 11.14 (b). Thus the total geometric phase slightly deviates from π and is complex in accordance with [418]. When encircling this double loop again and again a drift of γ_1 is observed in the complex plane away from the origin, which may be interpreted as an observation of the predicted reversible geometric pumping process [67]. The dependence on the choice of the path signifies that the complex phases $\gamma_{1,2}$ are geometric and not topological when the time reversal invariance is broken and the effective Hamiltonian is represented by a complex non-Hermitian and nonsymmetric matrix.

Chapter 12

Magnetorotational instability

. . . much of the fluid and stellar community was aware of the instability, however, and of its curious behavior of ostensibly changing the Rayleigh criterion discontinuously . . .

S. A. Balbus [28]

12.1 Magnetorotational instability in axial and helical magnetic fields

12.1.1 Cylindrical Couette–Taylor flow

In 1890 Maurice Couette, a student of Gabriel Lippmann, defended his thesis "Etudes sur le frottement des liquides" and was awarded his doctorate at the Sorbonne "with all white balls" and *cum laude* for the experiments with a viscometer of his own design [311]. Seventy years later Evgeny Velikhov, then a physics student of Stanislav Braginsky at the Moscow State University, discovered the magnetorotational instability of the *Couette–Taylor flow* [581].

The fates of the first scientific works of both young scientists were similar in a sense that the reaction of the scientific community in both cases was quiescent for almost 30 years, until Geoffrey Taylor investigated stability of the rotating Couette flow in 1923 [566] and Steven Balbus and John Hawley demonstrated in 1991 the crucial role of magnetorotational instability for the explanation of transition to turbulence and thus the anomalous viscosity in accretion disks surrounding gravitating bodies [28].

The aim of Couette was to measure the kinematic viscosity of water. In 1888 [135] he reported on the design of a viscometer that he presented at the 1889 Universal Exhibition in Paris [478]. In the Couette viscometer the liquid occupied a space between two co-axial cylinders, the outer one rotating while the inner one remained fixed, Figure 12.1. Couette found that at small speeds of rotation the moment of the drag which the fluid exerted on the inner cylinder was indeed proportional to the velocity of the outer cylinder, from which the kinematic viscosity was determined. At higher speeds the drag increased at a greater rate than the velocity, indicating the onset of turbulent motion.

In his thesis Couette referred [478] to the work of Arnulph Mallock from Rayleigh's laboratory [403] who independently designed a similar device with either the inner or

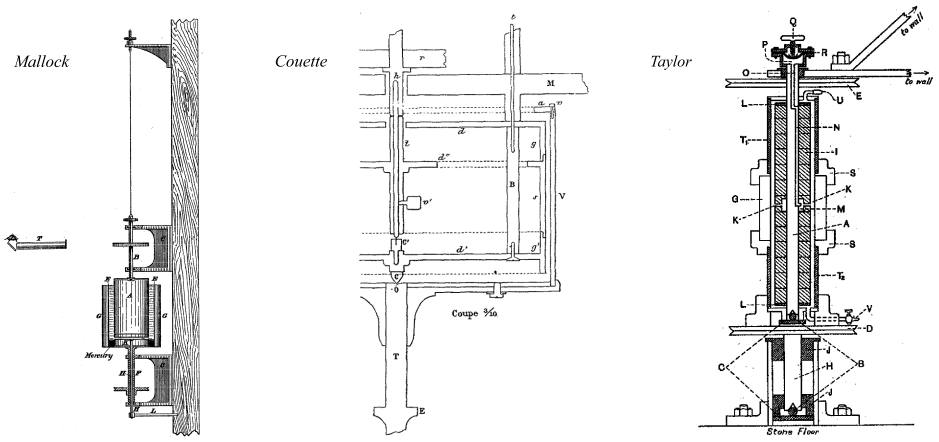

Figure 12.1. Original drawings of the viscometers of (left) Mallock [403, 404] with either outer or inner rotating cylinder and (center) Couette [136,478] with rotating outer cylinder and (right) the experimental apparatus of Taylor [566] in which both cylinders could rotate [311].

the outer cylinder rotating, Figure 12.1. Mallock confirmed Couette's results, but in the case when the inner cylinder rotated and the outer one not, he surprisingly observed instability of the fluid at all speeds that he used [403, 404]. Although the effect had been anticipated by Stokes already in 1848 [160], it was explained (in the inviscid approximation) by Rayleigh[1] only in 1917 [494]. According to *Rayleigh's criterion*, an inviscid rotating flow is stable with respect to axisymmetric perturbations provided that its angular momentum increases radially

$$\frac{1}{R^3}\frac{d}{dR}(\Omega R^2)^2 > 0. \tag{12.1}$$

When this criterion is not fulfilled, the balance between the centrifugal force and a pressure gradient is broken and the flow is centrifugally unstable. In particular, the inviscid fluid between two co-rotating and co-axial cylinders of infinite lengths and radii $R_1 < R_2$ is unstable if and only if

$$\Omega_1 R_1^2 > \Omega_2 R_2^2, \tag{12.2}$$

where Ω_1 and Ω_2 are the angular velocities of the inner and outer cylinders, respectively, see Figure 12.2.

Limitations in the design of the experiments by Couette and Mallock did not allow the full verification of the criterion (12.2). Besides, the steady flow in their viscometers was not close enough to two-dimensional because of a relatively small length-to-diameter ratio. This motivated Geoffrey Taylor to construct a slimmer Couette cell

[1] Note also that Maxwell proposed the centrifugal instability criterion as a problem for the Cambridge Mathematical Tripos as early as 1866 [424].

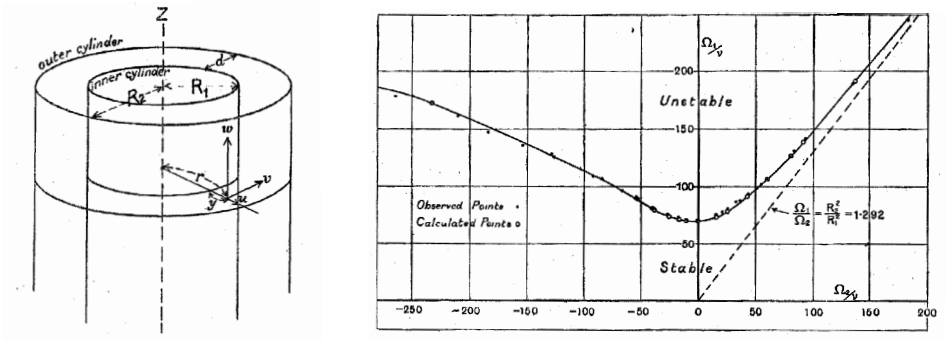

Figure 12.2. Original drawings of the geometry of Taylor's model and of the stability diagram in the $(\Omega_2/\nu, \Omega_1/\nu)$-plane for $R_1 = 3.55$ cm and $R_2 = 4.035$ cm [566]. Dashed line is Rayleigh's inviscid stability boundary [494].

making both co-rotation and counter-rotation of the cylinders possible, Figure 12.1. In his 1923 work [566] Taylor performed a linear stability analysis of the Navier–Stokes equations in case of infinite length cylinders and managed to find a stability diagram in the $(\Omega_2/\nu, \Omega_1/\nu)$-plane, see Figure 12.2. It turned out that the viscosity, ν, modifies the Rayleigh criterion in such a manner that it becomes only a sufficient stability condition and that the viscous stability boundary asymptotically tends to the Rayleigh line in the case of co-rotating cylinders, Figure 12.2. Moreover, the viscous flow is stable at small speeds of the inner cylinder when the outer one is at rest or in motion, while it inevitably becomes unstable when the velocity of the inner cylinder exceeds a critical value. This is in contradiction with the observations of Couette and Mallock that the viscous flow becomes unstable for large velocities of the outer cylinder when the inner does not move and is unstable at all speeds of the inner cylinder when the outer is at rest. The latter discrepancy is due to the fact that Mallock's lowest speed of rotation, 2 rpm, was still larger than the critical value calculated for the size of the cylinders he used [160], while the former is essentially caused by the insufficient axial elongation of the viscometers of Mallock and Couette.

The stability boundary extracted from Taylor's experimental data [566] perfectly agreed with that which followed from his linear stability analysis, Figure 12.2. Furthermore, Taylor's experiments revealed that with the violation of the stability threshold, the rotating Couette flow bifurcates to a secondary steady state characterized by counter-rotating toroidal vortices (the Taylor vortex flow). Extending the parameters deeper inside the instability domain results in flows with even more complicated spatiotemporal patterns [165, 478, 566]. Therefore, the instability of the Couette–Taylor (CT) flow is analogous to the static (divergence) instability in structural mechanics [239, 528].

The excellent correspondence that Taylor obtained between theory and experiment demonstrated the correctness of the Navier–Stokes equations and of the no-slip bound-

ary condition for the fluid at the cylinder walls [160] as well as proving the applicability of linear stability analysis to the CT-flow. After the influential work [566], Couette–Taylor cells belong to the standard equipment for laboratory testing hydrodynamical and magnetohydrodynamical (MHD) theories.

12.1.2 Paradox of Velikhov and Chandrasekhar

In 1953 Chandrasekhar considered the CT-flow of a weakly electrically conducting viscous fluid in the presence of the uniform magnetic field that is parallel to the axis of rotation of the cylinders [119]. He demonstrated that in this case characterized by the very small ratio of the kinematic viscosity coefficient, ν, to the magnetic diffusivity coefficient, η, i.e. by the *magnetic Prandtl number* $\mathrm{Pm} := \nu\eta^{-1} \ll 1$, the magnetic field stabilizes the hydrodynamically unstable CT-flow [119]. Chandrasekhar's article was brought to the attention of Evgeny Velikhov by his supervisor Stanislav Braginsky who posed a problem on the influence of the axial magnetic field on the hydrodynamically stable CT-flow – the very question that had not been addressed in [119].

In contrast to Chandrasekhar, Velikhov assumed that the liquid is both inviscid and perfectly conducting. In 1959 he established a new sufficient criterion of stability with respect to the *axisymmetric* perturbations[2] in the form

$$\frac{d\Omega^2}{dR} > 0, \tag{12.3}$$

or, in terms of the angular velocities of the cylinders,

$$\Omega_2 > \Omega_1, \tag{12.4}$$

see the left panel of Figure 12.3. In a subsequent work from 1960 Chandrasekhar confirmed this result [120].

Both Velikhov and Chandrasekhar pointed out that the new stability conditions (12.3) and (12.4) do not depend on the magnetic field strength B which implies that in the limit $B \to 0$ they do not converge to Rayleigh's criteria (12.1) and (12.2) valid for $B = 0$, as illustrated by the left panel of Figure 12.3. In the presence of dissipation convergence is possible [1, 599]. This dependence of the instability threshold on the sequence of taking the two limits of vanishing magnetic field and vanishing electrical resistivity constitutes the famous *Velikhov–Chandrasekhar paradox*. Its physical explanation has been given in terms of Alfvén's theorem [121] that in a fluid of zero resistivity the magnetic field lines are frozen into the fluid, independent of the strength of the magnetic field [120, 581]. However, the weak point of this argument is that the actual boundary of MRI does depend on the magnetic field strength even in the case of ideal magnetohydrodynamics and tends to that of solid body rotation only when the

[2] It is instructive to note that the instability of the magnetized Couette–Taylor flow with respect to *nonaxisymmetric* perturbations may occur via a coupling of positive and negative energy modes [264].

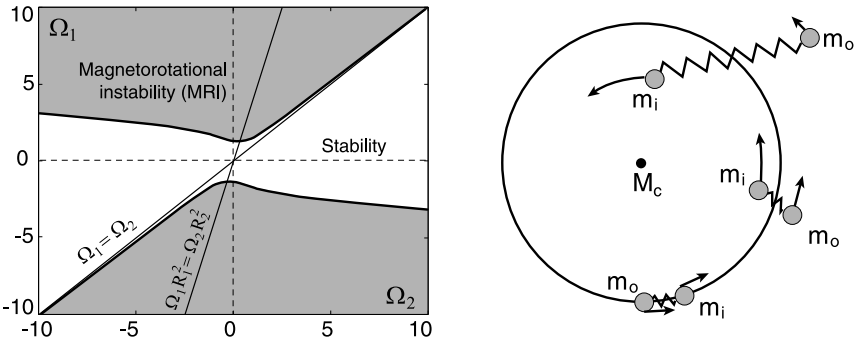

Figure 12.3. (Left) A diagram of stability with respect to axisymmetric perturbations with the axial wave number $k_z = 1$ of the Couette–Taylor flow of ideally electrically conducting inviscid fluid between the cylinders of the radii $R_1 = 1$ and $R_2 = 2$ when an axial magnetic field $B = 0.4$ is applied [308]; the stability boundary shown in bold black converges to the line $\Omega_1 = \Omega_2$ rather than to the Rayleigh line as $B \to 0$. (Right) A mechanical analogue of MRI in accretion disks [31]. The action of the magnetic field is equivalent to that of elastic springs that lead to the exchange of angular momentum between the fast inner mass m_i and the slow outer mass m_o.

field is vanishing, see Figure 12.3 (left).[3] This indicates that the roots of the paradox are more hidden [128, 308].

12.1.3 Magnetorotational instability in astrophysics and its analogues in celestial mechanics

Even half a century after the publications of Velikhov and Chandrasekhar the 'dubious' jump in the threshold of the *magnetorotational instability* (MRI) has not been fully understood and the paradox remained unresolved [1, 28, 199, 316]. Maybe this is not so surprising when taking into account that even the astrophysical relevance of MRI to destabilize a differentially rotating flow in accretion disks around gravitating celestial bodies remained underappreciated during a long period until it was rehabilitated by Balbus and Hawley in 1991.

The central problem here is that accretion disks typically rotate according to Kepler's law, $\Omega(R) \sim R^{-3/2}$ which results in an angular momentum $R^2\Omega(R) \sim R^{1/2}$ that fulfills Rayleigh's stability criterion (12.1). Such stable, nonturbulent disks would not allow the outward directed angular momentum transport that is necessary for the infalling disk matter to accrete into the central object. In their seminal paper [30], Balbus and Hawley highlighted the key role of the MRI in this process by showing that a weak, externally applied magnetic field is a trigger for the instability that actually taps into the rotational energy of the flow.

[3] It strikingly resembles the classical Taylor diagram reproduced in Figure 12.2 (right) except that the stability boundary asymptotically tends to the line of solid body rotation ($\Omega_1 = \Omega_2$).

In a perfectly conducting fluid, the magnetic field lines are 'frozen' into it, tethering fluid elements like a spring [28], see Figure 12.3 (right). If such a couple is perturbed, the magnetic 'tether' retards the faster inner element that has to move to the lower Keplerian orbit and simultaneously it accelerates the slower outer fluid element that thus has to move to the higher orbit. The separation between the elements grows with time yielding instability. Remarkably, this simple mechanical analogue of MRI proposed by Balbus and Hawley [28], is a working principle of numerous engineering projects developed since the 1960s that involve momentum exchange tethers for the orbital transfer of satellites [44]. Well known is the instability of an orbiting ring of connected satellites as well as of the orbiting flexible and extensible ring in the context of studies of formation of planetary rings [43, 87, 455, 481]. In the same context, the mechanism of the gravitational instability of a stream of co-orbital particles was recently shown to be similar to that of MRI [360].

In the reference frame comoving with a small patch of the magnetized accretion disk and rotating at the angular velocity $\Omega_0 = \Omega(R_0)$, the leading order WKB equations governing the evolution of its local radial (x) and azimuthal (y) displacements in the vicinity of a fiducial point with the radius R_0 are [28]

$$\begin{aligned} &\ddot{x} - 2\Omega_0 \dot{y} + \left(R_0 \left. \frac{d\Omega^2}{dR} \right|_{R=R_0} + \omega_A^2 \right) x = 0, \\ &\ddot{y} + 2\Omega_0 \dot{x} + \omega_A^2 y = 0, \end{aligned} \tag{12.5}$$

where the *Alfvén frequency*, ω_A, measures the intensity of the magnetic tension force. With $\omega_A = 0$ and Keplerian rotation $\Omega(R) \sim R^{-3/2}$ the equations (12.5) are reduced to the Hill–Clohessy–Wiltshire ones [132, 225] that describe in particular the relative motion of two satellites,[4] see also [360].

Writing down the characteristic equation of system (12.5) and taking into account that at the onset of MRI with only an axial magnetic field applied (which is a nonoscillatory instability) the critical eigenvalue is vanishing [308], we get the instability threshold (see also [120])

$$\mathrm{Ro} := \frac{1}{2} \frac{R}{\Omega} \frac{d\Omega}{dR} = -\frac{\omega_A^2}{4\Omega_0^2}, \tag{12.6}$$

where Ro is the *Rossby number*[5] (evaluated at $R = R_0$ in (12.6)) that indicates the deviation of the rotating shear flow from the solid body rotation, $\mathrm{Ro} = 0$. The latter is the

[4] A nice illustration is contained in the books by Beletsky [42] and Arnold [18]. During his space walk on March 18, 1965, the kosmonaut Alexei Leonov threw the lens cap of his movie camera towards the Earth: "the small object, shining in the Sun, began to distance itself rapidly and soon vanished from sight" [42]. The motion of the lens cap with respect to the spaceship is described by the Hill–Clohessy–Wiltshire equations. The lens cap will move relative to the kosmonaut approximately in an ellipse. The center of the ellipse will be situated in front of the kosmonaut in his orbit and the period of circulation around the ellipse will be equal to the period of motion around the spaceship's orbit.

[5] Karl-Gustaf Arvid Rossby (1898–1957) – a Swedish-American meteorologist.

threshold resulting from the sufficient stability criterion of Velikhov–Chandrasekhar (Ro > 0). The actual threshold of MRI given by equation (12.6) depends on the magnetic field strength through ω_A and therefore it coincides with the criterion (12.3) in the limit $\omega_A = 0$ which deviates from the nonmagnetic value Ro $= -1$ following from Rayleigh's criterion (12.1). This nonuniqueness of the critical Rossby number in the nonmagnetic limit is another manifestation of the Velikhov–Chandrasekhar paradox.

12.1.4 Laboratory experiments with CT-flow in axial and helical magnetic fields

In contrast to the nonmagnetic Couette–Taylor case, the theory of MRI was ahead of laboratory experiments [311]. First interesting experimental results were obtained only in 2004 in a spherical Couette flow of liquid sodium [532]. In this experiment, the authors observed correlated modes of velocity and magnetic field perturbation in parameter regions which are quite typical for MRI. However, the background state in this spherical Couette experiment was already fully turbulent, so that the original goal to show the basic destabilizing effect of a magnetic field was not met.

At Princeton University, work is going on to identify MRI in a CT-experiment with liquid gallium, and first encouraging results, including the observation of nonaxisymmetric *magneto-Coriolis waves*, have been recently reported [453]. The Princeton facility had been designed to investigate the *standard* version of MRI (SMRI) with only a vertical magnetic field being applied. SMRI is known to work only with magnetic Reynolds numbers (Rm) in the order of 1 or larger. Rm is proportional to the hydrodynamic Reynolds number according to Rm = PmRe, where Pm is the magnetic Prandtl number. For liquid metals Pm is typically in the range $10^{-6}-10^{-5}$. Therefore, in order to achieve Rm ~ 1, we need Re $= 10^5-10^6$, and wall-constrained flows (in contrast to wall-free Keplerian flows) with such high Re are usually turbulent, whatever the linear stability analysis might tell [309]. This is the point which makes SMRI experiments, and their interpretation, so cumbersome [29].

This situation changed drastically when Hollerbach and Rüdiger considered the effect of adding an azimuthal magnetic field to the axial one [227]. Indeed, it was shown [227] that the resulting *helical MRI* (HMRI) is then possible at far smaller Reynolds numbers and magnetic field amplitudes than SMRI, making HMRI an ideal playground for liquid metal experiments.

First experimental evidence for HMRI was obtained in 2006 at the liquid metal facility PROMISE (Potsdam ROssendorf Magnetic InStability Experiment) which is basically a CT-cell made of concentric rotating copper walls, filled with GaInSn (a eutectic which is liquid at room temperatures). In [546] it was shown that the HMRI traveling wave appears only in the predicted finite window of magnetic field intensity, with a frequency of the traveling wave that was in rather good accordance with numerical simulations.

Despite SMRI being a nonoscillatory instability and HMRI being an oscillatory one, there is a continuous and monotonic transition between them when Re and the magnetic field strength are increased simultaneously [227]. This is all the more remarkable in that HMRI has been identified with the destabilization of an inertial wave in apparent contrast to SMRI that is a destabilized slow magneto-Coriolis wave [453]. The transition from SMRI to HMRI, which is characterized by substantially different scaling laws, involves the origination of a spectral exceptional point [517] and a transfer of instability between the modes [309].

It is remarkable, too, that even in the limit of vanishing electrical conductivity ($\mathrm{Pm} \to 0$), the helical magnetic field is able to trigger an instability although the instantaneous growth of the energy of any perturbation must be smaller than in the field-free case – the *paradox of inductionless HMRI* [486]. In this inductionless case, however, the local WKB analysis in the small-gap approximation prohibits helical magnetorotational instability when Ro exceeds the Liu limit of $2-2\sqrt{2} \approx -0.828$ [383]. Thus the inductionless HMRI works only for comparably steep rotation profiles (i.e. slightly above the Rayleigh line of $\mathrm{Ro} = -1$) and disappears for profiles as flat as the Keplerian one with $\mathrm{Ro} = -0.75$. This behavior has been experimentally confirmed in the PROMISE experiment [311]. Nevertheless, HMRI at the Rossby numbers slightly above the Liu limit was observed already in the WKB approximation at small but finite Pm in [309]. The ultimate upper limit of the critical Ro in this case is an intriguing question because of its high sensitivity with respect to the variation of parameters.

Despite a more than a century-long history, hydrodynamic and hydromagnetic stability of rotating shear flows remains a vibrant area of research, full of intriguing paradoxes and mathematical, computational, and experimental challenges. Below we link some of the mentioned effects to singularities existing on the stability boundaries.

12.2 Mathematical setting

12.2.1 Nonlinear equations and a steady state

The standard nonlinear equations of dissipative incompressible magnetohydrodynamics consist of the Navier–Stokes equation for the fluid velocity $\mathbf{u}$

$$\frac{\partial \mathbf{u}}{\partial t} + (\mathbf{u}\cdot\nabla)\mathbf{u} = -\frac{1}{\rho}\nabla\left(p + \frac{\mathbf{B}^2}{2\mu_0}\right) + \frac{1}{\mu_0\rho}(\mathbf{B}\cdot\nabla)\mathbf{B} + \nu\nabla^2\mathbf{u}, \tag{12.7}$$

and of the induction equation for the magnetic field $\mathbf{B}$

$$\frac{\partial \mathbf{B}}{\partial t} = \nabla\times(\mathbf{u}\times\mathbf{B}) + \eta\,\nabla^2\,\mathbf{B}, \tag{12.8}$$

where p is the pressure, $\rho = \mathrm{const}$ the density, $\nu = const$ the kinematic viscosity, $\eta = (\mu_0\sigma)^{-1}$ the magnetic diffusivity, σ the conductivity of the fluid, and μ_0 the

magnetic permeability of free space [121]. Additionally, the mass continuity equation for incompressible flows and the solenoidal condition yield

$$\nabla \cdot \mathbf{u} = 0, \quad \nabla \cdot \mathbf{B} = 0. \tag{12.9}$$

We consider the rotational fluid flow in the gap between the radii R_1 and $R_2 > R_1$, with an imposed magnetic field sustained by currents external to the fluid. Introducing the cylindrical coordinates (R, ϕ, z) we consider the stability of a steady-state background liquid flow with the angular velocity profile $\Omega(R)$ in a helical background magnetic field (a magnetized CT-flow)

$$\mathbf{u}_0 = R\,\Omega(R)\,\mathbf{e}_\phi, \quad p = p_0(R), \quad \mathbf{B}_0 = B_\phi^0(R)\mathbf{e}_\phi + B_z^0\mathbf{e}_z, \tag{12.10}$$

with the azimuthal component

$$B_\phi^0(R) = \frac{\mu_0 I}{2\pi R}, \tag{12.11}$$

which can be thought as being produced by an axial current I. Note that

$$\frac{dB_\phi^0}{dR} = -\frac{\mu_0 I}{2\pi R^2} = -\frac{B_\phi^0}{R}, \quad \frac{d(RB_\phi^0)}{dR} = 0.$$

Therefore,

$$\nabla \times \mathbf{B}_0 = 0. \tag{12.12}$$

The angular velocity profile of the background CT-flow is [162]

$$\Omega(R) = \frac{\Omega_1 R_1^2 - \Omega_2 R_2^2}{R_1^2 - R_2^2} + \frac{1}{R^2}\frac{(\Omega_2 - \Omega_1)R_1^2 R_2^2}{R_1^2 - R_2^2}. \tag{12.13}$$

The centrifugal acceleration of the background flow (12.13) is compensated by the pressure gradient

$$\frac{1}{\rho}\frac{\partial p_0}{\partial R} = R\Omega^2. \tag{12.14}$$

12.2.2 Linearization with respect to nonaxisymmetric perturbations

Let us linearize the equations (12.7)–(12.9) of the magnetized Couette–Taylor flow in the vicinity of the stationary solution (12.10)–(12.12) assuming general perturbations $\mathbf{u} = \mathbf{u}_0 + \mathbf{u}'$, $p = p_0 + p'$, and $\mathbf{B} = \mathbf{B}_0 + \mathbf{B}'$ and leaving only the terms of first order with respect to the primed quantities. The perturbed fluid velocity and magnetic field fulfill the constraints

$$\nabla \cdot \mathbf{u}' = 0, \quad \nabla \cdot \mathbf{B}' = 0. \tag{12.15}$$

After introducing the matrices $\mathcal{U}(R) := \nabla \mathbf{u}_0$ and $\mathcal{B}(R) := \nabla \mathbf{B}_0$

$$\mathcal{U} = \begin{pmatrix} 0 & -\Omega & 0 \\ \Omega + R\frac{d\Omega}{dR} & 0 & 0 \\ 0 & 0 & 0 \end{pmatrix}, \quad \mathcal{B} = \begin{pmatrix} 0 & -\frac{B_\phi^0}{R} & 0 \\ \frac{dB_\phi^0}{dR} & 0 & 0 \\ 0 & 0 & 0 \end{pmatrix} \tag{12.16}$$

and taking into account the property (12.12), we get the linearized equations

$$(\partial_t + \mathcal{U} + \mathbf{u}_0 \cdot \nabla)\mathbf{u}' + \frac{1}{\rho}\nabla p' + \frac{1}{\rho\mu_0}\mathbf{B}_0 \times (\nabla \times \mathbf{B}') = \nu\nabla^2\mathbf{u}',$$
$$(\partial_t - \mathcal{U} + \mathbf{u}_0 \cdot \nabla)\mathbf{B}' + (\mathcal{B} - \mathbf{B}_0 \cdot \nabla)\mathbf{u}' = \eta\nabla^2\mathbf{B}'. \tag{12.17}$$

12.3 Geometrical optics approximation

We look for solutions of the linearized equations (12.17) in the form of a rapid oscillation with slowly varying amplitude of its envelope [179]

$$\mathbf{u}'(\mathbf{x}, t, \epsilon) = e^{i\Phi(\mathbf{x},t)/\epsilon}\left(\mathbf{u}^{(0)}(\mathbf{x}, t) + \epsilon\mathbf{u}^{(1)}(\mathbf{x}, t)\right) + \epsilon\mathbf{u}^{(r)}(\mathbf{x}, t),$$
$$\mathbf{B}'(\mathbf{x}, t, \epsilon) = e^{i\Phi(\mathbf{x},t)/\epsilon}\left(\mathbf{B}^{(0)}(\mathbf{x}, t) + \epsilon\mathbf{B}^{(1)}(\mathbf{x}, t)\right) + \epsilon\mathbf{B}^{(r)}(\mathbf{x}, t),$$
$$p'(\mathbf{x}, t, \epsilon) = e^{i\Phi(\mathbf{x},t)/\epsilon}\left(p^{(0)}(\mathbf{x}, t) + \epsilon p^{(1)}(\mathbf{x}, t)\right) + \epsilon p^{(r)}(\mathbf{x}, t), \tag{12.18}$$

with $i = \sqrt{-1}$, $0 < \epsilon \ll 1$ a small parameter, $\mathbf{x}$ denoting the vector of coordinates, Φ a real-valued phase of the oscillations, and $\mathbf{u}^{(j)}$, $p^{(j)}$, and $\mathbf{B}^{(j)}$, where $j = 0, 1, r$, the complex-valued amplitudes corresponding to fluid velocity, pressure, and magnetic field.

Assuming $\nu = \epsilon^2\tilde{\nu}$ and $\eta = \epsilon^2\tilde{\eta}$ [350, 381] and introducing the derivative

$$\frac{D}{Dt} := \partial_t + \mathbf{u}_0 \cdot \nabla \tag{12.19}$$

along the fluid stream lines, we substitute expressions (12.18) into equations (12.17), collect terms at ϵ^{-1} and ϵ^0 and expand the cross products, which yields

$$\frac{D\Phi}{Dt}\mathbf{u}^{(0)} + \frac{p^{(0)}}{\rho}\nabla\Phi = \frac{1}{\rho\mu_0}\mathbf{B}^{(0)}(\mathbf{B}_0 \cdot \nabla\Phi) - \frac{1}{\rho\mu_0}\nabla\Phi(\mathbf{B}_0 \cdot \mathbf{B}^{(0)}),$$
$$\frac{D\Phi}{Dt}\mathbf{B}^{(0)} - (\mathbf{B}_0 \cdot \nabla\Phi)\mathbf{u}^{(0)} = 0,$$
$$i\frac{D\Phi}{Dt}\mathbf{u}^{(1)} + i\frac{p^{(1)}}{\rho}\nabla\Phi = -\left(\frac{D}{Dt} + \tilde{\nu}(\nabla\Phi)^2 + \mathcal{U}\right)\mathbf{u}^{(0)},$$
$$-\frac{1}{\rho}\nabla p^{(0)} - \frac{1}{\rho\mu_0}\mathbf{B}_0 \times \nabla \times \mathbf{B}^{(0)} + i\frac{1}{\rho\mu_0}\mathbf{B}_0 \times \mathbf{B}^{(1)} \times \nabla\Phi,$$
$$i\frac{D\Phi}{Dt}\mathbf{B}^{(1)} - i(\mathbf{B}_0 \cdot \nabla\Phi)\mathbf{u}^{(1)} = -\left(\frac{D}{Dt} + \tilde{\eta}(\nabla\Phi)^2 - \mathcal{U}\right)\mathbf{B}^{(0)} - (\mathcal{B} - \mathbf{B}_0 \cdot \nabla)\mathbf{u}^{(0)}. \tag{12.20}$$

The solenoidality and incompressibility conditions (12.15) take the form

$$\mathbf{u}^{(0)} \cdot \nabla\Phi = 0, \quad \nabla \cdot \mathbf{u}^{(0)} + i\mathbf{u}^{(1)} \cdot \nabla\Phi = 0,$$
$$\mathbf{B}^{(0)} \cdot \nabla\Phi = 0, \quad \nabla \cdot \mathbf{B}^{(0)} + i\mathbf{B}^{(1)} \cdot \nabla\Phi = 0. \tag{12.21}$$

The dot product of the first two of the equations (12.20) with $\nabla\Phi, \mathbf{u}^{(0)}, \mathbf{B}^{(0)}$ together with the constraints (12.21) result in the system of equations

$$\begin{aligned}
(\nabla\Phi)^2\left(\frac{p^{(0)}}{\rho}+\frac{1}{\rho\mu_0}(\mathbf{B}_0\cdot\mathbf{B}^{(0)})\right)&=0,\\
\frac{D\Phi}{Dt}\mathbf{B}^{(0)}\cdot\mathbf{B}^{(0)}-(\mathbf{B}_0\cdot\nabla\Phi)\mathbf{u}^{(0)}\cdot\mathbf{B}^{(0)}&=0,\\
\frac{D\Phi}{Dt}\mathbf{B}^{(0)}\cdot\mathbf{u}^{(0)}-(\mathbf{B}_0\cdot\nabla\Phi)\mathbf{u}^{(0)}\cdot\mathbf{u}^{(0)}&=0,\\
\frac{D\Phi}{Dt}\mathbf{u}^{(0)}\cdot\mathbf{B}^{(0)}-\frac{1}{\rho\mu_0}\mathbf{B}^{(0)}\cdot\mathbf{B}^{(0)}(\mathbf{B}_0\cdot\nabla\Phi)&=0,\\
\frac{D\Phi}{Dt}\mathbf{u}^{(0)}\cdot\mathbf{u}^{(0)}-\frac{1}{\rho\mu_0}\mathbf{B}^{(0)}\cdot\mathbf{u}^{(0)}(\mathbf{B}_0\cdot\nabla\Phi)&=0.
\end{aligned}\tag{12.22}$$

For $\nabla\Phi\neq 0$, $\mathbf{B}^{(0)}\neq 0$, and $\mathbf{u}^{(0)}\neq 0$ it has a unique solution

$$p^{(0)}=-\frac{1}{\mu_0}(\mathbf{B}_0\cdot\mathbf{B}^{(0)}),\quad \frac{D\Phi}{Dt}=0,\quad \mathbf{B}_0\cdot\nabla\Phi=0.\tag{12.23}$$

The relations (12.23) allow us to simplify the last two of the equations (12.20) by eliminating pressure and taking into account the constraints (12.21)

$$\begin{aligned}
&\left(\frac{D}{Dt}+\tilde{\nu}(\nabla\Phi)^2+\mathcal{U}\right)\mathbf{u}^{(0)}-\frac{1}{\rho\mu_0}(\mathcal{B}+\mathbf{B}_0\cdot\nabla)\mathbf{B}^{(0)}=\\
&\qquad\frac{\nabla\Phi}{|\nabla\Phi|^2}\cdot\left[\left(\frac{D}{Dt}+\mathcal{U}\right)\mathbf{u}^{(0)}-\frac{1}{\rho\mu_0}(\mathcal{B}+\mathbf{B}_0\cdot\nabla)\mathbf{B}^{(0)}\right]\nabla\Phi,\\
&\left(\frac{D}{Dt}+\tilde{\eta}(\nabla\Phi)^2-\mathcal{U}\right)\mathbf{B}^{(0)}+(\mathcal{B}-\mathbf{B}_0\cdot\nabla)\mathbf{u}^{(0)}=0.
\end{aligned}\tag{12.24}$$

Differentiating the first of the identities (12.21) yields

$$\frac{D}{Dt}(\nabla\Phi\cdot\mathbf{u}^{(0)})=\frac{D\nabla\Phi}{Dt}\cdot\mathbf{u}^{(0)}+\nabla\Phi\cdot\frac{D\mathbf{u}^{(0)}}{Dt}=0.\tag{12.25}$$

Using the identity (12.25), we write

$$\begin{aligned}
&\left(\frac{D}{Dt}+\tilde{\nu}(\nabla\Phi)^2+\mathcal{U}\right)\mathbf{u}^{(0)}-\frac{1}{\rho\mu_0}(\mathcal{B}+\mathbf{B}_0\cdot\nabla)\mathbf{B}^{(0)}=\\
&\qquad\frac{\nabla\Phi}{|\nabla\Phi|^2}\cdot\left[\mathcal{U}\mathbf{u}^{(0)}-\frac{1}{\rho\mu_0}(\mathcal{B}+\mathbf{B}_0\cdot\nabla)\mathbf{B}^{(0)}\right]\nabla\Phi-\frac{\nabla\Phi}{|\nabla\Phi|^2}\frac{D\nabla\Phi}{Dt}\cdot\mathbf{u}^{(0)},\\
&\left(\frac{D}{Dt}+\tilde{\eta}(\nabla\Phi)^2-\mathcal{U}\right)\mathbf{B}^{(0)}+(\mathcal{B}-\mathbf{B}_0\cdot\nabla)\mathbf{u}^{(0)}=0.
\end{aligned}\tag{12.26}$$

Now we take the gradient of the identity $D\Phi/Dt = 0$

$$\nabla\partial_t\Phi + \nabla(\mathbf{u}_0\cdot\nabla)\Phi = \partial_t\nabla\Phi + (\mathbf{u}_0\cdot\nabla)\nabla\Phi + \mathcal{U}^T\nabla\Phi$$
$$= \frac{D}{Dt}\nabla\Phi + \mathcal{U}^T\nabla\Phi = 0. \tag{12.27}$$

Hence, the time evolution of the wave vector $\mathbf{k} := \nabla\Phi$ is given by the equation

$$\frac{D\mathbf{k}}{Dt} = -\mathcal{U}^T\mathbf{k}. \tag{12.28}$$

Given the wave vector $\mathbf{k}(t)$, equations (12.26) yield the *transport equations*

$$\frac{D\mathbf{u}^{(0)}}{Dt} = \left[2\frac{\mathbf{k}\mathbf{k}^T}{|\mathbf{k}|^2} - \mathcal{I}\right]\mathcal{U}\mathbf{u}^{(0)} - \tilde{\nu}|\mathbf{k}|^2\mathbf{u}^{(0)} + \frac{1}{\rho\mu_0}\left[\mathcal{I} - \frac{\mathbf{k}\mathbf{k}^T}{|\mathbf{k}|^2}\right](\mathcal{B} + \mathbf{B}_0\cdot\nabla)\,\mathbf{B}^{(0)},$$
$$\frac{D\mathbf{B}^{(0)}}{Dt} = \mathcal{U}\mathbf{B}^{(0)} - \tilde{\eta}|\mathbf{k}|^2\mathbf{B}^{(0)} - (\mathcal{B} - \mathbf{B}_0\cdot\nabla)\mathbf{u}^{(0)}. \tag{12.29}$$

The transport equations (12.29), where $\mathcal{I}$ is a 3×3 identity matrix, are a system of partial differential equations [178] that determine evolution of the amplitudes $\mathbf{u}^{(0)}$ and $\mathbf{B}^{(0)}$. In the absence of the magnetic field they are reduced to the hydrodynamical ones derived in [156, 164, 350, 381].

With the matrix $\mathcal{U}$ from (12.16), and $\Omega' = \frac{d\Omega}{dR}$, the equations (12.28) are

$$\dot{k}_R = -R\Omega' k_\phi, \quad \dot{k}_\phi = 0, \quad \dot{k}_z = 0. \tag{12.30}$$

Consider a solution to equations (12.30) with $k_\phi \equiv 0$, so that the wave numbers k_R and k_z are arbitrary constants [164]. Taking into account that

$$(\mathbf{B}_0\cdot\nabla)\mathbf{u}^{(0)} = \begin{pmatrix} \frac{B^0_\phi}{R}(\partial_\phi u^{(0)}_R - u^{(0)}_\phi) + B^0_z\partial_z u^{(0)}_R \\ \frac{B^0_\phi}{R}(\partial_\phi u^{(0)}_\phi + u^{(0)}_R) + B^0_z\partial_z u^{(0)}_\phi \\ \frac{B^0_\phi}{R}\partial_\phi u^{(0)}_z + B^0_z\partial_z u^{(0)}_z \end{pmatrix},$$
$$(\mathbf{B}_0\cdot\nabla)\mathbf{B}^{(0)} = \begin{pmatrix} \frac{B^0_\phi}{R}\partial_\phi B^{(0)}_R + B^0_z\partial_z B^{(0)}_R - \frac{B^0_\phi B^{(0)}_\phi}{R} \\ \frac{B^0_\phi}{R}\partial_\phi B^{(0)}_\phi + B^0_z\partial_z B^{(0)}_\phi + \frac{B^0_\phi B^{(0)}_R}{R} \\ \frac{B^0_\phi}{R}\partial_\phi B^{(0)}_z + B^0_z\partial_z B^{(0)}_z \end{pmatrix}, \tag{12.31}$$

we find that the system (12.29) in cylindrical coordinates (R, ϕ, z) has the form

$$
\begin{aligned}
(\partial_t + \Omega\partial_\phi + \tilde{\nu}|\mathbf{k}|^2)u_R^{(0)} &= 2\alpha^2\Omega u_\phi^{(0)} - \frac{2\alpha^2 B_\phi^0}{\rho\mu_0 R}B_\phi^{(0)} \\
&\quad + \alpha\frac{B_\phi^0}{R}\frac{\alpha\partial_\phi B_R^{(0)} - \sqrt{1-\alpha^2}\partial_\phi B_z^{(0)}}{\rho\mu_0} \\
&\quad + \alpha B_z^0\frac{\alpha\partial_z B_R^{(0)} - \sqrt{1-\alpha^2}\partial_z B_z^{(0)}}{\rho\mu_0}, \\
(\partial_t + \Omega\partial_\phi + \tilde{\nu}|\mathbf{k}|^2)u_\phi^{(0)} &= -2\Omega(1+\mathrm{Ro})u_R^{(0)} + \frac{B_\phi^0\partial_\phi B_\phi^{(0)}}{\rho\mu_0 R} + \frac{B_z^0\partial_z B_\phi^{(0)}}{\rho\mu_0}, \\
(\partial_t + \Omega\partial_\phi + \tilde{\nu}|\mathbf{k}|^2)u_z^{(0)} &= -2\sqrt{1-\alpha^2}\alpha\Omega u_\phi^{(0)} - \frac{B_\phi^0(\alpha^2-1)\partial_\phi B_z^{(0)}}{\rho\mu_0 R} \\
&\quad - \frac{\alpha\sqrt{1-\alpha^2}B_\phi^0(\partial_\phi B_R^{(0)} - 2B_\phi^{(0)})}{\rho\mu_0 R} \\
&\quad - B_z^0\frac{\sqrt{1-\alpha^2}\alpha\partial_z B_R^{(0)} - (1-\alpha^2)\partial_z B_z^{(0)}}{\rho\mu_0}, \\
(\partial_t + \Omega\partial_\phi + \tilde{\eta}|\mathbf{k}|^2)B_R^{(0)} &= B_z^0\partial_z u_R^{(0)} + \frac{B_\phi^0}{R}\partial_\phi u_R^{(0)}, \\
(\partial_t + \Omega\partial_\phi + \tilde{\eta}|\mathbf{k}|^2)B_\phi^{(0)} &= B_z^0\partial_z u_\phi^{(0)} + \frac{B_\phi^0}{R}\partial_\phi u_\phi^{(0)} + 2\Omega\mathrm{Ro}B_R^{(0)} + 2\frac{B_\phi^0}{R}u_R^{(0)}, \\
(\partial_t + \Omega\partial_\phi + \tilde{\eta}|\mathbf{k}|^2)B_z^{(0)} &= B_z^0\partial_z u_z^{(0)} + \frac{B_\phi^0}{R}\partial_\phi u_z^{(0)},
\end{aligned}
\tag{12.32}
$$

where $\alpha = k_z|\mathbf{k}|^{-1}$.

Seeking for a solution of the system (12.32) in the form $e^{\gamma t + ik_z z}$ and taking into account the solenoidality condition $B_R^{(0)}k_R + B_z^{(0)}k_z = 0$, we arrive at the system of algebraic equations on $u_R^{(0)}$, $u_\phi^{(0)}$, $B_R^{(0)}$ and $B_\phi^{(0)}$

$$
\begin{aligned}
(\gamma + \tilde{\nu}|\mathbf{k}|^2)u_R^{(0)} - 2\alpha^2\Omega u_\phi^{(0)} + \frac{2\alpha^2 B_\phi^0}{\rho\mu_0 R}B_\phi^{(0)} - ik_z\frac{B_z^0}{\rho\mu_0}B_R^{(0)} &= 0, \\
(\gamma + \tilde{\nu}|\mathbf{k}|^2)u_\phi^{(0)} + 2\Omega(1+\mathrm{Ro})u_R^{(0)} - ik_z\frac{B_z^0}{\rho\mu_0}B_\phi^{(0)} &= 0, \\
(\gamma + \tilde{\eta}|\mathbf{k}|^2)B_R^{(0)} - ik_z B_z^0 u_R^{(0)} &= 0, \\
(\gamma + \tilde{\eta}|\mathbf{k}|^2)B_\phi^{(0)} - 2\Omega\mathrm{Ro}B_R^{(0)} - ik_z B_z^0 u_\phi^{(0)} - 2\frac{B_\phi^0}{R}u_R^{(0)} &= 0.
\end{aligned}
\tag{12.33}
$$

Introducing the viscous, resistive, and Alfvén frequencies as $\omega_\nu = \tilde{\nu}|\mathbf{k}|^2$, $\omega_\eta = \tilde{\eta}|\mathbf{k}|^2$, $\omega_A = k_z B_z^0(\rho\mu_0)^{-1/2}$, and $\omega_{A_\phi} = B_\phi^0(\rho\mu_0)^{-1/2}R^{-1}$, respectively, we find that γ in equations (12.33) is an eigenvalue of the matrix $\mathbf{H}$, where [309]

$$\mathbf{H} = \begin{pmatrix} -\omega_\nu & 2\alpha^2\Omega & i\frac{\omega_A}{\sqrt{\rho\mu_0}} & -\frac{2\omega_{A_\phi}\alpha^2}{\sqrt{\rho\mu_0}} \\ -2\Omega(1+\mathrm{Ro}) & -\omega_\nu & 0 & i\frac{\omega_A}{\sqrt{\rho\mu_0}} \\ i\omega_A\sqrt{\rho\mu_0} & 0 & -\omega_\eta & 0 \\ 2\omega_{A_\phi}\sqrt{\rho\mu_0} & i\omega_A\sqrt{\rho\mu_0} & 2\Omega\mathrm{Ro} & -\omega_\eta \end{pmatrix}. \tag{12.34}$$

12.4 Stability analysis

Stability of the solutions to the equation (12.32) is determined by the roots γ of the dispersion relation

$$p(\gamma) := \det(\mathbf{H} - \gamma\mathbf{I}) = \gamma^4 + a_1\gamma^3 + a_2\gamma^2 + (a_3 + ib_3)\gamma + a_4 + ib_4 = 0, \tag{12.35}$$

where $\mathbf{I}$ is the unit matrix and

$$\begin{aligned}
a_1 &= 2(\omega_\nu + \omega_\eta),\\
a_2 &= (\omega_\nu + \omega_\eta)^2 + 2(\omega_A^2 + \omega_\nu\omega_\eta) + 4\alpha^2\Omega_0^2(1+\mathrm{Ro}) + 4\alpha^2\omega_{A_\phi}^2,\\
a_3 &= 2(\omega_\eta + \omega_\nu)(\omega_A^2 + \omega_\eta\omega_\nu) + 8\alpha^2\Omega_0^2(1+\mathrm{Ro})\omega_\eta + 4\alpha^2(\omega_\eta + \omega_\nu)\omega_{A_\phi}^2,\\
a_4 &= (\omega_A^2 + \omega_\nu\omega_\eta)^2 - 4\alpha^2\omega_A^2\Omega_0^2 + 4\alpha^2\Omega_0^2(1+\mathrm{Ro})(\omega_A^2 + \omega_\eta^2) + 4\alpha^2\omega_\nu\omega_\eta\omega_{A_\phi}^2,\\
b_3 &= -8\alpha^2\Omega_0\omega_A\omega_{A_\phi},\\
b_4 &= -4\alpha^2\Omega_0\omega_A\omega_{A_\phi}(\omega_\eta + \omega_\nu) - 4\alpha^2\Omega_0(1+\mathrm{Ro})\omega_A\omega_{A_\phi}(\omega_\eta - \omega_\nu).
\end{aligned} \tag{12.36}$$

12.4.1 The threshold of the standard MRI

With $\omega_{A_\phi} = 0$ the coefficients b_3 and b_4 vanish while the others simplify. Composing the Hurwitz matrix (2.51) of the polynomial, we write the Liénard–Chipart criterion of asymptotic stability [409]

$$a_4 > 0, \quad a_2 > 0, \quad h_1 = a_1 > 0, \quad h_3 = a_1a_2a_3 - a_1^2a_4 - a_3^2 > 0, \tag{12.37}$$

see Theorem 2.34. Under the physical assumption that $\omega_\nu \geq 0$ and $\omega_\eta \geq 0$, the last two inequalities are automatically satisfied, because

$$\begin{aligned}
h_3 = {} & 4\omega_A^2(\omega_\eta + \omega_\nu)^2((\omega_\eta + \omega_\nu)^2 + 4\Omega^2\alpha^2)\\
& + 4\omega_\eta\omega_\nu((\omega_\eta + \omega_\nu)^2 + 4\Omega^2\alpha^2(1+\mathrm{Ro}))^2 > 0.
\end{aligned} \tag{12.38}$$

On the other hand, condition $a_4 > 0$ implies that

$$\mathrm{Ro} > \mathrm{Ro}_c := -\frac{(\omega_A^2 + \omega_\nu\omega_\eta)^2 + 4\Omega^2\omega_\eta^2\alpha^2}{4\Omega^2\alpha^2(\omega_A^2 + \omega_\eta^2)} > -1 - \frac{1}{4\mathrm{Re}^2}, \tag{12.39}$$

where $\mathrm{Re} = \alpha\Omega\omega_\nu^{-1}$ is the *Reynolds number*. Therefore, the four stability conditions (12.37) are reduced to only (12.39) that yields the critical Rossby number (Ro_c) of SMRI (above which the flow is stable).

It is instructive that the equations (12.33) can be rewritten as an eigenvalue problem for a *nonconservative gyroscopic system*

$$\ddot{\mathbf{u}} + (\mathbf{D} + \Omega_0(1+\alpha^2)\mathbf{J})\dot{\mathbf{u}} + (\mathbf{N} + \mathbf{K})\mathbf{u} = 0, \tag{12.40}$$

where $\mathbf{u} = (\hat{u}_R, \hat{u}_\phi)^T$, $\mathbf{N} = \Omega_0(\omega_\eta(1+\alpha^2) + \mathrm{Ro}(\omega_\eta - \omega_\nu))\mathbf{J}$,

$$\mathbf{K} = \begin{pmatrix} \omega_A^2 + \omega_\nu\omega_\eta & k_{12} \\ k_{12} & \omega_A^2 + \omega_\nu\omega_\eta + 4\alpha^2\Omega_0^2\mathrm{Ro} \end{pmatrix} \tag{12.41}$$

with $k_{12} = \Omega_0(\omega_\eta(1-\alpha^2) + \mathrm{Ro}(\omega_\eta - \omega_\nu))$, and

$$\mathbf{J} = \begin{pmatrix} 0 & -1 \\ 1 & 0 \end{pmatrix}, \quad \mathbf{D} = \begin{pmatrix} \omega_\nu + \omega_\eta & \Omega_0(1-\alpha^2) \\ \Omega_0(1-\alpha^2) & \omega_\nu + \omega_\eta \end{pmatrix}. \tag{12.42}$$

For $\alpha = 1$, $\omega_\nu = 0$, and $\omega_\eta = 0$, equation (12.40) is similar to the model (12.5) and has the same dispersion relation.

Stable perturbations have $\Re\,\gamma \le 0$ provided that γ with $\Re\,\gamma = 0$ is a semisimple eigenvalue of the eigenvalue problem associated with the system (12.40). The growing solutions of SMRI are nonoscillatory with $\Im\gamma = 0$. Therefore, $\gamma = 0$ implies that $\det(\mathbf{N} + \mathbf{K}) = 0$ at the threshold of SMRI which gives exactly the critical Rossby number, Ro_c, determined by equation (12.39).

12.4.2 Singularities and the Velikhov–Chandrasekhar paradox

The Velikhov–Chandrasekhar paradox occurs at infinite $\mathrm{Pm} = \omega_\nu\omega_\eta^{-1}$ and means that in the ideal MHD case ($\omega_\eta = 0$, $\omega_\nu = 0$) the limit $\omega_A \to 0$ yields Velikhov's value $\mathrm{Ro_c} = 0$ as the instability threshold rather than Rayleigh's limit $\mathrm{Ro_c} = -1$ of the nonmagnetic case ($\omega_A = 0$, $\omega_\nu = 0$). Thus, we have a counterintuitive effect of two *noncommuting limits*[6]

$$\lim_{\omega_A\to 0}\lim_{\omega_\eta\to 0}\mathrm{Ro_c}(\omega_A,\omega_\eta) \neq \lim_{\omega_\eta\to 0}\lim_{\omega_A\to 0}\mathrm{Ro_c}(\omega_A,\omega_\eta).$$

With $\omega_A = \varepsilon\cos\varphi$ and $\omega_\eta = \varepsilon\sin\varphi$ in (12.39), we obtain

$$\mathrm{Ro_c} = -\frac{(\varepsilon\cos^2\varphi + \omega_\nu\sin\varphi)^2 + 4\alpha^2\Omega_0^2\sin^2\varphi}{4\alpha^2\Omega_0^2}, \tag{12.43}$$

which for $\varepsilon \to 0$ reduces to

$$\mathrm{Ro_c^0} = -\left(1 + \frac{1}{4\mathrm{Re}^2}\right)\sin^2\varphi = -\frac{1 + (2\mathrm{Re})^{-2}}{1 + \mathrm{Lu}^2}, \tag{12.44}$$

[6] Note that similar noncommutativity phenomena exist in the buckling problems of structural mechanics, see e.g. [445] and [373].

where $\mathrm{Lu} = \omega_A \omega_\eta^{-1}$ is the Lundquist number. Introducing the new parameter $\mathrm{Ro}' = (1 + 4\mathrm{Re}^2(1 + 2\mathrm{Ro}))(1 + 4\mathrm{Re}^2)^{-1}$ we find that in the $(\omega_A, \omega_\eta, \mathrm{Ro}')$-space equation (12.44) defines a ruled surface $(\varepsilon, \varphi) \mapsto (\varepsilon \cos\varphi, \varepsilon \sin\varphi, \cos n\varphi)$ with $n = 2$, which is a canonical equation for the Plücker conoid of degree $n = 2$ [231]. The surface (12.43) tends to the Plücker conoid when $\varepsilon = \sqrt{\omega_A^2 + \omega_\eta^2} \to 0$.

The threshold surface of SMRI is shown in the $(\omega_A, \omega_\eta, \mathrm{Ro})$-space in Figure 12.4 (a) and in projection to the (ω_A, ω_η)-plane in Figure 12.4 (b) for $\mathrm{Re} = 1$. For each α, ω_ν, and Ω_0 it has the same Plücker conoid singularity, i.e. an interval of self-intersection along the Ro-axis and two Whitney umbrella singular points at its ends. This singular structure implies nonuniqueness for the critical Rossby number when simultaneously $\omega_A = 0$ and $\omega_\eta = 0$.

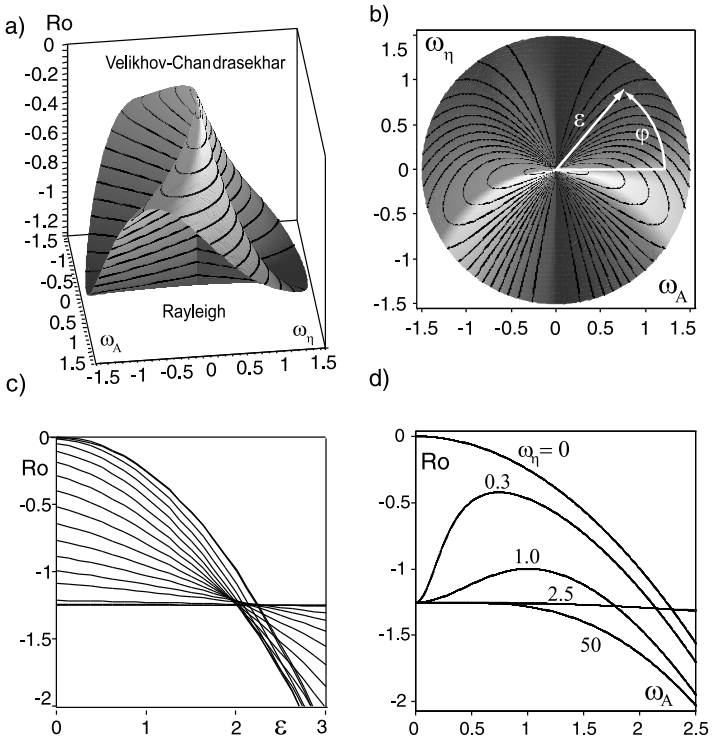

Figure 12.4. (a) The critical Rossby number of SMRI as a function of $\omega_A \sim \mathrm{LuPm}^{-1}$ and $\omega_\eta \sim \mathrm{Pm}^{-1}$ for $\omega_\nu = 1, \alpha = 1, \Omega_0 = 1$, i.e. for $\mathrm{Re} = 1$. (b) Top view of the surface. (c) Cross-sections of the surface along the rays specified by the Lundquist number, or, equivalently, by the angle φ that varies from 0 to 1.5 through the equal intervals $\Delta\varphi = 0.1$; the horizontal line corresponds to $\varphi = \pi/2$. (d) Transition between the case of low (Velikhov 1959) and high (Chandrasekhar 1953) resistivity.

Indeed, for a given Lu, tending the magnetic field to zero along a ray $\omega_A = \omega_\eta \mathrm{Lu}$ in the (ω_A, ω_η)-plane results in a value of the Rossby number specified by equation (12.44), see Figure 12.4 (c). The limit value of the critical Rossby number oscillates between the ideal MHD value $\mathrm{Ro}_c^0 = 0$ for $\mathrm{Lu} = \infty$ ($\varphi = 0$) and the nonmagnetic (Taylor) value $\mathrm{Ro}_c^0 = -1 - (2\mathrm{Re})^{-2}$ for $\mathrm{Lu} = 0$ ($\varphi = \pi/2$), which resolves the Velikhov–Chandrasekhar paradox.

Physically, the Lundquist number determines the 'lifetime' of the magnetic field line that is frozen into the fluid. In the ideal MHD case $\mathrm{Lu} = \infty$ means that the field does not diffuse from the fluid. At the lower values of Lu, resistivity destroys the magnetic tension effect which prevents Ro from reaching the solid body rotation value in the limit of vanishing magnetic field.

Figure 12.4 (d) demonstrates transition between the cases of high conductivity (Velikhov 1959) and of low conductivity (Chandrasekhar 1953) separated by the threshold $\omega_\eta = (\omega_\nu^2 + 4\Omega_0^2\alpha^2)(2\omega_\nu)^{-1}$. In the latter case the axial magnetic field stabilizes the hydrodynamically unstable CT-flow. Figure 12.4 (d) also illustrates the conclusions of Acheson and Hide that in the presence of small but finite resistivity in the limit of vanishing ω_A "the stability or otherwise of the system will then be decided essentially by Rayleigh's criterion" [1].

What eigenvalue behavior corresponds to the singular threshold of SMRI? In the absence of the magnetic field the roots of the dispersion relation (12.35) are exactly

$$\gamma_{1,2} = -\omega_\nu \pm i\,2\alpha\Omega_0\sqrt{\mathrm{Ro}+1}, \quad \gamma_{3,4} = -\omega_\eta. \tag{12.45}$$

The first two roots bifurcate and one of them becomes positive at the critical Rossby number $\mathrm{Ro}_c = -1 - (2\mathrm{Re})^{-2}$, see Figure 12.5 (a, b, e). The dark gray curves there represent the *inertial waves* whose interaction yields the centrifugal instability in the inviscid case [164, 308]. The Rayleigh line is thus characterized by the double zero eigenvalue with the Jordan block. Viscosity shifts this doublet to the left part of the complex plane [192]. This scenario corresponds to the lower Whitney umbrella singularity on the SMRI threshold shown in Figure 12.4 (a).

With $\omega_A \neq 0$ the merging of the inertial waves becomes imperfect, see Figure 12.5 (c, d), while the formerly damped roots $\gamma_{3,4}$ experience a bifurcation at the Rossby number that is close to the Velikhov–Chandrasekhar value. In Figure 12.5 (d) the light gray branches correspond to the slow magneto-Coriolis (MC) waves and the dark gray ones to the fast MC waves. Bifurcation of the slow MC-waves precedes the onset of SMRI (equation (12.39)) with the decrease of Ro. In the absence of viscosity and resistivity the roots of the dispersion relation (12.35) corresponding to slow- and fast MC-waves are exactly

$$\gamma^2 = -2\Omega_0^2\alpha^2(1+\mathrm{Ro}) - \omega_A^2 \pm 2\Omega_0\alpha\sqrt{\Omega_0^2\alpha^2(1+\mathrm{Ro})^2 + \omega_A^2}. \tag{12.46}$$

The corresponding double zero eigenvalue at $\omega_A = 0$ and $\mathrm{Ro} = 0$ is related to the upper Whitney umbrella singularity at the SMRI threshold in Figure 12.4 (a).

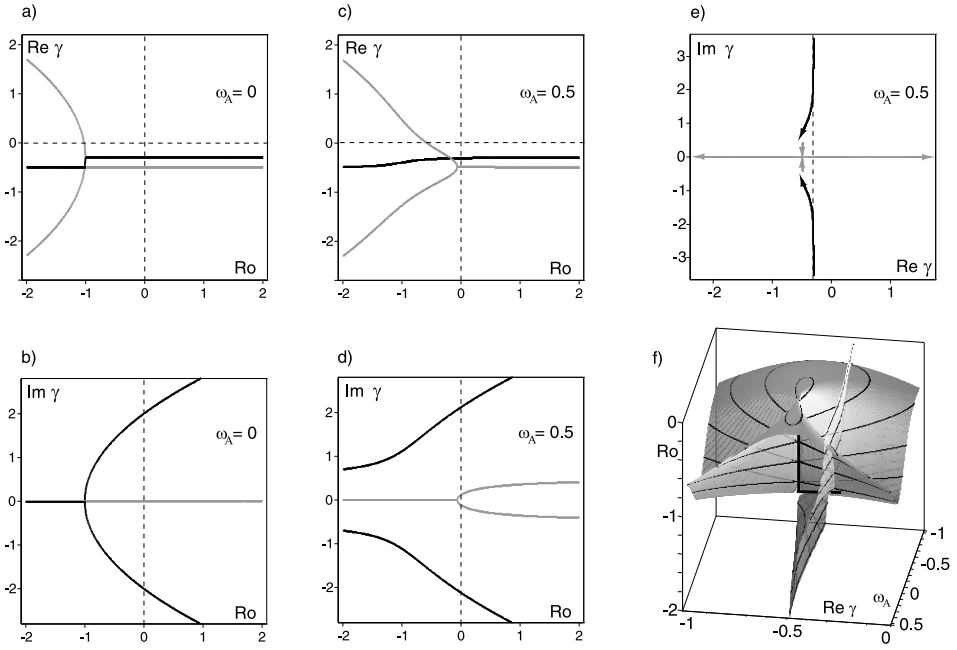

Figure 12.5. Growth rates and frequencies of the perturbation for $\Omega_0 = 1$, $\alpha = 1$, $\omega_\nu = 0.3$, $\omega_\eta = 0.5$ and (a, b) $\omega_A = 0$ and (c, d, e) $\omega_A = 0.5$; (f) growth rates surfaces in the $(\Re\gamma, \omega_A, \mathrm{Ro})$-space.

Transition between these two bifurcations happens in the presence of resistivity and viscosity and is described by means of the slices of two singular eigenvalue surfaces shown in Figure 12.5 (f). The surface corresponding to the roots $\gamma_{1,2}$ is locally equivalent to the Plücker conoid of degree $n = 2$ and that of the roots $\gamma_{3,4}$ to the Plücker conoid of degree $n = 1$ [231].

12.4.3 The singular threshold of the HMRI and connection of HMRI and SMRI through a spectral exceptional point

After scaling the spectral parameter as $\gamma = \lambda\sqrt{\omega_\nu\omega_\eta}$, we express the appropriately normalized coefficients (12.36) by means of the dimensionless Rossby number (Ro), magnetic Prandtl number (Pm), helicity parameter $\beta = \alpha\omega_{A_\phi}\omega_A^{-1}$ of the external magnetic field, Hartmann ($\mathrm{Ha} = \mathrm{LuPm}^{-1/2}$), and Reynolds (Re) numbers. Additional transformations yield the coefficients of the dispersion relation $p(\lambda) = 0$

$$
\begin{aligned}
a_1 &= 2(1 + \mathrm{Pm}^{-1})\sqrt{\mathrm{Pm}},\\
a_2 &= 2(1 + (1 + 2\beta^2)\mathrm{Ha}^2) + 4\mathrm{Re}^2(1 + \mathrm{Ro})\mathrm{Pm} + a_1^2/4,\\
a_3 &= a_1(1 + (1 + 2\beta^2)\mathrm{Ha}^2) + 8\mathrm{Re}^2(1 + \mathrm{Ro})\sqrt{\mathrm{Pm}},
\end{aligned}
$$

$$a_4 = \left(1+\mathrm{Ha}^2\right)^2 + 4\beta^2\mathrm{Ha}^2 + 4\mathrm{Re}^2(1 + \mathrm{Ro}(\mathrm{Pm}\mathrm{Ha}^2 + 1)),$$
$$b_3 = -8\beta\mathrm{Ha}^2\mathrm{Re}\sqrt{\mathrm{Pm}},\quad b_4 = b_3(1 + (1 - \mathrm{Pm})\mathrm{Ro}/2)/\sqrt{\mathrm{Pm}}. \tag{12.47}$$

The analogue of the Routh–Hurwitz conditions for the complex polynomials – the Bilharz criterion [62] – requires positiveness of all diagonal even-ordered minors of the so-called Bilharz matrix (see Theorem (2.35)) composed of the coefficients (12.47)

$$\begin{aligned} m_1 &= a_3a_4 + b_3b_4 > 0, \quad m_2 = (a_2a_3 - a_1a_4)m_1 - a_2^2b_4^2 > 0,\\ m_3 &= (a_1a_2 - a_3)m_2 - (a_1^2a_4a_2 + (a_1b_3 - b_4)^2)m_1\\ &\quad + a_1a_4(b_4a_2(2b_4 - a_1b_3) + a_1^2a_4^2) > 0,\\ m_4 &= a_1m_3 - a_1a_3m_2 + (a_3^3 + a_1^2b_4b_3 - 2a_1b_4^2)m_1\\ &\quad + a_1b_4^2a_4(a_1a_2 - a_3) - b_4^2a_3^2a_2 + b_4^4 > 0. \end{aligned} \tag{12.48}$$

When the last of the stability conditions (12.48) is fulfilled, the remaining inequalities are satisfied automatically [309]. Therefore, the threshold of HMRI is defined by the equation $m_4(\beta, \mathrm{Re}, \mathrm{Ha}, \mathrm{Pm}, \mathrm{Ro}) = 0$. For $\beta = 0$ the dispersion relation and thus the threshold for HMRI reduce to that of SMRI [309].

In the inductionless limit $\mathrm{Pm} \to 0$ the critical Rossby number for the onset of HMRI follows from the equation $m_4 = 0$ in the explicit form

$$\mathrm{Ro} = \frac{(1+\mathrm{Ha}^2)^2 + 4\beta^2\mathrm{Ha}^2(1+\beta^2\mathrm{Ha}^2)}{2\mathrm{Ha}^4\beta^2} - \frac{2\beta^2\mathrm{Ha}^2+\mathrm{Ha}^2+1}{2\mathrm{Ha}^4\beta^2} \tag{12.49}$$
$$\times \sqrt{(1+\mathrm{Ha}^2)^2 + 4\beta^2\mathrm{Ha}^2(1+\beta^2\mathrm{Ha}^2) + \frac{\mathrm{Ha}^4\beta^2}{\mathrm{Re}^2}\left((1+\mathrm{Ha}^2)^2 + 4\beta^2\mathrm{Ha}^2\right)}.$$

In the limit $\mathrm{Re} \to \infty$ and $\mathrm{Ha} \to \infty$ this critical value is majorated by

$$\mathrm{Ro}(\beta) = \frac{1 + 4\beta^4 - (1 + 2\beta^2)\sqrt{1 + 4\beta^4}}{2\beta^2}, \tag{12.50}$$

with the maximum at the well-known Liu limit $\mathrm{Ro_c} = 2 - 2\sqrt{2} \approx -0.828$ when $\beta = \sqrt{2}/2 \approx 0.707$ [309]. The line (12.50) is shown dashed in Figure 12.6 (left). Nevertheless, at small but finite Pm, the HMRI domain shown in dark gray in Figure 12.6 (left) can exceed the Liu limit for some choice of Ha and Re.

To understand how far beyond the Liu limit HMRI can exist, we show in Figure 12.7 a typical critical surface $m_4 = 0$ in the $(\mathrm{Pm}, \mathrm{Re}^{-1}, \mathrm{Ro})$-space for the special parameter choice $\mathrm{Ha} = 15$ and $\beta = 0.7$. On the Ro-axis we find a self-intersection and two Whitney umbrella singularities at its ends. At the upper singular point, i.e. exactly at $\mathrm{Pm} = 0$, the critical Rossby number is given by equation (12.49) in the limit $\mathrm{Re} \to \infty$.

In Figure 12.7 we see that the case with $\mathrm{Pm} = 0$ is connected to the case $\mathrm{Pm} \neq 0$ by the Plücker conoid singularity, quite similar as it was discussed for the paradox of Velikhov and Chandrasekhar. Interestingly, $\mathrm{Ro_c}$ for the onset of HMRI can indeed increase when Pm departs from zero which happens along curved pockets of HMRI.

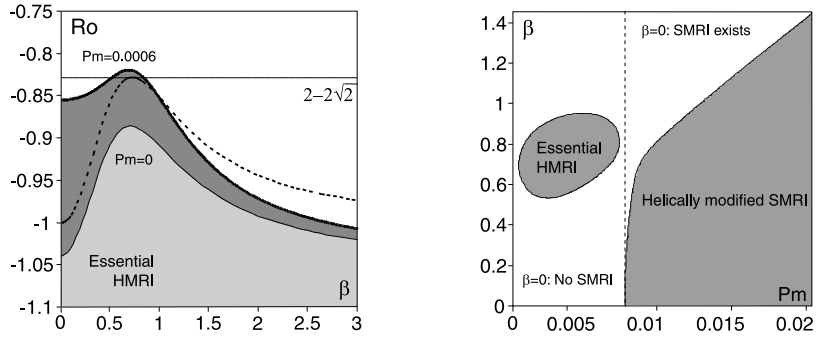

Figure 12.6. (Left) In the inductionless case $\mathrm{Pm} = 0$ the instability domain (light gray, at $\mathrm{Ha} = 19$ and $\mathrm{Re} = 900$) is always under the majorating dashed curve given by equation (12.50) that touches the Liu limit $\mathrm{Ro} = 2 - 2\sqrt{2}$ at $\beta = \sqrt{2}/2$; for $\mathrm{Pm} \neq 0$ this is no longer true and the instability domain (dark gray, shown for $\mathrm{Ha} = 19$ and $\mathrm{Re} = 900$) can partly lie above the Liu limit. (Right) HMRI island ($\mathrm{Ha} = 5$, $\mathrm{Re} = 100$, $\mathrm{Ro} = -0.85$) in the (Pm, β)-plane exists at such low Pm at $\beta \neq 0$ where SMRI at $\beta = 0$ does not [309, 311].

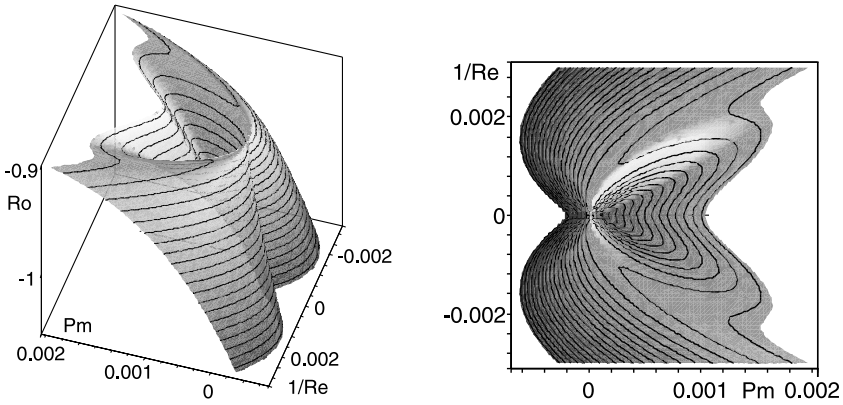

Figure 12.7. HMRI threshold at $\mathrm{Ha} = 15$ and $\beta = 0.7$ in the $(\mathrm{Pm}, \mathrm{Re}^{-1}, \mathrm{Ro})$-space and in projection to the $(\mathrm{Pm}, \mathrm{Re}^{-1})$-plane [311].

The two side bumps of the curve $\mathrm{Re}^{-1}(\mathrm{Pm})$ in a horizontal slice of the surface correspond to the domains[7] of the *essential HMRI* while the central hill marks the *helically modified SMRI* domain, according to the classification introduced in [309], see also Figure 12.6 (right). The *exchange of stability* [145] from standard MRI to the essential HMRI when β departs from zero takes place by means of the origination of a double complex eigenvalue with the negative real part (exceptional point) and its subsequent splitting, Figure 12.8.

[7] Islands of instability similar to the essential HMRI island of Figure 12.6 (right) were found in a pure hydrodynamical CT problem [8] as well as in other settings [438].

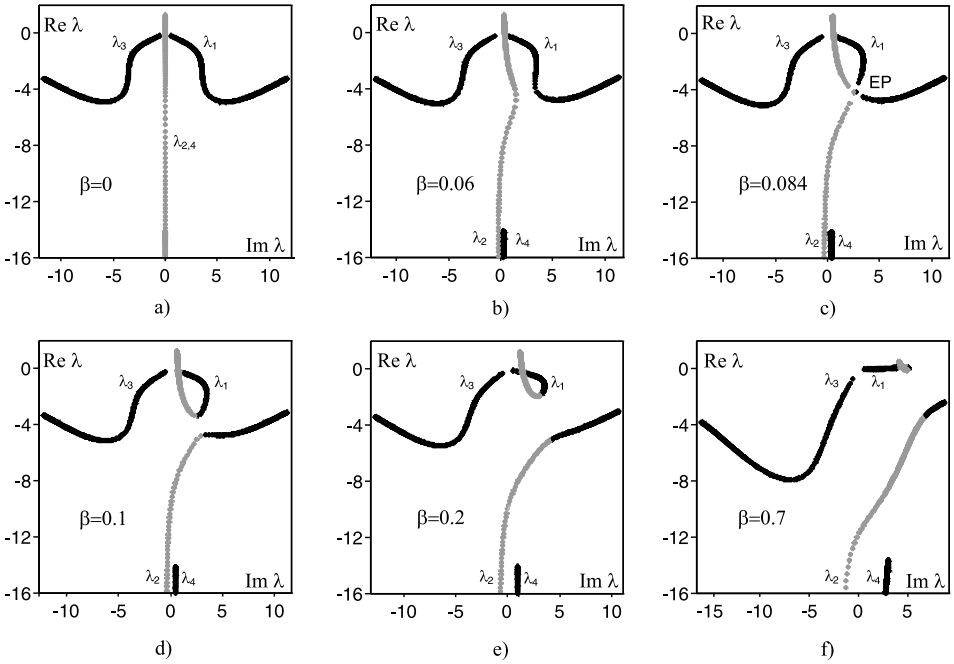

Figure 12.8. Ha $= 5$, Re $= 100$, Ro $= -0.85$: Eigenvalue trajectories in the complex plane when $0 \leq \mathrm{Pm} \leq 0.011$ show the effect of *transfer of instability between branches* through an exceptional point (EP). (a) SMRI is caused by the transition of a pure real eigenvalue from negative values to positive. (b) Deformation of the critical branch (gray) for $\beta \neq 0$; (c) merging of the critical and stable branches with the origination of the double complex eigenvalue with the Jordan block at the EP; (d–f) splitting of the EP and bifurcation of the eigenvalue trajectories: after surgery the stable complex branch acquires an unstable tail of the critical branch (gray) and becomes unstable near the origin, which corresponds to an unstable traveling wave of HMRI [309].

For small Pm the essential HMRI occurs at higher Ro than the helically modified SMRI, while for some finite value of Pm the central hill and the side bumps get the same value of $\mathrm{Ro_c}$. Most remarkably, there is a value of $\mathrm{Ro_c}$ at which the two side bumps of the curve $\mathrm{Re}^{-1}(\mathrm{Pm})$ disappear completely. This is the maximal possible value for the essential HMRI, at least at the given β and Ha. Now we can ask: how does this limit behave if we send Ha to infinity, and to which value of Lu does this correspond?

Actually, with the increase in Ha the stability boundary preserves its shape and simultaneously it compresses in the direction of zero Pm. Substituting $\mathrm{Ha} = \mathrm{LuPm}^{-1/2}$ into the equations (12.47), we plot again the surface $m_4 = 0$ in the $(\mathrm{Pm}, \mathrm{Re}^{-1}, \mathrm{Ro})$-space, but now for a given β and Lu, Figure 12.8 (left).

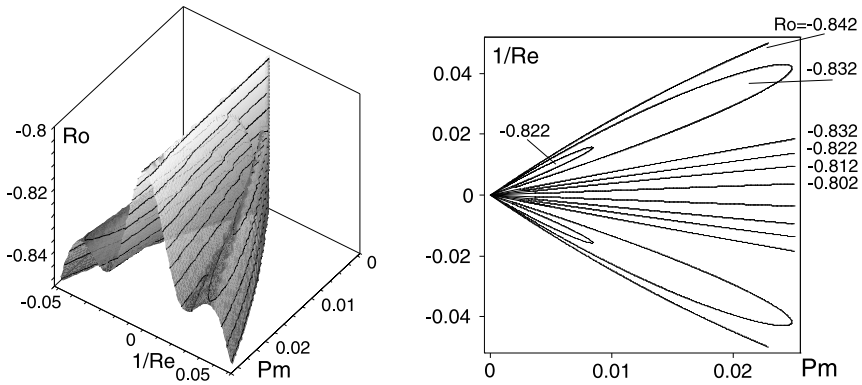

Figure 12.9. (Left) The critical Ro at Lu $= 0.5$ and $\beta = 0.6$ in the $(\mathrm{Pm}, \mathrm{Re}^{-1}, \mathrm{Ro})$-space and (right) its cross-sections in the $(\mathrm{Pm}, \mathrm{Re}^{-1})$-plane at Ro $= -0.842$, Ro $= -0.832$, Ro $= -0.822$, Ro $= -0.812$, and Ro $= -0.802$ [310].

The corresponding cross-sections of the instability domain in the $(\mathrm{Re}^{-1}, \mathrm{Pm})$-plane are shown in Figure 12.9 (right). At a given value of Ro there exist three domains of instability. Two sub-domains that have the form of a petal correspond to the HMRI. They are bounded by closed curves with a self-intersection singularity at the origin. They are also elongated in a preferred direction that in the $(\mathrm{Re}^{-1}, \mathrm{Pm})$-plane corresponds to a limited range of the magnetic Reynolds number Rm $=$ PmRe. The central domain, which corresponds to the helically modified SMRI, has a similar singularity at the origin and is unbounded in the positive Pm-direction. In comparison with the central domain where Rm > 1, within the side petals Rm < 1.

Now we reconsider again the limit Pm $\to 0$, while keeping Lu as a free parameter. At the origin all the boundaries of the petals can be approximated by the straight lines Pm $=$ RmRe^{-1}. Substituting this expression into equation $m_4 = 0$, we find that the only term that does not depend on Pm is a polynomial $Q(\mathrm{Rm}, \mathrm{Lu}, \beta, \mathrm{Ro}) = p_0 + p_1\mathrm{Rm}^2 + p_2\mathrm{Rm}^4 + p_3\mathrm{Rm}^6$, with the coefficients

$$
\begin{aligned}
p_0 &= \mathrm{Lu}^4(4\beta^4\mathrm{Lu}^2 + 2\beta^2 + 4\mathrm{Lu}^2\beta^2 + 1)^2,\\
p_1 &= 4(-\beta^2(1 + 20\mathrm{Lu}^4\beta^2 + 2\mathrm{Lu}^4 + 8\beta^2\mathrm{Lu}^6\\
&\quad + 16\beta^6\mathrm{Lu}^6 + 24\mathrm{Lu}^6\beta^4 + 4\mathrm{Lu}^2 + 8\beta^2\mathrm{Lu}^2 + 20\beta^4\mathrm{Lu}^4)\mathrm{Ro}^2\\
&\quad + (16\mathrm{Lu}^6\beta^4 + 16\beta^6\mathrm{Lu}^2 + \mathrm{Lu}^2 + 4\beta^4 + 16\beta^8\mathrm{Lu}^4 + 1 - 16\beta^8\mathrm{Lu}^6 + 4\mathrm{Lu}^2\beta^4)\mathrm{Ro}\\
&\quad + 1 - 8\mathrm{Lu}^2\beta^2(\mathrm{Lu}^4\beta^2 - \beta^2 + \mathrm{Lu}^4 - \beta^2\mathrm{Lu}^2 + \mathrm{Lu}^2)\\
&\quad + 16\beta^6\mathrm{Lu}^2(1 + \beta^2\mathrm{Lu}^2 + \mathrm{Lu}^2 + \mathrm{Lu}^4) + 4\beta^4 + 2\mathrm{Lu}^4),\\
p_2 &= 16(\mathrm{Lu}^4\beta^4\mathrm{Ro}^4 - \beta^2(-2 + 4\beta^4\mathrm{Lu}^4 - 3\mathrm{Lu}^2 + 4\mathrm{Lu}^4\beta^2)\mathrm{Ro}^3\\
&\quad + 2\beta^2(3 + 4\beta^2 + 6\beta^4\mathrm{Lu}^4 + 4\mathrm{Lu}^2 + 16\beta^2\mathrm{Lu}^2 + 3\mathrm{Lu}^4 + 8\mathrm{Lu}^2\beta^4 + 12\mathrm{Lu}^4\beta^2)\mathrm{Ro}^2\\
&\quad + (32\beta^4\mathrm{Lu}^4 + 16\beta^4 + 40\mathrm{Lu}^2\beta^4 + 2 + 2\mathrm{Lu}^2 + 4\beta^2 + 32\beta^6\mathrm{Lu}^4 + 32\beta^6\mathrm{Lu}^2)\mathrm{Ro}\\
&\quad + 2 + 4\mathrm{Lu}^4\beta^2 + 8\mathrm{Lu}^2\beta^4 + 16\beta^6\mathrm{Lu}^2 + 8\beta^4 + 16\beta^6\mathrm{Lu}^4 + \mathrm{Lu}^4 + 4\beta^4\mathrm{Lu}^4),\\
p_3 &= 64((2\mathrm{Ro}\beta^2 + 1)^2 + 8\mathrm{Ro}\beta^4 + 4\beta^4 + 3\mathrm{Ro}^2\beta^2 - \mathrm{Ro}^3\beta^2)(\mathrm{Ro} + \mathrm{RoLu}^2 + 1).
\end{aligned}
\tag{12.51}
$$

The roots of the polynomial are coefficients Rm of the linear approximation to the instability domains at the origin in the $(\mathrm{Re}^{-1}, \mathrm{Pm})$-plane. Simple roots mean nondegenerate self-intersection of the stability boundary at the origin. Double roots correspond to a degeneration of the angle of self-intersection when it collapses to zero which happens only at the maximal critical Rossby number, Figure 12.9 (left). In the $(\mathrm{Lu}, \beta, \mathrm{Ro})$-space a set of points that correspond to multiple roots of the polynomial Q is given by the discriminant surface $64\Delta^2 p_0 p_3 = 0$, where

$$\Delta(\mathrm{Lu}, \beta, \mathrm{Ro}) := 18 p_0 p_1 p_2 p_3 - 4 p_1^3 p_3 + p_1^2 p_2^2 - 4 p_0 p_2^3 - 27 p_0^2 p_3^2. \qquad (12.52)$$

The surface $p_3 = 0$ consists of a sheet $\mathrm{Ro} = -(1 + \mathrm{Lu}^2)^{-1}$ corresponding to the doubly degenerate infinite values of Rm at the maxima of the helically modified SMRI. It smoothly touches along the β-axis the surface $\Delta = 0$ that consists of two smooth sheets that touch each other along a spatial curve – the cuspidal edge – corresponding to triple roots of the polynomial Q, Figure 12.10 (a).

Every point on the upper sheet of the surface $\Delta = 0$ represents a degenerate linear approximation to the essential HMRI domain and therefore a maximal Ro at the corresponding values of β and Lu. Numerical optimization results in the new ultimate limit for HMRI $\mathrm{Ro_c} \approx -0.802$ at $\mathrm{Lu} \approx 0.618$, $\beta \approx 0.634$, and $\mathrm{Rm} \approx 0.770$, see Figure 12.10 (b). This new limit of $\mathrm{Ro_c}$ on the cuspidal edge is smoothly connected to the inductionless Liu limit by the upper sheet of the discriminant surface, which converges to the curve (12.50) when $\mathrm{Lu} = 0$. We point out that the new limit is achieved at $\mathrm{Ha} \to \infty$ when the optimal Pm tends to zero in such a way that $\mathrm{Lu} \approx 0.618$.

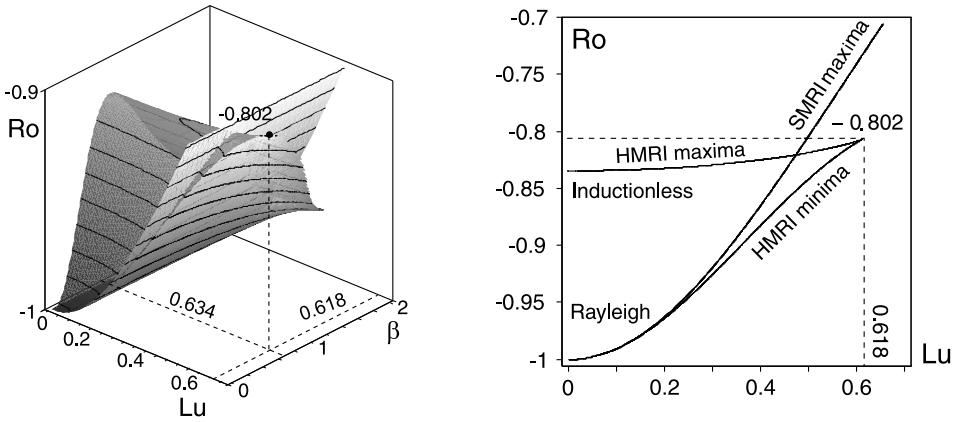

Figure 12.10. (a) Discriminant surface $\Delta = 0$ in the $(\mathrm{Lu}, \beta, \mathrm{Ro})$-space and (b) its cross-section at $\beta = 0.634$ [310].

References

[1] D. J. Acheson and R. Hide, Hydromagnetics of rotating fluids, *Rep. Prog. Phys.* **36** (1973), 159–221.

[2] L. Y. Adrianova, *Introduction to Linear Systems of Differential Equations*, Translations of Mathematical Monographs 146, American Mathematical Society, Providence, RI, 1998.

[3] D. Afolabi, Sylvester's eliminant and stability criteria for gyroscopic systems, *J. Sound Vibr.* **182** (1995), 229–244.

[4] S. A. Agafonov, Stability and motion stabilization of nonconservative mechanical systems, *J. Math. Sci.* **112** (2002), 4419–4497.

[5] S. A. Agafonov, Stability of nonconservative systems and applications, *J. Math. Sci.* **125** (2005), 556–578.

[6] A. Akay, Acoustics of friction, *J. Acoust. Soc. Amer.* **111** (2002), 1525–1548.

[7] R. Alam, S. Bora, R. Byers and M. L. Overton, Characterization and construction of the nearest defective matrix via coalescence of pseudospectral components, *Linear Algebra and its Applications* **435** (2011), 494–513.

[8] S. Altmeyer, C. Hoffmann and M. Lücke, Islands of instability for growth of spiral vortices in the Taylor-Couette system with and without axial through flow, *Phys. Rev. E* **84** (2011), 046308.

[9] L. J. An and D. G. Schaeffer, The flutter instability in granular flow, *Journal of the Mechanics and Physics of Solids* **40** (1992), 683–698.

[10] D. R. Andersen, S. Datta and R. L. Gunshor, A coupled mode approach to modulation instability and envelope solitons, *J. App. Phys.* **54** (1983), 5608–5612.

[11] B. D. O. Anderson, The reduced Hermite criterion with application to the proof of the Lienard–Chipart criterion, *IEEE Trans. AC* **17** (1972), 669–672.

[12] S. B. Andersson, *Geometric Phases in Sensing and Control*, Ph.D. thesis, University of Maryland, College Park, 2003.

[13] S. B. Andersson and P. S. Krishaprasad, *The Hannay–Berry Phase of the Vibrating Ring Gyroscope*, Center for Dynamics and Control of Smart Structures, Technical Research Report no. CDCSS TR 2004-2, University of Maryland, College Park, 2004.

[14] I. P. Andreichikov and V. I. Yudovich, The stability of visco-elastic rods, *Izv. Acad. Nauk SSSR, MTT* **1** (1975), 150–154.

[15] V. Antropov, E. Boltushkin, A. Ivanov, Y. Korotaev, V. Lohmatov, I. Meshkov, V. Pavlov, R. Pivin, I. Seleznev, A. Sidorin, A. Smirnov, E. Syresin, G. Trubnikov

and S. Yakovenko, Positron storage ring LEPTA, *Nuclear Instruments and Methods in Physics Research Section A: Accelerators, Spectrometers, Detectors and Associated Equipment* **532** (2004), 172–176.

[16] V. Apostolyuk and F. E. H. Tay, Dynamics of micromechanical Coriolis vibratory gyroscopes, *Sensor Letters* **2** (2004), 252–259.

[17] V. I. Arnold, On matrices depending on parameters, *Russian Mathematical Surveys* **26** (1971), 29–43.

[18] V. I. Arnold, *Mathematical Methods of Classical Mechanics*, 2nd edn., Graduate Texts in Mathematics 60, Springer, Berlin, 1989.

[19] V. I. Arnold, Spaces of functions with moderate singularities, *Funct. Anal. Appl.* **23** (1989), 169–177.

[20] V. I. Arnold, Remarks on eigenvalues and eigenvectors of Hermitian matrices, Berry phase, adiabatic connections and quantum Hall effect, *Selecta Mathematica, New Series* **1** (1995), 1–19.

[21] V. I. Arnold and B. A. Khesin, *Topological Methods in Hydrodynamics*, Applied Mathematical Sciences 125, Springer, New York, 1998.

[22] V. I. Arnold, V. V. Kozlov and A. I. Neishtadt, *Mathematical Aspects of Classical and Celestial Mechanics*, Encyclopaedia of Mathematical Sciences 3, Springer, New York, 2006.

[23] V. Arnold, A. Varchenko and S. Gusein-Zade, *Singularities of Differentiable Maps*, 1st edn., Monographs in Mathematics 1, Birkhäuser, Boston, 1985.

[24] F. V. Atkinson and A. B. Mingarelli, *Multiparameter Eigenvalue Problems: Sturm–Liouville Theory*, CRC Press, Boca Raton, Florida, 2010.

[25] D. Avitabile and T. J. Bridges, Numerical implementation of complex orthogonalization, parallel transport on Stiefel bundles, and analyticity, *Physica D* **239** (2010), 1038–1047.

[26] A. E. Baikov and P. S. Krasil'nikov, The Ziegler effect in a non-conservative mechanical system, *PMM J. Appl. Math. Mech.* **74** (2010), 51–60.

[27] J. Baillieul and M. Levi, Constrained relative motions in rotational mechanics, *Archive for Rational Mechanics and Analysis* **115** (1991), 101–135.

[28] S. A. Balbus, Enhanced angular momentum transport in accretion disks, *Ann. Rev. Astron. Astroph.* **41** (2003), 555–597.

[29] S. A. Balbus, A turbulent matter, *Nature* **470** (2011), 475–476.

[30] S. A. Balbus and J. F. Hawley, A powerful local shear instability in weakly magnetized disks: I. Linear analysis, *The Astrophysical Journal* **376** (1991), 214–233.

[31] S. A. Balbus and J. F. Hawley, Instability, turbulence, and enhanced transport in accretion disks, *Rev. Mod. Phys.* **70** (1998), 1–53.

[32] N. V. Banichuk, A. S. Bratus and A. D. Myshkis, On the destabilizing action of small dissipative forces on non-conservative systems, *Doklady Akademii Nauk SSSR* **309** (1989), 1325–1327.

[33] N. V. Banichuk, A. S. Bratus and A. D. Myshkis, Stabilizing and destabilizing effects in nonconservative systems, *PMM J. Appl. Math. Mech.* **53** (1989), 158–164.

[34] L. Barkwell and P. Lancaster, Overdamped and gyroscopic vibrating systems, *Trans. ASME J. Appl. Mech.* **59** (1992), 176–181.

[35] S. Barnett, A new formulation of the theorems of Hurwitz, Routh and Sturm, *J. Inst. Maths. Appl.* **8** (1971), 240–250.

[36] S. Barnett, Leverrier's algorithm – a new proof and extensions, *SIAM J. Matrix Anal. Appl.* **10** (1989), 551–556.

[37] H. Baumgärtel, *Analytic Perturbation Theory for Matrices and Operators*, Operator Theory: Advances and Applications 15, Birkhäuser Verlag, Basel, 1985.

[38] B. J. Bayly, Three-dimensional instability of elliptical flow, *Phys. Rev. Lett.* **57** (1986), 2160–2163.

[39] M. Beck, Die Knicklast des einseitig eingespannten, tangential gedruckten Stabes, *ZAMP Z. angew. Math. Phys.* **3** (1952), 225–228.

[40] M. Becker, W. Hauger and W. Winzen, Influence of internal and external damping on the stability of Beck's column on an elastic foundation, *J. Sound Vibr.* **54** (1977), 468–472.

[41] V. V. Beletsky, Some stability problems in applied mechanics, *Applied Mathematics and Computation* **70** (1995), 117–141.

[42] V. V. Beletsky, *Essays on the Motion of Celestial Bodies*, Springer, Basel, 2001.

[43] V. V. Beletsky and E. M. Levin, Stability of a ring of connected satellites, *Acta Astron.* **12** (1985), 765–769.

[44] V. V. Beletsky and E. M. Levin, *Dynamics of Space Tether Systems*, Advances in the Astronautical Sciences 83, American Astronautical Society, San Diego, 1993.

[45] V. V. Belov, S. Y. Dobrokhotov and T. Y. Tudorovskiy, Operator separation of variables for adiabatic problems in quantum and wave mechanics, *Journal of Engineering Mathematics* **55** (2006), 183–237.

[46] C. M. Bender and H. F. Jones, WKB Analysis of PT -Symmetric Sturm–Liouville problems, *J. Phys. A: Math. Theor.* **45** (2012), 444004.

[47] C. M. Bender and P. D. Mannheim, PT symmetry and necessary and sufficient conditions for the reality of energy eigenvalues, *Phys. Lett. A* **374** (2010), 1616–1620.

[48] T. B. Benjamin and J. E. Feir, Disintegration of wave trains on deep water. 1. Theory, *J. Fluid Mech.* **27** (1967), 417–430.

[49] M. V. Berry, Quantal phase factors accompanying adiabatic changes, *Proc. R. Soc. Lond. Ser. A. Math. Phys. Sci.* **392** (1984), 45–57.

[50] M. V. Berry, Physics of nonhermitian degeneracies, *Czech. J. Phys.* **54** (2004), 1039–1047.

[51] M. V. Berry, Optical polarization evolution near a non-Hermitian degeneracy, *J. Opt.* **13** (2011), 115701.

[52] M. V. Berry and M. R. Dennis, The optical singularities of birefringent dichroic chiral crystals, *Proc. R. Soc. Lond. Ser. A. Math. Phys. Sci.* **459** (2003), 1261–92.

[53] M. V. Berry and M. R. Jeffrey, *Conical diffraction: Hamilton's diabolical point at the heart of crystal optics*, in: Progress in Optics 50, pp. 13–50, Elsevier, New York, 2007.

[54] M. V. Berry and P. Shukla, Slow manifold and Hannay angle in the spinning top, *European Journal of Physics* **32** (2011), 115–127.

[55] M. V. Berry and P. Shukla, Classical dynamics with curl forces, and motion driven by time-dependent flux, *Journal of Physics A: Mathematical and Theoretical* **45** (2012), 305201.

[56] M. V. Berry and M. Wilkinson, Diabolical points in the spectra of triangles, *Proc. R. Soc. Lond. A* **392** (1984), 15–43.

[57] V. Bespalov and V. Talanov, Filamentary structure of light beams in nonlinear liquids, *JETP Letters-USSR* **3** (1966), 307–310.

[58] S. P. Bhattacharyya, H. Chapellat and L. H. Keel, *Robust Control. The Parametric Approach*, Information & System Science, Prentice Hall, NJ, 1995.

[59] D. Bigoni, On flutter instability in elastoplastic constitutive models, *International Journal of Solids and Structures* **32** (1995), 3167–3189.

[60] D. Bigoni, *Nonlinear Solid Mechanics: Bifurcation Theory and Material Instability*, Cambridge, Cambridge University Press, 2012.

[61] D. Bigoni and G. Noselli, Experimental evidence of flutter and divergence instabilities induced by dry friction, *Journal of the Mechanics and Physics of Solids* **59** (2011), 2208–2226.

[62] H. Bilharz, Bemerkung zu einem Satze von Hurwitz, *ZAMM Z. angew. Math. Mech.* **24** (1944), 77–82.

[63] P. Binding and P. J. Browne, Two parameter eigenvalue problems for matrices, *Linear Algebra and its Applications* **113** (1989), 139–157.

[64] P. Binding and H. Volkmer, Eigencurves for two-parameter Sturm–Liouville equations, *SIAM Rev.* **38** (1996), 27–48.

[65] P. Birtea, I. Casu and D. Comanescu, Instability conditions for circulatory and gyroscopic conservative systems, *Physica D* **241** (2012), 1655–1659.

[66] C. C. Bissell, Stodola, Hurwitz and the genesis of the stability criterion, *Int. J. Contr.* **50** (1989), 2313–2332.

[67] K. Y. Bliokh, The appearance of a geometric-type instability in dynamic systems with adiabatically varying parameters, *Journal of Physics A-Mathematical and General* **32** (1999), 2551–2565.

[68] K. Y. Bliokh, Geometric amplitude, adiabatic invariants, quantization, and strong stability of Hamiltonian systems, *J. Math. Phys.* **43** (2002), 25–42.

[69] K. Y. Bliokh, Geometrodynamics of polarized light: Berry phase and spin Hall effect in a gradient-index medium, *Journal of Optics A: Pure and Applied Optics* **11** (2009), 094009.

[70] K. Y. Bliokh, Y. P. Bliokh, V. Freilikher, S. Savel'ev and F. Nori, Colloquium: Unusual resonators: Plasmonics, metamaterials, and random media, *Reviews of Modern Physics* **80** (2008), 1201–1213.

[71] K. Y. Bliokh, Y. Gorodetski, V. Kleiner and E. Hasman, Coriolis effect in optics: Unified geometric phase and spin-Hall effect, *Phys. Rev. Lett.* **101** (2008) 030404.

[72] K. Y. Bliokh, A. Niv, V. Kleiner and E. Hasman, Geometrodynamics of spinning light, *Nature Photonics* **2** (2008), 748–753.

[73] A. M. Bloch, P. Hagerty, A. G. Rojo and M. I. Weinstein, Gyroscopically stabilized oscillators and heat baths, *Journal of Statistical Physics* **115** (2004), 1073–1100.

[74] A. M. Bloch, P. S. Krishnaprasad, J. E. Marsden and T. S. Ratiu, Dissipation induced instabilities, *Annales de L'Institut Henri Poincare – Analyse Non Lineaire* **11** (1994), 37–90.

[75] V. V. Bolotin, *Nonconservative Problems of the Theory of Elastic Stability*, Pergamon Press, Oxford, London, New York, Paris, 1963.

[76] V. V. Bolotin, A. A. Grishko and M. Y. Panov, Effect of damping on the postcritical behaviour of autonomous non-conservative systems, *International Journal of Non-Linear Mechanics* **37** (2002), 1163 –1179.

[77] V. V. Bolotin and N. I. Zhinzher, Effects of damping on stability of elastic systems subjected to nonconservative forces, *International Journal of Solids and Structures* **5** (1969), 965–989.

[78] M. Born and E. Wolf, *Principles of Optics*, 6th edn., Pergamon, London, 1989.

[79] O. Bottema, On the small vibrations of non-holonomic systems, *Indagationes Mathematicae* **11** (1949), 296–298.

[80] O. Bottema, On the stability of the equilibrium of a linear mechanical system, *ZAMP Z. angew. Math. Phys.* **6** (1955), 97–104.

[81] O. Bottema, The Routh-Hurwitz condition for the biquadratic equation, *Indagationes Mathematicae* **18** (1956), 403–406.

[82] O. Bottema, Stability of equilibrium of a heavy particle on a rotating surface, *ZAMP Z. angew. Math. Phys.* **27** (1976), 663–669.

[83] N. M. Bou-Rabee, J. E. Marsden and L. A. Romero, A geometric treatment of Jellet's egg, *ZAMM Z. angew. Math. Mech.* **85** (2005), 618–642.

[84] N. M. Bou-Rabee, J. E. Marsden and L. A. Romero, Dissipation-induced heteroclinic orbits in tippe tops, *SIAM Rev.* **50** (2008), 325–344.

[85] N. M. Bou-Rabee, L. A. Romero and A. G. Salinger, A multiparameter, numerical stability analysis of a standing cantilever conveying fluid, *SIAM J. Appl. Dyn. Syst.* **1** (2002), 190–214.

[86] R. N. Bracewell and O. K. Garriott, Rotation of artificial Earth satellites, *Nature* **182** (1958), 760–762.

[87] J. V. Breakwell, Stability of an orbiting ring, *J. Guid. and Contr.* **4** (1981), 197–200.

[88] L. Brevdo and T. J. Bridges, Absolute and convective instabilities of spatially periodic flows, *Phil. Trans. R. Soc. Lond. Ser. A Math. Phys. Eng. Sci.* **354** (1996), 1027–1064.

[89] T. J. Bridges, A geometric formulation of the conservation of wave action and its implications for signature and the classification of instabilities, *Proc. R. Soc. Lond. Ser. A Math. Phys. Eng. Sci.* **453** (1997), 1365–1395.

[90] T. J. Bridges and F. Dias, Enhancement of the Benjamin-Feir instability with dissipation, *Physics of Fluids* **19** (2007), 104104.

[91] R. W. Brockett, *Finite Dimensional Linear Systems*, Wiley, New York, 1970.

[92] E. Brommundt, High-frequency self-excitation in paper calenders, *Technische Mechanik* **29** (2009), 60–85.

[93] L. E. J. Brouwer, Beweging van een materieel punt op den bodem eener draaiende vaas onder den invloed der zwaartekracht, *N. Arch. v. Wisk.* **2** (1918), 407–419.

[94] L. E. J. Brouwer, The motion of a particle on the bottom of a rotating vessel under the influence of the gravitational force, in: H. Freudenthal (ed.), *Collected Works*, II, pp. 665–686, North-Holland, Amsterdam, 1975.

[95] J. W. Bruce and P. G. Giblin, *Curves and Singularities*, Cambridge University Press, Cambridge, UK, 1984.

[96] G. Bryan, On the beats in the vibrations of a revolving cylinder or bell, *Proc. Cambridge Philos. Soc.* **7** (1890), 101–111.

[97] A. D. Bryuno, The normal form of a Hamiltonian system, *Russian Mathematical Surveys* **43** (1988), 25–66.

[98] R. M. Bulatovic, A stability theorem for gyroscopic systems, *Acta Mechanica* **136** (1999), 119–124.

[99] R. M. Bulatovic, On the heavily damped response in viscously damped dynamic systems, *Trans. ASME J. Appl. Mech.* **71** (2004), 131–134.

[100] R. M. Bulatovic, A sufficient condition for instability of equilibrium of nonconservative undamped systems, *Phys. Lett. A* **375** (2011), 3826–3828.

[101] J. V. Burke, A. S. Lewis and M. L. Overton, Optimal stability and eigenvalue multiplicity, *Foundations of Computational Mathematics* **1** (2001), 205–225.

[102] J. V. Burke, A. S. Lewis and M. L. Overton, Optimizing matrix stability, *Proc. Amer. Math. Soc.* **129** (2001), 1635–1642.

[103] J. V. Burke, A. S. Lewis and M. L. Overton, Optimization and pseudospectra, with applications to robust stability, *SIAM J. Matrix Anal. Appl.* **25** (2003), 80–104.

[104] R. Burridge and J. Qian, The fundamental solution of the time-dependent system of crystal optics, *Euro. Jnl of Applied Mathematics* **17** (2006), 63–94.

[105] F. H. Busse, Convective flows in rapidly rotating spheres and their dynamo action, *Physics of Fluids* **14** (2002), 1301–1314.

[106] F. H. Busse and A. C. Or, Convection in a rotating cylindrical annulus – thermal Rossby waves, *J. Fluid Mech.* **166** (1986), 173–187.

[107] T. Butlin and J. Woodhouse, Friction-induced vibration: Should low-order models be believed?, *J. Sound Vibr.* **328** (2009), 92–108.

[108] R. A. Cairns, Role of negative energy waves in some instabilities of parallel flows, *J. Fluid Mech.* **92** (1979), 1–14.

[109] W. Campbell, The protection of steam-turbine disk wheels from axial vibration, *Trans. ASME* **46** (1924), 31–160.

[110] S. V. Canchi and R. G. Parker, Parametric instability of a circular ring subjected to moving springs, *J. Sound Vibr.* **293** (2006), 360–379.

[111] P. W. Carpenter, Current status of the use of wall compliance for laminar-flow control, *Experimental Thermal and Fluid Science* **16** (1998), 133–140.

[112] P. W. Carpenter, C. Davies and A. D. Lucey, Hydrodynamics and compliant walls: Does the dolphin have a secret? *Current Science* **79** (2000), 758–765.

[113] J. Carr and M. Z. M. Malhardeen, Beck's problem, *SIAM J. Appl. Math.* **37** (1979), 261–262.

[114] H. Casimir, On Onsager's principle of microscopic reversibility, *Reviews of Modern Physics* **17** (1945), 343–350.

[115] A. R. R. Casti, P. J. Morrison and E. A. Spiegel, Negative energy modes and gravitational instability of interpenetrating fluids, in: J. R. Buchler, S. T. Gottesman, and H. E. Kandrup (eds.), *Nonlinear Dynamics and Chaos in Astrophysics: Festschrift in Honor of George Contopoulos*), Annals of the New York Academy of Sciences 867, pp. 93–108, New York Academy of Science, New York, 1998.

[116] N. Challamel, C. Casandjian and J. Lerbet, On the occurrence of flutter in the lateral-torsional instabilities of circular arches under follower loads, *J. Sound Vibr.* **320** (2009), 617–631.

[117] N. Challamel, F. Nicot, J. Lerbet and F. Darve, Stability of non-conservative elastic structures under additional kinematics constraints, *Engineering Structures* **32** (2010), 3086–3092.

[118] S. Chan, J. Mottershead and M. Cartmell, Parametric resonances at subcritical speeds in discs with rotating frictional loads, *Proc. Inst. Mech. Eng. C* **208** (1994), 417–425.

[119] S. Chandrasekhar, The stability of viscous flow between rotating cylinders in the presence of a magnetic field, *Proc. R. Soc. Lond. A* **216** (1953), 293–309.

[120] S. Chandrasekhar, The stability of non-dissipative Couette flow in hydromagnetics, *Proc. Natl. Acad. Sci. USA* **46** (1960), 253–257.

[121] S. Chandrasekhar, *Hydrodynamic and Hydromagnetic Stability*, International Series of Monographs on Physics, Oxford University Press, Oxford, 1961.

[122] G. Chen, S. A. Fulling, F. J. Narkowich and S. Sun, Exponential decay of energy of evolution equations with locally distributed damping, *SIAM J. Appl. Math.* **51** (1991), 266–301.

[123] J.-S. Chen and D. B. Bogy, Mathematical structure of modal interactions in a spinning disk-stationary load system, *J. Appl. Mech.* **59** (1992), 390–397.

[124] J. Chen, P. Fu, S.-I. Niculescu and Z. Guan, An eigenvalue perturbation approach to stability analysis, part I: Eigenvalue series of matrix operators, *SIAM J. Control Optim.* **48** (2010), 5564–5582.

[125] S.-J. Chern, Stability theory for linear dissipative Hamiltonian systems, *Linear Algebra and its Applications* **357** (2002), 143–162.

[126] F. L. Chernous'ko, Motion of a solid containing a spherical damper, *Zhurnal prikladnoi Mekhaniki i Teckhnicheskoi Fiziki* **9** (1968), 73–79.

[127] N. G. Chetaev, *The Stability of Motion*, Pergamon Press, New York, 1961.

[128] D. M. Christodoulou, J. Contopoulos and D. Kazanas, Interchange method in incompressible magnetized Couette flow: Structural and magnetorotational instabilities, *The Astrophysical Journal* **462** (1996), 865–873.

[129] M. Chugunova and D. Pelinovsky, Count of eigenvalues in the generalized eigenvalue problem, *J. Math. Phys.* **51** (2010), 052901.

[130] L. Chumakova and E. G. Tabak, Simple waves do not avoid eigenvalue crossings, *Comm. Pure Appl. Math.* **63** (2010), 119–132.

[131] F. S. Chute, F. E. Vermeulen and E. A. Youssef, A twisted electrostatic quadrupole for guiding heavy charged particles, *Nuclear Instruments and Methods* **82** (1970), 86–92.

[132] W. Clohessy and R. Wiltshire, Terminal guidance system for satellite rendezvous, *J. of the Aerospace Sciences* **27** (1960), 653–658, 674.

[133] R. Cordeiro and R. Viera Martins, Effect of Krein signatures on the stability of relative equilibria, *Celestial Mechanics and Dynamical Astronomy* **61** (1995), 217–238.

[134] E. Cotton and M. M. Yuan, Sur les criteres de stabilite de Routh et de Hurwitz, *Bull. Sci. Math.* **72** (1948), 115–128.

[135] M. Couette, Sur un nouvel appareil pour l'etude du frottement des fluids, *Comptes Rend.* **107** (1888), 388–390.

[136] M. Couette, Etudes sur le frottement des liquides, *Ann. Chim. Phys.* **6** (1890), 433–510.

[137] S. H. Crandall, The role of damping in vibration theory, *J. Sound Vibr.* **11** (1970), 3–18, IN1.

[138] S. H. Crandall, Rotordynamics, in: *Nonlinear Dynamics and Stochastic Mechanics*, pp. 1–44, CRC Press, Boca Raton, 1995.

[139] S. H. Crandall, The effect of damping on the stability of gyroscopic pendulums, *ZAMP Z. angew. Math. Phys.* **46** (1995), S761–S780.

[140] B. Cushman-Roisin, Motion of a free particle on a beta-plane, *Geophys. Astrophys. Fluid. Dynamics* **22** (1982), 85–102.

[141] J. L. Daleckii and M. G. Krein, *Stability of Solutions of Differential Equations in Banach Space*, Translations of Mathematical Monographs 43, American Mathematical Sociaety, Providence, RI, 1974.

[142] B. N. Datta, Stability and inertia, *Linear Algebra and its Applications* **302-303** (1999), 563–600.

[143] S. Datta, C. T. Chan, K. M. Ho and C. M. Soukoulis, Effective dielectric constant of periodic composite structures, *Phys. Rev. B* **48** (1993), 14936–14943.

[144] A. David and S. C. Sinha, Versal deformation and local bifurcation analysis of time-periodic nonlinear systems, *Nonlinear Dynamics* **21** (2000), 317–336.

[145] S. H. Davis, On the principle of exchange of stabilities, *Proc. R. Soc. Lond. Ser. A, Math. Phys. Sci.* **310** (1969), 341–358.

[146] M. Dellnitz, I. Melbourne and J. E. Marsden, Generic bifurcation of Hamiltonian vector-fields with symmetry, *Nonlinearity* **5** (1992), 979–996.

[147] M. Dellnitz and I. Melbourne, Generic movement of eigenvalues for equivariant self-adjoint matrices, *Journal of Computational and Applied Mathematics* **55** (1994), 249–259.

[148] G. Demange and E.-M. Graefe, Signatures of three coalescing eigenfunctions, *Journal of Physics A: Mathematical and Theoretical* **45** (2012), 025303.

[149] C. Dembowski, H.-D. Gräf, H. L. Harney, A. Heine, W. D. Heiss, H. Rehfeld and A. Richter, Experimental observation of the topological structure of exceptional points, *Phys. Rev. Lett.* **86** (2001), 787–790.

[150] B. P. Demidovich, *Lectures on the Mathematical Theory of Stability*, Nauka, Moscow, 1967 (in Russian).

[151] G. G. Denisov, V. V. Novikov and A. E. Fedorov, To the problem of a passive levitation of bodies in physical fields, *Trans. ASME J. Appl. Mech.* **77** (2010), 031017.

[152] G. Derks and T. Ratiu, Unstable manifolds of relative equilibria in Hamiltonian systems with dissipation, *Nonlinearity* **15** (2002), 531.

[153] L. Dieci and A. Pugliese, Hermitian matrices depending on three parameters: Coalescing eigenvalues, *Linear Algebra and its Applications* **436** (2012), 4120–4142.

[154] B. Dietz, H. L. Harney, O. N. Kirillov, M. Miski-Oglu, A. Richter and F. Schaefer, Exceptional points in a microwave billiard with time-reversal invariance violation, *Phys. Rev. Lett.* **106** (2011), 150403.

[155] R. C. DiPrima and P. Hall, Complex eigenvalues for the stability of Couette flow, *Proc. R. Soc. Lond. Ser. A, Math. Phys. Sci.* **396** (1984), 75–94.

[156] S. Dobrokhotov and A. Shafarevich, Parametrix and the asymptotics of localized solutions of the Navier–Stokes equations in R^3, linearized on a smooth flow, *Math. Notes* **51** (1992), 47–54.

[157] I. Dobson, J. Zhang, S. Greene, H. Engdahl and P. W. Sauer, Is strong modal resonance a precursor to power system oscillations? *IEEE Trans. Circ. Syst. I* **48** (2001), 340–349.

[158] J. M. Domingos, Time reversal in classical and quantum mechanics, *International Journal of Theoretical Physics* **18** (1979), 213–230.

[159] G. T. S. Done, Damping configurations that have a stabilizing influence on nonconservative systems, *International Journal of Solids and Structures* **9** (1973), 203–215.

[160] R. J. Donnelly, Taylor-Couette flow: The early days, *Phys. Today.* **44** (1991), 32–39.

[161] E. H. Dowell, Can solar sails flutter?, *AIAA Journal* **49** (2011), 1305–1307.

[162] P. G. Drazin and W. H. Reid, *Hydrodynamic Stability*, Cambridge Monographs on Mechanics and Applied Mathematics, Cambridge University Press, Cambridge, UK, 1981.

[163] G. Y. Dzhanelidze, On the stability of rods due to the action of follower forces, *Trudy Leningradskogo Politekhnicheskogo Instytuta* **192** (1958), 21–27.

[164] B. Eckhardt and D. Yao, Local stability analysis along Lagrangian paths, *Chaos Solitons & Fractals* **5** (1995), 2073–2088.

[165] W. S. Edwards, S. R. Beane and S. Varma, Onset of wavy vortices in the finite-length Couette–Taylor problem, *Physics of Fluids A-Fluid Dynamics* **3** (1991), 1510–1518.

[166] H. Eleuch and I. Rotter, Avoided level crossings in open quantum systems, *Fortschritte der Physik* **61(2-3)** (2013), 194–204.

[167] I. Elishakoff, Controversy associated with the so-called "follower force": critical overview, *Appl. Mech. Revs.* **58** (2005), 117–142.

[168] A. L. Fabrikant and Y. A. Stepaniants, *Propagation of Waves in Shear Flows*, World Scientific Series on Nonlinear Science, Series A 18, World Scientific, Singapore, 1998.

[169] J. D. Fieldhouse, W. P. Steel, C. J. Talbot and M. A. Siddiqui, Rotor asymmetry used to reduce disc brake noise, in: *Brake Colloquium and Exhibition, Oct. 2004, Anaheim, CA, USA*, SAE Paper 2004-01-2797, SAE, Warrendale, 2004.

[170] A. Figotin and I. Vitebsky, Spectra of periodic nonreciprocal electric circuits, *SIAM J. Appl. Math.* **61** (2001), 2008–2035.

[171] F. Fish and G. Lauder, Passive and active flow control by swimming fishes and mammals, *Ann. Rev. Fluid Mech.* **38** (2006), 193–224.

[172] A. Föppl, Das Problem der Lavalschen Turbinenwelle, *Der Civilingenieur* **41** (1895), 333–342.

[173] E. Frank, On the zeros of polynomials with complex coefficients, *Bull. Amer. Math. Soc.* **52** (1946), 144–157.

[174] P. Freitas, Quadratic matrix polynomials with Hamiltonian spectrum and oscillatory damped systems, *ZAMP Z. angew. Math. Phys.* **50** (1999), 64–81.

[175] P. Freitas, M. Grinfeld and P. A. Knight, Stability of finite-dimensional systems with indefinite damping, *Adv. Math. Sci. Appl.* **17** (1997), 435–446.

[176] P. Freitas and P. Lancaster, On the optimal value of the spectral abscissa for a system of linear oscillators, *SIAM J. Matrix Anal. Appl.* **21** (1999), 195–208.

[177] P. Freitas and E. Zuazua, Stability results for the wave equation with indefinite damping, *Journal of Differential Equations* **132** (1996), 338–353.

[178] S. Friedlander and M. M. Vishik, On stability and instability criteria for magnetohydrodynamics, *Chaos* **5** (1995), 416–423.

[179] S. J. Friedlander and A. Lipton-Lifschitz, Localized instabilities in fluids in: *Handbook of Mathematical Fluid Dynamics*, vol. 2, pp. 289–353, Elsevier, Amsterdam, 2003.

[180] Y. Fukumoto and Y. Hattori, Curvature instability of a vortex ring, *J. Fluid Mech.* **526** (2005), 77–115.

[181] T. Gabrielson, Frequency constants for transverse vibration of annular disks, *J. Acoust. Soc. Am.* **105** (1999), 3311–3317.

[182] A. Gajewski and M. Zyczkowski, *Optimal Structural Design under Stability Constraints*, Kluwer, Dordrecht, 1988.

[183] G. P. Galdi and B. Straughan, Exchange of stabilities, symmetry, and nonlinear stability, *Archive for Rational Mechanics and Analysis* **89** (1985), 211–228.

[184] G. Galilei, *Dialogues Concerning Two New Sciences*, William Andrew Publishing, Norwich, NY, 2001.

[185] D. M. Galin, Real matrices depending on parameters, *Uspekhi Mat. Nauk* **27** (1972), 241–242.

[186] D. M. Galin, Versal deformations of linear Hamiltonian systems, *AMS Transl.* **118** (1982), 1–12.

[187] P. Gallina, About the stability of non-conservative undamped systems, *J. Sound Vibr.* **262** (2003), 977–988.

[188] D. Galloway, ABC flows then and now, *Geophysical & Astrophysical Fluid Dynamics* **106** (2012), 450–467.

[189] L. Garding, History of the mathematics of double refraction, *Archive for History of Exact Sciences* **40** (1989), 355–385.

[190] J. C. Garrison and E. M. Wright, Complex geometrical phases for dissipative systems, *Phys. Lett. A* **128** (1988), 177–181.

[191] A. M. Gasparini, A. V. Saetta and R. V. Vitaliani, On the stability and instability regions of non-conservative continuous system under partially follower forces, *Computer Methods in Applied Mechanics and Engineering* **124** (1995), 63–78.

[192] T. Gebhardt and S. Grossmann, The Taylor–Couette eigenvalue problem with independently rotating cylinders, *Zeitschrift für Physik B Condensed Matter* **90** (1993), 475–490.

[193] I. M. Gelfand and V. B. Lidskii, On the structure of the regions of stability of linear canonical differential equations with periodic coefficients, *Uspekhi Matem. Nauk* **10** (1955), 3–40.

[194] G. Genta, *Dynamics of Rotating Systems*, Mechanical Engineering Series, Springer, New York, 2007.

[195] A. Giesecke, F. Stefani and G. Gerbeth, Spectral properties of oscillatory and non-oscillatory α^2-dynamos, *Geophysical & Astrophysical Fluid Dynamics* **107(1-2)** (2012), 45–57.

[196] G. Gladwell, Follower forces – Leipholz early researches in elastic stability, *Canadian Journal of Civil Engineering* **17** (1990), 277–286.

[197] G. A. Glatzmaier, Geodynamo simulations – How realistic are they? *Ann. Rev. Earth Planet. Sci.* **30** (2002), 237–257.

[198] G. A. Glatzmaier and P. H. Roberts, A three dimensional self-consistent computer simulation of a geomagnetic field reversal, *Nature* **377** (1995), 203–209.

[199] H. Goedbloed, R. Keppens and S. Poedts, *Advanced Magnetohydrodynamics*, Cambridge University Press, Cambridge, UK, 2010.

[200] I. Gohberg, P. Lancaster and L. Rodman, *Matrix Polynomials*, Academic Press, San Diego, CA, 1982.

[201] I. Gohberg, P. Lancaster and L. Rodman, Perturbation of analytic Hermitian matrix functions, *Appl. Anal.* **20** (1985), 23–48.

[202] I. Gohberg, P. Lancaster and L. Rodman, *Indefinite Linear Algebra with Applications*, Birkhauser, Basel, 2005.

[203] I. C. Gohberg and M. G. Krein, *Introduction to the Theory of Linear Nonselfadjoint Operators*, Translations of Mathematical Monographs, AMS, Providence, RI, 1969.

[204] J. Goodman and H. Ji, Magnetorotational instability of dissipative Couette flow, *J. Fluid Mech.* **462** (2002), 365–382.

[205] A. G. Greenhill, On the general motion of a liquid ellipsoid under the graviatation of its own parts, *Proc. Cambridge Philos. Soc.* **4** (1880), 4–14.

[206] A. G. Greenhill, On the strength of shafting when exposed both to torsion and to end thrust, *Proc. Inst. Mech. Eng.* **34** (1883), 182–225.

[207] U. Günther and F. Stefani, Isospectrality of spherical MHD dynamo operators: Pseudohermiticity and a non-go theorem, *J. Math. Phys.* **44** (2003), 3097–3111.

[208] U. Günther and O. N. Kirillov, A Krein space related perturbation theory for MHD α^2-dynamos and resonant unfolding of diabolical points, *Journal of Physics A: Mathematical and General* **39** (2006), 10057–10076.

[209] U. Günther and O. N. Kirillov, Asymptotic methods for spherically symmetric MHD α^2-dynamos, *PAMM* **7** (2007), 4140023–4140024.

[210] U. Günther and O. N. Kirillov, Homotopic Arnold tongues deformation of the MHD α^2-dynamo, *PAMM* **8** (2008), 10719–10720.

[211] U. Günther, F. Stefani and M. Znojil, MHD α^2-dynamo, Squire equation and PT-symmetric interpolation between square well and harmonic oscillator, *J. Math. Phys.* **46** (2005), 063504.

[212] F. Haake, *Quantum Signatures of Chaos*, 3rd edn., Springer Series in Synergetics 54, Springer, Berlin, 2010.

[213] W. Hahn, *Stability of Motion*, Die Grundlehren der mathematischen Wissenschaften, Band 138, Springer, Berlin, 1967.

[214] J. H. Hannay, Angle variable holonomy in adiabatic excursion of an integrable Hamiltonian, *J. Phys. A: Math. Gen.* **18** (1985) 221–230.

[215] Y. Hattori and Y. Fukumoto, Short-wavelength stability analysis of thin vortex rings, *Phys. Fluids* **15** (2003), 3151–3163.

[216] M. Heil and A. L. Hazel, Fluid-structure interaction in internal physiological flows, *Ann. Rev. Fluid Mech.* **43** (2011), 141–162.

[217] J. Heilig and J. Wauer, Stability of a nonlinear brake system at high operating speeds, *Nonlinear Dynamics* **34** (2003), 235–247.

[218] W. D. Heiss, The physics of exceptional points, *Journal of Physics A: Mathematical and Theoretical* **45** (2012), 444016.

[219] D. Henrion and J.-B. Laseerre, Inner approximations for polynomial matrix inequalities and robust stability regions, *IEEE Transactions on Automatic Control* **57** (2012), 1456–1467.

[220] D. Henrion, D. Peaucelle, D. Arzelier and M. Sebek, Ellipsoidal approximation of the stability domain of a polynomial, *IEEE Transactions on Automatic Control* **48** (2003), 2255–2259.

[221] C. Hermite, On the number of roots of an algebraic equation contained between given limits (English translation by P. C. Parks), *Int. J. Control* **26** (1977), 183–195.

[222] G. Herrmann and I. C. Jong, On the destabilizing effect of damping in nonconservative elastic systems, *Trans. ASME J. Appl. Mech.* **32** (1965), 592–597.

[223] I. H. Herron and H. N. Ali, The principle of exchange of stabilities for Couette flow, *Quarterly of Applied Mathematics* **61** (2003) 279–293.

[224] K. Higuchi and E. H. Dowell, Effect of structural damping on flutter of plates with a follower force, *AIAA Journal* **30** (1992), 820–825.

[225] G. W. Hill, Researches in the lunar theory, *Am. J. Math.* **1** (1878), 5–26.

[226] N. Hoffmann and L. Gaul, Effects of damping on mode-coupling instability in friction induced oscillations, *ZAMM Z. angew. Math. Mech.* **83** (2003), 524–534.

[227] R. Hollerbach and G. Rüdiger, New type of magnetorotational instability in cylindrical Taylor–Couette flow, *Phys. Rev. Lett.* **95** (2005), 124501.

[228] E. O. Holopainen, On the effect of friction in baroclinic waves, *Tellus* **13** (1961), 363–367.

[229] W. Hoover, Time reversibility in nonequilibrium thermomechanics, *Physica D* **112** (1998), 225–240.

[230] I. Hoveijn, Versal deformations and normal forms for reversible and Hamiltonian linear systems, *Journal of Differential Equations* **126** (1996), 408–442.

[231] I. Hoveijn and O. N. Kirillov, Singularities on the boundary of the stability domain near 1:1-resonance, *Journal of Differential Equations* **248** (2010), 2585–2607.

[232] I. Hoveijn and M. Ruijgrok, The stability of parametrically forced coupled oscillators in sum resonance, *ZAMP Z. angew. Math. Phys.* **46** (1995), 384–392.

[233] R. Hryniv and P. Lancaster, On the perturbation of analytic matrix functions, *Int. Equ. Oper. Theor.* **34** (1999), 325–338.

[234] R. Hryniv and P. Lancaster, Stabilization of gyroscopic systems, *ZAMM Z. angew. Math. Mech.* **81** (2001), 675–681.

[235] P. Huerre and P. A. Monkewitz, Local and global instabilities in spatially developing flows, *Ann. Rev. Fluid Mech.* **22** (1990), 473–537.

[236] A. Hurwitz, Über die Bedingungen unter welchen eine Gleichung nur Würzeln mit negativen reellen Teilen besitzt, *Math. Ann.* **46** (1895), 273–284.

[237] K. Huseyin, P. Hagedorn and W. Teschner, On the stability of linear conservative gyroscopic systems, *ZAMP Z. angew. Math. Phys.* **34** (1983), 807–815.

[238] K. Huseyin, Standard forms of the eigenvalue problems associated with gyroscopic systems, *J. Sound Vibr.* **45** (1976), 29–37.

[239] K. Huseyin, *Vibrations and Stability of Multiple Parameter Systems*, Kluwer Academic Publishers, The Netherlands, 1978.

[240] R. A. Ibrahim, Overview of mechanics of pipes conveying fluids. Part I: Fundamental Studies, *Trans. ASME Journal of Pressure Vessel Technology* **132** (2010) 034001.

[241] D. J. Inman, A sufficient condition for the stability of conservative gyroscopic systems, *Trans. ASME J. Appl. Mech.* **55** (1988), 895–898.

[242] W. D. Iwan and K. J. Stahl, The response of an elastic disc with a moving mass system, *Trans. ASME J. Appl. Mech.* **40** (1973), 445–451.

[243] E. Jarlebring, S. Kvaal and W. Michiels, Computing all pairs (λ, μ) such that λ is a double eigenvalue of $A + \mu B$, *SIAM J. Matrix Anal. Appl.* **32** (2011), 902–927.

[244] H. H. Jeffcott, The lateral vibration of the loaded shaft in the neighbourhood of a whirling speed, *Phil. Mag. Ser.* **6(37)** (1919), 304–314.

[245] J. Jeronen, *On the mechanical stability and out-of-plane dynamics of a travelling panel submerged in axially flowing ideal fluid: a study into paper production in mathematical terms*, University of Juvaskyla, Finland, 2011.

[246] C. A. Jones, Multiple eigenvalues and mode classification in plane Poiseuille flow, *Quart. J. Mech. Appl. Math.* **41** (1988), 363–382.

[247] C. A. Jones, Dynamo theory, in: *Lecture Notes, Les Houches "Dynamos" Summer School, July 30–August 24, 2007*, pp. 44–136, Elsevier, Amsterdam, 2008.

[248] S. V. Joubert, M. Y. Shatalov and T. H. Fay, Rotating structures and Bryan's effect, *American Journal of Physics* **77** (2009), 520–525.

[249] C. M. Jung and B. F. Feeny, On the discretization of an elastic rod with distributed sliding friction, *J. Sound Vibr.* **252** (2002), 409–428.

[250] W. Kahan, Spectra of nearly Hermitian matrices, *Proc. Amer. Math. Soc.* **48** (1975), 11–17.

[251] R. Kalaba, K. Spingarn and L. Tesfatsion, Individual tracking of an eigenvalue and eigenvector of a parameterized matrix, *Nonlinear Analysis, Theory, Methods and Applications* **5** (1981), 337–340.

[252] R. Kalaba, K. Spingarn and L. Tesfatsion, Variational equations for the eigenvalues and eigenvectors of nonsymmetric matrices, *Journal of Optimization Theory and Applications* **33** (1981), 1–8.

[253] R. E. Kalman and J. E. Bertram, Control system analysis and design via the second method of Lyapunov, *ASME Trans. D* **82** (1960), 371–400.

[254] J. Kang, C. Krousgrill and F. Sadeghi, Dynamic instability of a thin circular plate with friction interface and its application to disc brake squeal, *J. Sound Vibr.* **316** (2008), 164–179.

[255] J. Kang, Theoretical model of ball joint squeak, *J. Sound Vibr.* **330** (2011), 5490–5499.

[256] P. L. Kapitsa, Stability and passage through the critical speed of the fast spinning rotors in the presence of damping, *Z. Tech. Phys.* **9** (1939), 124–147.

[257] A. V. Karapetjan, The stability of nonconservative systems, *Vestn. Mosk. Univ., Ser. 1: Mat. Mekh.* **30** (1975), 109–113.

[258] T. Kato, *Perturbation Theory for Linear Operators*, 2nd edn., Grundlehren der mathematischen Wissenschaften 132, Springer, Berlin–Heidelberg–New York, 1980.

[259] J. T. Katsikadelis and G. C. Tsiatas, Optimum design of structures subjected to follower forces, *International Journal of Mechanical Sciences* **49** (2007), 1204–1212.

[260] F. Keck, H.-J. Korsch and S. Mossmann, Unfolding a diabolic point: a generalized crossing scenario, *Journal of Physics A: Mathematical and General* **36** (2003), 2125–2137.

[261] M. V. Keldysh, On eigenvalues and eigenfunctions of some classes of nonselfadjoint equations, *Dokl. AN SSSR* **77** (1951), 11–14.

[262] W. Kerr, On the whirling speeds of loaded shafts, *Engineering* (1916), 150.

[263] P. Kessler, O. M. O'Reilly, A.-L. Raphael and M. Zworski, On dissipation-induced destabilization and brake squeal: A perspective using structured pseudospectra, *J. Sound Vibr.* **308** (2007), 1–11.

[264] I. V. Khalzov, A. I. Smolyakov and V. I. Ilgisonis, Energy of eigenmodes in magnetohydrodynamic flows of ideal fluids, *Physics of Plasmas* **15** (2008), 054501.

[265] V. L. Kharitonov, Asymptotic stability of an equilibrium position of a family of systems of differential equations, *Differentsialnye Uravnenija* **14** (1978), 2086–2088.

[266] A. L. Kimball, Internal friction as a cause of shaft whirling, *Phil. Mag.* **49** (1925), 724–727.

[267] A. L. Kimball and D. E. Lovell, Internal friction in solids, *Phys. Rev.* **30** (1927), 948–959.

[268] N. M. Kinkaid, O. M. O'Reilly and P. Papadopoulos, Automotive disc brake squeal, *J. Sound Vibr.* **267** (2003), 105–166.

[269] O. N. Kirillov, A. A. Mailybaev and A. P. Seyranian, Singularities of energy surfaces under non-Hermitian perturbations, *Doklady Physics* **50** (2005), 577–582.

[270] O. N. Kirillov, A. A. Mailybaev and A. P. Seyranian, Unfolding of eigenvalue surfaces near a diabolic point due to a complex perturbation, *Journal of Physics A: Mathematical and General* **38** (2005), 5531–5546.

[271] O. N. Kirillov and A. P. Seyranian, Optimization of Stability of a Flexible Missile under Follower Thrust, in: *7th AIAA/USAF/NASA/ISSMO Symposium on Multidisciplinary Analysis and Optimization. St.Louis. Missouri (USA). September 2-4. 1998.*, AIAA Paper 98-4969, pp. 2063–2073, AIAA, Reston, VA, 1998.

[272] O. N. Kirillov and A. P. Seyranian, Optimality conditions in nonconservative stability problems, in: G. I. N. Rozvany and N. Olhof (eds.), *Topology Optimization of Structures and Composite Continua*, NATO Science Series, Series II: Mathematics, Physics and Chemistry 7, pp. 363–365, Springer, Dordrecht, Netherlands, 2000.

[273] O. N. Kirillov and A. P. Seyranian, Collapse of Keldysh chains and the stability of nonconservative systems, *Doklady Mathematics* **66** (2002), 127–131.

[274] O. N. Kirillov and A. P. Seyranian, Metamorphoses of characteristic curves in circulatory systems, *J. Appl. Math. Mech.* **66** (2002), 371–385.

[275] O. N. Kirillov and A. P. Seyranian, A nonsmooth optimization problem, *Moscow University Mechanics Bulletin* **57** (2002), 1–6.

[276] O. N. Kirillov and A. P. Seyranian, Solution to the Herrmann–Smith problem, *Doklady Physics* **47** (2002), 767–771.

[277] O. N. Kirillov and A. P. Seyranian, Collapse of the Keldysh chains and stability of continuous nonconservative systems, *SIAM J. Appl. Math.* **64** (2004), 1383–1407.

[278] O. N. Kirillov and A. P. Seyranian, Dissipation induced instabilities in continuous nonconservative systems, *Proc. Appl. Math. Mech.* **5(1)** (2005), 97–98.

[279] O. N. Kirillov and A. P. Seyranian, Effect of small internal and external damping on the stability of continuous non-conservative systems, in: *Proceedings CDROM of the ENOC-2005, Eindhoven, The Netherlands, 7-12 August 2005*, pp. 2428–2436, 2005.

[280] O. N. Kirillov and A. P. Seyranian, Instability of distributed nonconservative systems caused by weak dissipation, *Doklady Mathematics* **71** (2005), 470–475.

[281] O. N. Kirillov and A. P. Seyranian, Stabilization and destabilization of a circulatory system by small velocity-dependent forces, *J. Sound Vibr.* **283** (2005), 781–800.

[282] O. N. Kirillov and A. P. Seyranian, The effect of small internal and external damping on the stability of distributed non-conservative systems, *PMM J. Appl. Math. Mech.* **69** (2005), 529–552.

[283] O. N. Kirillov, Optimization of stability of the flying bar, *Young Scientists Bulletin. Appl. Maths Mechs.* **1** (1999), 64–78.

[284] O. N. Kirillov, *Analysis of Stability Boundaries and Optimization of Circulatory Systems*, Ph.D. thesis, M. V. Lomonosov State University, Moscow, 2000.

[285] O. N. Kirillov, *How do Small Velocity-dependent Forces (De)stabilize a Nonconservative System?* DCAMM Report. 681, Technical University of Denmark, Lyngby, Denmark, 2003.

[286] O. N. Kirillov, How do small velocity-dependent forces (de)stabilize a nonconservative system? in: *2003 International Conference Physics and Control, vols. 1–4, Proceedings*, pp. 1090–1095, IEEE, 2003.

[287] O. N. Kirillov, Destabilization paradox, *Doklady Physics* **49** (2004), 239–245.

[288] O. N. Kirillov, A theory of the destabilization paradox in non-conservative systems, *Acta Mechanica* **174** (2005), 145–166.

[289] O. N. Kirillov, Gyroscopic stabilization of non-conservative systems, *Phys. Lett. A* **359** (2006), 204–210.

[290] O. N. Kirillov, Destabilization paradox due to breaking the Hamiltonian and reversible symmetry, *International Journal of Non-Linear Mechanics* **42** (2007), 71–87.

[291] O. N. Kirillov, Gyroscopic stabilization in the presence of nonconservative forces, *Doklady Mathematics* **76** (2007), 780–785.

[292] O. N. Kirillov, On the stability of nonconservative systems with small dissipation, *J. Math. Sci.* **145** (2007), 5260–5270.

[293] O. N. Kirillov, Subcritical flutter in the acoustics of friction, *Proc. R. Soc. Lond. Ser. A Math. Phys. Eng. Sci.* **464** (2008), 2321–2339.

[294] O. N. Kirillov, Campbell diagrams of weakly anisotropic flexible rotors, *Proc. R. Soc. Lond. Ser. A Math. Phys. Eng. Sci.* **465** (2009), 2703–2723.

[295] O. N. Kirillov, Perspectives and obstacles for optimization of brake pads with respect to stability criteria, *Int. J. Vehicle Design* **51** (2009), 143–167.

[296] O. N. Kirillov, Sensitivity analysis of Hamiltonian and reversible systems prone to dissipation-induced instabilities, in: E. E. Tyrtyshnikov and V. Olshevsky, (eds.), *Matrix Methods: Theory, Algorithms, Applications. Proceedings of the 2nd International Conference on Matrix Methods and Operator Equations, July 23-27, 2007, Moscow, Russia*, pp. 31–68, World Scientific, Singapore, 2009.

[297] O. N. Kirillov, Unfolding the conical zones of the dissipation-induced subcritical flutter for the rotationally symmetrical gyroscopic systems, *Phys. Lett. A* **373** (2009), 940–945.

[298] O. N. Kirillov, Eigenvalue bifurcation in multiparameter families of non-self-adjoint operator matrices, *ZAMP Z. angew. Math. Phys.* **61** (2010), 221–234.

[299] O. N. Kirillov, Brouwer's problem on a heavy particle in a rotating vessel: Wave propagation, ion traps, and rotor dynamics, *Phys. Lett. A* **375** (2011), 1653–1660.

[300] O. N. Kirillov, Re-visiting structural optimization of the Ziegler pendulum: singularities and exact optimal solutions, *PAMM* **11** (2011), 717–718.

[301] O. N. Kirillov, Sensitivity of sub-critical mode-coupling instabilities in non-conservative rotating continua to stiffness and damping modifications, *Int. J. Vehicle Struct. Syst.* **3** (2011), 1–14.

[302] O. N. Kirillov, Singularities in structural optimization of the Ziegler pendulum, *Acta Polytechnica* **51** (2011), 32–43.

[303] O. N. Kirillov, $\mathcal{PT}$-symmetry, indefinite damping and dissipation-induced instabilities, *Phys. Lett. A* **376** (2012), 1244–1249.

[304] O. N. Kirillov, Exceptional and diabolical points in stability questions, *Fortschritte der Physik* **61** (2013), 205–224.

[305] O. N. Kirillov, Stabilizing and destabilizing perturbations of $\mathcal{PT}$-symmetric indefinitely damped systems, *Phil. Trans. R. Soc. A* **371** (2013), 20120051.

[306] O. N. Kirillov and U. Günther, On Krein space related perturbation theory for MHD α^2-dynamos, *PAMM* **6** (2006), 637–638.

[307] O. N. Kirillov, U. Günther and F. Stefani, Determining role of Krein signature for three-dimensional Arnold tongues of oscillatory dynamos, *Phys. Rev. E* **79** (2009), 016205.

[308] O. N. Kirillov, D. E. Pelinovsky and G. Schneider, Paradoxical transitions to instabilities in hydromagnetic Couette–Taylor flows, *Phys. Rev. E* **84** (2011), 065301(R).

[309] O. N. Kirillov and F. Stefani, On the relation of standard and helical magnetorotational instability, *Astrophysical Journal* **712** (2010), 52–68.

[310] O. N. Kirillov and F. Stefani, Paradoxes of magnetorotational instability and their geometrical resolution, *Phys. Rev. E* **84** (2011), 036304.

[311] O. N. Kirillov and F. Stefani, Standard and helical magnetorotational instability: How singularities create paradoxal phenomena in MHD, *Acta Applicanda Mathematicae* **120** (2012), 177–198.

[312] O. N. Kirillov and F. Verhulst, Paradoxes of dissipation-induced destabilization or who opened Whitney's umbrella? *ZAMM Z. angew. Math. Mech.* **90** (2010), 462–488.

[313] Y. S. Kivshar and M. Peyrard, Modulational instabilities in discrete lattices, *Phys. Rev. A* **46** (1992), 3198–3207.

[314] W. Kliem and C. Pommer, Indefinite damping in mechanical systems and gyroscopic stabilization, *ZAMP Z. angew. Math. Phys.* **60** (2009), 785–795.

[315] C. Klingshirn, *Semiconductor Optics*, 3rd edn., Springer, Berlin, 2007.

[316] E. Knobloch, On the stability of magnetized accretion discs, *Mon. Not. R. Astron. Soc.* **255** (1992), 25–28.

[317] V. Kobelev, Sensitivity analysis of the linear nonconservative systems with fractional damping, *Structural and Multidisciplinary Optimization* **33** (2007), 179–188.

[318] R. Kollar, Homotopy method for nonlinear eigenvalue pencils with applications, *SIAM J. Math. Anal.* **43** (2011), 612–633.

[319] R. Kollar and P. D. Miller, Graphical Krein signature theory and Evans–Krein functions, *SIAM Rev.*, arXiv:1209.3185 (2013), to appear.

[320] N. D. Kopachevskii and S. G. Krein, *Operator Approach in Linear Problems of Hydrodynamics. Self-adjoint Problems for an Ideal Fluid*, Operator Theory: Advances and Applications 1, Birkhäuser, Basel, 2001.

[321] Z. Kordas and M. Zyczkowsky, On the loss of stability of a rod under a super-tangential force, *Archiwum Mechaniki Stosowanej* **15** (1963), 7–31.

[322] V. N. Koshlyakov and V. L. Makarov, Mechanical systems, equivalent in Lyapunov's sense to systems not containing non-conservative positional forces, *J. Appl. Math. Mech.* **71** (2007), 10–19.

[323] A. Kounadis and J. Katsikadelis, On the discontinuity of the flutter load for various types of cantilevers, *International Journal of Solids and Structures* **16** (1980), 375–383.

[324] V. V. Kozlov, Linear systems with a quadratic integral, *J. Appl. Math. Mech.* **56** (1992), 803–809.

[325] V. V. Kozlov, Gyroscopic stabilization and parametric resonance, *PMM J. Appl. Math. Mech.* **65** (2001), 715–721.

[326] V. V. Kozlov, Restrictions of quadratic forms to Lagrangian planes, quadratic matrix equations, and gyroscopic stabilization, *Functional Analysis and its Applications* **39** (2005), 271–283.

[327] V. V. Kozlov, Kelvin's instability theorem: Topological meaning and generalizations, *Doklady Mathematics* **79** (2009), 25–28.

[328] V. V. Kozlov, On the mechanism of stability loss, *Differential Equations* **45** (2009), 510–519.

[329] Kimball, noted G. E. physicist, dies suddenly, *Schenectady Gazette* (March 22, 1943), 1,8.

[330] V. V. Kozlov and A. A. Karapetyan, On the stability degree, *Differential Equations* **41** (2005), 195–201.

[331] F. Krause and K.-H. Rädler, *Mean-field Magnetohydrodynamics and Dynamo Theory*, Pergamon Press, Oxford, 1980.

[332] R. Krechetnikov and J. E. Marsden, On destabilizing effects of two fundamental nonconservative forces, *Physica D: Nonlinear Phenomena* **214** (2006), 25–32.

[333] R. Krechetnikov and J. E. Marsden, Dissipation-induced instabilities in finite dimensions, *Rev. Mod. Phys.* **79** (2007), 519–553.

[334] R. Krechetnikov and J. E. Marsden, Dissipation-induced instability phenomena in infinite-dimensional systems, *Archive for Rational Mechanics and Analysis* **194** (2009), 611–668.

[335] M. A. Krein, M. G. Naimark, The method of symmetric and Hermitian forms in the theory of the separation of the roots of algebraic equations (Translated from Russian by O. Boshko and J. L. Howland), *Linear and Multilinear Algebra* **10** (1981), 265–308.

[336] M. G. Krein, A generalization of several investigations of A. M. Liapunov on linear differential equations with periodic coefficients, *Dokl. Acad. Nauk SSSR.* **73** (1950), 445–448.

[337] M. G. Krein, *Topics in Differential and Integral Equations and Operator Theory*, Operator Theory 7, Birkhauser, Basel, Switzerland, 1983.

[338] M. G. Krein and G. I. Liubarskii, On the theory of transmission bands of periodic waveguides, *PMM J. Appl. Math. Mech.* **25** (1961), 24–37.

[339] M. I. Krivoruchenko, Rotation of the swing plane of Foucault's pendulum and Thomas spin precession: Two sides of one coin, *Physics-Uspekhi* **52** (2009), 821–829.

[340] M. Kroeger, M. Neubauer and K. Popp, Experimental investigation on the avoidance of self-excited vibrations, *Philos. Trans. R. Soc. A, Math. Phys. Eng. Sci.* **366** (2008), 785–810.

[341] P. Kuchment, *Floquet Theory for Partial Differential Equations*, Operator Theory: Advances and Applications 60, Birkhauser, Basel, 1993.

[342] V. Lakhadanov, On stabilization of potential systems, *Prikl. Mat. Mekh.* **39** (1975), 53–58.

[343] H. Lamb, On kinetic stability, *Proc. R. Soc. Lond. A* **80** (1908), 168–177.

[344] J. S. W. Lamb and J. A. G. Roberts, Time-reversal symmetry in dynamical systems: A survey, *Physica D* **112** (1998), 1–39.

[345] P. Lancaster, Explicit solutions of linear matrix equations, *SIAM Rev.* **12** (1970), 544–566.

[346] P. Lancaster, *Lambda-Matrices and Vibrating Systems*, Dover Books on Mathematics, Dover, New York, 2002.

[347] P. Lancaster, A. Markus and F. Zhou, Perturbation theory for analytic matrix functions: the semisimple case, *SIAM J. Matrix Anal. Appl.* **25** (2003), 606–626.

[348] P. Lancaster and M. Tismenetsky, Inertia characteristics of self-adjoint matrix polynomials, *Linear Algebra and its Applications* **52-53** (1983), 479–496.

[349] M. Landahl, On the stability of a laminar incompressible boundary layer over a flexible surface, *J. Fluid Mech.* **13** (1962), 609–632.

[350] M. J. Landman and P. G. Saffman, The three-dimensional instability of strained vortices in a viscous fluid, *Phys. Fluids* **30** (1987), 2339–2342.

[351] A. S. Landsberg, Geometrical phases and symmetries in dissipative systems, *Phys. Rev. Lett.* **69** (1992), 865–868.

[352] H. Langer and B. Naiman, Remarks on the perturbation of analytic matrix functions, II, *Int. Equ. Oper. Theor.* **12** (1989), 392–407.

[353] H. Langer and C. Tretter, A Krein space approach to PT-symmetry, *Czech. J. Phys.* **54** (2004), 1113–1120.

[354] W. F. Langford, Hopf meets Hamilton under Whitney's umbrella, in: S. N. Namachchivaya, (ed.), *IUTAM Symposium on Nonlinear Stochastic Dynamics. Proceedings of the IUTAM Symposium, Monticello, IL, USA, Augsut 26-30, 2002*, Solid Mech. Appl. 110, pp. 157–165, Kluwer, Dordrecht, 2003.

[355] M. A. Langthjem, On the influence of damping in a problem of dynamic stability optimization, *Structural Optimization* **7** (1994), 227–236.

[356] M. A. Langthjem and Y. Sugiyama, Dynamic stability of columns subjected to follower loads: A survey, *J. Sound Vibr.* **238** (2000), 809–851.

[357] M. A. Langthjem and Y. Sugiyama, Optimum design of cantilevered columns under the combined action of conservative and nonconservative loads Part I: The undamped case, *Computers and Structures* **74** (2000), 385–398.

[358] C. N. Lashmore-Davies, Negative energy waves, *Journal of Plasma Physics* **71** (2005), 101–109.

[359] D. P. Lathrop and C. B. Forest, Magnetic dynamos in the lab, *Phys. Today* **64** (2011), 40–45.

[360] H. N. Latter, H. Rein and G. I. Ogilvie, The gravitational instability of a stream of co-orbital particles, *Mon. Not. R. Astron. Soc.* **423** (2012), 1267–1276.

[361] K. A. Lazopoulos and A. K. Lazopoulos, Stability of a gradient elastic beam compressed by non-conservative forces, *ZAMM Z. angew. Math. Mech.* **90** (2010), 174–184.

[362] S. Le Dizes and P. Billant, Radiative instability in stratified vortices, *Physics of Fluids* **21** (2009), 096602.

[363] N. R. Lebovitz and E. Zweibel, Magnetoelliptic instabilities, *The Astrophysical Journal* **609** (2004), 301–312.

[364] Y. S. Ledyaev and Q. J. Zhu, Nonsmooth analysis on smooth manifolds, *Trans. Amer. Math. Soc.* **359** (2007), 3687–3732.

[365] R. Lefebvre and O. Atabek, Exceptional points in multichannel resonance quantization, *The European Physical Journal D - Atomic, Molecular, Optical and Plasma Physics* **56** (2010), 317–324.

[366] V. Legostayev, A. Subbotin, S. Timakov and Y. Cheremnykh, Normal modes of oscillations of a rotating membrane with a rigid central insert (an application of Heun functions), *J. Appl. Math. Mech.* **75** (2011), 154–164.

[367] H. Leipholz and H. Ziegler, *Stability: Fourteen Special Lectures Presented at the University of Waterloo, 1970-71*, SM Studies Series, Solid Mechanics Division, University of Waterloo, 1972.

[368] H. Leipholz, On conservative elastic systems of the first and second kind, *Archive of Applied Mechanics* **43** (1974), 255–271.

[369] H. Leipholz, *Stability Theory: An Introduction to the Stability of Dynamic Systems and Rigid Bodies*, 2nd edn., B. G. Teubner/John Wiley and Sons, Stuttgart, Chichester (England) and New York, 1987.

[370] A. Leissa, On a curve veering aberration, *ZAMP Z. angew. Math. Phys.* **25** (1974), 99–111.

[371] G. A. Leonov, *Strange Attractors and Classical Stability Theory*, Ex Libris Universitatis Petropolitanae, St. Petersburg University Press, 2008.

[372] G. A. Leonov and N. V. Kuznetsov, Time-varying linearization and the Perron effects, *International Journal of Bifurcation and Chaos* **17** (2007), 1079–1107.

[373] J. Lerbet, O. Kirillov, M. Aldowaji, N. Challamel, F. Nicot and F. Darve, Additional constraints may soften a non-conservative structural system: Buckling and vibration analysis, *International Journal of Solids and Structures* **50** (2013), 363–370.

[374] L. V. Levantovskii, The boundary of a set of stable matrices, *Usp Mat. Nauk* **35** (1980), 212–214.

[375] L. V. Levantovskii, Singularities of the boundary of a region of stability, *Funktsional. Anal. i Prilozhen.* **16** (1982), 44–48, 96.

[376] M. Levi, *The Mathematical Mechanic: Using Physical Reasoning to Solve Problems*, Princeton University Press, Princeton, NJ, 2009.

[377] M. Lewin, On the coefficients of the characteristic polynomial of a matrix, *Discrete Mathematics* **125** (1994), 255–262.

[378] A. S. Lewis, The mathematics of eigenvalue optimization, *Mathematical Programming, Ser. B* **97** (2003), 155–176.

[379] V. Lidskii, Perturbation theory of non-conjugate operators, *U.S.S.R. Comput. Math. and Math. Phys.* **6** (1966), 73–85.

[380] M. Liertzer, L. Ge, A. Cerjan, A. D. Stone, H. E. Türeci and S. Rotter, Pump-induced exceptional points in lasers, *Phys. Rev. Lett.* **108** (2012), 173901.

[381] A. Lifschitz, Short wavelength instabilities of incompressible three-dimensional flows and generation of vorticity, *Phys. Lett. A* **157** (1991), 481–487.

[382] S. G. Lipson, Berry's phase in optical interferometry: a simple derivation, *Optics Letters* **15** (1990), 154–155.

[383] W. Liu, J. Goodman, I. Herron and H. Ji, Helical magnetorotational instability in magnetized Taylor–Couette flow, *Phys. Rev. E* **74** (2006), 056302.

[384] A. Loria and E. Panteley, *Stability, Told by its Developers*, Advanced Topics in Control Theory, pp. 199–258, Springer, LNCIS, London, 2006.

[385] D. Ludwig, Conical refraction in crystal optics and hydromagnetics, *Comm. Pure Appl. Math.* **14** (1961), 113–124.

[386] K. A. Lurie, *An Introduction to the Mathematical Theory of Dynamic Materials*, Advances in Mechanics and Mathematics, Springer, New York, 2007.

[387] A. M. Lyapunov, The general problem of the stability of motion (translated into English by A. T. Fuller), *Int. J. Control* **55** (1992), 531–773.

[388] A. A. Lyashenko and S. J. Friedlander, A sufficient condition for instability in the limit of vanishing dissipation, *J. Math. Anal. Appl.* **221** (1998), 544–558.

[389] B. R. Mace and E. Manconi, Wave motion and dispersion phenomena: Veering, locking and strong coupling effects, *J. Acoust. Soc. Amer.* **131** (2012), 1015–1028.

[390] R. S. MacKay, Stability of equilibria of Hamiltonian systems, in: S. Sarkar (ed.), *Nonlinear Phenomena and Chaos*, pp. 254–270, Adam Hilger, Bristol, 1986.

[391] R. S. MacKay, Movement of eigenvalues of Hamiltonian equilibria under non-Hamiltonian perturbation, *Phys. Lett. A* **155** (1991), 266–268.

[392] R. S. MacKay and P. G. Saffman, Stability of water-waves, *Proc. R. Soc. Lond. Ser. A Math. Phys. Eng. Sci.* **406** (1986), 115–125.

[393] R. S. MacKay and J. A. Sepulchre, Stability of discrete breathers, *Physica D-Nonlinear Phenomena* **119** (1998), 148–162.

[394] J. H. Maddocks, *Stability in Hamiltonian Systems and the Calculus of Variations*, EPFL, Lausanne, 1998.

[395] J. H. Maddocks and M. L. Overton, Stability theory for dissipatively perturbed Hamiltonian-systems, *Comm. Pure Appl. Math.* **48** (1995), 583–610.

[396] O. Mahrenholtz and R. Bogacz, On the shape of characteristic curves for optimal structures under non-conservative loads, *Archive of Applied Mechanics* **50** (1981), 141–148.

[397] A. A. Mailybaev, O. N. Kirillov and A. P. Seyranian, Geometric phase around exceptional points, *Phys. Rev. A* **72** (2005), 014104.

[398] A. A. Mailybaev, O. N. Kirillov and A. P. Seyranian, Berry phase around degeneracies, *Doklady Mathematics* **73** (2006), 129–133.

[399] A. A. Mailybaev, Transformation to versal deformations of matrices, *Linear Algebra and its Applications* **337** (2001), 87–108.

[400] I. G. Malkin, *Theory of Stability of Motion*, Nauka, Moscow, 1966 (in Russian).

[401] W. V. R. Malkus, Precession of Earth as cause of geomagnetism, *Science* **160** (1968), 259–264.

[402] C. Mallagh, *Naval Architecture: Mid-period Theory and Ideology*, http://homepage.ntlworld.com/christopher.mallagh/INCKy/Hist/NavArch/MidPeriodIdeol.html.

[403] A. Mallock, Determination of the viscosity of water, *Proc. R. Soc. Lond.* **45** (1888-1889), 126–132.

[404] A. Mallock, Experiments on fluid viscosity, *Phil. Trans. R. Soc. Lond. A* **187** (1896), 41–56.

[405] S. Mandre and L. Mahadevan, A generalized theory of viscous and inviscid flutter, *Proc. R. Soc. Lond. Ser. A Math. Phys. Eng. Sci.* **466** (2010), 141–156.

[406] M. Mansour and B. D. O. Anderson, Kharitonov's theorem and the second method of Lyapunov, in: *Proceedings of the Workshop on Robust Control and Stability*, pp. 3–11, Ascona, Switzerland, 1992.

[407] M. Mansour and B. D. O. Anderson, Kharitonov's theorem and the second method of Lyapunov, *Systems and Control Letters* **20** (1993), 39–47.

[408] A. S. Marathay, Propagation of polarized light in a cholesteric structure, *Optics Commun.* **3** (1971), 369–373.

[409] M. Marden, *Geometry of Polynomials*, 2nd edn., Mathematical Surveys and Monographs, Number 3, American Mathematical Society, Providence, RI, 1966.

[410] J. E. Marsden, R. Montgomery and T. Ratiu, Reduction, symmetry, and phases in mechanics, *Memoirs of the American Mathematical Society* **88** (1990), 1–110.

[411] J. E. Marsden, O. M. O'Reilly, F. J. Wicklin and B. W. Zombro, Symmetry, stability, geometric phases and mechanical integrators (Part II), *Nonlin. Sci. Today* **1** (1991), 14–21.

[412] J. E. Marsden and T. S. Ratiu, *Introduction to Mechanics and Symmetry: A Basic Exposition of Classical Mechanical Systems*, Texts in Applied Mathematics 17, Springer, Berlin, 1999.

[413] L. M. Martyushev, The maximum entropy production principle: two basic questions, *Philos. Trans. R. Soc. Ser. B Biol. Sci.* **365** (2010), 1333–1334.

[414] L. M. Martyushev and V. D. Seleznev, Maximum entropy production principle in physics, chemistry, and biology, *Physics Reports* **426** (2006), 1–45.

[415] F. Massi, O. Giannini and L. Baillet, Brake squeal as dynamic instability: an experimental investigation, *J. Acoust. Soc. Am.* **120** (2006), 1388–1398.

[416] J. C. Maxwell, On governors, *Proc. R. Soc.* **16** (1868), 270–283.

[417] J. C. Maxwell, *The Scientific Letters and Papers of James Clerk Maxwell*, 3, Cambridge University Press, Cambridge, UK, 2009.

[418] H. Mehri-Dehnavi and A. Mostafazadeh, Geometric phase for non-Hermitian Hamiltonians and its holonomy interpretation, *Journal of Mathematical Physics* **49** (2008), 082105.

[419] L. Meirovitch and P. Hagedorn, A new approach to the modeling of distributed non-self-adjoint systems, *J. Sound Vibr.* **178** (1994), 227–241.

[420] J. D. Meiss, *Differential Dynamical Systems*, Mathematical Modeling and Computation 14, SIAM, Philadelphia, 2007.

[421] R. Mennicken and M. Moeller, *Non-Self-Adjoint Boundary Eigenvalue Problems*, North-Holland Mathematics Studies 192, Elsevier, 2003.

[422] D. R. Merkin, *Gyroscopic Sytems*, Gostekhizdat, Moscow, 1956 (in Russian).

[423] D. R. Merkin, *Introduction to the Theory of Stability*, Texts in Applied Mathematics 24, Springer, Berlin, 1997.

[424] H. K. Moffatt, The fluid dynamics of James Clerk Maxwell, in: R. Flood, M. McCartney, and A. Whitaker, (eds.), *James Clerk Maxwell*, Oxford University Press, 2013 (in press).

[425] H. K. Moffatt and Y. Shimomura, Spinning eggs – a paradox resolved, *Nature* **416** (2002), 385–386.

[426] N. Moiseyev, *Non-Hermitian Quantum Mechanics*, Cambridge University Press, Cambridge, UK, 2011.

[427] M. Montagnier, C. C. Paige and R. J. Spiteri, Real Floquet factors of linear time-periodic systems, *Systems and Control Letters* **50** (2003), 251–262.

[428] J. Moro, J. V. Burke and M. L. Overton, On the Lidskii–Vishik–Lyusternik perturbation theory for eigenvalues of matrices with arbitrary Jordan structure, *SIAM J. Matrix Anal. Appl.* **18** (1997), 793–817.

[429] P. J. Morrison, A paradigm for joined Hamiltonian and dissipative systems, *Physica D* **18** (1986), 410–419.

[430] P. J. Morrison, Hamiltonian description of the ideal fluid, *Reviews of Modern Physics* **70** (1998), 467–521.

[431] J. Moser, New aspects in the theory of stability of Hamiltonian systems, *Comm. Pure Appl. Math.* **11** (1958), 81–114.

[432] J. E. Mottershead and S. N. Chan, Brake squeal – an analysis of symmetry and flutter instability, in: R. A. Ibrahim and A. Soom (eds.), *Proceedings of the Winter Annual Meeting of the ASME, Anaheim, CA, USA, Nov. 8-13, 1992, DE-vol. 49, Friction-Induced Vibration, Chatter, Squeal and Chaos*, pp. 87–97, ASME Publications, New York, 1992.

[433] J. Mottershead, Vibration- and friction-induced instabilities in discs, *The Shock and Vibration Digest* **30** (1998), 14–31.

[434] T. S. Motzkin and O. Taussky, Pairs of matrices with the property L, *Trans. Amer. Math. Soc.* **73** (1952), 108–114.

[435] T. S. Motzkin and O. Taussky, Pairs of matrices with the property L. II, *Trans. Amer. Math. Soc.* **80** (1955), 387–401.

[436] D. F. Moyer, Energy, dynamics, hidden machinery: Rankine, Thomson and Tait, Maxwell, *Studies in History and Philosophy of Science Part A* **8** (1977), 251–268.

[437] P. C. Müller, *Stabilität und Matrizen*, Springer, Berlin, 1977.

[438] I. Mutabazi and A. Bahloul, Stability analysis of a vertical curved channel flow with a radial temperature gradient, *Theoretical and Computational Fluid Dynamics* **16** (2002), 79–90.

[439] U. Nackenhorst and M. Brinkmeier, On the dynamics of rotating and rolling structures, *Archive of Applied Mechanics* **78** (2008), 477–488.

[440] W. Nagata and N. Namachchivaya, Bifurcations in gyroscopic systems with an application to rotating shafts, *Proc. R. Soc. Lond. A* **454** (1998), 543–585.

[441] B. Naiman, Remarks on the perturbation of analytic matrix functions, *Int. Equ. Oper. Theor.* **9** (1986), 593–599.

[442] M. Naimark, *Linear differential operators. Part I: Elementary theory of linear differential operators.* With additional material by the author, Frederick Ungar Publishing Co., 1967.

[443] Y. I. Neimark, On the problem of the distribution of the roots of polynomials, *Doklady Akad. Nauk SSSR (N.S.)* **58** (1947), 357–360.

[444] F. C. Nelson, A brief history of early rotor dynamics, *Sound and Vibration* **37** (2003), 8–11.

[445] S. Neukirch, J. Frelat, A. Goriely and C. Maurini, Vibrations of post-buckled rods: The singular inextensible limit, *J. Sound Vibr.* **331** (2012), 704–720.

[446] M. V. Nezlin, Negative-energy waves and the anomalous Doppler effect, *Soviet Physics Uspekhi* **19** (1976), 946.

[447] E. L. Nicolai, On the stability of a circular ring and of a circular arch under uniformly distributed normal loading (in Russian), *Izv. Petrogradskogo Polit. Inst.* **27** (1918) 232–378.

[448] E. L. Nicolai, On the stability of the rectilinear form of equilibrium of a bar in compression and torsion, *Izvestia Leningradskogo Politechnicheskogo Instituta* **31** (1928), 201–231.

[449] E. L. Nicolai, On the problem of the stability of a bar in torsion, *Vestnik Mechaniki i Prikladnoi Matematiki* **1** (1929), 41–58.

[450] E. L. Nicolai, Über den Einfluss der Torsion auf die Stabilität rotierender Wellen, in: *Proc. of the 3rd Congr. Appl. Mech.*, pp. 103–104, Stockholm, 1930.

[451] S. M. Nikolskii, *Memoirs (in Russian)*, Steklov Mathematical Institute, Moscow, 2003.

[452] E. Nissim, Effect of linear damping on flutter speed. I. Binary systems, *Aeronautical Quarterly* **16** (1965), 159–178.

[453] M. D. Nornberg, H. Ji, E. Schartman, A. Roach and J. Goodman, Observation of magnetocoriolis waves in a liquid metal Taylor–Couette experiment, *Phys. Rev. Lett.* **104** (2010), 074501.

[454] M. North, Disc brake squeal, in: *Braking of Road Vehicles*, Automobile Division of the Institution of Mechanical Engineers, pp. 169–176, Mechanical Engineers Publications Limited, London, England, 1976.

[455] G. I. Ogilvie, James Clerk Maxwell and the dynamics of astrophysical discs, *Phil. Trans. R. Soc. A* **366** (2008), 1707–1715.

[456] K. Ono, J.-S. Chen and D. B. Bogy, Stability analysis for the head-disk interface in a flexible disk drive, *Trans. ASME J. Appl. Mech.* **58** (1991), 1005–1014.

[457] L. Onsager, Reciprocal relations in irreversible processes. I., *Phys. Rev.* **37** (1931), 405–426.

[458] A. C. Or, On the behaviour of a pair of complex eigenmodes near a crossing, *Quart. J. Mech. Appl. Math.* **44** (1991), 559–569.

[459] O. M. O'Reilly, N. K. Malhotra and N. S. Namachchivaya, Reversible dynamical-systems – dissipation-induced destabilization and follower forces, *Applied Mathematics and Computation* **70** (1995), 273–282.

[460] O. M. O'Reilly, N. K. Malhotra and N. S. Namachchivaya, Some aspects of destabilization in reversible dynamical systems with application to follower forces, *Nonlinear Dynamics* **10** (1996), 63–87.

[461] G. Ostermeyer and M. Müller, New insights into the tribology of brake systems, *IMechE Journal of Automobile Engineering* **222** (2008), 1167–1200.

[462] L. A. Ostrovskii, S. A. Rybak and L. S. Tsimring, Negative energy waves in hydrodynamics, *Sov. Phys. Uspekhi* **29** (1986), 1040–1052.

[463] H. Ouyang, W. Nack, Y. Yuan and F. Chen, Numerical analysis of automotive disc brake squeal: A review, *Int. J. Veh. Noise and Vibr.* **1** (2005), 207–231.

[464] N. Paldor and A. Sigalov, The mechanics of inertial motion on the Earth and on a rotating sphere, *Physica D* **160** (2001), 29–53.

[465] Y. G. Panovko and I. I. Gubanova, *Stability and Oscillations of Elastic Systems*, Consultants Bureau, New York, 1965.

[466] Y. G. Panovko and S. V. Sorokin, On quasi-stability of viscoelastic systems with the follower forces, *Izv. Acad. Nauk SSSR. Mekh. Tverd. Tela.* **5** (1987), 135–139.

[467] Y. P. Park and C. D. Mote, The maximum controlled follower force on a free-free beam carrying a concentrated mass, *J. Sound Vibr.* **98** (1985), 247–256.

[468] P. C. Parks, A new look at the Routh–Hurwitz problem using Lyapunov's second method, *Bull. de l'Acad. Polon. des Sciences, Ser. des Sciences Techniques* **12** (1964), 19–21.

[469] P. C. Parks, A. M. Lyapunov's stability theory – 100 years on, *IMA Journal of Mathematical Control and Information* **9** (1992), 275–303.

[470] P. C. Parks and V. Hahn, *Stability Theory*, Prentice Hall International Series in Systems and Control Engineering, Prentice Hall, New York, 1993.

[471] W. Paul, Electromagnetic traps for charged and neutral particles, *Rev. Mod. Phys.* **62** (1990), 531–542.

[472] R. M. Pearce, Strong focusing in a magnetic helical quadrupole channel, *Nuclear Instruments and Methods* **83** (1970), 101–108.

[473] P. Pedersen and A. P. Seyranian, Sensitivity analysis for problems of dynamic stability, *International Journal of Solids and Structures* **19** (1983), 315–335.

[474] P. Pedersen, Influence of boundary conditions on the stability of a column under nonconservative load, *International Journal of Solids and Structures* **13** (1977), 445–455.

[475] F. M. Penning, Die Glimmentladung bei niedrigem Druck zwischen koaxialen Zylindern in einem axialen Magnetfeld, *Physica* **3** (1936), 873–894.

[476] N. Perkins and C. Mote, Comments on curve veering in eigenvalue problems, *J. Sound Vibr.* **106** (1986), 451–463.

[477] M. Philipp, P. von Brentano, G. Pascovici and A. Richter, Frequency and width crossing of two interacting resonances in a microwave cavity, *Phys. Rev. E* **62** (2000), 1922–1926.

[478] J. M. Piau, M. Bremond, J. M. Couette and M. Piau, Maurice Couette, one of the founders of rheology, *Rheol. Acta* **33** (1994), 357–368.

[479] R. H. Plaut, Determining the nature of instability in nonconservative problems, *AIAA Journal* **10** (1972), 967–968.

[480] R. Plaut, New destabilization phenomenon in nonconservative systems, *ZAMM Z. angew. Math. Mech.* **51** (1971), 319–321.

[481] H. Poincare, Note sur la stabilite de l'anneau de Saturne, *Bulletin Astronomique* **Serie I, 2** (1885), 507–508.

[482] S. Ponti, J. A. Reyes and C. Oldano, Homogeneous models for bianisotropic crystals, *Journal of Physics: Condensed Matter* **14** (2002), 10173.

[483] L. Pontryagin, Hermitian operators in a space with indefinite metric, *Izv. Akad. Nauk. SSSR Ser. Mat.* **8** (1944), 243–280.

[484] C. G. Poulton, L. C. Botten, R. C. McPhedran, N. A. Nicorovici and A. B. Movchan, Noncommuting limits in electromagnetic scattering: Asymptotic analysis for an array of highly conducting inclusions, *SIAM J. Appl. Math.* **61** (2001), 1706–1730.

[485] L. Prandtl, Beiträge zur Frage der kritischen Drehzahlen, *Dinglers Polytechnisches Journal* **20** (1918), 179–182.

[486] J. Priede, I. Grants and G. Gerbeth, Inductionless magnetorotational instability in a Taylor–Couette flow with a helical magnetic field, *Phys. Rev. E* **75** (2007), 047303.

[487] M. Proctor, The role of mean circulation in parity selection by planetary magnetic fields, *Geophys. Astrophys. Fluid Dynamics* **8** (1977), 311–324.

[488] B. I. Rabinovich, *A discussion upon the talk of M. L. Pivovarov "Rotating motion of satellites with a weak self-excitation, a survey"*, http://www.iki.rssi.ru/seminar/200011/piv_ans.htm, 30 November 2000, in Russian.

[489] K.-H. Rädler, Mean-field dynamo theory: Early ideas and today's problems, in: S. Molokov, R. Moreau, K. Moffatt, and K.-H. Rädler (eds.), *Magnetohydrodynamics*, Fluid Mechanics and its Applications 80, pp. 55–72, Springer Netherlands, 2007.

[490] A. Ralston, A symmetric formulation of the Hurwitz–Routh criterion, *Trans. I.R.E. on Automatic Control* **AC-7** (1962), 50–51.

[491] W. J. M. Rankine, On the centrifugal force of rotating shafts, *The Engineer* **27** (1869), 249.

[492] J. S. Rao, *History of Rotating Machinery Dynamics*, History of Mechanism and Machine Science 20, Springer, Berlin, 2011.

[493] J. W. S. Rayleigh, *The Theory of Sound*, 1, Macmillan, London, 1877.

[494] J. W. S. Rayleigh, On the dynamics of revolving fluids, *Proc. R. Soc. Lond. A* **93** (1917), 148–154.

[495] F. Rellich, Störungstheorie der Spektralzerlegung, *Mathematische Annalen* **113** (1937), 600–619.

[496] F. Rellich, *Perturbation Theory of Eigenvalue Problems*, Gordon and Breach, New York, 1968.

[497] U. Ringertz, On the design of Beck's column, *Structural Optimization* **8** (1994), 120–124.

[498] C. W. Roberson, A. Mondelli and D. Chernin, High-current betatron with stellarator fields, *Phys. Rev. Lett.* **50** (1983), 507–510.

[499] P. Y. Rocard, *Dynamic Instability: Automobiles, Aircraft, Suspension Bridges*, F. Ungar Publication, New York, NY, 1957.

[500] A. Rohlmann, T. Zander, M. Rao and G. Bergmann, Applying a follower load delivers realistic results for simulating standing, *J. Biomech.* **42** (2009), 1520–1526.

[501] R. Romea, Effects of friction and beta on finite-amplitude baroclinic waves, *Journal of the Atmospheric Sciences* **34** (1977), 1689–1695.

[502] T. Rossing, Acoustics of the glass harmonica, *J. Acoust. Soc. Am.* **95** (1994), 1106–1111.

[503] N. Rouche, P. Habets and M. Laloy, *Stability Theory by Liapunov's Direct Method*, Applied Mathematical Sciences 22, Springer-Verlag, New York Heidelberg Berlin, 1977.

[504] E. J. Routh, Stability of a dynamical system with two independent motions, *Proc. Lond. Math. Soc.* **5** (1874), 97–99.

[505] E. J. Routh, *Treatise on the Stability of a Given State of Motion, Particularly, Steady Motion*, MacMillan, London, 1877.

[506] M. S. Ruderman, L. Brevdo and R. Erdelyi, Kelvin–Helmholtz absolute and convective instabilities of, and signalling in, an inviscid fluid-viscous fluid configuration, *Proc. R. Soc. Lond. A* **460** (2004), 847–874.

[507] C. E. Ruter, K. G. Makris, R. El-Ganainy, D. N. Christodoulides, M. Segev and D. Kip, Observation of parity-time symmetry in optics, *Nature Physics* **6** (2010), 192–195.

[508] A. K. Samantaray, R. Bhattacharyya and A. Mukherjee, On the stability of Crandall gyropendulum, *Phys. Lett. A* **372** (2008), 238–243.

[509] G. R. Sarson and C. A. Jones, A convection driven geodynamo reversal model, *Phys. Earth Planet. Int.* **111** (1999), 3–20.

[510] G. S. Schajer, The vibration of a rotating circular string subject to a fixed end restraint, *J. Sound Vibr.* **92** (1984), 11–19.

[511] J. Schindler, A. Li, M. C. Zheng, F. M. Ellis and T. Kottos, Experimental study of active LRC circuits with PT-symmetries, *Phys. Rev. A* **84** (2011), 040101(R).

[512] R. Sedney, A survey of the fluid dynamic aspects of liquid-filled projectiles, in: *AIAA, Atmospheric Flight Mechanics Conference, 12th, Snowmass, CO, Aug. 18-21, 1985.*, AIAA-85-1822-CP, pp. 1–19, 1985.

[513] C. Semler, H. Alighanbari and M. Paidoussis, A physical explanation of the destabilizing effect of damping, *Trans. ASME J. Appl. Mech.* **65** (1998), 642–648.

[514] M. B. Sevryuk, *Reversible Systems*, Lecture Notes in Mathematics 1211, Springer-Verlag, New York, 1986.

[515] M. B. Sevryuk, Reversible linear systems and their versal deformations, *Journal of Mathematical Sciences* **60** (1992), 1663–1680.

[516] A. P. Seyranian, Bifurcations in single-parameter circulatory systems, *Izv. RAN Mekhanika Tverdogo Tela* **29** (1994), 142–148.

[517] A. P. Seyranian, O. N. Kirillov and A. A. Mailybaev, Coupling of eigenvalues of complex matrices at diabolic and exceptional points, *J. Phys. A: Math. Gen.* **38** (2005), 1723–1740.

[518] A. P. Seyranian and A. A. Mailybaev, *Multiparameter Stability Theory with Mechanical Applications*, Series on Stability, Vibration and Control of Systems, Series A 13, World Scientific, Singapore, 2003.

[519] A. P. Seyranian and A. A. Mailybaev, Paradox of Nicolai and related effects, *ZAMP Z. angew. Math. Phys.* **62** (2011), 539–548.

[520] A. P. Seyranian and P. Pedersen, On two effects in fluid/structure interaction theory, in: *Flow-induced Vibration*, pp. 565–576, Balkema, Rotterdam, 1995.

[521] A. P. Seyranian and O. N. Kirillov, Bifurcation diagrams and stability boundaries of circulatory systems, *Theoret. Appl. Mech.* **26** (2001), 135–138.

[522] V. E. Shapiro, Rotating class of parametric resonance processes in coupled oscillators, *Phys. Lett. A* **290** (2001), 288–296.

[523] M. Y. Shatalov, A. G. Every and A. S. Yenwong-Fai, Analysis of non-axisymmetric wave propagation in a homogeneous piezoelectric solid circular cylinder of transversely isotropic material, *International Journal of Solids and Structures* **46** (2009), 837–850.

[524] R. C. Shieh and E. F. Masur, Some general principles of dynamic instability of solid bodies, *ZAMP Z. angew. Math. Phys.* **19** (1968), 927–941.

[525] A. A. Shkalikov, Operator pencils arising in elasticity and hydrodynamics: The instability index formula, *Oper. Theory Adv. Appl.* **87** (1996), 358–385.

[526] A. A. Shkalikov, Invariant subspaces of dissipative operators in Krein space and Sobolev problem on a rotating top, *Funct. Anal. Appl.* (2004), 273–286.

[527] A. Shuvalov and N. Scott, On singular features of acoustic wave propagation in weakly dissipative anisotropic thermoviscoelasticity, *Acta Mechanica* **140** (2000), 1–15.

[528] G. J. Simitses and D. H. Hodges, *Nonconservative Systems*, Fundamentals of Structural Stability, Butterworth-Heinemann, Burlington, 2006, pp. 297 – 328.

[529] S. C. Sinha, E. A. Butcher and A. Dávid, Construction of dynamically equivalent time-invariant forms for time-periodic systems, *Nonlinear Dynamics* **16** (1998), 203–221.

[530] J.-J. Sinou, F. Thouverez and L. Jezequel, Stability analysis and non-linear behaviour of structural systems using the complex non-linear modal analysis, *Comput. Struct.* **84** (2006), 1891–1905.

[531] J.-J. Sinou and L. Jezequel, Mode coupling instability in friction-induced vibrations and its dependency on system parameters including damping, *European Journal of Mechanics - A/Solids* **26** (2007), 106 – 122.

[532] D. R. Sisan, N. Mujica, W. A. Tillotson, Y.-M. Huang, W. Dorland, A. B. Hassam, T. M. Antonsen, and D. P. Lathrop, Experimental observation and characterization of the magnetorotational instability, *Phys. Rev. Lett.* **93** (2004), 114502.

[533] D. Sjöberg, C. Enström, G. Kristensson, D. J. N. Wall and N. Wellander, A Floquet–Bloch decomposition of Maxwell's equations applied to homogenization, *Multiscale Model. Simul.* **4** (2005), 149–171.

[534] D. M. Smith, The motion of a rotor carried by a flexible shaft in flexible bearings, *Proc. R. Soc. Lond. A* **142** (1933), 92–118.

[535] T. E. Smith and G. Herrmann, Stability of a beam on an elastic foundation subjected to a follower force, *Trans. ASME J. Appl. Mech.* **39** (1972), 628–629.

[536] S. Sobolev, On motion of a symmetric top with a cavity filled with fluid, in: G. V. Demidenko and V. L. Vaskevich (eds.), *Selected Works of S. L. Sobolev*, pp. 333–382, Springer, 2006.

[537] G. Spelsberg-Korspeter, D. Hochlenert and P. Hagedorn, Self-excitation mechanisms in paper calenders formulated as a stability problem, *Technische Mechanik* **31** (2011), 15–24.

[538] G. Spelsberg-Korspeter, D. Hochlenert, O. N. Kirillov and P. Hagedorn, In- and out-of-plane vibrations of a rotating plate with frictional contact: Investigations on squeal phenomena, *Trans. ASME J. Appl. Mech.* **76** (2009), 041006.

[539] G. Spelsberg-Korspeter, O. N. Kirillov and P. Hagedorn, Modeling and stability analysis of an axially moving beam with frictional contact, *Trans. ASME J. Appl. Mech.* **75** (2008), 031001.

[540] R. J. Spiteri and M. Montagnier, The real story behind Floquet–Lyapunov theory, in: N. Mastorakis (ed.), *Problems in Modern Applied Mathematics*, pp. 276–281, World Scientific and Engineering Society Press, 2000.

[541] R. Spurr, The ringing of wine glasses, *Wear* **4** (1961), 150–153.

[542] R. Spurr, A theory of brake squeal, *Proc. Inst. Mech. Eng.* **AD** (1961), 33–52.

[543] M. Steenbeck, F. Krause and K.-H. Rädler, Berechnung der mittleren Lorentz-Feldstärke $\overline{\mathbf{v} \times \mathbf{b}}$ für ein elektrisch leitendes Medium in turbulenter, durch Coriolis–Kräfte beeinfluter Bewegung, *Z. Naturforsch.* **21a** (1966), 369–376.

[544] F. Stefani, S. Eckert, G. Gerbeth, A. Giesecke, T. Gundrum, C. Steglich, T. Weier and B. Wustmann, DRESDYN – A new facility for MHD experiments with liquid sodium, *Magnetohydrodynamics* **48** (2012), 103–113.

[545] F. Stefani, A. Gailitis and G. Gerbeth, Magnetohydrodynamic experiments on cosmic magnetic fields, *ZAMM Z. angew. Math. Mech.* **88** (2008), 930–954.

[546] F. Stefani, T. Gundrum, G. Gerbeth, G. Rüdiger, M. Schultz, J. Szklarski and R. Hollerbach, Experimental evidence for magnetorotational instability in a Taylor-Couette flow under the influence of a helical magnetic field, *Phys. Rev. Lett.* **97** (2006), 184502.

[547] F. Stefani and G. Gerbeth, Asymmetric polarity reversals, bimodal field distribution, and coherence resonance in a spherically symmetric mean-field dynamo model, *Phys. Rev. Lett.* **94** (2005), 184506.

[548] G. W. Stewart and J. G. Sun, *Matrix Perturbation Theory*, Computer Science and Scientific Computing, Academic Press, Boston, 1990.

[549] K. Stewartson, On the stability of a spinning top containing liquid, *J. Fluid Mech.* **5** (1959), 577–592.

[550] A. Struthers and G. Jayaraman, Elastic stability of columns on partial elastic foundations under subtangential loading, *J. Sound Vibr.* **329** (2010), 3856–3865.

[551] P. A. Sturrock, Kinematics of growing waves, *Phys. Rev.* **112** (1958), 1488–1503.

[552] P. A. Sturrock, In what sense do slow waves carry negative energy, *J. Appl. Phys.* **31** (1960), 2052–2056.

[553] Y. Sugiyama, *Experimental Approach to Nonconservative Stability Problems*, Modern Problems of Structural Stability, pp. 341–394, Springer, Vienna, 2002.

[554] Y. Sugiyama, K. Katayama and K. Kiriyama, Experimental verification of dynamic stability of vertical cantilevered columns subjected to a sub-tangential force, *J. Sound Vibr.* **236** (2000), 193–207.

[555] Y. Sugiyama, T. Katayama, T. Yosimura and H. Kawagoe, Stability of Reut's columns having a damper, *Transactions of the Japan Society of Mechanical Engineers. C* **57(537)** (1991), 1575–1579.

[556] Y. Sugiyama and M. A. Langthjem, Physical mechanism of the destabilizing effect of damping in continuous non-conservative dissipative systems, *International Journal of Non-Linear Mechanics* **42** (2007), 132–145.

[557] Y. Sugiyama, M. Langthjem and B.-J. Ryu, Realistic follower forces, *J. Sound Vibr.* **225** (1999), 779–782.

[558] Y. Sugiyama, M. Langthjem and B.-J. Ryu, Beck's column as the ugly duckling, *J. Sound Vibr.* **254** (2002), 407–410.

[559] Y. Sugiyama, M. A. Langthjem, T. Iwama, M. Kobayashi, K. Katayama and H. Yutani, Shape optimization of cantilevered columns subjected to a rocket-based follower force and its experimental verification, *Structural and Multidisciplinary Optimization* **46** (2012), 829–838.

[560] J. Sun, Eigenvalues and eigenvectors of a matrix dependent on several parameters, *J. Comput. Math.* **3** (1985), 351–364.

[561] J. Sun, Multiple eigenvalue sensitivity analysis, *Linear Algebra and Applications* **137/138** (1990), 183–211.

[562] C. Sundararajan, Optimization of a nonconservative elastic system with stability constraint, *Journal of Optimization Theory and Applications* **16** (1975), 355–378.

[563] G. E. Swaters, Modal interpretation for the Ekman destabilization of inviscidly stable baroclinic flow in the Phillips model, *J. Phys. Oceanogr.* **40** (2010), 830–839.

[564] E. Tassi and P. J. Morrison, Mode signature and stability for a Hamiltonian model of electron temperature gradient turbulence, *Physics of Plasmas* **18** (2011), 032115.

[565] H. Tasso, Linear and nonlinear stability in resistive magnetohydrodynamics, *Annals of Physics* **234** (1994), 211–224.

[566] G. I. Taylor, Stability of a viscous liquid contained between two rotating cylinders, *Phil. Trans. R. Soc. Lond. A* **223** (1923), 289–343.

[567] B. D. H. Tellegen, The gyrator, a new electric network element, *Philips Res. Rep.* **3** (1948), 81–101.

[568] E. Teller, The crossing of potential surfaces, *J. Phys. Chem.* **41** (1937), 109–116.

[569] M. Teytel, How rare are multiple eigenvalues? *Comm. Pure Appl. Math.* **52** (1999), 917–934.

[570] J. M. T. Thompson, *Instabilities and Catastrophes in Science and Engineering*, Wiley, New York, 1982.

[571] R. I. Thompson, T. J. Harmon and M. G. Ball, The rotating-saddle trap: A mechanical analogy to RF-electric-quadrupole ion trapping?, *Canadian Journal of Physics* **80** (2002), 1433–1448.

[572] W. Thomson, On the precessional motion of a liquid, *Nature (London)* **15** (1877), 297–298.

[573] W. Thomson and P. G. Tait, *Treatise on Natural Philosophy, vol. I, part I, New Edition*, Cambridge University Press, Cambridge, 1879.

[574] J. Tian and S. Hutton, On the mechanisms of vibrational instability in a constrained rotating string, *J. Sound Vibr.* **225** (1999), 111–126.

[575] V. N. Tkhai, On stability of mechanical systems under the action of position forces, *PMM J. Appl. Math. Mech.* **44** (1980), 24–29.

[576] L. N. Trefethen and M. Embree, *Spectra and Pseudospectra: The Behavior of Nonnormal Matrices and Operators*, Princeton University Press, Princeton, NJ, 2005.

[577] G. S. Triantafillou, Note on the Kelvin-Helmholtz instability of stratified fluids, *Phys. Fluids* **6** (1994), 164–171.

[578] D. Tsiklauri, On the conical refraction of hydromagnetic waves in plasma with anisotropic thermal pressure, *Physics of Plasmas* **3** (1996), 800–803.

[579] J. van der Meer, *Hamiltonian Hopf Bifurcation*, Lect. Notes Math. 1160, Springer-Verlag, Berlin, 1985.

[580] C. F. van Loan, How near is a stable matrix to an unstable matrix? *Contemp. Math.* **47** (1985), 465–477.

[581] E. P. Velikhov, Stability of an ideally conducting liquid flowing between cylinders rotating in a magnetic field, *Sov. Phys. JETP-USSR* **9** (1959), 995–998.

[582] K. Veselic, On the stability of rotating systems, *ZAMM Z. angew. Math. Mech.* **75** (1995), 325–328.

[583] S. Vidoli and F. Vestroni, Veering phenomena in systems with gyroscopic coupling, *Trans. ASME, J. Appl. Mech.* **72** (2005), 641–647.

[584] M. Vishik and L. Lyusternik, Solution of some perturbation problems in the case of matrices and selfadjoint or non-selfadjoint equations, *Russian Math. Surveys* **15** (1960), 1–74.

[585] H. Volkmer, *Multiparameter Eigenvalue Problems and Expansion Theorems*, Springer, Berlin, 2009.

[586] T. von Karman, *Festigkeitsprobleme im Maschinenbau*, in: Encyklopaedie der Mathematischen Wissenschaften, IV:4, pp. 311–385, Teubner, Leipzig, 1910.

[587] J. von Neumann and E. Wigner, Concerning the behaviour of eigenvalues in adiabatic processes, *Physikalische Zeitschrift* **30** (1929), 467–470.

[588] U. von Wagner, D. Hochlenert and P. Hagedorn, Minimal models for disk brake squeal, *J. Sound Vibr.* **302** (2007), 527–539.

[589] J. A. Walker, A note on stabilizing damping configurations for linear nonconservative systems, *International Journal of Solids and Structures* **9** (1973), 1543–1545.

[590] J. A. Walker, *Dynamical Systems and Evolution Equations: Theory and Applications*, Mathematical Concepts and Methods in Science and Engineering 20, Plenum Press, New York, 1980.

[591] J. Wallis, *Cono-cuneus, or, The shipwright's circular wedge that is, a body resembling in part a conus, in part a cuneus, geometrically considered*, in a letter to the honourable Sir Robert Moray, printed by John Playford for Richard Davis, London, 1684.

[592] G. Wang and Y. Lin, A new extension of Leverrier's algorithm, *Linear Algebra and Applications* **180** (1993), 227–238.

[593] A. Welters, On explicit recursive formulas in the spectral perturbation analysis of a Jordan block, *SIAM J. Matrix Anal. Appl.* **32** (2011), 1–22.

[594] F. J. W. Whipple, The motion of a particle on the surface of a smooth rotating globe, *Phil. Mag., 6th series* **33** (1917), 457–471.

[595] E. P. Wigner, Ueber die Operation der Zeitumkehr in der Quantenmechanik, *Nachrichten von der Gesellschaft der Wissenschaften zu Gottingen, Mathematisch-Physikalische Klasse* (1932), 546–559.

[596] J. C. Willems and P. A. Fuhrmann, Stability theory for high order equations, *Linear Algebra and its Application* **167** (1992), 131–149.

[597] J. Williamson, On the algebraic problem concerning the normal forms of linear dynamical systems, *American Journal of Mathematics* **58** (1936), 141–163.

[598] J. Williamson, On the normal forms of linear canonical transformations in dynamics, *American Journal of Mathematics* **59** (1937), 599–617.

[599] A. P. Willis and C. F. Barenghi, Magnetic instability in a sheared azimuthal flow, *Astronomy and Astrophysics* **388** (2002), 688–691.

[600] H. Wimmer, Inertia theorems for matrices, controllability and linear vibrations, *Linear Algebra and its Applications* **8** (1974), 337–343.

[601] Y. Xie, S.-S. Li, Y.-W. Lin, Z. Ren and C. T.-C. Nguyen, UHF micromechanical extensional wine-glass mode ring resonators, in: *Techical Digest, 2003 IEEE International Electron Devices Meeting, Washington, DC, Dec. 8–10*, pp. 953–956, IEEE, 2003.

[602] Y. Xiong and S. G. Hutton, Vibration and stability analysis of a multi-guided rotating string, *J. Sound Vibr.* **169** (1994), 669–683.

[603] V. A. Yakubovich and V. M. Starzinskii, *Linear Differential Equations with Periodic Coefficients*, vols. 1 and 2, Wiley, New York, 1975.

[604] L. Yang and S. Hutton, Interactions between an idealized rotating string and stationary constraints, *J. Sound Vibr.* **185** (1995), 139–154.

[605] E. A. Youssef, F. S. Chute and F. E. Vermeulen, A note on particle trajectories in a Helical Electrostatic Quadrupole, *Nuclear Instruments and Methods* **93** (1971), 181–186.

[606] M. Y. Yurkin, The finite dimension property of small oscillations of a top with a cavity filled with an ideal fluid, *Functional Analysis and its Applications* **31** (1997), 40–51.

[607] M. Y. Yurkin, On the stability of small oscillations of a spinning asymmetrical top with liquid inside, *Doklady Akademii Nauk* **362** (1998), 170–173.

[608] E. E. Zajac, Kelvin–Tait–Chetaev theorem and extensions, *Journal of the Astronautical Sciences* **11** (1964), 46–49.

[609] V. E. Zakharov, Stability of periodic waves of finite amplitude on the surface of a deep fluid, *Journal of Applied Mechanics and Technical Physics* **9** (1968), 190–194.

[610] V. E. Zakharov and L. A. Ostrovsky, Modulation instability: The beginning, *Physica D-Nonlinear Phenomena* **238** (2009), 540–548.

[611] A. Zettl, *Sturm–Liouville Theory*, Mathematical Surveys and Monographs 121, AMS, Providence, RI, 2005.

[612] A. A. Zevin, A theory of linear non-conservative systems, *J. Appl. Math. Mech.* **52** (1988), 300–304.

[613] A. A. Zevin, On the theory of linear gyroscopic systems, *J. Appl. Math. Mech.* **60** (1996), 227–232.

[614] Z. Zhang, J. Neubauer and D. Berry, Physical mechanisms of phonation onset: A linear stability analysis of an aeroelastic continuum model of phonation, *J. Acoust. Soc. Am.* **122** (2007), 2279–2295.

[615] N. I. Zhinzher, Effect of dissipative forces with incomplete dissipation on the stability of elastic systems, *Izv. Ross. Akad. Nauk. MTT* **1** (1994), 149–155.

[616] J. Zhou, Classification and characteristics of Floquet factorisations in linear continuous-time periodic systems, *International Journal of Control* **81** (2008), 1682–1698.

[617] V. F. Zhuravlev, Generalization of the Rayleigh theorem to gyroscopic systems, *PMM J. Appl. Math. Mech.* **40** (1976), 606–610.

[618] V. F. Zhuravlev, Decomposition of nonlinear generalized forces into potential and circulatory components, *Doklady Physics* **52** (2007), 339–341.

[619] V. F. Zhuravlev, Analysis of the structure of generalized forces in the Lagrange equations, *Mechanics of Solids* **43** (2008), 837–842.

[620] V. F. Zhuravlev and D. M. Klimov, Theory of the shimmy phenomenon, *Mechanics of Solids* **45** (2010), 324–330.

[621] H. Ziegler, Stabilitätsprobleme bei geraden Staben und Wellen, *ZAMP Z. angew. Math. Phys.* **2** (1951), 265–289.

[622] H. Ziegler, Die Stabilitätskriterien der Elastomechanik, *Archive of Applied Mechanics* **20** (1952), 49–56.

[623] H. Ziegler, Linear elastic stability. A critical analysis of methods, First part, *ZAMP Z. angew. Math. Phys.* **4** (1953), 89–121.

[624] H. Ziegler, Linear elastic stability. A critical analysis of methods, Second part, *ZAMP Z. angew. Math. Phys.* **4** (1953), 167–185.

[625] H. Ziegler, An attempt to generalize Onsager's principle, and its significance for rheological problems, *ZAMP Z. angew. Math. Phys.* **9** (1958), 748–763.

[626] H. Ziegler, *Principles of structural stability*, Blaisdell Publ. Co., Waltham, Massachusetts, Toronto, 1968.

Index